frontiers | Research Topics

Advancements in stem cell differentiation and disease applications

Edited by
Yu Liu

Published in
Frontiers in Cell and Developmental Biology
Frontiers in Genetics

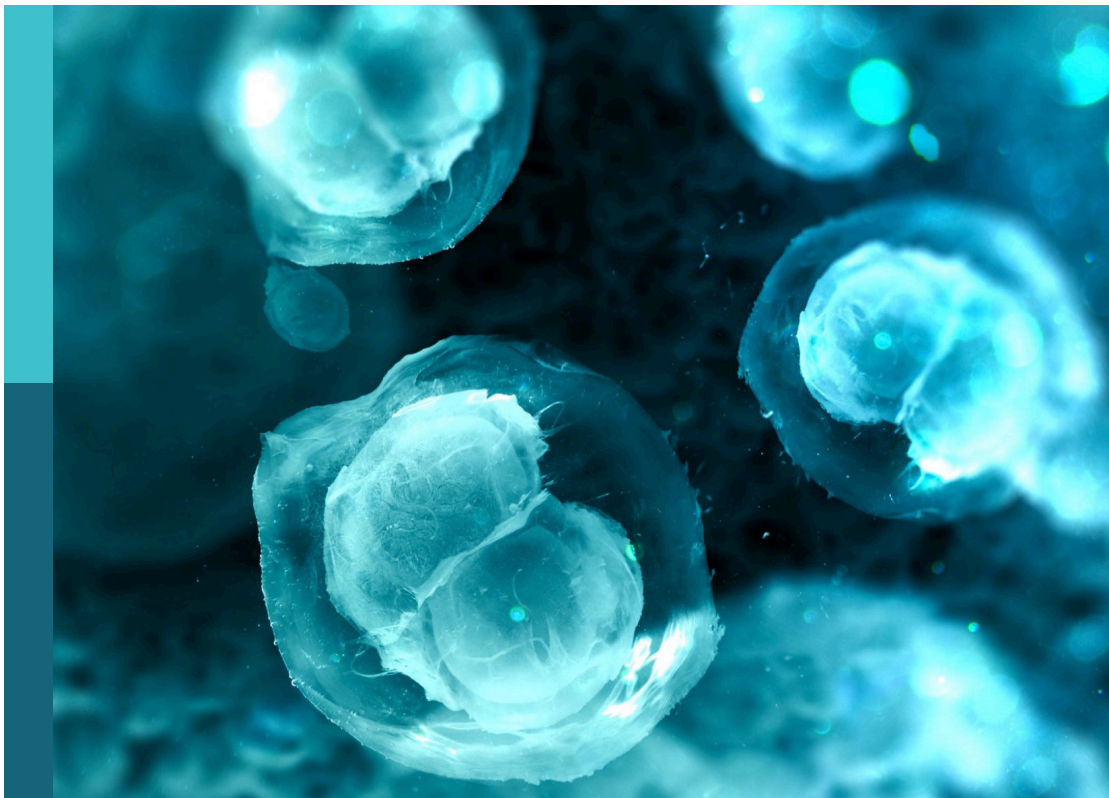

ISSN 1664-8714
ISBN 978-2-8325-7455-3
DOI 10.3389/978-2-8325-7455-3

Generative AI statement
Any alternative text (Alt text) provided alongside figures in the articles in this ebook has been generated by Frontiers with the support of artificial intelligence and reasonable efforts have been made to ensure accuracy, including review by the authors wherever possible. If you identify any issues, please contact us.

About Frontiers

Frontiers is more than just an open access publisher of scholarly articles: it is a pioneering approach to the world of academia, radically improving the way scholarly research is managed. The grand vision of Frontiers is a world where all people have an equal opportunity to seek, share and generate knowledge. Frontiers provides immediate and permanent online open access to all its publications, but this alone is not enough to realize our grand goals.

Frontiers journal series

The Frontiers journal series is a multi-tier and interdisciplinary set of open-access, online journals, promising a paradigm shift from the current review, selection and dissemination processes in academic publishing. All Frontiers journals are driven by researchers for researchers; therefore, they constitute a service to the scholarly community. At the same time, the *Frontiers journal series* operates on a revolutionary invention, the tiered publishing system, initially addressing specific communities of scholars, and gradually climbing up to broader public understanding, thus serving the interests of the lay society, too.

Dedication to quality

Each Frontiers article is a landmark of the highest quality, thanks to genuinely collaborative interactions between authors and review editors, who include some of the world's best academicians. Research must be certified by peers before entering a stream of knowledge that may eventually reach the public - and shape society; therefore, Frontiers only applies the most rigorous and unbiased reviews. Frontiers revolutionizes research publishing by freely delivering the most outstanding research, evaluated with no bias from both the academic and social point of view. By applying the most advanced information technologies, Frontiers is catapulting scholarly publishing into a new generation.

What are Frontiers Research Topics?

Frontiers Research Topics are very popular trademarks of the *Frontiers journals series*: they are collections of at least ten articles, all centered on a particular subject. With their unique mix of varied contributions from Original Research to Review Articles, Frontiers Research Topics unify the most influential researchers, the latest key findings and historical advances in a hot research area.

Find out more on how to host your own Frontiers Research Topic or contribute to one as an author by contacting the Frontiers editorial office: frontiersin.org/about/contact

Advancements in stem cell differentiation and disease applications

Topic editor
Yu Liu — University of Houston, United States

Citation
Liu, Y., ed. (2026). *Advancements in stem cell differentiation and disease applications*. Lausanne: Frontiers Media SA. doi: 10.3389/978-2-8325-7455-3

Table of contents

frontiers | Frontiers in Genetics

TYPE Original Research
PUBLISHED 02 April 2025
DOI 10.3389/fgene.2025.1516626

OPEN ACCESS

EDITED BY
Valerie Kouskoff,
The University of Manchester, United Kingdom

REVIEWED BY
Armel Hervé Nwabo Kamdje,
University of Garoua, Cameroon
Seo Rin Kim,
Pusan National University, Republic of Korea

*CORRESPONDENCE
Xinghua Lv,
ldyylxh18@163.com

RECEIVED 24 October 2024
ACCEPTED 11 March 2025
PUBLISHED 02 April 2025

CITATION
He J, Yao Y, Wang R, Liu Y, Wan X, Wang H, Zhou Y, Wang W, Ma Y and Lv X (2025) Enhanced renal ischemia/reperfusion injury repair potential of exosomes derived from B7-H1^{high} mesenchymal stem cells.
Front. Genet. 16:1516626.
doi: 10.3389/fgene.2025.1516626

Enhanced renal ischemia/reperfusion injury repair potential of exosomes derived from B7-H1^{high} mesenchymal stem cells

Jiahui He[1], Yawei Yao[1], Ruiyan Wang[1], Yujia Liu[1], Xingyu Wan[1], Hao Wang[2], Yuqiang Zhou[1], Wenjing Wang[1], Yan Ma[1] and Xinghua Lv[2]*

[1]Department of Anaesthesia, The First Clinical Medical College of Lanzhou University, Lanzhou, China, [2]Department of Day Surgery Center, The First Hospital of Lanzhou University, Lanzhou, Gansu, China

Two subgroups with high expression of B7-H1 and low expression of B7-H1 were successfully isolated from primitive human umbilical cord mesenchymal stem cells. And exosomes with high B7-H1 expression and low B7-H1 expression were successfully isolated. In comparison to the sham-operated group, mice in the IRI group demonstrated elevated serum levels of blood urea nitrogen (BUN) and serum creatinine (Scr), accompanied by a more pronounced degree of renal tissue damage. The administration of exosomes via the tail vein markedly accelerated the recovery of renal function in IRI mice, with the therapeutic effect beingmore pronounced in those treated with B7-H1high-Exo. Moreover RNA sequencing of mouse kidney treated with B7-H1high-Exo and B7-H1low-Exo showed that eight genes (C3, IRF7, AREG, CXCL10, Aldh1l2, Fnip2, Vcam1, St6galnac3) were involved in the pathophysiological process of ischemia-reperfusion injury. The *in vitro* and *in vivo* experiments showed that the expression level of C3 protein was significantly decreased, which indicated that B7-H1high-Exo played a therapeutic role by down-regulating C3.

KEYWORDS

renal ischemia-reperfusion injury, exosomes, B7-H1, cell sorting, C3, NF-κB

Introduction

The occurrence of acute kidney injury (AKI) following cardiac surgery can reach up to 40% among patients undergoing such procedures. Even mild and transient forms of AKI are associated with an increased risk of prolonged intensive care unit (ICU) stay, as well as elevated morbidity and mortality rates (Lassnigg et al., 2004; Wang and Bellomo, 2017). Renal ischemia-reperfusion injury (IRI) represents the predominant etiology of perioperative AKI and has emerged as a critical determinant of patient prognosis. In a variety of clinical settings, including major vascular, cardiac, and hepatic surgeries, as well as conditions such as shock, sepsis, trauma, and renal transplantation, renal IRI arises from the cessation of renal blood flow, followed by reperfusion. This process initiates a signaling cascade that mediates necrosis, apoptosis, and inflammation of renal cells, leading to AKI, which is characterized by the activation of endothelial cells, leukocyte recruitment and infiltration, and death of tubular epithelial cells (Bonventre and Weinberg, 2003; Han and Lee, 2019).

Despite the extensive knowledge and depth of existing studies on IRI, there remains no clear consensus regarding the precise role of immune system dysfunction in hypoxia-induced multiorgan injury. Programmed cell death protein 1 (PD-1) and its primary endogenous ligand, programmed death ligand 1 (PD-L1), which is also known as B7-H1 or CD274, are pivotal immune checkpoint molecules that play a critical role in regulating apoptosis. B7-H1, part of the B7 family of co-stimulatory molecules, is an important target for immune regulation (Ishida et al., 1992). Recent research has shown that changes in B7-H1 expression are linked to IRI, with increased levels observed in various hypoxia experimental models and in patients experiencing IRI (Hakroush et al., 2021; Sumiyoshi et al., 2021; Wang et al., 2022). As early as 2003, Fondevila et al. suggested that liver damage from prolonged ischemia followed by reperfusion should be viewed as an inflammatory response driven by the innate immune system (Fondevila et al., 2003). They later provided initial evidence that the co-stimulation of PD-1-negative T-cells influenced a local innate immune-driven inflammatory response, leading to hepatic IRI. Indeed, while disruption of PD-1 signaling exacerbated hepatocyte injury, the engagement of B7-H1 following intentional stimulation conferred protection against fulminant IRI through a localized IL-10-mediated mechanism. These findings indicate that the engagement of negative PD-1/B7-H1 signaling is essential for maintaining liver homeostasis during IR-induced hepatocyte injury (Ji et al., 2010). While the numbers of studies in this domain is still limited, B7-H1 has demonstrated considerable potential as a clinical therapeutic target.

As novel mediators of intercellular communication, exosomes (Exo) play a pivotal role in stem cell-mediated tissue repair. Direct interaction with target cells enables the delivery of genetic materials, including mRNA and miRNA, bypassing the potential risks associated with stem cell transplantation (Gho and Lee, 2017; Guo et al., 2021).

Mesenchymal stem cells (MSCs) can be sourced from a variety of tissues, with hucMSCs being particularly advantageous for cell therapy due to their readily accessible origin from umbilical cords (Xiao et al., 2022). Despite the registration of approximately 300 clinical trials investigating the therapeutic potential of hucMSCs, their efficacy remains constrained by the inherent heterogeneity of MSCs and the adverse effects reported in some clinical trials (Phinney, 2012; Tyndall, 2011). Utilizing different MSCs can reduce negative effects, remove confounding factors, and improve the effectiveness of their specific roles, which in turn aids in creating more effective treatment options. Consequently, it is essential to further categorize and characterize MSCs according to their functional diversity to support the creation of standardized MSC-based approaches for treating various diseases (Wu et al., 2020).

Recent research has elucidated that human gingival mesenchymal stem cells (GMSCs) can be categorized into B7-H1^{high} and B7-H1^{low} subpopulations, with the immunomodulatory function of GMSCs being significantly associated with B7-H1 signaling. In a murine model of type II collagen-induced arthritis (CIA), the increased expression of B7-H1 led to a significant reduction in the activity of inflammatory cells activity compared to the B7-H1^{low} subpopulation, thereby mitigating inflammation in the CIA model. The presence of a GMSC subpopulation with elevated B7-H1 expression could offer a distinctive and complementary approach for stem cell-based treatments targeting autoimmune and inflammatory diseases.

The findings of these studies suggest that a subset of MSCs with elevated B7-H1 expression may offer a promising avenue for the treatment of IRI. However, the precise function of the CD274+ hucMSCs subset, along with the assessment of its Exo origin in the management of renal IRI and its underlying molecular processes, remains uninvestigated. In this study, subpopulations of B7-H1^{high} and B7-H1^{low} hucMSCs were isolated using flow cytometry, and Exo was subsequently extracted for further analysis. Advanced experiments have identified ST6GalNac3 as a critical mediator of B7-H1^{high}-Exo function, with the *in vitro* effects on HK-2 cells attributed to the elevated expression of B7-H1. Our research discloses a novel role for B7-H1^{high}-Exo, suggesting its potential in promoting renal tissue repair and functional recovery, thereby opening up promising avenues for cell-free therapeutic strategies in the treatment of IRI.

Materials and methods

Mice

Six-to eight-week-old male SPF-grade C57BL/6 mice were procured from the Animal Experiment Center of Lanzhou University [License: SCXK (GAN) 2023-0003] and housed in an SPF-grade laboratory. The mice were free to ingest food and water throughout the duration of the experiment. Environmental conditions, including constant temperature and humidity, were rigorously maintained.

Mouse renal I/R model

Mouse renal I/R model was performed in male C57BL/6 mice. Briefly, the mice were anesthetized with pentobarbital sodium by intraperitoneal injection and lay on the platform. B7-H1^{high}-Exo (50 μg), B7-H1^{low}-Exo (50 μg) and PBS was separately injected into the tail vein of the fixed mice using a mouse tail vein injection imager before the start of surgery. Dorsal incisions of both left and right sides were made to expose kidneys. The right kidney artery was gently separated with cotton swabs and occluded with a microvascular clamp to induce renal ischemia for 45 min. The left renal pedicle clamping and ischemia were the same as right. After ischemia, the micro-aneurysm clips were removed to start the reperfusion. The wounds were sutured and resuscitated with warm sterile saline intraperitoneally. All operations were the same in the sham group except for clamping and ischemia. The mice were sacrificed 24 h after reperfusion and the specimens were collected. All animal experimental protocols were performed according to the guidelines of the Ethical Committee of the First Hospital Lanzhou University.

Cell culture

HucMSCs, provided by Yinfeng Biologicals and validated by the bioassay laboratory of Shaanxi Stem Cell Engineering Co., Ltd., were cultured in Dulbecco's Modified Eagle Medium (DMEM) supplemented with 10% fetal bovine serum (FBS), 1% penicillin, and streptomycin, and subsequently digested with 0.25% trypsin. After 48 h, the supernatant of MSCs cells transfected with B7-H1^{high} and B7-H1^{low} were collected for exosomes extraction. All cell cultures were maintained in a saturated humidity incubator at 37°C with 5% CO_2, with the culture medium being replaced daily.

HK2 cell culture and H/R model

HK2 cells purchased from Procell were cultured in DMEM/Nutrient Mixture F12 supplemented with 10% FBS, 500 U/mL penicillin, and 500 μg/mL streptomycin (Gibco) at 37 °C in a humidified atmosphere containing 5% CO2. For H/R treatment, HK2 cells were exposed to hypoxia condition with 1% O2, 5% CO2, and 94% N2 for 24 h in the absence or presence of B7-H1^{high}-Exo and B7-H1^{low}-Exo (50 μg/mL). Then reoxygenation (21% O2, 5% CO2, and 74% N2) for 4 h. Samples were collected after modeling for analyses.

MACSQuant®Tyto® cell flow sorting and flow cytometry

hucMSCs were digested with 0.25% trypsin and subsequently incubated with anti-CD90-APC and anti-CD274-PE antibodies (Biolegend, United States) at 25°C for 30 min. The fluorescent cells that had been labeled with anti-CD90 antibody and anti-CD274 antibody were transferred to a MACSQuant® Tyto® sorting bin. The MACSQuant Tyto Running Buffer contained 1 × 10^7 hucMSCs per 10 mL. Before sorting, logical gating hierarchies were established using MACSQuant Tyto software. Cell debris, doublets, and dead cells were excluded, and a gate was set to isolate the target cell population. Samples were sorted at a flow rate of 4 mL/h under a pressure of approximately 140 mbar. Upon completion of the sorting process, B7-H1 expression in both positive and negative cell populations was analyzed using a NovoCyte Advanteon Dx VBR flow cytometer.

RT–qPCR

A volume of 1 μL of extracted RNA was employed to ascertain the concentration of the sample (ng/μL) through the utilisation of an ultra-micro spectrophotometer. The A260/A280 ratio was found to be between 1.8 and 2.1, indicative of high-quality RNA. The RNA-to-DNA reaction mixture was prepared in RNase-free 200 μL microcentrifuge tubes and thoroughly mixed to a total volume of 10 μL. The mixture was then incubated at 42°C for 2 min and subsequently maintained at 4°C. The cDNA synthesis reaction system was similarly prepared on ice in RNase-free 200 μL microcentrifuge tubes, mixed to a total volume of 20 μL. The reactions were conducted in accordance with the specified protocol using a gradient PCR instrument and subsequently stored at 4°C. The cDNA products were prepared individually in RNase-free microcentrifuge tubes, employing the following PCR reaction system, with three replicate wells per template, all configured on ice. A two-step PCR reaction programme was implemented.

Primers are as follows.

Extraction and identification of exosomes

Exosomes were isolated through a series of processes including centrifugation, column filtration, and purification. B7-H1^{high}-MSCs and B7-H1^{low}- MSCs supernatant was centrifuged at 2000 g for 30 min at 4°C. Then, the supernatant was transferred to a new centrifuge tube, and centrifuged at 10,000 × g for 45 min at 4°C to remove larger vesicles. Subsequently, the supernatant was filtered with a 0.45-μm filter membrane (Millipore, R6BA09493), and the filtrate was collected which was centrifuged again at 10,000 × g for 60 min at 4°C in a centrifuge. The supernatant was discarded, and the pellets were resuspended with 5 mL pre-cooled PBS. The pellets were centrifuged at 12,000 × g at 4°C for 2 min. The supernatant, which was rich in exosome particles, was retained. The harvested exosomes were transferred into the upper chamber of Exosome Purification Filter (Umibio) and centrifuged at 3,000 × g for 10 min at 4 °C. After centrifugation, the liquid at the bottom of the EPF column was collected, which was the purified exosomes. The isolated

Primer name	Primer sequence5′- 3′	PCR product length/bp
β-actin	CCTGGCACCCAGCACAAT GGGCCGGACTCGTCATAC	144
C3	ACTCAGGCAGTGACATGGTG TGATGCTCAAGGGCTTCTGG	270
IRF7	ATGGGCAAGTGCAAGGTGTA GATGGTATAGCGTGGGGAGC	180
Vcam1	AATGCCTGGGAAGATGGTCG AGGAAAAGAGCCTGTGGTGC	163
CXCL10	AGCTCTACTGAGGTGCTATGT GTACCCTTGGAAGATGGGAAAG	85
AREG	CGCTCTTGATACTCGGCTCA CCCCAGAAAATGGTTCACGC	87
Fnip2	GCATCATCCCAAGAAGGCTATGA CGCAGTCAGTAAGGCAGCAA	277
ST6	TGAGGTCACGATCTGGTGGA TACAAGACGCACAACCAGCA	162
Aldh1l2	ACCAAGAAAGAGCCACTCGG CCAAACACGCAGCACTCTTC	91

exosomes were subsequently stored at −80°C. Transmission electron microscopy (TEM) was employed to examine the morphological characteristics of the exosomes. Furthermore, the size and concentration of the exosomes were assessed utilizing a flow nanoanalyzer. The expression levels of CD9 and CD63 were determined via Western blot analysis.

Scr and BUN measurements

The collected whole blood samples were subjected to centrifugation at 3,000 rpm for a duration of 15 min. Subsequently, Scr and BUN levels were quantified utilizing specific assay kits (Scr: RXWB0459-96, RUIXIN BIOTECH; BUN: RXWB0153-96, RUIXIN BIOTECH).

Hematoxylin and eosin (H&E) staining

Kidney tissues were fixed in 4% paraformaldehyde for over 24 h and subsequently embedded in paraffin. The 5 μm thick sections were deparaffinised by immersion in xylene for 20 min, followed by rehydration through a graded series of anhydrous ethanol. H&E staining was conducted on the 5 μm-thick sections, which were deparaffinized using xylene and stained with H&E reagent (Sigma, United States). In brief, the sections were incubated with hematoxylin for 5 min at room temperature, rinsed, and then incubated with eosin for approximately 2 min at room temperature. The histomorphology of the kidney tissues was subsequently examined under a microscope.

Western blot

Sample Preparation: Following the quantification of protein concentration, 20 μg of protein from each well was aliquoted (with an equivalent volume of culture supernatant serving as a control). The protein samples were then combined with 5× SDS-PAGE loading buffer, thoroughly mixed, and subjected to heat treatment at 95°C for 5 min. A 12% acrylamide separating gel was utilized, and the heated supernatant was loaded into each sample well for electrophoresis, conducted at 70 V for 30 min followed by 120 V for 60 min. Proteins were transferred onto a membrane using a constant current of 250 mA in a wet transfer system for 90 min. Closure: A 5% skimmed milk powder solution was sealed and maintained at room temperature for 1 hour. Incubation of the primary antibody involved diluting the antibody with 5% skimmed milk powder at a dilution ratio of 1: 1000, followed by incubation at 4°C overnight. For the incubation of the secondary antibody, the primary antibody was aspirated, and the membrane was washed three times with TBST (5 min per wash). Subsequently, an HRP-labeled secondary antibody, diluted at a ratio of 1:5000, was added and incubated at room temperature for 1 h. For imaging development, following the secondary antibody incubation, the membrane was again washed three times with TBST (5 min per wash) and then developed using an ELC luminescent solution.

ELISA

The concentrations of IL-1β (RX203063M, RUIXIN BIOTECH), IL-10 (RX203075M, RUIXIN BIOTECH), TNF-α (RX202412M, RUIXIN BIOTECH) and IL-18 (RX203064M, RUIXIN BIOTECH) in kidney tissues or macrophages were measured by enzyme-linked immunosorbent assay (ELISA) kits according to the manufacturer's protocols. The OD values were read using a plate reader (Bio Rad).

Whole transcriptome sequencing (RNA-seq)

The cDNA libraries were generated utilizing the NEBNext® Ultra™ RNA Library Prep Kit for Illumina, provided by New England Biolabs, United States. Following this, the RNA quality was evaluated using an Agilent 2,100 Bioanalyzer from Agilent Technologies, United States. Sequencing of the samples was conducted on an Illumina HiSeq 6,000 system, manufactured by Illumina, United States. Differential expression genes (DEGs) had an average fold change of at least 2, and a q-value (FDR) less than 0.05. The sequences of.

Statistical analysis

Statistical analyses were conducted utilizing R software (version 4.1.0). The assessment of normality was carried out via the Shapiro-Wilk test. Group comparisons were executed using the independent samples t-test for data exhibiting normal distribution and the Mann-Whitney U-test for data not conforming to normal distribution. For comparisons involving multiple groups, a one-way analysis of variance (ANOVA) was employed, supplemented by *post hoc* analyses using Tukey's Honest Significant Difference (HSD) test where applicable. Categorical variables were analyzed through the chi-square test. A p-value of less than 0.05 was deemed indicative of statistical significance. All statistical analyses were conducted using two-tailed tests, and data visualization was performed utilizing GraphPad Prism software.

Results

Sorting of hucMSCs and expression of B7-H1 in positive and negative cells

Initially, we assessed the expression level of B7-H1 in hucMSCs via flow cytometry. The results indicated that the expression level of B7-H1 in hucMSCs was 47% (Figure 1A). Subsequently, we performed cell sorting on the hucMSCs (Figure 1B), resulting in the isolation of cell clusters with high and low B7-H1 expression, respectively. The post-sorting cell survival rates were 57% and 63%, respectively. In the low-expressing B7-H1 group, the expression of B7-H1 in cell clusters decreased from 47% to 11.26%, whereas in the high-expressing B7-H1 group, the proportion increased from 47% to 91.66% (Figures 1C,D).

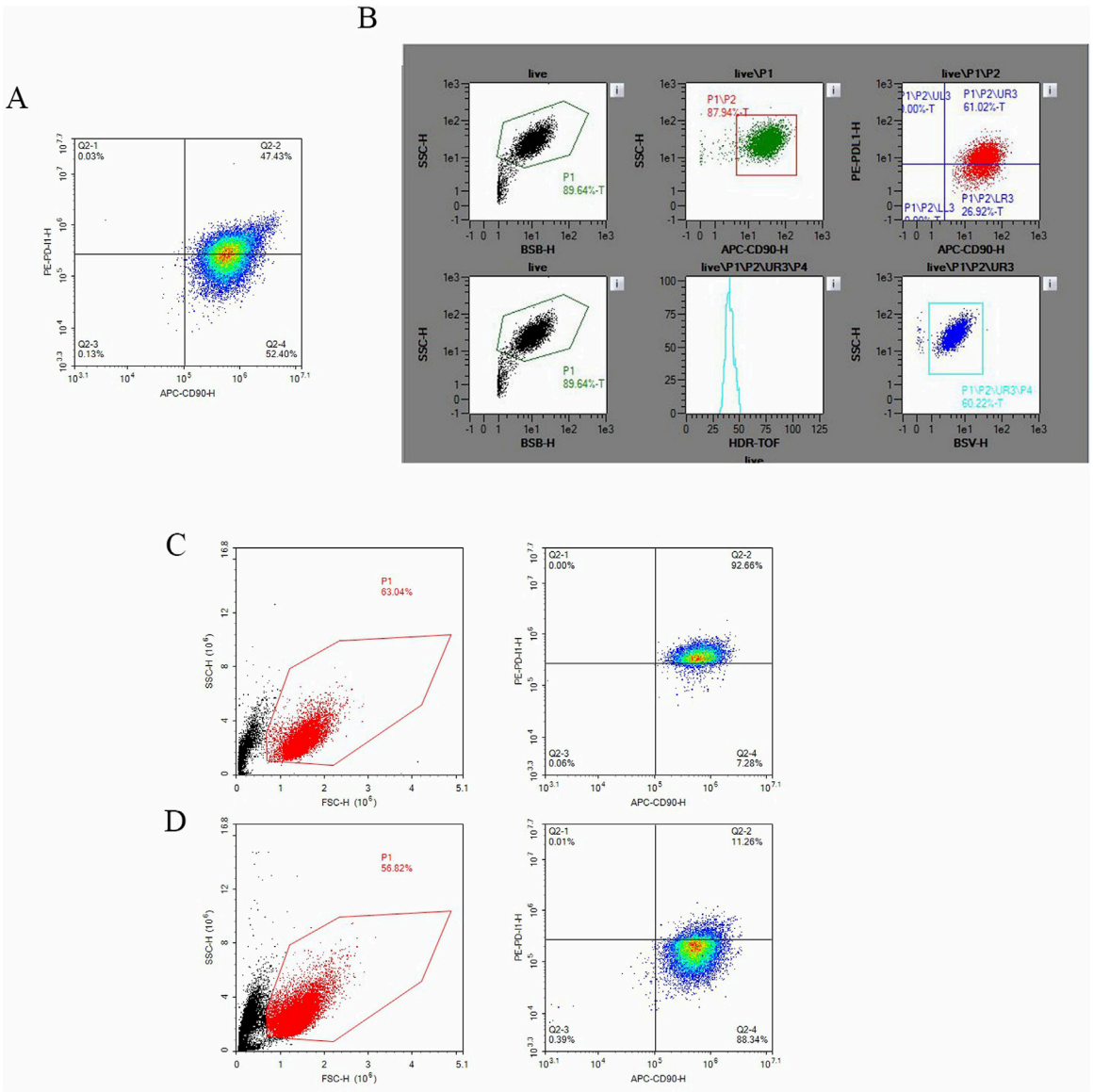

FIGURE 1
The sorting of hucMSCs and the expression of B7-H1 in both positive and negative cell populations. **(A)** Depicts the expression of B7-H1 in hucMSCs as determined by flow cytometry prior to sorting, **(B)** shows the flow cytometry sorting process for B7-H1^{high} and B7-H1^{low} hucMSCs, **(C)** the expression of B7-H1 in B7-H1^{high} hucMSCs as assessed by flow cytometry post-sorting and **(D)** the expression of B7-H1 in B7-H1^{low} hucMSCs as assessed by flow cytometry post-sorting.

Identification of B7-H1^{high}-Exo and B7-H1^{low}-Exo

B7-H1^{high}-Exo and B7-H1^{low}-Exo were characterized using TEM, NTA, and Western blotting. Under TEM, both groups of exosomes exhibited vesicle-like structures with a round or oval morphology (Figure 2A). NTA analysis further revealed that these exosomes had an average diameter of approximately 100 nm (Figure 2B). Western blot also confirmed that TSG101, CD9 and CD63 were positive in B7-H1^{high}-Exo and B7-H1^{low}-Exo (Figure 2C). Subsequently, Western blot analysis was conducted to assess the expression of B7-H1 in the two Exo groups. The results demonstrated that the B7-H1^{high}-Exo group exhibited significantly elevated levels of B7-H1 protein compared to the B7-H1^{low}-Exo group (Figure 2D). These findings indicated that B7-H1^{high}-Exo was efficiently isolated from hucMSCs with high levels of B7-H1 expression, whereas B7-H1^{low}-Exo was obtained from hucMSCs with lower expression levels of B7-H1.

B7-H1^{high}-Exo significantly enhances the restoration of renal function in mice subjected to renal ischemia-reperfusion injury

Our prior research demonstrated that exosomes derived from hucMSCs can be effectively targeted to the injured kidney, where they exerted significant therapeutic effects (Wei et al., 2024). In the

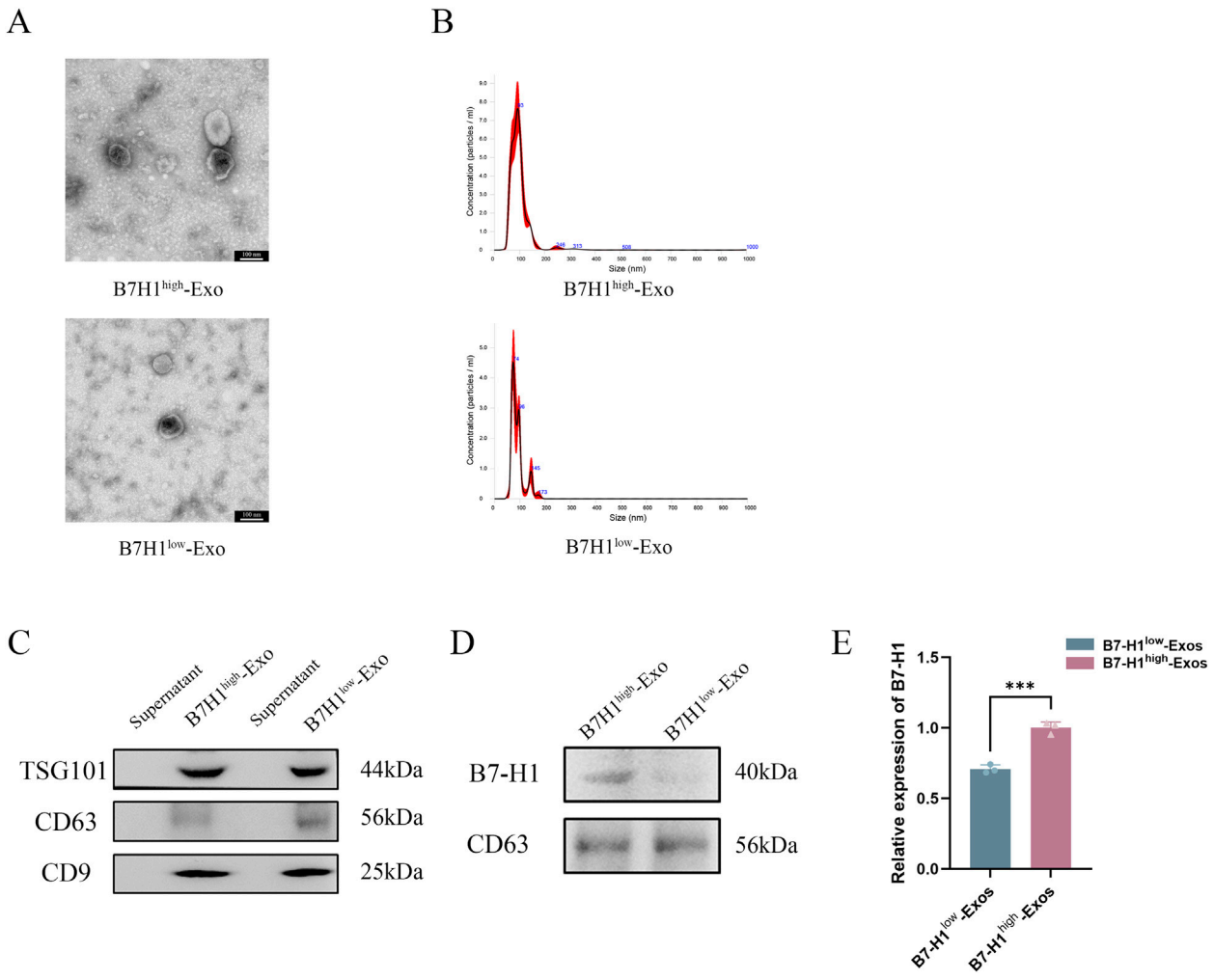

FIGURE 2
Characterization of B7-H1^{high}-Exo and B7-H1^{low}-Exo. **(A, B)** TEM and NTA were conducted to assess the size distribution of B7-H1^{high}-Exo and B7-H1^{low}-Exo. The scale bars 100 nm. **(C)** The expression levels of TSG101, CD63, and CD9 in the two groups. **(D)** The protein content of B7-H1 in B7-H1^{high}-Exo and B7-H1^{low}-Exo. **(E)** Quantification of the data presented in panel D was shown on the right. Data were expressed as mean ± standard error. Statistical significance was indicated as follows: ***P < 0.001 (n = 3).

present study, we employed a renal ischemia-reperfusion model to evaluate the impact of B7-H1^{high}-Exo and B7-H1^{low}-Exo treatments on BUN and Scr levels following renal IRI. The B7-H1^{low}-Exo group exhibited a marked improvement compared to the Sham group (Figures 3A, B). Importantly, the B7-H1^{high}-Exo group demonstrated superior functional recovery relative to the B7-H1^{low}-Exo group. To further explore the therapeutic potential of Exo in IRI, we conducted histological analyses. Post-IRI, the extent of renal injury was markedly diminished in the group treated with B7-H1^{low}-Exo compared to the IRI control group (Figures 3C, D). Remarkably, mice administered with B7-H1^{high}–Exo demonstrated a reduced injury area compared to those receiving B7-H1^{low}-Exo. Although the renal tubules remained sparsely packed, the tubular walls exhibited gradual homogenization, and the glomerular size progressively returned to normal in the B7-H1^{low}-Exo group relative to the IRI group. In summary, our results indicated that kidneys treated with B7-H1^{high}-Exo achieved superior functional recovery compared to those treated with B7-H1^{low}-Exo.

RNA-seq revealed multiple differentially expressed genes and pathways emerged in renal ischemia-reperfusion injury

To investigate the mechanisms underlying the B7-H1^{high}-Exo-mediated repair of renal injury, we conducted a comparative analysis of the transcriptome profiles of renal tissues from mice in the four groups utilizing RNA-Seq. KEGG pathway enrichment analyses (Figures 4A, B) revealed that the differentially expressed genes between the B7-H1^{high}-Exo and B7-H1^{low}-Exo groups were predominantly enriched in pathways related to NF-κB signaling and TNF signaling pathway, among others. Meanwhile, we conducted a differential gene expression analysis on the B7-H1^{high}-Exo and B7-H1^{low}-Exo groups, revealing 181 upregulated and 208 downregulated genes (Figure 4C). Subsequently, we identified the top 10 most significantly upregulated and downregulated genes. Among these, eight genes—C3, IRF7, AREG, Cxcl10, Aldh1l2, Fnip2, Vcam1, and St6Galnac3—had

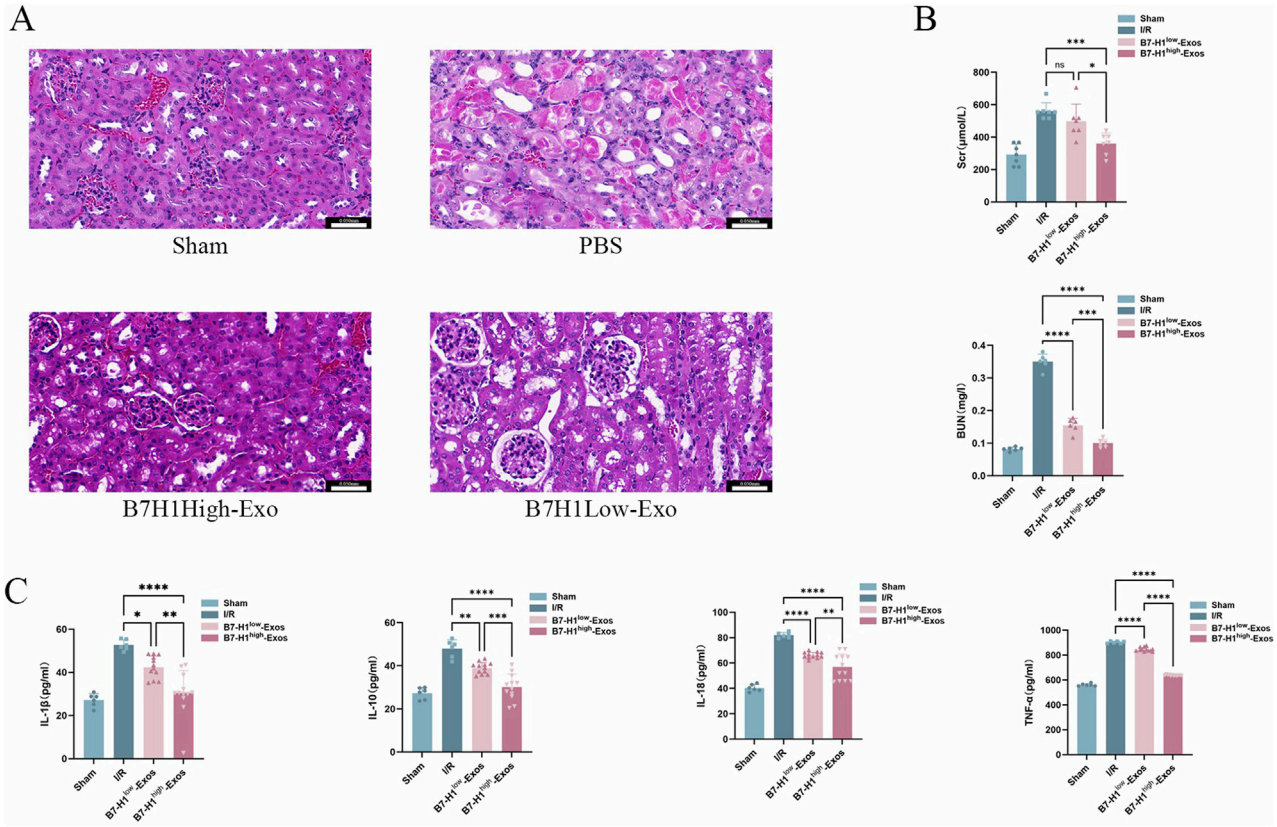

FIGURE 3
B7-H1^{high}-Exo significantly enhanced the restoration of renal function in mice subjected to renal ischemia-reperfusion injury **(A)** Kidney tissues from four experimental groups were collected for histopathological analysis using H&E staining. Scale bars 0.050 mm **(B)** BUN and Scr levels were quantified using specific ELISA kits **(C)** The concentrations of interleukin-1β (IL-1β), interleukin-10 (IL-10), interleukin-18 (IL-18), and tumor necrosis factor-alpha (TNF-α) were measured with appropriate assay kits. Data are expressed as mean ± standard error. Statistical significance is indicated as follows: *P < 0.05, **P < 0.01, ***P < 0.001, ****P < 0.0001, ns denotes no significant difference (n = 5).

been previously investigated in the context of ischemia-reperfusion injury. Venn can show the overlap of differential genes among different comparison combinations, and the differential genes that are common or unique to several comparison combinations can be screened by Venn diagram. Our analysis of differential genes in these four groups by Venn revealed a total of 34 overlapping differential genes (Figure 4D).

B7-H1^{high}-Exo mitigates the expression of C3 induced by renal ischemia-reperfusion injury

To further ascertain which genes exhibited the most significant enhancement in functional recovery following IRI, we assessed their expression in renal IRI and hypoxia/reoxygenation-induced HK-2 cells using quantitative RT-qPCR. the expression level of the C3 protein was markedly reduced in HK-2 cells treated with B7-H1^{high}-Exo compared to those treated with B7-H1^{low}-Exo (Figure 5A). Surprisedly, consistent with the results of hypoxia/reoxygenation-induced HK-2 cells, expression of C3 was reduced in renal IRI (Figure 5B). The result suggested that B7-H1^{high}-Exo might ameliorate renal IRI by downregulating C3 expression. A secondary validation of predictions from the RNA-seq analysis by RNAscope in Western blot confirmed a strong downregulation of NF-κB signaling (Figures 5C, D). This suggests that the downregulation of NF-κB is inseparable from the treatment of B7-H1^{high}-Exo.

Discussion

In this study, we have firstly identified a subpopulation of human umbilical cord MSCs characterized by high expression of B7-H1. We successfully isolated exosomes with elevated levels of B7-H1 from these cells. Our findings demonstrated that B7-H1^{high}-Exo exhibit superior efficacy in repairing IRI. Through a series of experiments, we observed that B7-H1^{high}-Exo facilitate the repair of renal tissues and the recovery of renal function by down-regulating complement C3. Similarly, B7-H1^{high}-Exo compared to B7-H1^{low}-Exo also showed repair of renal tissue by downregulation of NF-κB. These results strongly indicated the potential of B7-H1^{high} exosomes as a promising cell-free therapeutic approach for the treatment of IRI.

IRI is the primary contributor to AKI (Bonventre and Yang, 2011). Typically, the pathophysiological process of ischemia-

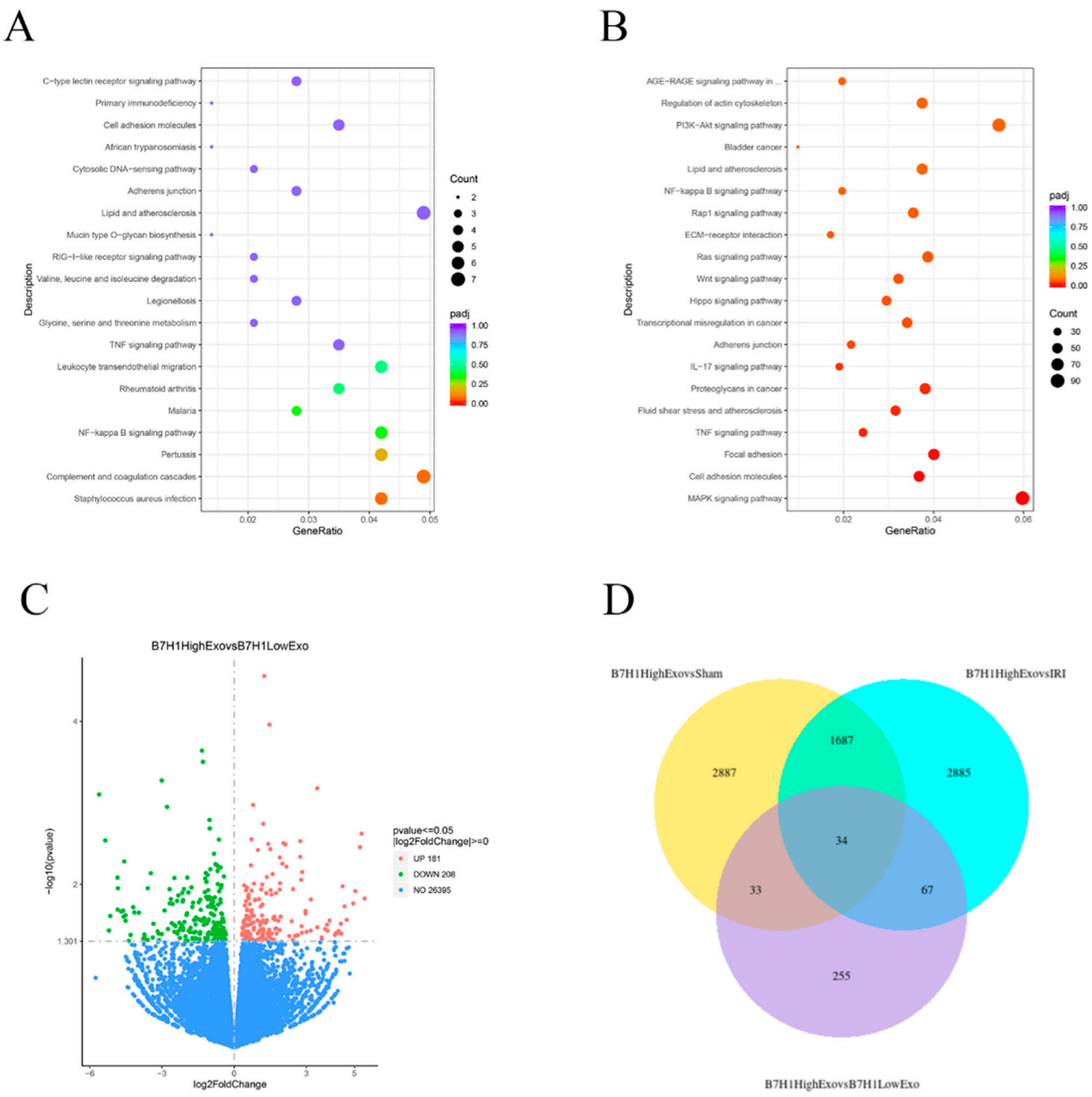

FIGURE 4
The effects of B7-H1^{high}-Exo on renal ischemia-reperfusion injury-induced C3 expression. **(A)** Top 20 enriched KEGG pathways in the difference between B7-H1^{high}-Exo and B7-H1^{low}-Exo. **(B)** Top 20 enriched KEGG pathways in the difference between Sham and I/R. **(C)** Analysis of renal gene expression differences between the mouse B7-H1^{high}-Exo and B7-H1^{low}-Exo groups. **(D)** Venn of the four groups of differentially expressed genes.

reperfusion injury is delineated into six key components: vascular leakage, programmed cell death, transcriptional reprogramming, autoimmunity, activation of both innate and adaptive immune responses, and the no-reflow phenomenon (Eltzschig et al., 2011). Nevertheless, research focusing on the immune cell mechanisms underlying AKI remains scarce. During the initial phases of ischemia/reperfusion (I/R) injury, a substantial number of cells undergo necrosis as a result of hypoxic conditions. Necrotic cells, displaying potent immunostimulatory properties, promote the infiltration of inflammatory cells and cytokine production, leading to the subsequent release or upregulation of damage-associated molecular patterns (DAMPs), which are ligands associated with cellular injury or death (Hotchkiss et al., 2009). DAMPs interact with innate immune receptors, including toll-like receptors (TLRs), thereby activating the innate immune response (Chen et al., 2010; Iyer et al., 2009). In contrast to the well-documented immune response observed in I/R injury, the mechanisms by which the adaptive immune response is activated under sterile conditions remain inadequately understood. Existing research indicates that CD4$^+$ and CD8$^+$ T cells primarily mediate I/R injury (Day et al., 1950; Shen et al., 2009; Yilmaz et al., 2006). In contrast, recent studies suggest that regulatory T cells (Tregs) confer

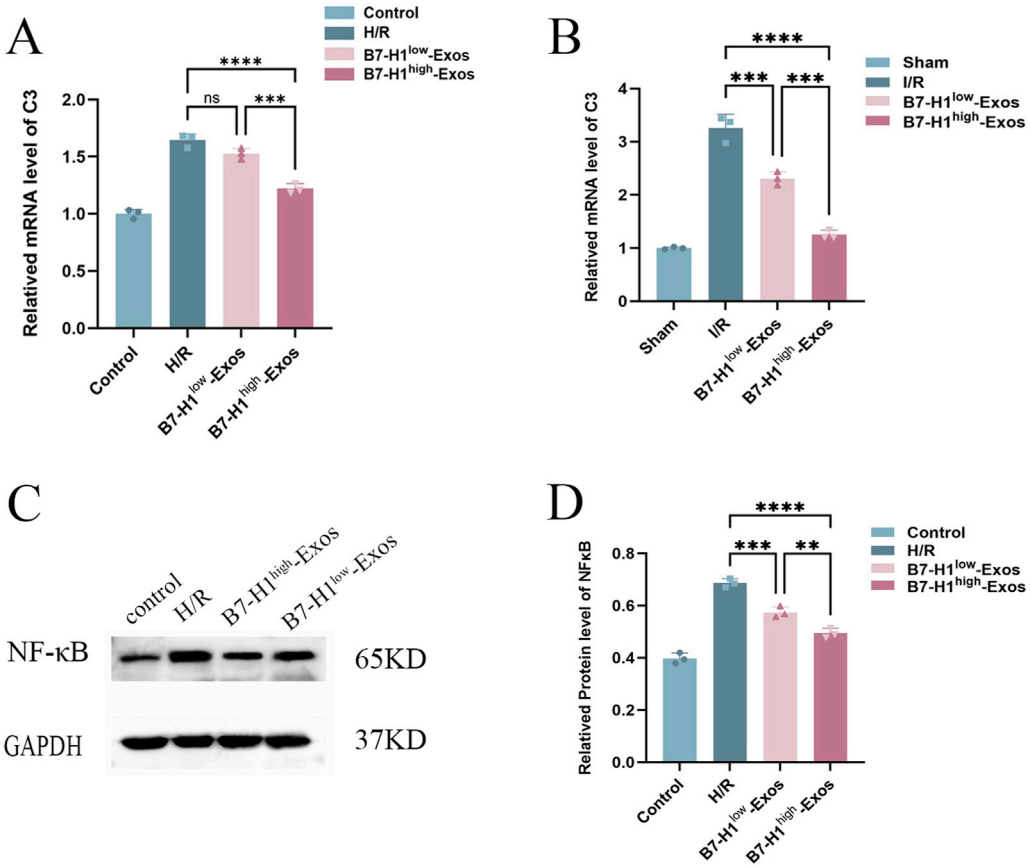

FIGURE 5
The effects of B7-H1^{high}-Exo on renal ischemia-reperfusion injury-induced C3 expression, **(A, B)** the results of the RT-qPCR (n = 3). **(C, D)** Western blot analysis of NF-κB expression in normal HK-2 cells or hypoxia/reoxygenation-induced HK-2 cells with different treatments. The data were expressed as mean ± standard error. Statistical significance was indicated as follows: ***$P < 0.001$, ****$P < 0.0001$, ns denotes no significant difference.

protection to the kidney against IR-induced inflammation and injury. However, the blockade of PD-1 on the surface of Tregs prior to graft transfer impairs their protective function against ischemic kidney injury. Additionally, the inhibition of B7-H1 or PD-L2 results in exacerbated kidney injury and inflammation (Jaworska et al., 2015). Consequently, B7-H1 presents significant potential for further investigation in the context of I/R injury.

MSCs can be obtained from a diverse array of sources, such as bone marrow, adipose tissue, umbilical cord, human placenta, dental pulp, skin, blood, and urine, in addition to induced pluripotent stem cells (iPSCs) (Huang and Yang, 2021). Clinical trials conducted thus far have demonstrated their substantial therapeutic potential (Abumoawad et al., 2019). Nevertheless, the variability in donor condition, cell type, differentiation capacity, and other influencing factors contributes to considerable heterogeneity, thereby constraining the effectiveness of MSC-based therapies (Kim et al., 2021). Growing evidence substantiates the role of Exo in stem cell-mediated repair through the modulation of immunomodulatory functions. In various models of kidney injury, Exo has been shown to facilitate the repair of damaged cells, promote the proliferation of renal tubular cells, and inhibit apoptosis and inflammation (Grange et al., 2019). Over time, MSC-Exo have gained prominence as a significant alternative therapeutic approach for diseases traditionally treated with MSCs. This is particularly evident in the pretreatment of stem cells, which allows for more precise disease management and minimizes treatment-related complications.

As previously noted, the heterogeneity among MSCs is regarded as a significant impediment to their clinical translation into therapies that are reproducible, predictable, and standardized (Zhou et al., 2021). This heterogeneity pertains to the variability in their molecular markers, differentiation potential, and biological functions. Such variation arises not only from diverse tissue sources but also from distinct cell subpopulations within the same tissue source (Hass et al., 2011; Mastri et al., 2014). While numerous studies have compared and analyzed the functional differences of MSCs derived from various tissue sources—encompassing aspects such as multidirectional differentiation potential and immunomodulatory functions—research focusing on the functional characteristics of MSC subpopulations within the same tissue remains limited (Baksh, 2007). Consequently, identifying subpopulations with specific functions and appropriately applying them could offer a viable strategy for tissue repair and functional restoration.

In this study, we identified a subpopulation of hucMSCs with the potential to enhance renal tissue repair and restore renal function using flow cytometry. However, it was observed that this subpopulation did not maintain stable expression during cell

proliferation, eventually reverting to the expression profile of unsorted hucMSCs. So we isolated the subpopulation immediately after sorting and utilized them at passages 2–4 for both *in vivo* and *in vitro* experiments to solve the problem. The findings demonstrated that the *in vivo* administration of B7-H1^{high}-Exo facilitated tissue restoration in regions affected by IRI and enhanced the recovery of renal function. Furthermore, *in vitro* experiments corroborated that the application of B7-H1^{high}-Exo to HK-2 cells significantly attenuated apoptosis in renal tubular cells. Simultaneously, we conducted RNA-seq on the renal tissues of mice and identified differential expression in a total of 389 genes when comparing the B7-H1^{high}-Exo and B7-H1^{low}-Exo groups. Further validation using PCR *in vivo* and vitro revealed that the gene C3 demonstrated significant differential expression between the B7-H1^{high}-Exo and B7-H1^{low}-Exo groups. Notably, C3 is a critical complement protein situated at the convergence of all complement activation pathways. Extracellular, tissue, cell-derived, and intracellular C3 are pivotal in the dysregulated immune response observed in numerous diseases, rendering them promising therapeutic targets (Kolev et al., 2022). IRI represents an inevitable and severe consequence of renal transplantation, which significantly elevates the risk of delayed graft function and graft loss. The primary catalyst of detrimental response in the kidney is the activation of the complement system, a critical element of the innate immune system. The activation results in the deposition of complement C3 on renal tubules and the infiltration of immune cells, culminating in tubular damage and a consequent decline in renal function (Howard et al., 2021). In murine models, C3 deficiency confers a protective effect against renal IRI and diminishes immune cell infiltration (Zhou et al., 2000). Evidence suggests that following the induction of acute kidney injury in C3 knockout mice, the impairment of renal function is less pronounced compared to wild-type mice (Boudhabhay et al., 2020). Furthermore, Tregs are crucial in the context of IRI. Research demonstrated that the complement system also modulates the induction, function, and stability of Tregs (Van der Touw et al., 2013). A particular research group discovered that peripheral, murine, and natural regulatory T cells (nTregs) express the receptors C3aR and C5aR, which, through their signaling pathways, inhibit Tregs function (Kwan et al., 2013). CD4 Tregs are immunosuppressive T cells, and research has demonstrated that Tregs can mitigate AKI (Lee et al., 2010). Jaworska K et al. reported an improvement in IRI following Tregs transplantation, an effect contingent upon Tregs expression of programmed death ligands 1 and 2, i.e., B7-H1 and PD-L2. Concurrently, experimental evidence indicating PD-1 expression by renal tubular epithelial cells (Jaworska et al., 2015), along with clinical observations of renal adverse events in patients undergoing treatment with immune checkpoint inhibitors targeting the PD-1/B7-H1 axis (Wanchoo et al., 2017), underscores the significance of PD-1 in renal inflammation. Consequently, we hypothesize that B7-H1^{high}-Exo may enhance the function of Tregs by down-regulating C3 and the associated complement cascade pathway, thereby inhibiting renal inflammation. This hypothesis warrants validation in future studies.

However, this study is not without limitations. Firstly, although we have verified how B7-H1^{high}-Exo acts on C3 and NF-κB to repair damage separately, the interaction mechanisms among B7-H1, C3, and NF-κB required further elucidation. Furthermore, the *in vivo* administration of exosomes through the tail vein did not constitute a non-invasive or direct method of drug delivery. Future research could explore transnasal drug delivery, which is currently favored as the preferred method for exosome-based drug delivery due to its numerous advantages. Initially, it offers a non-invasive and direct approach to drug delivery, complemented by its rapid therapeutic effects (Long et al., 2017). Ultimately, this study concentrated on the mechanisms associated with renal tissue repair and functional recovery following IRI.

Conclusion

In summary, our study represented the inaugural investigation to elucidate the roles of C3 and NF-κB through B7-H1^{high}-Exo in the context of IRI, unveiling their potential as therapeutic targets in this pathological setting. The reparative capacity of hucMSCs-derived exosomes with high B7-H1 expression was significantly greater than that of exosomes with low B7-H1 expression. Furthermore, these exosomes facilitated renal tissue repair and functional recovery by down-regulating C3 and NF-κB. Therefore, the therapeutic strategy centered on B7-H1 might effectively augment the ameliorative impact of hucMSCs-derived exosomes on renal injury resulting from IRI.

Data availability statement

The original contributions presented in the study are publicly available. This data can be found here: https://pan.baidu.com/s/1CYgX-egq6MiOHx5CeDT_-w?pwd=ryf6 Access code: ryf6.

Ethics statement

The animal study was approved by the Animal Experiment Center of Lanzhou University [License: SCXK (GAN) 2023-0003]. The study was conducted in accordance with the local legislation and institutional requirements.

Author contributions

JH: Conceptualization, Data curation, Methodology, Software, Writing–original draft, Writing–review and editing. XL: Funding acquisition, Resources, Supervision, Visualization, Writing–review and editing. YY: Conceptualization, Data curation, Writing–original draft. YL: Formal Analysis, Methodology, Writing–original draft. RW: Software, Writing–original draft. XW: Validation, Writing–original draft. HW: Investigation, Writing–original draft. WW: Data curation, Writing–original draft. YZ: Data curation, Writing–original draft. YM: Software, Writing–original draft.

Funding

The author(s) declare that financial support was received for the research and/or publication of this article. This study was in

part supported by grants from the Natural Science Foundation of Gansu Province Program of China (23JRRA0932 to XL); the First Hospital of Lanzhou University Foundation (ZX-62000002-2022-723 to XL); the United Scientific Research Fund of Gansu Province (24JRRA914 to XL).

Conflict of interest

The authors declare that the research was conducted in the absence of any commercial or financial relationships that could be construed as a potential conflict of interest.

Generative AI statement

The author(s) declare that no Generative AI was used in the creation of this manuscript.

Publisher's note

All claims expressed in this article are solely those of the authors and do not necessarily represent those of their affiliated organizations, or those of the publisher, the editors and the reviewers. Any product that may be evaluated in this article, or claim that may be made by its manufacturer, is not guaranteed or endorsed by the publisher.

References

Abumoawad, A., Saad, A., Ferguson, C. M., Eirin, A., Herrmann, S. M., Hickson, L. J., et al. (2019). In a Phase 1a escalating clinical trial, autologous mesenchymal stem cell infusion for renovascular disease increases blood flow and the glomerular filtration rate while reducing inflammatory biomarkers and blood pressure. *Kidney Int.* 97, 793–804. doi:10.1016/j.kint.2019.11.022

Baksh, D. (2007). Comparison of proliferative and multilineage differentiation potential of human mesenchymal stem cells derived from umbilical cord and bone marrow. *Stem Cells* 45, 99–106. doi:10.1634/stemcells.2006-0709

Bonventre, J., and Yang, L. (2011). Cellular pathophysiology of ischemic acute kidney injury. *J. Clin. investigation* 121, 4210–4221. doi:10.1172/JCI45161

Bonventre, J. V., and Weinberg, J. M. (2003). *Recent Adv. Pathophysiol. ischemic acute Ren. Fail.* 14 8, 2199–2210. doi:10.1097/01.asn.0000079785.13922.f6

Boudhabhay, I., Poillerat, V., Grunenwald, A., Torset, C., Leon, J., Daugan, M. V., et al. (2020). Complement activation is a crucial driver of acute kidney injury in rhabdomyolysis. *Kidney Int.* 99 (3), 581–597. doi:10.1016/j.kint.2020.09.033

Chen, G., Nunez, G., and Chen, G. Y. (2010). Nunez GSterile inflammation: sensing and reacting to damage. *Nat Rev Immunol* 10:826–837. doi:10.1038/nri2873

Day, Y.-J., Huang, L., Ye, H., Li, L., Linden, J., and Okusa, M. D. (1950). Renal ischemia-reperfusion injury and adenosine 2A receptor-mediated tissue protection: the role of CD4+ T cells and IFN-gamma. *J. Immunol. Baltim. Md.* 176 (176), 3108–3114. doi:10.4049/jimmunol.176.5.3108

Eltzschig, H., Eckle, T., Eltzschig, H. K., and Eckle, T. (2011). Ischemia reperfusion-from mechanism to translation. Nat Med. *Nature medicine* 17: 1391–1401. doi:10.1038/nm.2507

Fondevila, C., Busuttil, R. W., and Kupiec-Weglinski, J. W. (2003). Hepatic ischemia/reperfusion injury—a fresh look. *Exp. Mol. Pathology* 74 (2), 86–93. doi:10.1016/s0014-4800(03)00008-x

Gho, Y., and Lee, C. (2017). Emergent properties of extracellular vesicles: a holistic approach to decode the complexity of intercellular communication networks. *Mol. Biosyst.* 13, 1291–1296. doi:10.1039/c7mb00146k

Grange, C., Skovronova, R., Marabese, F., and Bussolati, B. (2019). Stem cell-derived extracellular vesicles and kidney regeneration. *Cells* 8, 1240. doi:10.3390/cells8101240

Guo, S., Redenski, I., and Levenberg, S. (2021). Spinal cord repair: from cells and tissue engineering to extracellular vesicles. *Cells* 10, 1872. doi:10.3390/cells10081872

Hakroush, S., Wulf, S., Gallwas, J., and Tampe, B. (2021). Variable expression of programmed cell death protein 1-ligand 1 in kidneys independent of immune checkpoint InhibitionCase report: collapsing focal segmental glomerulosclerosis after initiation of ado-trastuzumab emtansine therapy. *Front. Oncol.*, 11, 796223, doi:10.3389/fonc.2021.796223

Han, S., and Lee, H. (2019). Mechanisms and therapeutic targets of ischemic acute kidney injury. *Kidney Res. Clin. Pract.* 38, 427–440. doi:10.23876/j.krcp.19.062

Hass, R., Kasper, C., Böhm, S., and Jacobs, R. (2011). Different populations and sources of human mesenchymal stem cells (MSC): a comparison of adult and neonatal tissue-derived MSC. *Cell Commun. Signal. CCS* 9, 12. doi:10.1186/1478-811X-9-12

Hotchkiss, R. S., Strasser, A., McDunn, J. E., and Swanson, P. E. (2009). Cell death. *N. Engl. J. Med.* 361 (16), 1570–1583. doi:10.1056/NEJMra0901217

Howard, M. C., Nauser, C. L., Vizitiu, D. A., and Sacks, S. H. (2021). Fucose as a new therapeutic target in renal transplantation. *Pediatr. Nephrol.* 36 (5), 1065–1073. doi:10.1007/s00467-020-04588-2

Huang, Y., and Yang, L. J. S. C. R. (2021). *Therapy, Mesenchymal stem cells and extracellular vesicles in therapy against kidney diseases*, 12.

Ishida, Y., Agata, Y., Shibahara, K., and Honjo, T. (1992). Induced expression of PD-1, a novel member of the immunoglobulin gene superfamily, upon programmed cell death. *EMBO J.* 11 (11), 3887–3895. doi:10.1002/j.1460-2075.1992.tb05481.x

Iyer, S., Pulskens, W. P., Sadler, J. J., Butter, L. M., Teske, G. J., Ulland, T. K., et al. (2009). Necrotic cells trigger a sterile inflammatory response through the NLRP3 inflammasome. *Proc. Natl. Acad. Sci. U. S. A.* 106, 20388–20393. doi:10.1073/pnas.0908698106

Jaworska, K., Ratajczak, J., Huang, L., Whalen, K., Yang, M., Stevens, B. K., et al. (2015). Both PD-1 ligands protect the kidney from ischemia reperfusion injury. *J. Immunol.* 194 (1), 325–333. doi:10.4049/jimmunol.1400497

Ji, H., Shen, X., Gao, F., Ke, B., Freitas, M. C. S., Uchida, Y., et al. (2010). Programmed death-1/B7-H1 negative costimulation protects mouse liver against ischemia and reperfusion injury. *Hepatol. Baltim. Md.* 52, 1380–1389. doi:10.1002/hep.23843

Kim, G., Shon, O. J., Seo, M. S., Choi, Y., Park, W. T., and Lee, G. W. (2021). Mesenchymal stem cell-derived exosomes and their therapeutic potential for osteoarthritis. *Biology* 10, 285. doi:10.3390/biology10040285

Kolev, M., Barbour, T., Baver, S., Francois, C., and Deschatelets, P. (2022). With complements: C3 inhibition in the clinic. *Immunol. Rev.* 313, 358–375. doi:10.1111/imr.13138

Kwan, W.-h., van der Touw, W., Paz-Artal, E., Li, M. O., and Heeger, P. S. (2013). Signaling through C5a receptor and C3a receptor diminishes function of murine natural regulatory T cells. *J. Exp. Med.* 210, 257–268. doi:10.1084/jem.20121525

Lassnigg, A., Schmidlin, D., Mouhieddine, M., Bachmann, L. M., Druml, W., Bauer, P., et al. (2004). Minimal changes of serum creatinine predict prognosis in patients after cardiothoracic surgery: a prospective cohort study. *J. Am. Soc. Nephrol. JASN* 15, 1597–1605. doi:10.1097/01.asn.0000130340.93930.dd

Lee, H., Nho, D., Chung, H. S., Lee, H., Shin, M. K., Kim, S. H., et al. (2010). CD4+CD25+ regulatory T cells attenuate cisplatin-induced nephrotoxicity in mice. *Kidney Int.* 78, 1100–9. doi:10.1038/ki.2010.139

Long, Q., Upadhya, D., Hattiangady, B., Kim, D. K., An, S.Y., Shuai, B., et al. (2017). Intranasal MSC-derived A1-exosomes ease inflammation, and prevent abnormal neurogenesis and memory dysfunction after status epilepticus. *Proc. Natl. Acad. Sci.* 114, E3536-E3545. doi:10.1073/pnas.1703920114

Mastri, M., Lin, H., and Lee, T. (2014). Enhancing the efficacy of mesenchymal stem cell therapy. *World J. stem cells* 6, 82–93. doi:10.4252/wjsc.v6.i2.82

Phinney, D. (2012). Functional heterogeneity of mesenchymal stem cells: implications for cell therapy. *J. Cell. Biochem.* 113, 2806–2812. doi:10.1002/jcb.24166

Shen, X., Wang, Y., Gao, F., Ren, F., Busuttil, R. W., Kupiec-Weglinski, J. W., et al. (2009). CD4 T cells promote tissue inflammation via CD40 signaling without *de novo* activation in a murine model of liver ischemia/reperfusion injury. *Hepatol. Baltim. Md.* 50 (5), 1537–1546. doi:10.1002/hep.23153

Sumiyoshi, M., Kawamoto, E., Nakamori, Y., Esumi, R., Ikejiri, K., Shinkai, T., et al. (2021). Elevated plasma soluble PD-L1 levels in out-of-hospital cardiac arrest patients, *J. Clin. Med.*, 10, 4188, doi:10.3390/jcm10184188

Tyndall, A. (2011). "*Successes and failures of stem cell transplantation in autoimmune diseases*,", 2011. Hematology/the Education Program of the American Society of Hematology. American Society of Hematology. Education Program, 280–284. doi:10.1182/asheducation-2011.1.280

van der Touw, W., Cravedi, P., Kwan, W. H., Paz-Artal, E., Merad, M., and Heeger, P. S. (2013). Cutting edge: receptors for C3a and C5a modulate stability of alloantigen-reactive induced regulatory T cells. *J. Immunol.* (Baltimore, Md: 1950), 190. doi:10.4049/jimmunol.1300847

Wanchoo, R., Karam, S., Uppal, N. N., Barta, V. S., Deray, G., Devoe, C., et al. (2017). Adverse renal effects of immune checkpoint inhibitors: a narrative review. *Am. J. Nephrol.* 45, 160–169. doi:10.1159/000455014

Wang, J., Zheng, X., Jiang, Y., Jia, H., Shi, X., Han, Y., et al. (2022). Soluble programmed cell death protein 1 and its ligand: potential biomarkers to predict acute kidney injury after surgery in critically ill patients. *J. Inflamm. Res.* 15, 1995–2008. doi:10.2147/JIR.S356475

Wang, Y., and Bellomo, R. (2017). Cardiac surgery-associated acute kidney injury: risk factors, pathophysiology and treatment. *Nat. Rev. Nephrol.* 13 (11), 697–711. doi:10.1038/nrneph.2017.119

Wei, H., Li, L., Luo, H., Wang, H., He, J., Yao, Y., et al. (2024). Role of Nrf2/HO-1 signaling pathway in human umbilical cord mesenchymal stem cells-derived exosomes-induced reduction of renal ischemia-reperfusion injury in mice. *Chin. J. Anesthesiol.* 44 (1), 97–103. doi:10.3760/cma.j.cn131073.20230912.00120

Wu, W., Xiao, Z. X., Zeng, D., Huang, F., Wang, J., Liu, Y., et al. (2020). B7-H1 promotes the functional effect of human gingiva-derived mesenchymal stem cells on collagen-induced arthritis murine model. *Mol. Ther.* 28, 2417–2429. doi:10.1016/j.ymthe.2020.07.002

Xiao, X., Li, W., Xu, Z., Sun, Z., Ye, H., Wu, Y., et al. (2022). Extracellular vesicles from human umbilical cord mesenchymal stem cells reduce lipopolysaccharide-induced spinal cord injury neuronal apoptosis by mediating miR-29b-3p/PTEN. *Connect. Tissue Res.* 63 (6), 634–649. doi:10.1080/03008207.2022.2060826

Yilmaz, G., Arumugam, T. V., Stokes, K. Y., and Granger, D. N. (2006). Role of T Lymphocytes and interferon-γ in ischemic stroke. *Circulation* 113 (17), 2105–2112. doi:10.1161/CIRCULATIONAHA.105.593046

Zhou, T., Yuan, Z., Weng, J., Pei, D., Du, X., He, C., et al. (2021). Challenges and advances in clinical applications of mesenchymal stromal cells. *J. Hematol. and Oncol.* 14, 24. doi:10.1186/s13045-021-01037-x

Zhou, W., Farrar, C. A., Abe, K., Pratt, J. R., Marsh, J. E., Wang, Y., et al. (2000). Predominant role for C5b-9 in renal ischemia/reperfusion injury. *J. Clin. investigation* 105, 1363–1371. doi:10.1172/JCI8621

frontiers | Frontiers in Cell and Developmental Biology

TYPE Original Research
PUBLISHED 09 May 2025
DOI 10.3389/fcell.2025.1513163

OPEN ACCESS

EDITED BY
Atsushi Asakura,
University of Minnesota Twin Cities,
United States

REVIEWED BY
Ye Xie,
Icahn School of Medicine at Mount Sinai,
United States
Fei Zheng,
St. Jude Children's Research Hospital,
United States

*CORRESPONDENCE
Shinichi Fukuda,
s-fukuda@md.tsukuba.ac.jp

†These authors have contributed equally to this work and share first authorship

RECEIVED 18 October 2024
ACCEPTED 23 April 2025
PUBLISHED 09 May 2025

CITATION
Tran T-H, Lukmanto D, Chen M, Strauß O, Yamashita T, Ohneda O and Fukuda S (2025) Characterization and neurogenic responses of primary and immortalized Müller glia. *Front. Cell Dev. Biol.* 13:1513163. doi: 10.3389/fcell.2025.1513163

Characterization and neurogenic responses of primary and immortalized Müller glia

Thi-Hang Tran[1,2,3†], Donny Lukmanto[1†], Mei Chen[4], Olaf Strauß[5], Toshiharu Yamashita[1,2], Osamu Ohneda[2] and Shinichi Fukuda[1*]

[1]Laboratory of Advanced Vision Science, Institute of Medicine, University of Tsukuba, Tsukuba, Japan, [2]Laboratory of Regenerative Medicine and Stem Cell Biology, Institute of Medicine, University of Tsukuba, Tsukuba, Japan, [3]Ph.D. program in Human Biology, School of Integrative and Global Majors, University of Tsukuba, Tsukuba, Japan, [4]The Wellcome-Wolfson Institute for Experimental Medicine, School of Medicine, Dentistry and Biomedical Sciences, Queen's University Belfast, Belfast, United Kingdom, [5]Experimental Ophthalmology, Department of Ophthalmology, Charité - Universitätsmedizin Berlin, Corporate Member of Freie Universität, Berlin Institute of Health, Humboldt-University, Berlin, Germany

Primary Müller glia (MG) have been reported to exhibit a neurogenic capacity induced by small molecules. However, whether immortalized mouse MG cell lines exhibit neurogenic capacities similar to those of primary mouse MG remains unclear. In this study, we examined the morphology, proliferation rate, and marker profile of primary MG cells isolated from postnatal mouse pups with two immortalized mouse MG cell lines, QMMuC-1 and ImM10, in a standard growth medium. After chemical induction, we compared the morphology, markers, direct neuronal reprogramming efficiency, and axon length of these cell types in two culture media: Neurobasal and DMEM/F12. Our results showed that in standard growth medium, QMMuC-1 and ImM10 cells displayed similar morphology and marker profiles as primary MG cells, with the only differences observed in nestin expression. However, QMMuC-1 and ImM10 cells exhibited much higher proliferation rates than the primary MG cells. Following chemical treatment in both Neurobasal and DMEM/F12 media, a subset of primary MG, QMMuC-1, and ImM10 cells was induced to differentiate into immature neuron-like cells by day 7. While primary MG cells showed similar neuronal reprogramming efficiency and axon length extension in both media, QMMuC-1 and ImM10 cells displayed variations between the two culture media. Moreover, some of the induced neuronal cells derived from primary MG cells expressed HuC/D and Calbindin markers, whereas none of the cells derived from QMMuC-1 and ImM10 cells expressed these markers. Subsequent observations revealed that induced immature neuron-like cells derived from primary MG cells in both types of media and those derived from ImM10 cells cultured in DMEM/F12 survived until day 14. Taken together, our findings suggest that the two immortalized cell lines, QMMuC-1 and ImM10, exhibited neurogenic capacities similar to those of primary MG cells to some extent but did not fully recapitulate all their characteristics. Therefore, careful consideration should be given to culture conditions and the validation of key results when using immortalized cells as a substitute for primary MG cells.

KEYWORDS

Müller glia, QMMuC-1 cell line, ImM10 cell line, neurogenic responses, chemical induction, neuronal reprogramming

1 Introduction

Many retinal degenerative diseases are characterized by the progressive degeneration of retinal neurons, including photoreceptors and retinal ganglion cells, which eventually leads to irreversible blindness (Kaur and Singh, 2023). Cell replacement is a promising strategy for replacing lost neurons and restoring vision (Coco-Martin et al., 2021). However, cell replacement through transplantation poses several challenges in clinical applications, including the complicated process of creating a reliable cell source, poor survival and integration rates of cells, and other potential side effects (Coco-Martin et al., 2021). In contrast, cell replacement via *in vivo* direct reprogramming from an endogenous cell source to neurons can overcome these challenges (Coco-Martin et al., 2021; Wang et al., 2021). Direct reprogramming of resident cells to replace damaged neurons is faster and avoids the risk of immune rejection (Wang et al., 2021). Nonetheless, this strategy requires further investigation to address significant limitations such as the low proliferative ability of the endogenous cell source, low conversion efficiency, and immaturity of the converted neurons (Wang et al., 2021). More importantly, several studies that successfully achieved *in vivo* direct reprogramming lack definitive validation of the origin of the converted neurons, leading to controversy or issues with reproducibility (Yao et al., 2018; Zhou et al., 2020; Xu et al., 2023). To address this limitation, genetic lineage tracing of the starting cells involved in direct reprogramming should be used to ensure the accurate identification and validation of the reprogrammed neurons (Hoang et al., 2022; Xie and Chen, 2022; Xie et al., 2022).

Several studies have successfully converted Müller glia (MG), the radial glia in the retina, into retinal neurons by overexpressing neuronal transcription factor genes in adult mice (Jorstad et al., 2017; Yao et al., 2018; Todd et al., 2021; Todd et al., 2022). However, for clinical use, inducing neuronal conversion using small molecules is desirable because this approach is cost-effective, safe, and easy to control in terms of concentration and timing (Wang et al., 2021). Two studies showed that chemical compounds can convert primary MG cells isolated from rat and mouse pups into bipolar-like cells (Xia et al., 2021; Yang et al., 2022). Interestingly, one study found that the intravitreal injection of four small molecules induced some MG to migrate into the outer nuclear layer and express rhodopsin, a specific gene of rod photoreceptors (Fujii et al., 2023). Despite these encouraging findings, the efficiency of chemically induced direct reprogramming remains low, and it is not yet understood how small-molecule combinations can be adjusted to achieve the desired retinal neurons.

In 2015, through two successive rounds of chemical screening with 5,000 and 1,500 small molecules, a set of five small molecules was found to effectively induce mouse fibroblasts into functional neurons *in vitro* (Li et al., 2015). This compound combination was optimized to convert astrocytes into neurons in the mouse brain (Ma et al., 2021). Thus, *in vitro* implementation offers many advantages for screening drug candidates owing to its cost-effectiveness and rapid procedures. Nonetheless, to obtain a pure primary MG population for *in vitro* experiments, retinas are usually dissociated using several enzymes, cultured, and passaged at least twice (Liu et al., 2017; Pereiro et al., 2020b). Using this method, only a small number of primary MG cells can be obtained; however, they proliferate slowly and early undergo senescence after four to eight passages (Liu et al., 2017; Pereiro et al., 2020b). Thus, it requires the use of many postnatal mouse pups to obtain enough cells for experiments, which raises ethical concerns regarding animal welfare. Several MG cell lines have been established and used to study the characteristics and functions of MG, owing to their high proliferative capacity (Sarthy et al., 1998; Limb et al., 2002; Tomi et al., 2003; Otteson and Joseph Phillips, 2010; Augustine et al., 2018; Kittipassorn et al., 2019). Despite the similar characteristics of these cell lines to those of primary MG cells, the immortalization process may change their physiology and behavior compared to primary cells. However, it remains unknown whether these cell lines can serve as useful tools for studying neurogenic characteristics instead of primary MG cells. Here, we show similar and distinct characteristics between primary MG, ImM10, and QMMuC-1 cells grown in growth and chemical induction media. These findings provide useful information on the use of primary MG or immortalized cells to study the neurogenic capacity of MG.

2 Materials and methods

2.1 Experimental animals

Wild-type C57BL/6J female and male mice were purchased from CLEA Japan Inc (Tokyo, Japan). The mice were kept at the laboratory of the Animal Resource Center facility of the University of Tsukuba under standard conditions, including controlled temperatures (23°C ± 1°C) and a 12-h light/dark cycle (7 a.m.–7 p.m.). The mice had *ad libitum* access to water and chow. The animal experimental procedure were reviewed and approved by the Animal Experimental Ethical Review Committee of the University of Tsukuba.

2.2 Isolation and culture of Primary Müller glia

Primary MG were isolated from the retinas of postnatal day 2 C57BL/6J mouse pups using a Papain Dissociation System (Worthington Biochemical, Cat. #LK003150), following previously established protocols with some modifications (Liu et al., 2017). Briefly, retinas were dissected from the eyes and then incubated with Papain for 10 min in a water bath at 37°C. Every 5 min, the tubes containing the dissociated solutions were gently shaken by rotating them up and down several times. Once incubation was completed, ovomucoid and DNase I were added to the tissue solution to halt the dissociation process. The cell suspension was centrifuged at 400 *g* for 5 min at room temperature. Subsequently, the cell pellet was washed and resuspended in high-glucose DMEM medium (Gibco, Cat. #12100061) supplemented with 10% Fetal Bovine Serum (FBS; Gibco, Cat. #10270-106) and 1% penicillin-streptomycin (Fujifilm

Abbreviations: Müller glia, MG, glial fibrillary acidic protein, GFAP, 4′,6-diamino-2-phenylindole, DAPI, sex determining region Y (SRY)-box9, Sox9, glutamine synthetase, GS, glutamate aspartate transporter, GLAST, paired box 6, Pax6, class III beta-tubulin, TuJ1, RNA-binding protein with multiple splicing, Rbpms, microtubule-associated protein 2 (Map2).

Wako Pure Chemical, Cat. #168-23191), followed by centrifugation at 300 *g* for 5 min at room temperature. Finally, the cell pellet was resuspended in in high-glucose DMEM medium supplemented with 10% FBS and 1% penicillin-streptomycin and seeded onto 0.1% gelatin-coated dishes. After two passages, the primary cells were utilized for characterization and chemical reprogramming.

2.3 Culture of two immortalized müller glia cell lines

The QMMuC-1 cell line was generously provided by Dr. Mei Chen, Queen's University Belfast. The ImM10 cell line was kindly provided by Dr. Olaf Strauß, Charité Universitäts Medizin Berlin, with approval from Dr. Deborah C. Ottenson, University of Houston. Both cell lines were cultured in high-glucose DMEM medium supplemented with 10% FBS and 1% penicillin-streptomycin. QMMuC-1 and ImM10 cells at passages 30-40 were used in this study.

2.4 Proliferation rate assay

The proliferation rates of primary MG, QMMuC-1 and ImM10 cells were determined using the Cell Counting Kit 8 (Dojindo, Japan) following the manufacturer's instructions. Initially, primary MG, QMMuC-1 and ImM10 cells were seeded in 96-well plates at a density of 1×10^3 cells/well and cultured in high-glucose DMEM supplemented with 10% FBS and 1% penicillin/streptomycin. Cell proliferation was measured every 24 h for 7 days. At the designated time point, 10 μL of Cell Counting Kit 8 reagent was added to each well and mixed uniformly. All cells were incubated for an hour, and the optical absorbance at 450 nm was measured and averaged from six wells for each cell type using a Varioskan Lux multiplate reader (Thermo Fisher Scientific, United States).

2.5 Small-molecule-induced direct reprogramming of primary and immortalized MG

Primary MG, QMMuC-1, and Imm10 cells were chemically reprogrammed according to a previously reported method with some modifications (Yang et al., 2022). Briefly, primary MG, ImM10, and QMMuC-1 cells were seeded into 96-well plates coated with 2% Matrigel (Corning, Cat. #354234) and cultured in a growth medium. After primary MG and QMMuC-1 cells reached over 90% confluence and ImM10 cells reached 70% confluence, cells were changed into neuronal induction medium (100 μL of medium per well), consisting of Neurobasal (Gibco, Cat. #21103-049) or DMEM/F12 medium (Gibco, Cat. #11320-033) supplemented with 0.5% N2 (Thermo Fisher Scientific, Cat. #17502048), and 1% B27 (Thermo Fisher Scientific, Cat. #17504,044), 1% L-glutamine (Gibco, Cat. #25030081), 1% penicillin-streptomycin, basic fibroblast growth factor (100 ng/mL; Peprotech, Cat. #100-18B) (100 ng/mL), cAMP (100 μM; Nacalai Tesque, Cat. #23840-16), forskolin (10 μM; Sigma-Aldrich, Cat. #F6886), ISX9 (40 μM; Selleck Chemicals, Cat. #1300031-49-5), CHIR99021 (20 μM; AdooQ BioScience, Cat. #A10199), I-BET151 (2 μM; Medchem Express, Cat. #HY-12323), and Y-27632 (5 μM; Merck Millipore, Cat. #688001). On day 2 after chemical treatment, the concentrations of three small molecules were reduced (ISX9, 20 μM; CHIR99021, 3 μM; I-BET151, 1 μM). On day 7 after chemical induction, the cells were fixed and subjected to immunofluorescence analysis.

For the control groups, only DMSO or individual small molecules were added to the medium. Specifically, ISX9 (day 0 to day 2: 40 μM, day 2 to day 7: 20 μM) or I-BET151 (day 0 to day 2: 2 μM, day 2 to day 7: 1 μM) was used as a control treatment.

2.6 Immunofluorescence staining

The cells were fixed in 4% paraformaldehyde for 20 min at room temperature, followed by three washes with PBS, each lasting 5 min. Subsequently, the cells were permeabilized with 0.3% Triton in PBS for 10 min. After incubation with a blocking buffer containing 1% bovine serum albumin (Sigma-Aldrich, Cat. #9048-46-8) and 0.3% Triton in PBS for 1 h, the cells were incubated with primary antibodies diluted in the blocking buffer overnight at 4°C. The cells were washed with 0.05% Tween in PBS three times, each for 5 min before incubation with secondary antibodies and 4′,6-diamino-2-phenylindole (DAPI; Invitrogen Corporation, Carlsbad, CA; 1:1,000 dilution) diluted in the blocking buffer for 1 h at room temperature. After another round of washing with 0.05% Tween in PBS three times for 5 min each, the cells were mounted with non-hardening Fluoro-KEEPER Antifade Reagent (Nacalai Tesque, Japan) and imaged using a Keyence BZ-X700 All-in-One microscope (Keyence, Osaka, Japan).

The primary antibodies used in this study were rabbit sex determining region Y (SRY)-box9 (Sox9; Merck, Cat. #AB5535, 1:100), rabbit glutamine synthetase (GS; Abcam, Cat. #ab73593, 1:100), rabbit glutamate aspartate transporter (GLAST; Frontier Institute, Cat. #GLAST-Rb-Af660, 1:100), rabbit glial fibrillary acidic protein (GFAP; CST, Cat. #12389, 1:100), mouse nestin (Invitrogen, Cat. #14-5,843-82, 1:500), rabbit paired box 6 (Pax6; BioLegend, Cat. #BL-901301, 1:300), mouse class III beta-tubulin (TuJ1; Genetex, GT11710, 1:500), rabbit RNA-binding protein with multiple splicing (Rbpms; Abcam, Cat. # Ab194213, 1:200), rabbit Brn3a (Abcam, Cat. # Ab245230, 1:500), rabbit Calbindin (Proteintech, Cat. # 14479-1-AP, 1:200), mouse Rhodopsin (Abcam, Cat. # ab3267, 1:200), rabbit microtubule-associated protein 2 (Map2; EMD Millipore, Cat. # AB5622, 1:200), mouse HuC/D (Santa Cruz Biotechnology, Cat. # sc-515624, 1:200), rabbit NeuroD1 (CST, Cat. #D90G12-7,019, 1:200), and rabbit Otx2 (PGI, Cat. #13497-1-AP, 1: 500).

The secondary antibodies used in the present study included Alexa Fluor® 488 goat anti-rabbit IgG H&L (Abcam, Cat. #ab150077) and Alexa Fluor® 594 goat anti-mouse IgG H&L (Abcam, Cat. #ab150116) at a 1:200 dilution.

2.7 Quantification and statistical analysis

The fluorescence intensity was measured using NIH ImageJ/Fiji software, following a previously published method with some modifications (Echeverria et al., 2025). Images taken under the same settings across cell types were converted to grayscale. The

freehand tool was used to isolate individual cells, and features such as the "area," "area of integrated intensity," and "mean gray value" were measured. A similar area was drawn in a region without cells to measure the background fluorescence intensity. The corrected total cell fluorescence for each cell was calculated by subtracting the product of the "mean gray value" of the background and the "area" of each single cell from the "area integrated density" of that cell. To account for differences in cell size, the corrected total cell fluorescence was normalized by dividing it by the "area" of the respective cell to obtain the fluorescence intensity ratio. The fluorescence intensity ratio of the three cell types in the growth medium was assessed using 3 to 5 cells per image, with 15 images analyzed for each cell line. The fluorescence intensity ratio of TuJ1 at day 14 was evaluated for 1 to 5 cells per image, with 5–10 images analyzed for each cell line.

The conversion efficiency and axon length were analyzed using the Simple Neurite Tracer plugin in the NIH ImageJ/Fiji software (Arshadi et al., 2021). For each treatment, 10-15 images at ×20 magnification were analyzed to obtain average values. Three independent experiments were conducted.

The percentages of primary MG cells positive for Calbindin/TuJ1 or HuC/D among total cells were quantified on day 7 after chemical treatment, using 15 images captured at ×20 magnification.

Data processing and analyses were performed using Python (version 3.8). Statistical significance was determined using the Kruskal–Wallis test, followed by Dunn's *post hoc* test for multiple comparisons ($^{*}p < 0.05$).

3 Results

3.1 Cellular morphology

After isolation and two passages, the cellular morphology of primary MG was examined and compared with that of QMMuC-1 and ImM10 cells under light microscopy (Figure 1A). All cell cultures exhibited a typical MG morphology, with large adherent cells and multiple broad processes. However, the ImM10 cells showed a slight difference in morphology, with elongated rather than broad processes.

3.2 Proliferation rate

The proliferation rates of primary MG, QMMuC-1, and ImM10 cells at 1 week were determined using a Cell Counting Kit 8 (Figure 1B). For the first 3 days, all cell types showed comparable proliferation rates. However, from day 3, ImM10 cells proliferated remarkably, and on day 7, the mean absorbance at 450 nm of ImM10 cells was approximately 19 times and 2.65 times greater than that of primary MG and QMMuC-1 cells, respectively. The proliferation rate of QMMuC-1 cells increased gradually, with the mean absorbance at day 7 being 7.3 times higher than that of primary MG cells. In contrast, primary MG cells only proliferated for the first 2 days and then maintained a similar number of cells until day 7. This suggests that QMMuC-1 and ImM10 cells have a higher proliferative capacity than primary MG cells, as expected.

3.3 Cellular marker profile

We investigated the expression of primary MG, QMMuC-1, and ImM10 cells with various markers, including marker specific for MG, neuronal progenitor cells, and neurons by immunocytochemistry (Figure 2). All cell cultures expressed three MG markers: sex-determining region Y-box 9 (Sox9), glutamine synthetase (GS), and glutamate aspartate transporter (GLAST). ImM10 cells exhibited significantly higher fluorescence signal intensities for all three markers compared to primary MG. Glial fibrillary acidic protein (GFAP), a marker of MG in the activated state, especially after retinal damage, was expressed by all three cell types. However, primary MG showed higher variability in GFAP expression, indicating heterogeneous characteristics.

Interestingly, both primary MG and ImM10 cells were positive for a neuronal progenitor cell marker nestin, whereas QMMuC-1 cells were negative. All three cell types expressed Pax6. None of the primary MG, QMMuC-1, or ImM10 cells expressed class III beta-tubulin (TuJ1), a marker of immature neurons. These results suggest that QMMuC-1 and ImM10 cells exhibit a marker profile highly similar to that of primary MG cells, except for nestin marker, with some variation in fluorescence signal intensity.

3.4 Morphological change and marker expression during chemical reprogramming

Next, we examined whether QMMuC-1 and ImM10 cells exhibited similar neurogenic characteristics induced by small molecules as primary MG cells. We treated primary MG, QMMuC-1, and ImM10 cells with six compounds, including db-cAMP (D, 100 μM), Forskolin (F, 10 μM), Y-27632 (Y, 5 μM), ISX9 (I, 40 μM), CHIR99021 (C, 20 μM), and I-BET151 (B, 2 μM), that have been reported to induce the differentiation of primary mouse MG cells into neuron-like cells (Yang et al., 2022). Unexpectedly, we observed massive cell death during a preliminary experiment (data not shown), particularly in QMMuC-1 and ImM10 cells. Cell death is a major limiting factor in direct reprogramming (Gascón et al., 2016). A high concentration of small molecules induces rapid neuronal conversion but also causes significant cell death (Feng et al., 2021). Thus, we aimed to improve the survival rate by reducing the concentrations of three compounds on day 2 after chemical induction (Figure 3A). Additionally, we tested the neurogenic capacity of these cell cultures in two different media: Neurobasal and DMEM/F12. With this new concentration modification, we observed rapid cellular morphological changes in a subset of primary MG, QMMuC-1, and ImM10 cells after chemical treatment in both media (Figures 3B, C). A few QMMuC-1 cells acquired smaller cell bodies with thin extensions by day 3. By day 7, in both types of culture media, numerous primary MG, QMMuC-1, and ImM10 cells adopted neuron-like shapes with small cell bodies and long extensions. In contrast, in the control group with DMSO or with only IBET-151 or ISX9, all three cell types maintained typical MG-like morphology. Interestingly, in DMEM/F12 medium supplemented with DMSO, most of the ImM10 cells underwent cell death, while these cells still survived and proliferated in Neurobasal medium supplemented with DMSO.

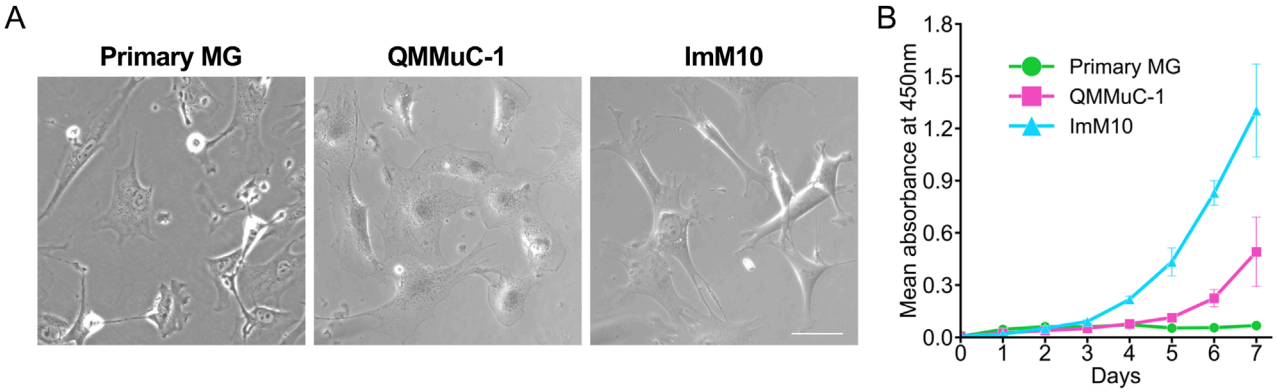

FIGURE 1
Morphology and proliferation rate of primary MG, QMMuC-1, and ImM10 cells in growth media. **(A)** The cellular morphology of primary MG, QMMuC-1, and ImM10 cells was observed under light microscopy. Scale Bars, 50 μm. **(B)** The proliferation rate of primary MG, QMMuC-1, and ImM10 cells in growth media for 7 days. Both immortalized cell lines exhibited a higher proliferation rate than primary MG. Error bars show mean ± SD.

This result indicates that DMEM/F12 medium lacks certain factors or nutrients necessary for the survival and proliferation of ImM10 cells, unlike Neurobasal medium.

On day 7, all cell types were fixed and subjected to immunostaining with the MG marker Sox9 and the neuronal marker TuJ1 (Figure 4). As expected, many TuJ1-positive cells were detected in all cell cultures treated with the 6 chemicals. We observed three distinct types of morphologies of TuJ1-positive cells: neuron-like, intermediate-like, and MG-like shapes in all cultures of primary MG, QMMuC-1, and ImM10 cells (Figure 4A). In contrast, in the control groups, all cells were negative for the TuJ1 marker (Figure 4B and data not shown), with the exception of QMMuC-1 cells treated with only ISX9 compound in Neurobasal medium. A few TuJ1-positive cells with MG-like morphology were detected in this group. Notably, these TuJ1-positive cells still expressed Sox9 marker in their nuclei, indicating that the cells were still in an immature stage (Figures 4C, D).

We quantified the number of TuJ1-positive cells among the total number of cells for each morphological type (Figures 4E, F). The results showed that, in both Neurobasal and DMEM/F12 media supplemented with 6 small molecules, most TuJ1-positive cells derived from QMMuC-1 and primary MG cells acquired neuron-like shapes. In contrast, in the Neurobasal medium supplemented with 6 compounds, approximately half of the TuJ1-positive cells derived from ImM10 cells exhibited an MG-like shape (Figure 4E). In DMEM/F12, this rate was lower but still accounted for approximately one-third of the total number of TuJ1-positive cells (Figure 4F). Interestingly, in Neurobasal medium supplemented with only ISX9 compound, QMMuC-1 cells showed a comparable rate of TuJ1-positive cells with MG-like morphology to those in Neurobasal medium supplemented with 6 chemicals. This result suggests that ISX9, in combination with Neurobasal medium, has a modest effect on neuronal induction in QMMuC-1 cells. When comparing the neuronal conversion efficiencies of the three cell types induced by 6 small molecules (Figures 4E, F), QMMuC-1 cells showed a higher tendency to become TuJ1-positive and acquire a neuron-like shape. However, a significant difference in this rate was observed only between QMMuC-1 and ImM10 cells cultured in the Neurobasal medium. Analysis of the total axon length per cell showed that neuron-like/TuJ1-positive cells from primary MG and ImM10 cells extended to similar lengths in both media (Figure 4G). However, the axons of neuron-like TuJ1-positive cells derived from QMMuC-1 cells were shorter in the Neurobasal medium. In general, the total axonal length per cell was similar across all cell types. Thus, these results indicate that while the culture medium did not significantly affect neuronal conversion efficiency and axon growth in primary MG cells, chemical induction in DMEM/F12 medium induced more neuron-like cells in ImM10 cells and promoted better axon growth in QMMuC-1 cells than in Neurobasal medium.

To confirm the neuronal identity of neuron-like cells derived from primary MG, QMMuC-1, and ImM10 cells, we stained these cells with neuronal cell markers (Figures 5A, 6A, 7A) and retinal neuron markers (Figures 5B,C, 6B-C, and 7B-C). None of the TuJ1+ cells in all three cell types were positive for NeuroD1, a member of the basic helix-loop-helix transcription factor family that highly expressed in developing neurons (Cho and Tsai, 2004). In addition, TuJ1+ cells in all three cell types were negative for Map2, a marker of mature neurons, confirming that these cells remained at an immature stage. Interestingly, a few TuJ1+ cells derived from primary MG cells were positive for Calbindin in both types of media (Figure 5B). Moreover, we detected cells expressing the HuC/D marker in the primary MG cells treated with 6 compounds (Figure 5C). Due to limitations with the host antibody, we could not confirm whether these HuC/D+ cells were also TuJ1+; however, because none of the primary MG cells cultured in growth medium were positive for HuC/D, it is likely that these HuC/D+ cells were induced by the 6 chemicals. Calbindin is a calcium-binding protein primarily expressed in horizontal cells, as well as in some subtypes of amacrine and retinal ganglion cells in the mouse retina (Poché et al., 2007; Gu et al., 2016). Similarly, HuC/D is expressed in amacrine and retinal ganglion cells, with transient expression in horizontal cells during development (Ekström and Johansson, 2003). However, primary MG-derived TuJ1+ cells were negative for Brn3a and Rbpms, two markers of retinal ganglion cells. Therefore, these results suggest that a subset of neuron-like cells derived from primary MG cells were likely directed toward amacrine cells or horizontal cells rather than retinal ganglion cells. There was no difference in the percentage of primary MG cells positive for

10.3389/fcell.2025.1513163

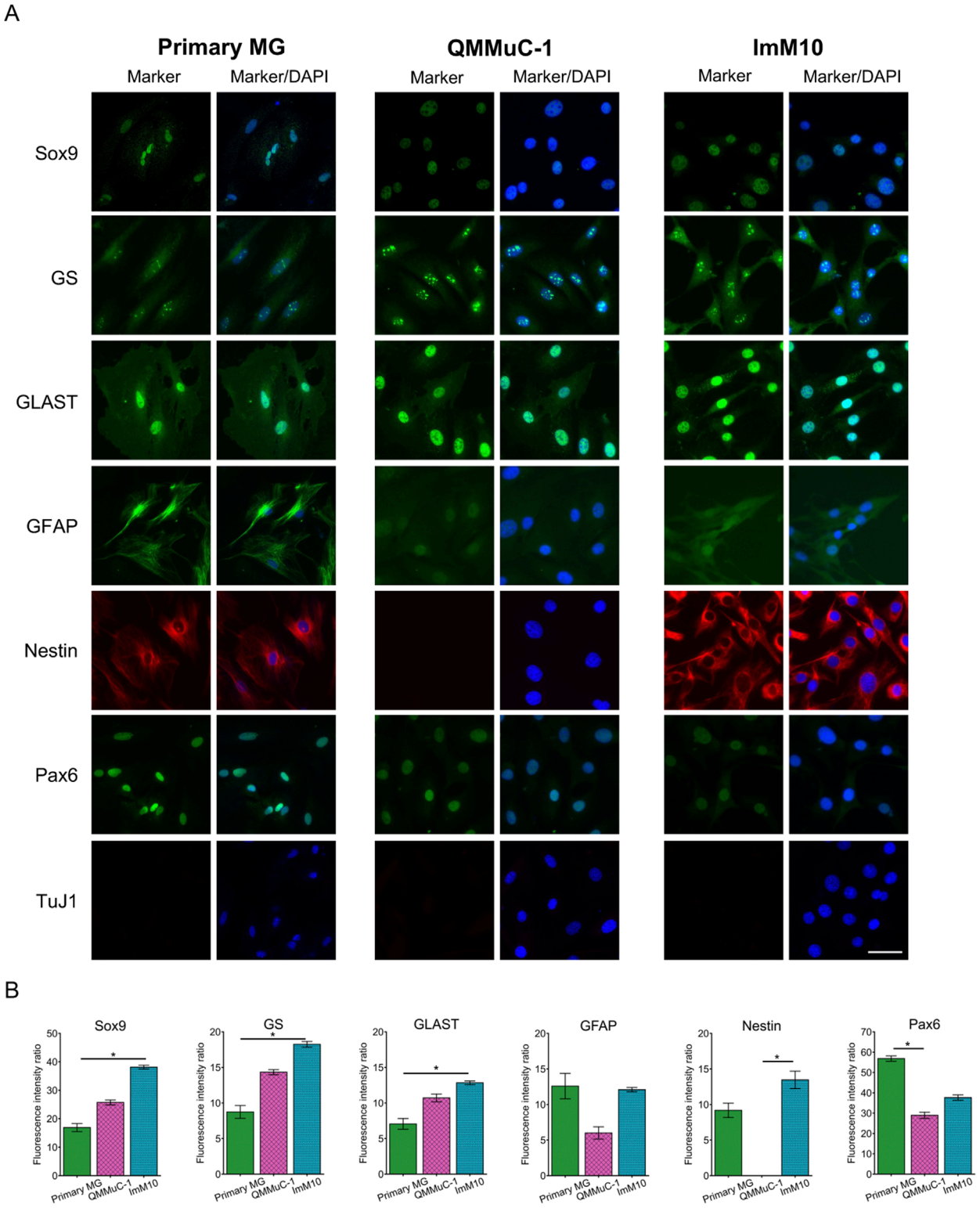

FIGURE 2
Marker profile of primary MG, QMMuC-1, and ImM10 cells in growth media. **(A)** Representative images of primary MG, QMMuC-1, and ImM10 cells stained with MG markers (Sox9, GS, GLAST, and GFAP), retinal progenitor markers (nestin, Pax6), and a neuronal marker (TuJ1). Scale Bars, 50 μm. **(B)** The fluorescence intensity ratio for each marker. The data are presented as mean ± SD.

10.3389/fcell.2025.1513163

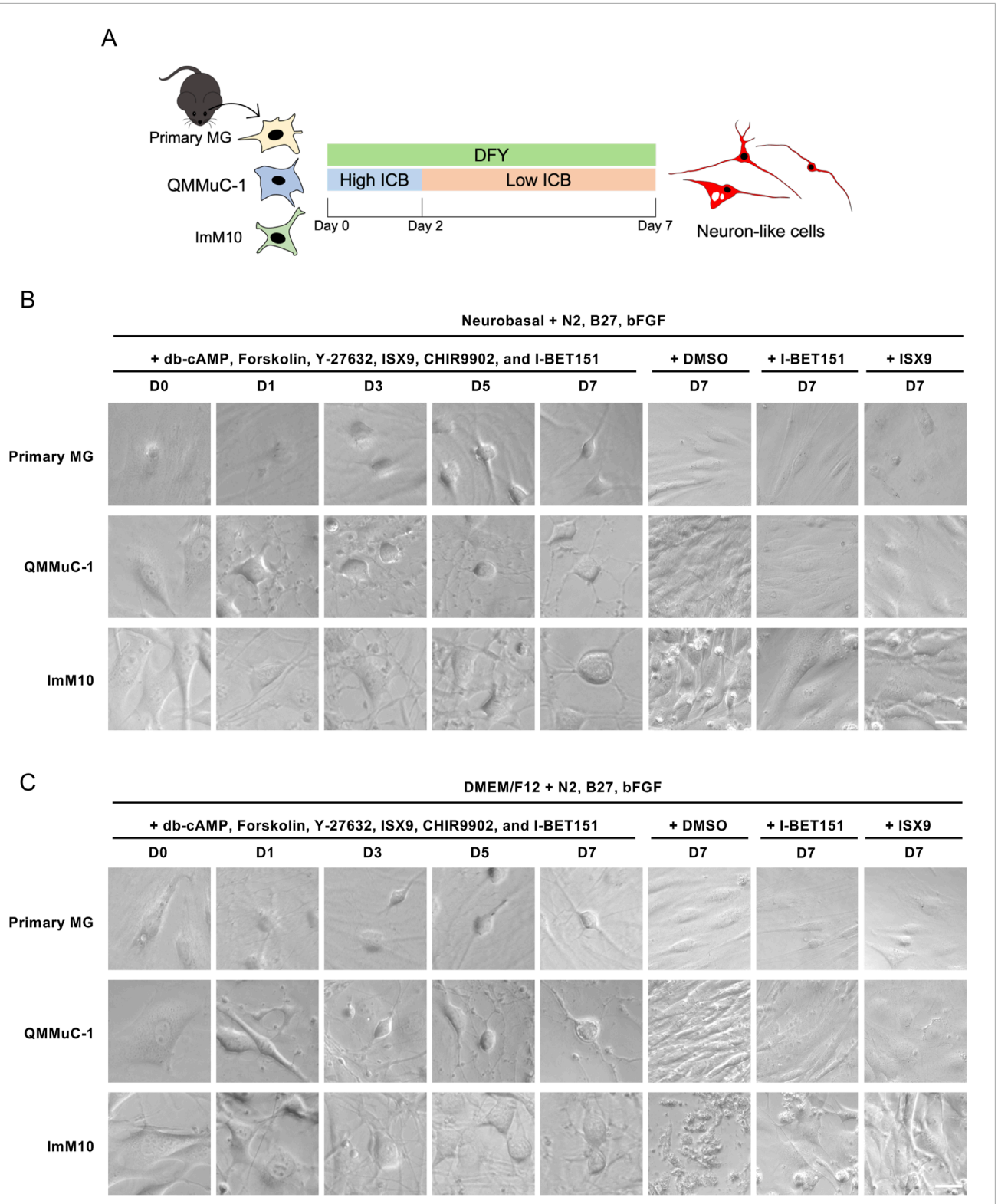

FIGURE 3
Morphological changes of primary MG, QMMuC-1, and ImM10 cells after chemical treatment. **(A)** The scheme of the chemical induction procedure. Primary MG, QMMuC-1, and ImM10 cells were seeded onto matrigel-coated wells and then cultured with an induction medium consisting of db-cAMP (D, 100 μM), Forskolin (F, 10 μM), Y-27632 (Y, 5 μM), ISX9 (I, 40 μM), CHIR99021 (C, 20 μM), and I-BET151 (B, 2 μM). After 2 days, the concentrations of three compounds were reduced (ISX9, 20 μM; CHIR99021, 3 μM; I-BET151, 1 μM). **(B)** Phase-contrast images of cells on days 0, 1, 3, 5, and 7 in a Neurobasal medium supplemented with 6 small molecules and the phase-contrast images of cells on days 7 in a Neurobasal medium supplemented with DMSO or only I-BET151 or only ISX9. **(C)** Phase-contrast images of cells on days 0, 1, 3, 5, and 7 in DMEM/F12 medium and the phase-contrast images of cells on days 7 in a DMEM/F12 medium supplemented with DMSO or only I-BET151 or only ISX9. Primary MG, QMMuC-1, and ImM10 cells changed their cell shape from glial morphology to neuron-like morphology during the chemical induction process in both media supplemented with 6 compounds. Scale Bars, 25 μm.

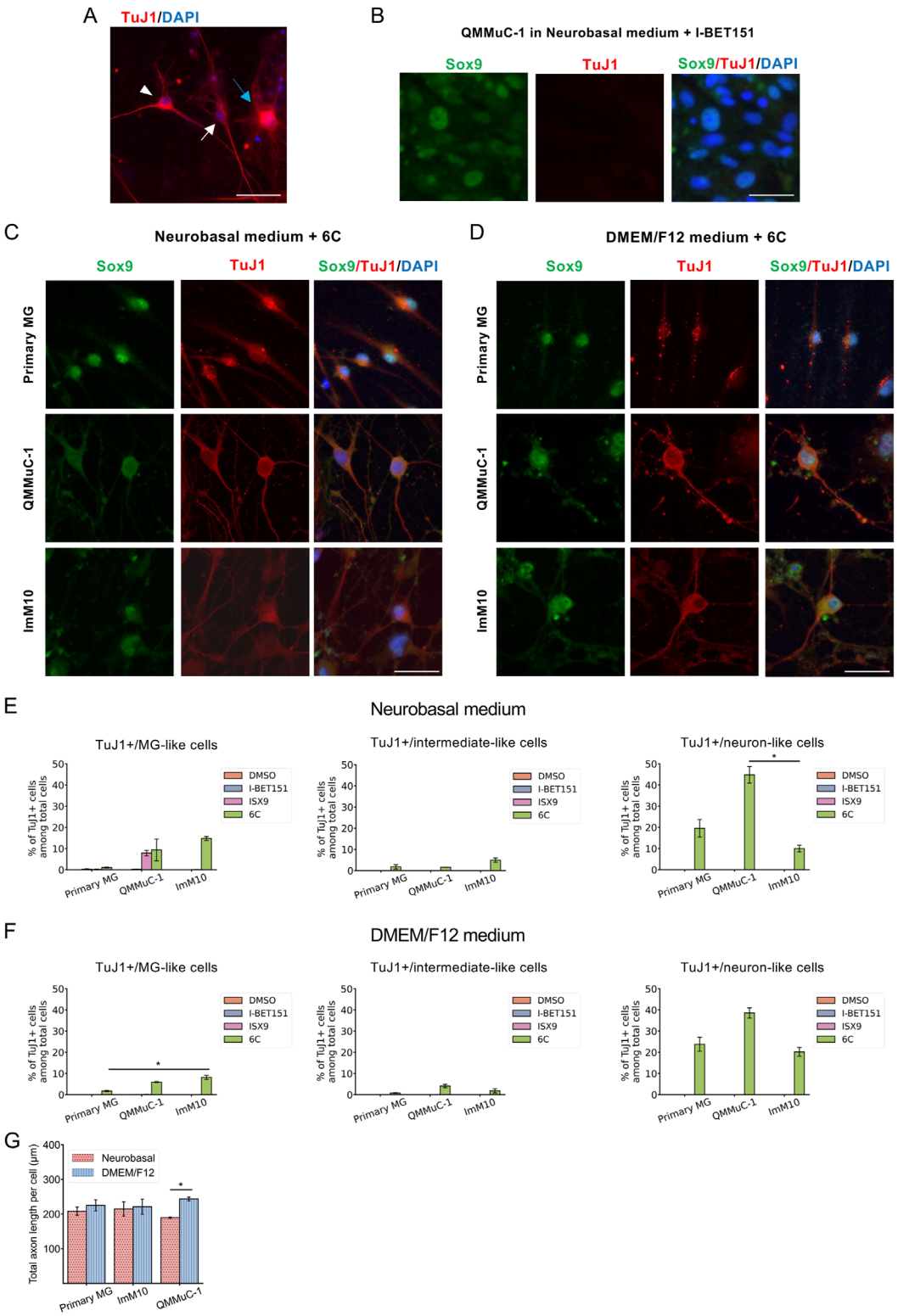

FIGURE 4
Analysis of TuJ1-positive cells derived from primary MG, QMMuC-1, and ImM10 cells at day 7 after chemical treatment. **(A)** Representative images of three morphologically distinct types of TuJ1+ cells derived from primary MG at day 7. TuJ1+ cell with neuron-like morphology is indicated by a white arrowhead. TuJ1+ cell with intermediate-like morphology is indicated by a white arrow. TuJ1+ cell with MG-like morphology is indicated by a blue arrow. Scale bars, 100 μm. **(B)** A representative image of cells in the control group that were not induced into TuJ1+ cells: QMMuC-1 cells cultured in Neurobasal medium supplemented with I-BET151 only. Scale bars, 50 μm. **(C, D)** Immunostaining of primary MG, QMMuC-1, and ImM10 cells with TuJ1 and Sox9 markers at day 7 in Neurobasal medium **(C)** and DMEM/F12 medium **(D)**. Scale bars, 50 μm. **(E–F)** The percentage of neuron-like morphology/TuJ1+ cells, intermediate-like morphology/TuJ1+ cells, and MG-like morphology/TuJ1+ cells derived from primary MG, QMMuC-1, and ImM10 cells among total number of cells at day 7 in Neurobasal medium **(E)** and DMEM/F12 medium **(F)**. The data are presented as mean ± SEM (n = 3). **(G)** The total axonal length per cell of neuron-like morphology/TuJ1+ cells at day 7. The data are presented as mean ± SEM (n = 3). 6C–Medium supplemented with 6 small molecules.

Calbindin/TuJ1 or HuC/D markers on day 7 between Neurobasal and DMEM/F12 media. Surprisingly, unlike primary MG cells, none of the neuron-like cells derived from ImM10 or QMMuC-1 cells expressed Calbindin or HuC/D. All cell types were negative for Otx2, a marker of bipolar cells and immature photoreceptors, as well as Rhodopsin, a marker of mature photoreceptors. Taken together, these results on day 7 indicate that QMMuC-1 and ImM10 cells can be induced into immature TuJ1+/neuron-like cells, similar to primary MG cells. However, unlike primary MG cells, they did not differentiate into amacrine or horizontal cell fates by day 7.

Primary MG, QMMuC-1, and ImM10 cells were cultured until day 14 in both Neurobasal and DMEM/F12 media supplemented with 6 small molecules (Figure 8). Interestingly, neuron-like cells derived from primary MG cells survived until day 14 in both media (Figure 8A). In contrast, none of the neuron-like cells derived from QMMuC-1 cells survived until day 14 (data not shown). For ImM10 cells, some neuron-like cells remained in the DMEM/F12 medium on day 14, whereas only cells with MG-like morphology were observed in the Neurobasal medium (Figure 8B). Immunostaining results (Figures 8C– E) showed that the surviving MG-like cells in the Neurobasal medium slightly expressed the TuJ1 marker compared to neuron-like cells, suggesting that these cells could have been induced by the small molecules, but the effects were insufficient to achieve noticeable morphological changes. *In vitro* cells expressing TuJ1 without acquiring a neuron-like shape have also been reported in previous studies (Gascón et al., 2016; Todd et al., 2022). Surprisingly, TuJ1-positive cells derived from primary MG cells in both Neurobasal and DMEM/F12 media, as well as from ImM10 cells in DMEM/F12, expressed GS, a marker of MG. These results indicate that induced neuron-like cells derived from QMMuC-1 cells in both types of media and from ImM10 cells in the Neurobasal medium may require additional supplements to survive beyond day 7. Furthermore, the surviving induced neuron-like cells on day 14 were still in an immature stage.

4 Discussion

Our research demonstrates that QMMuC-1 and ImM10 cells share similar morphology and marker profiles with primary MG cells in the growth medium and can be chemically induced into immature neuron-like cells. However, QMMuC-1 and ImM10 cells showed unique characteristics, including higher proliferation rates, distinct survival abilities after chemical induction, and different responses to Neurobasal and DMEM/F12 media supplemented with 6 small molecules.

The QMMuC-1 cell line was generated via spontaneous immortalization, while the ImM10 cell line was established by the conditional overexpression of a proto-oncogene called simian virus 40 large tumor antigen (Otteson and Joseph Phillips, 2010; Augustine et al., 2018). Both cell lines were cultured for up to 50 passages (Otteson and Joseph Phillips, 2010; Augustine et al., 2018). In contrast, primary MG cells stop proliferation and undergo senescence after only 4 to 8 passages (Liu et al., 2017; Pereiro et al., 2020b). Thus, it is not surprising that QMMuC-1 and ImM10 cells have a higher proliferation capacity than primary MG cells in the growth medium. Simian virus 40 large tumor antigen activation in primary mouse embryonic fibroblasts showed a shorter doubling rate and greater viability than in cells cultured under spontaneously immortalized conditions (Amand et al., 2016). Thus, conditional overexpression of simian virus 40 large tumor antigen may induce the ImM10 cell line to acquire a higher capacity to overcome contact inhibition and a faster proliferation rate than the QMMuC-1 cell line.

Immunostaining of cell cultures in the growth medium revealed that primary MG, QMMuC-1 and ImM10 cells expressed GFAP marker. In normal retinas, MG typically show no gene expression or very low gene expression of GFAP (Xue et al., 2006a). After the retinal injury, MG upregulate GFAP expression, indicating their activation and stress (Xue et al., 2006a). A previous study reported that freshly dissociated rabbit Müller glial cells did not express the GFAP gene, but after 2 days of culturing, the cells displayed high levels of GFAP marker expression (Mcgillem et al., 1998). Other studies have also shown that primary MG cells express GFAP markers even when the primary cells are isolated from normal, healthy pups (Augustine et al., 2018; Kittipassorn et al., 2019). In contrast, several research groups have reported that primary MG cells do not express GFAP (Hicks and Courtois, 1990; Limb et al., 2002). The cell isolation protocols used in these studies have many differences, including the type of enzyme used for dissociation and the duration of enzyme incubation. One study suggested that extended soaking during cell isolation in their protocol may reduce the cellular adhesion and the severity of tissue dissociation, resulting in low GFAP gene expression (Hicks and Courtois, 1990). Thus, the differences in GFAP expression in primary cells in previous reports may be due to the differences in the effects of the dissociation step on MG. The W21M MG cell line, an immortalized whale MG, strongly expresses GFAP at passages lower than 10 but starts to reduce GFAP expression after passage 10 (Pereiro et al., 2022). Although in this study, the fluorescence signal intensity of GFAP marker in primary MG was comparable to two immortalized cell lines, primary MG displayed a higher variability. Hence, the lower expression of GFAP in QMMuC-1 and more stable expression of GFAP in ImM10 cells compared to that in primary MG cells may be due to the high passage number of the two immortalized cell lines used in the present study.

The primary MG cells isolated from postnatal mouse pups in the present study expressed nestin and Pax6, consistent with previous studies (Xue et al., 2006b; Pereiro et al., 2020a). MG express nestin and Pax6 during postnatal development but diminish the expression of these markers in the adult stage (Xue et al., 2006b; Kato et al., 2022). Notably, a study has demonstrated that a subset of MG cells continues to express Pax6 during the adult stage (Joly et al., 2011). Several studies have shown that MG upregulate nestin and Pax6 expression following retinal injury (Xue et al., 2006b; Suga et al., 2014; Kato et al., 2022). Both QMMuC-1 and ImM10 cell lines were established from primary MG cells isolated at the postnatal stage; however, QMMuC-1 cells were negative for nestin marker. Interestingly, one study observed that only primary human MG that coexpress nestin and cellular retinaldehyde-binding protein, a MG marker, can become spontaneously immortalized in culture (Lawrence et al., 2007). Thus, it is possible that at early passages of QMMuC-1 cells, these cells express nestin. However, after several passages, these cells may lose nestin expression for unknown reasons.

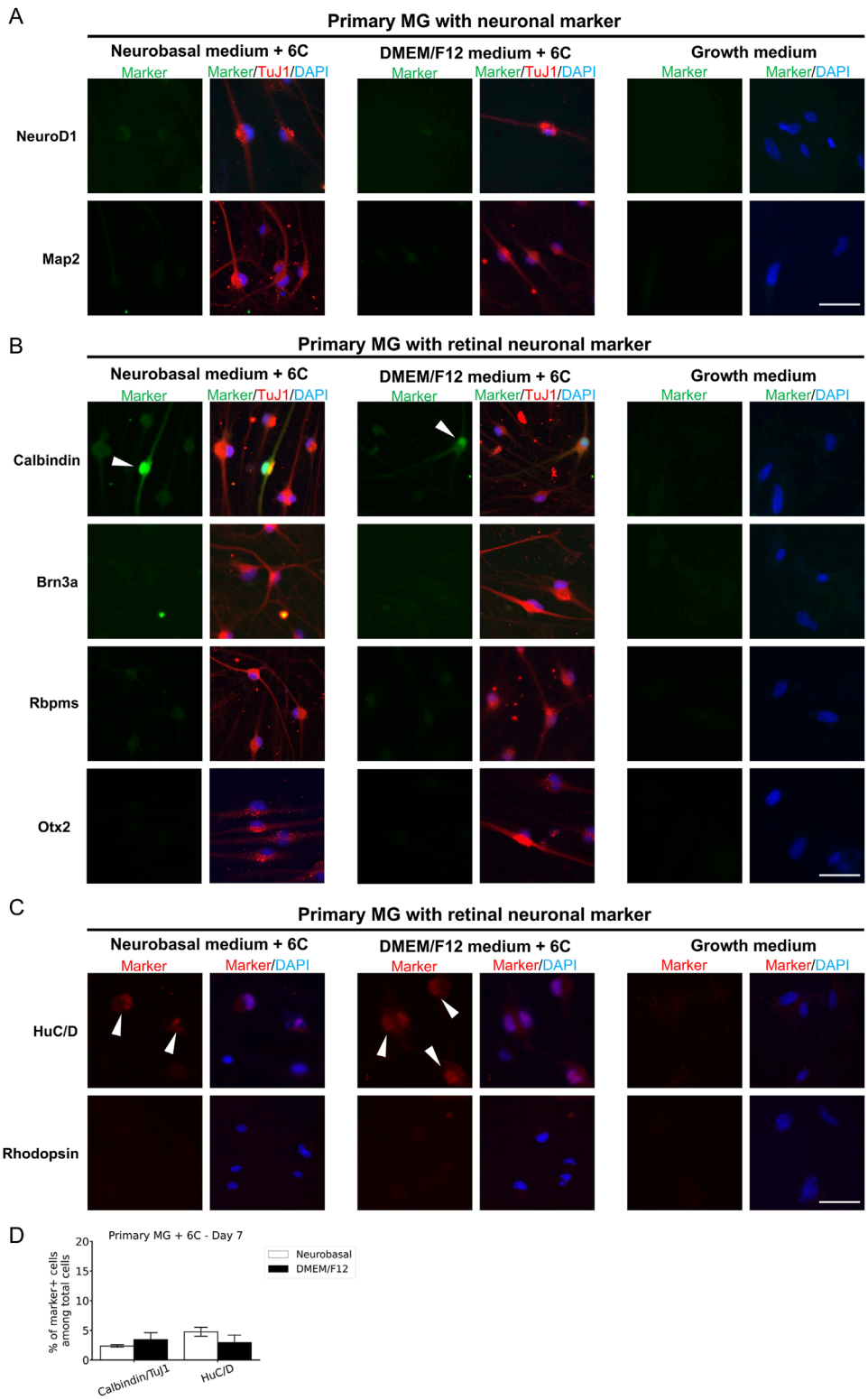

FIGURE 5
Immunostaining results of neuron-like cells derived from primary MG cells with various neuronal markers and retinal neuron markers. **(A)** Cells were stained with TuJ1 marker and neuronal markers: NeuroD1 and Map2. Scale Bars, 50 μm. **(B)** Cells were stained with TuJ1 marker and retinal neuron markers: Calbindin (primarily expressed in horizontal cell, as well as in some subtypes of amacrine and retinal ganglion cells); Brn3a and Rbpms (markers of retinal ganglion cells); Otx2 (marker of bipolar and immature photoreceptor). Scale Bars, 50 μm. **(C)** Cells were stained retinal neuron markers: HuC/D (expressed in amacrine and retinal ganglion cells, with transient expression in horizontal cells during development), Rhodopsin (marker of mature rod photoreceptor). **(D)** The percentage of cells derived from primary MG that were positive for Calbindin/TuJ1 or HuC/D among total cells on day 7. The data are presented as mean ± SD (n = 3). Scale Bars, 50 μm. 6C–Medium supplemented with 6 small molecules.

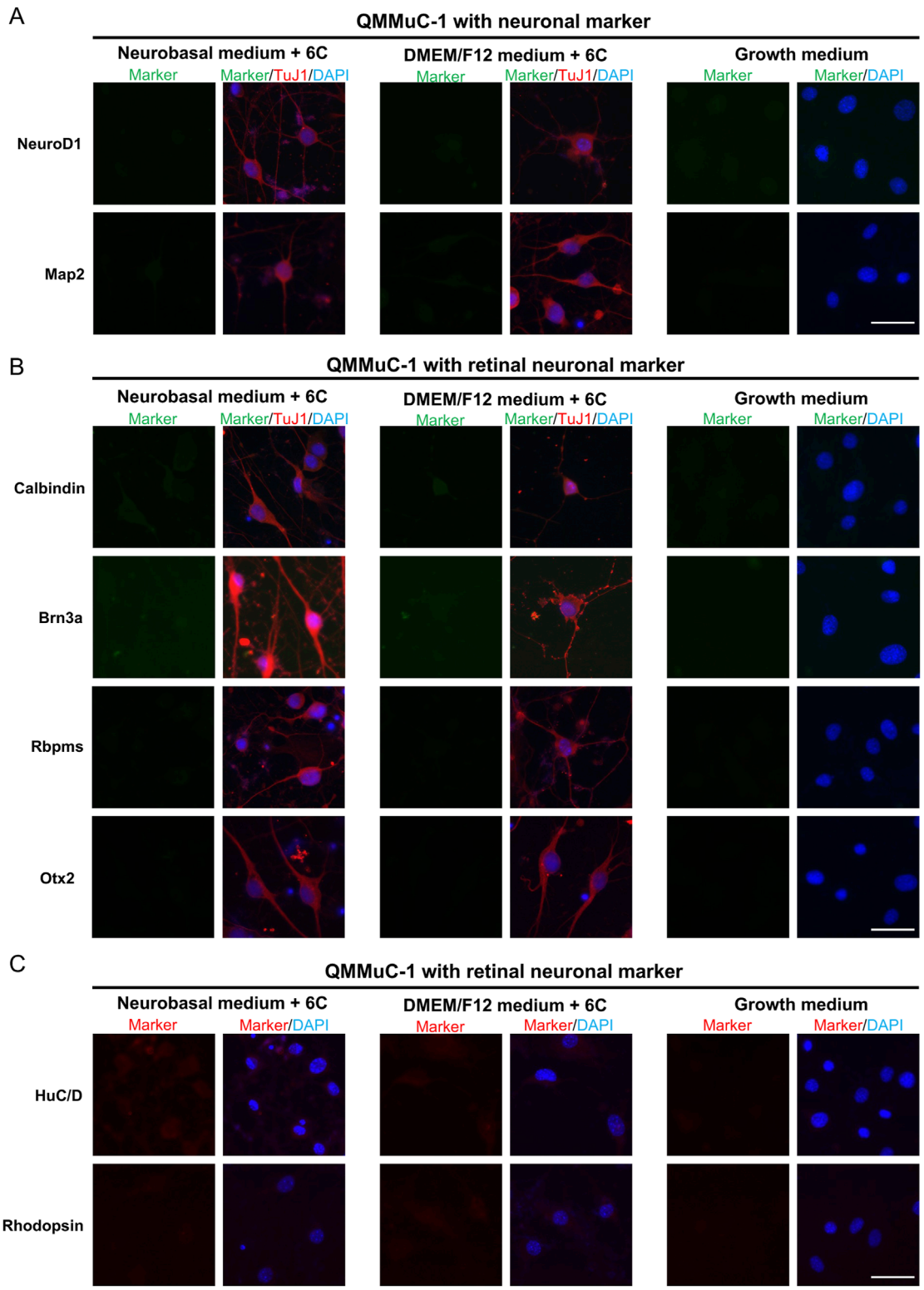

FIGURE 6
Immunostaining results of neuron-like cells derived from QMMuC-1 cells with various neuronal markers and retinal neuron markers. **(A)** Cells were stained with TuJ1 marker and neuronal markers: NeuroD1 and Map2. Scale Bars, 50 μm. **(B)** Cells were stained with TuJ1 marker and retinal neuron markers: Calbindin (primarily expressed in horizontal cell, as well as in some subtypes of amacrine and retinal ganglion cells); Brn3a and Rbpms (markers of retinal ganglion cells); Otx2 (marker of bipolar and immature photoreceptor). Scale Bars, 50 μm. **(C)** Cells were stained retinal neuron markers: HuC/D (expressed in amacrine and retinal ganglion cells, with transient expression in horizontal cells during development), Rhodopsin (marker of mature rod photoreceptor). Scale Bars, 50 μm. 6C–Medium supplemented with 6 small molecules.

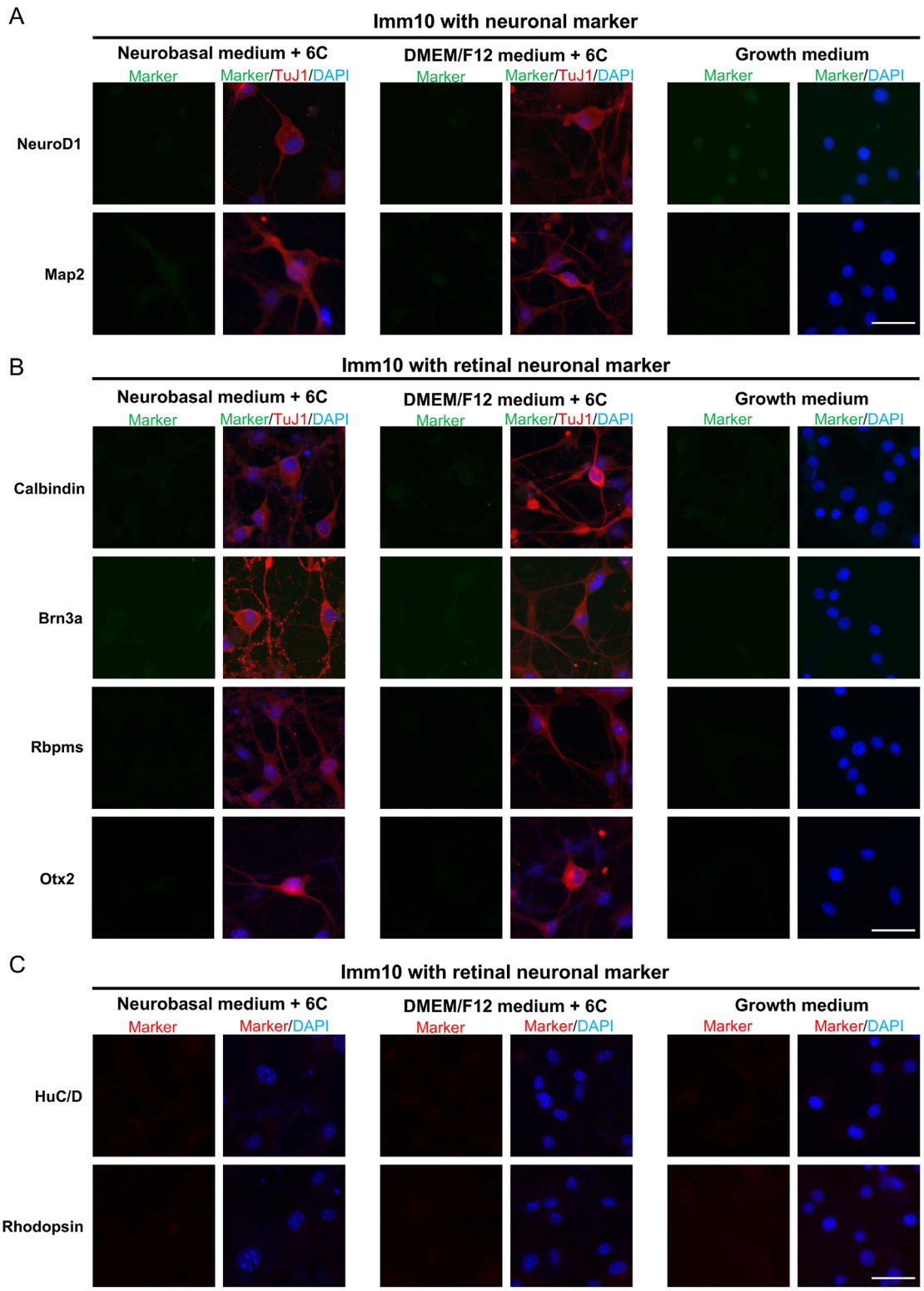

FIGURE 7
Immunostaining results of neuron-like cells derived from ImM10 cells with various neuronal markers and retinal neuron markers. **(A)** Cells were stained with TuJ1 marker and neuronal markers: NeuroD1 and Map2. Scale Bars, 50 μm. **(B)** Cells were stained with TuJ1 marker and retinal neuron markers: Calbindin (primarily expressed in horizontal cell, as well as in some subtypes of amacrine and retinal ganglion cells); Brn3a and Rbpms (markers of retinal ganglion cells); Otx2 (marker of bipolar and immature photoreceptor). Scale Bars, 50 μm. **(C)** Cells were stained retinal neuron markers: HuC/D (expressed in amacrine and retinal ganglion cells, with transient expression in horizontal cells during development), Rhodopsin (marker of mature rod photoreceptor). Scale Bars, 50 μm. 6C–Medium supplemented with 6 small molecules.

10.3389/fcell.2025.1513163

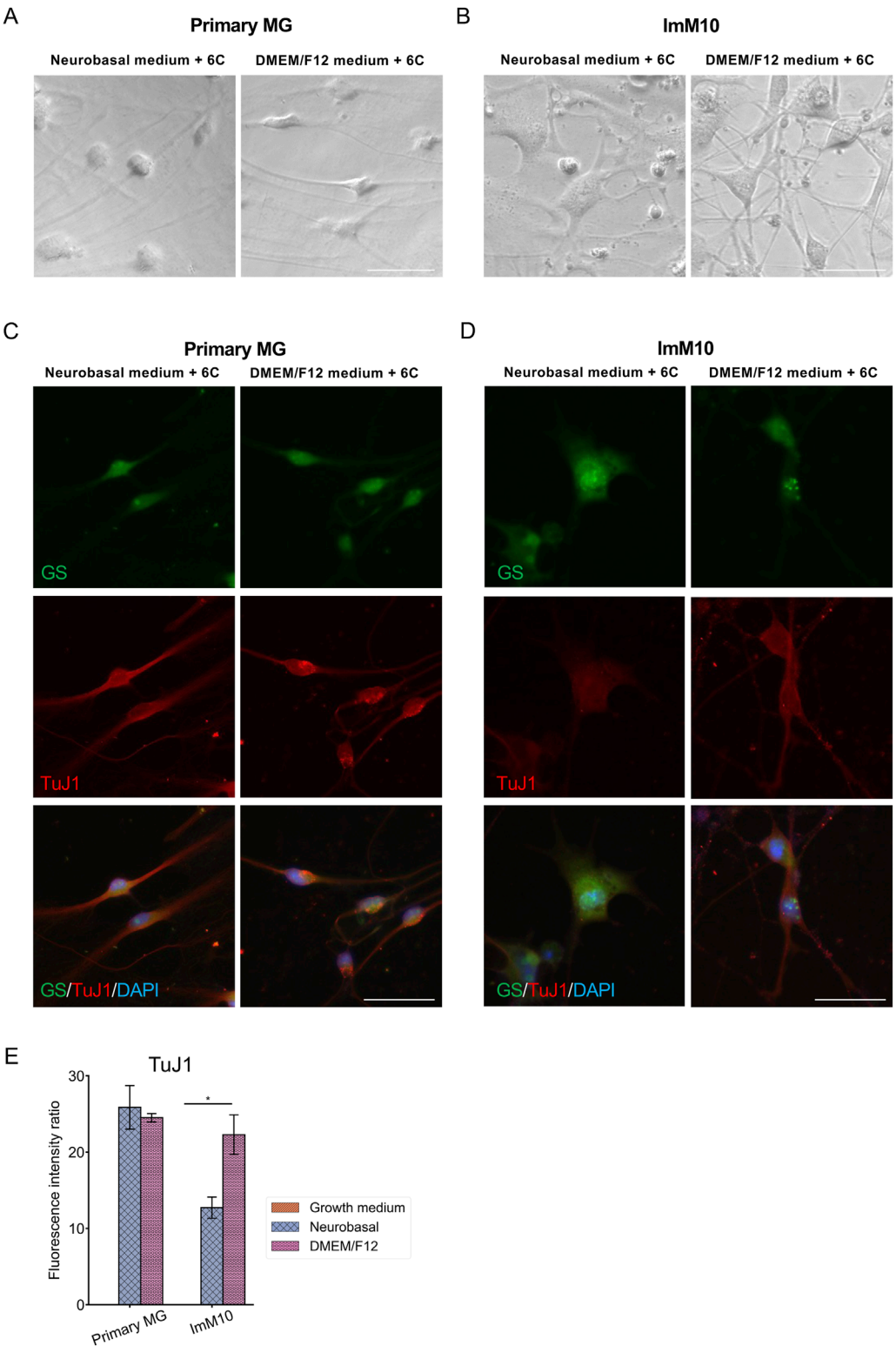

FIGURE 8
Morphology and immunocytochemistry staining of primary MG and ImM10 cells at day 14 after chemical induction. **(A)** Morphology of primary MG cells at day 14 in Neurobasal and DMEM/F12 media. Scale Bars, 50 μm. **(B)** Morphology of ImM10 cells at day 14 in Neurobasal and DMEM/F12 media. Scale Bars, 50 μm. Primary MG **(C)** and ImM10 cells **(D)** were stained with GS and TuJ1 markers at day 14 post-chemical treatment. Scale Bars, 50 μm **(E)** The fluorescence intensity ratio for TuJ1 marker. 6C–Medium supplemented with 6 small molecules.

The concentration of small molecules greatly affects neuronal conversion and the survival rate of induced neurons. A previous study halved the concentration of I-BET151 and ISX9 on day 2 after chemical induction and later added neurotrophins, antioxidants, and a broad-spectrum caspase inhibitor on day 6 to increase the survival of reprogrammed cells (Xia et al., 2021). Another study established a strategy to balance the neuronal conversion efficiency and survival rate by adding small molecules in a stepwise manner, with one group of small molecules inducing neuronal reprogramming, while the other group promoting cell survival and improving reprogramming efficiency (Yang et al., 2019). To reduce cell death, we adjusted the concentrations of I-BET151, ISX9, and CHIR99021 on day 2 after chemical induction. In addition to the small molecule concentration, we found that the volume of the induction medium greatly affected the survival rate of converted neurons. Typically, the volume of the medium has not been reported in direct reprogramming studies. In our preliminary experiments, we observed that a higher volume of induction medium accelerated the direct reprogramming process and caused more cell death, even with the same concentration as in a smaller volume. This observation may explain the differences between our results and those of previous study (Yang et al., 2022). When we first tested the same concentration of small-molecule combinations to convert primary mouse MG cells into neuron-like cells, we observed low cell survival. The previous study utilized 6-well plates, whereas we used 96-well plates, which are more suitable for drug screening and reduce the number of primary MG cells required for experiments (Yang et al., 2022). However, although we improved the cell survival with our treatment, the induced neuron-like cells remained in an immature stage at day 14 after chemical induction. Reduced concentrations of these compounds could potentially lead to a slower neuronal reprogramming process or incomplete downregulation of MG gene expression. Thus, our results highlight the importance of small molecule concentrations in cell survival and reprogramming efficiency.

Although immortalized glial cell lines undergo changes during the immortalization process, many retain a neurogenic capacity that is, to some extent, similar to that of primary glial cells. One study treated primary mouse MG cells with four chemicals and found that this combination upregulated the rhodopsin gene, a specific photoreceptor marker (Fujii et al., 2023). This finding was validated using a rat immortalized MG cell line, which showed a similar upregulation (Fujii et al., 2023). Another study screened 93 small molecules in a spontaneously transformed mouse astrocyte cell line and identified a combination that converted these cells into glutamatergic neurons (Fernandes et al., 2022). In this study, we investigated the neurogenic characteristics of two mouse immortalized MG cell lines, QMMuC-1 and ImM10, in two types of culture media, Neurobasal and DMEM/F12. Previous studies on direct neuronal reprogramming commonly used these media individually or in a 1:1 ratio (Li et al., 2015; Yang et al., 2019; 2022; Ma et al., 2021; Xia et al., 2021; Fernandes et al., 2022; Fujii et al., 2023). Our findings demonstrated that QMMuC-1 and ImM10 cells were chemically converted into neuron-like TuJ1-positive cells similar to primary cells by day 7 in both media. Interestingly, QMMuC-1 cells showed a higher tendency to convert induced neuron-like cells than primary MG and ImM10 cells. Notably, only ISX9 supplementation in Neurobasal medium was able to induce a subset of QMMuC-1 cells to upregulate TuJ1 expression. Nestin is a marker protein for central nervous system stem cells and progenitor cells, and its expression decreases when these cells differentiate into neurons and glial cells (Dahlstrand et al., 1995). The absence of nestin expression in QMMuC-1 cells may facilitate neuronal differentiation following chemical treatments. Similar to primary MG cells, QMMuC-1 and ImM10 cells did not upregulate NeuroD1, a basic helix-loop-helix transcription factor crucial for neuronal generation and cell fate (Cho and Tsai, 2004), nor Map2, a marker of mature neurons after chemical treatment at day 7.

Although QMMuC-1 and ImM10 cells can be induced into immature neuron-like cells similar to primary MG cells, the induced neuronal cells from these two immortalized lines may not differentiate in the same way as primary MG cells. After stimulation with six compounds, a subset of primary MG-derived neuron-like cells appears to differentiate into amacrine or horizontal cell fates, as indicated by HuC/D and calbindin markers. In contrast, neuron-like cells derived from QMMuC-1 and ImM10 cells had not reached the differentiation stage. Another possibility is that TuJ1+ cells derived from QMMuC-1 and ImM10 cells could differentiate in the same direction as primary MG cells, but at a slower rate. Therefore, future work is needed to evaluate cell identity at a more mature stage. However, based on these results, we could at least conclude that QMMuC-1 and ImM10 cells did not respond to the six compounds in the same way as primary MG cells. The high variability of the GFAP marker in primary MG cells suggests that these cells were quite heterogeneous, which may explain the differences in response between the cell types. Firstly, the primary MG cells isolated from postnatal day 2 pups may contain a small subset that is susceptible to neurogenic stimulation, allowing these cells to differentiated into retinal neurons more easily. In contrast, the QMMuC-1 and ImM10 cell lines underwent many passages, thus may have lost these characteristics.

We observed that the induced neuron-like cells derived from QMMuC-1 cells could not be maintained beyond day 7 in either Neurobasal or DMEM/F12 media. In contrast, the induced neuron-like cells derived from ImM10 cells in DMEM/F12 survived until day 14 post-treatment, albeit with a gradual reduction in cell numbers after day 7. Primary MG-derived neuron-like cells, on the other hand, survived until day 14 in both types of media. In the retina, MG support retinal neurons by releasing various factors, including neurotrophins (Tworig and Feller, 2022). Given that only a subset of primary MG cells is converted into induced neuron-like cells, non-converted MG cells may release neurotrophic factors, thereby supporting the survival of converted neuron-like cells. In contrast, immortalized cell lines lose this characteristic during the immortalization process, as exemplified by QMMuC-1's significantly lower expression of neurotrophic genes than in primary MG cells (Augustine et al., 2018). The study mentioned above, which used a spontaneously transformed mouse astrocyte cell line, also included neurotrophins in the induction medium from day 0, whereas previous studies typically added neurotrophic factors after transitioning to a mature medium (Li et al., 2015; Ma et al., 2021; Fernandes et al., 2022). It remains unclear why neuron-like cells derived from QMMuC-1 and ImM10 exhibit distinct survival abilities, despite both being immortalized cell lines. Differences in the methods used for immortalization may influence their characteristics.

Our results suggest that the two immortalized MG cell lines, QMMuC-1 and ImM10, to some extent, can be used to study

the neurogenic characteristics of MG and address the limitations associated with the use of primary MG cells. Using the ImM10 cell line can be particularly beneficial for screening purposes because it carries a GFP reporter gene under the rhodopsin promoter, enabling the robust detection of GFP signals when ImM10 cells are converted into photoreceptor cells (Otteson and Joseph Phillips, 2010). Immortalized cell lines are also particularly valuable for studying the neurogenic capacity of MG in human due to the limited availability of primary human MG cells. However, since the induced neuronal cells from these two immortalized lines did not respond to the six small molecules in the same differentiation direction as primary MG cells, validating key findings from immortalized cells using primary MG cells is essential. In addition, the inclusion of neurotrophic factors or other supportive factors in the induction media is crucial for maintaining the survival of induced neuron-like cells derived from immortalized cells.

While this study provides valuable insights into the neurogenic capacity of immortalized MG cell lines, certain limitations must be acknowledged. Firstly, due to the lack of access to early-passage QMMuC-1 and ImM10 cell lines, we were unable to assess and compare their neurogenetic capacity at early and late passages. This limitation prevents a comprehensive understanding of how genetic or epigenetic drift during immortalization may influence neurogenesis. Future studies focusing on early-passage immortalized MG cell lines will be essential for clarifying the impact of passage number on small-molecule-induced neurogenesis and improving the generalizability of these findings. Secondly, the induced neuronal cells in this study are predominantly at an immature stage. Therefore, further work will be necessary to promote their maturation and evaluate their functional characteristics, such as synaptic connectivity and electrophysiological responses. Finally, while our study highlighted differences in cell survival between the induced neuronal cells derived from primary Müller glia, QMMuC-1 cells, and ImM10 cells in two different media, and suggested potential factors contributing to these differences, we did not perform experiments aimed at improving cell survival. Optimizing conditions to enhance cell survival is a complex task that would require careful adjustments of various factors, and thus, represents an important area for future research.

5 Conclusion

In conclusion, we examined and compared the characteristics of primary MG cells and two immortalized mouse MG cell lines, QMMuC-1 and ImM10, in standard growth and neurogenic induction media. In standard growth medium, QMMuC-1 and ImM10 cells showed similar morphology and marker profiles, with differences only in the nestin markers. However, the QMMuC-1 and ImM10 cells exhibited significantly higher proliferation rates. In the chemical induction medium, QMMuC-1 cells and ImM10 cells were converted into immature neuron-like cells, such as primary MG cells with variations in reprogramming efficiency. However, induced neuronal cells derived from QMMuC-1 and ImM10 cells exhibited differences in their differentiation capacity into retinal neurons compared to primary MG cells. Our experiments also showed differences in the cell survival of induced neuron-like cells derived from the three cell types and the effect of the culture medium on direct neuronal reprogramming.

Data availability statement

The raw data supporting the conclusions of this article will be made available by the authors, without undue reservation.

Ethics statement

The animal study was approved by The Animal Experimental Ethical Review Committee of the University of Tsukuba. The study was conducted in accordance with the local legislation and institutional requirements.

Author contributions

T-HT: Data curation, Formal Analysis, Investigation, Methodology, Visualization, Writing – original draft, Writing – review and editing, Validation. DL: Conceptualization, Investigation, Methodology, Validation, Writing – review and editing. MC: Resources, Writing – review and editing, Validation. OS: Resources, Writing – review and editing, Validation. TY: Investigation, Methodology, Writing – review and editing, Validation. OO: Writing – review and editing, Resources, Validation. SF: Funding acquisition, Project administration, Supervision, Writing – review and editing, Validation, Conceptualization.

Funding

The author(s) declare that financial support was received for the research and/or publication of this article. SF was supported by supported by JST FOREST Program Grant Number JPMJFR200T, JSPS KAKENHI Grant Number JP22H03241, JP23K24500, JP18K19961, AMED Grant Number JP23bm1123024, Takeda Science Foundation, TANO Young Investigator's Award, JRVS basal research support program, JST Grant Number JPMJPF 2017; DL by the Mishima Saiichi Memorial Foundation, Hirose Foundation; T.H.T by Support for Pioneering Research Initiated by the Next-Generation (SPRING).

Conflict of interest

The authors declare that the research was conducted in the absence of any commercial or financial relationships that could be construed as a potential conflict of interest.

Generative AI statement

The author(s) declare that no Generative AI was used in the creation of this manuscript.

Publisher's note

References

Amand, M. M., Hanover, J. A., and Shiloach, J. (2016). A comparison of strategies for immortalizing mouse embryonic fibroblasts. *J. Biol. Methods* 3, e41. doi:10.14440/jbm.2016.110

Arshadi, C., Günther, U., Eddison, M., Harrington, K. I. S., and Ferreira, T. A. (2021). SNT: a unifying toolbox for quantification of neuronal anatomy. *Nat. Methods* 18, 374–377. doi:10.1038/s41592-021-01105-7

Augustine, J., Pavlou, S., O'hare, M., Harkin, K., Stitt, A., Curtis, T., et al. (2018). Characterization of a spontaneously immortalized murine müller glial cell line QMMuC-1. *Invest. Ophthalmol. Vis. Sci.* 59, 1666–1674. doi:10.1167/iovs.17-23293

Cho, J.-H., and Tsai, M.-J. (2004). The role of BETA2/NeuroD1 in the development of the nervous system. *Mol. Neurobiol.* 30, 035–047. doi:10.1385/MN:30:1:035

Coco-Martin, R. M., Pastor-Idoate, S., and Pastor, J. C. (2021). Cell replacement therapy for retinal and optic nerve diseases: cell sources, clinical trials and challenges. *Pharmaceutics* 13, 865. doi:10.3390/pharmaceutics13060865

Dahlstrand, J., Lardelli, M., and Lendahl, U. (1995). Nestin mRNA expression correlates with the central nervous system progenitor cell state in many, but not all, regions of developing central nervous system. *Brain Res. Dev. Brain Res.* 84, 109–129. doi:10.1016/0165-3806(94)00162-s

Echeverria, C. V., Leathers, T. A., and Rogers, C. D. (2025). Comparative analysis of fixation techniques for signal detection in avian embryos. *Dev. Biol.* 517, 13–23. doi:10.1016/j.ydbio.2024.09.002

Ekström, P., and Johansson, K. (2003). Differentiation of ganglion cells and amacrine cells in the rat retina: correlation with expression of HuC/D and GAP-43 proteins. *Dev. Brain Res.* 145, 1–8. doi:10.1016/S0165-3806(03)00170-6

Feng, Y., Bai, S., Li, G., Nie, H., Chen, S., Pan, C., et al. (2021). Reprogramming rat astrocytes into neurons using small molecules for cell replacement following intracerebral hemorrhage. *Brain Sci. Adv.* 7, 184–198. doi:10.26599/bsa.2021.9050009

Fernandes, G. S., Singh, R. D., and Kim, K. K. (2022). Generation of a pure culture of neuron-like cells with a glutamatergic phenotype from mouse astrocytes. *Biomedicines* 10, 928. doi:10.3390/biomedicines10040928

Fujii, Y., Arima, M., Murakami, Y., and Sonoda, K. H. (2023). Rhodopsin-positive cell production by intravitreal injection of small molecule compounds in mouse models of retinal degeneration. *PLoS One* 18, e0282174. doi:10.1371/journal.pone.0282174

Gascón, S., Murenu, E., Masserdotti, G., Ortega, F., Russo, G. L., Petrik, D., et al. (2016). Identification and successful negotiation of a metabolic checkpoint in direct neuronal reprogramming. *Cell. Stem Cell.* 18, 396–409. doi:10.1016/j.stem.2015.12.003

Gu, Y.-N., Lee, E.-S., and Jeon, C.-J. (2016). Types and density of calbindin D28k-immunoreactive ganglion cells in mouse retina. *Exp. Eye Res.* 145, 327–336. doi:10.1016/j.exer.2016.02.001

Hicks, D., and Courtois, Y. (1990). The growth and behaviour of rat retinal miiller cells *in vitro* 1. An improved method for isolation and culture.

Hoang, T., Kim, D. W., Appel, H., Pannullo, N. A., Leavey, P., Ozawa, M., et al. (2022). Genetic loss of function of Ptbp1 does not induce glia-to-neuron conversion in retina. *Cell. Rep.* 39, 110849. doi:10.1016/j.celrep.2022.110849

Joly, S., Pernet, V., Samardzija, M., and Grimm, C. (2011). Pax6-positive müller glia cells express cell cycle markers but do not proliferate after photoreceptor injury in the mouse retina. *Glia* 59, 1033–1046. doi:10.1002/glia.21174

Jorstad, N. L., Wilken, M. S., Grimes, W. N., Wohl, S. G., Vandenbosch, L. S., Yoshimatsu, T., et al. (2017). Stimulation of functional neuronal regeneration from Müller glia in adult mice. *Nature* 548, 103–107. doi:10.1038/nature23283

Kato, M., Sudou, N., Nomura-Komoike, K., Iida, T., and Fujieda, H. (2022). Age- and cell cycle-related expression patterns of transcription factors and cell cycle regulators in Müller glia. *Sci. Rep.* 12, 19584. doi:10.1038/s41598-022-23855-w

Kaur, G., and Singh, N. (2023). Inflammation and retinal degenerative diseases. *Neural Regen. Res.* 18, 513–518. doi:10.4103/1673-5374.350192

Kittipassorn, T., Haydinger, C. D., Wood, J. P. M., Mammone, T., Casson, R. J., and Peet, D. J. (2019). Characterization of the novel spontaneously immortalized rat Müller cell line SIRMu-1. *Exp. Eye Res.* 181, 127–135. doi:10.1016/j.exer.2019.01.013

Lawrence, J. M., Singhal, S., Bhatia, B., Keegan, D. J., Reh, T. A., Luthert, P. J., et al. (2007). MIO-M1 cells and similar muller glial cell lines derived from adult human retina exhibit neural stem cell characteristics. *Stem Cells* 25, 2033–2043. doi:10.1634/stemcells.2006-0724

Li, X., Zuo, X., Jing, J., Ma, Y., Wang, J., Liu, D., et al. (2015). Small-molecule-Driven direct reprogramming of mouse fibroblasts into functional neurons. *Cell. Stem Cell.* 17, 195–203. doi:10.1016/j.stem.2015.06.003

Limb, G. A., Salt, T. E., Munro, P. M. G., Moss, S. E., and Khaw, P. T. (2002). *In vitro* characterization of a spontaneously immortalized human müller cell line (MIO-M1). *Invest. Ophthalmol. Vis. Sci.* 43, 864–869.

Liu, X., Tang, L., and Liu, Y. (2017). Mouse müller cell isolation and culture. *Bio Protoc.* 7, e2429. doi:10.21769/bioprotoc.2429

Ma, Y., Xie, H., Du, X., Wang, L., Jin, X., Zhang, Q., et al. (2021). *In vivo* chemical reprogramming of astrocytes into neurons. *Cell. Discov.* 7, 12. doi:10.1038/s41421-021-00243-8

Mcgillem, G. S., Guidry, C., and Dacheux, R. F. (1998). Antigenic changes of rabbit retinal miiller cells in culture.

Otteson, D. C., and Joseph Phillips, M. (2010). A conditional immortalized mouse muller glial cell line expressing glial and retinal stem cell genes. *Invest. Ophthalmol. Vis. Sci.* 51, 5991–6000. doi:10.1167/iovs.10-5395

Pereiro, X., Beriain, S., Rodriguez, L., Roiz-Valle, D., Ruzafa, N., and Vecino, E. (2022). Characteristics of whale müller glia in primary and immortalized cultures. *Front. Neurosci.* 16, 854278. doi:10.3389/fnins.2022.854278

Pereiro, X., Miltner, A. M., La Torre, A., and Vecino, E. (2020a). Effects of adult müller cells and their conditioned media on the survival of stem cell-derived retinal ganglion cells. *Cells* 9, 1759. doi:10.3390/cells9081759

Pereiro, X., Ruzafa, N., Acera, A., Urcola, A., and Vecino, E. (2020b). Optimization of a method to isolate and culture adult porcine, rats and mice müller glia in order to study retinal diseases. *Front. Cell. Neurosci.* 14, 7. doi:10.3389/fncel.2020.00007

Poché, R. A., Kwan, K. M., Raven, M. A., Furuta, Y., Reese, B. E., and Behringer, R. R. (2007). Lim1 is essential for the correct laminar positioning of retinal horizontal cells. *J. Neurosci.* 27, 14099–14107. doi:10.1523/JNEUROSCI.4046-07.2007

Sarthy, V. P., Brodjian, S. J., Dutt, K., Kennedy, B. N., French, R. P., and Crabb, J. W. (1998). Establishment and characterization of a retinal muller cell line.

Suga, A., Sadamoto, K., Fujii, M., Mandai, M., and Takahashi, M. (2014). Proliferation potential of Müller glia after retinal damage varies between mouse strains. *PLoS One* 9, e94556. doi:10.1371/journal.pone.0094556

Todd, L., Hooper, M. J., Haugan, A. K., Finkbeiner, C., Jorstad, N., Radulovich, N., et al. (2021). Efficient stimulation of retinal regeneration from Müller glia in adult mice using combinations of proneural bHLH transcription factors. *Cell. Rep.* 37, 109857. doi:10.1016/j.celrep.2021.109857

Todd, L., Jenkins, W., Finkbeiner, C., Hooper, M. J., Donaldson, P. C., Pavlou, M., et al. (2022). D E V E LO P M E N TA L B I O LO G Y Reprogramming Mu¨ ller glia to regenerate ganglion-like cells in adult mouse retina with developmental transcription factors. Available online at: https://www.science.org.

Tomi, M., Funaki, T., Abukawa, H., Katayama, K., Kondo, T., Ohtsuki, S., et al. (2003). Expression and regulation of L-cystine transporter, system X c-in the newly developed rat retinal Müller cell line (TR-MUL). *Glia* 43, 208–217. doi:10.1002/glia.10253

Tworig, J. M., and Feller, M. B. (2022). Müller glia in retinal development: from specification to circuit integration. *Front. Neural Circuits* 15, 815923. doi:10.3389/fncir.2021.815923

Wang, H., Yang, Y., Liu, J., and Qian, L. (2021). Direct cell reprogramming: approaches, mechanisms and progress. *Nat. Rev. Mol. Cell. Biol.* 22, 410–424. doi:10.1038/s41580-021-00335-z

Xia, X., Teotia, P., Patel, H., Van Hook, M. J., and Ahmad, I. (2021). Chemical induction of neurogenic properties in mammalian Müller glia. *Stem Cells* 39, 1081–1090. doi:10.1002/stem.3370

Xie, Y., and Chen, B. (2022). Critical examination of müller glia-derived *in vivo* neurogenesis in the mouse retina. *Front. Cell. Dev. Biol.* 10, 830382. doi:10.3389/fcell.2022.830382

Xie, Y., Zhou, J., and Chen, B. (2022). Critical examination of Ptbp1-mediated glia-to-neuron conversion in the mouse retina. *Cell. Rep.* 39, 110960. doi:10.1016/j.celrep.2022.110960

Xu, D., Zhong, L.-T., Cheng, H.-Y., Wang, Z.-Q., Chen, X.-M., Feng, A.-Y., et al. (2023). Overexpressing NeuroD1 reprograms Müller cells into various types of retinal neurons. *Neural Regen. Res.* 18, 1124–1131. doi:10.4103/1673-5374.355818

Xue, L. P., Lu, J., Cao, Q., Hu, S., Ding, P., and Ling, E. A. (2006a). Müller glial cells express nestin coupled with glial fibrillary acidic protein in experimentally induced glaucoma in the rat retina. *Neuroscience* 139, 723–732. doi:10.1016/j.neuroscience.2005.12.032

Xue, L. P., Lu, J., Cao, Q., Kaur, C., and Ling, E. A. (2006b). Nestin expression in Müller glial cells in postnatal rat retina and its upregulation following optic nerve transection. *Neuroscience* 143, 117–127. doi:10.1016/j.neuroscience.2006.07.044

Yang, P., Cao, Q., Liu, Y., Wang, K. W., and Zhu, W. (2022). Small-molecule-driven direct reprogramming of Müller cells into bipolar-like cells. *Cell. Prolif.* 55, e13184. doi:10.1111/cpr.13184

Yang, Y., Chen, R., Wu, X., Zhao, Y., Fan, Y., Xiao, Z., et al. (2019). Rapid and efficient conversion of human fibroblasts into functional neurons by small molecules. *Stem Cell. Rep.* 13, 862–876. doi:10.1016/j.stemcr.2019.09.007

Yao, K., Qiu, S., Wang, Y. V., Park, S. J. H., Mohns, E. J., Mehta, B., et al. (2018). Restoration of vision after *de novo* genesis of rod photoreceptors in mammalian retinas. *Nature* 560, 484–488. doi:10.1038/s41586-018-0425-3

Zhou, H., Su, J., Hu, X., Zhou, C., Li, H., Chen, Z., et al. (2020). Glia-to-Neuron conversion by CRISPR-CasRx alleviates symptoms of neurological disease in mice. *Cell.* 181, 590–603.e16. doi:10.1016/j.cell.2020.03.024

frontiers | Frontiers in Cell and Developmental Biology

TYPE Brief Research Report
PUBLISHED 21 May 2025
DOI 10.3389/fcell.2025.1569187

OPEN ACCESS

EDITED BY
Yu Liu,
University of Houston, United States

REVIEWED BY
Takahiro Kunisada,
Gifu University, Japan
Angelo Canciello,
University of Teramo, Italy

*CORRESPONDENCE
Elena Gonzalez-Muñoz,
egonmu@uma.es

RECEIVED 31 January 2025
ACCEPTED 02 May 2025
PUBLISHED 21 May 2025

CITATION
Dučić T, Rodriguez-Yañez F and Gonzalez-Muñoz E (2025) Synchrotron radiation FTIR microspectroscopy enables measuring dynamic cell identity patterning during human 3D differentiation.
Front. Cell Dev. Biol. 13:1569187.
doi: 10.3389/fcell.2025.1569187

Synchrotron radiation FTIR microspectroscopy enables measuring dynamic cell identity patterning during human 3D differentiation

Tanja Dučić[1], Francisco Rodriguez-Yañez[2] and Elena Gonzalez-Muñoz[2,3]*

[1]ALBA Synchrotron Light Source, Barcelona, Spain, [2]Instituto de Investigacion Biomedica de Malaga y Plataforma en Nanomedicina-IBIMA Plataforma BIONAND, Malaga, Spain, [3]Department of Cell Biology, Genetics and Physiology, Universidad de Malaga, Malaga, Spain

Human cell fate specification, particularly in neural development, is difficult to study due to limited access to embryonic tissues and differences from animal models. Human induced pluripotent stem cells (hiPSCs) and 3D organoid models enable the study of early human neural development, surpassing limitations of 2D cultures by incorporating crucial cell-cell and cell-matrix interactions. In this study, we used synchrotron radiation-based Fourier transform infrared (SR-FTIR) microspectroscopy to examine biomolecular profiles of 3D-differentiated organoids, specifically embryoid bodies (EBs) and neural spheroids (NS), derived from hiPSCs. SR-FTIR allowed us to analyze these organoids' cellular identity at a biomolecular level, offering a holistic view that complements specific cell markers. Our findings reveal distinct biomolecular identities in 3D organoids, with differences in DNA structure, lipid saturation, phospholipid composition, and protein conformations. This approach highlights that cellular identity is shaped by more than gene expression alone; it involves unique biomolecular compositions that can be detected even in complex, multicellular environments. By demonstrating the role of molecular configuration in cell differentiation, our findings suggest that differentiation processes extend beyond genetics, involving interdependent biochemical signals. This study demonstrates the unique efficacy SR-FTIR in analyzing human-specific 3D models for investigating complex multicellular differentiation mechanisms, offering new avenues for understanding the biochemical basis of human development and disease.

KEYWORDS

SR-FTIR, biomolecular conformation, IPSC, 3D embryoid bodies, neural spheroids, human morphogenesis, cell identity

1 Introduction

The variety of mechanisms involved in human development during early cell fate specification has only recently begun to be elucidated due the relative inaccessibility of human embryo tissues and biological differences with animal models. This is

specially challenging in brain development that requires an elaborate succession of cellular events that, when disrupted, can lead to neuropsychiatric disease which present great difficulty in studying and understanding their origin and possible therapeutic alternatives.

Neural specification of human induced pluripotent stem cells (hiPSCs), offers unprecedented opportunities for studying human neural development (Avior et al., 2016). The recent development of 3D neural cultures derived from hiPSCs offers a promising approach to understanding human brain development and disease (Pasca, 2018), surpassing the lack of cell-cell/cell-matrix interactions in monolayer cultures.

Our understanding has improved recently thanks to techniques allowing single-cell resolution in studying cell states (Hagey et al., 2016). Nevertheless, cell commitment during development has mainly been investigated in isolation at the population level by analyzing the effects of individual factors or, when using non-targeted approaches, the analysis is focused on cell expression profiles based on specific gene or protein identity markers (Jovic et al., 2022). This approach is not ideal due to the interdependent nature of the processes and the significant cellular transformations involved.

Although the use of cell identity markers is very useful and allows the analysis of specific cell populations, their use is not free of controversy regarding their fidelity or causality in determining cell identity, and it is becoming increasingly necessary to understand cellular transformation as a whole in order to achieve a deep understanding of the specification process during development and the factors that constitute the identity of a cell (McKinley et al., 2020).

Fourier transform infrared (FTIR) microspectroscopy is a highly effective analytical method used to examine various cellular components, including polysaccharides, nucleic acids, proteins, and lipids at the subcellular level. It leverages the natural ability of molecular systems to vibrate in resonance with different infrared light frequencies, creating unique spectra for each component (Miller and Dumas, 2010). Synchrotron radiation (SR)-FTIR microspectroscopy offers exceptional spectral resolution at the single-cell level, enabling the detailed analysis of cellular diversity within complex systems. Its micrometer-scale resolution, allows for monitoring the overall biochemical makeup of bulk samples (spanning tens of cubic microns). This method can detect subtle shifts in the composition of biological macromolecules, making it a valuable tool across various biological research fields for studying changes in chemical structure and conformation (Dumas, 2020).

The high spectral clarity and stable, fast measurements provided by synchrotron source FTIR (SR-FTIR) make it ideal for accurately resolving organic compounds, especially when compared to conventional globar sources. SR-FTIR spectroscopy provides approximately 1000 times the brightness of standard sources, enhancing the signal-to-noise ratio and enabling rapid acquisition of thousands of spectra over large sample areas with high peak precision (Baker et al., 2014). Additionally, SR-FTIR combines the high spatial resolution required to reach diffraction limits with excellent spectral detail, linking specific chemical groups to their vibrational peaks in IR spectra—thus aiding in the study of chemical properties in biological molecules and complexes.

Mid-infrared (IR) spectroscopy offers high sensitivity for analyzing the structure and conformation of proteins, lipids status, and nucleic acids, as well as complex biological substances like body fluids, cell cultures and tissues, often used in biomarker research (reviewed in (Dumas, 2020; Malek and Bambery, 2014; Finlayson et al., 2019)). Infrared spectroscopy is a crucial tool in "functional biology," revealing extensive information from FTIR spectra, such as protein secondary structures through Amide I (1,600–1,700 cm^{-1}) and Amide II (1,500–1,060 cm^{-1}) bands, which reflect peptide backbone vibrations. These bands are sensitive to structural differences in proteins, such as α-helices, β-sheets, turns, and random coils, as influenced by hydrogen bonding environments. Beyond conformational analysis of proteins, FTIR provides detailed biochemical insights into samples, with prominent absorption patterns from lipids (2,800–3,020 cm^{-1}), carbonyl (C=O) groups in lipids and proteins (1,480–1,780 cm^{-1}), and nucleic acids (900–1,480 cm^{-1}), which involve PO_2^- stretching vibrations.

FTIR spectroscopy has broad applications beyond biological research and diagnostics, including material science, extreme environmental studies, archaeology, and planetary sciences. It is also pivotal in forensic science, as the biochemical makeup of fingerprints provides essential evidence. As a non-destructive technique sensitive to biomolecular conformational changes, FTIR microspectroscopy has been used to study mouse and rat healthy or injured brain tissue and there is still a limited number of studies using human brain tissue that confirm the capacity of this technology to be used as a potential diagnostic tool for disease mainly focused in brain tumors (Boseley et al., 2024; Liao et al., 2013; Steiner et al., 2023). However, one limitation in advancing neuroscience research lies, on one hand, in the relative difficulty of accessing human neural tissue samples, especially from pathologies where surgical interventions are highly unlikely, and on the other, in the challenge of tracking early stages of diseases or understanding the developmental characteristics of the nervous system itself. To address this issue, differentiated cell models derived from induced pluripotent stem cells provide a valuable alternative to animal models, allowing for the study of unique human-specific traits. The application of FTIR microspectroscopy in studying cell models derived from pluripotent cells remains limited and has largely focused on homotypic differentiations in 2D cultures (Ami et al., 2008; Heraud et al., 2010; Cao et al., 2014). Expanding its use to more complex systems, such as 3D cultures or *in vivo* models, could provide deeper insights into cellular differentiation and the dynamic biochemical changes that occur during development. While few research has explored its use in analyzing 3D structures, this has mainly focused on tumor organoids (Sun et al., 2024; Shao et al., 2024), with little information available regarding its use in understanding complex 3D multicellular differentiation. Such studies will not only enhance our understanding of the molecular features of this intricate process but also help identify potential abnormalities associated with these tissues.

In this study, we utilized both spontaneous and directed 3D differentiation of iPS cells: spontaneous differentiation to generate embryoid bodies (EBs) containing cell derivatives from the three germ layers, and directed differentiation formed neural spheroids with characteristic glial and neuronal profiles. We applied SR-FTIR technology to analyze cellular identity in terms of the

composition and conformation of key/fundamental biomolecules, providing a holistic perspective that complements specific cell-type markers. Our findings reveal that 3D organoids exhibit notable differences in their biomolecular profiles, and conformational changes reflect a distinct macromolecular identity, including unique characteristics in DNA backbone structure, phospholipid abundance, lipid unsaturation levels, and predominant protein structures.

2 Methods

2.1 Cell culture and 3D spheres generation

We used previously generated iPS cell lines from female donors (3 cell lines) with clearances from the bioethical committee and Review Board of the Spanish National Research Ethics Service (#PR-03-2018). They were cultured in hES medium on mitomycin-C-treated mouse fibroblasts as previously described (Gonzalez-Munoz et al., 2014; Lopez-Caraballo et al., 2020a; Lopez-Caraballo et al., 2020b). For 3D neural spheroid (NS) generation we used already published protocol (Marton et al., 2019) with some modifications. iPSCs were dissociated and plated in low-attachment 96-well U-bottom plates in mTeSR1 medium with ROCK inhibitor Y-27632. Spheroids were differentiated into neuroectodermal lineage using SMAD inhibitors (and maintained in differentiation medium supplemented with growth factors (EGF, bFGF) and SHH agonist. From day 25, NS were cultured with T3, biotin and neurotrophic factors (NT-3, BDNF), to promote maturation. For embryoid body (EB) formation, iPSCs were aggregated in AggreWell-800^{TM} and cultured in hES medium without bFGF as previously described (Gonzalez-Munoz et al., 2014; Lopez-Caraballo et al., 2020a).

At day 40, three dimensional NS and EB were either used for RNA isolation or fixed using 4% paraformaldehyde incubation for 20 min at 25°C. Data correspond to the average of 3 independent differentiation experiments done in triplicate (EB) or quadruplicate (NS) from three different iPSC clones (n = 9 for EB and n = 12 for NS).

2.2 Immunofluorescence

NS and EB were fixed in 4% paraformaldehyde, cryoprotected in 30% sucrose, and embedded in OCT compound. Cryosections were blocked and incubated with primary and secondary antibodies, counterstained with Hoechst 33258, and imaged using a Leica SP5 II confocal system. Fluorescence intensity was quantified using Fiji software (Shihan et al., 2021; Schindelin et al., 2012).

2.3 Quantitative PCR

RNA was isolated using the NucleoSpin RNA Mini kit, and cDNA was synthesized using SuperScript II SuperMix. qPCR was performed with SYBR Green on a CFX96 Real-Time System, using actin, gapdh, and tbp as reference genes (Supplementary Table S4).

2.4 SR-FTIR measurements and analysis

Samples were analyzed at the MIRAS beamline (ALBA Synchrotron) using a Hyperion 3,000 microscope. Spectra were collected in transmission mode (10 μm × 10 μm aperture) across the 4,000–900 cm^{-1} range. Principal component analysis (PCA) was performed using Orange software (Demšar et al., 2013; Toplak et al., 2017; Toplak et al., 2021).

3 Results

3.1 Three-dimensional organoids derived from the spontaneous and directed differentiation of induced pluripotent stem cells (iPSCs) exhibit characteristic molecular markers of specific trilineage and neural differentiation

Embryoid bodies (EBs) were generated as 3D trilineage differentiation organoids by allowing iPSCs to spontaneously differentiate in suspension cultures without growth factors, promoting simultaneous and spontaneous differentiation into cell types representing the three germ layers: endoderm, mesoderm, and ectoderm. Neural spheroids (NS) were produced through a modified protocol (Marton et al., 2019) that included inhibiting the SHH signaling pathway after neuronal induction. This approach activates oligodendrogenesis, generating therefore the three main neural cell types of the central nervous system—neurons, astrocytes, and oligodendrocytes—that co-develop both spatially and temporally, mirroring endogenous cellular diversity.

After 6 weeks, RNA from NS and EBs was extracted for quantitative PCR analysis targeting cell-type markers: *AFP* and *GATA4* for endoderm, *BRACHYURY* and *RUNX1* for mesoderm, and for ectoderm and neural differentiation, *NCAM* for neurons, *GFAP* for astrocytes, and *OLIG1* and *OLIG2* for oligodendrocytes (Figure 1A). Additionally, NS and EBs were fixed, cryosectioned, and immunostained to detect proteins associated with specific cell identities, including MYF5 for mesoderm, GATA4 and AFP for endoderm, NG2 and OLIG2 for oligodendrocyte progenitors, MBP for oligodendrocytes, GFAP for astrocytes, and MAP2, DCX, TUJ1, NESTIN, and MECP2 for neuronal progenitors and early neurons (Figure 1B).

Quantitative PCR and immunofluorescence data, supported by fluorescence intensity quantification (Figure 1C), reveal significant differential marker expression aligned with trilineage identities in EBs and neural cell types in NS. These data confirm the reliability of the 3D model in accurately reflecting the distinctive co-differentiation processes.

10.3389/fcell.2025.1569187

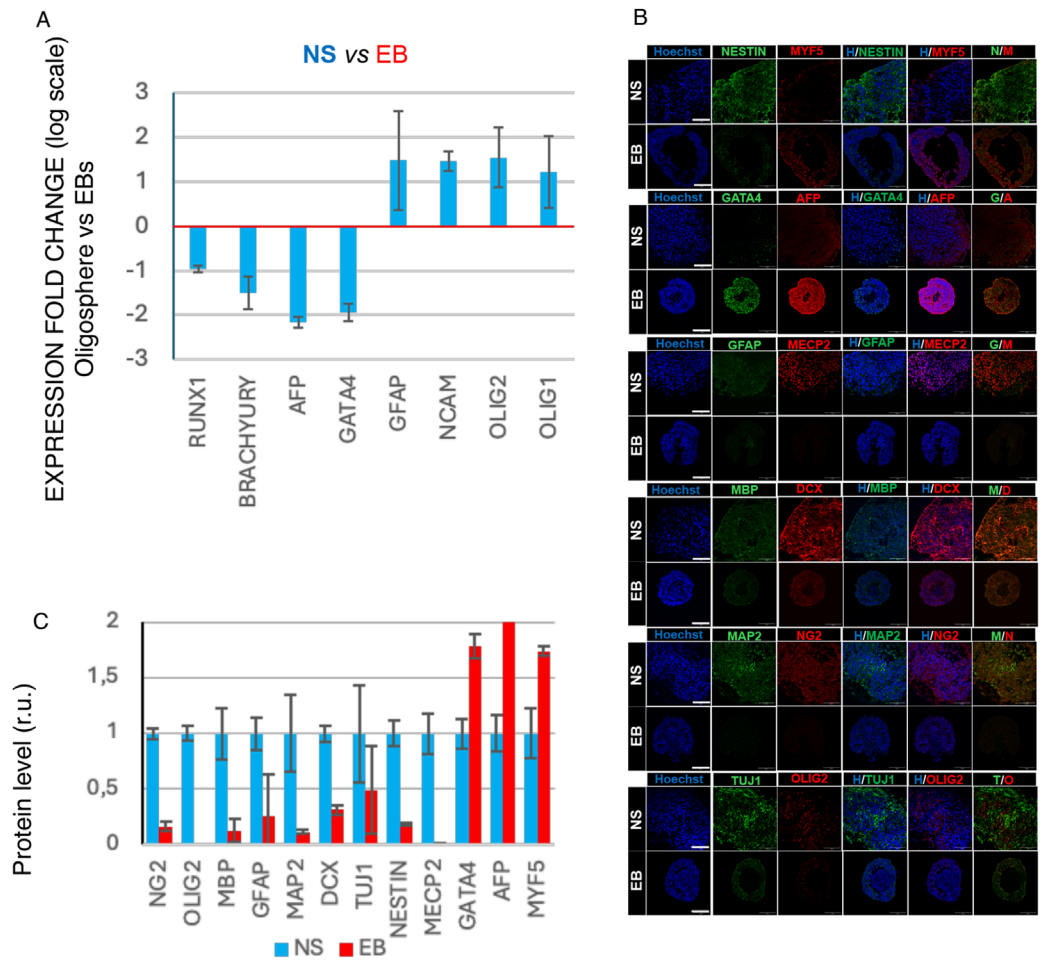

FIGURE 1
Cell marker characterization of NS and EB 3D organoids differentiated from human iPSC lines. **(A)** qRT-PCR data showing regulation of differentiation markers *GATA4* and *AFP* (endoderm), BRACHYURY and *RUNX1* (Mesoderm), and for ectoderm and neural differentiation, *NCAM* for neurons, *GFAP* for astrocytes, and *OLIG1* and *OLIG2* for oligodendrocytes at day 40 of either *in vitro* differentiation. Average folding change expression values ± STD (relative to spontaneous differentiated EB) are represented (logarithmic scale). **(B)** Representative immunofluorescence analysis image of markers of mesoderm (MYF5), GATA4 and AFP for endoderm, NG2 and OLIG2 for oligodendrocyte progenitors, MBP for oligodendrocytes, GFAP for astrocytes, and MAP2, DCX, TUJ1, NESTIN, and MECP2 for neuronal progenitors and early neurons (scale bar 100 μm). **(C)** Protein level quantification based on relative fluorescence intensity.

3.2 SR-FTIR spectroscopy enables the identification of complex differentiated 3D structures based on characteristic biomolecular profiles that reflect their interconnected cellular identities

EBs and NS cryosections were analyzed using SR FTIR microspectroscopy, revealing primary absorption features of key biomolecules: proteins (Amide I and II: 1,480–1,700 cm^{-1}), lipids (2,800–3,000 cm^{-1}) carbonyl (C=O) groups, and nucleic acids and sugars that predominantly absorb between 1,000 and 1,500 cm^{-1} (Dumas, 2020) (Supplementary Figure S1). In Figure 2, the second-derivative spectra show the lipid region (A), Amides I and II and carboxyl group (B), and nucleic acids (C), highlighting distinctive spectral variations between EB and NS samples across all regions (Figures 2A–C), confirmed by PCA grouping of these sample types (Figures 2D–F; Supplementary Table S2).

In the lipid region, the differences are evident in bands at ~2,850, ~2,874, ~2,925, and ~2,960 cm^{-1}, corresponding to $\nu_s CH_2$, $\nu_s CH_3$, $\nu_{as} CH_2$ and $\nu_{as} CH_3$ respectively (Loutherback et al., 2016), along with the ~3,010 cm^{-1} peak ($\nu(H{-}C$ =), indicating fatty acid unsaturation (Figure 2A; Supplementary Table S1). The PCA analysis further substantiates these distinctions, as these bands significantly contribute to the separation of the EB and NS groups (Figures 2D,G; Supplementary Table S2). For the protein/ester region, variations primarily involve the Amide I and II band positions (Figure 2B; Supplementary Table S1), where PCA loadings indicate shifts in secondary protein structures, notably around ~1,620, ~1,650, and ~1,680 cm^{-1}, representing intramolecular β-sheet, α-helix, and turn and loops structures, respectively, alongside the ~1,740 cm^{-1} carbonyl peak from phospholipid acyl chains or carbonylated proteins (Loutherback et al., 2016) (Figures 2E,H; Supplementary Table S2). Within Amide II, differences emerge at ~1,545 to 1,555 cm^{-1} for α-helix and random

10.3389/fcell.2025.1569187

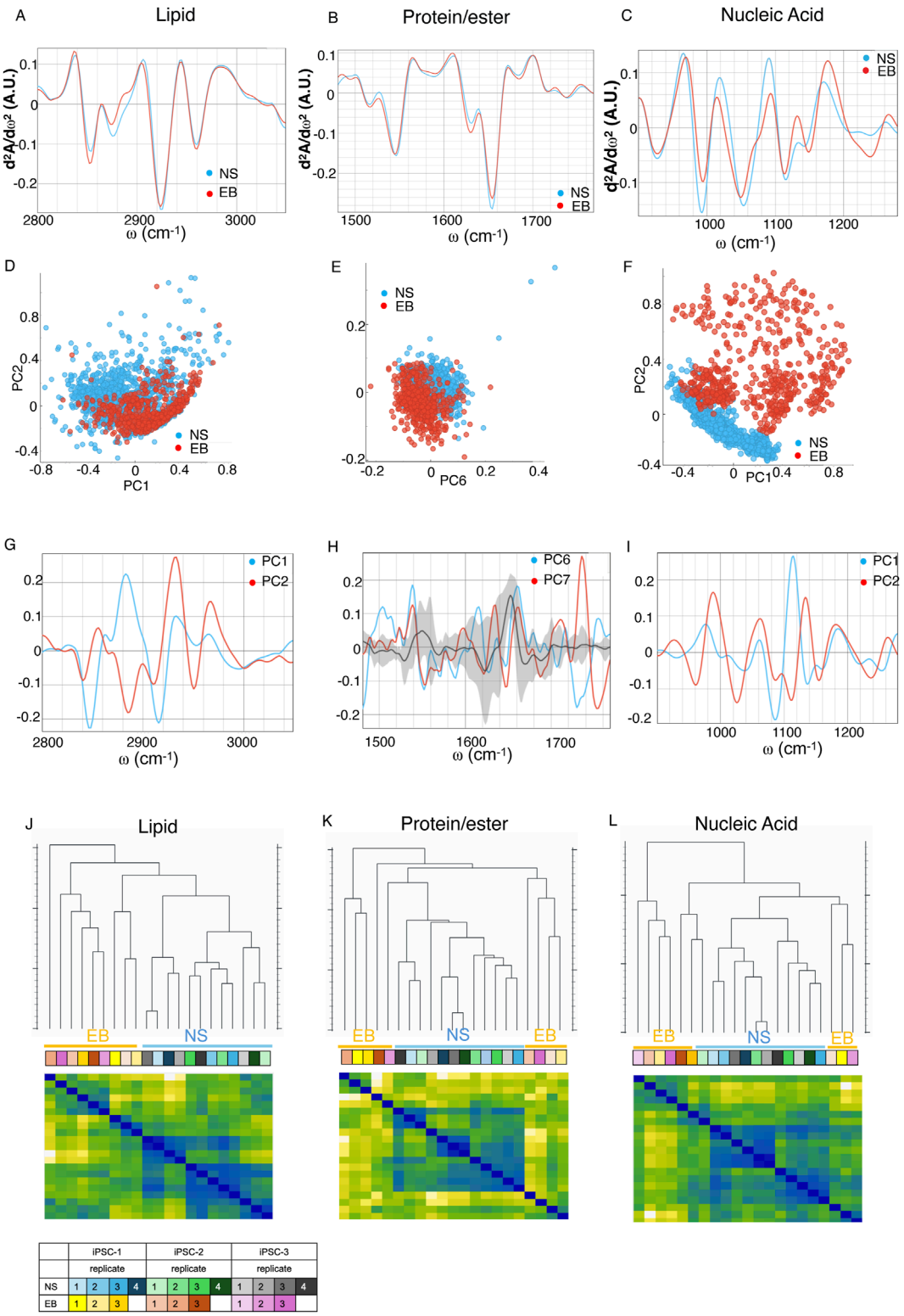

FIGURE 2
Second derivative of the FTIR averaged spectra of fixed neural spheroids (NS) (blue) and trilineage (EB) (red) differentiated iPSC in the **(A)** lipids' spectral region of 3,020–2,800 cm^{-1}, **(B)** proteins and carbonyl area, 1,800–1,480 cm^{-1}, and **(C)** the nucleic acids region, 1,200–900 cm^{-1}. Graphs in **(D,F,H)** represent the PCA analysis and values of the PC scores for each region assigned above; graphs **(E,G,I)** show the contribution of individual absorbance to the PCAs (loading values) of the specified principal components in blue and red. Black line and grey shadow represents the average and SD contribution of all principal components explaining 80% of the variance. **(J–L)** Hierarchical clustering (top dendrograms) and leveraged heatmaps (bottom matrices) of NS and EB organoids, based on the average FTIR absorption spectra of each biological replicate. Clustering was performed using Euclidean distances calculated across three distinct spectral regions: lipid-associated bands **(J)**, protein and carbonyl-associated bands **(K)**, and nucleic

(*Continued*)

FIGURE 2 (Continued)
acid-associated bands **(L)**. In the heatmaps, warmer colors indicate greater similarity (lower distance) between replicates, while cooler colors indicate greater dissimilarity. This visualization allows grouping of biologically related samples based on their biochemical spectral profiles. The color-coded table indicates the identity and grouping of the biological replicates. Data represent independent differentiation experiments performed in triplicate for EBs and quadruplicate for NSs, derived from three different iPSC clones (n = 9 for EB and n = 12 for NS).

coil structures (Malek and Bambery, 2014; Dučić et al., 2022) and at intramolecular β-sheet structure peak near ~1,570 cm^{-1} (Figure 2B; Supplementary Table S2).

In the nucleic acid and carbohydrate absorbtion region (1,200–900 cm^{-1}), multiple bands show differences (Figure 2C; Supplementary Table S1). PCA indicates distinct vibrational band contributions at ~975, ~1,027, ~1,060 cm^{-1}, corresponding to DNA, Z-form DNA, with the latter particularly enhanced in Z-form DNA (Zhang et al., 2016). Shifts at ~1,110–1,115 cm^{-1} and ~1,130–1,135 cm^{-1} relate to DNA methylation (Li et al., 2018) and RNA (Gioacchini et al., 2014), respectively (Figures 2F,I; Supplementary Table S2), suggesting notable DNA reorganization and epigenetic variation based on organoid type (Knaupp et al., 2017; Li et al., 2021).

Euclidean distances were calculated for each spectral region's averages to create a hierarchical clustering of the different samples (Figures 2J–L), that derived from distinct experimental replicates from three different iPSCs to ensure robustness and reproducibility of the results. We found differential segregation of samples within each spectral region according to their differentiation group, confirming that the molecular configuration profile based on their spectral features varies and is therefore definitive of cellular identity within the organoids.

These differences were supported by the analysis of the integral area of the specific peaks, indicative of abundance of specific biomolecule and conformation (shown in Figure 3; Supplementary Table S2). For DNA backbone conformation, peak areas around ~990 and ~1,060 cm^{-1}, associated with DNA-backbone and Z-form DNA that has been associated with histone acetylation and epigenetic modifications (Zhang et al., 2016; Gioacchini et al., 2014; Beknazarov et al., 2020), were statistically higher in the NS group, while ~1,150 and ~1,250 cm^{-1} peaks, indicative of different C-O bound carbohydrates (glycogen) (Malek and Bambery, 2014; Heraud et al., 2010) content and RNA/DNA structures respectively (Martinez-Rovira et al., 2020), were more prominent in EB organoids. Although most molecular events during cell specification have traditionally been studied in the context of specific transcriptional regulator activity, the epigenetic roles associated with nucleic acid conformational changes and molecular bonding remain underexplored. Z-DNA has gained attention for its potential role in transcriptional regulation; it is thought to form in the promoter region within open chromatin, induced by chromatin remodeling factors, and to stabilize this open structure through binding with proteins such as ADAR1 or Nrf2, thereby facilitating downstream transcriptional events (Liu et al., 2001; Maruyama et al., 2013). The distinct DNA conformations observed between EB and NS organoids suggest a potential relationship between these conformational changes and the involvement of specific proteins, either as causative factors or as a consequence of these changes. This includes the possible roles of histone acetyltransferases and Z-DNA binding proteins, such as mentioned ADAR1, Nrf2, or DLM-1 (Kim et al., 2018) for cell fate decisions. While the identification of Z-DNA is based on previously reported vibrational signatures in the ~1,060 cm^{-1} region, we acknowledge that this remains a putative spectral assignment. Nonetheless, experimental studies using isotopically labeled oligonucleotides and induced B-to-Z transitions have provided direct evidence linking these IR bands to the Z-DNA conformation (Banyay et al., 2003; Duan et al., 2023). *In vivo* formation of Z-DNA under histone acetilation conditions (Zhang et al., 2016) or after histone remodeling complex overexpression (Li et al., 2020), further supports its functional relevance. However, complementary structural approaches such as NMR or crystallography would be required to definitively confirm its presence in our system.

Additionally, the ~1,070 cm^{-1} peak area, representing –CO–O–C stretching in cholesterol esters and phospholipids, was elevated in EBs *versus* NS (Supplementary Figure S1G).

In the protein region, significant differences were found in Amide I and II integral areas (Supplementary Table S2), indicating changes in protein quantity, structure, or function. Protein conformation variations were also observed in peak areas near ~1,650 cm^{-1}, ~1,645 cm^{-1}, and ~1,635 cm^{-1}, attributed to α-helix, random coil, and β-sheet structures, respectively (Pezolet et al., 1992; Wellner et al., 1996; Sarroukh et al., 2011; Bhatia et al., 2015; SAJ and Joye, 2020) (Figures 3C,D; Supplementary Table S2). Notably, NS samples exhibited a higher presence of α-helix structures, while EBs had more β-sheet structures. The β-sheet/α-helix ratio is linked to proteins' responses to mechanical stimuli (Rustem et al., 2012), presenting a potential avenue for examining the connection between mechanical influences, recently described as regulators of morphogenetic events (Goodwin and Nelson, 2021), and the underlying molecular mechanisms that involve changes in the composition and conformation of biomolecules involved in this regulation.

Although part of this difference likely reflects the distinct proteomic profiles of each organoid type, as also indicated by marker expression patterns (Figures 1A,C), it may also result from conformational shifts driven by mechanobiological context. Mechanical forces are known to regulate protein folding and aggregation states, often without altering gene expression, by influencing the energy landscape of protein structure (Discher et al., 2009; Vining and Mooney, 2017). Thus, the β-sheet/α-helix ratio observed here may represent an integrated biochemical signature of both protein composition and mechanotransductive regulation, reinforcing the value of SR-FTIR in capturing subtle, functionally relevant structural properties in differentiating cells.

In the lipid region, a significant increase in methylene groups (both $\nu_s CH_2$ and $\nu_{as} CH_2$) was observed during trilineage development compared to neural differentiation (Figures 3G,H; Supplementary Table S2). This increase suggests longer acyl chains,

10.3389/fcell.2025.1569187

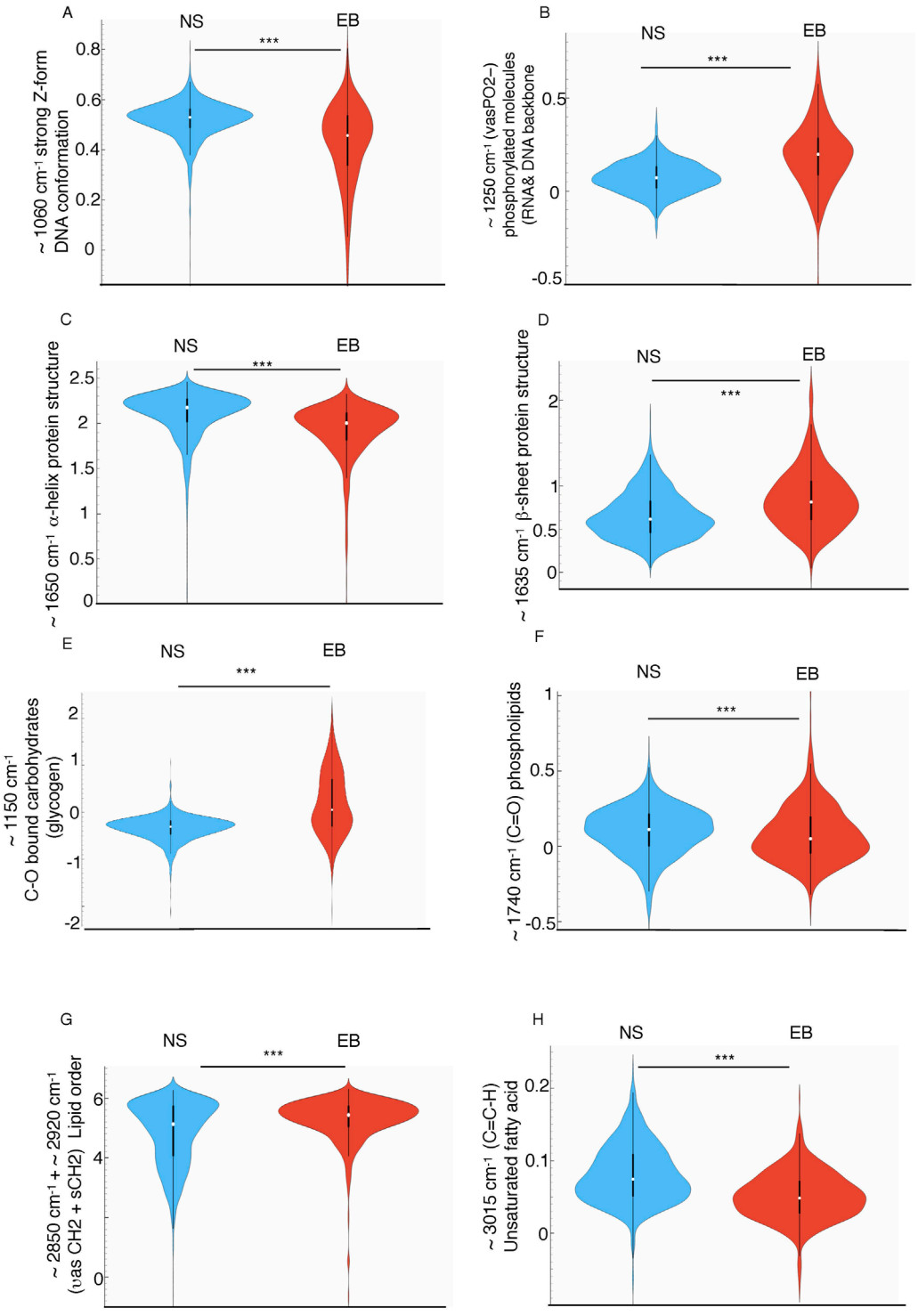

FIGURE 3
Violin plots showing the normalized mean integral area values of second derivative average spectra of NS and EB organoids at selected spectral regions: **(A)** ~1,060 cm^{-1} assigned to strongly enhanced Z-form DNA **(B)** ~1,250 cm^{-1} assigned to ($\nu asPO^{2-}$) related to DNA backbone conformation **(C)** ~1,650 cm^{-1} assigned to α-helix protein conformation, **(D)** ~1,635 cm^{-1} related to β-sheet protein conformation, **(E)** ~1,150 cm^{-1} corresponding to –CO– stretching related to glycogen, **(F)** ~1,740 cm^{-1} assigned to the ester carbonyl groups (νC = O) related to phospholipids, **(G)** (~2,850 + 2,920 cm^{-1}) sum of asymmetric and symmetric CH2 picks area related to the total amount of lipid present in the cells, **(H)** ~3,010 cm^{-1} assigned to unsaturated fatty acids. Values were calculated from unit vector-normalized spectra following baseline correction and second derivative transformation. Integration was performed using the "integral from 0" method within Orange Spectroscopy software (ANOVA test ***$p < 0.005$). The y-axis represents unitless integral area values, enabling relative comparisons across groups. These measurements reflect the abundance of specific molecular features between NS and EB populations.

impacting membrane rigidity, and an overall rise in lipid content (Malek and Bambery, 2014) within these cells as confirmed by the higher cumulative methylene and methyl peak areas in EBs (Supplementary Table S2). Additionally, the significant increase in the ~3,010 cm^{-1} peak area (Figures 3G,H; Supplementary Table S2) —associated with fatty acid unsaturation—in NS, alongside the elevated symmetric/asymmetric methylene stretching ratio ($\nu_s CH_2/\nu_{as} CH_2$) in EBs (linked to membrane rigidity) (Sandt et al., 2013), aligns with the observation of greater membrane lipid fluidity during neural differentiation compared to trilineage differentiation.

Meanwhile, other lipid structural features, such as the abundance of ester carbonyl group stretching vibrations (ν C=O), associated with membrane permeability, and the ratio of this peak to the sum of methylene and methyl band areas (ν CH_2 and ν CH_3), which has been correlated with lipid peroxidation (Dučić et al., 2019; Mendelsohn et al., 2006; Kreuzer et al., 2020), remain similar across both trilineage and neural differentiation. These findings indicate that lipid composition and structural variations are not generalized but rather specifically targeted to certain aspects, such as membrane fluidity. These distinctions suggest that particular structural and functional adaptations in lipid membranes may underpin mechanisms or functional outcomes tied to the complex multicellular differentiation processes.

4 Discussion

Growing evidence implicates metabolic pathways as central regulators of cell fate and function, suggesting that these pathways not only supply energy for cellular activities but also shape and define cellular identity (Ghosh-Choudhary et al., 2020), influencing the epigenetic regulation of gene expression (Tatapudy et al., 2017). For instance, nicotinamide N-methyltransferase (NNMT) is a key enzyme in metabolic regulation, essential for establishing and maintaining the histone H3 repressive mark (H3K27me3) during pluripotency (Sperber et al., 2015). NNMT is particularly abundant in adipose tissue and the liver, where its expression impacts lipid accumulation during cell differentiation processes (Komatsu et al., 2018; Xu et al., 2022), highlighting the interconnection between cell identity and biomolecular composition. In the context of neural stem cells, glucose and lipid metabolism play critical roles in processes such as proliferation, differentiation, and quiescence, with several studies emphasizing the importance of lipid accumulation in human neurogenesis (reviewed in (Angelopoulos et al., 2022)). Our data add a new perspective to this connection, highlighting the qualitative profile of these macromolecules as part of a coordinated process during multicellular co-differentiation, suggesting their active role in this process.

Our data provide highly relevant insights into early cellular development and specification, shedding light on the critical role that biomolecular composition and conformation play in determining cellular identity. The cellular macromolecular profile can be detected not only in homogeneous cell populations (Ami et al., 2008; Heraud et al., 2010; Cao et al., 2014; Dučić et al., 2019; Sandt et al., 2012; Dučić et al., 2023), but even in extremely complex cellular environments like those used here, which involve the simultaneous and cooperative emergence of various cell types. These findings suggest that differentiation and specification extend beyond a complex gene expression regulatory network; they are closely linked to the biomolecular composition and structure of cells during differentiation, which is therefore tightly related to cellular identity. While our data do not clarify the direction of causality between molecular configuration and gene expression profiles, they certainly establish a connection and add a new layer of complexity to cellular identity, simultaneously providing a novel tool for its definition. Furthermore, they allow for compelling hypotheses in which molecular composition and configuration underlie the intercellular regulation occurring during multicellular differentiation.

Differential specification regulation in interacting cells remains a key topic in human developmental biology. Most approaches have focused on the role of morphogens and transcriptional regulation via ligands and receptors, progressively contributing to the transcriptional restriction that leads to cellular identity. Recently, however, attention has shifted to how mechanical forces shape developing tissues and to the physical mechanisms of morphogenesis, leveraging biophysical measurements (Goodwin and Nelson, 2021; Mammoto et al., 2013). Developing tissues are subject to both intrinsic mechanical signals from active forces and changes in tissue mechanical properties, as well as extrinsic mechanical signals, such as constraint, compression, pressure, and shear forces.

It is essential to highlight that mechanical forces also impact another key developmental aspect—cellular differentiation. Physical forces can activate intracellular signaling cascades or modify nuclear envelope mechanics, influencing the activation or nuclear localization of mechanosensitive transcription factors, which then lead to downstream changes in gene expression, altering cell behavior and fate (Vining and Mooney, 2017; Hampoelz and Lecuit, 2011; Kumar et al., 2017). Such nuclear-level changes could indirectly impact tissue material properties, ultimately resulting in morphological changes.

While the study provides robust evidence of group-specific spectral differences supported by multivariate analyses, it is important to acknowledge certain limitations. The number of biological replicates per group is modest and may limit the generalizability of the findings. Although each replicate was independently generated and analyzed, increasing the sample size in future studies would enhance statistical power and capture broader biological variability. Additionally, our conclusions are based on exploratory, unsupervised methods (e.g., hierarchical clustering and PCA) rather than predictive modeling. While this avoids risks of overfitting, it also limits the formal assessment of classification accuracy. Future work may benefit from combining larger replicate numbers with supervised approaches to validate and extend the current findings.

Furthermore, all cell lines used in this study were derived from female donors. Although no consistent sex-dependent effects have been reported in spontaneous or directed neural differentiation under standard culture conditions, subtle sex-linked variability in gene regulation, chromatin structure, has been described (Sugathan and Waxman, 2013; Ober et al., 2008). Importantly, recent studies have shown both no significant sex-related differences in early neural induction from human pluripotent stem cells (Strano et al., 2020) or limited effect on the expression of specific genes (Pottmeier et al., 2024), indicating minimal impact on the results presented here. Nonetheless, including cell lines from both sexes in future studies would strengthen the translational robustness of spectral phenotyping approaches.

Finally, although SR-FTIR spectroscopy provides spatial resolution in the range of ~3–10 μm, enabling single-cell level analysis (Dučić et al., 2022; Dučić et al., 2023; Andjus et al., 2019; Pascolo et al., 2014; Hackett et al., 2013; Doherty et al., 2016) this resolution is approximate and may integrate signals from adjacent cells in densely packed 3D structures such as organoids or embryoid bodies. Furthermore, the use of spectral averaging across many cells, while improving the signal-to-noise ratio, may mask the presence of rare subpopulations or transitional states. Although consistent spectral segregation between groups was observed, a more detailed exploration of cellular heterogeneity would benefit from increasing sampling density or combining SR-FTIR with higher-resolution or complementary single-cell techniques (Heraud et al., 2010; Wang et al., 2021).

Our approach employs a human model based on pluripotent stem cells 3D differentiation, proving to be extremely valuable for studying specific developmental characteristics of the nervous system, often not replicated in animal models (Walsh et al., 2024; Li et al., 2023). This model also enables simultaneous and comparative analysis of different experimentally controlled differentiation patterns.

Our findings indicate that biomolecular composition and configuration are also crucial factors during early developmental stages—an aspect that remains largely unexplored. Further studies are needed to establish causal relationships between genetic developmental patterns, the influence of mechanical forces, and molecular composition and structure. While the first two are beginning to be elucidated (Vining and Mooney, 2017; Hampoelz and Lecuit, 2011; Kumar et al., 2017), the role of molecular composition and conformation in this process remains uncharted. This study, therefore, serves as evidence of its significant role in human development.

5 Conclusion

This research underscores the value of SR-FTIR microspectroscopy for high-resolution biomolecular profiling in trilineage and neural hPSC-derived organoids, providing insights into cellular identity in 3D differentiation. The distinct biochemical and structural profiles observed among organoids reveal that cellular identity extends beyond traditional gene expression markers, implicating specific biomolecular composition and conformation besides mechanical forces in cell fate decisions. The study highlights SR-FTIR as a promising tool for investigating human developmental biology and understanding potential disease mechanisms that arise from differential and potentially aberrant cellular differentiation.

Data availability statement

The original contributions presented in the study are included in the article/Supplementary Material, further inquiries can be directed to the corresponding author.

Ethics statement

The studies involving humans were approved by Comité Coordinador de Ética de la Investigación Biomédica de Andalucía (CCEIBA) Consejería de Salud (Junta de Andalucia) Spain. The studies were conducted in accordance with the local legislation and institutional requirements. The participants provided their written informed consent to participate in this study.

Author contributions

TD: Formal Analysis, Investigation, Writing – review and editing. FR-Y: Investigation, Writing – review and editing. EG-M: Conceptualization, Formal Analysis, Funding acquisition, Investigation, Supervision, Visualization, Writing – original draft, Writing – review and editing.

Funding

The author(s) declare that financial support was received for the research and/or publication of this article. EG-M acknowledge financial support from Ministerio de Ciencia e Innovación del Gobierno de España (grant number PID 2021-124033OB-I00) and from IBIMA plataforma BIONAND (grant number PlanPropio-Area8-2023).

Acknowledgments

The authors thank ALBA Synchrotron facility for beamtime allocation and financial support from the in-house Proposal Nº 2023087702 and excellent working conditions and IBIMA Plataforma BIONAND ICTS Nambiosis U28. NanoImaging Unit for microscopy support.

Conflict of interest

The authors declare that the research was conducted in the absence of any commercial or financial relationships that could be construed as a potential conflict of interest.

Generative AI statement

The author(s) declare that no Gen AI was used in the creation of this manuscript.

Publisher's note

All claims expressed in this article are solely those of the authors and do not necessarily represent those of

their affiliated organizations, or those of the publisher, the editors and the reviewers. Any product that may be evaluated in this article, or claim that may be made by its manufacturer, is not guaranteed or endorsed by the publisher.

Supplementary material

The Supplementary Material for this article can be found online at: https://www.frontiersin.org/articles/10.3389/fcell.2025.1569187/full#supplementary-material

References

Ami, D., Neri, T., Natalello, A., Mereghetti, P., Doglia, S. M., Zanoni, M., et al. (2008). Embryonic stem cell differentiation studied by FT-IR spectroscopy. *Biochim. Biophys. Acta* 1783 (1), 98–106. doi:10.1016/j.bbamcr.2007.08.003

Andjus, P., Stamenkovic, S., and Dučić, T. (2019). Synchrotron radiation-based FTIR spectro-microscopy of the brainstem of the hSOD1 G93A rat model of amyotrophic lateral sclerosis. *Eur. Biophys. J.* 48 (5), 475–484. doi:10.1007/s00249-019-01380-5

Angelopoulos, I., Gakis, G., Birmpas, K., Kyrousi, C., Habeos, E. E., Kaplani, K., et al. (2022). Metabolic regulation of the neural stem cell fate: unraveling new connections, establishing new concepts. *Front. Neurosci.* 16, 1009125. doi:10.3389/fnins.2022.1009125

Avior, Y., Sagi, I., and Benvenisty, N. (2016). Pluripotent stem cells in disease modelling and drug discovery. *Nat. Rev. Mol. Cell. Biol.* 17 (3), 170–182. doi:10.1038/nrm.2015.27

Baker, M. J., Trevisan, J., Bassan, P., Bhargava, R., Butler, H. J., Dorling, K. M., et al. (2014). Using Fourier transform IR spectroscopy to analyze biological materials. *Nat. Protoc.* 9 (8), 1771–1791. doi:10.1038/nprot.2014.110

Banyay, M., Sarkar, M., and Graslund, A. (2003). A library of IR bands of nucleic acids in solution. *Biophys. Chem.* 104 (2), 477–488. doi:10.1016/s0301-4622(03)00035-8

Beknazarov, N., Jin, S., and Poptsova, M. (2020). Deep learning approach for predicting functional Z-DNA regions using omics data. *Sci. Rep.* 10 (1), 19134. doi:10.1038/s41598-020-76203-1

Bhatia, N. K., Srivastava, A., Katyal, N., Jain, N., Khan, M. A., Kundu, B., et al. (2015). Curcumin binds to the pre-fibrillar aggregates of Cu/Zn superoxide dismutase (SOD1) and alters its amyloidogenic pathway resulting in reduced cytotoxicity. *Biochim. Biophys. Acta* 1854 (5), 426–436. doi:10.1016/j.bbapap.2015.01.014

Boseley, R. E., Sylvain, N. J., Peeling, L., Kelly, M. E., and Pushie, M. J. (2024). A review of concepts and methods for FTIR imaging of biomarker changes in the post-stroke brain. *Biochim. Biophys. Acta Biomembr.* 1866 (3), 184287. doi:10.1016/j.bbamem.2024.184287

Cao, J., Ng, E. S., McNaughton, D., Stanley, E. G., Elefanty, A. G., Tobin, M. J., et al. (2014). Fourier transform infrared microspectroscopy reveals unique phenotypes for human embryonic and induced pluripotent stem cell lines and their progeny. *J. Biophot.* 7 (10), 767–781. doi:10.1002/jbio.201200217

Demšar, J. C. T., Erjavec, A., Gorup, Č., Hocevar, T., Milutinovič, M., Martin Možina, M., et al. (2013). Orange: data mining toolbox in Python. *J. Mach. Learn Res.* 14, 2349–2353.

Discher, D. E., Mooney, D. J., and Zandstra, P. W. (2009). Growth factors, matrices, and forces combine and control stem cells. *Science* 324 (5935), 1673–1677. doi:10.1126/science.1171643

Doherty, J., Cinque, G., and Gardner, P. (2016). Single-cell analysis using Fourier transform infrared microspectroscopy. *Appl. Spectrosc. Rev.* 52 (6), 560–587. doi:10.1080/05704928.2016.1250214

Duan, M., Li, Y., Zhang, F., and Huang, Q. (2023). Assessing B-Z DNA transitions in solutions via infrared spectroscopy. *Biomolecules* 13 (6), 964. doi:10.3390/biom13060964

Dučić, T., Ninkovic, M., Martinez-Rovira, I., Sperling, S., Rohde, V., Dimitrijevic, D., et al. (2022). Live-cell synchrotron-based FTIR evaluation of metabolic compounds in brain glioblastoma cell lines after riluzole treatment. *Anal. Chem.* 94 (4), 1932–1940. doi:10.1021/acs.analchem.1c02076

Dučić, T., Sanchez-Mata, A., Castillo-Sanchez, J., Algarra, M., and Gonzalez-Munoz, E. (2023). Monitoring oocyte-based human pluripotency acquisition using synchrotron-based FTIR microspectroscopy reveals specific biomolecular trajectories. *Spectrochim. Acta A Mol. Biomol. Spectrosc.* 297, 122713. doi:10.1016/j.saa.2023.122713

Dučić, T., Stamenkovic, S., Lai, B., Andjus, P., and Lucic, V. (2019). Multimodal synchrotron radiation microscopy of intact astrocytes from the hSOD1 G93A rat model of amyotrophic lateral sclerosis. *Anal. Chem.* 91 (2), 1460–1471. doi:10.1021/acs.analchem.8b04273

Dumas, P.M. (2020). "IR spectroscopy and spectromicroscopy with synchrotron radiation," in *Synchrotron light sources and free-electron lasers: accelerator physics, instrumentation and science applications*, 2059–2113.

Finlayson, D., Rinaldi, C., and Baker, M. J. (2019). Is infrared spectroscopy ready for the clinic? *Anal. Chem.* 91 (19), 12117–12128. doi:10.1021/acs.analchem.9b02280

Ghosh-Choudhary, S., Liu, J., and Finkel, T. (2020). Metabolic regulation of cell fate and function. *Trends Cell. Biol.* 30 (3), 201–212. doi:10.1016/j.tcb.2019.12.005

Gioacchini, G., Giorgini, E., Vaccari, L., Ferraris, P., Sabbatini, S., Bianchi, V., et al. (2014). A new approach to evaluate aging effects on human oocytes: fourier transform infrared imaging spectroscopy study. *Fertil. Steril.* 101 (1), 120–127. doi:10.1016/j.fertnstert.2013.09.012

Gonzalez-Munoz, E., Arboleda-Estudillo, Y., Otu, H. H., and Cibelli, J. B. (2014). Cell reprogramming. Histone chaperone ASF1A is required for maintenance of pluripotency and cellular reprogramming. *Science* 345 (6198), 822–825. doi:10.1126/science.1254745

Goodwin, K., and Nelson, C. M. (2021). Mechanics of development. *Dev. Cell.* 56 (2), 240–250. doi:10.1016/j.devcel.2020.11.025

Hackett, M. J., Borondics, F., Brown, D., Hirschmugl, C., Smith, S. E., Paterson, P. G., et al. (2013). Subcellular biochemical investigation of purkinje neurons using synchrotron radiation fourier transform infrared spectroscopic imaging with a focal plane array detector. *ACS Chem. Neurosci.* 4 (7), 1071–1080. doi:10.1021/cn4000346

Hagey, D. W., Zaouter, C., Combeau, G., Lendahl, M. A., Andersson, O., Huss, M., et al. (2016). Distinct transcription factor complexes act on a permissive chromatin landscape to establish regionalized gene expression in CNS stem cells. *Genome Res.* 26 (7), 908–917. doi:10.1101/gr.203513.115

Hampoelz, B., and Lecuit, T. (2011). Nuclear mechanics in differentiation and development. *Curr. Opin. Cell. Biol.* 23 (6), 668–675. doi:10.1016/j.ceb.2011.10.001

Heraud, P., Ng, E. S., Caine, S., Yu, Q. C., Hirst, C., Mayberry, R., et al. (2010). Fourier transform infrared microspectroscopy identifies early lineage commitment in differentiating human embryonic stem cells. *Stem Cell. Res.* 4 (2), 140–147. doi:10.1016/j.scr.2009.11.002

Jovic, D., Liang, X., Zeng, H., Lin, L., Xu, F., and Luo, Y. (2022). Single-cell RNA sequencing technologies and applications: a brief overview. *Clin. Transl. Med.* 12 (3), e694. doi:10.1002/ctm2.694

Kim, S. H., Lim, S. H., Lee, A. R., Kwon, D. H., Song, H. K., Lee, J. H., et al. (2018). Unveiling the pathway to Z-DNA in the protein-induced B-Z transition. *Nucleic Acids Res.* 46 (8), 4129–4137. doi:10.1093/nar/gky200

Knaupp, A. S., Buckberry, S., Pflueger, J., Lim, S. M., Ford, E., Larcombe, M. R., et al. (2017). Transient and permanent reconfiguration of chromatin and transcription factor occupancy drive reprogramming. *Cell. Stem Cell.* 21 (6), 834–845.e6. doi:10.1016/j.stem.2017.11.007

Komatsu, M., Kanda, T., Urai, H., Kurokochi, A., Kitahama, R., Shigaki, S., et al. (2018). NNMT activation can contribute to the development of fatty liver disease by modulating the NAD (+) metabolism. *Sci. Rep.* 8 (1), 8637. doi:10.1038/s41598-018-26882-8

Kreuzer, M., Stamenkovic, S., Chen, S., Andjus, P., and Dučić, T. (2020). Lipids status and copper in a single astrocyte of the rat model for amyotrophic lateral sclerosis: correlative synchrotron-based X-ray and infrared imaging. *J. Biophot.* 13 (10), e202000069. doi:10.1002/jbio.202000069

Kumar, A., Placone, J. K., and Engler, A. J. (2017). Understanding the extracellular forces that determine cell fate and maintenance. *Development* 144 (23), 4261–4270. doi:10.1242/dev.158469

Li, C., Fleck, J. S., Martins-Costa, C., Burkard, T. R., Themann, J., Stuempflen, M., et al. (2023). Single-cell brain organoid screening identifies developmental defects in autism. *Nature* 621 (7978), 373–380. doi:10.1038/s41586-023-06473-y

Li, D., Shu, X., Zhu, P., and Pei, D. (2021). Chromatin accessibility dynamics during cell fate reprogramming. *EMBO Rep.* 22 (2), e51644. doi:10.15252/embr.202051644

Li, L. L. S. F., Puretzky, A., Riehn, R., and Hallen, H. D. (2018). DNA methylation detection using resonance and nanobowtie-antenna-enhanced Raman spectroscopy. *Biophysical J.* 114 (11), 2498–2506. doi:10.1016/j.bpj.2018.04.021

Li, Y., Huang, Q., Yao, G., Wang, X., Zhang, F., Wang, T., et al. (2020). Remodeling chromatin induces Z-DNA conformation detected through fourier transform infrared spectroscopy. *Anal. Chem.* 92 (21), 14452–14458. doi:10.1021/acs.analchem.0c02432

Liao, C. R., Rak, M., Lund, J., Unger, M., Platt, E., Albensi, B. C., et al. (2013). Synchrotron FTIR reveals lipid around and within amyloid plaques in transgenic mice and Alzheimer's disease brain. *Analyst* 138 (14), 3991–3997. doi:10.1039/c3an00295k

Liu, R., Liu, H., Chen, X., Kirby, M., Brown, P. O., and Zhao, K. (2001). Regulation of CSF1 promoter by the SWI/SNF-like BAF complex. *Cell.* 106 (3), 309–318. doi:10.1016/s0092-8674(01)00446-9

Lopez-Caraballo, L., Martorell-Marugan, J., Carmona-Saez, P., and Gonzalez-Munoz, E. (2020a). Analysis of menstrual blood stromal cells reveals SOX15 triggers oocyte-based human cell reprogramming. *iScience* 23 (8), 101376. doi:10.1016/j.isci.2020.101376

Lopez-Caraballo, L., Martorell-Marugan, J., Carmona-Saez, P., and Gonzalez-Munoz, E. (2020b). iPS-derived early oligodendrocyte progenitor cells from SPMS patients reveal deficient *in vitro* cell migration stimulation. *Cells* 9 (8), 1803. doi:10.3390/cells9081803

Loutherback, K., Birarda, G., Chen, L., and Holman, H. Y. (2016). Microfluidic approaches to synchrotron radiation-based Fourier transform infrared (SR-FTIR) spectral microscopy of living biosystems. *Protein Pept. Lett.* 23 (3), 273–282. doi:10.2174/0929866523666160106154035

Malek, K. B. R., and Bambery, K. R. (2014). "FTIR imaging of tissues: techniques and methods of analysis," in *Optical spectroscopy and computational methods in biology and medicine* (Netherlands: Springer), 419–473.

Mammoto, T., Mammoto, A., and Ingber, D. E. (2013). Mechanobiology and developmental control. *Annu. Rev. Cell. Dev. Biol.* 29, 27–61. doi:10.1146/annurev-cellbio-101512-122340

Martinez-Rovira, I., Seksek, O., Dokic, I., Brons, S., Abdollahi, A., and Yousef, I. (2020). Study of the intracellular nanoparticle-based radiosensitization mechanisms in F98 glioma cells treated with charged particle therapy through synchrotron-based infrared microspectroscopy. *Analyst* 145 (6), 2345–2356. doi:10.1039/c9an02350j

Marton, R. M., Miura, Y., Sloan, S. A., Li, Q., Revah, O., Levy, R. J., et al. (2019). Differentiation and maturation of oligodendrocytes in human three-dimensional neural cultures. *Nat. Neurosci.* 22 (3), 484–491. doi:10.1038/s41593-018-0316-9

Maruyama, A., Mimura, J., Harada, N., and Itoh, K. (2013). Nrf2 activation is associated with Z-DNA formation in the human HO-1 promoter. *Nucleic Acids Res.* 41 (10), 5223–5234. doi:10.1093/nar/gkt243

McKinley, K. L., Castillo-Azofeifa, D., and Klein, O. D. (2020). Tools and concepts for interrogating and defining cellular identity. *Cell. Stem Cell.* 26 (5), 632–656. doi:10.1016/j.stem.2020.03.015

Mendelsohn, R., Flach, C. R., and Moore, D. J. (2006). Determination of molecular conformation and permeation in skin via IR spectroscopy, microscopy, and imaging. *Biochim. Biophys. Acta* 1758 (7), 923–933. doi:10.1016/j.bbamem.2006.04.009

Miller, L. M., and Dumas, P. (2010). From structure to cellular mechanism with infrared microspectroscopy. *Curr. Opin. Struct. Biol.* 20 (5), 649–656. doi:10.1016/j.sbi.2010.07.007

Ober, C., Loisel, D. A., and Gilad, Y. (2008). Sex-specific genetic architecture of human disease. *Nat. Rev. Genet.* 9 (12), 911–922. doi:10.1038/nrg2415

Pasca, S. P. (2018). Building three-dimensional human brain organoids. *Nat. Neurosci.*

Pascolo, L., Bortot, B., Benseny-Cases, N., Gianoncelli, A., Tosi, G., Ruozi, B., et al. (2014). Detection of PLGA-based nanoparticles at a single-cell level by synchrotron radiation FTIR spectromicroscopy and correlation with X-ray fluorescence microscopy. *Int. J. Nanomedicine* 9, 2791–2801. doi:10.2147/IJN.S58685

Pezolet, M., Bonenfant, S., Dousseau, F., and Popineau, Y. (1992). Conformation of wheat gluten proteins. Comparison between functional and solution states as determined by infrared spectroscopy. *FEBS Lett.* 299 (3), 247–250. doi:10.1016/0014-5793(92)80125-z

Pottmeier, P., Nikolantonaki, D., Lanner, F., Peuckert, C., and Jazin, E. (2024). Sex-biased gene expression during neural differentiation of human embryonic stem cells. *Front. Cell. Dev. Biol.* 12, 1341373. doi:10.3389/fcell.2024.1341373

Rustem, I., Litvinov, D. A. F., Zuev, Y. F., and Weisel, J. W. (2012). The α-helix to β-sheet transition in stretched and compressed hydrated fibrin clots. *Biophysical J.* 103 (5), 1020–1027. doi:10.1016/j.bpj.2012.07.046

Saj, I. J., and Joye, I. J. (2020). Peak fitting applied to fourier transform infraredand Raman spectroscopic analysis of proteins. *Appl. Sci.* 10 (17), 5918. doi:10.3390/app10175918

Sandt, C., Feraud, O., Oudrhiri, N., Bonnet, M. L., Meunier, M. C., Valogne, Y., et al. (2012). Identification of spectral modifications occurring during reprogramming of somatic cells. *PLoS One* 7 (4), e30743. doi:10.1371/journal.pone.0030743

Sandt, C., Frederick, J., and Dumas, P. (2013). Profiling pluripotent stem cells and organelles using synchrotron radiation infrared microspectroscopy. *J. Biophot.* 6 (1), 60–72. doi:10.1002/jbio.201200139

Sarroukh, R., Cerf, E., Derclaye, S., Dufrene, Y. F., Goormaghtigh, E., Ruysschaert, J. M., et al. (2011). Transformation of amyloid β(1-40) oligomers into fibrils is characterized by a major change in secondary structure. *Cell. Mol. Life Sci.* 68 (8), 1429–1438. doi:10.1007/s00018-010-0529-x

Schindelin, J., Arganda-Carreras, I., Frise, E., Kaynig, V., Longair, M., Pietzsch, T., et al. (2012). Fiji: an open-source platform for biological-image analysis. *Nat. Methods* 9 (7), 676–682. doi:10.1038/nmeth.2019

Shao, W., Yang, Y., Shen, W., Ren, L., and WenwenWang, Z. P. (2024). Hyaluronic acid-conjugated methotrexate and 5-fluorouracil for targeted drug delivery. *Int. J. Biol. Macromol.* 273 (Pt 1), 132671. doi:10.1016/j.ijbiomac.2024.132671

Shihan, M. H., Novo, S. G., Le Marchand, S. J., Wang, Y., and Duncan, M. K. (2021). A simple method for quantitating confocal fluorescent images. *Biochem. Biophys. Rep.* 25, 100916. doi:10.1016/j.bbrep.2021.100916

Sperber, H., Mathieu, J., Wang, Y., Ferreccio, A., Hesson, J., Xu, Z., et al. (2015). The metabolome regulates the epigenetic landscape during naive-to-primed human embryonic stem cell transition. *Nat. Cell. Biol.* 17 (12), 1523–1535. doi:10.1038/ncb3264

Steiner, G., Galli, R., Preusse, G., Michen, S., Meinhardt, M., Temme, A., et al. (2023). A new approach for clinical translation of infrared spectroscopy: exploitation of the signature of glioblastoma for general brain tumor recognition. *J. Neurooncol* 161 (1), 57–66. doi:10.1007/s11060-022-04204-3

Strano, A., Tuck, E., Stubbs, V. E., and Livesey, F. J. (2020). Variable outcomes in neural differentiation of human PSCs arise from intrinsic differences in developmental signaling pathways. *Cell. Rep.* 31 (10), 107732. doi:10.1016/j.celrep.2020.107732

Sugathan, A., and Waxman, D. J. (2013). Genome-wide analysis of chromatin states reveals distinct mechanisms of sex-dependent gene regulation in male and female mouse liver. *Mol. Cell. Biol.* 33 (18), 3594–3610. doi:10.1128/MCB.00280-13

Sun, L., Ji, M., Liu, Y., Zhang, M., Zheng, C., and Wang, P. (2024). XQZ3, a Chlorella pyrenoidosa polysaccharide suppresses cancer progression by restraining mitochondrial bioenergetics via HSP90/AKT signaling pathway. *Int. J. Biol. Macromol.* 264 (Pt 2), 130705. doi:10.1016/j.ijbiomac.2024.130705

Tatapudy, S., Aloisio, F., Barber, D., and Nystul, T. (2017). Cell fate decisions: emerging roles for metabolic signals and cell morphology. *EMBO Rep.* 18 (12), 2105–2118. doi:10.15252/embr.201744816

Toplak, M., Read, S. T., Sandt, C., and Borondics, F. (2021). Quasar: easy machine learning for biospectroscopy. *Cells* 10 (9), 2300. doi:10.3390/cells10092300

Toplak, M. B. G., Read, S., Sandt, C., Rosendahl, S. M., Vaccari, L., Demšar, J., et al. (2017). Infrared Orange: connecting hyperspectral data with machine learning. *Synchrotron Radiat. News* 30, 40–45. doi:10.1080/08940886.2017.1338424

Vining, K. H., and Mooney, D. J. (2017). Mechanical forces direct stem cell behaviour in development and regeneration. *Nat. Rev. Mol. Cell. Biol.* 18 (12), 728–742. doi:10.1038/nrm.2017.108

Walsh, R. M., Luongo, R., Giacomelli, E., Ciceri, G., Rittenhouse, C., Verrillo, A., et al. (2024). Generation of human cerebral organoids with a structured outer subventricular zone. *Cell. Rep.* 43 (4), 114031. doi:10.1016/j.celrep.2024.114031

Wang, Y., Dai, W., Liu, Z., Liu, J., Cheng, J., Li, Y., et al. (2021). Single-cell infrared microspectroscopy quantifies dynamic heterogeneity of mesenchymal stem cells during adipogenic differentiation. *Anal. Chem.* 93 (2), 671–676. doi:10.1021/acs.analchem.0c04110

Wellner, N., Belton, P. S., and Tatham, A. S. (1996). Fourier transform IR spectroscopic study of hydration-induced structure changes in the solid state of omega-gliadins. *Biochem. J.* 319 (Pt 3), 741–747. doi:10.1042/bj3190741

Xu, W., Hou, L., Li, P., and Li, L. (2022). Effect of nicotinamide N-methyltransferase on lipid accumulation in 3T3-L1 adipocytes. *Bioengineered* 13 (5), 12421–12434. doi:10.1080/21655979.2022.2074768

Zhang, F., Huang, Q., Yan, J., and Chen, Z. (2016). Histone acetylation induced transformation of B-DNA to Z-DNA in cells probed through FT-IR spectroscopy. *Anal. Chem.* 88 (8), 4179–4182. doi:10.1021/acs.analchem.6b00400

frontiers | Frontiers in Cell and Developmental Biology

TYPE Review
PUBLISHED 30 June 2025
DOI 10.3389/fcell.2025.1613378

OPEN ACCESS

EDITED BY
Valerie Kouskoff,
The University of Manchester,
United Kingdom

REVIEWED BY
Armel Hervé Nwabo Kamdje,
University of Garoua, Cameroon
Yangzi Zhu,
Xuzhou Central Hospital, China

*CORRESPONDENCE
Huayang Xu,
xhy8783668@163.com
Shangzhi Feng,
1131718266@qq.com

RECEIVED 17 April 2025
ACCEPTED 19 June 2025
PUBLISHED 30 June 2025

CITATION
Zhang Y, Yin Z, Zou Z, Feng S and Xu H (2025) Nanopathways modulating postoperative cognitive dysfunction: extracellular vesicles. *Front. Cell Dev. Biol.* 13:1613378. doi: 10.3389/fcell.2025.1613378

Nanopathways modulating postoperative cognitive dysfunction: extracellular vesicles

Yunmeng Zhang[1], Zengsheng Yin[1], Zhiyong Zou[1], Shangzhi Feng[2]* and Huayang Xu[1]*

[1]Department of Anesthesiology, Jiujiang College Hospital, Jiujiang, Jiangxi, China, [2]Department of Urology, Jiujiang University Clinic College/Hospital, Jiujiang, Jiangxi, China

Postoperative cognitive dysfunction is a common central nervous system complication after general anesthesia in the elderly, and when it occurs, it will seriously affect the patient's postoperative recovery and quality of life, which puts elderly postoperative general anesthesia patients at an extremely uncertain risk of postoperative psychiatric disorders or even death. It is currently believed that neuronal damage and inflammatory response due to cerebral ischemia/reperfusion injury induced by transient or repeated global cerebral ischemia during surgery are the key mechanisms for the development of postoperative cognitive dysfunction. Therefore, repairing postoperative neuronal damage and reducing neuroinflammatory responses may be an effective means of early intervention for postoperative cognitive dysfunction. Extracellular vesicles, a therapeutic tool with clear advantages in regenerative medicine, have been suggested as potential nanopathways to modulate postoperative cognitive dysfunction due to their pro-regenerative, pro-repair, and influence on immune responses. In this paper, we will summarize studies related to extracellular vesicles in the treatment of postoperative cognitive dysfunction and discuss the potential function of extracellular vesicles in nerve repair and inhibition of acute neurological inflammation, which will expand the therapeutic strategies for postoperative cognitive dysfunction and may represent the development of novel cell-free therapeutic pathways for modulating postoperative cognitive dysfunction.

KEYWORDS

postoperative cognitive dysfunction, extracellular vesicle, nano-targeted therapy, neuroinflammation, neurorestoration, cell-free therapeutic pathway

Introduction

Postoperative cognitive dysfunction (POCD) is a common complication of general anesthesia surgery, manifesting as agitation, confusion, and loss of learning and memory abilities, with memory loss being the most prominent feature (Liu et al., 2023). This condition can persist for months or even years, and untimely and inappropriate interventions may lead to dementia or even risk of death, which severely hampers postoperative recovery in elderly patients and makes the perioperative period extremely precarious for elderly patients undergoing general anesthesia surgical procedures. The occurrence of POCD is associated with a variety of factors, including age, education,

preoperative complications, type of anesthesia, degree of surgical trauma, type of surgery, and postoperative Pain (Oriby et al., 2023; Ding et al., 2021). Large-scale clinical studies have shown that POCD occurs in about 30% of cases at 7 days postoperatively and in about 10% of cases at 3 months postoperatively (Yang et al., 2022). In terms of type of surgery, patients undergoing cardiovascular and orthopedic surgeries had the highest prevalence of postoperative cognitive deficits, at about 40% (Progress of research in postoperative cognitive dysfunction in cardiac surgery patients: a review article), while non-cardiovascular surgeries accounted for about 23.8% (Silva et al., 2021). POCD can seriously affect patients' quality of life and increase the difficulty and burden of care, while soaring hospitalization costs as well as increased risk of mortality and dementia contribute to the adverse consequences of POCD. Therefore, early detection, diagnosis and intervention of POCD will effectively improve the quality of life of elderly surgical patients. However, the mechanism of POCD is unclear, and uniform clinical criteria for diagnosing POCD are still lacking. Therefore, it is imperative to find reliable and convenient clinical biomarkers. Currently, it is believed that the pathogenesis of POCD mainly focuses on the dysregulation of neuronal damage, neuroinflammation, oxidative stress, impairment of synaptic structural plasticity, and lack of neurotrophic support (Zhao et al., 2024; Lin et al., 2020). The most researched and considered major factors are neuronal damage and neuroinflammation, which are in fact considered to be the end result of other factors that ultimately trigger the onset and progression of POCD (Lin et al., 2020).

With the development of nanoscience and technology, extremely microscopic biomaterials are considered to be helpful in solving neurodegenerative disorders. With the regenerative repair, immune interference, and its unique cell affinity, targeting, and nano-delivery platform effects of extracellular vesicles, extracellular vesicles have been recognized as potential nanobio-pathways that can prevent and treat related neurological disorders (e.g., Alzheimer's disease, Parkinson's disease). For example, extracellular vesicles deliver therapeutic genetic material, such as miRNAs and proteins, which can exert neuroprotective effects and reduce cognitive impairment. As mediators of intercellular communication, extracellular vesicles are implicated in amyloid degradation, brain clearance, and intercellular diffusion of tau, and neuronal damage can be repaired by improving neuronal apoptosis through specific modifications of extracellular vesicles. The stem cell-derived extracellular vesicles also showed a strong regeneration-promoting function in brain injury due to their regenerative repair function (Hu et al., 2020). As far as neuroinflammation is concerned, extracellular vesicles in postoperative patients can act as a proactive mediator of postoperative cognitive dysfunction, and interfering with the development of these extracellular vesicles can help to impede and ameliorate COPD, e.g., treatment with GW4869 (an extracellular vesicle blocking agent) can be effective in preserving postoperative cognitive function by inhibiting the release of extracellular vesicles. In addition, extracellular vesicles from a variety of cellular sources also exhibit significant immunosuppressive functions, e.g., extracellular vesicles from mesenchymal stem cells reduce neuroinflammation (Cabrera-Pastor, 2024). Thus, extracellular vesicles may be a potential new modality for the prevention and treatment of postoperative cognitive dysfunction. Synthesizing the current studies and proposing the potential mechanism of extracellular vesicles for the treatment of POCD and preoperative medication pathway will greatly expand the prevention and treatment strategies for postoperative cognitive function.

Postoperative cognitive dysfunction

In November 2018, the first international definition of perioperative neurocognitive disorder (PND) was proposed (Evered et al., 2018). Traditionally POCD, postoperative delirium, and preexisting cognitive impairment have all been defined as PND, while also emphasizing that cognitive deficits are associated with the entire perioperative period (Kong et al., 2022). With the rapid development of medical technology, the proportion of elderly patients undergoing surgery continues to rise, and the incidence of POCD has gradually increased, POCD has become a research hotspot in perioperative medicine (Liu and Leung, 2000). Studies have found that the overall incidence of POCD in older postoperative patients is approximately 25.8% within 1 week, and approximately 30%–60% of POCD occurs with delirium or cognitive dysfunction within 1 week of cardiovascular surgery. Previously, it was thought that all forms of cognitive impairment after anesthesia could be referred to as POCD, including POD, but more recently it has been argued that POCD is different from POD because POD is accompanied by altered consciousness, whereas POCD is not (H et al., 2017). Perioperative neurocognitive disorders in humans can lead to significant complications in the lives of patients, and patients with POCD will experience disturbances in consciousness, cognition, orientation, thinking, memory, or sleep, as well as social impairments after anesthesia and surgery. Patients with POCD often exhibit anxiety, confusion, and a loss of learning and memory abilities. This may increase the risk of developing different brain dysfunctions, including Alzheimer's disease, long-term cognitive decline, and dementia, making POCD a highly worrisome condition, especially in the elderly population (Needham et al., 2017; Berger et al., 2019; Fong et al., 2021). Postoperative cognitive dysfunction can be triggered and exacerbated by a variety of factors, and the occurrence of postoperative cognitive dysfunction will seriously reduce postoperative recovery and lead to unavoidable medical disputes, but the relevant treatment methods are still very limited, and it is still necessary to find rapid and effective methods to prevent and control postoperative cognitive dysfunction, however, all the preventive and curative measures should be based on the premise that the etiology of the disease is clearly defined and the mechanism of the disease is clearly defined.

Etiology and mechanisms

Factors closely associated with POCD include perioperative factors such as age at surgery, preoperative education, basal status, duration of surgery, type of surgery, type of anesthesia, and intraoperative hemodynamic changes, as well as postoperative factors such as infections, pain, and sleep disorders (Le et al., 2014; Monk et al., 2008) (Table 1). Of these, advanced age was identified as the only risk factor for long-term POCD (>3 months postoperatively) (Le et al., 2014; Monk et al., 2008; Moller et al., 1998). Although surgery is effective in treating a wide range

of diseases, it can also lead to postoperative cognitive deficits, which may be associated with intraoperative and postoperative neuroinflammation induced by a variety of factors, neuronal injury, microecological dysregulation, defective autophagy in neuronal cells, and immune dysregulation (Huang et al., 2025). Different types of surgeries may also have an effect; older patients undergoing orthopedic and cardiovascular surgeries are more likely to develop POCD, possibly because such surgeries are more likely to cause widespread inflammation and neurologic changes (Wei et al., 2017; Hovens et al., 2016). Studies have found that POCD frequently occurs after coronary artery bypass grafting (CABG), and that the incidence of early cognitive dysfunction after CABG is high, at about 30%–60% (Boodhwani et al., 2006; Liu et al., 2009; Bishawi et al., 2018). For example, it has been found that transient or repeated cerebral ischemia during surgery can induce cerebral ischemia/reperfusion injury which in turn leads to neuronal damage and neuroinflammation, which is considered to be the key pathogenesis of POCD (van Harten et al., 2012; Lu et al., 2022). And massive intraoperative blood loss can lead to circulatory fluctuations and insufficient blood supply to the brain, which can affect oxygen supply, brain cell metabolism, and postoperative cognitive function (Zhang et al., 2019). For postoperative factors, postoperative pain and sleep disturbances are thought to be associated with the development of POCD, e.g., effective analgesia and adequate sleep may reduce the incidence of POCD (Wang et al., 2014). Although the mechanism is still unclear, it may involve the body's stress response due to pain to trigger an anxious and depressed state, and the sleep state can effectively promote the removal of metabolic waste. In addition, maintaining a positive preoperative state of mind may also help reduce postoperative delirium (POD) and promote postoperative cognitive improvement (Hudetz et al., 2010). It is evident that POCD is not only related to neurological disorders but also to psychiatric disorders. However, the relationship between anesthetic drugs and depth of anesthesia and the incidence of POCD is still controversial (Hou et al., 2018; Lu et al., 2018; Farag et al., 2006). Indeed, the etiology of POCD varies depending on the purpose of the study, which depends on the population included, assessment criteria, interventions, type of surgery and other factors. For example, studies have found that the fewer years of education and knowledge base a patient has, the higher the incidence of POCD, but this still needs to take into account geographic and gender differences (Scott et al., 2017).

Sleep disorders are thought to be an important contributor to POCD, with chronic reductions in sleep duration or complete lack of sleep leading to cognitive deficits. For example, maintaining sleep duration at 4–6 h per night can lead to neurobehavioral deficits during waking hours. In contrast, patients' reduced daytime strength, functional limitations, and emotional vulnerability after surgery will negatively affect postoperative cognitive recovery (Xie et al., 2013). In fact, postoperative cognitive dysfunction (POCD) and AD have similar pathogenesis (Hu et al., 2010).

During sleep, the interstitial volume of the cerebral cortex can increase by up to 60%, resulting in increased convection of ISF and CSF, which is effective in clearing Aβ. Pathological tau accumulation is more strongly associated with cognitive decline than Aβ, and sleep disorders can lead to hyperphosphorylation and aggregation of tau proteins, which in turn can lead to the formation of neural protofibrillar tangles, neurinflammatory plaques, and other structures (Brier et al., 2016). Sleep disturbances are also associated with hemodynamic instability and changes in pulmonary ventilation, which increase the incidence of postoperative fatigue, anxiety, depression, and pain sensitivity and thus decrease the rate of recovery from postoperative cognitive deficits, which leads to prolonged hospital stays. Postoperative pain can also severely affect postoperative cognitive recovery. Postoperative pain is a complex series of pathophysiological responses to surgical trauma involving cellular inflammation, nerve damage, and synaptic remodeling, which are closely related to the development of postoperative cognitive dysfunction. The hippocampus plays a key role in regulating emotion, learning and memory formation during cognitive processes, and postoperative pain significantly induces cellular stress and inflammatory responses and induces the release of inflammatory cytokines in the hippocampus, which in turn impairs hippocampal function (Chen et al., 2020; Conner et al., 2009). In addition, the toxicity of anesthetic drugs has been linked to postoperative cognitive dysfunction, and new evidence from experimental models in humans and rodents *in vivo* suggests neurobiological changes and lifelong cognitive deficits following exposure to anesthetic agents. Studies have shown that exposure to isoproterenol and sevoflurane causes cognitive deficits in mice (Lv et al., 2017). Anesthetics cause changes in the blood-brain barrier and cerebrovascular system by altering neuronal networks that may also contribute to long-term neurocognitive dysfunction in the brain. Since both intravenous and inhalational anesthetics currently in use produce anesthetic and sedative effects by binding to GABA receptors and/or N-methyl-D-aspartate receptors (NMDA, a subtype of glutamate receptors), due to these mechanisms of their use, all of these drugs may contribute to the development of neurocognitive deficits in the postoperative period (Orser and Wang, 2019).

Postoperative neuroinflammation, systemic immune activation, and oxidative stress in cells have been found to be key mechanisms in the development of postoperative cognitive dysfunction (Cibelli et al., 2010) (Figure 1). In terms of postoperative systemic inflammation, surgical trauma induces the release of proinflammatory cytokines and chemokines at the site of tissue injury, triggering a localized inflammatory response. These inflammatory mediators can activate peripheral immune cells and disrupt the tight junctions of the blood-brain barrier, and these peripheral immune cells (macrophages and monocytes) can then infiltrate the nervous system to and further contribute to the neuroinflammatory cascade. In the CNS, microglia play a critical role as immune cells, and their dysfunction can lead to neuroinflammation and negatively impact overall health. Microglia help reduce neuroinflammation by phagocytizing proteins such as Aβ, tau, and α-synuclein (Loh et al., 2024). Because central microglia are particularly sensitive to pathological injury and can respond immediately to infection, inflammation, and neurological injury, this inflammatory state can activate microglia to polarize toward inflammation (M1 phenotype) and lead to further release of proinflammatory cytokines and chemokines, thereby triggering a cascade of neuroinflammatory responses (Li et al., 2010). In contrast, microglia polarization responses have a huge impact on neuronal activity and synaptic plasticity in the hippocampus, ultimately affecting cognitive function. For example, a systematic evaluation of animal experiments has shown that microglia

TABLE 1 Risks of POCD and interventions.

Type of surgery	Risk factors	Intervention	References
Gastrointestinal Surgery	advanced age	Cognitive Training	Saleh et al. (2015)
Cesarean section	Surgical Stress	Stellate ganglion block	Deng et al. (2023)
Solid tumor resection	Educational background	Improvement of cognitive reserve	Kainz et al. (2023)
Thoracic surgery	Sleep disorders	Treatment of preoperative sleep disorders	Li et al. (2021a)
Tibial Fracture Surgery	Postoperative decline in mitochondrial function	Drugs to improve mitochondrial function	He et al. (2022)
Carotid artery exposure	Postoperative neuroinflammation, oxidative stress and synaptic dysfunction	Transcranial near infrared laser irradiation	Zhong et al. (2022)
Apical hepatectomy	Postoperative mitochondrial dysfunction	Dexmedetomidine to reduce mitochondrial damage	Sun et al. (2023)
Lobectomy	Pain	Dexmedetomidine preoperative sedation and analgesia	Shi et al. (2020)
Partial hepatectomy	Postoperative neuroinflammation	Dexmedetomidine inhibits hippocampal inflammation	Chen et al. (2019)
Hip replacement	Pain	Oxycodone for postoperative paroxysms	Gan et al. (2020)
Heart Surgery	Postoperative systemic inflammation	Ketamine to suppress systemic inflammation	Hudetz et al. (2009)
Partial hepatectomy	Postoperative neuroinflammation	Electroacupuncture inhibits neuroinflammation	Yuan et al. (2014)
Inhalation Anesthesia	Anesthetic Drug Toxicity	Nimodipine reverses sevoflurane toxicity	Cui et al. (2018)
Inhalation Anesthesia Surgery	Anesthesia Drug Toxicity	Cistanche extract inhibits neuroinflammation	Peng et al. (2020)
Carotid Artery Exposure	Postoperative neuroinflammation	Amantadine maintains neurotrophic	Zhong et al. (2020)

activation is associated with elevated levels of IL-1β, TNF-α, and Toll-like receptors (activated microglia release cytokines and chemokines, such as IL-1β, IL-6, and TNF-α), and may lead to delirium (Hoogland et al., 2015; Author Anonymous, 2024). Additional studies have also confirmed that the inflammatory response plays a key role in the onset and progression of POCD, and that activation of the systemic inflammatory cascade response will result in systemic cytokine dysregulation, which is thought to be an important factor in neurodegeneration and subsequent cognitive impairment in delirium (Momen-Heravi et al., 2014). This is because the elderly are often in a state of chronic low-grade inflammation and immunocompromise, which makes them more susceptible to the inflammatory effects of infection and trauma. When an elderly patient is subjected to major trauma (e.g., a serious injury or fracture), the systemic acute inflammatory response can be triggered rapidly and involves the release of cytokines and the aggregation of inflammatory cells, which is followed by a high likelihood of POCD after undergoing anesthesia and major surgery. POCD and major surgical procedures or anesthetic drugs can elicit a secondary inflammatory response that can exacerbate the severity of the inflammatory response. Such secondary inflammatory events can lead to immune dysregulation, disruption of cellular function, and negative effects on multiple systems, including an increased risk of POCD (Qin et al., 2024). In addition, this chronic inflammatory state can also lead to mild neuroinflammation characterized by upregulation of central proinflammatory cytokines and increased numbers of microglia (Li et al., 2022). In addition to aging itself, chronic diseases associated with aging, such as obesity, diabetes, cardiovascular disease, *etc.*, can also lead to the body in a state of "chronic low-grade inflammation" (Kawai et al., 2021). In fact, mice that underwent major surgery after a one-time inflammation showed a further decline in physical activity that also led to more severe cognitive impairment.

In addition to the inflammatory response, POCD has been found to be involved in a variety of pathological processes such as neuroinflammation, mitochondrial dysfunction, oxidative stress, blood-brain barrier damage, impaired neurotrophic support, and synaptic injury and has been well-studied. Evidence suggests that these associated molecular pathways may increase perioperative complications and mortality (Lin et al., 2020). However, at present, inflammatory response and nerve damage are considered to be the more recognized key mechanisms of postoperative POCD, and many therapeutic options are mainly based on this mechanism and have achieved some therapeutic effects, although the current therapeutic options are extremely limited. Therefore, summarizing and describing the potential new nanoscale solutions by inhibiting inflammation and repairing the most nerve damage will greatly expand the treatment options for postoperative POCD and may lead to new breakthroughs in nanotherapeutics.

Perioperative factors lead to the release of DaMPs from damaged cells that are recognized by the corresponding receptors in circulating macrophages. Binding to TLR and RAGE at

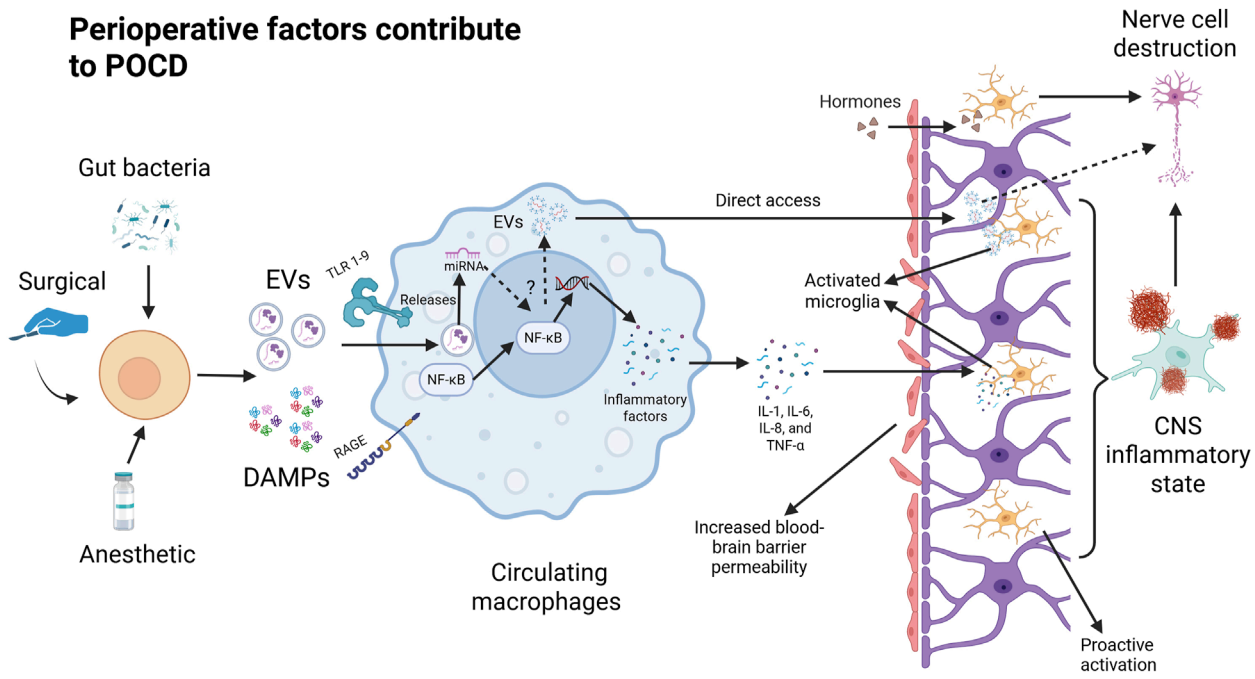

FIGURE 1
Perioperative factors contribute to POCD.

the macrophage membrane triggers the NF-κB pathway in the cytoplasm. Degradation by phosphorylation and ubiquitination exposed the nuclear translocation site in NF-κB and induced nuclear translocation of NF-κB. In the nucleus, NF-κB regulates the expression of proinflammatory genes and promotes the cellular secretion of inflammatory factors (IL-1, IL-6, IL-8, and TNF-α). Pro-inflammatory factors disrupt the tight junctions of the blood-brain barrier after which inflammatory factors, danger signaling molecules, and peripheral immune cells enter the brain through the damaged blood-brain barrier to further activate microglia. At the same time, the damaged cells may also release specific extracellular vesicles that prompt peripheral immune cells (including circulating macrophages) to produce inflammatory factors or extracellular vesicles that can directly damage neuronal cells through the blood-brain barrier.

Status of treatment

POCD is a complication of the central nervous system characterized by intellectual disability, anxiety, personality changes, and impaired memory that manifests as neurocognitive deficits, affecting many elderly patients recovering from surgical procedures, where declines in memory, attention, and executive functioning can significantly affect quality of life and increase the risk of long-term cognitive impairment. Currently, the treatment of POCD relies on medication and rehabilitation such as acupuncture (Table1), focusing on reducing inflammatory responses and maintaining neurotransmitter balance, such as the narcotic drugs dexmedetomidine, etomidate, and ketamine; the anti-inflammatory drugs parecoxib and cyclooxygenase-2; and the antipsychotic drugs galantamine and sarcosine methyl, haloperidol, and so on (Wang et al., 2021). Acupuncture, on the other hand, is mainly for electro-acupuncture stimulation of acupoints to reduce the postoperative stress response thereby alleviating the degree of nerve damage (Ho et al., 2020). In contrast, non-pharmacological options such as preoperative and postoperative cognitive training are usually preferred for the treatment of POCD in the clinical context (Butz et al., 2022; Saleh et al., 2015). This is due to the fact that various medications are not developed for POCD, which can have numerous adverse effects on patients. For example, postoperative use of non-steroidal anti-inflammatory drugs for pain relief may lead to gastric bleeding and kidney damage and is not suitable for long-term use; anesthetic drugs are not suitable for patients with chronic diseases such as heart, lungs and brain, especially for the elderly. Although some clinical reports suggest that the use of lidocaine (a local anesthetic) or parecoxib (a nonsteroidal anti-inflammatory drug) may reduce the incidence of POCD (Ho et al., 2024). Even though certain medications, such as cholinesterase inhibitors, N-methyl-d-aspartate receptor antagonists, and antipsychotics, have been used in clinical practice to improve cognitive function, there are no specific medications approved by the U.S. Food and Drug Administration for the treatment of POCD (Gao et al., 2024). Therefore, there is a need to study and develop effective control programs to help patients regain cognitive function at different stages of the postoperative period. Although anti-inflammation, inhibition of microglia activation and improvement of cerebral microcirculation are potential coping strategies for POCD, neither pharmacologic nor non-pharmacologic approaches have achieved satisfactory clinical results (Lin et al., 2020). There is an urgent need to explore reliable detection and treatment

methods, and the international community has called for systematic research on POCD.

Extracellular vesicles modulate postoperative cognitive dysfunction

Modulation of neuroinflammatory responses

Inflammatory responses play a key role in the development and progression of a variety of human diseases, including autoimmune, neurodegenerative, and other inflammatory disorders, and have also been recognized as a major feature of several neurological disease-related pathological conditions, such as Alzheimer's disease and postoperative cognitive dysfunction. Neuroinflammation has been identified as a key mechanism contributing to cognitive impairment, and a large body of clinical evidence highlights the significant impact of immune dysfunction on cognitive decline. Surgical activation of immune cells in the immune system (e.g., macrophages and neutrophils) infiltrates neural tissue through the disrupted blood-brain barrier and thus leads to neuroinflammation. Although the inflammatory response to tissue damage or destruction removes harmful substances and damaged tissue. However, excessive nervous system inflammation can lead to neurotoxicity and cell death. In turn, damaged neurons release Aβ to cause inflammation, thus initiating a vicious cycle of continuous Aβ release, similar to Alzheimer's disease (Krstic and Knuesel, 2013). In addition, central inflammation affects neurotrophic factor levels, which disrupts synaptic plasticity and leads to decreased nerve regeneration. The resulting excessive inflammation in the brain can lead to postoperative cognitive decline (Solas et al., 2017). Extracellular vesicles are important carriers that mediate the transfer of active substances and genetic information between cells. It was found that the preoperative message carried by exosomes released by peripheral monocytes/macrophages has been altered in older patients who have experienced major illness or trauma (Qin et al., 2024). Another study reported that extracellular vesicles released by macrophages, when injected *via* jugular vein, aggregated more prominently in the brains of mice with the presence of central nervous system inflammation than in normal mice (Dong et al., 2021). In contrast, postoperative mice treated with GW4869 had cognitive function and blood-brain barrier function closer to those of normal mice, and significant reductions in the levels of inflammatory factors in the peripheral blood and central hippocampus of the mice. Furthermore, injection of macrophage-released exosomes into healthy mice induced inflammation, hippocampal damage, and cognitive deficits, which were significantly alleviated by treatment with GW4869 (Qin et al., 2024). Thus, extracellular vesicles are likely to be important mediators in mediating the postoperative peripheral immune response to induce central inflammation. Twenty-five EVs associated with M1-type microglia have been reported to modulate neuronal inflammation involved in cognitive impairment (Medders et al., 2010; Zhou et al., 2016). For example, EVs released from M1-microglia overexpressing IL-1R1 can promote POCD development by modulating neuronal inflammation. Another study reported that extracellular vesicles released by macrophages, when injected *via* jugular vein, aggregated more prominently in the brains of mice with the presence of central nervous system inflammation than in normal mice (Dong et al., 2021). Extracellular vesicles may help deliver therapeutic genetic material, such as miRNAs and proteins, to exert neuroprotective effects and reduce cognitive impairment. For example, in an animal model of persistent pulmonary hypertension, extracellular vesicles inhibit macrophage infiltration and the release of proinflammatory mediators through miRNA-mediated decreases in the levels of monocyte chemotactic proteins and mitogens, which effectively control the inflammatory response caused by the surgery and thus reduce the occurrence of POCD. The release of extracellular vesicles containing miR-124-3p from microglial cells also exerts a protective effect against cognitive deficits by attenuating the inflammatory polarization process of hippocampal microglia in aged mice (Xin et al., 2017). Embryonic stem cell-derived extracellular vesicles also alleviate long-term diabetes-induced chronic inflammation in neural tissue to improve postoperative cognitive dysfunction in mice (Lang et al., 2023). Therefore, interfering with the generation of extracellular vesicles as mediators of postoperative cognitive dysfunction and special cellular sources with anti-inflammatory functions or utilizing their anti-inflammatory functions may be a potential pathway to ameliorate postoperative cognitive dysfunction.

Promotes neural tissue survival

The regenerative repair function of extracellular vesicles of specific cellular origin has been extensively studied, and their neurorestorative function is gradually being recognized. In postoperative cognitive dysfunction, neuronal damage is the direct cause of the onset of cognitive impairment (Lang et al., 2023). Repairing and promoting neuronal survival may help to inhibit the onset and slow the severity of postoperative cognitive dysfunction. Among them, stem cell-derived extracellular vesicles are most widely used in neural cell regeneration and repair therapy, mainly due to their high self-renewal capacity, high plasticity, low immunogenicity and effective cellular therapeutic efficacy (Andrzejewska et al., 2021). First, exogenous extracellular vesicles can target brain cells across the blood-brain barrier (Wang et al., 2020). Second, stem cell-derived extracellular vesicles exhibit robust neurogenesis and cognitive recycling (Lang et al., 2023). For example, embryonic stem cell-derived extracellular vesicles have shown potent regenerative functions in brain injury, and have also shown beneficial effects in promoting angiogenesis, stem cell proliferation and differentiation (Hu et al., 2020; Hu et al., 2015). In addition, extracellular vesicles that maintain neural repair and regeneration are also present in the central system. miR-124-3p-containing extracellular vesicles released by exogenous microglia in the hippocampus improve cognitive function by repairing axonal demyelination and overexpressing neurotrophic factors. Previous studies have demonstrated that microglia in the hippocampus continuously synthesize, assemble and secrete various types of extracellular vesicles into synapses to regulate synaptic plasticity and neural activity (Li Q. et al., 2021; E et al., 2022). Extracellular vesicles in the hippocampal microenvironment contain miR-124-3p that can also alter the expression of various neurotrophic factors that are essential for nerve growth. For example, BDNF promotes neuronal growth and differentiation and enhances

synaptic plasticity (Huang et al., 2018; Ge et al., 2020). Since miRNA expression is associated with surgery-induced neuronal injury, extracellular vesicles carrying and transporting miRNAs may be important elements in neuronal survival or death. For example, knockdown of extracellular vesicles of miR-206 inhibits neuronal apoptosis after acute brain injury. It is well known that microglia polarization has a huge impact on neuronal activity and synaptic plasticity in the hippocampus, which can ultimately affect cognitive function. Previous studies have demonstrated that microglia in the hippocampus can secrete miRNA-containing extracellular vesicles into the microenvironment to regulate microglia polarization and neurodegeneration (Qian et al., 2022). For example, central hippocampal microglia contain miR-124-3p extracellular vesicles involved in the process of autophagy and apoptosis in neurons to ameliorate postoperative cognitive dysfunction. In contrast some substances in microglia extracellular vesicles damage neurons at a later stage, such as IL-1β, soluble toxic Aβ peptide, and caspase-1 (Kong et al., 2024). Since miRNAs are involved in multiple pathophysiological processes involved in POCD occurrence, interfering with the extracellular vesicles that transmit miRNAs may be a new target for POCD therapy by enhancing neuronal survival.

Improvement of postoperative pain

Postoperative pain-induced cognitive impairment severely worsens the outcome of rehabilitation in elderly patients. Elderly patients are often sensitive to surgical trauma, stress, anesthesia, or pain, which greatly increases the incidence of postoperative cognitive impairment, especially after undergoing cardiovascular, orthopedic, or cerebrovascular surgery. Postoperative pain-induced cognitive deficits in elderly patients are becoming a pressing issue, and patients with cognitive deficits often experience severe impairments in social activities, learning, and memory, which are detrimental to the quality of recovery in elderly patients. Postoperative pain is associated with the development of POCD, and although the mechanisms involved are unclear, it may be related to the body's stress response due to pain, which triggers a state of anxiety and depression. Several studies have confirmed that effective analgesia can reduce the incidence of POCD (Wang et al., 2014). For example, postoperative morphine analgesia inhibits the expression of proinflammatory factors, cell cycle protein D1, in the hippocampus and promotes the expression of anti-inflammatory factors in the central system (Kong et al., 2024). As extracellular vesicles derived from stem cells are also effective in relieving postoperative pain, the use of these extracellular vesicles may be a way to improve postoperative cognitive dysfunction. Abnormally activated microglia act as an innate central immune cell, which can exacerbate inflammatory pain by upregulating inflammatory factors. Extracellular vesicles derived from human umbilical cord mesenchymal stem cells have been shown to alleviate inflammatory neuropathic pain caused by microglia activation (Hua et al., 2022). Neuroinflammation is a common feature of most neurologic dysfunctions and is also strongly associated with postoperative pain. By reducing neuroinflammation it is also effective in reducing postoperative pain and ultimately facilitating recovery from postoperative cognitive dysfunction. For example, miR-124-3p expression in microglial extracellular vesicles was shown to be downregulated in the hippocampus of mice with postoperative pain. Protective effect of postoperative pain production against cognitive impairment by modulating inflammatory polarization of hippocampal microglia in aged mice can be reduced (Kong et al., 2024). In addition, various forms of extracellular vesicles have been shown to reduce signs of neuronal inflammation thereby alleviating neuropathic pain in animal models. For example, extracellular vesicles from synovial MSCs, human placental stem cells, dental pulp stem cells, and bone marrow MSCs have all demonstrated the ability to reduce inflammation to relieve pain in animal models (Shipman et al., 2024). Interestingly, self-metabolically regulated processes (autophagy, pyroptosis) in neuronal cells are also associated with neuropathic pain, with activation of astrocyte autophagy decreasing the pain level and inhibition of autophagy exacerbating the pain, regardless of whether neuropathic pain is at any stage of induction or maintenance. The activation of cellular pyroptosis also exacerbates neuroinflammation and thus neuropathic pain. In contrast, human umbilical cord mesenchymal stem cell-derived extracellular vesicles have been found to attenuate inflammatory neuropathic pain by enhancing autophagy and inhibiting cellular focal death. Therefore, pain alleviation and thus effective reduction of POCD by utilizing the inhibitory neuroinflammatory effects of extracellular vesicles may be a potential approach for the treatment of POCD.

Reducing postoperative sleep disturbances

Postoperative sleep disorders are a common complication after major surgery, and patients usually present with a persistent decrease in the quality and duration of their sleep (Gögenur et al., 2008). Surgery is associated with sleep fragmentation and deprivation, as well as reduced rapid eye movement and slow wave sleep, which results in changes in postoperative brain function and increases the risk of postoperative cognitive decline, and prolonged reductions in postoperative sleep duration or complete sleep deprivation have been shown to result in cognitive deficits (Sipilä and Kalso, 2021). Therefore, early identification and intervention of sleep disorders may be effective in reducing postoperative cognitive dysfunction, ultimately improving prognosis and shortening hospital stay (Shokri-Kojori et al., 2018; Bah et al., 2019). In terms of mechanisms, postoperative sleep disturbances can lead to amyloid plaque accumulation, tau protein diffusion, increased neuroinflammation, and increased blood-brain barrier permeability leading to postoperative cognitive decline (Gu and Zhu, 2021). Modulation of these processes may be a pathway to reversing postoperative cognitive deficits. Extracellular vesicles are important mediators of the transfer of active substances and genetic information between cells, and are involved in the development of sleep disorders and their subsequent resultant cognitive deficits by increasing the formation of amyloid plaques, transmitting tau proteins, modulating neuroinflammation, and increasing the permeability of the blood-brain barrier (Gu and Zhu, 2021). For example, inhibition of total extracellular vesicular secretion secretion *in vivo* decreases AD-like pathological processes, but the mechanisms involved in this process still need to be refined (Dinkins et al., 2014). Plasma extracellular vesicles obtained from sleep-rhythm-disordered mice can act as a bridge between

peripheral clock-control genes and central rhythms and transmit the effects of circadian rhythm disruption to target organs, thereby disrupting end-organ homeostasis (Khalyfa et al., 2017). In terms of direct action, extracellular vesicles may be proteins that directly regulate signaling pathways or regulate proteins involved in signaling pathways or key enzymes. However, the specific molecular mechanisms behind these processes are still debatable. With the advantage that extracellular vesicle intervention and mediated miRNA modulation can reduce neurotoxic proteins produced by sleep disorders, extracellular vesicles, a nano-delivery pathway, may in the future provide new insights into the pathomechanisms and treatment of POCD. An *in vitro* study, for example, found that extracellular vesicles derived from N2a cells enhance Aβ uptake into microglia *via* their surface sphingolipids and ultimately reduce amyloid plaque formation (Perez-Gonza et al., 2012; An et al., 2013). Under hypoxic conditions, extracellular vesicles will help prevent and treat abnormally elevated Aβ levels caused by sleep disorders. In conclusion, sleep disorders are likely to be involved in the pathogenesis of postoperative cognitive impairment and increase the risk of postoperative dementia. And due to the advantages of extracellular vesicles in terms of reduced immunogenicity and better targeting. Delivery of therapeutic biomolecules to target cells *via* extracellular vesicles to correct physiological dysfunction is a potential therapeutic strategy for treating brain disorders characterized by exogenous disturbances (e.g., surgery, trauma).

Regulates the microecology of the body

Increased permeability of the blood-brain barrier in the postoperative period is the main pathologic mechanism of POCD (Wang et al., 2017). During surgery, the integrity of the blood-brain barrier (BBB) may be compromised, allowing harmful substances normally blocked by the barrier to enter the brain. This may lead to inflammation and brain cell damage, which ultimately induces the development of POCD (Keshavarz et al., 2021). Specifically, the entry of harmful substances triggers microglia activation, which in turn promotes the secretion of pro-inflammatory factors, which in turn exacerbates BBB damage, resulting in a vicious cycle of inflammation and neurodegeneration (Wang Y. et al., 2019). In fact, the factors associated with BBB permeability impairment are not only related to the gastrointestinal tract's communication with brain centers. The importance of the microbiome-gut-brain axis in central system disorders has gained prominence over the past 2 decades (Iyaswamy et al., 2023). It has been shown that alterations in gut flora reduce expression of tight junction proteins, leading to BBB leakage (Luo et al., 2021; Wen et al., 2020). Thus, surgically induced intestinal mucosal injury impairs the intestinal mucosal barrier function, allowing toxic metabolites and bacteria to enter the somatic circulation, which in turn enters the central system through the compromised BBB (Yang et al., 2023). Surgical and anesthetic procedures may alter the composition of the gut microbiota. Indeed, the gut microbiota of older mice with postoperative cognitive dysfunction was significantly different from that of normal mice (Zhang Sh et al., 2023). Changes in the abundance of various bacterial species and their metabolites before and after surgery may be associated with postoperative cognitive impairment (Zhang et al., 2024; Ren et al., 2024; Tsigalou et al., 2023). For example, increased abundance of pro-inflammatory gut microbiota triggers and worsens the systemic inflammatory response, promotes neuronal cell injury and inhibitory processes on neuroautophagy, and influences anti-inflammatory extracellular vesicle production and circulation, which collectively play a role in the onset and progression of cognitive deficits in the postoperative period. Interestingly, secretion of extracellular vesicles by some specific beneficial intestinal flora can also effectively reverse this process, e.g., mucinophilic Ackermannia-derived extracellular vesicles can ameliorate intestinal I/R-induced POCD in a mouse model by maintaining intestinal and BBB integrity. Therefore, analyzing perioperative changes in extracellular vesicles released by gut flora and exploring interventions based on these alterations could provide a promising approach to the prevention and management of neurocognitive disorders.

Extracellular vesicles of bacterial origin are important mediators of communication between different bacterial colonies as well as between colonies and hosts. These vesicles are mainly composed of lipopolysaccharides, lipids and proteins (Díaz-Garrido et al., 2021). They play an important role in maintaining the integrity of the host intestinal mucosal barrier, supporting the normal function of the host immune system, and regulating substance metabolism (Díez-Sainz et al., 2022; Tan et al., 2022). Changes in bacterial flora produce different types of extracellular vesicles, and dysbiosis can lead to abnormalities in these vesicles, which can have a more variable impact on host cognitive function. In a preclinical study, it was demonstrated that transferring fecal microbes from older to younger mice increases the likelihood of cognitive deficits and that such vesicles cause hippocampal damage (Lee et al., 2020). In addition, postoperative cognitive deficits may also be associated with an increase in pro-inflammatory bacteria, such as extracellular vesicles from the intestinal flora of AD patients that activate GSK-3β proteins, induce tau protein phosphorylation, and enhance the secretion of inflammatory cytokines in the hippocampus (Wei et al., 2020). All these processes suggest that extracellular vesicles are involved in the gut-brain axis to induce the onset and progression of POCD. Therefore, by interfering with the occurrence and release of extracellular vesicles may be a potential way to regulate the organism's microecology to effectively ameliorate POCD.

Reduced neurotoxicity of anesthetics

Anesthetic neurotoxicity is defined as damage to the structure and function of the nervous system caused by exposure to anesthetic drugs (Campo et al., 2024). *In vivo* experimental models have shown neurobiological changes and lifelong cognitive deficits following exposure to anesthetics. It is possible that anesthetics interfere with the proliferation and differentiation of immature neurons and that neurogenic changes can be observed after exposure to different anesthetics (including isoproterenol, isoflurane, and sevoflurane) in young and adult brains (Fang et al., 2012). For inducing postoperative cognitive dysfunction, this may be due to the fact that anesthetics can induce changes in the blood-brain barrier and the cerebrovascular system by altering the neuronal network of the brain for long-term neurocognitive dysfunction (Zanghi and Jevtovic-Todorovic, 2017). As the most widely used anesthetics, exposure to isoproterenol and sevoflurane will often exacerbate postoperative

cognitive impairment in patients (Lv et al., 2017). All currently used intravenous and inhaled general anesthetics produce anesthetic and sedative effects by binding to GABA receptors and/or N-methyl-D-aspartate receptors. This can lead to minor neurocognitive deficits in patients after surgery, such as postoperative delirium. First, this is because with the use of perioperative anesthetic drugs GABAA receptors are potentiated, which alters the opening of intracellular ion channels affecting the inflow and outflow of chloride ions leading to excessive neuronal inhibition that persists long after the drugs have been eliminated (Orser and Wang, 2019). Second, proinflammatory cytokines released during surgery also induce cell surface overexpression of extrasynaptic GABAA receptors. Both mechanisms may lead to permanent neurocognitive deficits in patients after surgery (Orser and Wang, 2019). Perioperative neurocognitive deficits may carry a serious risk of developing dementia, memory loss, loss of concentration and even death (Rudolph and Marcantonio, 2011). Therefore, intervening and ameliorating the neurotoxicity of anesthetics may be a necessary part of preventing POCD. Biomolecules that control adverse reactions to anesthetic drugs may help reduce the development of postoperative brain dysfunction, study finds. It was found that extracellular vesicles are capable of transporting active ingredients that represent the extracellular microenvironment, and that all cell types can communicate with each other through this pathway, exchanging molecules needed to maintain homeostasis. In this case, any alteration affecting each cell type can to a large extent be compensated by the other cell types, being able to provide the tissue with all the effective molecules needed to overcome the perturbation or to induce specific epigenetic modifications that allow the synthesis of molecules that restore the *in vivo* equilibrium or even prevent it from being altered (Campo et al., 2024). Of course, this does not preclude the transport of extracellular vesicles from providing the deleterious molecules needed to promote perturbation. In the *in vitro* circulation, extracellular vesicles can exert a protective effect against anesthetic-dependent adverse effects by transmitting overexpression of miR-34a and miR-124 in the central system. YRNA1 in circulating extracellular vesicles is significantly overexpressed in the postanesthetic state, and its upregulation correlates closely with the ability of the central system to compensate for anesthetic-induced inflammatory effects. In clinical practice, the incidence of POCD is higher in elderly patients anesthetized with sevoflurane (Ishii et al., 2016). This may be due to the higher utilization of sevoflurane compared to isoproterenol. It has been found that sevoflurane inhalation anesthesia promotes POCD in a dose-dependent manner, and that inhalation of sevoflurane can cause cognitive deficits and behavioral abnormalities in postoperative patients, accelerating the onset and progression of POCD (Cheng et al., 2018). This may be due to the fact that sevoflurane anesthesia produces associated extracellular vesicles involved in the activation of inflammatory and apoptotic neuronal pathways in the central system of the organism (Cui et al., 2018). For example, sevoflurane-induced associated extracellular vesicles can deliver miR-584-5p to promote the onset and progression of delirium by targeting BDNF to regulate Caspase3 and BDNF/TrkB signaling.

In addition, anesthetic drugs disrupt the balance of the gut microbiota through direct effects on the microbiota, potentially leading to dysbiosis, which in turn affects central neurocognitive function through the gut-brain axis (Iyaswamy et al., 2023; Liu et al., 2022). In addition, the effects of different anesthetic drugs and anesthetic methods on the microbiota may vary. Opioids can have significant effects on the gut microbiota that can lead to disruption of microbial and host metabolism. In addition, anesthesia-induced dysbiosis of the intestinal flora can lead to significant changes in the composition of extracellular vesicles and alter the ability of extracellular vesicles to enter the bloodstream, which ultimately affects systemic energy metabolism and thus the central system, which may be a potential mechanism for surgical damage to the intestinal microbial homeostasis leading to the development of POCD (Huh et al., 2019; Saeedi et al., 2019). Indeed, extracellular vesicles from different flora sources exert different effects on the host, which also include a protective effect on central cognitive functions (Diaz-Garrido et al., 2022). Therefore, implementation of appropriate preoperative and postoperative interventions to minimize damage to the microbiota ecosystem and repair disturbed microecology may be a future strategy for POCD treatment in the case of cognitive deficits caused by anesthetic drugs or surgery. Certainly, preventing or ameliorating the onset and progression of postoperative cognitive deficits by means of intervening on extracellular vesicles released after microecological disturbances, including inhibition of deleterious vesicles and promotion of protective vesicles (e.g., preoperative intestinal implantation of probiotic bacteria) may be an exploratory avenue of POCD nanotherapeutics.

Advantages of extracellular vesicles in modulating postoperative cognitive dysfunction

Biomolecular transfer function

There is growing evidence that circulating extracellular vesicles contain a large number of multifunctional RNAs (e.g., miRNAs, lncRNAs, circRNAs), which explains their key role in cellular communication. In this context, extracellular vesicles are considered important messengers that can transport a wide range of molecules at once, including cytokines, growth factors, various proteins, and even nucleic acids, thus determining their efficient delivery for transfer from 1 cell to another (Campo et al., 2024). These transported molecules may represent all the major components of the extracellular microenvironment, and all the biomolecular types that maintain homeostasis in the organism can communicate with each other through this mechanism, exchanging molecules required for correct homeostasis. Delivery of therapeutic RNA to target cells *via* extracellular vesicles to correct protein dysfunction is a potential therapeutic strategy for the treatment of brain disorders due to the low immunogenicity and good targeting properties of extracellular vesicles (Duan et al., 2021). For example, extracellular vesicle transferable miRNAs modulate the neuroinflammatory cascade response, Aβ production, and neuronal apoptosis to inhibit the development of postoperative cognitive dysfunction (Gu and Zhu, 2021). Decreased S-100β protein, neuron-specific enolase, and glial cell line-derived neurotrophic factor in the peripheral circulation are strongly associated with the development of POCD (McDonagh et al., 2010). These proteins may be modified and

increased or decreased through the extracellular vesicle pathway to accelerate recovery from postoperative cognitive impairment. Extracellular vesicle-mediated circRNAs can also be involved in the onset and progression of neurological diseases (Chen et al., 2016). For example, the pathogenesis of POCD may be related to abnormal levels of exosome-delivered circRNA-089763 caused by perioperative stimuli.

Furthermore, elucidating the mechanisms by which postoperative extracellular vesicle changes control neuroinflammation is critical for developing therapeutic strategies targeting postoperative neurodegeneration (Prinz and Priller, 2014; Gao and Hong, 2008; Izquierdo-Altarejos et al., 2020). In this context, extracellular vesicles have emerged as key mediators mediating circulatory and central inflammatory changes, facilitating the transfer of inflammatory bioactive molecules between cells and the regulation of immune responses. Extracellular vesicles act as carriers of specific cargoes, including microRNAs, proteins, and lipids, and are capable of modulating peripheral and central immune responses (Vella et al., 2016; Gallego et al., 2022). For example, extracellular vesicles from activated microglia can exacerbate central inflammation by transferring pro-inflammatory molecules to neighboring cells, while other studies have shown that extracellular vesicles can transport inflammation-suppressing substances to control excessive immune responses (Izquierdo-Altarejos et al., 2023).

Cell-free nanotherapeutic pathways

For the treatment of POCD, extracellular vesicles of specialized cellular origin may be good cell-free nanotherapeutic avenues (Figure 2). Compared to liposomes, extracellular vesicles have excellent targeting and alteration of pathophysiological processes due to their specific membrane proteins and contained biomolecules, while their low immunogenicity and biohazardous nature may be of greater value for use in purely cell-based therapies. For example, MSCs are pluripotent cells with potential regenerative repair potential, mainly by secreting growth factors and cytokines for paracrine effects. Extracellular vesicles with cellular repair function are one of their important paracrine factors, which may be a potential cell-free nanotherapeutic for the treatment of CNS diseases. Recent reports suggest that extracellular vesicles can prevent neuroinflammatory properties in the center (Zhuang et al., 2011). For example, MSC-derived extracellular vesicles prevented postoperative hippocampal tissue damage and significantly reduced serum NSE and S100-β levels. Extracellular vesicles derived from human mesenchymal stem cells have been shown to have anti-inflammatory effects on microglia in perinatal brain injury (Thomi et al., 2019) and the number of activated inflammatory microglia was significantly reduced compared to the control group (Zhuang et al., 2011). Similar to this result, adipose stem cell-derived extracellular vesicles inhibited microglia activation and prevented neuroinflammation by inhibiting NF-κB and MAPK pathways (Yang et al., 2017). Extracellular vesicles of antler MSCs can help improve cognitive function in rats undergoing extracorporeal circulation surgery by mediating the TLR2/TLR4 signaling pathway, which may be due to the fact that extracellular vesicles of AMSCs inhibit neuronal apoptotic ability in rats undergoing extracorporeal circulation surgery. In fact, in addition to stem cell-derived extracellular vesicles, more cell-derived extracellular vesicles exist to improve postoperative cognitive dysfunction, such as plant-derived extracellular vesicles (Nemati et al., 2022). Ginseng-derived extracellular vesicles were found to have special proteins that nourish nerve tissues to repair damaged neurons (Li et al., 2023). In contrast, extracellular vesicles of poplar origin function to inhibit the systemic inflammatory response (Shao et al., 2023). This may also be a potential tool to improve postoperative cognitive dysfunction.

Penetrating the blood-brain barrier to target cells

In fact, due to their phospholipid bilayer structure, extracellular vesicles can penetrate all current biological barriers, such as the blood-testis barrier, the blood-brain barrier, and the placental barrier. In the case of the blood-brain barrier, the mechanism by which extracellular vesicles cross the blood-brain barrier is through receptor-mediated endocytosis, e.g., extracellular vesicles derived from neural stem cells interact with brain endothelial cells *via* heparan sulfate proteoglycans and ultimately cross the blood-brain barrier through endocytosis (Yin et al., 2025). For the treatment of central diseases, the penetration rate of the blood-brain barrier of a drug is a key indicator for evaluating drug efficacy. This may not be necessary for extracellular vesicles, such as those administered intranasally, which can be rapidly transported to the mouse brain and taken up by microglia. It can also be engineered to modify its membrane proteins to enhance its central targeting ability. It has been found that receptor-mediated transcytosis is widespread at certain receptors (e.g., TfR, low-density lipoprotein receptor (LDLR), and insulin receptor (INSR)) on brain endothelial cells. Utilizing these receptor pathways, enhancement of extracellular vesicle penetration into the BBB can be designed. For example, extracellular vesicles harboring TfR ligands cross the BBB *via* receptor-mediated transcytosis (Wang et al., 2024). In addition, in clinical work, peripheral blood samples are easier to collect and accept than other samples such as cerebrospinal fluid and brain tissue, and extracellular vesicles in the extracorporeal circulation may be excellent diagnostic markers for central diseases. It has been found that brain tissue can release extracellular vesicles, which can carry non-coding RNAs (ncRNAs, microRNAs, circRNAs) and enter the circulation through the blood-brain barrier. Especially for circRNA, it is mainly transported in the form of extracellular vesicles and communicates between central and peripheral circulation through the blood-brain barrier. (Li et al., 2015). circRNA may play a key role in neurological disorders (Zhao et al., 2016; Sekar et al., 2018). For example, circRNA-associated ceRNA networks have been characterized in the susceptible brains of mice with accelerated aging, and these networks may influence the diagnosis and treatment of AD in the near future (Zhang et al., 2017). Furthermore, dysfunction of the extracellular vesicle-mediated circRNA-miRNA-mRNA regulatory system appears to represent an important aspect of epigenetic control of human CNS pathogenic genes. And POCD and AD have similar pathogenesis (Hu et al., 2010). Thus, the potential for the diagnostic and therapeutic role of extracellular vesicles in the treatment of central diseases is great.

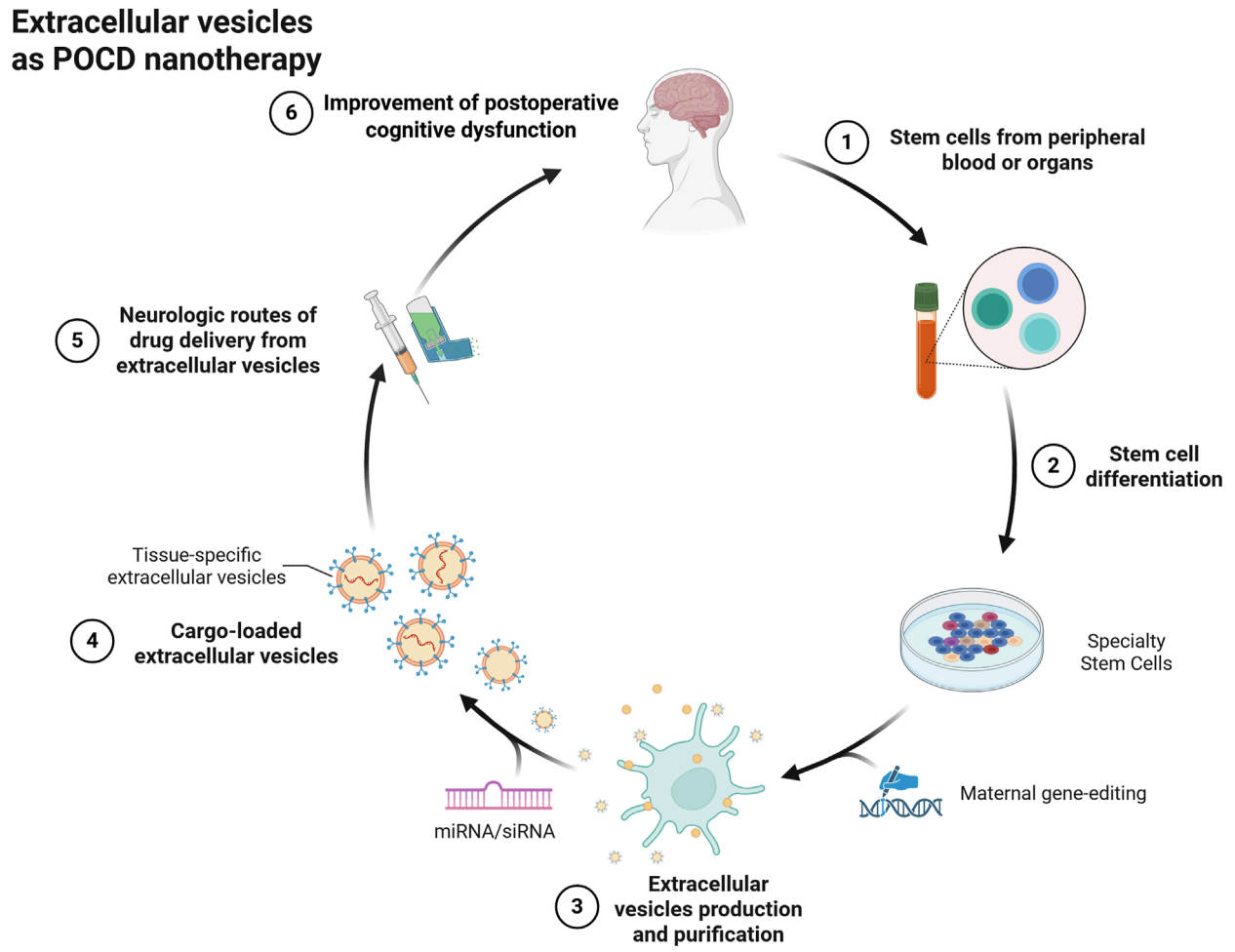

FIGURE 2
Extracellular vesicles as POCD nanotherapeutics.

Communicating whole body holistic conditioning

Extracellular vesicles act as mediators for communication between the periphery and the center, and pathophysiological changes in the peripheral circulation can interact through extracellular vesicles. Extracellular vesicles play a key role in intercellular and interorgan communication and influence disease progression. Peripheral immune signaling can influence brain function through extracellular vesicle-mediated communication, which can affect barrier function and neuroinflammatory responses. Extracellular vesicles contain key mediators in the immune system (Budnik et al., 2016). These mediators activate the peripheral inflammatory response to induce the production of pro-inflammatory factors, which, after blood transport and penetration of the disrupted blood-brain barrier, can enter the center and exacerbate the neuroinflammatory process in neurological disorders. Second, proinflammatory factors can also be transported directly to the center by extracellular vesicles, inducing a central inflammatory response (Cabrera-Pastor, 2024). In addition, there is evidence that extracellular vesicles play a role in facilitating communication between the brain and adipose tissue. Adipose tissue produces many bioactive substances that are involved in interactions with peripheral organs and the central system through extracellular vesicles. Adipokines transported by extracellular vesicles modulate neuroinflammation and oxidative stress, which have been implicated in central nervous system disorders. In addition, adipose tissue is an important source of circulating noncoding RNAs, many of which are carried by extracellular vesicles and are involved in regulating homeostasis in the peripheral and central systems (Hajer et al., 2008). For chronic diseases resulting in systemic pathological microchanges can also be transmitted centrally *via* extracellular vesicles, inducing atrophy and aging of neural tissues, e.g., POCD. POCD is also an important comorbidity and complication of diabetes (Biessels and Whitmer, 2020). Diabetic patients are at a significantly increased risk of developing cognitive dysfunction after surgery (Thourani et al., 1999). This may be related to diabetes modulating cognitive function and changes in brain structure, such as diabetics having lower total brain volume, more infarcts, greater white matter high signal volume, and lower gray matter volume (Callisaya et al., 2019). In contrast, extracellular vesicles may be involved in inducing

changes in the brain tissue of diabetic patients, possibly because they transmit signals of circulating chronic inflammation and abnormal glucose metabolism that lead to neurological tissue lesions (Wang M. et al., 2019). For example, glucagon signaling pathways have been shown to be associated with neuroinflammation, and these signals can also be transmitted by extracellular vesicles (van Harten et al., 2012; Gonçalves et al., 2016; van Praag et al., 2002; Zhang L. et al., 2023). And neuroinflammation has become an important cause of aging and cognitive decline. In addition, gut microbes play a role in the production of bioactive substances, such as extracellular vesicles (Mhanna et al., 2024; Zhai et al., 2024). These extracellular vesicles can enter the bloodstream and affect the central nervous system, subsequently affecting host cognition and behavior. The perioperative period is characterized by disturbances in the intestinal flora due to slow gastrointestinal motility and metabolic disturbances in the body, while the extracellular vesicles produced by the mother are altered, and these altered circulating extracellular vesicles ultimately affect central cognitive functions (Huang et al., 2025).

Discussion and outlook

Perioperative neurocognitive dysfunction is a major problem affecting the health of the population, compromising postoperative recovery and increasing the financial burden on patients. As survival life expectancy increases, POCD is a growing public health problem due to the need for surgery in many frail older adults, with approximately 20%–50% of people over the age of 60 years developing POCD after major surgery (Avidan et al., 2017; Vlisides et al., 2019). The pathogenesis of POCD involves a variety of neurobiological processes, including cerebrovascular dysfunction, neural tissue damage, neuroinflammation, and brain tissue alterations (Vlisides et al., 2019). For example, preoperative dexamethasone administration before cardiac surgery significantly reduced the incidence of postoperative neurocognitive deficits in patients. The mechanism of this protective effect is most likely through the reduction of the neuroinflammatory response (Glumac et al., 2017). This emphasizes the key role of neuroinflammation in the development of cognitive impairment. Therefore, ways to reduce neuroinflammation may be the most currently recognized effective way to improve POCD. However, at present, relying solely on drugs such as compounds that are not suitable for most elderly patients who need prophylactic or anti-infective drugs such as dexamethasone and immunosuppressants may have numerous side effects. These medications also fail to meet the practical requirements of sustained postoperative slowing of the inflammatory state in order to effectively prevent POCD. As far as extracellular vesicles are concerned, the role of extracellular vesicles in slowing down inflammation is more modest (Noonin and Thongboonkerd, 2021). It is also more suitable for perioperative maintenance medication. First, for the process of postoperative peripheral inflammation inducing central inflammation, blocking the mediator function of extracellular vesicles or utilizing extracellular vesicles can suppress peripheral immune activation which is also the initial state (Arabpour et al., 2021). Second, interfering with inflammatory activation of microglia as well as promoting the release of anti-inflammatory extracellular vesicles from the hippocampus through specific modifications targeting extracellular vesicles in the center (Qin et al., 2024; Xin et al., 2017; Kong et al., 2024; Xin et al., 2022; Feng et al., 2017). Finally, the regenerative function exhibited by extracellular vesicles of special origin contributes to the repair of nerve tissue damage caused by neuroinflammation (Lang et al., 2023). All these modalities suggest the great potential of extracellular vesicles for the prevention and treatment of POCD. For molecules of the delivery signaling pathway of extracellular vesicles, a role involving gut-brain communication could be interesting. By utilizing extracellular vesicles released by the cells may help to improve intestinal motility while improving central cognitive function (Diaz-Garrido et al., 2021). In fact, in elderly patients, the postoperative period is often accompanied by slow intestinal motility leading to the accumulation of harmful substances (metabolic wastes released by bacteria) in the intestines and into the bloodstream affecting central cognitive functions (Kim et al., 2024). Currently, the diagnosis of POCD is still based on the description of the patient's symptoms, assessment of mental status, and clinical behaviors, which are complex and take time to evaluate, especially in older patients with preoperative psychiatric disorders (Needham et al., 2017; Kapoor et al., 2019). This greatly delays POCD diagnosis and treatment. Recent studies have found that diseased tissue from the brain can release extracellular vesicles and can cross the blood-brain barrier into the circulation. These extracellular vesicles may be a new diagnostic marker for POCD (Li et al., 2018; Otero-Ortega et al., 2019). Currently there are few effective treatments for POCD, and improving postoperative pain is considered one of them, and opioids and NSAIDs are commonly used clinically to relieve pain caused by postoperative period (Ho et al., 2024). However, continued opioid use increases the risk of serious adverse effects, such as drug addiction, opioid tolerance, and opioid-induced pain hypersensitivity. It should be noted that certain miRNAs carried by extracellular vesicles have sustained analgesic effects (Hua et al., 2022). However, since miRNAs can act on different target genes and the expression of a gene can be regulated by multiple miRNAs. This suggests that interventions based on targeting the activity and/or treatment of individual genes have a limited effect. Thus, the use of multiple extracellular vesicles with analgesic effect miRNAs or the use of extracellular vesicles implanted with multiple miRNAs, *etc.*, may be considered. Indeed, the successive multiple injuries induced by surgery require a multipronged therapeutic approach to ameliorate cognitive deficits, which includes systemic modulation using extracellular vesicles as well as reduction of the neurotoxic effects of anesthetic drugs (Cui et al., 2018). Of course, whether the use of multiple extracellular vesicles poses biosafety or potential complications needs to be further explored, for example, most of the extracellular vesicles that are administered *via* blood vessels or orally are concentrated in the liver and kidneys, and it is still unknown whether the metabolism of these extracellular vesicles by the liver will impair liver and kidney functions. In fact, administration *via* intranasal or intrathecal administration may be an effective way to avoid the above or even to rapidly affect the center (Yang et al., 2020).

Summarize

Extracellular vesicles as a potential tool for the treatment of postoperative cognitive dysfunction. Extracellular vesicles may be effective in preventing the extent of postoperative neurocognitive deficits and contribute to the treatment of postoperative neural tissue damage by interfering with pathological mechanisms of postoperative cognitive dysfunction, such as inhibiting inflammation and repairing nerve damage. In particular, RNAs transmitted by extracellular vesicles modulate the systemic neuroinflammatory cascade response, neuronal injury, and signaling communication in systemic microecology. This suggests that the role of extracellular vesicles in the pathogenesis associated with postoperative cognitive dysfunction could provide an avenue for their role as potential biomarkers and therapeutic targets for neurocognitive deficits induced by surgical or anesthetic drugs. Continuing to elucidate the exact pathomechanisms of POCD, studies on the mechanisms of reliable action of extracellular vesicles in postoperative cognitive impairment, and how to use extracellular vesicles for rapid central onset of action may be the future direction of research in postoperative cognitive impairment. Future work should focus on how to obtain extracellular vesicles that have a significant effect and are conveniently sourced. For the present, particular attention could be paid to changes in the state of extracellular vesicles and intravesicular biomolecules in the presence of postoperative cognitive deficits for early diagnosis and intervention of the disease.

Author contributions

YZ: Methodology, Writing – review and editing. ZY: Investigation, Writing – original draft. ZZ: Writing – original draft. SF: Methodology, Writing – review and editing. HX: Writing – review and editing.

Funding

The author(s) declare that no financial support was received for the research and/or publication of this article.

Acknowledgments

All figures are created with BioRender.com.

Conflict of interest

The authors declare that the research was conducted in the absence of any commercial or financial relationships that could be construed as a potential conflict of interest.

Generative AI statement

The author(s) declare that no Generative AI was used in the creation of this manuscript.

Publisher's note

References

An, K., Klyubin, I., Kim, Y., Jung, J. H., Mably, A. J., O'Dowd, S. T., et al. (2013). Exosomes neutralize synaptic-plasticity-disrupting activity of Aβ assemblies *in vivo*. *Mol. Brain* 6, 47. doi:10.1186/1756-6606-6-47

Andrzejewska, A., Dabrowska, S., Lukomska, B., and Janowski, M. (2021). Mesenchymal stem cells for neurological disorders. *Adv. Sci. (Weinh)* 8 (7), 2002944. doi:10.1002/advs.202002944

Arabpour, M., Saghazadeh, A., and Rezaei, N. (2021). Anti-inflammatory and M2 macrophage polarization-promoting effect of mesenchymal stem cell-derived exosomes. *Int. Immunopharmacol.* 97, 107823. doi:10.1016/j.intimp.2021.107823

Author Anonymous (2024). Correction to "modulating neuroinflammation and cognitive function in postoperative cognitive dysfunction *via* CCR5-GPCRs-Ras-MAPK pathway targeting with microglial EVs". *CNS Neurosci. Ther.* 30 (9), e70063. doi:10.1111/cns.70063

Avidan, M. S., Maybrier, H. R., Abdallah, A. B., Jacobsohn, E., Vlisides, P. E., Pryor, K. O., et al. (2017). Intraoperative ketamine for prevention of postoperative delirium or pain after major surgery in older adults: an international, multicentre, double-blind, randomised clinical trial. *Lancet* 390 (10091), 267–275. doi:10.1016/S0140-6736(17)31467-8

Bah, T. M., Goodman, J., and Iliff, J. J. (2019). Sleep as a therapeutic target in the aging brain. *Neurotherapeutics* 16 (3), 554–568. doi:10.1007/s13311-019-00769-6

Berger, M., Oyeyemi, D., Olurinde, M. O., Whitson, H. E., Weinhold, K. J., Woldorff, M. G., et al. (2019). The INTUIT study: investigating neuroinflammation underlying postoperative cognitive dysfunction. *J. Am. Geriatr. Soc.* 67 (4), 794–798. doi:10.1111/jgs.15770

Biessels, G. J., and Whitmer, R. A. (2020). Cognitive dysfunction in diabetes: how to implement emerging guidelines. *Diabetologia* 63 (1), 3–9. doi:10.1007/s00125-019-04977-9

Bishawi, M., Hattler, B., Almassi, G. H., Spertus, J. A., Quin, J. A., Collins, J. F., et al. (2018). Preoperative factors associated with worsening in health-related quality of life following coronary artery bypass grafting in the randomized On/Off bypass (ROOBY) trial. *Am. Heart J.* 198, 33–38. doi:10.1016/j.ahj.2017.12.014

Boodhwani, M., Rubens, F. D., Wozny, D., Rodriguez, R., Alsefaou, A., Hendry, P. J., et al. (2006). Predictors of early neurocognitive deficits in low-risk patients undergoing on-pump coronary artery bypass surgery. *Circulation* 114 (1 Suppl. l), I461–I466. doi:10.1161/CIRCULATIONAHA.105.001354

Brier, M. R., Gordon, B., Friedrichsen, K., McCarthy, J., Stern, A., Christensen, J., et al. (2016). Tau and Aβ imaging, CSF measures, and cognition in alzheimer's disease. *Sci. Transl. Med.* 8 (338), 338ra66. doi:10.1126/scitranslmed.aaf2362

Budnik, V., Ruiz-Cañada, C., and Wendler, F. (2016). Extracellular vesicles round off communication in the nervous system. *Nat. Rev. Neurosci.* 17 (3), 160–172. doi:10.1038/nrn.2015.29

Butz, M., Meyer, R., Gerriets, T., Sammer, G., Doerr, J. M., El-Shazly, J., et al. (2022). Increasing preoperative cognitive reserve to prevent postoperative delirium and postoperative cognitive decline in cardiac surgical patients (INCORE): study protocol for a randomized clinical trial on cognitive training. *Front. Neurol.* 13, 1040733. doi:10.3389/fneur.2022.1040733

Cabrera-Pastor, A. (2024). Extracellular vesicles as mediators of neuroinflammation in intercellular and inter-organ crosstalk. *Int. J. Mol. Sci.* 25 (13), 7041. doi:10.3390/ijms25137041

Callisaya, M. L., Beare, R., Moran, C., Phan, T., Wang, W., and Srikanth, V. K. (2019). Type 2 diabetes mellitus, brain atrophy and cognitive decline in older people: a longitudinal study. *Diabetologia* 62 (3), 448–458. doi:10.1007/s00125-018-4778-9

Campo, A., Aliquò, F., Velletri, T., Scuruchi, M., Avenoso, A., Campo, G. M., et al. (2024). Involvement of selected circulating ncRNAs in the regulation of cognitive dysfunction induced by anesthesia. *Gene* 928, 148806. doi:10.1016/j.gene.2024.148806

Chen, B. J., Mills, J. D., Takenaka, K., Bliim, N., Halliday, G. M., and Janitz, M. (2016). Characterization of circular RNAs landscape in multiple system atrophy brain. *J. Neurochem.* 139 (3), 485–496. doi:10.1111/jnc.13752

Chen, N., Chen, X., Xie, J., Wu, C., and Qian, J. (2019). Dexmedetomidine protects aged rats from postoperative cognitive dysfunction by alleviating hippocampal inflammation. *Mol. Med. Rep.* 20 (3), 2119–2126. doi:10.3892/mmr.2019.10438

Chen, Y., Zhang, P., Lin, X., Zhang, H., Miao, J., Zhou, Y., et al. (2020). Mitophagy impairment is involved in sevoflurane-induced cognitive dysfunction in aged rats. *Aging (Albany NY)* 12 (17), 17235–17256. doi:10.18632/aging.103673

Cheng, Y., Jiang, Y., Zhang, L., Wang, J., Chai, D., Hu, R., et al. (2018). Mesenchymal stromal cells attenuate sevoflurane-induced apoptosis in human neuroglioma H4 cells. *BMC Anesthesiol.* 18 (1), 84. doi:10.1186/s12871-018-0553-1

Cibelli, M., Fidalgo, A. R., Terrando, N., Ma, D., Monaco, C., Feldmann, M., et al. (2010). Role of interleukin-1beta in postoperative cognitive dysfunction. *Ann. Neurol.* 68 (3), 360–368. doi:10.1002/ana.22082

Conner, J. M., Franks, K. M., Titterness, A. K., Russell, K., Merrill, D. A., Christie, B. R., et al. (2009). NGF is essential for hippocampal plasticity and learning. *J. Neurosci.* 29 (35), 10883–10889. doi:10.1523/JNEUROSCI.2594-09.2009

Cui, R. S., Wang, K., and Wang, Z. L. (2018). Sevoflurane anesthesia alters cognitive function by activating inflammation and cell death in rats. *Exp. Ther. Med.* 15 (5), 4127–4130. doi:10.3892/etm.2018.5976

Deng, X., Sun, T., Zhao, D., Sana, S., and Li, W. (2023). Stellate ganglion block potentially ameliorates postoperative cognitive decline in aged rats by regulating the neuroendocrine response to stress. *Heliyon* 9 (3), e14337. doi:10.1016/j.heliyon.2023.e14337

Díaz-Garrido, N., Badia, J., and Baldomà, L. (2021). Microbiota-derived extracellular vesicles in interkingdom communication in the gut. *J. Extracell. Vesicles* 10 (13), e12161. doi:10.1002/jev2.12161

Diaz-Garrido, N., Badia, J., and Baldomà, L. (2022). Modulation of dendritic cells by microbiota extracellular vesicles influences the cytokine profile and exosome cargo. *Nutrients* 14 (2), 344. doi:10.3390/nu14020344

Diaz-Garrido, N., Cordero, C., Olivo-Martinez, Y., Badia, J., and Baldomà, L. (2021). Cell-to-Cell communication by host-released extracellular vesicles in the gut: implications in health and disease. *Int. J. Mol. Sci.* 22 (4), 2213. doi:10.3390/ijms22042213

Díez-Sainz, E., Milagro, F. I., Riezu-Boj, J. I., and Lorente-Cebrián, S. (2022). Effects of gut microbiota-derived extracellular vesicles on obesity and diabetes and their potential modulation through diet. *J. Physiol. Biochem.* 78 (2), 485–499. doi:10.1007/s13105-021-00837-6

Ding, X., Gao, X., Wang, Z., Jiang, X., Lu, S., Xu, J., et al. (2021). Preoperative chronic and acute pain affects postoperative cognitive function mediated by neurotransmitters. *J. Mol. Neurosci.* 71 (3), 515–526. doi:10.1007/s12031-020-01673-x

Dinkins, M. B., Dasgupta, S., Wang, G., Zhu, G., and Bieberich, E. (2014). Exosome reduction *in vivo* is associated with lower amyloid plaque load in the 5XFAD mouse model of alzheimer's disease. *Neurobiol. Aging* 35 (8), 1792–1800. doi:10.1016/j.neurobiolaging.2014.02.012

Dong, B., Wang, C., Zhang, J., Zhang, J., Gu, Y., Guo, X., et al. (2021). Exosomes from human umbilical cord mesenchymal stem cells attenuate the inflammation of severe steroid-resistant asthma by reshaping macrophage polarization. *Stem Cell Res. Ther.* 12 (1), 204. doi:10.1186/s13287-021-02244-6

Duan, L., Xu, L., Xu, X., Qin, Z., Zhou, X., Xiao, Y., et al. (2021). Exosome-mediated delivery of gene vectors for gene therapy. *Nanoscale* 13 (3), 1387–1397. doi:10.1039/d0nr07622h

Esteves, M., Abreu, R., Fernandes, H., Serra-Almeida, C., Martins, P. A. T., Barão, M., et al. (2022). MicroRNA-124-3p-enriched small extracellular vesicles as a therapeutic approach for parkinson's disease. *Mol. Ther.* 30 (10), 3176–3192. doi:10.1016/j.ymthe.2022.06.003

Evered, L., Silbert, B., Knopman, D. S., Scott, D. A., DeKosky, S. T., Rasmussen, L. S., et al. (2018). Recommendations for the nomenclature of cognitive change associated with anaesthesia and Surgery-2018. *Anesthesiology* 129 (5), 872–879. doi:10.1097/ALN.0000000000002334

Fang, F., Xue, Z., and Cang, J. (2012). Sevoflurane exposure in 7-day-old rats affects neurogenesis, neurodegeneration and neurocognitive function. *Neurosci. Bull.* 28 (5), 499–508. doi:10.1007/s12264-012-1260-4

Farag, E., Chelune, G. J., Schubert, A., and Mascha, E. J. (2006). Is depth of anesthesia, as assessed by the bispectral index, related to postoperative cognitive dysfunction and recovery? *Anesth. Analg.* 103 (3), 633–640. doi:10.1213/01.ane.0000228870.48028.b5

Feng, X., Valdearcos, M., Uchida, Y., Lutrin, D., Maze, M., and Koliwad, S. K. (2017). Microglia mediate postoperative hippocampal inflammation and cognitive decline in mice. *JCI Insight* 2 (7), e91229. doi:10.1172/jci.insight.91229

Fong, T. G., Vasunilashorn, S. M., Gou, Y., Libermann, T. A., Dillon, S., Schmitt, E., et al. (2021). Association of CSF alzheimer's disease biomarkers with postoperative delirium in older adults. *Alzheimers Dement. (N Y).* 7 (1), e12125. doi:10.1002/trc2.12125

Gallego, J. J., Fiorillo, A., Casanova-Ferrer, F., Urios, A., Ballester, M. P., Durbán, L., et al. (2022). Plasma extracellular vesicles play a role in immune system modulation in minimal hepatic encephalopathy. *Int. J. Mol. Sci.* 23 (20), 12335. doi:10.3390/ijms232012335

Gan, J., Tu, Q., Miao, S., Lei, T., Cui, X., Yan, J., et al. (2020). Effects of oxycodone applied for patient-controlled analgesia on postoperative cognitive function in elderly patients undergoing total hip arthroplasty: a randomized controlled clinical trial. *Aging Clin. Exp. Res.* 32 (2), 329–337. doi:10.1007/s40520-019-01202-w

Gao, H. M., and Hong, J. S. (2008). Why neurodegenerative diseases are progressive: uncontrolled inflammation drives disease progression. *Trends Immunol.* 29 (8), 357–365. doi:10.1016/j.it.2008.05.002

Gao, X., Lin, C., Feng, Y., You, Y., Jin, Z., Li, M., et al. (2024). Akkermansia muciniphila-derived small extracellular vesicles attenuate intestinal ischemia-reperfusion-induced postoperative cognitive dysfunction by suppressing microglia activation *via* the TLR2/4 signaling. *Biochim. Biophys. Acta Mol. Cell Res.* 1871 (2), 119630. doi:10.1016/j.bbamcr.2023.119630

Ge, X., Guo, M., Hu, T., Li, W., Huang, S., Yin, Z., et al. (2020). Increased microglial exosomal miR-124-3p alleviates neurodegeneration and improves cognitive outcome after rmTBI. *Mol. Ther.* 28 (2), 503–522. doi:10.1016/j.ymthe.2019.11.017

Glumac, S., Kardum, G., Sodic, L., Supe-Domic, D., and Karanovic, N. (2017). Effects of dexamethasone on early cognitive decline after cardiac surgery: a randomised controlled trial. *Eur. J. Anaesthesiol.* 34 (11), 776–784. doi:10.1097/EJA.0000000000000647

Gögenur, I., Wildschiøtz, G., and Rosenberg, J. (2008). Circadian distribution of sleep phases after major abdominal surgery. *Br. J. Anaesth.* 100 (1), 45–49. doi:10.1093/bja/aem340

Gonçalves, J. T., Schafer, S. T., and Gage, F. H. (2016). Adult neurogenesis in the hippocampus: from stem cells to behavior. *Cell* 167 (4), 897–914. doi:10.1016/j.cell.2016.10.021

Gu, X., and Zhu, J. (2021). Roles of exosomes and exosomal MicroRNAs in postoperative sleep disturbance. *Nat. Sci. Sleep.* 13, 1363–1375. doi:10.2147/NSS.S310351

H, O. B., Mohan, H., Hare, C. O., Reynolds, J. V., and Kenny, R. A. (2017). Mind over matter? The hidden epidemic of cognitive dysfunction in the older surgical patient. *Ann. Surg.* 265 (4), 677–691. doi:10.1097/SLA.0000000000001900

Hajer, G. R., van Haeften, T. W., and Visseren, F. L. (2008). Adipose tissue dysfunction in obesity, diabetes, and vascular diseases. *Eur. Heart J.* 29 (24), 2959–2971. doi:10.1093/eurheartj/ehn387

He, K., Zhang, J., Zhang, W., Wang, S., Li, D., Ma, X., et al. (2022). Hippocampus-based mitochondrial respiratory function decline is responsible for perioperative neurocognitive disorders. *Front. Aging Neurosci.* 14, 772066. doi:10.3389/fnagi.2022.772066

Ho, Y. S., Cheng, W. Y., Lai, M. S., Lau, C. F., Wong, G. T., Yeung, W. F., et al. (2024). Postoperative electroacupuncture boosts cognitive function recovery after laparotomy in mice. *Biomolecules* 14 (10), 1274. doi:10.3390/biom14101274

Ho, Y. S., Zhao, F. Y., Yeung, W. F., Wong, G. T., Zhang, H. Q., and Chang, R. C. (2020). Application of acupuncture to attenuate immune responses and oxidative stress in postoperative cognitive dysfunction: what do we know So far? *Oxid. Med. Cell Longev.* 2020, 9641904. doi:10.1155/2020/9641904

Hoogland, I. C., Houbolt, C., van Westerloo, D. J., van Gool, W. A., and van de Beek, D. (2015). Systemic inflammation and microglial activation: systematic review of animal experiments. *J. Neuroinflammation* 12, 114. doi:10.1186/s12974-015-0332-6

Hou, R., Wang, H., Chen, L., Qiu, Y., and Li, S. (2018). POCD in patients receiving total knee replacement under deep vs light anesthesia: a randomized controlled trial. *Brain Behav.* 8 (2), e00910. doi:10.1002/brb3.910

Hovens, I. B., van Leeuwen, B. L., Mariani, M. A., Kraneveld, A. D., and Schoemaker, R. G. (2016). Postoperative cognitive dysfunction and neuroinflammation; cardiac surgery and abdominal surgery are not the same. *Brain Behav. Immun.* 54, 178–193. doi:10.1016/j.bbi.2016.02.003

Hu, G. W., Li, Q., Niu, X., Hu, B., Liu, J., Zhou, S. M., et al. (2015). Exosomes secreted by human-induced pluripotent stem cell-derived mesenchymal stem cells attenuate limb ischemia by promoting angiogenesis in mice. *Stem Cell Res. Ther.* 6 (1), 10. doi:10.1186/scrt546

Hu, G., Xia, Y., Zhang, J., Chen, Y., Yuan, J., Niu, X., et al. (2020). ESC-sEVs rejuvenate senescent hippocampal NSCs by activating lysosomes to improve cognitive dysfunction in vascular dementia. *Adv. Sci. (Weinh)* 7 (10), 1903330. doi:10.1002/advs.201903330

Hu, Z., Ou, Y., Duan, K., and Jiang, X. (2010). Inflammation: a bridge between postoperative cognitive dysfunction and alzheimer's disease. *Med. Hypotheses* 74 (4), 722–724. doi:10.1016/j.mehy.2009.10.040

Hua, T., Yang, M., Song, H., Kong, E., Deng, M., Li, Y., et al. (2022). Huc-MSCs-derived exosomes attenuate inflammatory pain by regulating microglia pyroptosis and autophagy *via* the miR-146a-5p/TRAF6 axis. *J. Nanobiotechnology* 20 (1), 324. doi:10.1186/s12951-022-01522-6

Huang, J., Qin, T. S., Bo, Y., Li, Y. J., Liu, R. S., Yu, Y., et al. (2025). The role of the intestinal flora and its derivatives in neurocognitive disorders: a narrative review from surgical perspective. *Mol. Neurobiol.* 62 (2), 1404–1414. doi:10.1007/s12035-024-04322-1

Huang, S., Ge, X., Yu, J., Han, Z., Yin, Z., Li, Y., et al. (2018). Increased miR-124-3p in microglial exosomes following traumatic brain injury inhibits neuronal inflammation and contributes to neurite outgrowth *via* their transfer into neurons. *Faseb J.* 32 (1), 512–528. doi:10.1096/fj.201700673R

Hudetz, J. A., Hoffmann, R. G., Patterson, K. M., Byrne, A. J., Iqbal, Z., Gandhi, S. D., et al. (2010). Preoperative dispositional optimism correlates with a reduced incidence of postoperative delirium and recovery of postoperative cognitive function in cardiac surgical patients. *J. Cardiothorac. Vasc. Anesth.* 24 (4), 560–567. doi:10.1053/j.jvca.2010.01.004

Hudetz, J. A., Iqbal, Z., Gandhi, S. D., Patterson, K. M., Byrne, A. J., Hudetz, A. G., et al. (2009). Ketamine attenuates post-operative cognitive dysfunction after cardiac surgery. *Acta Anaesthesiol. Scand.* 53 (7), 864–872. doi:10.1111/j.1399-6576.2009.01978.x

Huh, Y. J., Seo, J. Y., Nam, J., Yang, J., McDowell, A., Kim, Y. K., et al. (2019). Bariatric/metabolic surgery induces noticeable changes of microbiota and their secreting extracellular vesicle composition in the gut. *Obes. Surg.* 29 (8), 2470–2484. doi:10.1007/s11695-019-03852-1

Ishii, K., Makita, T., Yamashita, H., Matsunaga, S., Akiyama, D., Toba, K., et al. (2016). Total intravenous anesthesia with propofol is associated with a lower rate of postoperative delirium in comparison with sevoflurane anesthesia in elderly patients. *J. Clin. Anesth.* 33, 428–431. doi:10.1016/j.jclinane.2016.04.043

Iyaswamy, A., Lu, K., Guan, X. J., Kan, Y., Su, C., Liu, J., et al. (2023). Impact and advances in the role of bacterial extracellular vesicles in neurodegenerative disease and its therapeutics. *Biomedicines* 11 (7), 2056. doi:10.3390/biomedicines11072056

Izquierdo-Altarejos, P., Cabrera-Pastor, A., Gonzalez-King, H., Montoliu, C., and Felipo, V. (2020). Extracellular vesicles from hyperammonemic rats induce neuroinflammation and motor incoordination in control rats. *Cells* 9 (3), 572. doi:10.3390/cells9030572

Izquierdo-Altarejos, P., Cabrera-Pastor, A., Martínez-García, M., Sánchez-Huertas, C., Hernández, A., Moreno-Manzano, V., et al. (2023). Extracellular vesicles from mesenchymal stem cells reduce neuroinflammation in hippocampus and restore cognitive function in hyperammonemic rats. *J. Neuroinflammation* 20 (1), 1. doi:10.1186/s12974-022-02688-4

Kainz, E., Juilfs, N., Harler, U., Kahl, U., Mewes, C., Zöllner, C., et al. (2023). The impact of cognitive reserve on delayed neurocognitive recovery after major non-cardiac surgery: an exploratory substudy. *Front. Aging Neurosci.* 15, 1267998. doi:10.3389/fnagi.2023.1267998

Kapoor, I., Prabhakar, H., and Mahajan, C. (2019). Postoperative cognitive dysfunction. *Indian J. Crit. Care Med.* 23 (Suppl. 2), S162–S164. doi:10.5005/jp-journals-10071-23196

Kawai, T., Autieri, M. V., and Scalia, R. (2021). Adipose tissue inflammation and metabolic dysfunction in obesity. *Am. J. Physiol. Cell Physiol.* 320 (3), C375–C391. doi:10.1152/ajpcell.00379.2020

Keshavarz, A. R. S., Ashrafian, F., Yadegar, A., Lari, A., Moradi, H. R., Shahriary, A., et al. (2021). The protective effects of live and pasteurized Akkermansia muciniphila and its extracellular vesicles against HFD/CCl4-Induced liver injury. *Microbiol. Spectr.* 9 (2), e0048421. doi:10.1128/Spectrum.00484-21

Khalyfa, A., Poroyko, V. A., Qiao, Z., Gileles-Hillel, A., Khalyfa, A. A., Akbarpour, M., et al. (2017). Exosomes and metabolic function in mice exposed to alternating dark-light cycles mimicking night shift work schedules. *Front. Physiol.* 8, 882. doi:10.3389/fphys.2017.00882

Kim, N. Y., Lee, H. Y., Choi, Y. Y., Mo, S. J., Jeon, S., Ha, J. H., et al. (2024). Effect of gut microbiota-derived metabolites and extracellular vesicles on neurodegenerative disease in a gut-brain axis chip. *Nano Converg.* 11 (1), 7. doi:10.1186/s40580-024-00413-w

Kong, E., Geng, X., Wu, F., Yue, W., Sun, Y., and Feng, X. (2024). Microglial exosome miR-124-3p in hippocampus alleviates cognitive impairment induced by postoperative pain in elderly mice. *J. Cell Mol. Med.* 28 (3), e18090. doi:10.1111/jcmm.18090

Kong, H., Xu, L. M., and Wang, D. X. (2022). Perioperative neurocognitive disorders: a narrative review focusing on diagnosis, prevention, and treatment. *CNS Neurosci. Ther.* 28 (8), 1147–1167. doi:10.1111/cns.13873

Krstic, D., and Knuesel, I. (2013). Deciphering the mechanism underlying late-onset alzheimer disease. *Nat. Rev. Neurol.* 9 (1), 25–34. doi:10.1038/nrneurol.2012.236

Lang, H. L., Zhao, Y. Z., Xiao, R. J., Sun, J., Chen, Y., Hu, G. W., et al. (2023). Small extracellular vesicles secreted by induced pluripotent stem cell-derived mesenchymal stem cells improve postoperative cognitive dysfunction in mice with diabetes. *Neural Regen. Res.* 18 (3), 609–617. doi:10.4103/1673-5374.350205

Le, Y., Liu, S., Peng, M., Tan, C., Liao, Q., Duan, K., et al. (2014). Aging differentially affects the loss of neuronal dendritic spine, neuroinflammation and memory impairment at rats after surgery. *PLoS One* 9 (9), e106837. doi:10.1371/journal.pone.0106837

Lee, K. E., Kim, J. K., Han, S. K., Lee, D. Y., Lee, H. J., Yim, S. V., et al. (2020). The extracellular vesicle of gut microbial Paenalcaligenes hominis is a risk factor for vagus nerve-mediated cognitive impairment. *Microbiome* 8 (1), 107. doi:10.1186/s40168-020-00881-2

Li, B., Arime, Y., Hall, F. S., Uhl, G. R., and Sora, I. (2010). Impaired spatial working memory and decreased frontal cortex BDNF protein level in dopamine transporter knockout mice. *Eur. J. Pharmacol.* 628 (1-3), 104–107. doi:10.1016/j.ejphar.2009.11.036

Li, H., Meng, Y., He, S., Tan, X., Zhang, Y., Zhang, X., et al. (2022). Macrophages, chronic inflammation, and insulin resistance. *Cells* 11 (19), 3001. doi:10.3390/cells11193001

Li, Q., Liu, S., Yan, J., Sun, M. Z., and Greenaway, F. T. (2021b). The potential role of miR-124-3p in tumorigenesis and other related diseases. *Mol. Biol. Rep.* 48 (4), 3579–3591. doi:10.1007/s11033-021-06347-4

Li, R., Chen, N., Wang, E., and Tang, Z. (2021a). Correlation between preoperative sleep disorders and postoperative delayed neurocognitive recovery in elderly patients. *Zhong Nan Da Xue Xue Bao Yi Xue Ban.* 46 (11), 1251–1259. doi:10.11817/j.issn.1672-7347.2021.210015

Li, S., Li, Y., Chen, B., Zhao, J., Yu, S., Tang, Y., et al. (2018). exoRBase: a database of circRNA, lncRNA and mRNA in human blood exosomes. *Nucleic Acids Res.* 46 (D1), D106–D112. doi:10.1093/nar/gkx891

Li, S., Zhang, R., Wang, A., Li, Y., Zhang, M., Kim, J., et al. (2023). Panax notoginseng: derived exosome-like nanoparticles attenuate ischemia reperfusion injury *via* altering microglia polarization. *J. Nanobiotechnology* 21 (1), 416. doi:10.1186/s12951-023-02161-1

Li, Y., Zheng, Q., Bao, C., Li, S., Guo, W., Zhao, J., et al. (2015). Circular RNA is enriched and stable in exosomes: a promising biomarker for cancer diagnosis. *Cell Res.* 25 (8), 981–984. doi:10.1038/cr.2015.82

Lin, X., Chen, Y., Zhang, P., Chen, G., Zhou, Y., and Yu, X. (2020). The potential mechanism of postoperative cognitive dysfunction in older people. *Exp. Gerontol.* 130, 110791. doi:10.1016/j.exger.2019.110791

Liu, L., Shang, L., Jin, D., Wu, X., and Long, B. (2022). General anesthesia bullies the gut: a toxic relationship with dysbiosis and cognitive dysfunction. *Psychopharmacol. Berl.* 239 (3), 709–728. doi:10.1007/s00213-022-06096-7

Liu, L. L., and Leung, J. M. (2000). Predicting adverse postoperative outcomes in patients aged 80 years or older. *J. Am. Geriatr. Soc.* 48 (4), 405–412. doi:10.1111/j.1532-5415.2000.tb04698.x

Liu, Y., Yang, W., Xue, J., Chen, J., Liu, S., Zhang, S., et al. (2023). Neuroinflammation: the central enabler of postoperative cognitive dysfunction. *Biomed. Pharmacother.* 167, 115582. doi:10.1016/j.biopha.2023.115582

Liu, Y. H., Wang, D. X., Li, L. H., Wu, X. M., Shan, G. J., Su, Y., et al. (2009). The effects of cardiopulmonary bypass on the number of cerebral microemboli and the incidence of cognitive dysfunction after coronary artery bypass graft surgery. *Anesth. Analg.* 109 (4), 1013–1022. doi:10.1213/ane.0b013e3181aed2bb

Loh, J. S., Mak, W. Q., Tan, L. K. S., Ng, C. X., Chan, H. H., Yeow, S. H., et al. (2024). Microbiota-gut-brain axis and its therapeutic applications in neurodegenerative diseases. *Signal Transduct. Target Ther.* 9 (1), 37. doi:10.1038/s41392-024-01743-1

Lu, B., Yuan, H., Mo, L., Sun, D., Liu, R., Zhou, H., et al. (2022). Effects of different types of non-cardiac surgical trauma on hippocampus-dependent memory and neuroinflammation. *Front. Behav. Neurosci.* 16, 950093. doi:10.3389/fnbeh.2022.950093

Lu, X., Jin, X., Yang, S., and Xia, Y. (2018). The correlation of the depth of anesthesia and postoperative cognitive impairment: a meta-analysis based on randomized controlled trials. *J. Clin. Anesth.* 45, 55–59. doi:10.1016/j.jclinane.2017.12.002

Luo, A., Li, S., Wang, X., Xie, Z., Li, S., and Hua, D. (2021). Cefazolin improves anesthesia and surgery-induced cognitive impairments by modulating blood-brain barrier function, gut bacteria and short chain fatty acids. *Front. Aging Neurosci.* 13, 748637. doi:10.3389/fnagi.2021.748637

Lv, X., Yan, J., Jiang, J., Zhou, X., Lu, Y., and Jiang, H. (2017). MicroRNA-27a-3p suppression of peroxisome proliferator-activated receptor-γ contributes to cognitive impairments resulting from sevoflurane treatment. *J. Neurochem.* 143 (3), 306–319. doi:10.1111/jnc.14208

McDonagh, D. L., Mathew, J. P., White, W. D., Phillips-Bute, B., Laskowitz, D. T., Podgoreanu, M. V., et al. (2010). Cognitive function after major noncardiac surgery, apolipoprotein E4 genotype, and biomarkers of brain injury. *Anesthesiology* 112 (4), 852–859. doi:10.1097/ALN.0b013e3181d31fd7

Medders, K. E., Sejbuk, N. E., Maung, R., Desai, M. K., and Kaul, M. (2010). Activation of p38 MAPK is required in monocytic and neuronal cells for HIV glycoprotein 120-induced neurotoxicity. *J. Immunol.* 185 (8), 4883–4895. doi:10.4049/jimmunol.0902535

Mhanna, A., Martini, N., Hmaydoosh, G., Hamwi, G., Jarjanazi, M., Zaifah, G., et al. (2024). The correlation between gut microbiota and both neurotransmitters and mental disorders: a narrative review. *Med. Baltim.* 103 (5), e37114. doi:10.1097/MD.0000000000037114

Moller, J. T., Cluitmans, P., Rasmussen, L. S., Houx, P., Rasmussen, H., Canet, J., et al. (1998). Long-term postoperative cognitive dysfunction in the elderly ISPOCD1 study. ISPOCD investigators. International study of post-operative cognitive dysfunction. *Lancet* 351 (9106), 857–861. doi:10.1016/s0140-6736(97)07382-0

Momen-Heravi, F., Bala, S., Bukong, T., and Szabo, G. (2014). Exosome-mediated delivery of functionally active miRNA-155 inhibitor to macrophages. *Nanomedicine.* 10 (7), 1517–1527. doi:10.1016/j.nano.2014.03.014

Monk, T. G., Weldon, B. C., Garvan, C. W., Dede, D. E., van der Aa, M. T., Heilman, K. M., et al. (2008). Predictors of cognitive dysfunction after major noncardiac surgery. *Anesthesiology* 108 (1), 18–30. doi:10.1097/01.anes.0000296071.19434.1e

Needham, M. J., Webb, C. E., and Bryden, D. C. (2017). Postoperative cognitive dysfunction and dementia: what we need to know and do. *Br. J. Anaesth.* 119 (Suppl. l_1), i115–i125. doi:10.1093/bja/aex354

Nemati, M., Singh, B., Mir, R. A., Nemati, M., Babaei, A., Ahmadi, M., et al. (2022). Plant-derived extracellular vesicles: a novel nanomedicine approach with advantages and challenges. *Cell Commun. Signal* 20 (1), 69. doi:10.1186/s12964-022-00889-1

Noonin, C., and Thongboonkerd, V. (2021). Exosome-inflammasome crosstalk and their roles in inflammatory responses. *Theranostics* 11 (9), 4436–4451. doi:10.7150/thno.54004

Oriby, M. E., Elrashidy, A. A., Elsharkawy, A., and Ahmed, S. A. (2023). Effects of ketamine or dexmedetomidine on postoperative cognitive dysfunction after cataract surgery: a randomized controlled trial. *Indian J. Anaesth.* 67 (2), 186–193. doi:10.4103/ija.ija_429_22

Orser, B. A., and Wang, D. S. (2019). GABAA receptor theory of perioperative neurocognitive disorders. *Anesthesiology* 130 (4), 618–619. doi:10.1097/ALN.0000000000002562

Otero-Ortega, L., Laso-García, F., Gómez-de Frutos, M., Fuentes, B., Diekhorst, L., Díez-Tejedor, E., et al. (2019). Role of exosomes as a treatment and potential biomarker for stroke. *Transl. Stroke Res.* 10 (3), 241–249. doi:10.1007/s12975-018-0654-7

Peng, S., Li, P., Liu, P., Yan, H., Wang, J., Lu, W., et al. (2020). Cistanches alleviates sevoflurane-induced cognitive dysfunction by regulating PPAR-γ-dependent antioxidant and anti-inflammatory in rats. *J. Cell Mol. Med.* 24 (2), 1345–1359. doi:10.1111/jcmm.14807

Perez-Gonzalez, R., Gauthier, S. A., Kumar, A., and Levy, E. (2012). The exosome secretory pathway transports amyloid precursor protein carboxyl-terminal fragments from the cell into the brain extracellular space. *J. Biol. Chem.* 287 (51), 43108–43115. doi:10.1074/jbc.M112.404467

Prinz, M., and Priller, J. (2014). Microglia and brain macrophages in the molecular age: from origin to neuropsychiatric disease. *Nat. Rev. Neurosci.* 15 (5), 300–312. doi:10.1038/nrn3722

Qian, L., Rawashdeh, O., Kasas, L., Milne, M. R., Garner, N., Sankorrakul, K., et al. (2022). Cholinergic basal forebrain degeneration due to sleep-disordered breathing exacerbates pathology in a mouse model of alzheimer's disease. *Nat. Commun.* 13 (1), 6543. doi:10.1038/s41467-022-33624-y

Qin, J., Yuan, H., An, X., Liu, R., and Meng, B. (2024). Macrophage-derived exosomes exacerbate postoperative cognitive dysfunction in mice through inflammation. *J. Neuroimmunol.* 394, 578403. doi:10.1016/j.jneuroim.2024.578403

Ren, L., Liang, H., Zhu, L., Yang, X., Zhang, H., Sun, N., et al. (2024). Dietary restriction improves perioperative neurocognitive disorders by inhibiting neuroinflammation and gut microbial dysbiosis. *Neuroscience* 540, 48–67. doi:10.1016/j.neuroscience.2024.01.012

Rudolph, J. L., and Marcantonio, E. R. (2011). Review articles: postoperative delirium: acute change with long-term implications. *Anesth. Analg.* 112 (5), 1202–1211. doi:10.1213/ANE.0b013e3182147f6d

Saeedi, P., Petersohn, I., Salpea, P., Malanda, B., Karuranga, S., Unwin, N., et al. (2019). Global and regional diabetes prevalence estimates for 2019 and projections for 2030 and 2045: results from the international diabetes Federation diabetes atlas, 9(th) edition. *Diabetes Res. Clin. Pract.* 157, 107843. doi:10.1016/j.diabres.2019.107843

Saleh, A. J., Tang, G. X., Hadi, S. M., Yan, L., Chen, M. H., Duan, K. M., et al. (2015). Preoperative cognitive intervention reduces cognitive dysfunction in elderly patients after gastrointestinal surgery: a randomized controlled trial. *Med. Sci. Monit.* 21, 798–805. doi:10.12659/MSM.893359

Scott, J. E., Mathias, J. L., Kneebone, A. C., and Krishnan, J. (2017). Postoperative cognitive dysfunction and its relationship to cognitive reserve in elderly total joint replacement patients. *J. Clin. Exp. Neuropsychol.* 39 (5), 459–472. doi:10.1080/13803395.2016.1233940

Sekar, S., Cuyugan, L., Adkins, J., Geiger, P., and Liang, W. S. (2018). Circular RNA expression and regulatory network prediction in posterior cingulate astrocytes in elderly subjects. *BMC Genomics* 19 (1), 340. doi:10.1186/s12864-018-4670-5

Shao, M., Jin, X., Chen, S., Yang, N., and Feng, G. (2023). Plant-derived extracellular vesicles -a novel clinical anti-inflammatory drug carrier worthy of investigation. *Biomed. Pharmacother.* 169, 115904. doi:10.1016/j.biopha.2023.115904

Shi, H. X., Du, X. J., Wu, F., Hu, Y. J., and Mi, W. D. (2020). Dexmedetomidine for early postoperative cognitive dysfunction after video-assisted thoracoscopic lobectomy in elderly Male patients with lung cancer. *Med. Baltim.* 99 (36), e21691. doi:10.1097/MD.0000000000021691

Shipman, W. D., Fonseca, R., Dominguez, M., Bhayani, S., Gilligan, C., Diwan, S., et al. (2024). An update on emerging regenerative medicine applications: the use of extracellular vesicles and exosomes for the management of chronic pain. *Curr. Pain Headache Rep.* 28 (12), 1289–1297. doi:10.1007/s11916-024-01309-4

Shokri-Kojori, E., Wang, G. J., Wiers, C. E., Demiral, S. B., Guo, M., Kim, S. W., et al. (2018). β-Amyloid accumulation in the human brain after one night of sleep deprivation. *Proc. Natl. Acad. Sci. U. S. A.* 115 (17), 4483–4488. doi:10.1073/pnas.1721694115

Silva, A. R., Regueira, P., Albuquerque, E., Baldeiras, I., Cardoso, A. L., Santana, I., et al. (2021). Estimates of geriatric delirium frequency in noncardiac surgeries and its evaluation across the years: a systematic review and meta-analysis. *J. Am. Med. Dir. Assoc.* 22 (3), 613–20.e9. doi:10.1016/j.jamda.2020.08.017

Sipilä, R. M., and Kalso, E. A. (2021). Sleep well and recover faster with less Pain-A narrative review on sleep in the perioperative period. *J. Clin. Med.* 10 (9), 2000. doi:10.3390/jcm10092000

Solas, M., Milagro, F. I., Ramírez, M. J., and Martínez, J. A. (2017). Inflammation and gut-brain axis link obesity to cognitive dysfunction: plausible pharmacological interventions. *Curr. Opin. Pharmacol.* 37, 87–92. doi:10.1016/j.coph.2017.10.005

Sun, L., Niu, K., Guo, J., Tu, J., Ma, B., and An, J. (2023). Dexmedetomidine attenuates postoperative spatial memory impairment after surgery by reducing cytochrome C. *BMC Anesthesiol.* 23 (1), 85. doi:10.1186/s12871-023-02035-x

Tan, J., Ni, D., Taitz, J., Pinget, G. V., Read, M., Senior, A., et al. (2022). Dietary protein increases T-cell-independent sIgA production through changes in gut microbiota-derived extracellular vesicles. *Nat. Commun.* 13 (1), 4336. doi:10.1038/s41467-022-31761-y

Thomi, G., Surbek, D., Haesler, V., Joerger-Messerli, M., and Schoeberlein, A. (2019). Exosomes derived from umbilical cord mesenchymal stem cells reduce microglia-mediated neuroinflammation in perinatal brain injury. *Stem Cell Res. Ther.* 10 (1), 105. doi:10.1186/s13287-019-1207-z

Thourani, V. H., Weintraub, W. S., Stein, B., Gebhart, S. S., Craver, J. M., Jones, E. L., et al. (1999). Influence of diabetes mellitus on early and late outcome after coronary artery bypass grafting. *Ann. Thorac. Surg.* 67 (4), 1045–1052. doi:10.1016/s0003-4975(99)00143-5

Tsigalou, C., Paraschaki, A., Bragazzi, N. L., Aftzoglou, K., Bezirtzoglou, E., Tsakris, Z., et al. (2023). Alterations of gut microbiome following gastrointestinal surgical procedures and their potential complications. *Front. Cell Infect. Microbiol.* 13, 1191126. doi:10.3389/fcimb.2023.1191126

van Harten, A. E., Scheeren, T. W., and Absalom, A. R. (2012). A review of postoperative cognitive dysfunction and neuroinflammation associated with cardiac surgery and anaesthesia. *Anaesthesia* 67 (3), 280–293. doi:10.1111/j.1365-2044.2011.07008.x

van Praag, H., Schinder, A. F., Christie, B. R., Toni, N., Palmer, T. D., and Gage, F. H. (2002). Functional neurogenesis in the adult hippocampus. *Nature* 415 (6875), 1030–1034. doi:10.1038/4151030a

Vella, L. J., Hill, A. F., and Cheng, L. (2016). Focus on extracellular vesicles: exosomes and their role in protein trafficking and biomarker potential in alzheimer's and parkinson's disease. *Int. J. Mol. Sci.* 17 (2), 173. doi:10.3390/ijms17020173

Vlisides, P., Avidan, M., Leis, A., Schoettinger, A., Hickey, K., McKinney, A., et al. (2019). Recommendations and alerting for delirium alleviation in real-time (RADAR): protocol for a pilot randomized controlled trial. *F1000Res* 8, 1683. doi:10.12688/f1000research.20597.2

Wang, B., Li, S., Cao, X., Dou, X., Li, J., Wang, L., et al. (2017). Blood-brain barrier disruption leads to postoperative cognitive dysfunction. *Curr. Neurovasc Res.* 14 (4), 359–367. doi:10.2174/1567202614666171009105825

Wang, C. M., Chen, W. C., Zhang, Y., Lin, S., and He, H. F. (2021). Update on the mechanism and treatment of sevoflurane-induced postoperative cognitive dysfunction. *Front. Aging Neurosci.* 13, 702231. doi:10.3389/fnagi.2021.702231

Wang, M., Su, P., Liu, Y., Zhang, X., Yan, J., An, X., et al. (2019b). Abnormal expression of circRNA_089763 in the plasma exosomes of patients with post-operative cognitive dysfunction after coronary artery bypass grafting. *Mol. Med. Rep.* 20 (3), 2549–2562. doi:10.3892/mmr.2019.10521

Wang, R., Wang, X., Zhao, H., Li, N., Li, J., Zhang, H., et al. (2024). Targeted delivery of hybrid nanovesicles for enhanced brain penetration to achieve synergistic therapy of glioma. *J. Control Release* 365, 331–347. doi:10.1016/j.jconrel.2023.11.033

Wang, W., Wang, Y., Wu, H., Lei, L., Xu, S., Shen, X., et al. (2014). Postoperative cognitive dysfunction: current developments in mechanism and prevention. *Med. Sci. Monit.* 20, 1908–1912. doi:10.12659/MSM.892485

Wang, X., Zhou, Y., Gao, Q., Ping, D., Wang, Y., Wu, W., et al. (2020). The role of exosomal microRNAs and oxidative stress in neurodegenerative diseases. *Oxid. Med. Cell Longev.* 2020, 3232869. doi:10.1155/2020/3232869

Wang, Y., Luo, J., and Li, S. Y. (2019a). Nano-curcumin simultaneously protects the blood-brain barrier and reduces M1 microglial activation during cerebral ischemia-reperfusion injury. *ACS Appl. Mater Interfaces* 11 (4), 3763–3770. doi:10.1021/acsami.8b20594

Wei, C., Luo, T., Zou, S., Zhou, X., Shen, W., Ji, X., et al. (2017). Differentially expressed lncRNAs and miRNAs with associated ceRNA networks in aged

mice with postoperative cognitive dysfunction. *Oncotarget* 8 (34), 55901–55914. doi:10.18632/oncotarget.18362

Wei, S., Peng, W., Mai, Y., Li, K., Wei, W., Hu, L., et al. (2020). Outer membrane vesicles enhance tau phosphorylation and contribute to cognitive impairment. *J. Cell Physiol.* 235 (5), 4843–4855. doi:10.1002/jcp.29362

Wen, J., Ding, Y., Wang, L., and Xiao, Y. (2020). Gut microbiome improves postoperative cognitive function by decreasing permeability of the blood-brain barrier in aged mice. *Brain Res. Bull.* 164, 249–256. doi:10.1016/j.brainresbull.2020.08.017

Xie, L., Kang, H., Xu, Q., Chen, M. J., Liao, Y., Thiyagarajan, M., et al. (2013). Sleep drives metabolite clearance from the adult brain. *Science* 342 (6156), 373–377. doi:10.1126/science.1241224

Xin, H., Wang, F., Li, Y., Lu, Q. E., Cheung, W. L., Zhang, Y., et al. (2017). Secondary release of exosomes from astrocytes contributes to the increase in neural plasticity and improvement of functional recovery after stroke in rats treated with exosomes harvested from MicroRNA 133b-Overexpressing multipotent mesenchymal stromal cells. *Cell Transpl.* 26 (2), 243–257. doi:10.3727/096368916X693031

Xin, J., Shan, W., Li, J., Yu, H., and Zuo, Z. (2022). Activation of the lateral habenula-ventral tegmental area neural circuit contributes to postoperative cognitive dysfunction in mice. *Adv. Sci. (Weinh)* 9 (22), e2202228. doi:10.1002/advs.202202228

Yang, C., Sun, S., Zhang, Q., Guo, J., Wu, T., Liu, Y., et al. (2020). Exosomes of antler mesenchymal stem cells improve postoperative cognitive dysfunction in cardiopulmonary bypass rats through inhibiting the TLR2/TLR4 signaling pathway. *Stem Cells Int.* 2020, 2134565. doi:10.1155/2020/2134565

Yang, J., He, Y., Liao, X., Hu, J., and Li, K. (2023). Does postoperative pulmonary infection correlate with intestinal flora following gastric cancer surgery? - A nested case-control study. *Front. Microbiol.* 14, 1267750. doi:10.3389/fmicb.2023.1267750

Yang, Y., Liu, Y., Zhu, J., Song, S., Huang, Y., Zhang, W., et al. (2022). Neuroinflammation-mediated mitochondrial dysregulation involved in postoperative cognitive dysfunction. *Free Radic. Biol. Med.* 178, 134–146. doi:10.1016/j.freeradbiomed.2021.12.004

Yang, Y., Ye, Y., Su, X., He, J., Bai, W., and He, X. (2017). MSCs-Derived exosomes and neuroinflammation, neurogenesis and therapy of traumatic brain injury. *Front. Cell Neurosci.* 11, 55. doi:10.3389/fncel.2017.00055

Yin, W., Ma, H., Qu, Y., Ren, J., Sun, Y., Guo, Z. N., et al. (2025). Exosomes: the next-generation therapeutic platform for ischemic stroke. *Neural Regen. Res.* 20 (5), 1221–1235. doi:10.4103/NRR.NRR-D-23-02051

Yuan, S., Zhang, X., Bo, Y., Li, W., Zhang, H., and Jiang, Q. (2014). The effects of electroacupuncture treatment on the postoperative cognitive function in aged rats with acute myocardial ischemia-reperfusion. *Brain Res.* 1593, 19–29. doi:10.1016/j.brainres.2014.10.005

Zanghi, C. N., and Jevtovic-Todorovic, V. (2017). A holistic approach to anesthesia-induced neurotoxicity and its implications for future mechanistic studies. *Neurotoxicol Teratol.* 60, 24–32. doi:10.1016/j.ntt.2016.12.004

Zhai, T., Ren, W., Ji, X., Wang, Y., Chen, H., Jin, Y., et al. (2024). Distinct compositions and functions of circulating microbial DNA in the peripheral blood compared to fecal microbial DNA in healthy individuals. *mSystems* 9 (3), e0000824. doi:10.1128/msystems.00008-24

Zhang, J., Liu, G., Zhang, F., Fang, H., Zhang, D., Liu, S., et al. (2019). Analysis of postoperative cognitive dysfunction and influencing factors of dexmedetomidine anesthesia in elderly patients with colorectal cancer. *Oncol. Lett.* 18 (3), 3058–3064. doi:10.3892/ol.2019.10611

Zhang, L., Cheng, X., Xia, L., Liu, N., Liu, L., Liu, S., et al. (2024). Analysis of 16s rRNA gene sequencing in feces: the impact of bariatric surgery on the gut microbiota in patients with obesity. *Obes. Surg.* 34 (4), 1185–1195. doi:10.1007/s11695-024-07087-7

Zhang, L., Li, D., Yi, P., Shi, J., Guo, M., Yin, Q., et al. (2023b). Peripheral origin exosomal microRNAs aggravate glymphatic system dysfunction in diabetic cognitive impairment. *Acta Pharm. Sin. B* 13 (7), 2817–2825. doi:10.1016/j.apsb.2023.03.018

Zhang, S., Jia, X., Wu, Q., Jin, J., Xu, L., Yang, L., et al. (2023a). The involvement of the gut microbiota in postoperative cognitive dysfunction based on integrated metagenomic and metabolomics analysis. *Microbiol. Spectr.* 11 (6), e0310423. doi:10.1128/spectrum.03104-23

Zhang, S., Zhu, D., Li, H., Li, H., Feng, C., and Zhang, W. (2017). Characterization of circRNA-Associated-ceRNA networks in a senescence-accelerated mouse prone 8 brain. *Mol. Ther.* 25 (9), 2053–2061. doi:10.1016/j.ymthe.2017.06.009

Zhao, Q., Wan, H., Pan, H., and Xu, Y. (2024). Postoperative cognitive dysfunction-current research progress. *Front. Behav. Neurosci.* 18, 1328790. doi:10.3389/fnbeh.2024.1328790

Zhao, Y., Alexandrov, P. N., Jaber, V., and Lukiw, W. J. (2016). Deficiency in the ubiquitin conjugating enzyme UBE2A in Alzheimer's disease (AD) is linked to deficits in a natural circular miRNA-7 sponge (circRNA; ciRS-7). *Genes (Basel)* 7 (12), 116. doi:10.3390/genes7120116

Zhong, J., Li, J., Ni, C., and Zuo, Z. (2020). Amantadine alleviates postoperative cognitive dysfunction possibly by preserving neurotrophic factor expression and dendritic arborization in the hippocampus of old rodents. *Front. Aging Neurosci.* 12, 605330. doi:10.3389/fnagi.2020.605330

Zhong, J., Zhao, L., Wu, W., Chen, J., Yuan, S., Zhang, X., et al. (2022). Transcranial near-infrared laser improves postoperative neurocognitive disorder in aged mice *via* SIRT3/AMPK/Nrf2 pathway. *Front. Neurosci.* 16, 1100915. doi:10.3389/fnins.2022.1100915

Zhou, M., Greenhill, S., Huang, S., Silva, T. K., Sano, Y., Wu, S., et al. (2016). CCR5 is a suppressor for cortical plasticity and hippocampal learning and memory. *Elife* 5, e20985. doi:10.7554/eLife.20985

Zhuang, X., Xiang, X., Grizzle, W., Sun, D., Zhang, S., Axtell, R. C., et al. (2011). Treatment of brain inflammatory diseases by delivering exosome encapsulated anti-inflammatory drugs from the nasal region to the brain. *Mol. Ther.* 19 (10), 1769–1779. doi:10.1038/mt.2011.164

frontiers | Frontiers in Cell and Developmental Biology

TYPE Original Research
PUBLISHED 11 July 2025
DOI 10.3389/fcell.2025.1634945

OPEN ACCESS

EDITED BY
Yu Liu,
University of Houston, United States

REVIEWED BY
Armel Hervé Nwabo Kamdje,
University of Garoua, Cameroon
Chuanhui Song,
Nanjing University, China

*CORRESPONDENCE
Yingjie Xu,
xyjdywe@163.com
Yingtao Wu,
347107303@qq.com

RECEIVED 25 May 2025
ACCEPTED 27 June 2025
PUBLISHED 11 July 2025

CITATION
Wang Y, Zhang H, Yu J, Jing J, Fu Z, Hao Y, Huang Q, Ma R, Xu Y and Wu Y (2025) Psoralen-mediated regulation of osteogenic differentiation of periodontal ligament stem cells: involvement of the mTOR pathway. *Front. Cell Dev. Biol.* 13:1634945. doi: 10.3389/fcell.2025.1634945

Psoralen-mediated regulation of osteogenic differentiation of periodontal ligament stem cells: involvement of the mTOR pathway

Yujia Wang[1], Hongbo Zhang[1], Jie Yu[2], Jin Jing[1], Zhaojiang Fu[1], Yuanping Hao[1], Qihang Huang[3], Ruibin Ma[3], Yingjie Xu[1]* and Yingtao Wu[1]*

[1]Qingdao Stomatological Hospital Affiliated to Qingdao University, Qingdao, Shandong, China, [2]Zibo Stomatological Hospital, Zibo, China, [3]School of Stomatology, Shandong Second Medical University, Weifang, China

Background: Chronic periodontitis is a prevalent inflammatory and destructive oral disease, and its primary treatment is to control the development of inflammation and promote the regeneration of periodontal tissue. Psoralen (Pso) has been shown to promote the osteogenic differentiation of periodontal ligament stem cells (PDLSCs), suggesting its potential as a therapeutic agent for osteogenic regeneration.

Methods: Network pharmacology and transcriptomic sequencing were exploited to screen target genes of Pso in PDLSCs, lentiviruses were employed to interfere with the target gene, and RT-qPCR was conducted to assess the expression levels of osteogenesis-related factors. Pso-loaded mesoporous polydopamine (MPDA-Pso) nanoparticles were constructed and evaluated *in vitro*, and *in vivo* osteogenesis was assessed in rats with alveolar bone defects.

Results: Network pharmacology analysis revealed that the mammalian target of rapamycin (mTOR) was a potential target of Pso, and Pso significantly modulated the expression levels of mTOR in PDLSCs and markedly enhanced osteogenic differentiation. However, Pso did not significantly alter osteogenesis-related genes in PDLSCs after mTOR-inhibitor treatment. We also confirmed that MPDA-Pso nanoparticles promoted the expression of osteogenesis-related genes in PDLSCs; and compared with the control group, observed that the mass of new bone was augmented in the MPDA-Pso group.

Conclusion: Pso was shown to promote the osteogenic differentiation of PDLSCs, and we postulate that this differentiation was facilitated in the LPS-induced inflammatory microenvironment via inhibition of the autophagy-related mTOR-signaling pathway. Additionally, the MPDA-Pso nanoparticles we developed promoted osteogenesis.

KEYWORDS

PDLSCs, Psoralen, osteogenic differentiation, mTOR, periodontitis

1 Introduction

Periodontitis is a chronic, progressive inflammatory disease that affects periodontal tissue, and its primary clinical manifestations include the formation of periodontal pockets and varying degrees of alveolar bone resorption. In advanced cases, periodontitis can lead to tooth loosening, displacement, or even total loss (Kinane, 2000; Sanz et al., 2020a; Teles et al., 2022). As the predominant cause of tooth loss in adults, significantly impacting patient quality of life. Epidemiologic data reveal its worldwide prevalence, affecting approximately 11% of the population in its severe form, ranking as the sixth most prevalent disease worldwide (Kinane, 2000; Kwon et al., 2021). The primary goal of periodontitis treatment is to control inflammation, prevent further destruction of periodontal tissue, and promote regeneration. Primary treatments such as supragingival scaling and root planning are considered the gold standard for chronic periodontitis (Sanz et al., 2012; Herrera et al., 2022; Sanz et al., 2020b). However, periodontitis is also closely related to various systemic diseases such as diabetes and chronic kidney disease. To effectively manage inflammation and prevent infections resulting from systemic factors, adjunctive treatment with antibiotics is often necessary (Graziani et al., 2000; Liccardo et al., 2019). Nonetheless, antibiotics can lead to drug resistance and other side effects, so it is urgent to uncover new drugs for periodontal local treatment that manifest anti-inflammatory and antibacterial properties while minimizing side effects in order to facilitate the regeneration of periodontal bone tissue.

Psoralen (Pso), a linear furanocoumarin compound, is the principal bioactive constituen of the traditional Chinese herb *Psoralea corylifolia L.*, and is a member of the linear furanocoumarin family. Pso is recognized for its diverse biologic activities, including anti-inflammatory, antibacterial, anti-tumor, and estrogen-like effects—specifically facilitating the promotion of osteogenic differentiation (Li et al., 2018; Jamalis et al., 2020); and has been applied widely to the clinical arena. Researchers indicate that Pso enhances the proliferation and vitality of bone marrow mesenchymal stem cells while also promoting their osteogenic differentiation (Huang et al., 2021; Yuan et al., 2016). We previously revealed that Pso elevated levels of the anti-inflammatory factor IL-10 in serum and reduced the secretion of the pro-inflammatory factor TNF-α (Liu et al., 2021). However, the precise mechanism by which Pso promotes osteogenic differentiation of periodontal ligament stem cells (PDLSCs) remains unclear.

Autophagy functions as a self-protective mechanism that cells use to against oxidative stress, hypoxia, and exogenous microorganisms. It facilitates the removal of harmful substances and factors generated during alveolar bone resorption, and occupies a crucial role in regulating the differentiation and functions of cells involved in bone metabolism (Guo et al., 2021; Wang et al., 2023; Liu et al., 2015). Autophagy also facilitates cellular metabolism and assists in maintaining homeostasis within the intracellular environment. Studies have revealed that autophagy is essential for the proliferation and osteogenic differentiation of bone marrow mesenchymal stem cells (BMSCs), with the mammalian target of rapamycin (mTOR)-signaling pathway significantly contributing to this process (Nuschke et al., 2014). Network pharmacology studies have also identified mTOR as a potential target for Pso. We therefore speculate that Pso mediates the osteogenic regulatory effect through the mTOR signal-transduction pathway.

Pso, however, exhibits limited solubility in water, rendering it unsuitable for topical periodontal administration. Consequently, optimizing its delivery methods and surface properties are challenges that must be addressed prior to clinical application. Mesoporous polydopamine (MPDA) has been demonstrated to serve as a drug carrier that manifests favorable mechanical compatibility, with the aromatic rings on the surface of the polydopamine facilitating drug loading via hydrophobic-hydrophobic interactions (Jiang et al., 2022; Hu et al., 2022). Furthermore, the substantial surface area of the pores enhances drug-loading capacity and encapsulation efficiency, providing a foundation for effective drug delivery and targeted release (Zhu et al., 2021; Ma et al., 2022; Ch et al., 2016); this then enables the precise localization for periodontal drug therapy. Additionally, MPDA demonstrates excellent water solubility, significantly improving the water dispersibility of hydrophobic drugs post-loading. These physicochemical properties have therefore recently led to the extensive exploration of MPDA as a drug carrier.

Thus, to improve the properties of Pso, we encapsulated hydrophobic Pso within MPDA to create novel MPDA-Pso nanoparticles, and incorporated them into PDLSCs *in vitro* and alveolar bone defects in rats *in vivo*. We hypothesized that Pso would promote osteogenic differentiation *in vivo and in vitro*, and that it would reflect a potential for development into a novel drug for clinical application.

2 Materials and methods

2.1 Effect of pso on osteogenic differentiation of PDLSCs

2.1.1 Culture of PDLSCs

PDLSCs were isolated from the periodontal membrane of healthy first premolars reserved for extraction due to orthodontic needs of patients with no prior history of periodontal disease. The subjects, aged between 18 and 25 years, received treatment at the Oral and Maxillofacial Surgery Department of Qingdao Stomatological Hospital and showed no underlying systemic conditions. Primary PDLSCs were cultured in medium supplemented with 20% fetal bovine serum (FBS, Pricella, China), and all other cultures were maintained with a 10% concentration. This study was approved by the Ethics Committee of Qingdao University (QDU-HEC-2024266).

2.1.2 Adipogenic differentiation

When PDLSCs reached their third passage, they were plated at a density of 1×10^5 cells per well in a six-well plate and subjected to adipogenic differentiation using specific medium (Pricella, China), with medium refreshed every 3 days for 21 days. Following this period, the cells were fixed in 4% paraformaldehyde (Solarbio, China), rinsed with PBS, and stained with oil red O (Pricella, China) for subsequent microscopic examination.

2.1.3 Osteogenic differentiation

After the third passage, PDLSCs were similarly plated at a density of 1×10^5 cells per well in a six-well plate and induced with osteogenic differentiation medium (Pricella, China). The cells were then fixed with 4% paraformaldehyde, rinsed with PBS, and subjected to alizarin red (Pricella, China) and alkaline phosphatase (ALP) staining (Pricella, China) for microscopic examination.

2.1.4 Flow-cytometric identification

The cell density at the third-generation of PDLSCs was adjusted to 1×10^6 cells/mL. The cellular suspension was aliquoted into centrifuge tubes at 100 μL per tube, and antibodies generated against CD34, CD45, CD73, CD90, and CD105 (Pricella, China) (at 1:50 dilutions) were added separately, while the control group received an equivalent volume of PBS. All cells were then incubated at room temperature in the dark for 20 min. After centrifugation, the supernatant was discarded, and the pellet was washed twice with PBS. The cells were resuspended in 500 μL of PBS for analysis on a flow cytometer (CytoFLEX; Beckman Coulter, Fullerton, California, United States).

2.1.5 CCK-8 assay

PDLSCs were seeded at a density of 2×10^4 cells per well in a 96-well plate and cultured with a gradient of lipopolysaccharide (LPS) concentrations at 0 μg/mL, 20 ng/mL, 50 ng/mL, 100 ng/mL, 150 ng/mL,and 200 ng/mL to screen the concentration of LPS in the simulated periodontitis microenvironment. On this basis, the effective concentration of Pso was screened at concentrations of 2 μg/mL, 5 μg/mL, 10 μg/mL, 15 μg/mL, 20 μg/mL, and 25 μg/mL. We evaluated cellular proliferation using a microplate reader (Bio-Tek, United States).

2.1.6 Pso promotes osteogenesis of PDLSCs

PDLSCs were co-cultured with Pso after LPS-induction and the LPS-induced stem cells served as the control group. We followed the same experimental protocol as in section 2.1.2, with alizarin red staining and ALP staining performed.

2.2 Network construction of the drug-target pathway

2.2.1 Network pharmacology screening of drug targets

Network pharmacology analysis was employed to screen the potential targets of Pso in relation to chronic periodontitis (Beijing Allwegene Tech.). We implemented this approach to determine the specific targets that Pso may affect with respect to chronic periodontitis. Pathways with a significant enrichment of target genes were then analyzed to construct a drug-target-pathway network.

2.2.2 Transcriptomics

Cells were allocated to four groups: PDLSCs, PDLSCs induced by LPS, PDLSCs cultured with Pso, and cells cultured with both LPS/PSO. Total RNA was extracted using TRIzol reagent (Takara, Japan), and high-throughput sequencing was conducted by Beijing Allwegene Tech., with $P < 0.05$ designating differentially expressed genes (DEGs). We performed gene Ontology (GO) and Kyoto Encyclopedia of Genes and Genomes (KEGG) enrichment analyses to identify the pathways associated with the DEGs.

2.2.3 Detection of osteogenesis-related targeted protein

Total cell protein from all groups noted above were extracted using RIPA lysis solution (Elabscience, China) on ice, and a BCA kit (Elabscience, China) was employed to determine protein concentration. With GADPH as the internal reference, ALP (1: 1000; (Abcam, United Kingdom), OCN (1: 5000; Abcam, United Kingdom), Runt-related transcription factor 2 (RUNX2; 1: 1000; Abcam, United Kingdom), and mTOR (1: 1000; Boster, United States) were added sequentially and proteins incubated at 4°C overnight. After incubation with second antibody, ECL luminescent reagent (Elabscience, China) was added to observe HRP-labeled protein bands.

2.2.4 Detection of mTOR pathway-related genes

Total RNA from all groups noted above was extracted using TRIzol reagent, and the expression levels of PI3K, LC3, Deptor, PI3K, and WIPI 1 (Sangon Biotech, China) were determined by real-time q-PCR. GADPH (Sangon Biotech, China) was used as the internal reference, and relative expression levels were calculated using the $2^{-\Delta\Delta CT}$ method. All analyses were repeated three times. The primers that we used were PI3K, 101 CTT TGC GAC AAG ACT GCC GAG AG (forward) and 101 CGC CTG AAG CTG AGC AAC ATC C (reverse); WIPI 1, 114 TGC TTG GCT CAG GAA CAA CAG AAG (forward) and 114 GCA CCG TGG AGG CTG AAG ATG (reverse); LC3, 89 TCT GAG GGC GAG AAG ATC CGA AAG (forward) and 89 TCC AGG TCT CCT ATC CGA GCT TTG (reverse); RagC, 139 CAG CGG CAA GTC CTC CAT CC (forward) and 139 CAT GTA GTC ATC CTG TGC GTC AAT G (reverse); and Deptor, 118 TTG TGG TGC GAG GAA GTA AGC C (forward) and 118 AGG ACA TTG AGC CCG TTG ACA G (reverse).

2.3 The role of the mTOR-signaling axis in osteogenic differentiation

2.3.1 mTOR inhibitors

Rapamycin is a potent and specific mTOR inhibitor and an autophagic activator (Rangaraju et al., 2010; Edwards and Wandless, 2007), and can be used to effectively inhibit the expression of mTOR. PDLSCs were cultured with rapamycin (MCE, United States) and dissolved in DMSO (Solarbio, China), and PCR was conducted to verify mTOR gene expression.

2.3.2 Detection of osteogenesis-related factors

We added Pso to the control group to form the experimental group, extracted RNA, and implemented PCR to evaluate the changes in gene-expression levels. Cells were then allocated to the control group or mTOR-inhibitor group. The gene and protein expression levels for Rag C and for the osteogenic genes ALP and RUNX2 were ultimately ascertained.

2.3.3 Lentiviral transfection of PDLSCs

Lentiviruses for Rag C knockdown were constructed by Jikai Gene (Shanghai, China), and PDLSCs in optimal growth conditions

were selected for lentiviral transfection. After 16 h of PDLSC transfection with lentivirus, normal medium was replaced, cultures were continued for an additional 72 h, and cells were observed under a fluorescence microscope. Following successful transfection, puromycin was employed to select for cell lines with stable expression, and PCR was utilized to assess expression changes in ALP and RUNX2 genes.

2.4 Preparation and characterization of MPDA-Pso nanoparticles

2.4.1 Synthesis of MPDA nanoparticles

After mixing absolute ethanol and purified water, F127 and TMB were added and the mixture stirred for 30 min at room temperature. Dopamine hydrochloride (Aladdin, China) and Tris were then added, and the mixture was stirred for 24 h at room temperature. The mixture was centrifuged at 12,000 rpm for 10 min, and MPDA was obtained by washing the mixture of absolute ethanol/acetone (v/v = 2:1) three times by centrifugal precipitation.

2.4.2 Preparation of MPDA-Pso composites

MPDA and Pso were dispersed in absolute ethanol by ultrasonic shock. The evenly distributed MPDA and Pso were subsequently mixed and stirred in a magnetic stirrer for 24 h at room temperature.

2.4.3 Characterization of MPDA and MPDA-Pso

The surface morphology and diameter of MPDA and MPDA-Pso composites were determined by transmission electron microscopy (TEM). The zeta potential was used to assess the stability of MPDA and MPDA-Pso, and the peaks for MPDA and MPDA-Pso were characterized using a Fourier transform infrared spectrometer (NICOLET iS50 FT-IR) and ultraviolet spectrophotometer.

2.5 Effect of MPDA-Pso nanoparticles on osteogenic differentiation

2.5.1 Alizarin red staining

PDLSCs were added to six-well plates at 2×10^5 cells per well and divided into four groups: an MPDA group, Pso group, MPDA-Pso group, and blank control group. The medium was changed every 3 days for 21 days, and the cells were then fixed with 4% paraformaldehyde, washed with PBS, and stained with alizarin red.

2.5.2 Alkaline phosphatase staining

PDLSCs were added to six-well plates at a concentration of 2×10^5 cells per well and grouped as 2.5.1 cells, and we changed the solution every 3 days and co-cultured them for 14 days. The cells were then fixed in 4% paraformaldehyde (Solarbio, China) for 30 min, washed with PBS, and stained with an ALP staining kit.

2.5.3 Quantification of alkaline phosphatase

After 14 days, the existing medium was removed, and the cells were fixed with 4% paraformaldehyde and rinsed with PBS. The cells in each group were then lysed on ice. Protein concentration was assessed with a BCA kit, and absorbance was measured at 520 nm after treatment with an ALP kit, and ALP activity was calculated according to the formula.

2.5.4 Detection of osteogenesis-related gene expression in PDLSCs

PDLSCs were seeded in six-well plates and grouped as in 2.5.1 above. After 7 days of culture, the RNA was extracted and its concentration was analyzed. The expression of ALP was determined by q-PCR using QuantiNova PCR Kits (QIAGEN, Germany). We adopted GAPDH as an internal reference for all samples, and the results were quantified as relative expression using the $2^{-\Delta\Delta}$Ct method. The primers that we used for ALP were 92 ACT CTC CGA GAT GGT GGTGGT G (forward) and 92 CGT GGT CAA TTC TGC CTC CTT CC (reverse). Three replicates of the experiment were performed for each group.

2.5.5 Effects of MPDA-Pso nanoparticles on osteogenesis in rats with alveolar bone defects

To verify the osteogenic effects of MPDA-Pso nanoparticles *in vivo*, we anesthetized eight-week-old Sprague-Dawley rats using sodium pentobarbital, extracted their maxillary first molar, and established an alveolar bone-defect model. Following tooth extraction we applied a gelatin sponge, gelatin sponge combined with MPDA, gelatin sponge combined with MPDA-Pso, or a control group with no material to the alveolar socket. The maxilla (which included the alveolar bone-defect site) was dissected from the sacrificed rats on days seven and 28. Micro-computed tomography (micro-CT) was employed to reconstruct 3D images of alveolar bone defects and to conduct a quantitative analysis. We also performed hematoxylin and eosin (H&E) staining to evaluate the degree of alveolar bone healing. Our experimental procedures complied with the NIH Guide for the Care and Use of Laboratory Animals (United States); and the present study was approved by the Ethics Committee of Qingdao University (QDU-AEC-2024475).

3 Results

3.1 Effect of pso on osteogenic differentiation of PDLSCs

3.1.1 Culture and identification of PDLSCs

PDLSCs have the potential of self-renewal and multi-lineage differentiation, and are vital to the repair of periodontal tissue damage and the regenerative treatment of periodontal disease (Calabrese, 2021). These cells are also the primary source of newly attaching cells following periodontitis treatment (Yu et al., 2017). We first cultured PDLSCs and identified them, and observed that the primary stem cells grew radially around the tissue block and were arranged in a vortex shape, exhibiting a typically long spindle shape (S1 A). After osteogenic and adipogenic induction, mineralized red nodules (S1 C) and pink lipid droplets (S1 D) were observed microscopically. Flow-cytometric analysis showed that the primary stem cells exhibited characteristics of mesenchymal stem cells (MSCS)—i.e., the cells were positive for CD73, CD90, and CD105 (S1 F), while they were negative for CD34 and CD45 (S1 E). These results indicated that the cells we extracted were, in fact, PDLSCs, and that PDLSCs manifested the basic characteristics of BMSCs.

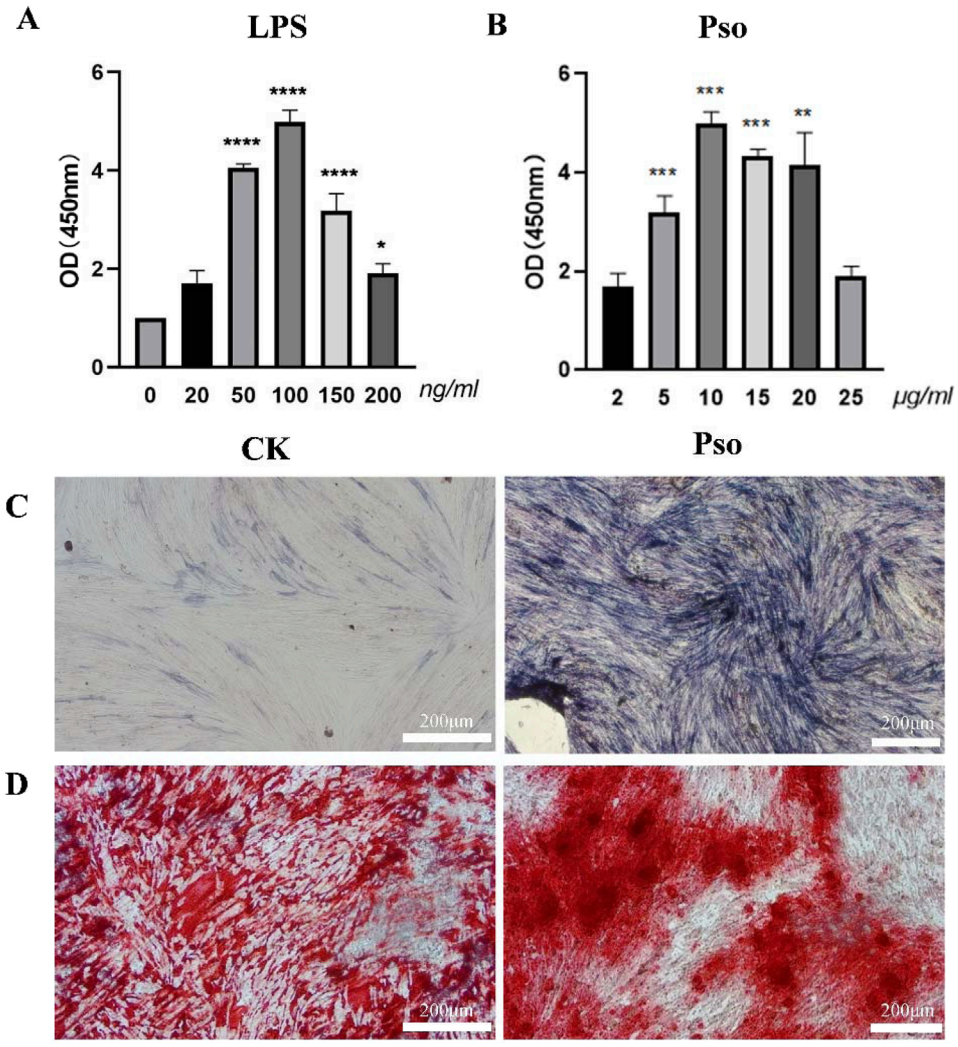

FIGURE 1
Effects of Pso on PDLSCs. **(A)** Impact of various concentrations of Pso on the viability of PDLSCs. **(B)** Influence of different concentrations of LPS on the viability of PDLSCs. **(C)** Representative images of ALP staining. CK, PDLSCs only; Pso, PDLSCs plus Pso. **(D)** Representative images of alizarin red staining (scale bar = 200 μm). Data are expressed as means ± SD. $^{*}P < 0.05$, $^{**}P < 0.01$, $^{***}P < 0.001$, and $^{****}P < 0.0001$.

3.1.2 Effects of Pso on PDLSCs

LPS is known to stimulate the production of pro-inflammatory cytokines *in vitro*, and has been employed to simulate periodontal inflammatory disease (Stemmler et al., 2021). In order to emulate the periodontal microenvironment, PDLSCs were co-cultured with LPS, according to the references and our CCK-8 assay showed that 100 ng/mL LPS can simulate periodontitis environment and did not inhibit the proliferation of PDLSCs (Figure 1A). On this basis, we found that 10 μg/mL Pso significantly promoted the activity of PDLSCs (Figure 1B). Additionally,We noted that as LPS concentration increased, the enhancement in cellular vitality became less pronounced. Consequently, we selected 10 μg/mL Pso and 100 ng/mL LPS for subsequent experiments. ALP staining revealed a distinct blue-black coloration in the Pso group relative to the control group (Figure 1C), denoting a higher production of ALP in the former group. Additionally, alizarin red staining demonstrated an increased presence of calcium nodules in the Pso group (Figure 1D), further supporting the conclusion that Pso promoted the osteogenic differentiation of PDLSCs.

3.2 Drug-target-pathway network construction

3.2.1 Network pharmacology screening of drug targets

To elucidate the mechanism underlying Pso-induced osteogenic differentiation of PDLSCs, we initially conducted a network pharmacology analysis to predict potential targets of Pso. After deduplication through database queries, we obtained 24 active compound targets and 1,800 chronic periodontitis-related therapeutic targets (Figure 2A). Eight genes were ultimately identified that served as both target genes of active

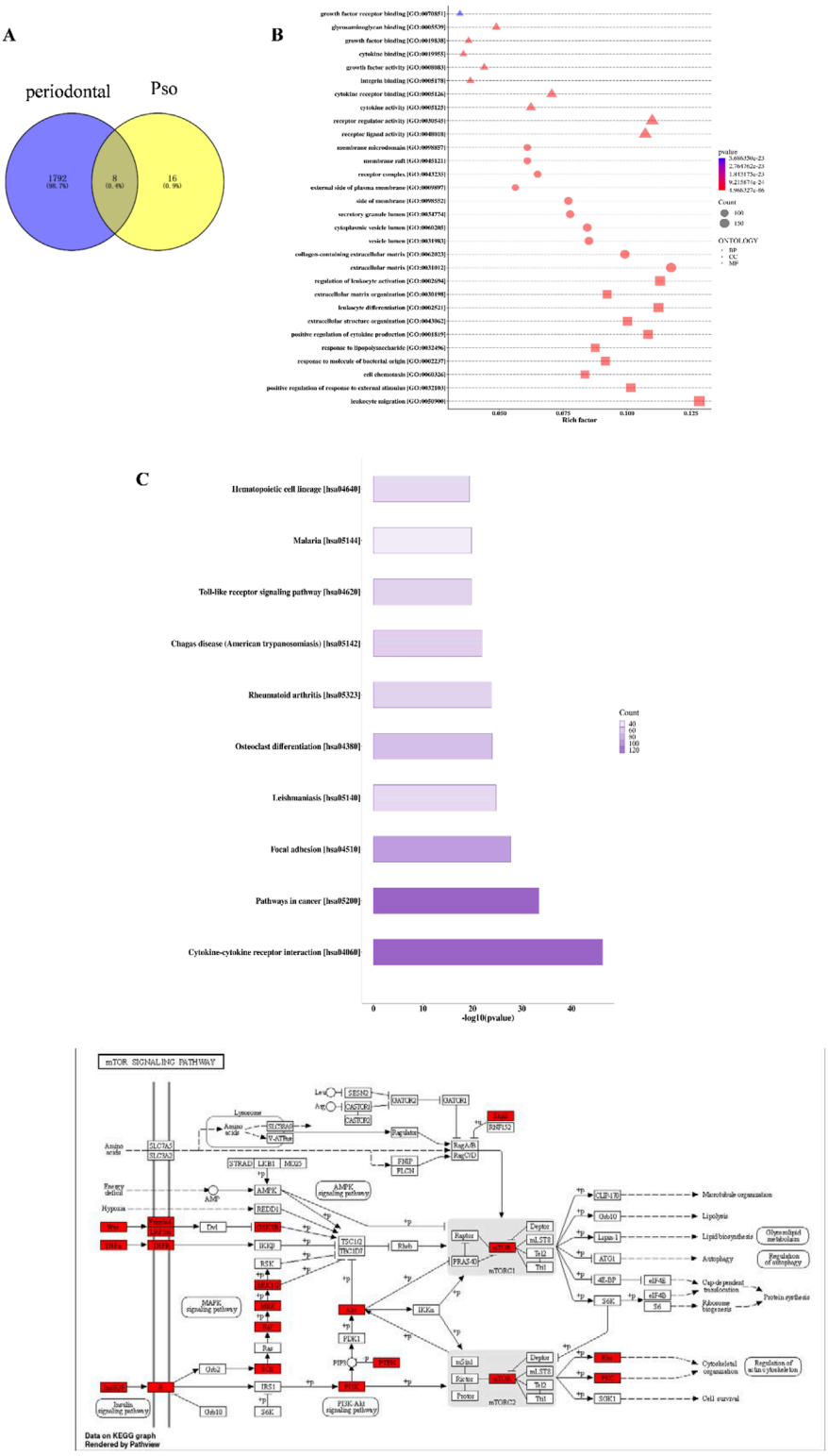

FIGURE 2
Network pharmacology results. **(A)** Venn diagram of Pso and chronic periodontitis targets. **(B)** Bubble chart of GO-enrichment analysis for Pso targets. The horizontal axis represents the rich factor value of the enrichment degree, and the vertical axis represents the GO Term. Of these, the size of the shape represents the number of differentially expressed proteins mapped. The larger the shape, the greater the number. The color of the shape represents the size of the corrected p-value; the redder the color, the smaller the p-value. BP, Biological Process; CC, Cellular Component; MF, Molecular Function. Diagram of the mTOR-signaling pathway in the KEGG database; red boxes indicate DEGs. **(C)** Histogram of KEGG-enrichment analysis of the top 10 target protein pathways affected by Pso. In the figure, the abscissa is –log10 (p-value) and the ordinate is the pathway name. The length of the column represents the size of the p-value; the longer the column, the smaller the p-value; and the darker the color, the more target proteins mapped to this pathway. **(D)** KEGG pathway analysis of metabolic mTOR diagram detailing target proteins; red denotes the target-expressed proteins.

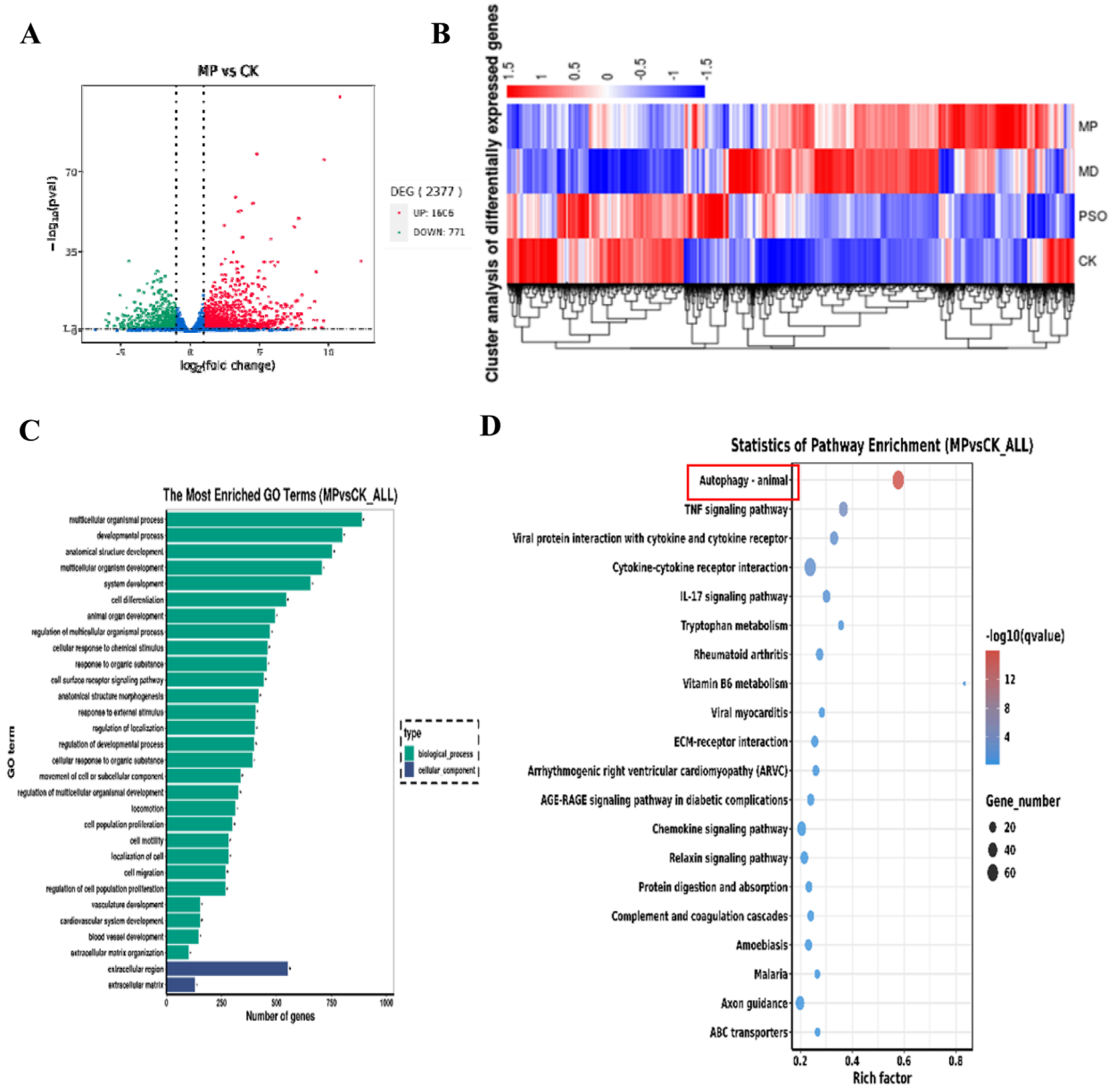

FIGURE 3
Transcriptomic-sequencing analysis as applied to investigate the effects of Pso on LPS-induced PDLSCs. **(A)** Volcano plot of the number of DEGs; red dots signify upregulated genes, and green dots denote downregulated genes with significant differential expression. **(B)** Differential expression-clustering diagram; the color-gradient transitions from red to blue indicate a diminution in log(FPKM+1) values. **(C)** Top 10 GO functional-enrichment analysis. Green denotes biological processes, while blue signifies cellular components. **(D)** KEGG functional-enrichment analysis features the pathway names on the vertical axis and the rich factor on the horizontal axis; the size of each point reflects the number of DEGs within the corresponding pathway, and the color of the points corresponds to different Q-value ranges. The top 20 significantly enriched pathways were sorted from smallest to largest by Q-value, and the red box in the figure denotes the most obvious pathway for enrichment for visual emphasis, and the red box in the figure denotes the most obvious pathway for enrichment for visual emphasis.

ingredients and genes associated with chronic periodontitis. Enrichment analysis of the target proteins revealed that Pso targeted a variety of immune- and inflammation-related signaling pathways, including the mTOR signaling pathway, Toll-like receptor signaling pathway, and MAPK signaling pathway (Figures 2B–D); and of these, the mTOR signaling pathway was specifically related to osteogenesis (Laplante and Sabatini, 2012).

3.2.2 Use of transcriptomic sequencing to screen pso targets

In order to explore the mechanism(s) underlying Pso influences on the osteogenic differentiation of PDLSCs, we sequenced RNA extracted from the cultured cells using an Illumina second-generation high-throughput sequencing platform. This approach allowed us to assess the impact of Pso on PDLSCs, particularly in the context of LPS-induced differential gene expression. In

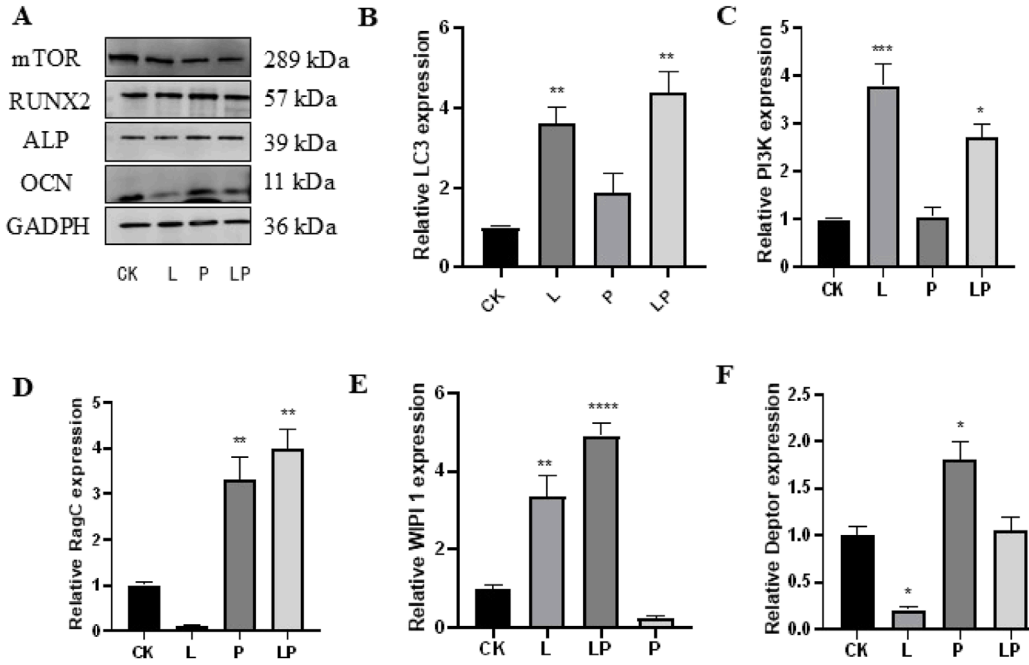

FIGURE 4
Verification of the effect of Pso on PDLSCs. **(A)** Representative protein expression bands for mTOR, OCN, RUNX2, ALP, and GADPH. **(B–F)**: Expression of LC3, PI3K, Rag C, WIPI 1, and Deptor genes. CK, blank control; L, LPS group; P, Pso group; LP, Pso/LPS co-culture group. Data are presented as mean ± SD. $^{*}P < 0.05$, $^{**}P < 0.01$, $^{***}P < 0.001$, and $^{****}P < 0.0001$ vs. control group.

comparison to the control group, we identified 2,377 DEGs in the cells cultured with both LPS/PSO, of which 1,606 were upregulated and 771 were downregulated (all $P < 0.05$) (Figure 3A). When Pso was administered to LPS-induced PDSLCs, the DEGs were predominantly enriched in biological processes, including developmental processes, cell differentiation, and cell regulation (Figure 3B).

In order to further identify the targeting pathway for Pso, we performed GO and KEGG functional-enrichment analyses of the DEGs, and noted that the most significantly enriched differences were observed in the pathways related to autophagy and mitophagy (Figure 3D). Among these factors, the enriched difference in the mTOR pathway was particularly significant, implying that this pathway was critical to the osteogenic process with respect to inflammatory PDLSCs. We therefore speculate that mTOR signaling may constitute a key pathway involved in the osteogenic differentiation of PDLSCs.

3.2.3 Effect of pso on PDLSCs

When we evaluated the expression of related proteins by Western blot analysis, we observed that the expression levels of the osteogenesis-related genes OCN, RUNX2, and ALP were significantly downregulated in the LPS group, while they were elevated following the addition of Pso. Relative to the control group, mTOR expression was notably downregulated in the PSO group. These results suggested that Pso promoted the osteogenic differentiation of PDLSCs, a process that may be associated with mTOR (Figure 4A).

3.2.4 Evaluation of mTOR pathway-related genes

In order to further clarify the mechanism by which mTOR regulated osteogenesis, we evaluated the differential expression of genes related to the mTOR pathway based on the results of transcriptomic sequencing. As can be viewed from the figure, after adding LPS and compared to the control group, the expression levels of LC3 and PI3K increased, while the expression of Deptor diminished; and again compared to the control group, the genes with augmented expression included Deptor, Rag C, and WIPI 1 in the Pso group (Figures 4B–F). These findings were thus consistent with our sequencing results.

3.3 Effects of mTOR on osteogenic differentiation in PDLSCs

3.3.1 Effects of an mTOR inhibitor on PDLSCs

In order to examine the relationship between the mTOR-signaling pathway and osteogenesis of PDLSCs, we added rapamycin as an mTOR inhibitor to cultured PDLSCs. Results indicated that the addition of the mTOR inhibitor significantly attenuated the gene-expression level of mTOR (Figure 5A) while simultaneously upregulating Rag C (Figure 5B). We also ascertained that after adding Pso to PDLSCs incubated with the mTOR inhibitor, the expression of Rag C protein was upregulated; and that the gene- and protein-expression levels for the osteogenic markers ALP and RUNX2 tended to increase, but not to a significant degree (Figures 5C–F). This indicated that Pso regulated osteogenic differentiation via mTOR.

10.3389/fcell.2025.1634945

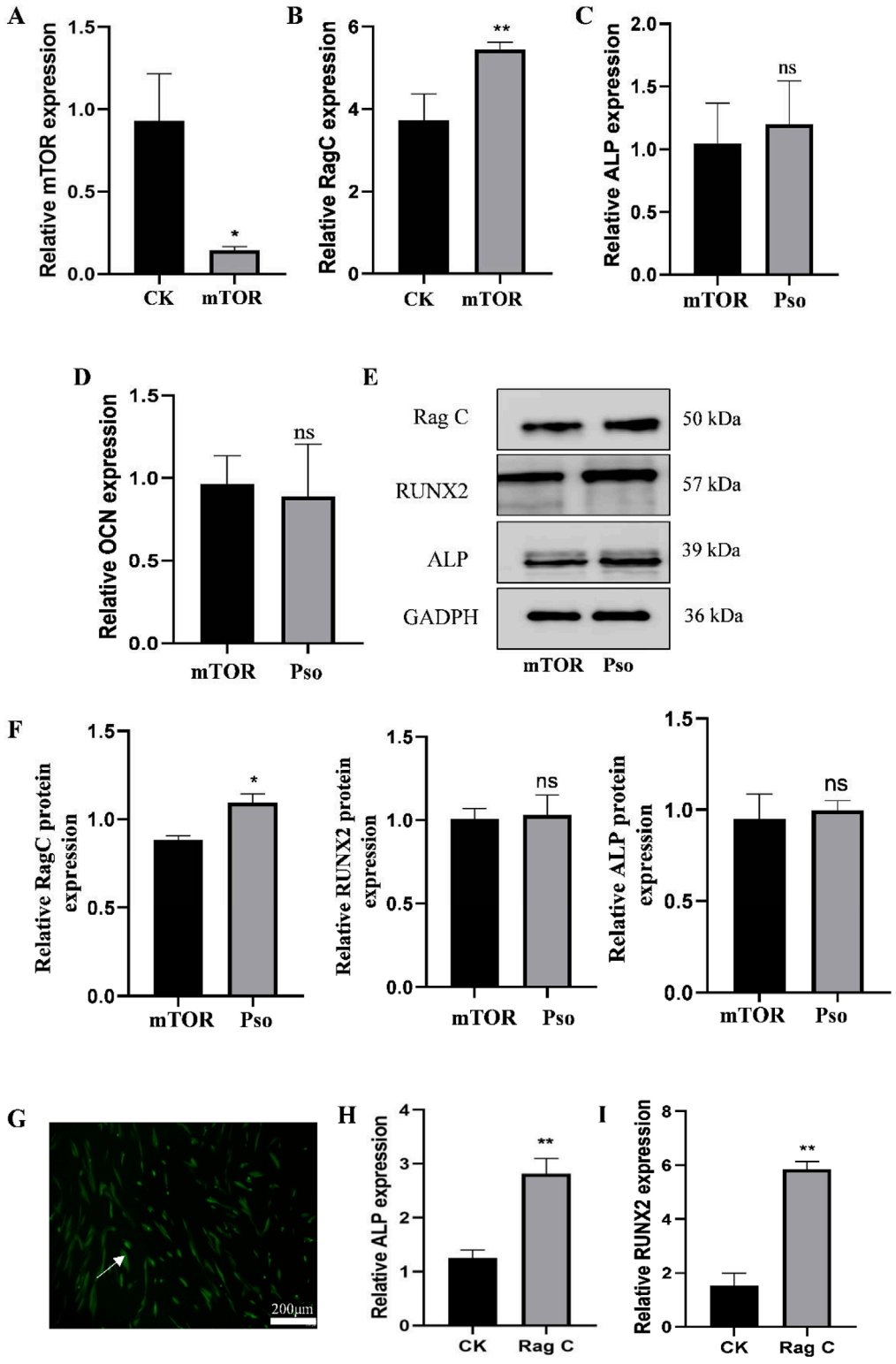

FIGURE 5
Expression of related genes and proteins after the addition of mTOR inhibitor. **(A)** Expression level of the mTOR gene after adding the inhibitor rapamycin. **(B)** Change in the expression levels of the Rag C gene. **(C–D)** Changes in the expression levels of the osteogenesis-related genes ALP and RUNX2. **(E)** Protein expression levels for of Rag C, Deptor, ALP, and RUNX2. CK, control group; mTOR, mTOR-inhibitor group. **(F)** Relative expression levels of Rag C, ALP, and RUNX2 proteins. mTOR, mTOR-inhibitor group; Pso, mTOR inhibitor + Pso group. **(G)** Representative images of PDLSCs with Rag C lentiviral knockdown; green fluorescence indicates the lentiviral vector particles. **(H–I)** Expression changes in ALP and RUNX2 in PDLSCs with Rag C knockdown. CK, control group; Rag C, PDLSCs (scale bar = 200 μm). Data are presented as mean ± SD. *P < 0.05, **P < 0.01, ***P < 0.001, and ****P < 0.0001 vs. the control group.

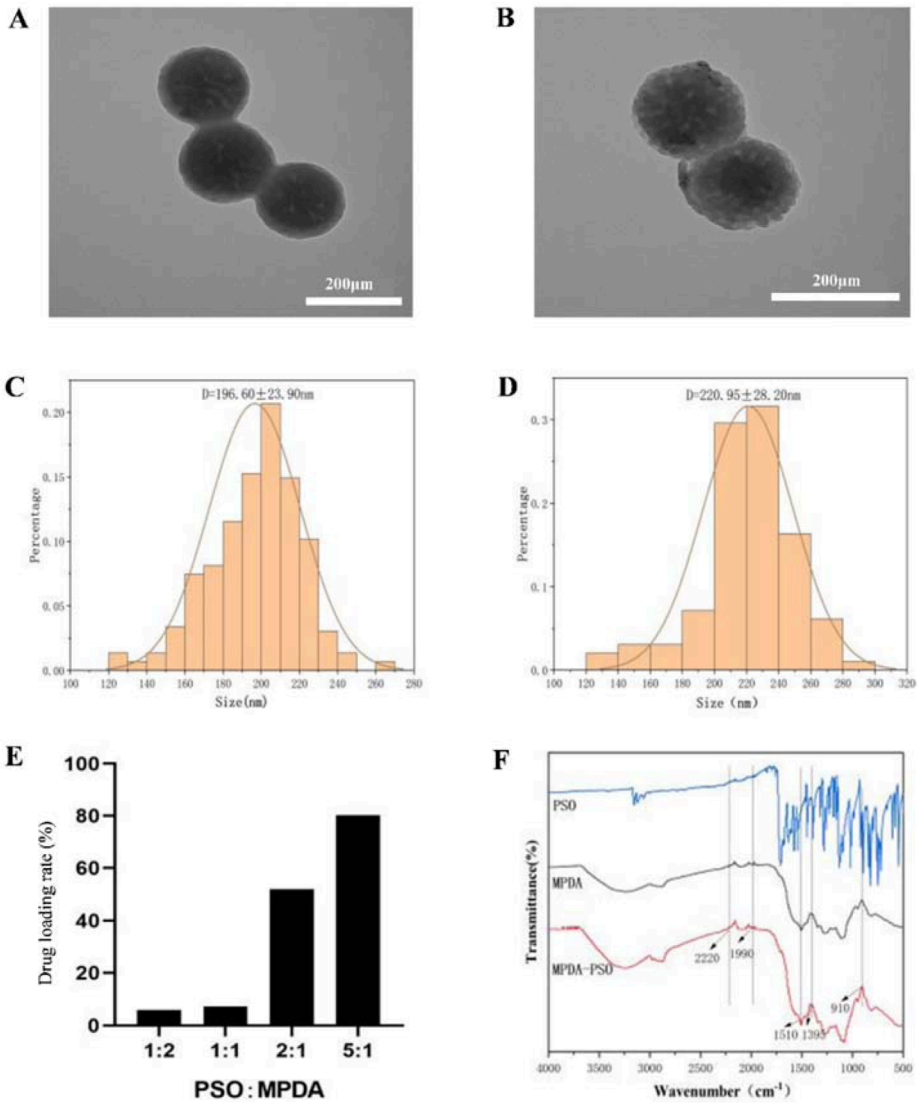

FIGURE 6
Characterization of MPDA-Pso nanoparticles. **(A)** Representative TEM image of MPDA nanoparticles. **(B)** Representative TEM image of MPDA-Pso nanoparticles. **(C)** Diagram of particle size distribution of MPDA. **(D)** Diagram of particle size distribution of MPDA-Pso nanoparticles. **(E)** Changes in the drug-loading rate of MPDA-Pso nanoparticles prepared with different ratios of Pso/MPDA. **(F)** Images of Fourier transform infrared spectrophotometry (FTIS); the three lines from top to bottom are the absorption peaks of Pso, MPDA, and MPDA-Pso.

3.3.2 Rag C knockdown by lentiviral transfection of PDLSCs

In order to further assess the underlying mechanism of action for Pso in the Rag C/mTOR-signaling axis and to investigate the role of mTOR in the osteogenic differentiation of PDLSCs, we constructed lentiviral vectors to establish PDLSCs with Rag C knockdown. The presence of green fluorescence in the cells validated the success of the lentiviral transfection (Figure 5G), and we observed that the osteogenic genes ALP and RUNX 2 were upregulated after lentiviral knockdown compared to the controls (Figures 5H,I). This result confirmed that Rag C functioned as an upstream regulator of mTOR and that Pso limited mTOR signaling via Rag C, thus modulating the osteogenic differentiation of PDLSCs.

3.4 Preparation and application of MPDA-Pso nanoparticles

3.4.1 Preparation and characterization of MPDA-Pso nanoparticles

In order to improve the physical properties of Pso, we prepared MPDA nanoparticles loaded with Pso. The optimal drug loading rate was approximately 80.30% when the Pso:MPDA ratio was 5:1 (Figure 6E). Under electron microscopy, the prepared MPDA nanoparticles were spherical and showed a pore structure (Figures 6A,C). The mean size of the MPDA nanoparticles was 196.60 ± 21.90 nm, and the zeta potential was −23 mv. Pso was encapsulated in MPDA mesopores, and the MPDA-Pso nanoparticles were spherical in shape (Figure 6B) and of various

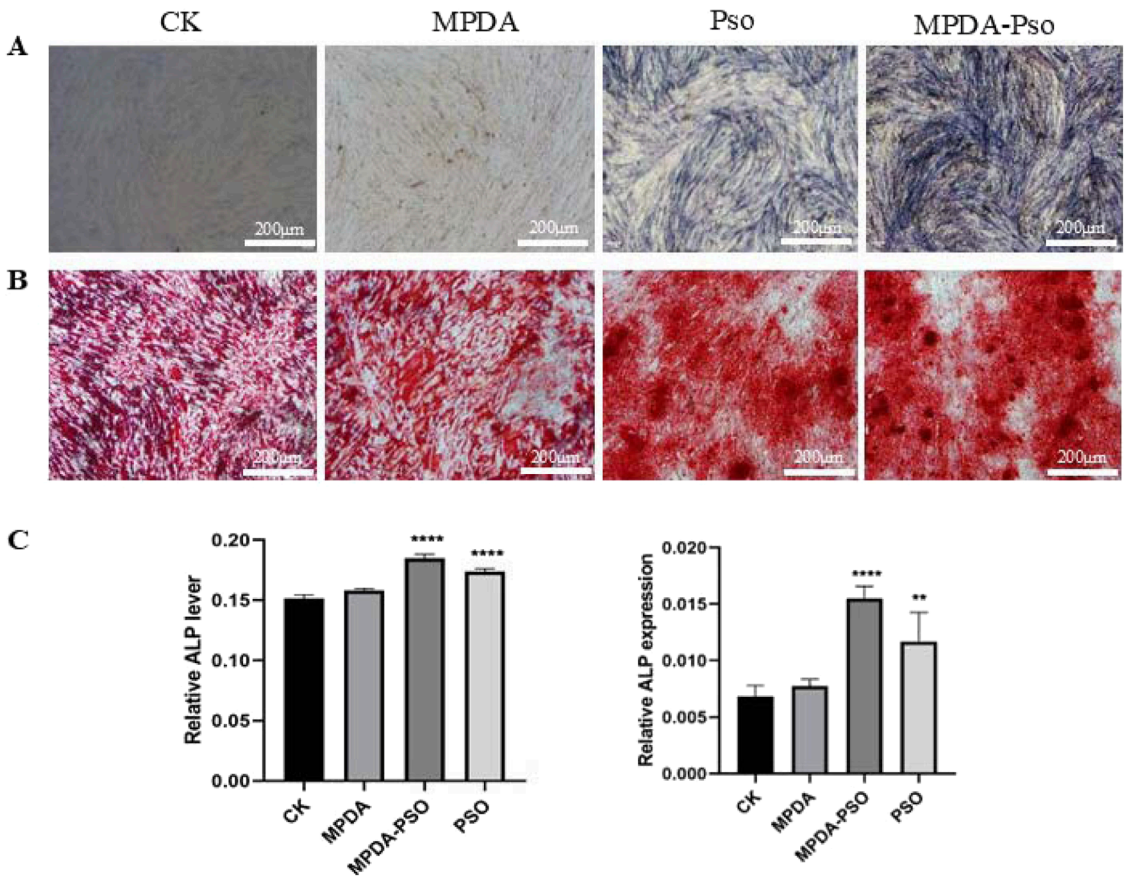

FIGURE 7
MPDA-Pso promotes osteogenesis of PDLSCs. **(A)** Images of ALP staining. **(B)** Alizarin red-stained images. **(C)** ALP activity and gene-expression analyses (scale bar = 200 μm). Data are presented as mean ± SD. $^{*}P < 0.05$, $^{**}P < 0.01$, $^{***}P < 0.001$, and $^{****}P < 0.0001$ vs. control group.

particle sizes with a mean ± SD of 220.95 ± 28.20 nm (Figure 6D). After drug loading, the particle size and shape did not change significantly, and the zeta potential was −22.7 mv.

Fourier infrared spectra (Figure 6F) showed a series of changes in the MPDA-Pso nanoparticles compared to MPDA alone. The characteristic peak change at 1395 cm-1 represented the bending and tensile vibration of the C-O-H bond, the peak change at 910 cm-1 represented the vibration of the C-O bond of the oxygen-containing functional group in MPDA, and the peak change at 1510 cm-1 represented the shear vibration of the N-H bond. In conclusion, these characteristic peak changes further proved that Pso was successfully loaded and that the MPDA-Pso nanomaterials were prepared successfully.

3.4.2 Effect of MPDA-Pso nanoparticles on osteogenic differentiation of PDLSCs

To verify an effect of the prepared MPDA-Pso nanomaterials on osteogenic differentiation of PDLSCs, MPDA-Pso nanoparticles were co-cultured with PDLSCs, with the control group and the MPDA group displaying no significant blue coloration. In contrast, the cells in both the Pso and MPDA-Pso groups were stained intensely bluish; however, the staining area of the Pso group was notably smaller than that of the MPDA-Pso group (Figure 7A). The results of alizarin red staining mirrored those of ALP staining, with the most prominent red calcium nodules observed in the MPDA-Pso group, while such nodules were infrequently observed in the control and MPDA groups (Figure 7B). After 14 days of cell culture, ALP activity and ALP gene expression were assessed, and we noted significant differences among the Pso group, the MPDA-Pso group, and the control group. Both the Pso group and the MPDA-Pso group exhibited significantly enhanced ALP activity and ALP gene expression in the cells (Figures 7C,D). These results indicated that MPDA-Pso nanomaterials and Pso promoted the osteogenic differentiation of PDLCs.

3.4.3 Effects of MPDA-Pso nanoparticles on osteogenesis in rats with alveolar bone defects

To evaluate the osteogenic effects of MPDA-Pso nanomaterials *in vivo*, we constructed a rat model of maxillary first molar defect, conducted micro-CT analysis 7 days and 28 days after the application of the materials, and noted that the amount of new bone in the MPDA-Pso group increased compared to the control group. Alveolar bone healing was also better at 28 days than at 7 days (Figures 8A,B).

To assess the extent of alveolar bone healing, we conducted histologic analyses to evaluate alveolar inflammation and cellular proliferation at seven and 28 days post-reaction, and observed that all groups manifested an inflammatory response at 7 days. Although the proportion of new bone within the alveolar socket

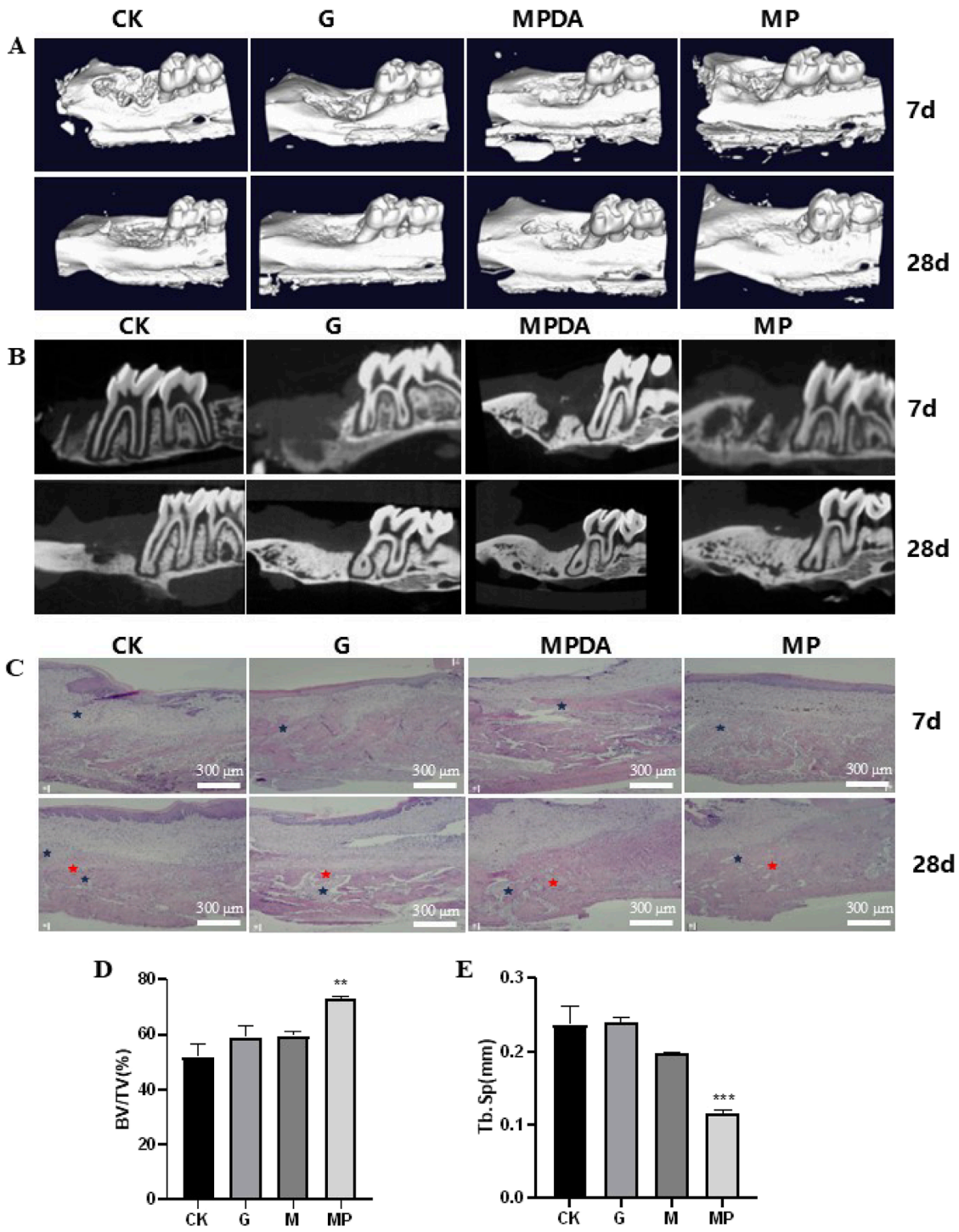

FIGURE 8
Effect of MPDA-Pso on osteogenesis in defective alveolar bone in rats. **(A–B)**: micro-CT images on days 7 and 28. **(C)**: H&E-stained images of alveolar bones; blue marks indicate inflammatory cell infiltration, and red marks indicate new bone tissue. **(D)**: Trabecular bone parameter BV/TV as obtained by micro-CT analysis. **(E)** Tb. Sp data analysis as obtained by micro-CT analysis. CK, control group; G, gelatin sponge; MPDA, gelatin sponge combined with MPDA; MP, gelatin sponge with MPDA-Pso BV/TV, bone volume per tissue volume; Tb. Sp, trabecular separation (scale bar = 300 μm). Data are expressed as mean ± SD. $^{**}P < 0.01$ and $^{***}P < 0.001$.

had increased significantly in the MPDA-Pso group by 28 days, the remaining three groups demonstrated more pronounced inflammatory responses in alveolar bone compared to the MPDA-Pso group (Figure 8C). We attribute the diminished inflammatory response observed in the MPDA-Pso group to the material's beneficial effect on the osteogenic differentiation of BMSCs, as it facilitated the transformation of granulation tissue into woven bone.

Our results also revealed that the bone volume fraction (BV/TV) in the MPDA-Pso group was significantly higher than that in the control group ($P < 0.01$) (Figure 8D). However, there was no significant difference in BV/TV between the gelfoam group or the MPDA group compared to the control group. Additionally, trabecular separation (Tb.Sp) in the MPDA-Pso group was significantly lower than in the control group ($P < 0.001$) (Figure 8E). These findings suggested that MPDA-Pso nanomaterials effectively promoted osteogenesis in rat alveolar sockets.

4 Discussion

Chronic periodontitis is at a high incidence in the human population, and can cause non-renewable inflammatory destruction of periodontal bone tissue (Van Der Velden, 2000). Additionally, LPS, the primary antigenic component of the outer membrane of Gram-negative bacteria such as Porphyromonas gingivalis, is able to stimulate local periodontal tissue cells and immune cells to produce a large number of inflammatory mediators, thus playing an important role in the pathogenesis of periodontitis (Gasmi et al., 2022; Xu et al., 2020; Zhang et al., 2023). PDLSCs are the principal source of newly attached cells after periodontitis treatment, manifest a variety of differentiative potentials, and can be employed as ideal model cells for regenerative engineering of periodontal tissue (Tomokiyo et al., 2019; Li et al., 2014).

Pso has been confirmed to exert anti-inflammatory, antibacterial, and osteogenic differentiative activities; and is widely applied to diseases such as psoriasis and vitiligo (Olafsson et al., 2023; Thakur et al., 2020). Our previous study also confirmed that systemic application of Pso significantly reduced alveolar bone loss in rats with periodontitis via modulation of the intestinal flora. Based upon the above considerations, we conducted a network pharmacology analysis to further explore the mechanism(s) by which Pso influences the osteogenic differentiation of PDLSCs. Network pharmacology results showed that Pso affected various biologic pathways and processes used by PDLSCs, including autophagy as related to osteogenesis. We therefore hypothesized that the effect of Pso on LPS-induced PDLSCs was associated with autophagy.

Autophagy is a process of cellular self-degradation and recycling of intracellular components, and plays an important role in the pathogenesis of immune regulation, infection, inflammation, tumors, and neurodegenerative and other diseases (Glick et al., 2010; Mizushima and Komatsu, 2011). It is currently postulated that autophagy is a defense-and-stress regulatory mechanism that is bidirectional (Onorati et al., 2018). Some studies have shown that *P.* gingivalis induces the production of autophagosomes (Lee et al., 2018), and there is also evidence that an enhanced autophagic response inhibits the intracellular survival of A. actinomycetes in a patient's THP-1 monocyte line infected with this bacterial species (Chung et al., 2018). In order to explore the relationships among Pso, autophagy, and periodontitis in an inflammatory environment, we simulated the inflammatory microenvironment characteristic of patients with periodontitis and performed transcriptomic sequencing. Through enrichment analysis and molecular function annotation of the differential genes involved, we discovered that the autophagic process in PDLCs was significantly affected by Pso, and that the mTOR-signaling pathway was crucial to the process. The mTOR-signaling pathway is an important cell-signaling pathway that participates in a variety of biologic processes such as cell growth, autophagy, and metabolism (Liu and Sabatini, 2020; Wang and Zhang, 2019; Kim and mtor, 2015); Yang G et al. found that MTORC1 is not only an executor of RagC phosphorylation, but also achieves feedback regulation of its own activity. This feedback regulation mechanism enables the mTORC1 signaling pathway to more accurately respond to changes in the intracellular and extracellular environment, maintaining the balance of cell growth, proliferation, and metabolism (Yang et al., 2019). and Abudu et al. ascertained that mTORG1 (a WD domain repeat protein of the mTOR family) inhibited mTOR signaling via Rag GTPases (Rags A–D), thereby promoting infrastructural autophagy (Abudu et al., 2024). The NLRP3 inflammasome produced by periodontitis can promote the maturation and secretion of inflammatory cytokines such as IL-1β and IL-18, while autophagosomes can recognize and encapsulate the NLRP3 inflammasome to degrade it, thereby inhibiting the large-scale production of inflammatory cytokines such as IL-1β and IL-18 from the source, effectively reducing inflammatory damage to periodontal tissue (Hashim et al., 2024; Isola et al., 2022). Recent evidence has shown that autophagy is involved in osteogenesis and bone development, and that AMP-activated protein kinase (AMPK) and mTOR are essential for autophagy (Cheng et al., 2019). Huang et al. also discerned that mTOR inactivation inhibited osteoblast proliferation and promoted differentiation (Huang et al., 2015).

To investigate the role of the mTOR-signaling pathway in the osteogenic differentiation of PDLSCs induced by Pso, we added the mTOR-inhibitor rapamycin to the cells. Our results demonstrated that after adding Pso to the PDLSCs and successfully inhibiting mTOR, the gene- and protein-expression levels of the osteogenesis-related factors ALP and RUNX2 tended to be upregulated (although they were not statistically different). In contradistinction, the expression levels of the Rag C gene increased significantly, indicating that Rag C was an upstream regulator of mTOR, and that the mTOR-signaling pathway was key to enhancing the differentiative capability of PDLSCs toward osteogenesis by Pso. This result also provides evidence for the application of Pso in the treatment of periodontitis.

In order to elucidate the upstream and downstream mechanisms underlying Pso effects on the mTOR pathway, we established a lentiviral Rag C-knockdown model using PDLSCs; and our analysis revealed that the expression of the osteogenesis-related genes ALP and RUNX2 was upregulated, indicating the impact of Rag C on mTOR signaling. We therefore speculate that Pso limited mTOR signaling by inhibiting Rag C, and that it modulated autophagy and stem cell osteogenesis by regulating the Rag C/mTOR-signaling axis.

Pso is slightly soluble in water, engendering a challenge to its use as an oral medication. To modify its physical properties so as to improve therapeutic efficacy, we selected MPDA as a carrier and prepared MPDA-Pso nanoparticles. This material exhibited a large surface area, facilitated surface modification, possessed favorable biocompatibility, and was convenient for loading drugs—making it widely available for use as a drug-delivery system (Liu et al., 2021). We synthesized MPDA-Pso nanoparticles that significantly increased the water solubility of Pso, and co-cultured these nanoparticles with PDLSCs. Our results indicated that MPDA-Pso nanoparticles promoted the osteogenic differentiation of PDLSCs, suggesting that, while MPDA-Pso altered

the physical properties of Pso, it did not affect the material's capacity to promote osteogenesis.

We subsequently performed micro-CT scan analysis on the maxillary bones of rats that were raised for 7 and 28 days following the application of the materials. The analysis revealed that alveolar bone healing encompassed several processes, including inflammatory cell infiltration, angiogenesis, fibroblast migration, collagen deposition, and bone remodeling (Thoma et al., 2017), of which the bone-remodeling process was the most significant. These results demonstrate that MPDA-Pso significantly increased the volume of bone mass and significantly reduced trabecular bone separation, demonstrating its potential for effectively promoting alveolar bone formation in rats.

5 Conclusion

In summary, we herein demonstrated that Pso promotes the osteogenic differentiation of PDLSCs. Specifically, Pso's promotional effect on the osteogenic differentiation of inflammatory PDLSCs was generated via its regulation of the Rag C/mTOR-signaling axis and the autophagic process, thus modulating stem cell osteogenesis. Furthermore, the MPDA-Pso nanoparticles we developed were shown to promote osteogenic differentiation of PDLSCs *in vitro* and to facilitate alveolar bone formation in rats *in vivo*. Collectively, our findings offer novel insights into the mechanisms by which Pso enhances osteogenic differentiation of PDLSCs within an inflammatory microenvironment, and potentially facilitates its application in the treatment of chronic periodontitis. Our experiments also revealed that the mechanism whereby Pso promoted osteogenic differentiation of PDLSCs involved a combination of multiple pathways, highlighting the necessity for the further examination of other potential underlying mechanisms.

Data availability statement

The original contributions presented in the study are included in the article/Supplementary Material, further inquiries can be directed to the corresponding authors.

Ethics statement

The studies involving humans were approved by Approval document of Ethics Committee Medical College of Qingdao University. The studies were conducted in accordance with the local legislation and institutional requirements. The participants provided their written informed consent to participate in this study. The animal study was approved by Approval document of Ethics Committee Medical college of Qingdao University. The study was conducted in accordance with the local legislation and institutional requirements.

Author contributions

YW: Visualization, Investigation, Software, Formal Analysis, Methodology, Writing – original draft. HZ: Resources, Writing – original draft, Supervision. JY: Methodology, Writing – original draft, Investigation. JJ: Investigation, Resources, Writing – original draft. ZF: Investigation, Validation, Resources, Writing – original draft. YH: Investigation, Writing – original draft, Supervision. QH: Supervision, Writing – original draft, Investigation. RM: Writing – review and editing, Investigation, Supervision. YX: Writing – review and editing, Supervision, Visualization, Methodology. YW: Funding acquisition, Validation, Supervision, Conceptualization, Writing – review and editing, Methodology.

Funding

The author(s) declare that financial support was received for the research and/or publication of this article. This work was supported by the National Natural Science Foundation of China (82301083), National Administration of Traditional Chinese Medicine - Health Commission of Shandong Provincel joint project (GZY-KJS-SD-2023-007), Shandong Traditional Chinese Medicine Science and Technology Project (2021Z030), Qingdao Key Health Discipline Development Fund (2025-2027), Qingdao Clinical Research Center for Oral Diseases (22–3-7-lczx-7-nsh), and Shandong Provincial Key Medical and Health Discipline of Oral Medicine (Qingdao University Affiliated Qingdao Stomatological Hospital) (2025-2027).

Acknowledgments

We thank LetPub (www.letpub.com.cn) for its linguistic assistance during the preparation of this manuscript.

Conflict of interest

The authors declare that the research was conducted in the absence of any commercial or financial relationships that could be construed as a potential conflict of interest.

Generative AI statement

The author(s) declare that no Generative AI was used in the creation of this manuscript.

Publisher's note

Supplementary material

The Supplementary Material for this article can be found online at: https://www.frontiersin.org/articles/10.3389/fcell.2025.1634945/full#supplementary-material

References

Abudu, Y. P., Kournoutis, A., Brenne, H. B., Lamark, T., and Johansen, T. (2024). MORG1 limits mTORC1 signaling by inhibiting rag GTPases. *Mol. Cell* 84 (3), 552–69.e11. doi:10.1016/j.molcel.2023.11.023

Calabrese, E. J. (2021). Human periodontal ligament stem cells and hormesis: enhancing cell renewal and cell differentiation. *Pharmacol. Res.* 173, 105914. doi:10.1016/j.phrs.2021.105914

Chen, F., Xing, Y., Wang, Z., Zheng, X., Zhang, J., and Cai, K. (2016). Nanoscale polydopamine (PDA) meets π-π interactions: an interface-directed coassembly approach for mesoporous nanoparticles. *Langmuir* 32 (46), 12119–12128. doi:10.1021/acs.langmuir.6b03294

Cheng, Y., Huang, L., Wang, Y., Huo, Q., Shao, Y., Bao, H., et al. (2019). Strontium promotes osteogenic differentiation by activating autophagy via the the AMPK/mTOR signaling pathway in MC3T3-E1 cells. *Int. J. Mol. Med.* 44 (2), 652–660. doi:10.3892/ijmm.2019.4216

Chung, J., Kim, S., Lee, H. A., Park, M. H., Kim, S., Song, Y. R., et al. (2018). Trans-cinnamic aldehyde inhibits aggregatibacter actinomycetemcomitans-induced inflammation in THP-1-derived macrophages via autophagy activation. *J. Periodontol.* 89 (10), 1262–1271. doi:10.1002/JPER.17-0727

Edwards, S. R., and Wandless, T. J. (2007). The rapamycin-binding domain of the protein kinase Mammalian target of rapamycin is a destabilizing domain. *J. Biol. Chem.* 282 (18), 13395–13401. doi:10.1074/jbc.M700498200

Gasmi, B. A., Kumar Mujawdiya, P., Noor, S., and Gasmi, A. (2022). Porphyromonas gingivalis in the development of periodontitis: impact on dysbiosis and inflammation. *Arch. Razi Inst.* 77 (5), 1539–1551. doi:10.22092/ARI.2021.356596.1875

Glick, D., Barth, S., and Macleod, K. F. (2010). Autophagy: cellular and molecular mechanisms. *J. Pathol.* 221 (1), 3–12. doi:10.1002/path.2697

Graziani, F., Karapetsa, D., Alonso, B., and Herrera, D. (2000). Nonsurgical and surgical treatment of periodontitis: how many options for one disease? *Periodontol* 75 (1), 152–188. doi:10.1111/prd.12201

Guo, Y. F., Su, T., Yang, M., Li, C. J., Guo, Q., Xiao, Y., et al. (2021). The role of autophagy in bone homeostasis. *J. Cell Physiol.* 236 (6), 4152–4173. doi:10.1002/jcp.30111

Hashim, N., Babiker, R., Mohammed, R., Rehman, M. M., Chaitanya, N. C., and Gobara, B. (2024). NLRP3 inflammasome in autoinflammatory diseases and periodontitis advance in the management. *J. Pharm. Bioallied Sci.* 16 (Suppl. 2), S1110–S1119. doi:10.4103/jpbs.jpbs_1118_23

Herrera, D., Sanz, M., Kebschull, M., Jepsen, S., Sculean, A., Berglundh, T., et al. (2022). Treatment of stage IV periodontitis: the EFP S3 level clinical practice guideline. *J. Clin. Periodontol.* 49 (Suppl. 24), 4–71. doi:10.1111/jcpe.13639

Huang, B., Wang, Y., Wang, W., Chen, J., Lai, P., Liu, Z., et al. (2015). mTORC1 prevents preosteoblast differentiation through the notch signaling pathway. *PLoS Genet.* 11 (8), e1005426. doi:10.1371/journal.pgen.1005426

Huang, Y., Liao, L., Su, H., Chen, X., Jiang, T., Liu, J., et al. (2021). Psoralen accelerates osteogenic differentiation of human bone marrow mesenchymal stem cells by activating the TGF-β/Smad3 pathway. *Exp. Ther. Med.* 22 (3), 940. doi:10.3892/etm.2021.10372

Hu, J., Ding, Y., Tao, B., Yuan, Z., Yang, Y., Xu, K., et al. (2022). Surface modification of titanium substrate via combining photothermal therapy and quorum-sensing-inhibition strategy for improving osseointegration and treating biofilm-associated bacterial infection. *Bioact. Mater* 18, 228–241. doi:10.1016/j.bioactmat.2022.03.011

Isola, G., Polizzi, A., Santonocito, S., Alibrandi, A., and Williams, R. C. (2022). Periodontitis activates the NLRP3 inflammasome in serum and saliva. *J. Periodontol.* 93 (1), 135–145. doi:10.1002/JPER.21-0049

Jamalis, J., Yusof, F. S. M., Chander, S., Wahab, R. A., P Bhagwat, D., Sankaranarayanan, M., et al. (2020). Psoralen derivatives: recent advances of synthetic strategy and pharmacological properties. *Antiinflamm. Antiallergy Agents Med. Chem.* 19 (3), 222–239. doi:10.2174/1871523018666190625170802

Jiang, S., Zhu, F., Ji, X., Li, J., Tian, H., Wang, B., et al. (2022). Mesoporous polydopamine-based nanovehicles as a versatile drug loading platform to enable tumor-sufficient synergistic therapy. *ChemMedChem* 17 (19), e202200360. doi:10.1002/cmdc.202200360

Kim, Y. C., and mTOR, G. K. L. (2015). A pharmacologic target for autophagy regulation. *J. Clin. Invest* 125 (1), 25–32. doi:10.1172/JCI73939

Kinane, D. F. (2000). Causation and pathogenesis of periodontal disease. *Periodontol* 2001 (25), 8–20. doi:10.1034/j.1600-0757.2001.22250102.x

Kwon, T., Lamster, I. B., and Levin, L. (2021). Current concepts in the management of periodontitis. *Int. Dent. J.* 71 (6), 462–476. doi:10.1111/idj.12630

Laplante, M., and Sabatini, D. M. (2012). mTOR signaling in growth control and disease. *Cell* 149 (2), 274–293. doi:10.1016/j.cell.2012.03.017

Lee, K., Roberts, J. S., Choi, C. H., Atanasova, K. R., and Yilmaz, Ö. (2018). Porphyromonas gingivalis traffics into endoplasmic reticulum-rich-autophagosomes for successful survival in human gingival epithelial cells. *Virulence* 9 (1), 845–859. doi:10.1080/21505594.2018.1454171

Liccardo, D., Cannavo, A., Spagnuolo, G., Ferrara, N., Cittadini, A., Rengo, C., et al. (2019). Periodontal disease: a risk factor for diabetes and cardiovascular disease. *Int. J. Mol. Sci.* 20 (6), 1414. doi:10.3390/ijms20061414

Liu, G. Y., Jiang, X. X., Zhu, X., He, W. y., Kuang, Y. l., Ren, K., et al. (2015). ROS activates JNK-mediated autophagy to counteract apoptosis in mouse mesenchymal stem cells *in vitro*. *Acta Pharmacol. Sin.* 36 (12), 1473–1479. doi:10.1038/aps.2015.101

Liu, G. Y., and Sabatini, D. M. (2020). mTOR at the nexus of nutrition, growth, ageing and disease. *Nat. Rev. Mol. Cell Biol.* 21 (4), 183–203. doi:10.1038/s41580-019-0199-y

Liu, H., Xu, Y., Cui, Q., Liu, N., Chu, F., Cong, B., et al. (2021). Effect of psoralen on the intestinal barrier and alveolar bone loss in rats with chronic periodontitis. *Inflammation* 44 (5), 1843–1855. doi:10.1007/s10753-021-01462-7

Li, X., Yu, C., Hu, Y., Xia, X., Liao, Y., Zhang, J., et al. (2018). New application of psoralen and angelicin on periodontitis with anti-bacterial, anti-inflammatory, and osteogenesis effects. *Front. Cell Infect. Microbiol.* 8, 178. doi:10.3389/fcimb.2018.00178

Li, Z., Jiang, C. M., An, S., Cheng, Q., Huang, Y. F., Wang, Y. T., et al. (2014). Immunomodulatory properties of dental tissue-derived mesenchymal stem cells. *Oral Dis.* 20 (1), 25–34. doi:10.1111/odi.12086

Ma, H., Peng, J., Zhang, J., Pan, L., Ouyang, J., Li, Z., et al. (2022). Frontiers in preparations and promising applications of mesoporous polydopamine for cancer diagnosis and treatment. *Pharmaceutics* 15 (1), 15. doi:10.3390/pharmaceutics15010015

Mizushima, N., and Komatsu, M. (2011). Autophagy: renovation of cells and tissues. *Cell* 147 (4), 728–741. doi:10.1016/j.cell.2011.10.026

Nuschke, A., Rodrigues, M., Stolz, D. B., Chu, C. T., Griffith, L., and Wells, A. (2014). Human mesenchymal stem cells/multipotent stromal cells consume accumulated autophagosomes early in differentiation. *Stem Cell Res. Ther.* 5 (6), 140. doi:10.1186/scrt530

Olafsson, S., Rodriguez, E., Lawson, A. R. J., Abascal, F., Huber, A. R., Suembuel, M., et al. (2023). Effects of psoriasis and psoralen exposure on the somatic mutation landscape of the skin. *Nat. Genet.* 55 (11), 1892–1900. doi:10.1038/s41588-023-01545-1

Onorati, A. V., Dyczynski, M., Ojha, R., and Amaravadi, R. K. (2018). Targeting autophagy in cancer. *Cancer* 124 (16), 3307–3318. doi:10.1002/cncr.31335

Rangaraju, S., Verrier, J. D., Madorsky, I., Nicks, J., Dunn, W. A., and Notterpek, L. (2010). Rapamycin activates autophagy and improves myelination in explant cultures from neuropathic mice. *J. Neurosci.* 30 (34), 11388–11397. doi:10.1523/JNEUROSCI.1356-10.2010

Sanz, I., Alonso, B., Carasol, M., Herrera, D., and Sanz, M. (2012). Nonsurgical treatment of periodontitis. *J. Evid. Based Dent. Pract.* 12 (Suppl. l), 76–86. doi:10.1016/S1532-3382(12)70019-2

Sanz, M., Herrera, D., Kebschull, M., Chapple, I., Jepsen, S., Beglundh, T., et al. (2020b). Treatment of stage I-III periodontitis-the EFP S3 level clinical practice guideline. *J. Clin. Periodontol.* 47 (22), 4–60. doi:10.1111/jcpe.13290(

Sanz, M., Marco Del Castillo, A., Jepsen, S., Gonzalez-Juanatey, J. R., D'Aiuto, F., Bouchard, P., et al. (2020a). Periodontitis and cardiovascular diseases: consensus report. *J. Clin. Periodontol.* 47 (3), 268–288. doi:10.1111/jcpe.13189

Stemmler, A., Symmank, J., Steinmetz, J., von Brandenstein, K., Hennig, C. L., and Jacobs, C. (2021). GDF15 supports the inflammatory response of PdL fibroblasts stimulated by P. gingivalis LPS and concurrent compression. *Int. J. Mol. Sci.* 22 (24), 13608. doi:10.3390/ijms222413608

Teles, F., Collman, R. G., Mominkhan, D., and Wang, Y. (2022). Viruses, periodontitis, and comorbidities. *Periodontol. 2000* 89 (1), 190–206. doi:10.1111/prd.12435

Thakur, A., Sharma, R., Jaswal, V. S., Nepovimova, E., Chaudhary, A., and Kuca, K. (2020). Psoralen: a biologically important coumarin with emerging applications. *Mini Rev. Med. Chem.* 20 (18), 1838–1845. doi:10.2174/1389557520666200429101053

Thoma, D. S., Naenni, N., Benic, G. I., Muñoz, F., Hämmerle, C. H. F., and Jung, R. E. (2017). Effect of ridge preservation for early implant placement - is there a need to remove the biomaterial? *J. Clin. Periodontol.* 44 (5), 556–565. doi:10.1111/jcpe.12709

Tomokiyo, A., Wada, N., and Maeda, H. (2019). Periodontal ligament stem cells: regenerative potency in periodontium. *Stem Cells Dev.* 28 (15), 974–985. doi:10.1089/scd.2019.0031

Van Der Velden, U. (2000). What exactly distinguishes aggressive from chronic periodontitis: is it mainly a difference in the degree of bacterial invasiveness? *Periodontol* 75 (1), 24–44. doi:10.1111/prd.12202

Wang, J., Zhang, Y., Cao, J., Wang, Y., Anwar, N., Zhang, Z., et al. (2023). The role of autophagy in bone metabolism and clinical significance. *Autophagy* 19 (9), 2409–2427. doi:10.1080/15548627.2023.2186112

Wang, Y., and Zhang, H. (2019). Regulation of autophagy by mTOR signaling pathway. *Adv. Exp. Med. Biol.* 1206, 67–83. doi:10.1007/978-981-15-0602-4_3

Xu, W., Zhou, W., Wang, H., and Liang, S. (2020). Roles of Porphyromonas gingivalis and its virulence factors in periodontitis. *Adv. Protein Chem. Struct. Biol.* 120, 45–84. doi:10.1016/bs.apcsb.2019.12.001

Yang, G., Humphrey, S. J., Murashige, D. S., Francis, D., Wang, Q. P., Cooke, K. C., et al. (2019). RagC phosphorylation autoregulates mTOR complex 1. *EMBO J.* 38 (3), e99548. doi:10.15252/embj.201899548

Yuan, X., Bi, Y., Yan, Z., Pu, W., Li, Y., and Zhou, K. (2016). Psoralen and isopsoralen ameliorate sex hormone deficiency-induced osteoporosis in female and Male mice. *Biomed. Res. Int.* 2016, 6869452. doi:10.1155/2016/6869452

Yu, M., Wang, L., Ba, P., Li, L., Sun, L., Duan, X., et al. (2017). Osteoblast progenitors enhance osteogenic differentiation of periodontal ligament stem cells. *J. Periodontol.* 88 (10), e159–e168. doi:10.1902/jop.2017.170016

Zhang, Z., Zhang, Y., Cai, Y., Li, D., He, J., Feng, Z., et al. (2023). NAT10 regulates the LPS-induced inflammatory response via the NOX2-ROS-NF-κB pathway in macrophages. *Biochim. Biophys. Acta Mol. Cell Res.* 1870 (7), 119521. doi:10.1016/j.bbamcr.2023.119521

Zhu, M., Shi, Y., Shan, Y., Guo, J., Song, X., Wu, Y., et al. (2021). Recent developments in mesoporous polydopamine-derived nanoplatforms for cancer theranostics. *J. Nanobiotechnology* 19 (1), 387. doi:10.1186/s12951-021-01131-9

frontiers | Frontiers in Cell and Developmental Biology

TYPE Original Research
PUBLISHED 21 July 2025
DOI 10.3389/fcell.2025.1618461

OPEN ACCESS

EDITED BY
Yu Liu,
University of Houston, United States

REVIEWED BY
Tiziana Anelli,
San Raffaele Scientific Institute (IRCCS), Italy
Soumya Ranjan Jena,
Ravenshaw University, India

*CORRESPONDENCE
Jin-Chung Shih,
jcshih@ntu.edu.tw
Thai-Yen Ling,
tyling@ntu.edu.tw

†These authors have contributed equally to this work

RECEIVED 26 April 2025
ACCEPTED 27 June 2025
PUBLISHED 21 July 2025
CORRECTED 11 November 2025

CITATION
Liu Y-Z, Lin H-H, Wu M-S, Shih J-C and Ling T-Y (2025) Dysregulation of decidual NK cell proliferation by impaired decidual cells: a potential contributor to excessive trophoblast invasion in placenta accreta spectrum. *Front. Cell Dev. Biol.* 13:1618461. doi: 10.3389/fcell.2025.1618461

Dysregulation of decidual NK cell proliferation by impaired decidual cells: a potential contributor to excessive trophoblast invasion in placenta accreta spectrum

You-Zhen Liu[1†], Hsin-Hung Lin[1,2,3†], Meng-Shiue Wu[1], Jin-Chung Shih[4*] and Thai-Yen Ling[1*]

[1]Graduate Institute of Pharmacology, National Taiwan University College of Medicine, Taipei, Taiwan, [2]MediDiamond Inc., Taipei, Taiwan, [3]LuminX Biotech Co. Ltd., Taipei, Taiwan, [4]Department of Obstetrics and Gynecology, National Taiwan University Hospital, Taipei, Taiwan

Aberrant interactions among decidual stromal cells, decidual natural killer (dNK) cells, and trophoblasts are implicated in placenta accreta spectrum (PAS) pathogenesis, though the underlying mechanisms remain unclear. This study investigates the relationship between defective decidualization of endometrial stromal cells and dysregulated dNK cell proliferation, which may contribute to excessive trophoblast invasion and the development of PAS. We established an *in vitro* system that mimics the decidual microenvironment to investigate these interactions. Maternal decidua-derived mesenchymal stem cells (MD-MSCs) from healthy pregnancies and PAS patients (PA-MSCs) were isolated and induced to undergo decidualization using hormonal and chemical stimuli. Peripheral natural killer (pNK) cells were then co-cultured with these MSCs to generate dNK-like cells. Cellular interactions among MSCs, dNK-like cells, and trophoblasts were evaluated using an *in vitro* co-culture system. Decidualization defects in PA-MSCs were marked by reduced morphological changes and dysregulated expression of decidual markers, potentially associated with estrogen receptor (ER) overexpression. Furthermore, both PA-MSCs and normal MD-MSCs similarly regulated trophoblast invasion, suggesting an indirect impact of impaired decidual cells on trophoblast behavior. Interestingly, decidualized MD-MSCs (De-MD-MSCs) showed the potential to induce the conversion of pNK cells into dNK-like cells, which displayed reduced cytotoxicity on trophoblasts and elevated KIR2DL4 expression. These dNK-like cells exhibited increased proliferation when co-cultured with PA-MSCs, enhancing trophoblast invasion and spiral artery remodeling. Conditioned medium derived from PA-MSCs-induced dNK-like cells demonstrated a higher capacity to promote trophoblast invasion in a dose-dependent manner. The abnormal proliferation of dNK cells induced by impaired decidual cells may contribute to the pathogenesis of PAS,

providing valuable insights into its mechanisms and potential therapeutic interventions.

KEYWORDS

decidualization, placenta accreta spectrum (PAS), trophoblast invasion, decidual natural killer cell, immune tolerace

Introduction

In the process of embryos implanting in the uterus, the interaction between the maternal decidual cells, leukocyte subpopulations like decidual natural killer (dNK) cells, and blastocyst trophoblasts is critical for healthy placental formation and successful pregnancy (Xu et al., 2017). During blastocyst development, trophoblasts differentiate into cytotrophoblasts (CTBs), the subsequent syncytiotrophoblasts (SCTs), and extravillous trophoblasts (EVTs), forming the primitive syncytium and lacunae (Kim et al., 2024; Kojima et al., 2022). Studies demonstrate that decidual and dNK cells regulate trophoblast invasion by secreting factors, maintaining a delicate balance (Yang et al., 2019). During pregnancy, decidual cells, part of the specialized endometrium, complete the decidual reaction post-implantation, supporting placentation through interactions with trophoblasts and producing specific proteins and factors (Hess et al., 2007). Throughout pregnancy, dNK cells, with unique killer cell immunoglobulin-like receptors (KIR) expression and interactions with decidual cells, play a crucial role in immune tolerance at the maternal-fetal interface and placentation through interactions with EVTs (Jabrane-Ferrat, 2019). The equilibrium among decidual, dNK, and trophoblast cells is vital in establishing an immune-regulated environment necessary for placental formation and fetal development, contributing significantly to maternal-fetal immune tolerance (Wang and Li, 2020; Hanna et al., 2006).

Various placental disorders, including the high-risk placenta accreta spectrum (PAS), are caused by disruptions in the regulation between these cells (Al-Khan et al., 2013). PAS is an abnormal placental development condition that encompasses placenta accreta, increta, and percreta and is a major cause of severe maternal morbidity and mortality (Bartels et al., 2018). PAS is particularly daunting for pregnant women and obstetricians due to the difficulty in early detection and the complexity of treatment even after diagnosis. The prevalence rate of PAS has increased in recent decades, from 1 in 1,250 births in the 1980s to as many as 1 in 272 births today (preventaccreta.org, 2024). From the cytological perspective, studies suggest that defects in the decidualization of endometrial stromal cells (ESCs) (Illsley et al., 2020; Gao et al., 2022), altered immune responses in maternal tissues (Adu-Gyamfi et al., 2021; Mirani et al., 2024), or a combination of both conditions (Velicky et al., 2016; Sharma et al., 2016; Moffett and Shreeve, 2023) are proposed as underlying factors contributing to excessive invasion of EVT. This can result in the pathologic adherence of the placenta and subsequent severe bleeding during delivery (Wang et al., 2021; Chang et al., 2020; Murata et al., 2022). However, due to the lack of appropriate animal models and even cellular models, studying the intricate mechanisms governing the aberrant placentation of PAS has presented challenges. Thus, the precise etiology of PAS remains incompletely understood, especially when investigating the early and mid-stages of human pregnancy, during which EVTs interact with decidual cells and dNK cells. Therefore, understanding the complex interactions among decidual cells, EVTs, and immune cells, particularly dNK cells within the uterus, is essential for developing diagnostic and therapeutic approaches to address PAS and its potentially life-threatening complications.

In our preliminary work, we isolated a unique cell population derived from the choriodecidual interface, where the decidua (developed from the endometrium) and the chorion (created from the trophoblast of the outer wall of the embryo) fuse. In order to clearly demonstrate the basic characteristics of MSCs, we adapted the results from previous studies (Su et al., 2017). These cells were identified from the precise decidua with the MSC markers (Supplementary Figure S1A) and differentiation potentials (Supplementary Figure S1B), known as human placenta maternal decidua-derived mesenchymal stem cells (MD-MSCs), replacing the previously confusing origin and nomenclature of human placenta choriodecidual membrane-derived mesenchymal stem cells (pcMSCs) (Su et al., 2017). They have shown significant potential for cell therapy due to their anti-inflammatory, immunomodulatory, and tissue repair capabilities (Chen et al., 2022). Beyond their roles in regenerative medicine, this study aims to explore the physiological functions of MD-MSCs in the endometrium to gain new insights into complex placental diseases. Consequently, we developed an MD-MSC-based decidualization and co-culture system. This advanced system facilitates the assessment of EVT invasion and dNK cell induction, thereby overcoming the limitations of traditional *in vitro* methods.

In this study, we established an MD-MSC-based co-culture system and utilized pathological MD-MSCs from patients with PAS (PA-MSCs) to investigate the underlying mechanism of PAS. Our findings suggest that MD-MSCs can potentially induce pNK cells to convert into dNK-like cells with lower cytolytic ability and enhanced expression of KIR2DL4, one of the polymorphic KIRs that interacts with HLA-G on EVTs (Rajagopalan and Long, 2012). Moreover, we observed that dNK-like cells proliferate significantly

Abbreviations: BMMSC, Bone marrow-derived mesenchymal stem/stromal cell; cAMP, Cyclic adenosine monophosphate; CTB, Cytotrophoblast; DC, Dendritic cell; dNK, Decidual natural killer cell; ER, Estrogen receptor, ESC, Endometrial stromal cell; EVT, Extravillous trophoblast; E2, Estradiol; HLA, Human leukocyte antigen; IGFBP1, Insulin-like growth factor binding protein 1; iCTB, Interstitial cytotrophoblast; KIR, Killer Ig-like Receptor; MD-MSC, Human placental maternal decidua-mesenchymal stem cell; MMP, Matrix metalloproteinase; MPA, Medroxyprogesterone acetate; PA-MSC, pathological MD-MSC from PAS patient; PAS, Placenta accreta spectrum; PBMC, Peripheral blood-derived mononuclear cell; pNK, Peripheral blood-derived natural killer cell; PR, Progesterone receptor; PRL, Prolactin; P4, Progesterone; SCARA5, Scavenger receptor class A type 5; SCT, Syncytiotrophoblast; TIMP, Tissue inhibitors of metalloproteinase.

when co-cultured with PA-MSCs and exhibit a greater capacity to promote trophoblast invasion when co-cultured with MD-MSCs. This discovery highlights the potential contribution of aberrant dNK cell numbers and decidualization defects to PAS development. This study proposes a novel approach to studying the intricate interactions among decidual, dNK, and trophoblast cells *in vitro* and offers new insights into the mechanism of PAS.

Materials and methods

Isolation and culture of MD-MSCs and PA-MSCs

MD-MSCs and PA-MSCs cells were obtained from the term placenta undergoing cesarean sections at Taipei Medical University Hospital and Dr. Jin-Chung Shih from National Taiwan University Hospital, respectively. All procedures were approved by the Institutional Review Board (IRB: 202308101RINC). The diagnostic criteria for selecting pathological placentas as clinical specimens in this study are outlined in Supplementary Table S1. Additionally, histopathological confirmation of PAS was performed, with Supplementary Figure S4 illustrating interstitial cytotrophoblast (iCTB) invasion into the myometrium in the three selected specimens. For cell isolation, the decidual membrane was isolated, chopped, and digested with a mixture of protease (Sigma, 9001-92-7), collagenase B (Sigma, COLLB-RO), and DNase I (Bioshop, DRB003). After overnight digestion at 4°C, the filtrate was centrifuged, washed, and resuspended in MCDB201 medium (Merck, M230428) supplemented with 1% insulin-transferrin-selenium (ScienCell, 0803), 10 ng/mL epidermal growth factor (EGF, Peprotech, AF10015), and 1% penicillin/streptomycin. Cells were seeded onto collagen-type IV-coated Petri dishes, and non-adherent cells were removed after 24 h. Upon reaching 90% confluency, cells were dissociated with trypsin (Gibco, 25-200-072), terminated with fetal bovine serum (FBS) (Gibco, 10-082-147), and seeded for further amplification.

In vitro decidualization

For *in vitro* decidualization using (a) hormone and (b) second messenger induction, MD-MSCs or PA-MSCs were initially seeded in a 10-cm Petri dish and allowed to attach for 48 h. Subsequently, the cells were stimulated with the combination of (a) 10 nM estradiol (E2, Sigma-Aldrich, E2785) and 1 μM progesterone (P4, Sigma-Aldrich, P8783) or (b) 0.5 mM 8-Bromo-cAMP sodium salt (MedChemExpress, HY-12306) and 1 μM medroxyprogesterone 17-acetate (MPA, Sigma-Aldrich, M1629) for 5 days. The morphology and the expression of decidualization markers were assessed at 5 days following induction. Throughout the decidualization process, the morphological changes of the cells were monitored using a phase-contrast microscope on the fifth day after induction. Furthermore, for further analysis, total protein and RNA were extracted from decidualized cultures and non-stimulated control samples at specified time points.

Decidual cell morphology quantification

MD-MSCs were initially seeded in a sterilized 12-well plate and subjected to two different decidualization cocktails. Following a 5-day decidualization period, cells were washed with PBS (pH 7.4) and fixed with 4% paraformaldehyde solution (BioLegend, 420801) in PBS for 10 min at room temperature. After fixation, cells underwent three PBS washes. They were stained with Wheat Germ Agglutinin (WGA) (Invitrogen, W11261) at a concentration of 5 μg/mL to target the cell membrane, enhance the visibility of cell boundaries, and facilitate the cell morphology quantification. For nuclear visualization, DAPI (BioLegend, 422801) was applied at a concentration of 1 μg/mL for 5 min. Stained cells were then observed using fluorescence microscopy to capture images, and ImageJ software was employed to quantify cell morphology. The circularities and roundness of 15 cells from each image were measured separately to assess cell shape, ensuring reliable statistical analysis.

Real-time PCR (RT-PCR)

Total RNA was extracted from MD-MSCs and PA-MSCs using the NucleoSpin® RNA isolation kit (740955.50, Macherey-Nagel). The concentration of RNA was determined using the Nanodrop 1000 (Thermo) spectrophotometer. Subsequently, reverse transcription was performed using the SuperScript first-strand synthesis system (Invitrogen, 48190-011) according to the manufacturer's instructions. The resulting cDNA samples were utilized for PCR amplification using the qPCRBIO SyGreen Blue Mix Lo-ROX (PB20.15). Quantitative PCR (qPCR) assays were conducted in triplicate on a Biometra Professional Basic 96 gradient detection system. To normalize the expression levels of target genes, the reference gene (18S rRNA) was used. The specific primers employed for each gene can be found in Supplementary Table S2. The average threshold cycle (Ct) was calculated from the Ct values obtained from three replicates of each sample. The normalized ΔCt value for each sample was computed as the mean Ct of the target gene minus the mean Ct of the reference gene. ΔΔCt was then calculated as the difference between the ΔCt values of the control and test samples. The fold change in gene expression for each sample relative to the control was determined using the $2^{(-\Delta\Delta Ct)}$ mathematical model for relative quantification in qPCR. The mean fold induction and standard error of the mean (SEM) were determined from a minimum of three or more independent experiments.

Enzyme-linked immunosorbent assay (ELISA)

To measure the concentration of secreted proteins, such as prolactin (PRL) and Insulin-like growth factor binding protein 1 (IGFBP1), the cell culture medium was collected and centrifuged at 2,000 g for 10 min at 4°C to remove any cellular debris. The resulting supernatant was immediately supplemented with a protease inhibitor cocktail and stored at −80°C for subsequent analysis. For the determination of scavenger receptor class A type 5 (SCARA5) protein levels, the cells were first lysed using RIPA

buffer supplemented with a 100-fold diluted protease inhibitor cocktail. The cell lysate was then collected and centrifuged at 16,500 g for 20 min. The resulting supernatant was transferred to a new Eppendorf tube and stored at −80°C until further use. To quantify the PRL and IGFBP1 secretion levels, specific ELISA kits were employed, such as the Human Prolactin DuoSet ELISA (R&D #DY682) and Human IGFBP1 DuoSet ELISA (R&D #DY871), in conjunction with the DuoSet ELISA Ancillary Reagent kit 2 (R&D #DY008B), following the manufacturer's instructions. Similarly, the SCARA5 levels were determined using an appropriate ELISA kit (AVIVA SYSTEMS BIOLOGY, OKCD00526).

Immunohistochemistry (IHC) in tissue sections

The human decidual tissue sections from normal and PAS placenta were formalin-fixed, paraffin-embedded, cut, and mounted at the Laboratory Animal Center, College of Medicine, National Taiwan University. The dissected sections were placed in a 60°C oven to soften the paraffin for the following steps. After 30 min, the sections were dewaxed with Xylene-clear citrus oil (National Diagnostics, HS-200), cleared in 100% ethanol, and rehydrated through gradients of ethanol in PBS (with gradients of 100%, 95%, 80%). Antigen retrieval was then conducted in 100°C citrate acid buffer for 20 min. Sections were sequentially incubated with 1% blocking BSA for 5 min and subsequently incubated with primary antibodies at 4°C overnight. After washing with PBS to remove unbound antibodies, biotinylated secondary antibodies were applied. Following that, HRP polymer was applied for 30 min at room temperature. After 30 min, diaminobenzidine (DAB) substrate (Chromogen: Substrate = 1:20) was added for precipitation for 1–3 min. Hematoxylin was then used to stain cell nuclei. Sections were mounted with Malinol (MUTO PURE CHEMICALS, 2040-2). The information on the antibodies used is provided in Supplementary Table S3. IHC staining reagents were used following the manufacturer's instructions (Novolink, RE7290-k).

Surface marker expression levels measured by flow cytometry

For the evaluation of ER, PR, and SCARA5 expression levels in MD-MSCs and PA-MSCs, live cells were trypsinized and fixed with a 4% paraformaldehyde solution (BioLegend, 420801) in PBS for 10 min at room temperature. Permeabilization was achieved using 0.1% Triton X-100 for 5 min at room temperature. Subsequently, fixed cells were incubated individually with ER, PR, and SCARA5 antibodies at manufacturer-specified concentrations for 15 min. For surface CD3, CD56, KIR2DL4, and HLA-G expression levels, the same protocols were followed without Triton X-100 permeabilization. Finally, cells were resuspended in FACS buffer (1X PBS supplemented with 1 mM EDTA, 25 mM HEPES, and 1% FBS) for subsequent analysis. Analytical flow cytometry was performed using an LSRFortessa, and FACS data were analyzed using FlowJo (version 10.8.01).

Trophoblast invasion assay

To perform the invasion assay, MD-MSCs and PA-MSCs were seeded and cultured in a 24-well plate. Subsequently, these cells underwent treatment with two distinct decidualization cocktails. Following a 5-day decidualization, trophoblast cell line 3A-sub-E (BCRC, 60302) was seeded onto transwell inserts with an 8 μm pore size to facilitate trophoblast invasion. Many mammalian cells can deform and squeeze through 8 μm pores, making this size appropriate for invasion studies. These inserts had been pre-coated with a Matrigel solution (Corning, #356231) diluted sixfold in serum-free MEM α (Minimum Essential Medium) (Gibco, 11900024). After a 3-day co-culture period, the transwell inserts were meticulously removed, and non-invaded cells present on the upper surface of the inserts were gently eliminated using a cotton swab. Subsequently, the invaded trophoblasts were lysed utilizing a CellTiter-Glo® 2.0 Cell Viability Assay (Promega #G9241) to facilitate the quantification of the relative trophoblast invasion rate.

Peripheral blood mononuclear cells (PBMCs) isolation and peripheral blood natural killer (pNK) cells purification

pNK cells were obtained from human peripheral blood following approved procedures by the IRB (202312090RINC). Mononuclear cells were isolated from human peripheral blood using the Mitenyl Biotec protocol for density gradient centrifugation. Peripheral blood was collected in a 10 mL vacutainer containing heparin and centrifuged at 550 g for 10 min to separate plasma from blood cells. The plasma was inactivated at 56°C for 30 min, followed by centrifugation at 3,000 g for 10 min to remove precipitate. For PBMC isolation, blood cells were diluted with four times the volume of commercial 1X PBS (Gibco, 00187) and layered over Ficoll-Paque (Cytiva, 17144002) in a 50 mL conical tube, then centrifuged at 400 g for 40 min. The PBMC layer was carefully transferred to a new tube, washed with 1X PBS, and centrifuged at 300 g for 10 min. Platelets were removed by resuspending the cell pellet in 1X PBS and centrifuging at 200 g for 15 min, repeating the step twice. The resulting cell pellet was resuspended, and a cell count was performed. A total of 10^7 cells were seeded in a T75 flask and cultured in a DSNK medium (BioMab, 020-A010-001) supplemented with inactivated plasma for pNK cell purification and expansion. After a 14-day selection period, the purity of pNK cells was assessed by flow cytometry by determining the expression of the pNK cell marker $CD3^-CD56^+$. Once purity reached 95%, pNK cells were considered suitable for subsequent experiments.

Cytotoxicity assay for pNK cell and dNK-like cells

The pNK cells and dNK-like cells induced by MD-MSCs were prepared according to the aforementioned protocols. In the cytotoxic assay, 3A-subE trophoblasts were initially seeded into a 96-well plate. Following a 6-h attachment period, the pNK cells and dNK-like cells were seeded to co-culture with the attached trophoblasts. The ratios of effector cells (NK cells) to target cells

(trophoblasts) were set at five different proportions: 1:1, 2:1, 4:1, 1:2, and 1:4. After co-culturing for 12 h, the NK cells were removed with the cell culture medium, and the remaining attached trophoblasts were lysed using the CellTiter-Glo® 2.0 Cell Viability Assay and measured for luminescence. The cytolytic ability of NK cells was quantified using the formula:

$$\left(\frac{Luminescence\ endpoint\ of\ (Trophoblast\ only\ group - NK\ with\ trophoblast\ group)}{Luminescence\ endpoint\ of\ trophoblast\ only\ group}\right)\times 100\%$$

.

dNK-like cell proliferation assay

MD-MSCs and PA-MSCs were seeded in 96-well plates at a density of 5×10^3 cells/well and cultured for 48 h. These cells were then treated with two different decidualization cocktails. Following a 5-day decidualization period, purified pNK cells were seeded at a density of 5×10^3 cells/well into the 96-well plates, establishing co-cultures with MD-MSCs, PA-MSCs, and the decidual cells. During the co-culture period, the suspended NK cells were collected at specific time points: 1, 4, 7, and 10 days. To quantify the proliferation of dNK-like cells, the CellTiter-Glo® 2.0 Cell Viability Assay (Promega #G9241) was employed. This assay allows measurement of cell viability based on ATP levels, providing insights into cell proliferation and overall cellular health.

RNA-sequencing and data analysis

MD-MSCs and PA-MSCs were cultured in 10 cm Petri dishes. Following treatment with various decidualization cocktails, the total RNA of these cells was extracted using the NucleoSpin ® RNA isolation kit (740955.50, Macherey-Nagel) and subsequently utilized for RNA-seq analysis. The RNA-seq procedure was carried out by BIOTOOLS (Taiwan). The genetic data obtained was analyzed using the Biotools RNAseq version 1.6.6 platform. This analysis yielded fold changes, Log_2 (fold changes), and p-values for each gene, allowing for the identification of differentially expressed genes (DEGs) based on Log_2 (fold changes) > 1 and p-values <0.05. The values presented on the heatmap are expressed as z-scores, which have been normalized relative to the gene expression levels. Gene expression plots were generated using the website SRplot, while Venn diagrams were created using Venny2.0.

Statistical analysis

Statistical analysis was performed using GraphPad Prism version 9.1.1 (GraphPad Software, La Jolla, CA, United States). The data were presented as mean ± SEM (standard error of the mean). Statistical comparisons were conducted using one-way ANOVA with Dunnett's *post hoc* correction or two-way ANOVA followed by Tukey's or Bonferroni's *post hoc* tests. A significance level of $P < 0.05$ was considered statistically significant ($^*P < 0.05$,$^{**}P < 0.01$,$^{***}P < 0.001$, n.s.: no significance).

Results

MD-MSCs represent a distinct cell type with the capability for *in vitro* decidualization

In this study, we have discovered a particular variety of MSCs known as MD-MSCs. These cells were meticulously extracted from the decidual membrane of the human placenta, a process accomplished through serum-free culture techniques. In addition, they displayed a remarkable capacity for amplification *in vitro*, with the ability to undergo approximately 20 passages (Su et al., 2017). Given their inherent expression of estrogen (ER) and progesterone receptors (PR), we hypothesized that they could respond to hormonal stimuli and undergo decidualization (Figure 1A).

To thoroughly assess the efficacy of the transition from MD-MSCs to decidual cells, we employed two well-established metrics: alterations in cell morphology and the upregulation of specific genes. Following a 5-day induction period with hormonal (E2/P4) or chemical (cAMP/MPA) agents (Figure 1A), MD-MSCs underwent significant morphological transformations, transitioning from a spindle-like to a rounded shape, as illustrated in Figure 1B-a. To quantify these observed changes in shape, we applied circularity and roundness parameters (Figure 1B-b) (Pan-Castillo et al., 2018). Remarkably, upon exposure to the second messenger induction, three distinct batches of MD-MSCs exhibited a pronounced shift in morphology (Supplementary Figure S2A).

To further investigate the genetic changes associated with decidualization in MD-MSCs, we conducted an RNA-seq analysis to explore potential decidual cell markers. We compared our dataset with two previously published single-cell RNA-seq databases (Lucas et al., 2020; Rawlings et al., 2021), aiming to identify upregulated genes that could serve as reliable biomarkers for decidual cells. This analysis resulted in the identification of 33 annotated genes (Figure 1C), the expression patterns of which were then visualized in heatmap format, as depicted in Figure 1D; Supplementary Data 1. Furthermore, 9 annotated genes are further investigated as potential decidual cell markers through comparison with the TISSUES database (BTO:0002770) (Supplementary Data 1). To validate the results obtained from RNA-seq, we conducted qPCR analysis on these 9 annotated genes (Figure 1E). Notably, three genes including prolactin (*Prl*), insulin-like growth factor binding protein 1 (*Igfbp1*), and scavenger receptor class A type 5 (*Scara5*) emerged as potential biomarkers for decidual cells. While IGFBP1 showed clear upregulation at both the transcript level, as confirmed by qPCR, and the protein level by ELISA, its differential expression appeared less prominent in the heatmap (Figure 1D). This discrepancy is likely due to the normalization method used in the transcriptomic analysis. Global scaling across all conditions can mask relative fold changes, especially when gene expression is compared against highly expressed reference transcripts (Supplementary Figure S3). As a result, genes that are genuinely upregulated may appear less visually distinct in the heatmap representation. Furthermore, the potential decidual cell markers were selected based on a 10-fold change observed in both E2/P4 and cAMP/MPA treatments to avoid the induction of nonspecific upregulation through chemical stimulation. Previous studies have shown that MSCs from either bone marrow or adipose tissue could also undergo decidualization

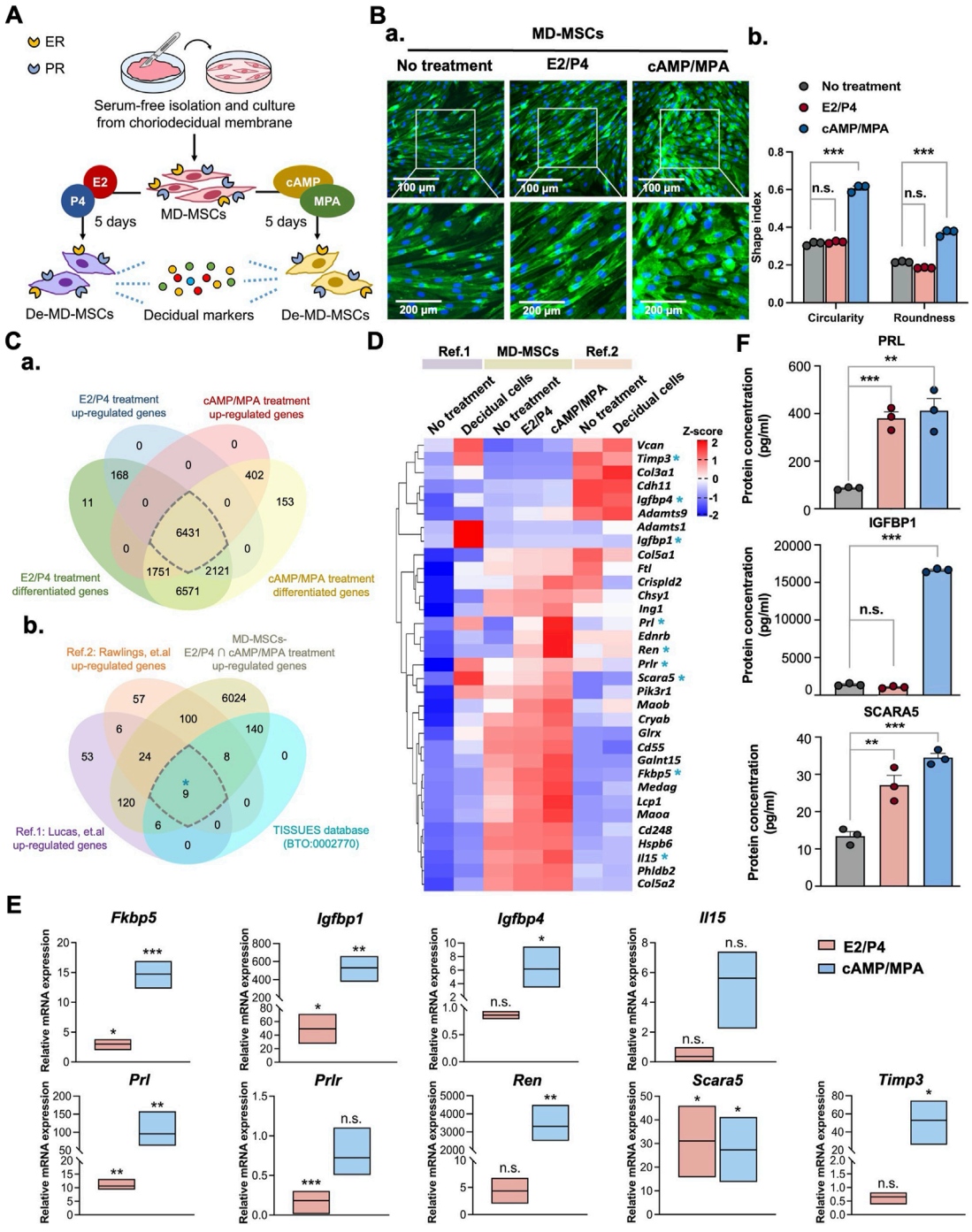

FIGURE 1
Characterization of MD-MSCs for decidualization potential through morphological changes and identification of decidual cell markers. **(A)** Schematic representation of the workflow for MD-MSCs isolation and culture for subsequent analysis. **(B) (a)** Representative images of normal MD-MSCs stained with WGA under E2/P4 and cAMP/MPA treatments. **(b)** Quantification of changes in circularity and roundness in normal MD-MSCs following decidualization treatment, assessed using ImageJ software. **(C) (a)** Venn diagrams display differentially upregulated genes' overlap in both E2/P4 and cAMP/MPA treatment groups. **(b)** A selection of 6431 upregulated genes was subsequently overlaid with two published databases to identify 33 potential decidual cell markers. 9 annotated genes are selected from the upregulated genes in decidual cells within the curated database TISSUES (BTO:0002770). **(D)** Heatmap presenting the expression levels of the 33 annotated upregulated genes during decidualization in MD-MSCs and two reference databases. Values are expressed as z-scores, which have been normalized to the gene expression levels. The asterisk key "*" signifies the annotation of 9 genes for potential validation as decidual cell markers. **(E)** Validation of 9 selected genes through qPCR analysis. *Prl*, *Igfbp1,* and *Scara5* are identified as potential marker genes for De-MD-MSCs. Values are normalized to **(F)** The protein expression levels of PRL, IGFBP1, and SCARA5 of MD-MSCs under E2/P4 and cAMP/MPA decidualization treatment. Values are expressed as mean ± SEM. $^{*}p < 0.05$, $^{**}p < 0.01$, and $^{***}p < 0.001$. *Prl*: Prolactin; *Igfbp1*: Insulin-like growth factor binding protein 1; *Scara5*: Scavenger receptor class A type 5.

through cAMP/MPA treatment. However, it's important to note that the cAMP signaling pathway can bypass the ER and PR, directly driving downstream processes and promoting nonspecific signal transduction (Yoshie et al., 2015). To address this concern, we also employed other types of MSCs to distinguish the decidualization potential of MD-MSCs. As anticipated, following E2/P4 treatment, the mRNA expression levels of *Prl*, *Igfbp1*, and *Scara5* were dramatically upregulated in MD-MSCs, compared with bone marrow-derived MSCs (BMMSCs) and adipose tissue-derived MSCs (Supplementary Figure S2B). Furthermore, the protein expression levels of these three decidual cell markers measured by ELISA were consistent (Figure 1F).

Decidualization defects in PA-MSCs have been observed in the MD-MSC-based decidualization system

Building upon previous research providing solid evidence for the decidualization potential of MD-MSCs, we aimed to delve deeper into the mechanisms underlying PAS, a condition associated with decidualization defects (Hecht et al., 2020). By utilizing PA-MSCs, we sought to unravel the detailed mechanisms of this disease through the decidualization system. We hypothesized that PA-MSCs might exhibit an inadequate degree of decidualization, rendering them unable to effectively resist trophoblast over-invasion (Aplin et al., 2020). First, as the representative images showed, we observed that PA-MSCs displayed fewer morphological changes compared to MD-MSCs (Figure 2A-a). Quantitative analysis revealed that PA-MSCs retained their spindle shape rather than adopting a round shape, as indicated by their low roundness and circularity values (Figure 2A-b). Additionally, we assessed the mRNA (Figure 2B) and protein (Figures 2C,D) expression levels of three annotated decidual cell marker genes in PA-MSCs. As shown in the figures, the mRNA expression levels of *Prl* and *Igfbp1* were significantly reduced in decidualized PA-MSCs (De-PA-MSCs) compared to De-MD-MSCs. Although there were no significant differences in protein levels between De-PA-MSCs and De-MD-MSCs by ELISA, immunohistochemistry staining of placental tissues revealed significantly reduced expression of PRL and IGFBP1 proteins in PAS samples compared to normal placenta. These findings indicate that the downregulation of *Prl* and *Igfbp1* at the mRNA level is reflected at the protein level in placental tissues, supporting a consistent trend across molecular and histological analyses. Conversely, the gene expression levels of *Scara5* were higher in De-PA-MSCs but reduced in protein levels. The inconsistency between SCARA5 mRNA and protein expression levels is likely attributable to post-transcriptional and translational regulation, which can modulate protein abundance independently of transcript levels. Nevertheless, these observations indicate a clear distinction in gene expression between PA-MSCs and MD-MSCs, suggesting a defective decidualization process in PA-MSCs. Notably, several annotated genes typically upregulated during decidualization were downregulated in E2/P4-treated PA-MSCs, as shown in Supplementary Figure S5A. To explore the potential upstream regulators of this impairment, we examined the expression levels of ER and PR. Therefore, we revisited the expression levels of ER and PR. Surprisingly, we discovered that ER was more expressed in PA-MSCs than in normal MD-MSCs, as evidenced by flow cytometry analysis (Supplementary Figure S5B). This finding was further corroborated by immunohistochemical (IHC) staining performed on PAS and normal placenta biopsy samples (Supplementary Figure S5C). The severe FIGO grade 3 PAS (placenta percreta) is characterized by extensive disruption of the decidual membrane. Therefore, we selectively obtained biopsies exhibiting FIGO grade 2 PAS (placenta increta), which is distinguished by the presence of residual decidua, as observed in IHC staining (Figure 2D; Supplementary Figure S5C).

Decidualization defects may not constitute the primary cause of dysregulation in trophoblast invasion, thereby leading to PAS

Considering the association between PAS and dysregulated decidual cells impacting trophoblast invasion, we established a co-culture system to evaluate the interaction between PA-MSCs and trophoblasts. The trophoblast invasion timeline is depicted in Figure 3A. In this system, we made a surprising discovery, as illustrated in Figure 3B. We found that MD-MSCs treated with cAMP/MPA inhibited trophoblast invasion, while normal and E2/P4-treated MD-MSCs enhanced trophoblast invasion. This implies that MD-MSCs and De-MD-MSCs can dynamically regulate trophoblast invasion, aligning with the concept proposed in clinical research that "decidual cells act as a natural stop signal to inhibit excessive trophoblast invasion." This phenomenon highlights the intricate interactions between decidual cells and trophoblasts and provides valuable insights into the regulation of trophoblast invasion during pregnancy.

E2/P4-treated De-PA-MSCs showed a statistically significant increase in the regulation of trophoblast invasion compared to the untreated group, as expected. In contrast, normal MD-MSCs did not show a significant difference in trophoblast invasion between E2/P4-treated and untreated conditions (Figure 3B). These results suggest that PA-MSCs may abnormally regulate trophoblast invasion under hormone decidualization. However, there was no significant difference in the regulation of trophoblast invasion between De-PA-MSCs and MD-MSCs under E2/P4 treatment. This finding challenges the assumption that impaired decidualization is one of the primary causes of PAS. Nevertheless, we investigated potential regulators and signaling pathways involved in trophoblast invasion regulation. The expression levels of 22 annotated genes associated with the regulation of trophoblast invasion are revealed through our RNA-seq database analysis. Notably, the genes negatively regulating trophoblast invasion, highlighted in red, were highly expressed in MD-MSCs under cAMP/MPA treatment (Figure 3C; Supplementary Data 2). Additionally, when comparing E2/P4-treated De-PA-MSCs to E2/P4-treated De-MD-MSCs, we observed lower expression levels of *Timp1*, *Timp3*, and *Timp4*, whereas *Timp2* was upregulated. *Timp2* inhibits active MMP-2 and helps activate pro-MMP-2 by forming a complex with MMP-2 and MMP-14 at the cell surface. Reduced TIMP-2 disrupts this balance, hindering trophoblast invasion (Bernardo and Fridman, 2003). In contrast, *Il33*, *Mmp12*, and *Mmp28* were significantly

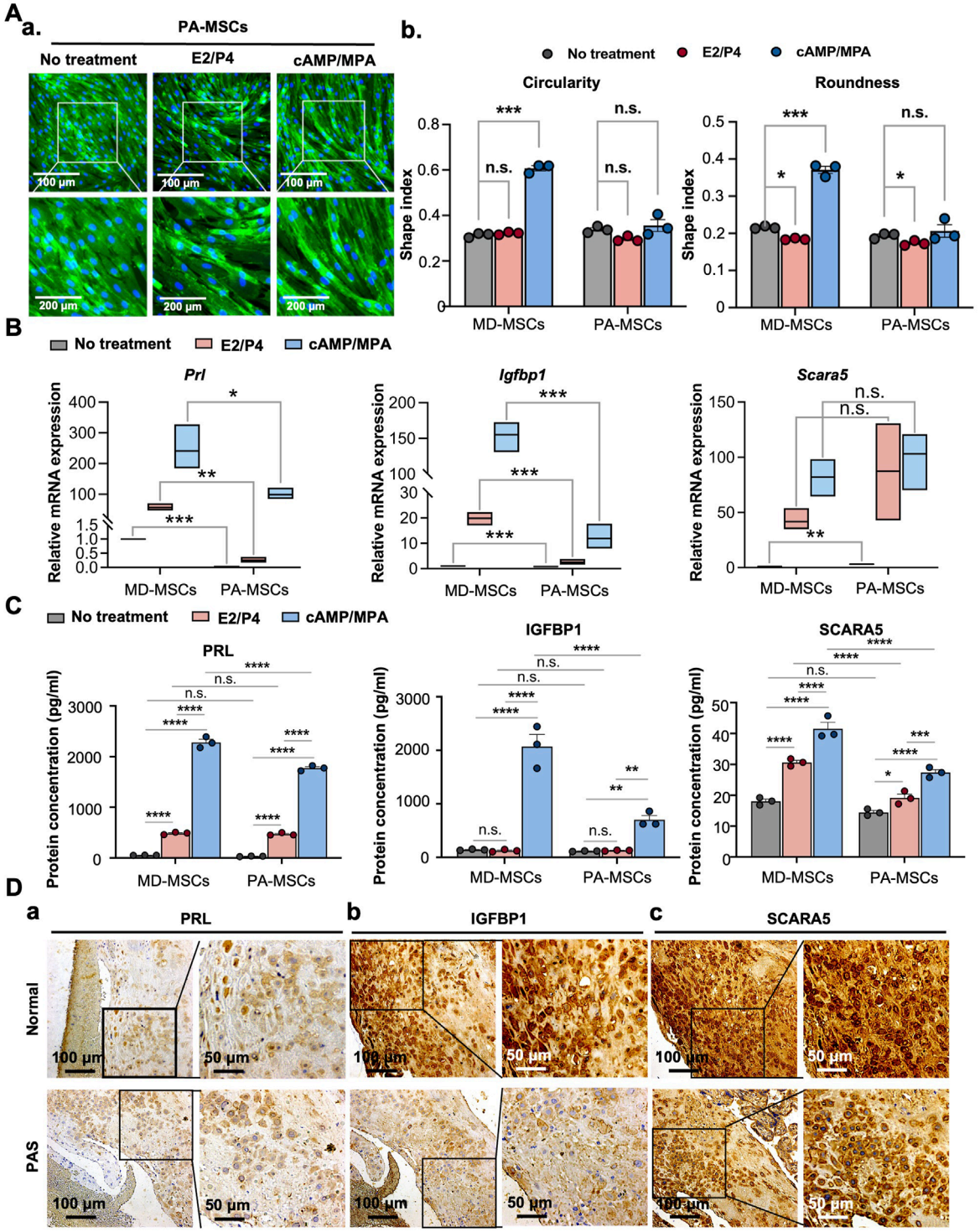

FIGURE 2
PA-MSCs demonstrate decidualization defects with reduced morphological changes and decidual cell marker expression levels. **(A) (a)** Representative images and quantification of **(b)** circularity and roundness changes in PA-MSCs stained with WGA under E2/P4 and cAMP/MPA treatments compared with MD-MSCs. **(B)** The mRNA expression levels of three potential decidual cell markers, *Prl*, *Igfbp1*, and *Scara5*, in PA-MSCs compared with MD-MSCs. **(C)** The protein expression levels of three potential decidual cell markers, PRL, IGFBP1, and SCARA5, in PA-MSCs compared with MD-MSCs. **(D)** Immunohistochemistry images showing the differential expression levels of **(a)** PRL, **(b)** IGFBP1, and **(c)** SCARA5 in decidual cells between normal and PAS patients. Values are expressed as mean ± SEM. $^{*}p < 0.05$, $^{**}p < 0.01$, and $^{***}p < 0.001$. PRL: Prolactin; IGFBP1: Insulin-like growth factor binding protein 1; SCARA5: Scavenger receptor class A type 5.

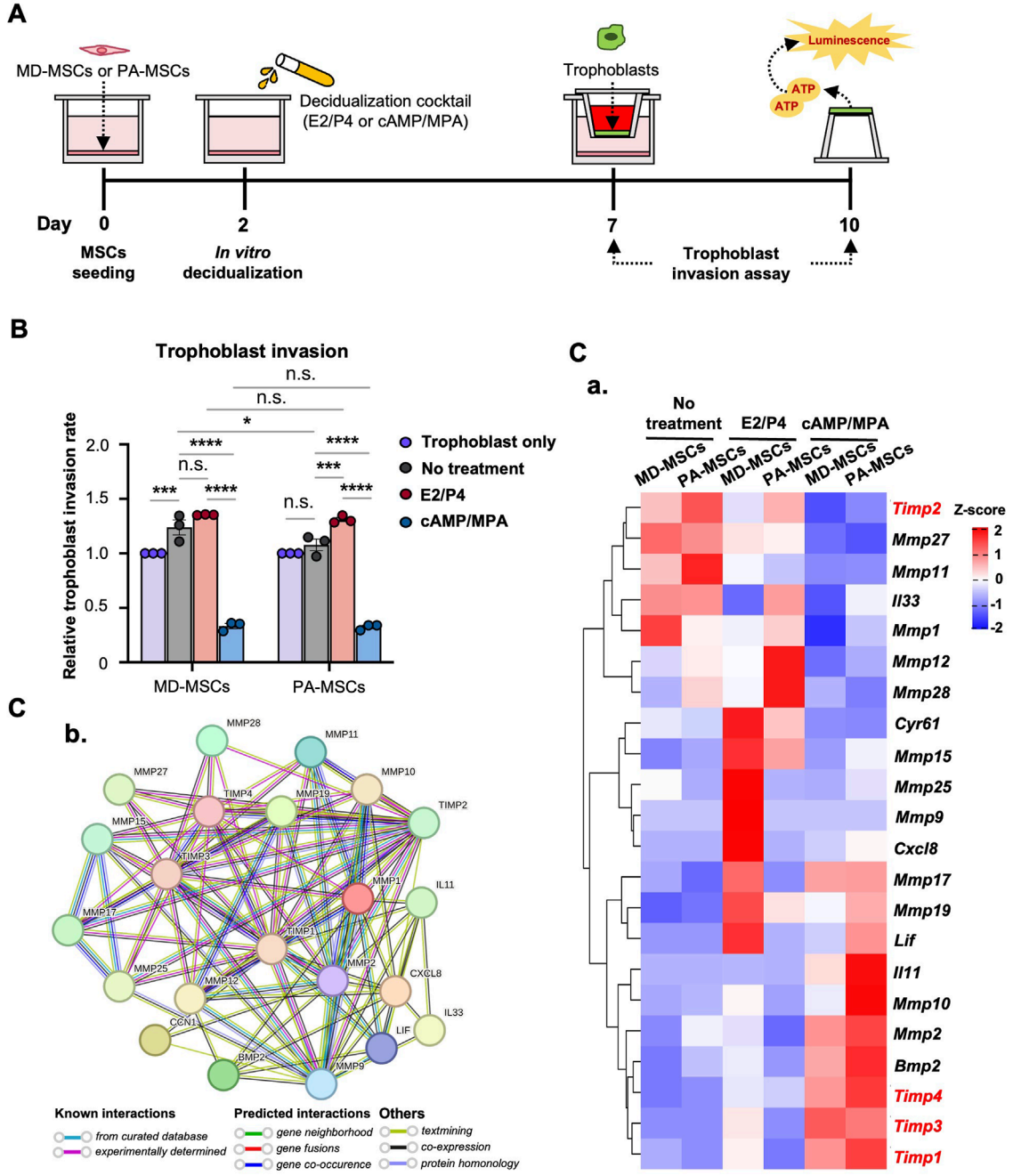

FIGURE 3
PA-MSCs and MD-MSCs have similar effects on trophoblast invasion through an MD-MSC-based co-culture system. **(A)** Schematic diagram of the co-culture system and timeline for the assessment of trophoblast invasion. **(B)** The effects of MD-MSCs and PA-MSCs under different decidualization treatments were compared to assess their impact on trophoblast invasion. Values are expressed as mean ± SEM. *p < 0.05, **p < 0.01, and ***p < 0.001, n.s.: not significant. **(C) (a)** The heatmap shows the potential molecules that are involved in the dynamic regulation of trophoblast invasion, annotated through the GEO database. Genes that negatively regulate trophoblast invasion were marked in red. Values are expressed as *z*-scores, which have been normalized to the gene expression levels. **(b)** Predicted networks of protein-protein interaction among annotated proteins through STRING analysis. The line between two nodes typically denotes the interaction between those two proteins, with the line's colors reflecting the available resources of interactions.

upregulated in the De-PA-MSCs under E2/P4 treatment (Figure 3C-a). The protein-protein interactions were analyzed by STRING for these proteins, encoded by these genes, and exhibited a high density of interactions involved in regulating trophoblast invasion. Particularly, tissue inhibitors of metalloproteinases (TIMPs) and matrix metalloproteinases (MMPs) exhibit a high level of evidence of known interactions (Figure 3C-b). These analyses suggest that the innate regulatory mechanisms governing trophoblast invasion through E2/P4 decidualization in PA-MSCs differ from those observed in normal MD-MSCs. However, the differential

expressions of these genes were not sufficient to account for the abnormal trophoblast invasion. Further research is necessary to fully understand the underlying mechanisms contributing to PAS. Particular attention should be given to dNK cells due to their pivotal role in pregnancy through their intrinsic interactions with decidual cells and trophoblasts within the physiological microenvironment.

The induction of dNK-like cells from pNK cells is potentially achievable through an MD-MSC-based co-culture system

It is well-established that, apart from decidual cells, dNK cells also play a crucial role in blastocyst implantation and placental formation. Due to limitations in acquiring dNK cells, we attempt to facilitate the *in vitro* conversion of dNK cells from pNK cells through co-culturing with MD-MSCs or De-MD-MSCs. The primary indicator of the successful conversion of dNK cells is the reduced cytotoxicity characteristic of dNK cells. The timeline of the dNK-like cell conversion and the assessments are depicted in Figure 4A. As the results showed, after co-culturing with MD-MSCs or De-MD-MSCs, the cytotoxicity of NK cells on trophoblasts decreased at each ratio of effector cells and target cells compared with pNK cells (Figure 4B). Particularly in the dNK cell batches, dNK2 and dNK3 cells, the cytolytic ability was dramatically reduced by about 20%–30% compared with pNK cells at the cell number ratio of 4:1 (Figure 4B).

To exclude the possibility that the decline in NK cell cytotoxicity is not attributable to functional loss post-co-culture MD-MSCs, we further investigated the upregulated expression levels of KIR2DL4, specifically expressed on dNK cell surfaces, to bind with HLA-G on trophoblast surfaces and activate the inhibitory signal contributing to immunotolerance to prevent trophoblasts from being cytolyzed. Firstly, we measured the levels of HLA-G on trophoblasts to confirm its presence (Supplementary Figure S7A). As anticipated, KIR2DL4 expression was notably higher, particularly on dNK cell batches, dNK2 and dNK3 cells, with percentages reaching 36.4% and 44.3% positive compared to the IgG control (Figure 4C-a). The quantified statistics, normalized with pNK cells, demonstrated a dramatic increase in the expression levels of KIR2DL4 after co-culturing with trophoblasts (Figure 4C-b; Supplementary Figure S7B). The upregulated expression level of KIR2DL4 was consistent with the reduced cytotoxic ability. Apart from the inhibitory receptor expression, the cytokines and chemokines associated with immunotolerance secreted by decidual cells are found in the RNA-seq database, including *Csf3*, *Il1β*, and *Tgfb1* (Figure 4D-a; Supplementary Data 3). The protein-protein interactions analyzed by STRING for these six secreted proteins exhibit interactions in regulating immune tolerance for dNK cells. Of noteworthy significance is the interaction between IL1β and CSF3, which is strongly supported by evidence from curated databases (Figure 4D-b). These results suggest that MD-MSCs can potentially convert pNK cells into dNK-like cells and potentially mimic the immunotolerance on trophoblasts *in vitro*. Moreover, we characterized dNK2 cells and compared them to pNK cells using CD56 and CD9 markers (Albini and Noonan, 2021; Zhang et al., 2024). As shown in Supplementary Figure S8, dNK2 cells exhibit a slight differentiation tendency, marked by $CD56^{bright}CD9^{high}$ expression, in contrast to pNK cells.

Identification of highly proliferated dNK-like cells in PA-MSCs

Following the successful induction of dNK-like cells *in vitro*, we conducted a further investigation to examine the differential effects of MD-MSCs and PA-MSCs on dNK-like cells in an attempt to find the potential causes of PAS. Initially, we assessed NK cell proliferation under co-culture conditions with MD-MSCs or PA-MSCs following various decidualization inductions (Figure 5A). The experimental timeline spanned 10 days, with day 7 corresponding to the dNK-like cell conversion period. In the NK cell proliferation assay, we made an intriguing observation: PA-MSCs demonstrated a greater capacity to enhance NK cell proliferation compared to normal MD-MSCs, particularly in the E2/P4-treated groups (Figure 5B-a). The quantified analysis clearly showed a three-fold increase in NK cell proliferation after co-culture with E2/P4-treated PA-MSCs compared to E2/P4-treated MD-MSCs on day 10 (Figure 5B-b). This observation prompted us to explore the relationship between NK cell proliferation and trophoblast invasion further. Additionally, our RNA-seq analysis identified cytokines, known as key regulators of NK cell proliferation, which were predominantly upregulated in the PA-MSCs groups. Significantly, five genes potentially enhancing NK cell proliferation in E2/P4-treated De-PA-MSCs were annotated, including *Cxcl12*, *Il33*, *Vegfa*, *Vegfc*, and *Tgfb1* (Figure 5C-a; Supplementary Data 4), with the predicted interactions of these secreted proteins shown in Figure 5C-b. VEGFA was not displayed in the interaction panel due to the absence of information in the STRING database. These findings suggested a potential association between abnormal NK cell proliferation and the development of PAS. Moreover, the increased proliferation of dNK cells in the placenta of PAS patients is also evident through immunofluorescence staining for CD56 and CD9 markers (Figure 5D). Consequently, we propose the hypothesis that Abnormal dNK cell proliferation may represent a significant contributing factor to the pathogenesis of PAS.

Increased dNK cell numbers may represent one of the key factors contributing to PAS

To assess the earlier presumption that PAS could be attributed to dysregulated trophoblast invasion, we modified the previously established co-culture system to investigate the distinct impact of increasing the dNK cell batch dNK2 cell numbers on trophoblast invasion. The experimental timeline for this study is depicted in Figure 6A. Given the complex interplay among the cells involved, we simplified the co-culture system by utilizing a dNK2 cell-conditioned medium. We anticipated that dNK2 cells would exhibit an enhanced capacity to promote trophoblast invasion with a dose-dependent correlation (Figure 6B). Furthermore, dNK2 cells induced by PA-MSCs demonstrated a greater capacity to enhance trophoblast invasion compared to those induced by MD-MSCs (Figure 6B). Statistical analysis was performed by normalizing the results with the control trophoblast alone group. This outcome

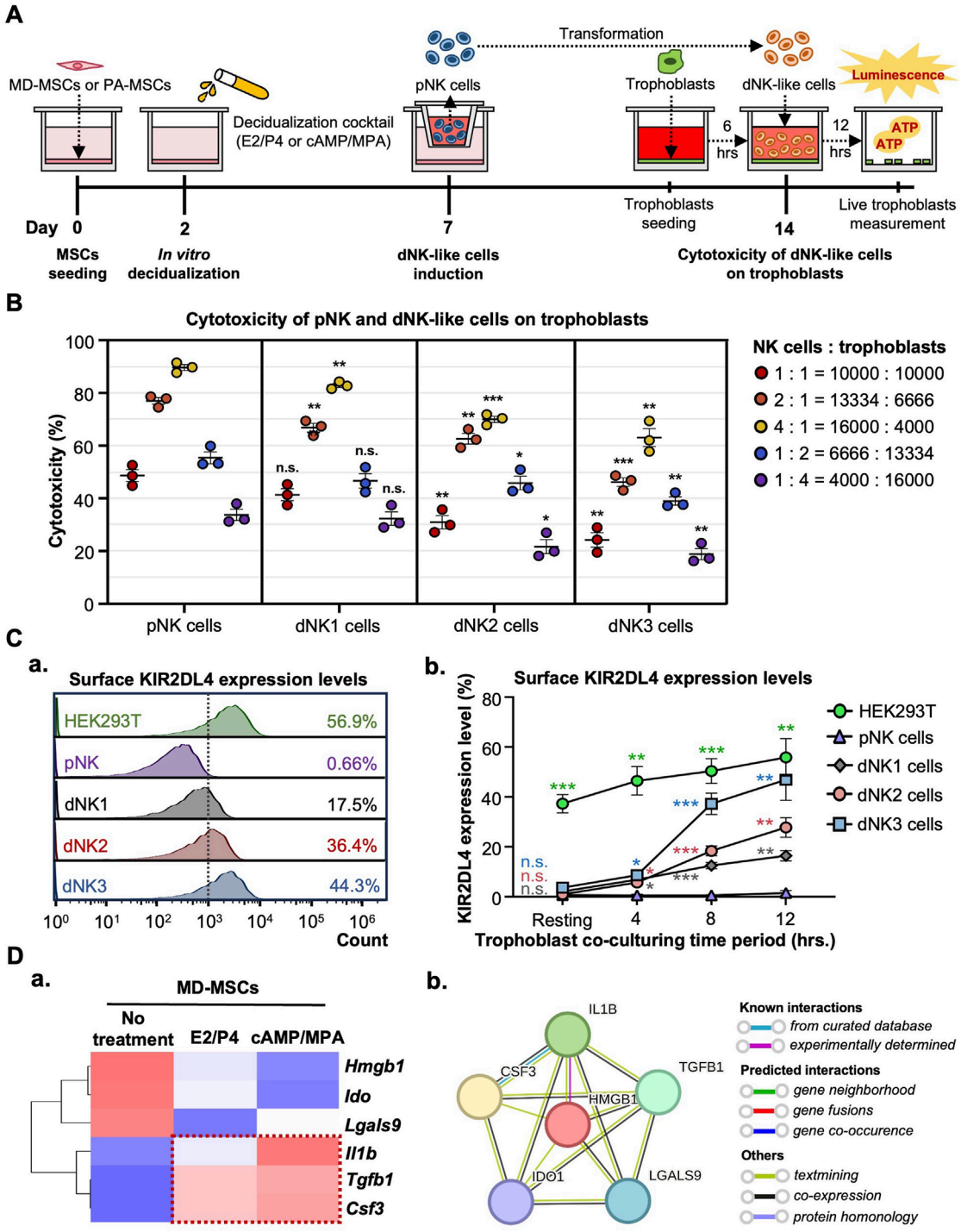

FIGURE 4
MD-MSCs can potentially convert dNK-like cells from pNK cells. **(A)** A schematic diagram and timeline depict the assessment of immune suppression in dNK-like cells using a co-culture system. **(B)** Evaluation of cytotoxicity involves three different MD-MSC-induced dNK-like cells interacting with trophoblasts. **(C) (a)** Flow cytometry analysis and **(b)** quantitative statistics represent surface KIR2DL4 expression levels on different subtypes of NK cells after co-culture with trophoblasts for 12 h. HEK293T serves as the positive control for KIR2DL4. Values are normalized to the IgG control and expressed as mean ± SEM. Significance levels are denoted as $^{*}p < 0.05$, $^{**}p < 0.01$, and $^{***}p < 0.001$, with all comparisons made against the pNK cell group. **(D) (a)** The heatmap illustrates three potential secreted proteins encoding genes that regulate the conversion of pNK cells into dNK-like cells. Values are expressed as z-scores, which have been normalized to the gene expression levels. **(b)** Predicted networks of protein-protein interaction among annotated proteins through STRING analysis. The line between two nodes typically represents the interaction between those two proteins, with the colors of the line reflecting the available resources for interactions. pNK cell: peripheral NK cells; dNK1 cells: MD-MSC-induced dNK-like cells; dNK2 cells: E2/P4-treated De-MD-MSC-induced dNK-like cells; dNK3 cells: cAMP/MPA-treated De-MD-MSC-induced dNK-like cells.

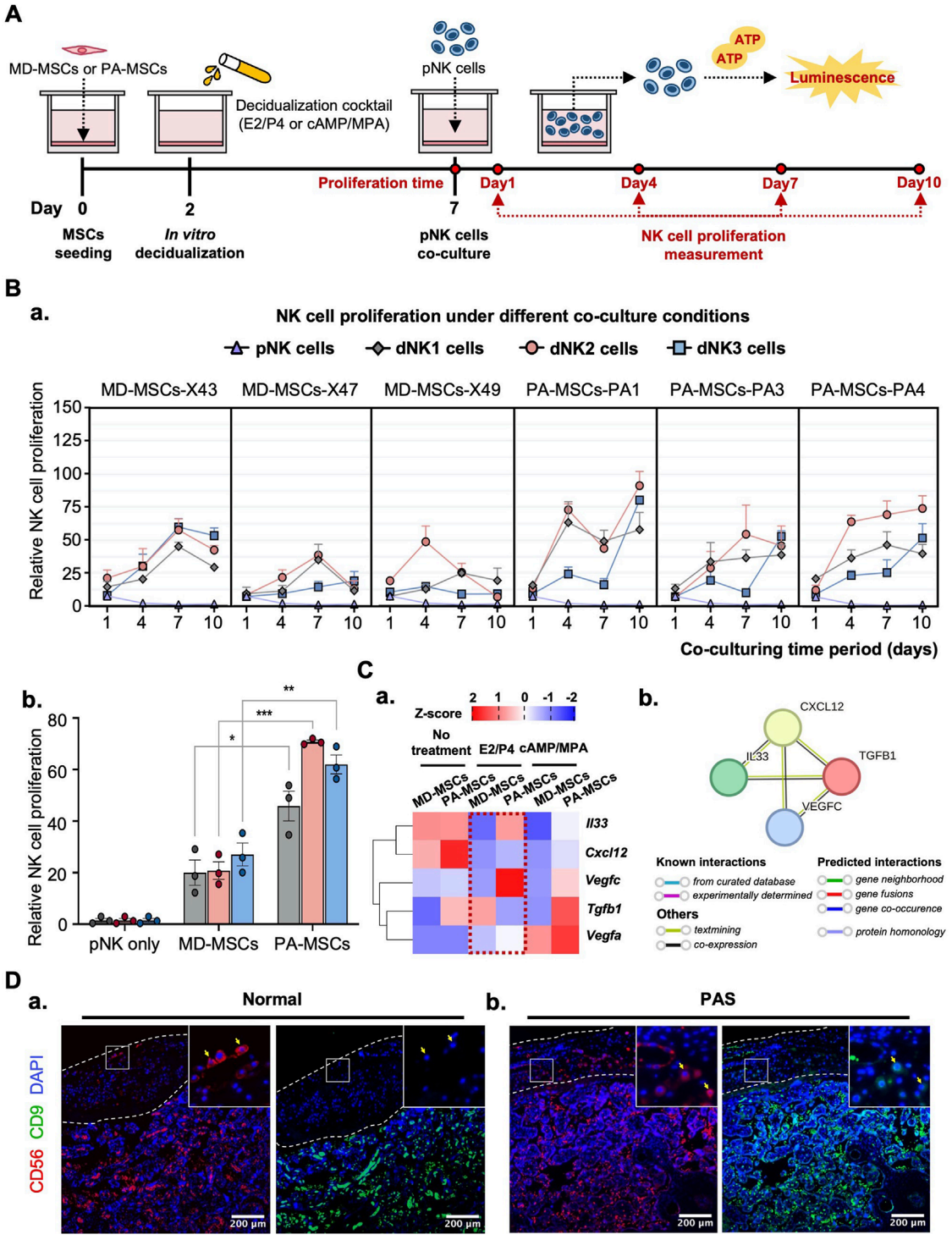

FIGURE 5
PA-MSCs demonstrate a greater capacity to enhance dNK-like cell proliferation than normal MD-MSCs. **(A)** A schematic diagram of the co-culture system for the dNK-like cell proliferation assay using MD-MSCs and PA-MSCs. **(B) (a)** The proliferation of dNK-like cells was measured at specific time points: 1, 4, 7, and 10 days under various conditions, including co-culture with MD-MSCs, PA-MSCs, and their corresponding decidual counterparts. **(b)** The effects of MD-MSCs, PA-MSCs, and their decidual counterparts on dNK-like cell proliferation were quantified at day 10. Values are expressed as mean ± SEM. $^{*}p < 0.05$, $^{**}p < 0.01$, and $^{***}p < 0.001$. **(C) (a)** The heat map illustrates the expression patterns of annotated secreted proteins responsible for stimulating dNK-like cell proliferation. Values are expressed as z-scores, which have been normalized to the gene expression levels. **(b)** Predicted networks of protein-protein interaction among annotated proteins through STRING analysis. The line between two nodes typically denotes the interaction between those two proteins, with the colors of the line reflecting the available resources of interactions. The thickness of the line is about the strength of the interactions. **(D)** Immunofluorescence staining of dNK cells in **(a)** a normal placenta and **(b)** a PAS placenta. The white-lined sections represent the decidual membrane. dNK cells are stained with CD56 (red) and CD9 (green). pNK cell: peripheral NK cells; dNK1 cells: MD-MSC-induced dNK-like cells; dNK2 cells: E2/P4-treated De-MD-MSC-induced dNK-like cells; dNK3 cells: cAMP/MPA-treated De-MD-MSC-induced dNK-like cells.

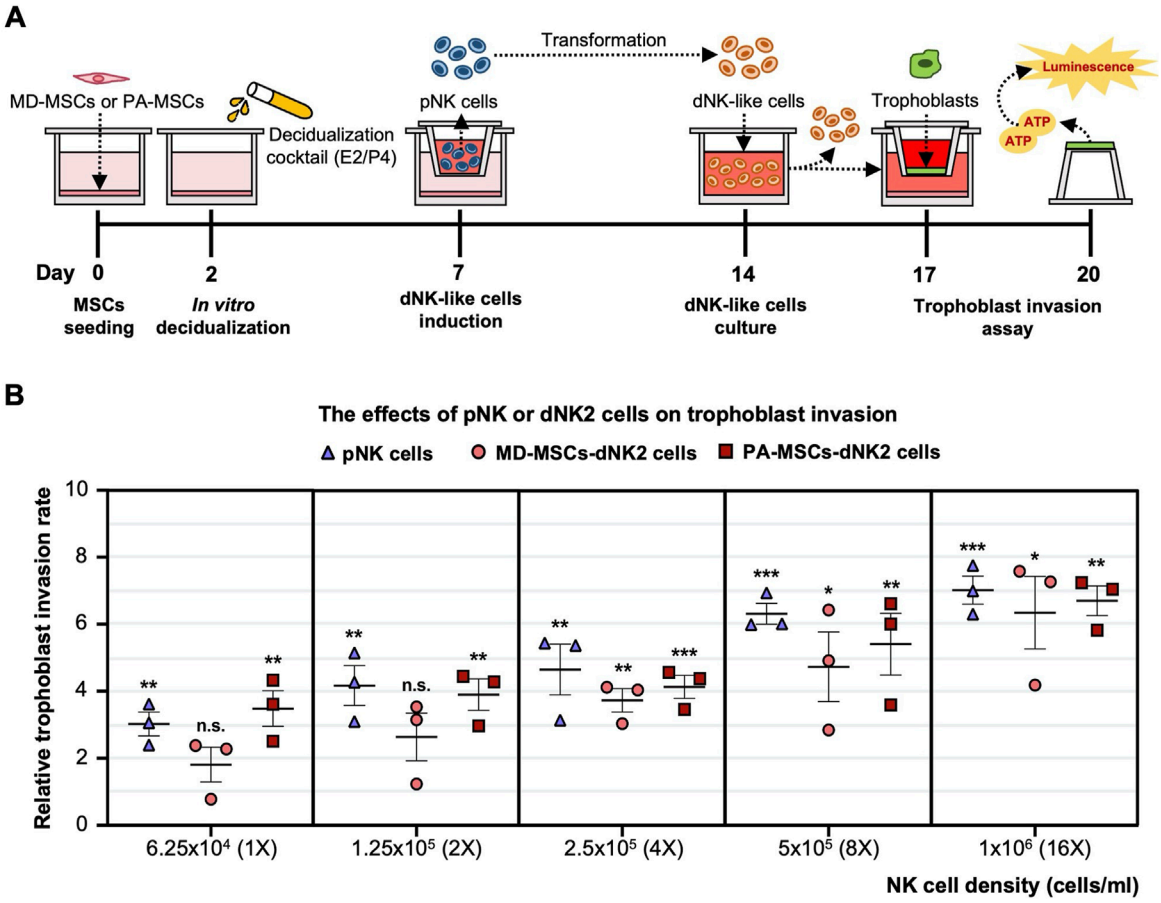

FIGURE 6
Enhanced trophoblast invasion was observed under E2/P4 treated PA-induced dNK-like cells with a dose-dependent correlation. **(A)** A schematic diagram and timeline depict the assessment of trophoblast invasion under MD-MSC or PA-induced dNK2 cell-derived conditioned medium. **(B)** Dose-dependent correlation in three subtypes of NK cells. Values are expressed as mean ± SEM. Significance levels are denoted as $^{*}p < 0.05$, $^{**}p < 0.01$, and $^{***}p < 0.001$, with all comparisons made against the pNK cell group. pNK cell: peripheral NK cells; dNK2 cells: E2/P4-treated De-MD-MSC-induced dNK-like cells.

indirectly suggests that increased dNK cell proliferation may be a pivotal factor in abnormal trophoblast invasion, potentially contributing to PAS as depicted in Figure 7. The novel finding sheds light on the mechanisms underlying PAS and lays the groundwork for the development of treatments for this condition.

Discussion

Previous studies have revealed the critical role that moderate trophoblast invasion plays in a successful pregnancy. Dysregulation of trophoblast invasion can lead to maternal lethal diseases, like the most severe pattern, PAS. PAS is associated with complicated interactions among decidual cells, trophoblasts, and dNK cells. The potential mechanisms of the PAS have not been clarified due to the limitations of the cell derivation.

In the published studies, primary ESCs and even decidual cells were predominantly obtained from menstrual blood (Sanche et al., 2021; Bozorgmehr et al., 2020) or endometrial biopsies, including curettage (Wu et al., 2017; Pei et al., 2019) and elective termination of pregnancy samples (Menkhorst et al., 2023; Lindau et al., 2021). However, these sources of ESCs have limitations regarding cell number and purity and involve invasive surgical procedures that may cause discomfort to the subjects. Furthermore, obtaining specimens from normal women has proven particularly challenging due to ethical concerns. In this study, we have identified a distinct cell type among ESCs from normal placenta characterized by its potential for decidualization and high capacity for *in vitro* amplification. Biomarker investigations validated the decidualization process of MD-MSCs, with particular attention to recognized decidual cell markers such as *Prl* and *Igfbp1* (Telgmann and Gellersen, 1998; Diniz-da-Costa et al., 2021). Our study observed a unique upregulation of *Scara5* (Lucas et al., 2020) in De-MD-MSCs, which has been suggested to play a pivotal role in crucial cellular functions during decidualization. Studies indicate that SCARA5 is downregulated in senescent decidual cells, suggesting its potential therapeutic implications in reproductive disorders (Rawlings et al., 2021; Hou et al., 2023; Szwarc et al., 2018). Further research is warranted to fully elucidate the mechanisms underlying the involvement of SCARA5 in decidualization and its implications for reproductive health. Given their unique *in vitro* decidualization potential and their ability to circumvent ethical issues, MD-MSCs

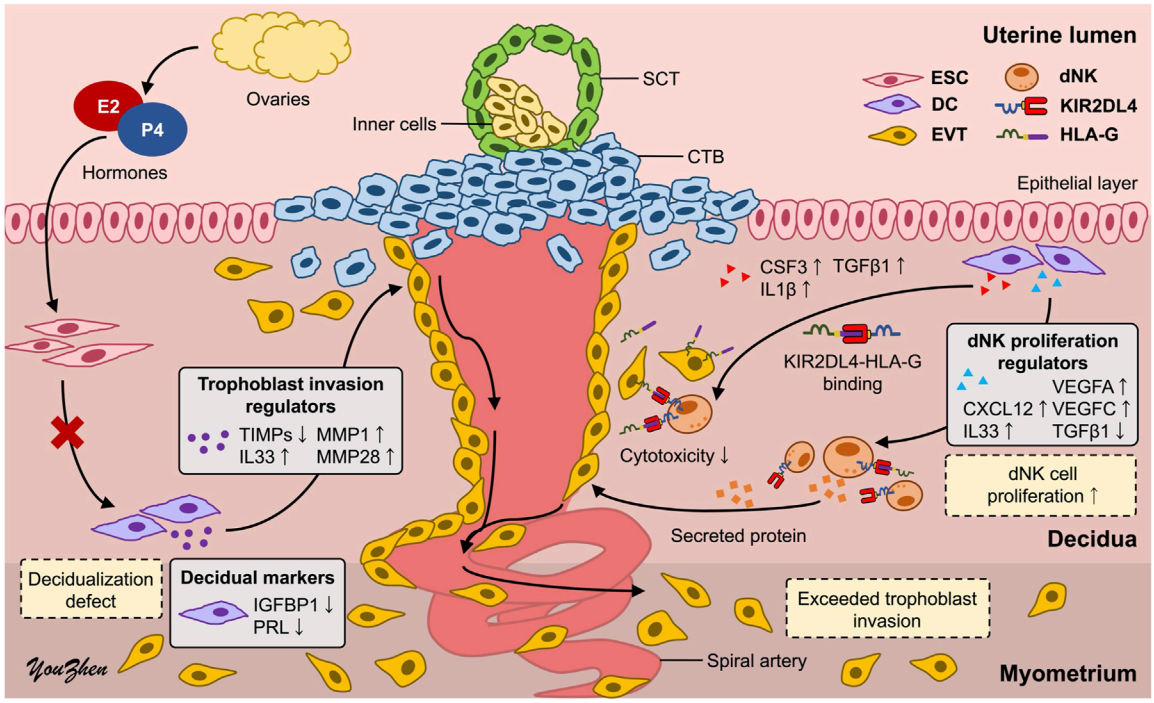

FIGURE 7
Schematic representation of the underlying mechanisms of PAS. The high proliferation of dNK cells induced by defective decidual cells may dysregulate trophoblast invasion, leading to PAS. CTB: cytotrophoblast; SCT: syncytiotrophoblast; ESC: endometrial stromal cell; DC: decidual cell; EVT: extravillous trophoblast; dNK: decidual natural killer cell.

stand out as a potentially valuable model for advancing the study of placental development and associated diseases.

In the trophoblast invasion assay, the validated EVT cell line 3A-subE was used in this study. We found that MD-MSCs treated with cAMP/MPA negatively regulate trophoblast invasion, in contrast to E2/P4-treated MD-MSCs, which enhance trophoblast invasion. The regulation of trophoblast invasion involves intricate cell-cell interactions and activation of multiple signaling pathways. Proteins secreted from decidual cells can either promote or inhibit trophoblast invasion, thus modulating trophoblast invasion levels. Gene expression analysis suggests that genes associated with trophoblast invasion enhancement (*Mmps*) are reduced, while genes associated with inhibiting trophoblast invasion (*Timps*) are upregulated in cAMP/MPA-treated MD-MSCs, consistent with their inhibitory effect on trophoblasts (Sharma et al., 2016; Zhu et al., 2012; Hamutoğlu et al., 2020; Li et al., 2021; Haider et al., 2022). In contrast, E2/P4 treatment sustains or increases *Mmp* expression relative to *Timps*, creating an environment that promotes trophoblast invasion. Of particular interest is the upregulation of *Timp2*, which uniquely contributes to both the inhibition and activation of MMP2, reflecting a finely balanced regulatory mechanism controlling matrix remodeling. These findings underscore how distinct hormonal signals differentially modulate the MMP/TIMP axis to influence trophoblast function and decidual remodeling.

Given that we observed that the decidual membrane was not absent in PAS patients, this finding contradicts the hallmark characteristic of PAS: the absence of the decidual membrane. Beyond the loss of the decidual membrane, poor decidualization and dysfunctional decidual cells may also play critical roles in the development of PAS (Afshar et al., 2024; Morlando and Collins, 2020; Arak et al., 2023). Consequently, we sought to further investigate the underlying mechanisms by utilizing pathological MD-MSCs, focusing on the remnants of the residual decidual membrane. We observed diminished morphological changes and decreased expression levels of PRL and IGFBP1, both at mRNA and protein levels, *in vitro* and *in vivo*. Additionally, besides these two decidual markers, other annotated upregulated genes under decidualization were found to be downregulated under E2/P4 treatment. This observation may be due to abnormally high ER expression, which has been associated with decidualization defects and endometriosis (Chantalat et al., 2020; Han et al., 2019). Elevated ERβ expression and activity in endometriosis promote lesion growth by inhibiting apoptosis, activating inflammatory pathways, defective decidualization, and enhancing invasion through epithelial–mesenchymal transition (Han et al., 2015). Regarding trophoblast invasion, no discernible effects on trophoblast invasion were observed between De-MD-MSCs and De-PA-MSCs. However, RNA-seq data revealed differential expression of molecules involved in trophoblast invasion regulation in E2/P4 treated De-PA-MSCs, notably downregulated *Timp1*, *Timp3* and *Timp4* (Szwarc et al., 2018), (Afshar et al., 2024; Morlando and Collins, 2020), (Tapia-Pizarro et al., 2013; Ma et al., 2014) and upregulated *Il33* (Chen et al., 2018; Valero-Pacheco et al., 2022), *Mmp1*, *Mmp12* and *Mmp28* (Deng et al., 2015; Li et al., 2003; Arora et al., 2023), which may promote trophoblast invasion. Based on these results, we propose two possible explanations. Firstly, it is conceivable that the drug potency of cAMP/MPA is too high to reveal the decidualization defect in PA-MSCs. Secondly, abnormal

trophoblast invasion may not be directly attributed to the inherent properties of defective decidual cells.

To investigate the indirect effects on trophoblast invasion, dNK cells were included in the co-culture system to explore their interactions with decidual cells and trophoblasts. At the maternal-fetal interface, dNK cells play a crucial role in promoting immune tolerance through specific interactions between KIRs on dNK cells and HLA expressed on trophoblasts (Bhattacharya et al., 2015). Notably, KIR2DL4 on maternal dNK cells can interact with soluble HLA-G (sHLA-G) from fetal trophoblast cells, potentially modulating immune responses and promoting tolerance to the semi-allogeneic fetus during pregnancy (Hanna et al., 2006; Velicky et al., 2016). This interaction is pivotal in regulating maternal immune responses and maintaining the integrity of the maternal-fetal interface. However, due to the challenge in deriving dNK cells, we opted for *in vitro* induction methods to address this issue. Instead of chemical induction using TGFβ and demethylation agents (Cerdeira et al., 2013), we employed decidual cell induction methods to closely mimic the physiological microenvironment (Vacca et al., 2011). Interestingly, De-MD-MSCs demonstrated the ability to induce dNK-like cells from pNK cells. Although these dNK-like cells did not exhibit markedly high expression of dNK cell surface markers, characterized by $CD56^{bright}CD16^{-}CD9^{bright}CD49a^{bright}$, their induction could potentially be enhanced under hypoxic conditions (Du et al., 2022). Despite the limited expression of surface markers, KIR2DL4 expression was significantly upregulated in dNK-like cells when co-cultured with De-MD-MSCs treated with either E2/P4 or cAMP/MPA. The observed reduction in immune response may be attributed to cytokines secreted by decidual cells, including *Csf3*, *Il-1β*, and *Tgfb1* (Dwyer et al., 2022; Wen et al., 2023), as suggested by RNA-seq data. Furthermore, we made a novel observation regarding the abnormal interaction between PA-MSCs and dNK-like cells. PA-MSCs exhibited a significant capacity to enhance dNK-like cell proliferation, as evidenced by the increased dNK cells in PAS placenta from immunofluorescence images. However, the underlying mechanisms driving this abnormal proliferation of dNK cells in PAS have yet to be fully elucidated. Only a few published studies proposed that the reduced proliferation of dNK cells may be one of the contributing factors to PAS (Khairy et al., 2017). Thus, further evidence is required to clarify the correlation between dNK cell proliferation and PAS.

Based on the observed decidualization defect and the highly proliferated dNK-like cells induced by PA-MSCs, several secreted proteins implicated in promoting dNK cell proliferation and correlating with trophoblast invasion are found to be upregulated and annotated in RNA-seq data from PA-MSCs compared to MD-MSCs. CXCL12 secreted by decidual cells can bind to CXCR4 receptors on dNK cells or trophoblasts, indirectly or directly inducing trophoblast differentiation, invasion, and spiral artery remodeling, which may be through activating downstream PI3K-Akt and MAPK-ERK signaling pathways (Supplementary Figure S6; Supplementary Data 5) (Zhu et al., 2012; Arck and Hecher, 2013; Wang et al., 2015; Li et al., 2024). In addition, IL33 has been found to activate the NF-κB and MAPK pathways and is essential for regulating trophoblast invasion and placental development by modulating the immune environment (Supplementary Figure S6) (Chen et al., 2018; Valero-Pacheco et al., 2022). Notably, TGFβ1, which has been suggested in evidence to suppress NK cell proliferation via SMAD-dependent signaling (Yang et al., 2021; Lamb et al., 2021), is downregulated in E2/P4-treated De-PA-MSCs, suggesting a reduction in immunoregulatory control that may permit excessive trophoblast activity. Interestingly, the TGF-β signaling pathway is enriched at the transcriptomic level, likely driven by upregulation of other pathway components, which may reflect compensatory or context-specific activation rather than direct TGFβ1-mediated signaling (Supplementary Figure S6). Furthermore, VEGFA and VEGFC, secreted by both decidual cells and dNK cells, not only enhance trophoblast invasion but also promote angiogenesis and spiral artery remodeling, potentially leading to significant bleeding in PAS (El-Badawy et al., 2023; Rekowska et al., 2023). In our study, the upregulated and downregulated genes suggest a positive correlation among dNK cell proliferation, trophoblast invasion, and spiral artery remodeling. Functional validation reveals that conditioned medium derived from dNK-cells induced by E2/P4-treated De-PA-MSCs has a greater capacity to enhance trophoblast invasion in a dose-dependent manner compared to dNK-like cells induced by De-MD-MSCs.

These findings provide new insights into the underlying mechanisms of PAS through the decidualization defect and subsequent abnormal interactions among decidual, dNK, and trophoblast cells. MD-MSCs have the potential to break the limitations of *in vitro* studies related to complex placental diseases and may significantly contribute to advancements in human health. However, the MD-MSCs-based co-culture model for studying placental disorders still presents challenges that require further efforts to overcome. The physiological identity of MD-MSCs in the endometrium requires more evidence to substantiate their correlation with decidualization and their role in placental formation, thereby highlighting the importance of this cell type. Due to a small clinical sample size, our results need further validation to ensure consistent findings through both *in vitro* cell assays and *in vivo* mouse models. The MD-MSC-based co-culture system needs to be augmented by co-culturing with various cell types to better mimic the complex microenvironment. Additionally, single-cell RNA-seq and cytokine array analyses should be conducted to validate the aforementioned results. Regarding trophoblast behavior, while this study focused on invasion capacity, the expression of differentiation markers also plays a critical role in regulating trophoblast function and warrants further investigation. We anticipate identifying specific molecular pathways to comprehensively elucidate the mechanisms underlying complex PAS in future research endeavors.

Conclusion

This study highlights the development of an MD-MSC-based system for *in vitro* investigation of the intricate interactions among decidual, dNK, and trophoblast cell induction and their implications for PAS. Utilizing the MD-MSC-based co-culture system, decidualization defects characterized by decreased morphological changes and expression of decidual markers were observed in the residual decidual membrane of PA-MSCs. Additionally, MD-MSCs demonstrated the capacity to induce the

differentiation of pNK cells into dNK-like cells, as evidenced by reduced cytotoxicity on trophoblasts and increased expression of KIR2DL4. Furthermore, PA-MSCs exhibited a high capacity to induce dNK-like cell proliferation, indirectly enhancing trophoblast invasion and spiral artery remodeling, possibly through CXCL12, TGFβ1, VEGFA, and VEGFC secretion. These findings provide new insights and lay the groundwork for further elucidating the complex pathophysiology of PAS through the novel MD-MSC cell type.

Data availability statement

The original contributions presented in the study are included in the article and/or Supplementary Material, further inquiries can be directed to the corresponding authors.

Ethics statement

The studies involving humans were approved by National Taiwan University Hospital Research Ethics Committee. The studies were conducted in accordance with the local legislation and institutional requirements. The participants provided their written informed consent to participate in this study. Written informed consent was obtained from the individual(s) for the publication of any potentially identifiable images or data included in this article.

Author contributions

Y-ZL: Validation, Data curation, Conceptualization, Investigation, Writing – review and editing, Writing – original draft. H-HL: Investigation, Data curation, Writing – review and editing, Validation. M-SW: Validation, Methodology, Investigation, Writing – review and editing. J-CS: Investigation, Validation, Formal analysis, Writing – review and editing, Conceptualization. T-YL: Funding acquisition, Writing – review and editing, Conceptualization.

Funding

The author(s) declare that financial support was received for the research and/or publication of this article. This work was supported by grant 110-2320-B-002-063-MY3, 113-2314-B-038-135- and 114-2314-B-038-011- from the National Science and Technology Council to T-YL.

Acknowledgments

Material and technical support: Placentas of PAS patients from J-CS, Department of Obstetrics and Gynecology, National Taiwan University Hospital, Taipei, Taiwan. NK cell expansion kit (DSNK) from BIOMAB, INC., Innovation Incubation Center of National Taiwan University, Taipei, Taiwan. Flow cytometry analysis was provided by the Flow Cytometric Analyzing and Sorting Core of the First Core Laboratory, National Taiwan University. Tissue section preparation was facilitated by the Laboratory Animal Center, College of Medicine, National Taiwan University.

Conflict of interest

Author H-HL was employed by MediDiamond Inc. Author H-HL was employed by LuminX Biotech Co. Ltd.

The remaining authors declare that the research was conducted in the absence of any commercial or financial relationships that could be construed as a potential conflict of interest.

Correction note

A correction has been made to this article. Details can be found at: 10.3389/fcell.2025.1696297.

Generative AI statement

The author(s) declare that no Generative AI was used in the creation of this manuscript.

Publisher's note

All claims expressed in this article are solely those of the authors and do not necessarily represent those of their affiliated organizations, or those of the publisher, the editors and the reviewers. Any product that may be evaluated in this article, or claim that may be made by its manufacturer, is not guaranteed or endorsed by the publisher.

Supplementary material

The Supplementary Material for this article can be found online at: https://www.frontiersin.org/articles/10.3389/fcell.2025.1618461/full#supplementary-material

References

Adu-Gyamfi, E. A., Lamptey, J., Chen, X. M., Li, F. F., Li, C., Ruan, L. L., et al. (2021). Iodothyronine deiodinase 2 (DiO2) regulates trophoblast cell line cycle, invasion and apoptosis; and its downregulation is associated with early recurrent miscarriage. *Placenta* 111, 54–68. doi:10.1016/j.placenta.2021.06.004

Afshar, Y., Yin, O., Jeong, A., Martinez, G., Kim, J., Ma, F., et al. (2024). Placenta accreta spectrum disorder at single-cell resolution: a loss of boundary limits in the decidua and endothelium. *Am. J. Obstet. Gynecol.* 230, 443.e1–443.e18. doi:10.1016/j.ajog.2023.10.001

Albini, A., and Noonan, D. M. (2021). Decidual-like NK cell polarization: from cancer killing to cancer nurturing. *Cancer Discov.* 11, 28–33. doi:10.1158/2159-8290.CD-20-0796

Al-Khan, A., Bulmer, J. N., Chantraine, F., Chen, C. P., Chen, Q., Collins, S., et al. (2013). IFPA Meeting 2012 Workshop Report III: trophoblast deportation, gestational trophoblastic disease, placental insufficiency and fetal growth restriction, trophoblast over-invasion and accreta-related pathologies, placental thrombosis and fibrinolysis. *Placenta* 34 (Suppl. 1), 11–16. doi:10.1016/j.placenta.2012.11.018

Aplin, J. D., Myers, J. E., Timms, K., and Westwood, M. (2020). Tracking placental development in health and disease. *Nat. Rev. Endocrinol.* 16, 479–494. doi:10.1038/s41574-020-0372-6

Arakaza, A., Zou, L., and Zhu, J. (2023). Placenta accreta spectrum diagnosis challenges and controversies in current obstetrics: a review. *Int. J. Womens Health.* 15, 635–654. doi:10.2147/IJWH.S395271

Arck, P. C., and Hecher, K. (2013). Fetomaternal immune cross-talk and its consequences for maternal and offspring's health. *Nat. Med.* 19, 548–556. doi:10.1038/nm.3160

Arora, P., Mochan, S., Gupta, S. K., Rani, N., Kshetrapal, P., Dwivedi, S., et al. (2023). Abnormal trophoblast invasion in early onset preeclampsia: involvement of cystathionine β-synthase, specificity protein 1 and miR-22. *bioRxiv 03*. doi:10.1101/2023.03.08.531728

Bartels, H. C., Postle, J. D., Downey, P., and Brennan, D. J. (2018). Placenta accreta spectrum: a review of pathology, molecular biology, and biomarkers. *Dis. Markers* 2018, 1507674. doi:10.1155/2018/1507674

Bernardo, M. M., and Fridman, R. (2003). TIMP-2 (tissue inhibitor of metalloproteinase-2) regulates MMP-2 (matrix metalloproteinase-2) activity in the extracellular environment after pro-MMP-2 activation by MT1 (membrane type 1)-MMP. *Biochem. J.* 374, 739–745. doi:10.1042/BJ20030557

Bhattacharya, P., Thiruppathi, M., Elshabrawy, H. A., Alharshawi, K., Kumar, P., and Prabhakar, B. S. (2015). GM-CSF: an immune modulatory cytokine that can suppress autoimmunity. *Cytokine* 75, 261–271. doi:10.1016/j.cyto.2015.05.030

Bozorgmehr, M., Gurung, S., Darzi, S., Nikoo, S., Kazemnejad, S., Zarnani, A. H., et al. (2020). Endometrial and menstrual blood mesenchymal stem/stromal cells: biological properties and clinical application. *Front. Cell Dev. Biol.* 8, 497. doi:10.3389/fcell.2020.00497

Cerdeira, A. S., Rajakumar, A., Royle, C. M., Lo, A., Husain, Z., Thadhani, R. I., et al. (2013). Conversion of peripheral blood NK cells to a decidual NK-like phenotype by a cocktail of defined factors. *J. Immunol.* 190, 3939–3948. doi:10.4049/jimmunol.1202582

Chang, R. Q., Zhou, W. J., Li, D. J., and Li, M. Q. (2020). Innate lymphoid cells at the maternal–fetal interface in human pregnancy. *Int. J. Biol. Sci.* 16, 957–969. doi:10.7150/ijbs.38264

Chantalat, E., Valera, M. C., Vaysse, C., Noirrit, E., Rusidze, M., Weyl, A., et al. (2020). Estrogen receptors and endometriosis. *Int. J. Mol. Sci.* 21, 2815. doi:10.3390/ijms21082815

Chen, H., Zhou, X., Han, T. L., Baker, P. N., Qi, H., and Zhang, H. (2018). Decreased IL-33 production contributes to trophoblast cell dysfunction in pregnancies with preeclampsia. *Mediat. Inflamm.* 2018, 9787239. doi:10.1155/2018/9787239

Chen, M. C., Lai, K. S. L., Chien, K. L., Teng, S. T., Lin, Y. R., Chao, W., et al. (2022). pcMSC modulates immune dysregulation in patients with COVID-19-induced refractory acute lung injury. *Front. Immunol.* 13, 871828. doi:10.3389/fimmu.2022.871828

Deng, C. L., Ling, S. T., Liu, X. Q., Zhao, Y. J., and Lv, Y. F. (2015). Decreased expression of matrix metalloproteinase-1 in the maternal umbilical serum, trophoblasts and decidua leads to preeclampsia. *Exp. Ther. Med.* 9, 992–998. doi:10.3892/etm.2015.2194

Diniz-da-Costa, M., Kong, C. S., Fishwick, K. J., Rawlings, T., Brighton, P. J., Hawkes, A., et al. (2021). Characterization of highly proliferative decidual precursor cells during the window of implantation in human endometrium. *Stem Cells* 39, 1067–1080. doi:10.1002/stem.3367

Du, X., Zhu, H., Jiao, D., Nian, Z., Zhang, J., Zhou, Y., et al. (2022). Human-induced CD49a+ NK cells promote fetal growth. *Front. Immunol.* 13, 821542. doi:10.3389/fimmu.2022.821542

Dwyer, G. K., D'Cruz, L. M., and Turnquist, H. R. (2022). Emerging functions of IL-33 in homeostasis and immunity. *Annu. Rev. Immunol.* 40, 15–43. doi:10.1146/annurev-immunol-101320-124243

El-Badawy, O., Abbas, A. M., Radwan, E., Makboul, R., Khamis, A. A., Ali, M., et al. (2023). Cross-talk between mucosal-associated invariant T, natural killer, and natural killer T cell populations is implicated in the pathogenesis of placenta accreta spectrum. *Inflammation* 46, 1192–1208. doi:10.1007/s10753-023-01799-1

Gao, L., Chen, H., Liu, J., Wang, M., Lin, F., Yang, G., et al. (2022). Extravillous trophoblast invasion and decidualization in cesarean scar pregnancies. *Acta Obstet. Gynecol. Scand.* 101, 1120–1128. doi:10.1111/aogs.14435

Haider, S., Lackner, A. I., Dietrich, B., Kunihs, V., Haslinger, P., Meinhardt, G., et al. (2022). Transforming growth factor-β signaling governs the differentiation program of extravillous trophoblasts in the developing human placenta. *Proc. Natl. Acad. Sci. USA.* 119, e2120667119. doi:10.1073/pnas.2120667119

Hamutoğlu, R., Bulut, H. E., Kaloğlu, C., Önder, O., Dağdeviren, T., Aydemir, M. N., et al. (2020). The regulation of trophoblast invasion and decidual reaction by matrix metalloproteinase-2, metalloproteinase-7, and metalloproteinase-9 expressions in the rat endometrium. *Reprod. Med. Biol.* 19, 385–397. doi:10.1002/rmb2.12342

Han, S. J., Jung, S. Y., Wu, S. P., Hawkins, S. M., Park, M. J., Kyo, S., et al. (2015). Estrogen receptor β modulates apoptosis complexes and the inflammasome to drive the pathogenesis of endometriosis. *Cell* 163, 960–974. doi:10.1016/j.cell.2015.10.034

Han, S. J., Lee, J. E., Cho, Y. J., Park, M. J., and O'Malley, B. W. (2019). Genomic function of estrogen receptor β in endometriosis. *Endocrinology* 160, 2495–2516. doi:10.1210/en.2019-00442

Hanna, J., Goldman-Wohl, D., Hamani, Y., Avraham, I., Greenfield, C., Natanson-Yaron, S., et al. (2006). Decidual NK cells regulate key developmental processes at the human fetal–maternal interface. *Nat. Med.* 12, 1065–1074. doi:10.1038/nm1452

Hecht, J. L., Baergen, R., Ernst, L. M., Katzman, P. J., Jacques, S. M., Jauniaux, E., et al. (2020). Classification and reporting guidelines for the pathology diagnosis of placenta accreta spectrum (PAS) disorders: recommendations from an expert panel. *Mod. Pathol.* 33, 2382–2396. doi:10.1038/s41379-020-0569-1

Hess, A. P., Hamilton, A. E., Talbi, S., Dosiou, C., Nyegaard, M., Nayak, N., et al. (2007). Decidual stromal cell response to paracrine signals from the trophoblast: amplification of immune and angiogenic modulators. *Biol. Reprod.* 76, 102–117. doi:10.1095/biolreprod.106.054791

Hou, R., Huang, R., Zhou, Y., Lin, D., Xu, J., Yang, L., et al. (2023). Single-cell profiling of the microenvironment in decidual tissue from women with missed abortions. *Fertil. Steril.* 119, 492–503. doi:10.1016/j.fertnstert.2022.12.016

Illsley, N. P., DaSilva-Arnold, S. C., Zamudio, S., Alvarez, M., and Al-Khan, A. (2020). Trophoblast invasion: lessons from abnormally invasive placenta (placenta accreta). *Placenta* 102, 61–66. doi:10.1016/j.placenta.2020.01.004

Jabrane-Ferrat, N. (2019). Features of human decidual NK cells in healthy pregnancy and during viral infection. *Front. Immunol.* 10, 1397. doi:10.3389/fimmu.2019.01397

Khairy, H. T., El-Mekkawi, S. F., Elsafty, M. S. E., Shial, E., and Kamal, A. S. (2017). Decidual natural killer cells (CD56+) population in the placental bed in accidental hemorrhage. *Egypt. J. Hosp. Med.* 69, 1582–1588. doi:10.12816/0040104

Kim, M., Jang, Y. J., Lee, M., Guo, Q., Son, A. J., Kakkad, N. A., et al. (2024). The transcriptional regulatory network modulating human trophoblast stem cells to extravillous trophoblast differentiation. *Nat. Commun.* 15, 1285. doi:10.1038/s41467-024-45669-2

Kojima, J., Ono, M., Kuji, N., and Nishi, H. (2022). Human chorionic villous differentiation and placental development. *Int. J. Mol. Sci.* 23, 8003. doi:10.3390/ijms23148003

Lamb, M. G., Rangarajan, H. G., Tullius, B. P., and Lee, D. A. (2021). Natural killer cell therapy for hematologic malignancies: successes, challenges, and the future. *Stem Cell Res. Ther.* 12, 211. doi:10.1186/s13287-021-02277-x

Li, Q., Sharkey, A., Sheridan, M., Magistrati, E., Arutyunyan, A., Huhn, O., et al. (2024). Human uterine natural killer cells regulate differentiation of extravillous trophoblast early in pregnancy. *Cell Stem Cell* 31, 181–195.e9. doi:10.1016/j.stem.2023.12.013

Li, Q. L., Illman, S. A., Wang, H. M., Liu, D. L., Lohi, J., and Zhu, C. (2003). Matrix metalloproteinase-28 transcript and protein are expressed in rhesus monkey placenta during early pregnancy. *Mol. Hum. Reprod.* 9, 205–211. doi:10.1093/molehr/gag028

Li, Y., Yan, J., Chang, H. M., Chen, Z. J., and Leung, P. C. (2021). Roles of TGF-β superfamily proteins in extravillous trophoblast invasion. *Trends Endocrinol. Metab.* 32, 170–189. doi:10.1016/j.tem.2020.12.005

Lindau, R., Vondra, S., Spreckels, J., Solders, M., Svensson-Arvelund, J., Berg, G., et al. (2021). Decidual stromal cells support tolerance at the human foetal-maternal interface by inducing regulatory M2 macrophages and regulatory T-cells. *J. Reprod. Immunol.* 146, 103330. doi:10.1016/j.jri.2021.103330

Lucas, E. S., Vrljicak, P., Muter, J., Diniz-da-Costa, M. M., Brighton, P. J., Kong, C. S., et al. (2020). Recurrent pregnancy loss is associated with a pro-senescent decidual response during the peri-implantation window. *Commun. Biol.* 3, 37. doi:10.1038/s42003-020-0763-1

Ma, R., Gu, B., Gu, Y., Groome, L. J., and Wang, Y. (2014). Down-regulation of TIMP 3 leads to increase in TACE expression and TNF α production by placental trophoblast cells. *Am. J. Reprod. Immunol.* 71, 427–433. doi:10.1111/aji.12205

Menkhorst, E., So, T., Rainczuk, K., Barton, S., Zhou, W., Edgell, T., et al. (2023). Endometrial stromal cell miR-19b-3p release is reduced during decidualization implying a role in decidual–trophoblast cross-talk. *Front. Endocrinol.* 14, 1149786. doi:10.3389/fendo.2023.1149786

Mirani, P., Lestari, P. M., Murti, K., Liberty, I. A., Andrina, H., Kesty, C., et al. (2024). CXC motif chemokine receptor 2: glimpses into the molecular pathogenesis of placenta accreta spectrum disorder. *Indones. J. Obstet. Gynecol. Sci.* 7, 16–22. doi:10.24198/obgynia.v7i1.481

Moffett, A., and Shreeve, N. (2023). Local immune recognition of trophoblast in early human pregnancy: controversies and questions. *Nat. Rev. Immunol.* 23, 222–235. doi:10.1038/s41577-022-00777-2

Morlando, M., and Collins, S. (2020). Placenta accreta spectrum disorders: challenges, risks, and management strategies. *Int. J. Womens Health.* 12, 1033–1045. doi:10.2147/IJWH.S224191

Murata, H., Tanaka, S., and Okada, H. (2022). The regulators of human endometrial stromal cell decidualization. *Biomolecules* 12, 1275. doi:10.3390/biom12091275

Pan-Castillo, B., Gazze, S. A., Thomas, S., Lucas, C., Margarit, L., Gonzalez, D., et al. (2018). Morphophysical dynamics of human endometrial cells during decidualization. *Nanomedicine* 14, 2235–2245. doi:10.1016/j.nano.2018.07.004

Pei, T., Huang, X., Long, Y., Duan, C., Liu, T., Li, Y., et al. (2019). Increased expression of YAP is associated with decreased cell autophagy in the eutopic endometrial stromal cells of endometriosis. *Mol. Cell. Endocrinol.* 491, 110432. doi:10.1016/j.mce.2019.04.012

preventaccreta.org. National Accreta foundation. (2024). Available online at: https://www.preventaccreta.org/. (Accessed 9 May 2024).

Rajagopalan, S., and Long, E. O. (2012). KIR2DL4 (CD158d): an activation receptor for HLA-G. *Front. Immunol.* 3, 258. doi:10.3389/fimmu.2012.00258

Rawlings, T. M., Makwana, K., Taylor, D. M., Molè, M. A., Fishwick, K. J., Tryfonos, M., et al. (2021). Modelling the impact of decidual senescence on embryo implantation in human endometrial assembloids. *Elife* 10, e69603. doi:10.7554/eLife.69603

Rekowska, A. K., Obuchowska, K., Bartosik, M., Kimber-Trojnar, Ż., Słodzińska, M., Wierzchowska-Opoka, M., et al. (2023). Biomolecules involved in both metastasis and placenta accreta spectrum—does the common pathophysiological pathway exist? *Cancers* 15, 2618. doi:10.3390/cancers15092618

Sanchez-Mata, A., and Gonzalez-Muñoz, E. (2021). Understanding menstrual blood-derived stromal/stem cells: definition and properties. Are we rushing into their therapeutic applications? *iScience* 24, 103501. doi:10.1016/j.isci.2021.103501

Sharma, S., Godbole, G., and Modi, D. (2016). Decidual control of trophoblast invasion. *Am. J. Reprod. Immunol.* 75, 341–350. doi:10.1111/aji.12466

Su, L. J., Wu, M. S., Hui, Y. Y., Chang, B. M., Pan, L., Hsu, P. C., et al. (2017). Fluorescent nanodiamonds enable quantitative tracking of human mesenchymal stem cells in miniature pigs. *Sci. Rep.* 7, 45607. doi:10.1038/srep45607

Szwarc, M. M., Hai, L., Gibbons, W. E., Peavey, M. C., White, L. D., Mo, Q., et al. (2018). Human endometrial stromal cell decidualization requires transcriptional reprogramming by PLZF. *Biol. Reprod.* 98, 15–27. doi:10.1093/biolre/iox161

Tapia-Pizarro, A., Argandona, F., Palomino, W. A., and Devoto, L. (2013). Human chorionic gonadotropin (hCG) modulation of TIMP1 secretion by human endometrial stromal cells facilitates extravillous trophoblast invasion *in vitro*. *Hum. Reprod.* 28, 2215–2227. doi:10.1093/humrep/det136

Telgmann, R., and Gellersen, B. (1998). Marker genes of decidualization: activation of the decidual prolactin gene. *Hum. Reprod. Update.* 4, 472–479. doi:10.1093/humupd/4.5.472

Vacca, P., Vitale, C., Montaldo, E., Conte, R., Cantoni, C., Fulcheri, E., et al. (2011). CD34+ hematopoietic precursors are present in human decidua and differentiate into natural killer cells upon interaction with stromal cells. *Proc. Natl. Acad. Sci.* 108, 2402–2407. doi:10.1073/pnas.1016257108

Valero-Pacheco, N., Tang, E. K., Massri, N., Lo, R., Chemerinski, A., Wu, T., et al. (2022). Maternal IL-33 critically regulates tissue remodeling and type 2 immune responses in the uterus during early pregnancy in mice. *Proc. Natl. Acad. Sci.* 119, e2123267119. doi:10.1073/pnas.2123267119

Velicky, P., Knöfler, M., and Pollheimer, J. (2016). Function and control of human invasive trophoblast subtypes: intrinsic vs. maternal control. *Cell Adhes. Migr.* 10, 154–162. doi:10.1080/19336918.2015.1089376

Wang, F., Qualls, A. E., Marques-Fernandez, L., and Colucci, F. (2021). Biology and pathology of the uterine microenvironment and its natural killer cells. *Cell. Mol. Immunol.* 18, 2101–2113. doi:10.1038/s41423-021-00739-z

Wang, L., Li, X., Zhao, Y., Fang, C., Lian, Y., Gou, W., et al. (2015). Insights into the mechanism of CXCL12-mediated signaling in trophoblast functions and placental angiogenesis. *Acta Biochim. Biophys. Sin.* 47, 663–672. doi:10.1093/abbs/gmv064

Wang, X. Q., and Li, D. J. (2020). The mechanisms by which trophoblast-derived molecules induce maternal–fetal immune tolerance. *Cell. Mol. Immunol.* 17, 1204–1207. doi:10.1038/s41423-020-0460-5

Wen, B., Liao, H., Lin, W., Li, Z., Ma, X., Xu, Q., et al. (2023). The role of TGF-β during pregnancy and pregnancy complications. *Int. J. Mol. Sci.* 24, 16882. doi:10.3390/ijms242316882

Wu, D., Kimura, F., Zheng, L., Ishida, M., Niwa, Y., Hirata, K., et al. (2017). Chronic endometritis modifies decidualization in human endometrial stromal cells. *Reprod. Biol. Endocrinol.* 15, 16–10. doi:10.1186/s12958-017-0233-x

Xu, Y. Y., Wang, S. C., Li, D. J., and Du, M. R. (2017). Co-signaling molecules in maternal–fetal immunity. *Trends Mol. Med.* 23, 46–58. doi:10.1016/j.molmed.2016.11.001

Yang, D., Dai, F., Yuan, M., Zheng, Y., Liu, S., Deng, Z., et al. (2021). Role of transforming growth factor-β1 in regulating fetal-maternal immune tolerance in normal and pathological pregnancy. *Front. Immunol.* 12, 689181. doi:10.3389/fimmu.2021.689181

Yang, F., Zheng, Q., and Jin, L. (2019). Dynamic function and composition changes of immune cells during normal and pathological pregnancy at the maternal–fetal interface. *Front. Immunol.* 10, 2317. doi:10.3389/fimmu.2019.02317

Yoshie, M., Kusama, K., and Tamura, K. (2015). Molecular mechanisms of human endometrial decidualization activated by cyclic adenosine monophosphate signaling pathways. *J. Mamm. Ova Res.* 32, 95–102. doi:10.1274/jmor.32.95

Zhang, Y., Yang, L., Yang, D., Cai, S., Wang, Y., Wang, L., et al. (2024). Understanding the heterogeneity of natural killer cells at the maternal–fetal interface: implications for pregnancy health and disease. *Mol. Hum. Reprod.* 30, gaae040. doi:10.1093/molehr/gaae040

Zhu, J. Y., Pang, Z. J., and Yu, Y. H. (2012). Regulation of trophoblast invasion: the role of matrix metalloproteinases. *Rev. Obstet. Gynecol.* 5, e137–e143. doi:10.3909/riog0196

frontiers | Frontiers in Cell and Developmental Biology

TYPE Correction
PUBLISHED 11 November 2025
DOI 10.3389/fcell.2025.1696297

OPEN ACCESS

APPROVED BY
Frontiers Editorial Office,
Frontiers Media SA, Switzerland

*CORRESPONDENCE
Jin-Chung Shih,
jcshih@ntu.edu.tw
Thai-Yen Ling,
tyling@ntu.edu.tw

†These authors have contributed equally to this work

RECEIVED 31 August 2025
REVISED 05 October 2025
ACCEPTED 27 October 2025
PUBLISHED 11 November 2025

CITATION
Liu Y-Z, Lin H-H, Wu M-S, Shih J-C and Ling T-Y (2025) Correction: Dysregulation of decidual NK cell proliferation by impaired decidual cells: a potential contributor to excessive trophoblast invasion in placenta accreta spectrum.
Front. Cell Dev. Biol. 13:1696297.
doi: 10.3389/fcell.2025.1696297

Correction: Dysregulation of decidual NK cell proliferation by impaired decidual cells: a potential contributor to excessive trophoblast invasion in placenta accreta spectrum

You-Zhen Liu[1†], Hsin-Hung Lin[1,2,3†], Meng-Shiue Wu[1], Jin-Chung Shih[4*] and Thai-Yen Ling[1*]

[1]Graduate Institute of Pharmacology, National Taiwan University College of Medicine, Taipei, Taiwan, [2]MediDiamond Inc., Taipei, Taiwan, [3]LuminX Biotech Co., Ltd., Taipei, Taiwan, [4]Department of Obstetrics and Gynecology, National Taiwan University Hospital, Taipei, Taiwan

KEYWORDS

decidualization, placenta accreta spectrum (PAS), trophoblast invasion, decidual natural killer cell, immune tolerace

A Correction on
Dysregulation of decidual NK cell proliferation by impaired decidual cells: a potential contributor to excessive trophoblast invasion in placenta accreta spectrum

by Liu Y-Z, Lin H-H, Wu M-S, Shih J-C and Ling T-Y (2025). Front. Cell Dev. Biol. 13:1618461. doi: 10.3389/fcell.2025.1618461

Affiliation [1]Graduate Institute of Pharmacology, National Taiwan University College of Medicine, Taipei, Taiwan was erroneously given as [1]Graduate Institute of Pharmacology, National Taiwan University College of Medicine, Taipei, Taiwan, United States.

The original article has been updated.

Publisher's note

All claims expressed in this article are solely those of the authors and do not necessarily represent those of their affiliated organizations, or those of the publisher, the editors and the reviewers. Any product that may be evaluated in this article, or claim that may be made by its manufacturer, is not guaranteed or endorsed by the publisher.

frontiers | Frontiers in Cell and Developmental Biology

TYPE Review
PUBLISHED 20 August 2025
DOI 10.3389/fcell.2025.1623959

OPEN ACCESS

EDITED BY
Valerie Kouskoff,
The University of Manchester,
United Kingdom

REVIEWED BY
Soumya Ranjan Jena,
Ravenshaw University, India
Vinod Reddy Lekkala,
University of California, San Francisco,
United States

*CORRESPONDENCE
Yujie He,
3272166124@qq.com

RECEIVED 06 May 2025
ACCEPTED 04 August 2025
PUBLISHED 20 August 2025

CITATION
Feng Y and He Y (2025) The secrets of menstrual blood: emerging frontiers from diagnostic tools to stem cell therapies. *Front. Cell Dev. Biol.* 13:1623959. doi: 10.3389/fcell.2025.1623959

The secrets of menstrual blood: emerging frontiers from diagnostic tools to stem cell therapies

Yige Feng[1,2] and Yujie He[1]*

[1]The First Clinical College, Shanxi Medical University, Taiyuan, Shanxi, China, [2]The Reproductive Medicine Center, The First Hospital of Shanxi Medical University, Taiyuan, Shanxi, China

Menstrual blood (MB), a biofluid rich in diverse cell types and biomolecules, has emerged as a vital resource for investigating female reproductive health and diseases because of its unique composition and noninvasive accessibility. This review explores the potential of MB in medical research and clinical applications, focusing on its diagnostic and therapeutic prospects. For disease diagnosis, MB offers a noninvasive sampling method for identifying biomarkers in endometriosis, cervical cancer, and other gynecological conditions. Therapeutically, stem cells derived from MB (menstrual blood-derived stem cells, MenSCs) exhibit pluripotency, high proliferative capacity, and low immunogenicity, positioning them as promising candidates in regenerative medicine. Preclinical and clinical studies have demonstrated the efficacy of MenSCs in treating infertility, premature ovarian insufficiency, intrauterine adhesions, hepatic disorders, cutaneous injuries, and neurological diseases. MenSCs also exert therapeutic effects through paracrine mechanisms by releasing cytokines and exosomes that modulate immunity, attenuate inflammation, and promote tissue repair. Despite existing challenges, MenSCs hold substantial promise for developing novel therapeutic strategies across multiple disease domains.

KEYWORDS

menstruation, diagnosis, therapy, stem cells, research progress

1 Background

Menstruation is a central physiological phenomenon of the female reproductive system characterized by cyclic shedding and bleeding of the endometrium triggered by ovarian cyclical changes. Throughout the reproductive lifespan, women typically undergo over 400 cycles of endometrial regeneration, differentiation, and shedding (Lv et al., 2018). These cyclic processes are regulated primarily by the hypothalamus-pituitary-ovary axis.

Menstrual blood (MB) is a complex biofluid containing blood from endometrial spiral arteries, vaginal secretions, and endometrial cells (van der Molen et al., 2014; Yang et al., 2012). Notably, MB results in significant differences in the concentrations of specific biomolecules and cellular compositions compared with those of peripheral blood (PB) (Iribarne-Durán et al., 2020; Hosseini et al., 2019). The shed endometrial cells encompass diverse types, including stromal cells, epithelial cells, vascular cells, and immune cells. These components not only reflect endometrial homeostasis but also provide critical insights for investigating reproductive health and disease mechanisms.

Given the heterogeneous and multifaceted composition of MB, research interest in this field has expanded substantially in recent years. This review systematically examines the applications of MB over the past decade in disease diagnostics, therapeutic development, pathogenesis elucidation, and genetic research. Furthermore, it evaluates the current challenges in clinical translation and outlines future directions to advance MB-based biomedical innovations.

2 Disease diagnosis

As a diagnostic specimen, MB offers multiple advantages, including ease of sampling, noninvasiveness, self-collection capability, periodic availability, and fewer ethical concerns (Hosoya et al., 2023). In terms of population acceptability, Wong et al. evaluated the willingness of 5,000 women to use MB as a diagnostic sample, with the results indicating that 87% of participants supported its utilization for testing (Wong et al., 2018). Another study by Budukh further validated the feasibility of MB as a screening specimen for cervical cancer (Budukh et al., 2018). This noninvasive collection method not only eliminates the discomfort associated with traditional sampling procedures but also empowers women to flexibly manage their daily activities. Consequently, MB has significant advantages as a diagnostic specimen applicable to all menstruating women.

2.1 Cervical cancer

Cervical cancer remains a leading cause of cancer-related mortality among women globally, accounting for approximately 25% of all female malignancies (Harro et al., 2001). With a mortality rate second only to that of breast cancer, it is a critical public health concern (Jin et al., 1999). Human papillomavirus (HPV) is the primary etiological agent, driving lesion progression from low-grade cervical intraepithelial neoplasia (CIN1) to high-grade neoplasia (CIN2/3) and microinvasive lesions, ultimately leading to invasive cervical cancer (Holowaty et al., 1999). Understanding this pathophysiological trajectory is essential for developing diagnostic, therapeutic, and preventive strategies. Early detection and intervention during the precancerous phase are pivotal to halting disease progression (Spitzer, 1998).

Current screening and diagnostic methods for cervical cancer rely primarily on cytology and histology. From the conventional Papanicolaou smear to improved liquid-based cytology and automated processes, these approaches have significantly reduced cervical cancer mortality in developed countries. However, owing to the high false-positive rates of cytology, colposcopy with directed biopsy is often required for further evaluation. While colposcopy can detect low- and high-grade dysplasia, its sensitivity for identifying microinvasive lesions remains limited. In cases with inconclusive findings or incomplete visualization of the squamocolumnar junction, cone biopsy is necessary to confirm diagnoses through histopathological identification of HPV-associated features. Additionally, molecular detection of high-risk HPV DNA sequences has been introduced in recent years, enhancing diagnostic sensitivity and specificity. Emerging HPV testing technologies, such as next-generation sequencing (NGS), enable hypothesis-free comprehensive genetic analysis, offering novel strategies for cervical cancer screening.

Currently, cervical cancer screening relies on cytology and histology. These methods, ranging from conventional Pap smears to advanced liquid-based cytology and automated systems, have significantly reduced mortality in developed nations (Hu and Ma, 2018). However, the high false-positive rates of cytology necessitate confirmatory colposcopy with directed biopsy. While colposcopy identifies dysplasia, its sensitivity for detecting microinvasive lesions is limited, particularly in cases with incomplete visualization of the squamocolumnar junction, which requires cone biopsy for histopathological confirmation (Burd, 2003). Molecular HPV DNA testing has emerged as a complementary tool, enhancing diagnostic accuracy (Burd, 2003). Next-generation sequencing (NGS) represents a novel frontier, enabling comprehensive genetic analysis without prior hypotheses (Tsang et al., 2022; Pei et al., 2023).

Despite these advancements, all current methods require invasive sampling, which can cause patient discomfort and psychological stress. Emerging studies on HPV detection in MB propose a noninvasive alternative. Zhang et al. (2021) collected MB via sanitary pads from premenopausal women with high-risk HPV positivity, extracted DNA, and performed next-generation sequencing (NGS)-based HPV genotyping. Compared with conventional cervical smears, MB-based testing achieved 97.7% sensitivity, identifying additional HPV genotypes, multiple infections, and true-negative cases. It also accurately detected high-risk HPV in routine false-negative test results.

Similarly, Tsang et al. (2024) used NGS to analyze MB samples from CIN/HPV-positive patients and reported a 66.7% sensitivity for high-risk HPV detection. Wong et al. (2018) further explored HPV DNA and genetic polymorphisms in MB from CIN/HPV patients and healthy controls. They reported that 83% of the participants tested HPV-positive and successfully genotyped, whereas 4% of the controls tested HPV-positive. Notably, TAP1 gene polymorphisms (I333V and D637G) in MB were linked to a reduced risk of high-grade intraepithelial neoplasia, offering actionable insights for clinical management and resource allocation.

2.2 Endometriosis

Endometriosis is a chronic disease characterized by the ectopic growth of endometrial-like tissue outside the uterine cavity, resulting in inflammatory, hormone dependent, immunological, systemic, and heterogeneous pathophysiological features, predominantly affecting reproductive-aged women (Sinaii et al., 2008). Its primary symptoms include pelvic pain, which may manifest as dysmenorrhea, dyspareunia, or chronic pelvic pain, often accompanied by overlapping symptoms (e.g., urinary or gastrointestinal manifestations), complicating clinical diagnosis (Parasar et al., 2017). Owing to symptom overlap with other gynecological conditions (e.g., ovarian cysts, uterine fibroids, or pelvic inflammatory disease sequelae) or chronic pain syndromes, a definitive diagnosis requires the integration of patient history, clinical examination, and imaging (Sinaii et al., 2008; Ballweg, 2004). However, the gold-standard diagnostic method—laparoscopy—is limited by its invasiveness (Parasar et al., 2017). Current research

on noninvasive biomarker-based diagnostic approaches remains underdeveloped (Falcone and Flyckt, 2018).

The discovery of aromatase has opened new avenues for noninvasive endometriosis diagnosis. Noble et al. (1996) demonstrated aromatase expression in both the eutopic endometria and ectopic lesions of endometriosis patients, whereas normal endometrial and nondiseased peritoneal tissues lacked detectable aromatase. Malik et al. (2018) performed immunohistochemical analysis of menstrual blood samples from endometriosis patients and nonendometriosis patients. They reported significantly increased P450 aromatase (CYP19A1) expression in endometriosis patients: 32.4% of the endometriosis patients presented moderate expression, and 67.6% presented strong expression, with no cases of negative or weak expression observed. These findings suggest that elevated aromatase levels in menstrual blood may serve as a potential noninvasive biomarker for endometriosis, offering insights for early diagnosis and disease management.

Ji et al. (2023) utilized data-independent acquisition coupled with mass spectrometry and bioinformatics to quantify differentially expressed proteins in menstrual blood. They reported significantly upregulated expression of Chemokine Ligand 5 and Interleukin-1 Receptor Antagonist in endometriosis patients. These findings highlight Chemokine Ligand 5 and Interleukin-1 Receptor Antagonist as promising candidates for endometriosis diagnosis, advancing biomarker research in this field.

2.3 Genital tuberculosis

Genital tuberculosis typically arises as a complication of pulmonary or extrapulmonary tuberculosis and spreads via blood or lymphatic pathways (Aliyu et al., 2004). Female genital tuberculosis (FGTB) is a clinically silent chronic disease that primarily involves the fallopian tubes in nearly all cases, leading to infertility, dyspareunia, menstrual irregularities, and chronic pelvic inflammation (Namavar et al., 2001). Owing to its atypical presentation, such as infertility or mild pelvic pain, which often overlaps with symptoms of other gynecological conditions, such as pelvic inflammatory disease or endometriosis, diagnosis requires the integration of patient history, imaging (e.g., ultrasound or MRI), and mycobacterial testing (Bose, 2011). Currently, no single diagnostic test is sufficient for FGTB confirmation, necessitating a multidisciplinary approach.

Paine et al. (2018) demonstrated that MB analysis via multiplex polymerase chain reaction offers a noninvasive alternative for FGTB diagnosis. The method achieved 90.2% sensitivity and 86.1% specificity, significantly outperforming traditional endometrial-based approaches. By analyzing MB samples without requiring invasive procedures such as dilation and curettage (D&C) or laparoscopy and delivering results within hours, this approach addresses the critical limitations of conventional diagnostics. Clinically, rapid, noninvasive MB testing enables early FGTB detection, allowing timely antitubercular therapy initiation to improve fertility outcomes and quality of life. In resource-limited settings, it circumvents costly and painful procedures such as D&C, reducing healthcare costs and patient discomfort. Additionally, the high sensitivity and specificity of multiplex polymerase chain reaction provide a reliable screening tool for asymptomatic or early-stage FGTB, particularly in reproductive-aged women, minimizing diagnostic delays and misdiagnosis risks while advancing clinical practice.

3 Disease treatment

MenSCs hold significant promise in the field of regenerative medicine (Figure 1). Clinically, MenSCs exhibit low immunogenicity and can be expanded for more than 20 passages *in vitro*. This immune privilege is attributed to their low expression of major histocompatibility complex class II molecules (MHC-II, specifically HLA-DR) and the absence of co-stimulatory molecules (CD80/CD86), supporting their capacity for immune evasion (Khoury et al., 2014). Both preclinical and clinical studies have demonstrated that MenSC transplantation does not elicit immune rejection or severe adverse effects (Khanjani et al., 2014; Zhong et al., 2009; Bockeria et al., 2013).

In addition to MenSCs, other cell types derived from menstrual blood—such as endometrial regenerative cells (ERCs) and endometrial stromal cells (ESCs)—can also be easily obtained and have been widely applied in the research and treatment of various diseases. Overall, menstrual blood-derived cells represent a valuable source for stem cell-based therapies, with broad therapeutic potential across a range of medical conditions.

3.1 Therapeutic potential of cell differentiation

MenSCs harness their pluripotency and self-renewal capacity to differentiate into various functional cell types under specific *in vitro* induction conditions, thereby restoring or replacing damaged tissues and achieving tissue regeneration. Their differentiation potential spans multiple tissue and cell types, demonstrating notable therapeutic potential in the treatment of a variety of diseases.

3.1.1 Treatment of gynecological disorders

3.1.1.1 Infertility

For women with unexplained infertility, endometrial functional abnormalities may contribute to the underlying pathology. Cell-based therapies, particularly those that leverage the capacity of stem cells for decidualization or epithelial differentiation, offer a potential solution to improve endometrial function. Such therapies promote endometrial tissue remodeling, creating optimal conditions for embryo implantation. Piersma et al. (2015) successfully induced decidualization in MenSCs, observing the upregulation of characteristic decidualization markers such as prolactin, progesterone receptor, estrogen receptor, and insulin-like growth factor-binding protein. Additionally, key genes involved in decidualization including FOXO1, NOTCH1, NANOG, WNT4, KLF4, OCT4, SOX2, and LIN28A, as well as angiogenesis-related genes such as HIF1A, VEGFR-2, and VEGFR-3, were significantly upregulated. This coordinated gene expression enhances endometrial functionality, providing a novel direction for cellular replacement therapies in the treatment of infertility.

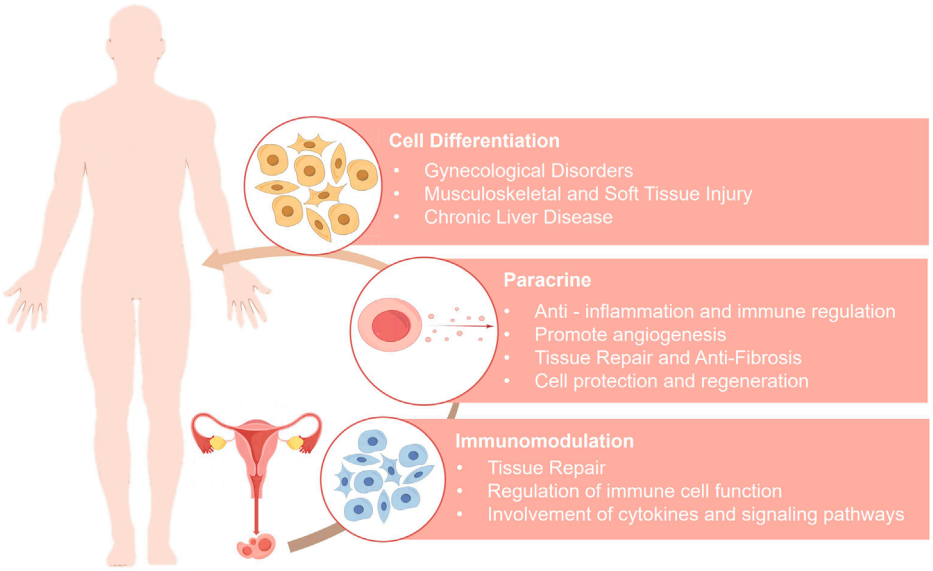

FIGURE 1
Mechanisms of menstrual blood-derived stem cells in disease treatment.

3.1.1.2 Ovarian disorders

Premature ovarian insufficiency (POI) is characterized by menstrual irregularities (amenorrhea, oligomenorrhea, or polymenorrhea) in women under 40 years of age and is accompanied by elevated follicle-stimulating hormone (FSH) levels (>25 U/L) and fluctuating estrogen decline (Feng et al., 2019). Studies have demonstrated that the transplantation of MenSCs improves ovarian function in POI models through multiple mechanisms. When transplanted via the tail vein into cyclophosphamide-induced POI model mice, MenSCs regulate follicular development, restore estrous cyclicity, reduce ovarian apoptosis, and maintain microenvironmental homeostasis via ECM-dependent FAK/AKT signaling activation (Feng et al., 2019). MenSCs also significantly improve physiological parameters in mice with ovarian damage, including serum hormone levels (e.g., FSH and estradiol (E2)), body weight, estrous cyclicity, ovarian reserve markers (e.g., anti-Müllerian hormone and FSH receptor (FSHR)), and follicle counts (Lai et al., 2015; Liu et al., 2014). Gene expression analysis revealed that posttransplantation ovarian gene expression profiles in mice closely resemble those of human ovarian tissue, suggesting that the POI microenvironment may induce MenSCss differentiation into ovarian-like cells (Liu et al., 2014).

Furthermore, the ability of MenSCs to promote germ cell differentiation has increased their therapeutic utility in treating ovarian disorders. Lai et al. (2016) demonstrated that MenSCs exposed to follicular fluid *in vitro* differentiate into oocyte-like cells and theca-like cells expressing FSHR and luteinizing hormone receptor, with steroidogenic capacity. Under coculture conditions, MenSCs further generate multinucleated embryoid structures, indicating their potential for oocyte development.

3.1.1.3 Intrauterine adhesions

Intrauterine adhesion (IUA), an acquired disorder following endometrial injury, is characterized by inadequate endometrial thickness, resulting in infertility and pregnancy loss even after assisted reproduction. Malik et al. (2018) demonstrated that MenSCs differentiated toward the endometrial lineage via PDGF, TGF-β, EGF, and 17β-estradiol expressed endometrial markers (cytokeratin (CK), vimentin, estrogen receptor, and progesterone receptor (PR)) in NOD-SCID mice posttransplantation, suggesting their capacity to reconstruct the endometrial architecture and restore fertility.

Fibrosis in IUA involves TGF-β-induced myofibroblast differentiation of endometrial stromal cells and the upregulation of α-smooth muscle actin (αSMA), type I collagen, CTGF, and fibronectin while impairing ESC migration (Deans and Abbott, 2010; Piersma et al., 2015; Zhu et al., 2019). Zhu et al. (Deans and Abbott, 2010) revealed that MenSCs-endometrial stromal cells coculture suppressed TGF-β-driven fibrosis by activating Hippo signaling (via TAZ phosphorylation), restoring ESC migratory capacity and promoting endometrial repair.

Clinical research has further verified the therapeutic potential of MenSCs. MenSCs isolated from the menstrual effluent of seven severe IUA patients were injected into the uterine cavity with hormone therapy, resulting in increased endometrial thickness in all patients (Malik et al., 2018). Among these, three achieved pregnancy with one live birth, demonstrating the efficacy of MenSCs in improving endometrial function and fertility outcomes (Malik et al., 2018; Chen et al., 2016).

3.1.2 Treatment of musculoskeletal and soft tissue injury

MenSCs exhibit remarkable potential in the treatment of musculoskeletal disorders and the repair of soft tissue injuries. Through directed differentiation, these cells can be induced to transform into osteoblasts, chondrocytes, and adipocytes, offering new therapeutic avenues for the repair of bone injuries, degenerative diseases, and congenital defects.

In the context of bone and cartilage regeneration, MenSCs cultured in osteogenic induction medium for 21 days presented marked morphological changes, along with significantly upregulated expression of key osteogenic markers such as alkaline phosphatase (ALP), secreted phosphoprotein 1 (SPP1), and bone gamma-carboxyglutamic acid-containing protein (BGLAP) (Skliutė et al., 2021). During chondrogenic differentiation, increased expression of the collagen type II alpha 1 (COL2A1) gene further supports its regenerative potential in skeletal and cartilage tissues.

With respect to muscle regeneration and pelvic organ prolapse (POP), the ability of MenSCs to differentiate into smooth muscle cells provides new insights for POP repair. The pathological basis of POP involves degeneration of vaginal smooth muscle, leading to loss of pelvic floor support (Chen et al., 2016). In a study by Chen et al. (2016), MenSCs were successfully induced to differentiate into smooth muscle cells under TGF-β1 stimulation via the TGFBR2/ALK5/Smad2/3 signaling pathway, laying the groundwork for cell-based therapies. Furthermore, in a clinical study of Duchenne muscular dystrophy (DMD), a patient who received an intramuscular injection of 116 million MenSCs presented significantly improved muscle strength and restored dystrophin expression (Ichim et al., 2010), highlighting the therapeutic potential of MenSCs in muscle repair.

In the context of soft tissue regeneration, the adipogenic potential of MenSCs is critical. Under rosiglitazone induction, the mRNA expression of adipogenic markers—including leptin receptor (LEPR), peroxisome proliferator-activated receptor gamma (PPAR-γ), and lipoprotein lipase (LPL)—was significantly upregulated (Khanmohammadi et al., 2014). Compared with BM-MSCs, MenSCs offer advantages in terms of accessibility and ethical acceptability, making them ideal candidates for repairing soft tissue defects resulting from burns or tumor resection.

The application of MenSCs also extends to cutaneous wound healing. These cells can differentiate into mature keratinocytes and express epidermal-specific markers *in vitro*, including keratin 14 (K14), p63, and involucrin (IVL) (Fard et al., 2018; Akhavan-Tavakoli et al., 2017). This epithelial differentiation capacity positions MenSCs as promising cell sources for the treatment of skin injuries such as burns and ulcers.

3.1.3 Treatment of chronic liver disease

MenSCs demonstrate significant potential for hepatocyte differentiation in the treatment of chronic liver diseases, suggesting a novel direction for regenerative medicine. Studies indicate that under the induction of factors such as hepatocyte growth factor (HGF) and Oncostatin M (OSM), MenSCs differentiate into hepatocyte-like cells, with the degree of differentiation showing a positive correlation with the concentrations of these factors (Malik et al., 2018). Differentiated cells express key hepatocyte markers—including albumin, tyrosine aminotransferase (TAT), and cytokeratin-18 (CK18)—at both the mRNA and protein levels and exhibit essential hepatocyte functions, such as albumin secretion, glycogen storage, and cytochrome P450 7A1 expression, thereby effectively mimicking the metabolic and detoxification functions of mature hepatocytes (Malik et al., 2018). Additionally, induced ERCs have been shown to differentiate into functional hepatocyte-like cells (Khademi et al., 2014). These findings suggest that menstrual blood-derived cells offer promising new avenues for cell-based therapies in chronic liver diseases, particularly in the regenerative treatment of hepatic fibrosis and cirrhosis.

3.1.4 Expanded therapeutic potential of MenSCs through multilineage differentiation

Multilineage-differentiating stress-enduring (Muse) cells, derived from mesenchymal stem cells (MSCs), are pluripotent cells with the capacity to differentiate into all three germ layers and exhibit enhanced resistance to environmental stress (Heneidi et al., 2013). Muse cells can evade immunological barriers, such as the pulmonary capillary network (Li et al., 2013a), and preferentially home to sites of tissue injury (Kushida et al., 2018), thereby overcoming the limitations associated with conventional MSCs in clinical applications. Li et al. (2024) successfully isolated Muse cells from MenSCs via prolonged trypsin digestion and demonstrated their significant therapeutic efficacy in animal models of acute liver injury and intracerebral hemorrhage, with superior homing ability and treatment outcomes compared with those of conventional MSCs.

Induced pluripotent stem cells (iPSCs) are pluripotent cells reprogrammed from somatic cells without relying on embryonic sources (Li et al., 2013b). iPSCs exhibit gene expression, pluripotency, and epigenetic profiles highly similar to those of embryonic stem cells (Park et al., 2008a; Ratajczak et al., 2008; Ye et al., 2009; Lengerke and Daley, 2010), providing an ethically acceptable cell resource for disease modeling, drug development, and regenerative medicine. Although iPSCs can be generated from various somatic cell sources (Takahashi et al., 2007; Yu et al., 2007; Hockemeyer et al., 2008; Huangfu et al., 2008; Lowry et al., 2008; Park et al., 2008b; Aasen et al., 2008; Kim et al., 2009; Sun et al., 2009; Li et al., 2010; Zhao et al., 2010; Zhou et al., 2011), traditional sources such as human dermal fibroblasts (HDFs) require invasive skin biopsies and prolonged *in vitro* expansion, limiting their practical utility. In contrast, MenSCs, owing to their noninvasive sourcing, ease of acquisition, robust proliferation, and stem cell-like phenotype (Malik et al., 2018; Patel et al., 2008), represent ideal candidates for iPSC generation.

3.2 Therapeutic potential via paracrine mechanisms

The therapeutic effects of MSCs are primarily mediated through their paracrine activity, which involves the secretion of bioactive factors—such as growth factors, chemokines, cytokines, and EVs—to modulate the local microenvironment (Pittenger et al., 2019; Fan et al., 2020; Wang et al., 2015; Seo et al., 2021; Liang et al., 2014; Chang et al., 2021; Razavi et al., 2020). With increasing research on MenSCs, the therapeutic potential of their paracrine mechanisms has been validated in various diseases. Factors secreted by MenSCs can modulate immune responses, promote tissue regeneration, inhibit inflammation and fibrosis, and enhance angiogenesis, thereby offering novel therapeutic strategies for chronic disease management and regenerative medicine.

3.2.1 Treatment of gynecological diseases

In the treatment of gynecological diseases, the paracrine activity of MenSCs has multiple therapeutic potential. The low success rate of *in vitro* fertilization (IVF) in older women is closely associated with abnormal reactive oxygen species (ROS) metabolism in oocytes (Mihalas et al., 2017). Studies have shown that EVs secreted by MenSCs can function as exogenous ROS scavengers, thereby reducing the dependence of embryos from aged female mice on endogenous antioxidant proteins such as superoxide dismutase 1 (SOD1) and glutathione peroxidase 1 (GPX1), ultimately improving IVF outcomes (Marinaro et al., 2018). Proteomic analyses further suggest that gene expression changes related to oxidative stress (GPX1, superoxide dismutase 1), metabolism (ACACA, GAPDH), placentation (PGF, VEGF-A), and stem cell differentiation (POU5F1, SOX2) may underlie the observed improvement in embryo quality (Marinaro et al., 2018; Marinaro et al., 2019).

In intrauterine adhesion (IUA) repair, MenSCs transplantation has been shown to accelerate endometrial regeneration. Zhang et al. (2016) reported that after being transplanted into a mouse model of endometrial injury, MenSCs activated the AKT and MAPK signaling pathways and upregulated angiogenesis-related proteins such as eNOS, VEGFA, VEGFR1, VEGFR2, and Tie2. These effects significantly shortened the repair time (complete regeneration within 7 days) and improved pregnancy rates and fetal counts (Huang et al., 2015; Lv et al., 2016). Additionally, fibroblast growth factor 2 secreted by MenSCs further promotes angiogenesis and cellular proliferation, thereby attenuating ovarian fibrosis and restoring sex hormone levels (Seo et al., 2013).

In the treatment of poor ovarian response (POR), paracrine factors from MenSCs modulate the local microenvironment to promote follicular development, as well as the differentiation of embryonic-like and ovarian stem cells. This leads to significant improvements in oocyte yield and quality, fertilization rates, embryo development rates, pregnancy rates, and live birth rates (Zafardoust et al., 2020; Rajabi et al., 2018; Bhartiya, 2018).

Moreover, the paracrine effects of MenSCs have shown their ability to inhibit epithelial ovarian cancer (EOC). Bu et al. (2016) demonstrated that MenSCs increased the proapoptotic Bax/Bcl-2 and Bad/Bcl-xL ratios, reduced the mitochondrial membrane potential, and activated the intrinsic apoptotic pathway to suppress EOC cell proliferation. Furthermore, they inhibited EOC cell cycle progression by blocking AKT phosphorylation. These findings suggest a promising strategy for the use of MenSCs in EOC therapy.

3.2.2 Treatment of liver diseases

The paracrine effects of MenSCs have significant potential in the treatment of liver diseases. In nonalcoholic fatty liver disease, the progression of which is closely associated with metabolic dysregulation—such as insulin resistance and lipid accumulation (Zhao et al., 2017)—MenSCs have been shown to modulate the expression of the key gene Rnf186 by secreting HGF. Rnf186 interferes with insulin signaling and lipid synthesis, and its abnormal expression is suppressed by the paracrine action of MenSCs, thereby alleviating metabolic disturbances (Du et al., 2023).

In models of cholestatic liver injury, MenSCs repair tissue damage via paracrine mechanisms. Yang et al. (2022) demonstrated that MenSCs significantly enhanced survival in mice while reducing the serum levels of liver injury markers (AST, ALT, ALP, DBIL). This effect is attributed to the upregulation of hepatic β-catenin, which helps to restore the integrity of tight junctions and normalize the expression of bile transport proteins (OATP2, BSEP, and NTCP1), ultimately inhibiting intrahepatic bile duct dilation, cholestasis, and the progression of fibrosis.

With respect to liver fibrosis, MenSCs secrete an array of factors that collectively form a synergistic paracrine network. For example, monocyte chemoattractant protein-1 recruits immune cells to the injured area for targeted inflammation regulation (Chen et al., 2017a), whereas Interleukin (IL)-6 and IL-8 stimulate proliferative pathways in hepatic cells and promote the recruitment of neutrophils and macrophages, thereby enhancing tissue repair (Qiu et al., 2012; Cai et al., 2008). Moreover, HGF secreted by MenSCs inhibits the activation of hepatic stellate cells (e.g., the LX-2 cell line), directly impeding fibrogenesis (Chen et al., 2017a). In addition, angiopoietin stimulates cell proliferation and survival (Li and Hu, 2012) and, together with Axl, coregulates apoptotic and proliferative signaling (D'Ar et al., 2002). IGFBP-6 prevents fibroblast apoptosis (Qiu et al., 2012; Micutkova et al., 2011), further mitigating the chronic inflammation that drives fibrosis. Collectively, these paracrine factors contribute to a therapeutic network that counteracts the progression of liver fibrosis.

For hepatocellular carcinoma (HCC) treatment, MenSCs exert their therapeutic effects through epigenetic modulation. In a time-dependent manner, their paracrine secretions can restore the levels of 5-hydroxymethylcytosine (5-hmC) and TET1 in HCC cells (Wu et al., 2019). TET1 and TET2 regulate DNA demethylation to suppress aberrant demethylation in HCC cells (Chen Q. et al., 2017; Ko et al., 2010). Upon activation by MenSCs, increased enrichment of 5-hmC and 5-mC in key enhancer regions leads to downregulation of the PI3K/AKT and RAF/ERK pathways, thereby inhibiting HCC cell proliferation and promoting apoptosis. Moreover, MenSCs modulate the DNA modification of chemoresistance-related genes, such as ID4 and HMGA1, enhancing their therapeutic efficacy against HCC(96). These findings suggest that the paracrine mechanisms of MenSCs, which involve the targeting of oncogenic gene expression through epigenetic regulation, constitute a novel therapeutic strategy for HCC.

3.2.3 Treatment of pulmonary diseases

Idiopathic pulmonary fibrosis is a chronic and progressive interstitial lung disease characterized by excessive fibrosis of the lung tissue and is associated with high morbidity and mortality rates (Blackwell et al., 2014). Although lung transplantation remains the most effective treatment, its clinical application is limited by donor scarcity, and existing pharmacological interventions provide only modest antifibrotic efficacy. Chen et al. (2020a) demonstrated that MenSCs transplantation alleviated fibrosis in bleomycin-induced Idiopathic pulmonary fibrosis models by homing to injured sites, suppressing epithelial cell apoptosis and proinflammatory cytokine (e.g., IL-1β and TNF-α) secretion, and inhibiting myofibroblast activation and collagen deposition.

ERCs also exhibit multipotent therapeutic potential in Idiopathic pulmonary fibrosis treatment (Zhao et al., 2018a). On the one hand, ERCs suppress TGF-β signaling and downregulate the proinflammatory cytokines IL-1β and TNF-α by upregulating IL-10 (Sziksz et al., 2015). They also restore total superoxide dismutase (T-SOD) activity to reduce oxidative stress and modulate

apoptotic signaling via downregulation of the Bax/Bcl-2 ratio, contributing to alveolar epithelial cell protection. On the other hand, ERCs upregulate antifibrotic genes such as HGF and matrix metalloproteinase-9 (MMP-9), further inhibiting fibrosis progression.

In acute lung injury animal models, MenSCs also exhibit therapeutic efficacy (Ren et al., 2018; Xiang et al., 2017). Through paracrine signaling, MenSCs increase proliferating cell nuclear antigen (PCNA) expression to promote cell proliferation, inhibit caspase-3-mediated apoptosis to reduce cell death, increase the secretion of anti-inflammatory factors such as IL-10 and keratinocyte growth factor (KGF), and simultaneously suppress proinflammatory cytokines such as IL-1β, neutrophil infiltration, and myeloperoxidase (MPO) activity, thereby attenuating pulmonary inflammation and restoring lung function.

3.2.4 Treatment of diabetic skin wounds

Under diabetic conditions, wound healing is disrupted through multiple mechanisms, including persistent inflammation, hypoxia, cellular dysfunction, impaired angiogenesis, and neuropathy (Guo and Dipietro, 2010). The chronic nature of diabetic wounds is closely associated with dysregulated inflammatory phase transitions. While inflammation is essential for initiating tissue repair (Aller et al., 2004), excessive activation of proinflammatory macrophages (M1) and the resulting prolonged inflammatory state significantly impede healing (Landén et al., 2016). The phenotypic switch from M1 to reparative macrophages (M2) is critical for tissue regeneration (Finley et al., 2016; Zhang et al., 2010; Emin et al., 2007; Murray et al., 2014); however, in the diabetic microenvironment, downregulation of M2-associated genes (e.g., Arg-1) leads to impaired polarization (Finley et al., 2016; Schwab et al., 2007). MenSC-Exos promote M2 polarization by modulating inducible nitric oxide synthase activity and the ARG: inducible nitric oxide synthase ratio, with a sustained increase in the M2/M1 ratio observed between days 7–14 posttreatment (Dalirfardouei et al., 2019; Mirzadegan et al., 2022).

Macrophage function is also closely linked to neural regeneration. As the primary source of neuroprotectin D1 (NPD1), M2 macrophages may facilitate axonal regeneration and contribute to wound repair (C et al., 2013; Hong et al., 2014). Mirzadegan et al. (Mirzadegan et al., 2022) demonstrated that MenSC intervention significantly increased the density of protein-gene product 9.5 (PGP9.5)-positive nerve fibers in diabetic wounds, suggesting the potential for reversing cutaneous neuropathy. At the molecular level, MenSC-Exos activate the NF-κB signaling pathway to increase keratinocyte proliferation and differentiation (Dalirfardouei et al., 2019; Brantley et al., 2001). Additionally, through interactions with the Notch pathway (Na et al., 2017; Shi et al., 2015) and Jumonji domain-containing protein D3, they may regulate epigenetic remodeling in keratinocytes (Na et al., 2016), thereby promoting migration and re-epithelialization.

The balance of collagen metabolism is crucial for optimal wound healing. MenSC-Exos induce the expression of type I collagen and type III collagen mRNAs, initially promoting type III collagen synthesis to support granulation tissue formation (Volk et al., 2011). At later stages, they reduce the type I collagen/type III collagen ratio to suppress scar hyperplasia (Yates et al., 2012; Cuttle et al., 2005; Larson et al., 2010; Zhang et al., 2015).

In terms of angiogenesis, MenSC-Exos dose-dependently upregulated key angiogenic markers, including vascular endothelial growth factor A (VEGFA), CD31, and von Willebrand factor (vWF), with 10 μg of MenSC-Exos demonstrating tenfold greater efficacy than exosomes from other stem cell sources (Dalirfardouei et al., 2019; Mirzadegan et al., 2022; Hu et al., 2016; Liang et al., 2016).

Importantly, although MenSCs exhibit strong migratory capacity due to high CXCR4 expression (Luz-Crawford et al., 2016), dysfunctional fibroblasts in diabetic wounds often fail to produce stromal cell-derived factor-1, thereby compromising MenSC homing efficiency (Mirzadegan et al., 2022; Brem et al., 2007). This paradox underscores the critical role of the local microenvironment in modulating stem cell-based therapies.

3.2.5 Treatment of central nervous system disorders

Spinal cord injury (SCI), characterized by sensory and motor dysfunction, continues to pose major clinical challenges because of the limited therapeutic efficacy of current treatment paradigms (Kunte et al., 2015). Recent studies have demonstrated that MenSCs transplantation promotes neural repair via multiple mechanisms. Wu et al. (2018) confirmed that MenSCs increase the expression of brain-derived neurotrophic factor, thereby supporting neuronal survival and axonal regeneration (Uchida et al., 2016). Additionally, MenSCs upregulate mature neuronal markers such as neurofilament-200 (NF-200) and microtubule-associated protein-2 (MAP-2), facilitating structural reconstruction of neural tissue (Li et al., 2013a). MenSCs also contribute to neural repair by attenuating glial scar formation, as evidenced by the reduced expression of inhibitory molecules such as chondroitin sulfate proteoglycans (CSPGs) (Anderson et al., 2016; Fan et al., 2017). Concurrently, MenSCs suppress the production of proinflammatory cytokines, including TNF-α and IL-1β, thereby alleviating neuroinflammation. In animal models, local injection of MenSCs significantly improved hindlimb motor function in rats with SCI(131).

Hjazi and colleagues (Hjazi et al., 2024) further advanced this therapeutic approach by combining MenSC-Exos with hyperbaric oxygen therapy (HBOT) in a model of traumatic SCI (TSCI). While MenSC-Exos exert anti-inflammatory and antiapoptotic effects (Dalirfardouei et al., 2019), HBOT reduces neuronal apoptosis by downregulating the expression of proinflammatory cytokines (e.g., IL-1β and TNF-α) (Ghaemi et al., 2023; Zhao et al., 2021). The combined therapy synergistically regulated apoptosis, oxidative stress, and inflammation, resulting in improved histopathological outcomes and functional recovery.

Alzheimer's disease, the most common type of dementia, is pathologically defined by amyloid-beta (Aβ) plaques and neurofibrillary tangles (NFTs). Aβ originates from proteolytic cleavage of the transmembrane amyloid precursor protein (APP), whereas NFTs consist of hyperphosphorylated and misfolded tau proteins (Ballard et al., 2011). Zhao et al. (2018b) reported that MenSCs transplantation reduced Aβ deposition in the hippocampus and cortex, potentially by regulating aberrant APP processing, enhancing Aβ clearance by microglia, and suppressing tau hyperphosphorylation. Moreover, MenSCs promoted the transformation of microglia into a neuroprotective phenotype,

facilitating anti-inflammatory cytokine secretion and markedly improving cognitive deficits in APP/PS1 transgenic mice.

Notably, Lopez-Verrilli et al. (2016) reported a biphasic effect of MenSCs on neurite outgrowth. While direct contact between MenSCs and neurons inhibited neurite elongation, their secreted factors—including VEGF, HGF, and brain-derived neurotrophic factor—promoted axonal extension. Further investigation revealed that the exosomal fractions of MenSC-EVs promoted neurite outgrowth, whereas the microvesicle fractions had inhibitory effects. This functional heterogeneity provides new insights into the application of MenSCs in treating neurodegenerative diseases.

3.2.6 Treatment of other systemic diseases

Myocardial infarction (MI), an acute cardiovascular emergency, is primarily treated by curtailing the progression of myocardial necrosis and promoting functional recovery (Lu et al., 2015). Wang et al. (2017) reported that extracellular vesicles derived from MenSC-EVs regulate the PTEN/Akt pathway through high expression of miR-21. This mechanism both inhibits cardiomyocyte apoptosis and promotes angiogenesis, thereby significantly improving cardiac function in infarcted rat models. This discovery provides a novel strategy for myocardial regeneration therapy.

In the field of prostate cancer (PC) treatment, Alcayaga-Miranda et al. (2016) revealed that MenSC-Exos reduce tumor cell ROS levels and downregulate the expression of vascular endothelial growth factor (VEGF) and hypoxia-inducible factor-1α (HIF-1α). This disrupts the tumor's hypoxic adaptation, thereby inhibiting tumor hemoglobin biosynthesis and neovascularization, which contributes to an antitumor effect. Such microenvironmental modulation offers a new avenue for targeted therapy in solid tumors.

With respect to ulcerative colitis (UC), (Malik et al., 2018) demonstrated that ERCs exert anti-inflammatory effects by rebalancing cytokine profiles—reducing IL-2 and TNF-α while increasing IL-4 and IL-10 levels. Further research has shown that preconditioning with stromal cell-derived factor-1 enhances CXCR4 expression in ERCs, promoting M2 macrophage polarization and Treg cell generation (Li et al., 2019); prestimulation with IL-1β inhibits the DKK1 protein and activates the Wnt/β-catenin pathway, thereby strengthening their immunomodulatory function (Yu et al., 2021); and melatonin preconditioning enhances ERC efficacy via antioxidant protection, significantly lowering both the disease activity index and tissue damage scores (Hao et al., 2024).

In the treatment of type 1 diabetes mellitus (T1DM), (Malik et al., 2018) confirmed that intravenous infusion of MenSCs results in targeted migration to the injured pancreas. This migration activates Ngn3-positive endocrine progenitor cells, facilitating β-cell regeneration, effectively reversing hyperglycemia, increasing insulin secretion, and restoring islet architecture. This finding provides a potential solution to the shortage of islet donors.

In sepsis treatment research, (Alcayaga-Miranda et al., 2015a) reported that MenSCs enhance host defense by increasing the expression of antimicrobial peptides and hepcidin. When combined with antibiotics, this approach significantly improves bacterial clearance and survival. Notably, MenSC-Exos exert a protective effect against LPS-induced liver injury by modulating abnormal natural killer (NK) cell activation (Chen et al., 2017c), thereby reducing inflammatory organ damage and demonstrating multitarget therapeutic potential.

3.2.7 Molecular mediators and signal transduction cascades

MenSCs exert reparative effects via the paracrine release of small extracellular vesicles (sEVs), which mediate multiple signaling pathways. miRNA profiling of exosomes has identified the enrichment of key microRNAs (miRNAs), such as miR-21 and miR-lethal-7 (let-7), in MenSC-derived sEVs. miR-21 enhances cell survival and improves cardiac function by targeting PTEN and activating the AKT/PKB signaling cascade (Wang et al., 2017). Let-7 modulates the NLRP3 pathway, enhancing the inhibition of ROS production and mitochondrial DNA damage via suppression of lectin-like oxidized low-density lipoprotein receptor-1 (LOX-1), thereby facilitating the repair of alveolar epithelial cells (Sun et al., 2019). In pancreatic regeneration, sEVs activate the PDX-1 signaling axis to promote β-cell regeneration and insulin secretion (Mahdipour et al., 2019).

In terms of immune regulation, MenSC-Exo induce phosphorylation of STAT3/STAT6, driving M2 macrophage polarization (Liu et al., 2017). Similarly, CD73 present in exosomes from endometrial regenerative cells promotes M2 polarization through a MAPK-dependent hydrolysis of ATP, thereby contributing to renal protection (Shao et al., 2025).

Regarding metabolic regulation, hepatocyte growth factor (HGF) secreted by MenSCs downregulates hepatic Rnf186 expression and modulates the AMPK-mTOR signaling pathway, improving glucose and lipid metabolism. In addition, HGF upregulates β-catenin, contributing to the repair of tight junctions and the expression of bile transporters (OATP2, BSEP, NTCP1), thereby attenuating the progression of hepatic fibrosis (Du et al., 2023; Yang et al., 2022).

At the epigenetic level, MenSCs restore the expression of TET1/2 and 5-hmC levels in hepatocellular carcinoma cells in a time-dependent manner. By modulating the 5-hmC/5-methylcytosine enrichment at enhancer regions of PI3K/AKT and RAF/ERK pathway target genes, MenSCs relieve repression of FOXO3, subsequently promoting downstream apoptotic processes (Wu et al., 2019).

3.3 Therapeutic effects mediated by immunomodulation

MenSCs exhibit unique advantages in the field of immunotherapy. Like BM-MSCs, MenSCs express low levels of HLA-B and HLA-C and lack HLA-DR expression, indicating potential immune privilege properties (Luz-Crawford et al., 2016). However, further investigations revealed distinct immunoregulatory features compared with those of BM-MSCs. Notably, MenSCs express lower levels of the Toll-like receptors TLR3 and TLR4 and exhibit weaker suppression of T cell subsets under low-concentration conditions (Luz-Crawford et al., 2016). In specific microenvironments, they may even stimulate lymphocyte proliferation (Nikoo et al., 2012). These distinctive immunomodulatory properties offer an important theoretical basis for the development of novel immunotherapeutic strategies.

3.3.1 Effects on tissue repair

ERCs demonstrate multifaceted immunomodulatory capabilities during tissue repair. Studies have shown that ERCs can induce the polarization of M2 macrophages, tolerogenic dendritic cells, and regulatory T and B cells both *in vivo* and *in vitro*. They also significantly suppress IgG and IgM antibody deposition and infiltration of $CD4^+$ and $CD8^+$ T cells. These immunoregulatory effects are closely associated with stromal cell-derived factor-1–mediated immunosuppressive mechanisms (Xu et al., 2017).

3.3.2 Regulation of immune cell function

MenSCs exert notable regulatory effects on various immune cell populations. In reproductive immunology, uterine NK cells play essential roles in early pregnancy tolerance through killer cell immunoglobulin-like receptors (Male and Moffett, 2023). Shokri et al. reported that IFN-γ- and IL-1β-pretreated MenSCs inhibited NK cell cytotoxicity via the IL-6 and TGF-β pathways, thereby reducing perforin and granzyme production and promoting an immune-tolerant microenvironment conducive to pregnancy (de Pedro et al., 2021). Additionally, Hosseini et al. reported a significant decrease in TCRγδ cell proportions in the menstrual blood of patients with recurrent spontaneous abortion, suggesting a possible link to pregnancy-related immune dysregulation (Hosseini et al., 2016). With respect to dendritic cells, Bozorgmehr and colleagues demonstrated that MenSCs dose-dependently suppress monocyte differentiation into immature dendritic cells, possibly through high secretion levels of IL-6 and IL-10 (Bozorgmehr et al., 2014). In antitumor immunity, menstrual blood-derived immune cells also show substantial potential. Qin et al. isolated DC-CIK cells from the menstrual blood of ovarian cancer patients and reported that these cells inhibited ovarian cancer stem cells by activating the TNFR1–ASK1–AIP1–JNK signaling pathway (Qin et al., 2018).

3.3.3 Involvement of cytokines and signaling pathways

Although MenSCs lack HLA-DR expression, limiting their antigen-presenting capacity, they exert immunoregulatory effects through the secretion of various paracrine molecules, including IL-6, TGF-β, COX-2, PGE2, indoleamine 2,3-dioxygenase, and programmed death ligand-1 (Malik et al., 2018; Luz-Crawford et al., 2016; Cuenca et al., 2018). Proteomic analysis revealed high expression levels of adhesion molecules such as activated leukocyte cell adhesion molecule and intercellular adhesion molecule-1 in MenSCs (Liu et al., 2018). These molecules interact with receptors such as LFA-1, directly participating in immune cell activation and regulation, and play critical roles in the immunomodulatory functions of MenSCs. Notably, MenSCs also secrete multiple angiogenic factors, including VEGF, HGF, angiogenin, and MMP-1, which contribute to both tissue regeneration and immune regulation.

4 Investigation of disease pathogenesis and therapeutic mechanisms

The pathogenesis of endometriosis remains incompletely understood; however, analysis of MenSCs from affected individuals has provided novel insights into its underlying mechanisms. Transcriptomic studies have shown significantly elevated levels of miR-200b-3p in MenSCs from patients with endometriosis (de Oliveira et al., 2022). This microRNA, which is commonly associated with tumor progression, regulates key cellular processes such as motility, proliferation, migration, and differentiation (Humphries and Yang, 2015). By suppressing the transcription factor ZEB1, miR-200b-3p reverses epithelial–mesenchymal transition, induces mesenchymal–epithelial transition, and modulates angiogenesis by targeting VEGF and epidermal growth factor receptor 2 (Wellner et al., 2009; Yang et al., 2016). These mechanisms may contribute to the proliferation, maintenance of stemness, and mesenchymal–epithelial transition of endometrial cells transported by retrograde menstruation, thereby promoting lesion formation and persistence.

The application of high-throughput technologies has further advanced our understanding of the molecular pathophysiology of endometriosis (Meola et al., 2010). However, these approaches require stable reference genes for accurate data interpretation. Zucherato et al. (2021) identified EIF2B1 and POP4 as the most stable reference genes in MenSCs derived from menstrual blood, whereas GAPDH and ACTB were found to be less reliable, providing an essential foundation for future experimental designs. Moreover, MenSCs from patients presented higher expression levels of the surface markers CD9, CD10, and CD29 than those from healthy individuals did, along with increased proliferative and invasive capacities (Nikoo et al., 2014). When cocultured with PB mononuclear cells, these MenSCs presented increased expression of indoleamine 2,3-dioxygenase-1 and COX-2, as well as elevated secretion of proinflammatory cytokines such as IFN-γ, IL-10, and monocyte chemoattractant protein-1, suggesting that MenSCs may contribute to disease progression through immunomodulation and altered cellular behavior (Nikoo et al., 2014).

High mobility group box-1 (HMGB1) also plays a critical role in endometriosis. HMGB1, a nonhistone nuclear protein abundant in mammalian chromatin, is involved in DNA transcription, repair, replication, and remodeling (Liu et al., 2010). Elevated HMGB1 levels have been detected in the blood of patients, where it interacts with receptors such as RAGE and TLR4, forming complexes with IL-1β or LPS to activate proinflammatory signaling pathways (Shimizu et al., 2017). Additionally, HMGB1 promotes endothelial cell proliferation and the release of angiogenic factors such as VEGF, thereby facilitating the implantation and survival of ectopic endometrial cells (Shimizu et al., 2017). Integrative omics analyses by Penariol et al. (2022) identified key genes (e.g., ATF3, ID1, ID3, and FOSB) and proteins (e.g., MT2A and COL1A1) involved in disease development. The chronic inflammatory microenvironment may disrupt MenSCs function, leading to dysregulation of gene and protein expression and contributing to the progression of endometriosis (Penariol et al., 2022).

In therapeutic investigations, the natural flavonoid components of Citrus latifolia have been utilized for their anti-inflammatory properties to alleviate dysmenorrhea and menorrhagia. Robeldo et al. (2020) demonstrated that Citrus latifolia increases the production of prostaglandin F2α, which acts on prostaglandin receptors to reduce the menstrual volume and inhibits the release of proinflammatory cytokines such as TNF-α (Ekström et al., 1991). This mechanism effectively blocks inflammatory signaling

and nociceptive sensitization. Compared with nonsteroidal anti-inflammatory drugs, this approach is particularly effective in patients with menstrual disorders associated with insufficient prostaglandin F2α secretion (Robeldo et al., 2020).

5 Comparison with other mesenchymal stem cells

Phenotypically, MenSCs share similar surface markers with other mesenchymal stem cells (MSCs), such as CD10, CD29, CD44, CD73, CD90, and CD105 (Cordeiro et al., 2022; Margiana et al., 2022), and possess multilineage differentiation potential. However, MenSCs display a significantly faster proliferation rate, with a population doubling time of approximately 19.4 hours—roughly twice as fast as that of bone marrow-derived MSCs (BM-MSCs) (Skliutė et al., 2021). Functionally, their colony-forming unit-fibroblast frequency is 2–4 times higher than that of BM-MSCs, and their *in vitro* migratory ability is also superior.

In terms of paracrine activity, MenSCs secrete higher levels of VEGF and basic fibroblast growth factor, leading to enhanced angiogenesis. Notably, MenSCs induce hemoglobin production at levels 8-fold greater than BM-MSCs. They also exhibit superior feeder layer characteristics, supporting the expansion and maintenance of $CD34^{+}CD133+$ hepatic stellate cells. MenSCs promote a 3-fold increase in cell expansion and generate more CFU-GEMM colonies (Alcayaga-Miranda et al., 2015b). By secreting growth factors and extracellular matrix proteins, MenSCs contribute to reconstructing the bone marrow microenvironment and support the *ex vivo* expansion of hematopoietic stem cells (Khoury et al., 2011).

Comparative studies in therapeutic applications also highlight MenSCs' advantages (Wang et al., 2017). evaluated the effects of intramyocardial injection of BM-MSCs, adipose-derived MSCs, and MenSCs in a murine MI model. MenSCs exhibited superior cardioprotective effects and increased microvascular density, attributed to high miR-21 levels in their exosomes that activate the PTEN/Akt signaling pathway (Lopez-Verrilli et al., 2016). compared the effects of MenSCs, BM-MSCs, umbilical cord, and chorionic MSCs on cortical neurite outgrowth. MenSC-derived exosomes showed the strongest neurite-promoting effect, whereas their microvesicles inhibited neurite extension, suggesting functional specificity among extracellular vesicle subtypes. In liver regeneration, Fathi-Kazerooni et al. (Malik et al., 2018) demonstrated that MenSC-derived hepatocyte progenitor-like cells more effectively improved liver injury markers compared to BM-MSCs, with greater reductions in inflammation, necrosis, and collagen deposition. Mechanistically, this was linked to stronger anti-inflammatory effects exerted by MenSCs.

6 Comparison of menstrual blood and peripheral blood

In studies directly comparing MB and PB, (Iribarne-Durán et al., 2020) reported that MB samples contain substantial levels of endocrine-disrupting chemicals, notably parabens and benzophenones. These endocrine-disrupting chemicals concentrations are correlated with specific sociodemographic and lifestyle factors, such as the use of cosmetics, skin oils/creams, and hair dyes (Jiménez-Díaz et al., 2016). Importantly, MB levels of parabens and benzophenones were found to be lower than those measured in PB serum (Matsumoto et al., 2007), providing evidence for a blood–uterine barrier: a physical and/or metabolic partition that may restrict certain compounds from reaching the endometrium, potentially via glucuronidation-mediated metabolism and increased excretion of endocrine-disrupting chemicals. Further research revealed marked differences in immune cell composition between MB and PB. Hosseini et al. (2019) demonstrated that the frequencies of NKT cell subsets and their associated cytokine profiles differ significantly between MB and PB in fertile women, infertile women, and those with unexplained recurrent spontaneous abortion. This finding underscores the profound influence of the endometrial immune microenvironment on the cellular makeup of MB. Together, these studies not only validate MB as a promising biomarker for assessing endocrine-disrupting chemicals exposure and its link to gynecological conditions but also highlight its unique utility in probing local uterine immune mechanisms.

7 Current status of clinical trial research

Although preclinical studies in cellular and animal models have confirmed the safety and efficacy of MenSC transplantation, the clinical application of MenSCs remains limited compared to other stem cell sources. This is primarily due to the restricted availability of menstrual blood donors and the lack of standardized *in vitro* culture protocols. To date, clinical trials involving MenSCs have primarily evaluated their therapeutic effects in diseases such as multiple sclerosis, H7N9 influenza virus infection, severe COVID-19, Asherman's syndrome, and ovarian insufficiency (Zhong et al., 2009; Zafardoust et al., 2020; Tan et al., 2016; Chen J. et al., 2020; Fathi-Kazerooni et al., 2022; Xu et al., 2021; Zafardoust et al., 2025; Zafardoust et al., 2023a; Zafardoust et al., 2023b). The results indicate that MenSC transplantation leads to marked clinical improvement in these conditions, with no serious adverse events or complications observed, underscoring the potential value of MenSCs in clinical applications.

In the context of ovarian insufficiency, the team led by Zafardoust has conducted long-term follow-up studies to assess the efficacy and potential complications of autologous MenSC therapy. Their clinical trial demonstrated that autologous MenSC transplantation can increase the rate of natural conception, improve ovarian function, and restore regular menstrual cycles. Importantly, no serious complications—such as endometriosis, ovarian malignancies, or autoimmune diseases—were reported, suggesting that autologous MenSC transplantation represents a safe and promising approach for improving reproductive outcomes in women with ovarian insufficiency (Table 1).

However, current clinical research on MenSCs still faces limitations. Most studies involve small sample sizes and short follow-up durations, which weakens the statistical power for evaluating long-term safety despite supporting evidence from basic research. Therefore, large-scale, multicenter clinical trials are necessary

TABLE 1 Menscs-related clinical trials.

Subject condition	Subject number	Subject gender	Donor information	Follow-up time	Follow-up outcome	References
Multiple Sclerosis	4	Female	healthy, non-smoking, female volunteers between 18 and 30 years of age	2–12 months	no abnormalities	Zhong et al. (2009)
Asherman's syndrome	7	Female	Autologous transplantation	3–6 months	recovery of endometrial morphology to a normal status	Tan et al. (2016)
Epidemic Influenza A (H7N9) Infection	17	Female	Healthy female donors (20–45 years old)	5 years	most clinical symptoms were ameliorative from 1 to 12 months	Chen et al. (2020b)
Severe COVID-19	14	Male and female	Master Cell Bank (derived from menses of at least five healthy women)	28 days	Reversal of hypoxia, immune reconstitution, and cytokine storm downregulation	Fathi-Kazerooni et al. (2022)
Severe and critically ill COVID-19	28	Male and female (no statistical difference at the gender level)	3 healthy female donors (20–45 years old)	1 months	Significantly improved dyspnea	Xu et al. (2021)
Poor ovarian response	105	Female	Autologous MenSCs	3 years	Spontaneous pregnancy rate was significantly higher without complications	Zafardoust et al. (2025)
Poor ovarian response	15	Female	Autologous MenSCs	1 years	Spontaneous pregnancy rate was higher	Zafardoust et al. (2020)
Poor ovarian response	180	Female	Autologous MenSCs	2 months	Spontaneous pregnancy rate, anti-Mullerian hormone levels, and antral follicle count were significantly increased	Zafardoust et al. (2023a)
Premature ovarian failure	15	Female	Autologous MenSCs	1 years	Ovarian function improved and menses resumed	Zafardoust et al. (2023b)

to comprehensively assess the efficacy and safety of MenSC-based therapies. In addition, the majority of enrolled participants have been female, and only the study by Xu et al. (2021) has conducted sex-stratified analyses. Given the female-specific origin of MenSCs, sex-based stratification should be considered an essential component of future clinical investigations.

8 Conclusion

This review provides a comprehensive overview of the potential of MB in both basic research and clinical applications, with a particular emphasis on its innovative roles in disease diagnosis and therapy. As a biologically rich fluid containing diverse cellular and molecular constituents, MB offers a non-invasive, highly acceptable platform for investigating women's reproductive health and pathology. In the therapeutic arena, MenSCs have emerged as a key resource in regenerative medicine owing to their pluripotency, low immunogenicity, and ease of procurement. Through mechanisms of direct differentiation, paracrine signaling, and immune modulation, MenSCs have demonstrated promising efficacy in preclinical models and early clinical studies.

9 Limitations

Nonetheless, the clinical translation of MenSC-based therapies faces several critical challenges—including *in vivo* cell tracking post

transplantation, donor-related variability in therapeutic outcomes, the establishment of robust quality control and standardization protocols, and the need for long-term safety data. In addition, unresolved ethical and sociocultural considerations remain. Although the use of menstrual blood (MB) as a research sample raises fewer ethical concerns compared to embryonic or fetal tissues, ethical guidelines for MB collection are still evolving.

Moreover, cultural norms, religious beliefs, and disparities in education continue to pose barriers to MB donation, especially in low- and middle-income countries. In Islamic jurisprudence, menstruation is considered a state of ritual impurity, which may discourage donation. Similarly, in Hindu traditions, menstrual blood is sometimes perceived as carrying "negative energy," potentially reducing donor willingness. In patriarchal societies, it is not uncommon for women to require spousal consent to donate biological materials, thereby limiting female autonomy. Trust may also be compromised when research teams are male-dominated, as some women may feel uncomfortable discussing menstrual health issues with male investigators.

10 Future directions

Despite these hurdles, ongoing technological and scientific advances are steadily unveiling the unique bioactive components and mechanisms of action of MB. To better preserve the three-dimensional architecture of the native extracellular matrix (ECM) and replicate the microenvironment required for cell proliferation and differentiation, scaffold-based technologies have been employed to facilitate the directed differentiation of MenSCs. Polylactic acid and multi-walled carbon nanotubes, as promising biomaterials, have been incorporated into scaffold designs due to their favorable mechanical properties and biocompatibility, enhancing MenSC differentiation toward germ cell lineages (Eyni et al., 2017).

A bilayer scaffold composed of amniotic membrane and silk fibroin has shown therapeutic potential in wound healing and skin regeneration. This scaffold mimics the skin ECM by providing optimized mechanical strength and 3D structure, significantly improving the regenerative capacity of MenSCs. On an immunomodulatory level, anti-inflammatory factors secreted by the amniotic membrane (e.g., SLPI/elafin) synergize with MenSC-derived paracrine cytokines such as IDO, PGE_2, and TGF-β, promoting the polarization of macrophages from the pro-inflammatory M1 phenotype to the regenerative M2 phenotype. This scaffold system has also been shown to induce MenSC differentiation into keratinocyte-like cells (Mirzadegan et al., 2022), while upregulating VEGFA to activate $CD34^+$ endothelial cells and stimulate angiogenesis. Concurrently, restoration of the SDF-1/CXCR4 signaling axis improves endothelial progenitor cell homing (Mirzadegan et al., 2020). *In vivo* studies in diabetic mouse models have demonstrated enhanced epidermal thickness and type I collagen synthesis following treatment, resulting in effective wound regeneration and healing (Araste et al., 2020).

Further translational progress has been made through large animal studies. For instance, (Emmerson et al., 2019) investigated the integration of endometrial MSCs with synthetic meshes in a sheep model of POP. Their findings showed that autologous eMSCs improved mesh biocompatibility and restored vaginal tissue strength, while exhibiting long-term survival *in vivo* and contributing to immune modulation, ECM remodeling, and fibrosis regulation.In parallel, organoid technologies are emerging as essential tools to study the menstrual cycle and endometrial diseases. Wiwatpanit et al. (2020) developed a scaffold-free endometrial organoid model consisting of epithelial and stromal components that closely mimics the physiology of native endometrium. This model provides a versatile 3D system to investigate hormone-induced pathological changes in the endometrium. Such insights are poised to drive the broader application of MB in regenerative and immune-based therapies, offering novel strategies to address persistent clinical needs.

Overall, MB represents a novel and promising tool for both disease diagnosis and therapeutic intervention. Its emerging applications in regenerative medicine and immunotherapy hold significant potential to address unresolved clinical challenges and advance the development of precision medicine.

Author contributions

YF: Writing – original draft, Conceptualization, Writing – review and editing. YH: Writing – review and editing, Supervision, Formal Analysis.

Funding

The author(s) declare that no financial support was received for the research and/or publication of this article.

Conflict of interest

The authors declare that the research was conducted in the absence of any commercial or financial relationships that could be construed as a potential conflict of interest.

Generative AI statement

The author(s) declare that no Generative AI was used in the creation of this manuscript.

Any alternative text (alt text) provided alongside figures in this article has been generated by Frontiers with the support of artificial intelligence and reasonable efforts have been made to ensure accuracy, including review by the authors wherever possible. If you identify any issues, please contact us.

Publisher's note

References

Aasen, T., Raya, A., Barrero, M. J., Garreta, E., Consiglio, A., Gonzalez, F., et al. (2008). Efficient and rapid generation of induced pluripotent stem cells from human keratinocytes. *Nat. Biotechnol.* 26 (11), 1276–1284. doi:10.1038/nbt.1503

Akhavan-Tavakoli, M., Fard, M., Khanjani, S., Zare, S., Edalatkhah, H., Mehrabani, D., et al. (2017). *In vitro* differentiation of menstrual blood stem cells into keratinocytes: a potential approach for management of wound healing. *Biol. J. Int. Assoc. Biol. Stand* 48, 66–73. doi:10.1016/j.biologicals.2017.05.005

Alcayaga-Miranda, F., Cuenca, J., Martin, A., Contreras, L., Figueroa, F. E., and Khoury, M. (2015a). Combination therapy of menstrual derived mesenchymal stem cells and antibiotics ameliorates survival in sepsis. *Stem Cell. Res. Ther.* 6, 199. doi:10.1186/s13287-015-0192-0

Alcayaga-Miranda, F., Cuenca, J., Luz-Crawford, P., Aguila-Díaz, C., Fernandez, A., Figueroa, F. E., et al. (2015b). Characterization of menstrual stem cells: angiogenic effect, migration and hematopoietic stem cell support in comparison with bone marrow mesenchymal stem cells. *Stem Cell. Res. Ther.* 6 (1), 32. doi:10.1186/s13287-015-0013-5

Alcayaga-Miranda, F., González, P. L., Lopez-Verrilli, A., Varas-Godoy, M., Aguila-Díaz, C., Contreras, L., et al. (2016). Prostate tumor-induced angiogenesis is blocked by exosomes derived from menstrual stem cells through the inhibition of reactive oxygen species. *Oncotarget* 7 (28), 44462–44477. doi:10.18632/oncotarget.9852

Aliyu, M. H., Aliyu, S. H., and Salihu, H. M. (2004). Female genital tuberculosis: a global review. *Int. J. Fertil. Womens Med.* 49 (3), 123–136. doi:10.1093/humupd/dmh018

Aller, M. A., Arias, J. L., Nava, M. P., and Arias, J. (2004). Posttraumatic inflammation is a complex response based on the pathological expression of the nervous, immune, and endocrine functional systems. *Exp. Biol. Med. Maywood N. J.* 229 (2), 170–181. doi:10.1177/153537020422900206

Anderson, M. A., Burda, J. E., Ren, Y., Ao, Y., O'Shea, T. M., Kawaguchi, R., et al. (2016). Astrocyte scar formation aids central nervous system axon regeneration. *Nature* 532 (7598), 195–200. doi:10.1038/nature17623

Arasteh, S., Khanjani, S., Golshahi, H., Mobini, S., Jahed, M. T., Heidari-Vala, H., et al. (2020). Efficient wound healing using a synthetic nanofibrous bilayer skin substitute in murine model. *J. Surg. Res.* 245, 31–44. doi:10.1016/j.jss.2019.07.017

Ballard, C., Gauthier, S., Corbett, A., Brayne, C., Aarsland, D., and Jones, E. (2011). Alzheimer's disease. *Lancet Lond Engl.* 377 (9770), 1019–1031. doi:10.1016/S0140-6736(10)61349-9

Ballweg, M. L. (2004). Impact of endometriosis on women's health: comparative historical data show that the earlier the onset, the more severe the disease. *Best. Pract. Res. Clin. Obstet. Gynaecol.* 18 (2), 201–218. doi:10.1016/j.bpobgyn.2004.01.003

Bhartiya, D. (2018). Stem cells survive oncotherapy and can regenerate non-functional gonads: a paradigm shift for oncofertility. *Indian J. Med. Res.* 148 (Suppl. l), S38-S49–49. doi:10.4103/ijmr.IJMR_2065_17

Blackwell, T. S., Tager, A. M., Borok, Z., Moore, B. B., Schwartz, D. A., Anstrom, K. J., et al. (2014). Future directions in idiopathic pulmonary fibrosis research. An NHLBI workshop report. *Am. J. Respir. Crit. Care Med.* 189 (2), 214–222. doi:10.1164/rccm.201306-1141WS

Bockeria, L., Bogin, V., Bockeria, O., Le, T., Alekyan, B., Woods, E. J., et al. (2013). Endometrial regenerative cells for treatment of heart failure: a new stem cell enters the clinic. *J. Transl. Med.* 11, 56. doi:10.1186/1479-5876-11-56

Bose, M. (2011). Female genital tract tuberculosis: how long will it elude diagnosis? *Indian J. Med. Res.* 134 (1), 13–14. doi:10.2217/IMT.11.80

Bozorgmehr, M., Moazzeni, S. M., Salehnia, M., Sheikhian, A., Nikoo, S., and Zarnani, A. H. (2014). Menstrual blood-derived stromal stem cells inhibit optimal generation and maturation of human monocyte-derived dendritic cells. *Immunol. Lett.* 162 (2 Pt B), 239–246. doi:10.1016/j.imlet.2014.10.005

Brantley, D. M., Chen, C. L., Muraoka, R. S., Bushdid, P. B., Bradberry, J. L., Kittrell, F., et al. (2001). Nuclear factor-kappaB (NF-kappaB) regulates proliferation and branching in mouse mammary epithelium. *Mol. Biol. Cell.* 12 (5), 1445–1455. doi:10.1091/mbc.12.5.1445

Brem, H., Stojadinovic, O., Diegelmann, R. F., Entero, H., Lee, B., Pastar, I., et al. (2007). Molecular markers in patients with chronic wounds to guide surgical debridement. *Mol. Med. Camb Mass* 13 (1–2), 30–39. doi:10.2119/2006-00054.Brem

Bu, S., Wang, Q., Zhang, Q., Sun, J., He, B., Xiang, C., et al. (2016). Human endometrial mesenchymal stem cells exhibit intrinsic anti-tumor properties on human epithelial ovarian cancer cells. *Sci. Rep.* 6, 37019. doi:10.1038/srep37019

Budukh, A., Palayekar, V., Maheshwari, A., Deodhar, K., Purwar, P., Bagal, S., et al. (2018). Menstrual pad, a cervical cancer screening tool, a population-based study in rural India. *Eur. J. Cancer Prev. Off. J. Eur. Cancer Prev. Organ ECP* 27 (6), 546–552. doi:10.1097/CEJ.0000000000000387

Burd, E. M. (2003). Human papillomavirus and cervical cancer. *Clin. Microbiol. Rev.* 16 (1), 1–17. doi:10.1128/cmr.16.1.1-17.2003

Cheng, C., Singh, V., Krishnan, A., Kan, M., Martinez, J. A., and Zochodne, D. W. (2013). Loss of innervation and axon plasticity accompanies impaired diabetic wound healing. *PloS One* 8 (9), e75877. doi:10.1371/journal.pone.0075877

Cai, J., Kehoe, O., Smith, G. M., Hykin, P., and Boulton, M. E. (2008). The angiopoietin/Tie-2 system regulates pericyte survival and recruitment in diabetic retinopathy. *Investig. Ophthalmol. Vis. Sci.* 49 (5), 2163–2171. doi:10.1167/iovs.07-1206

Chang, C., Yan, J., Yao, Z., Zhang, C., Li, X., and Mao, H. Q. (2021). Effects of mesenchymal stem cell-derived paracrine signals and their delivery strategies. *Adv. Healthc. Mater* 10 (7), e2001689. doi:10.1002/adhm.202001689

Chen, X., Kong, X., Liu, D., Gao, P., Zhang, Y., Li, P., et al. (2016). *In vitro* differentiation of endometrial regenerative cells into smooth muscle cells: A potential approach for the management of pelvic organ prolapse. *Int. J. Mol. Med.* 38 (1), 95–104. doi:10.3892/ijmm.2016.2593

Chen, L., Zhang, C., Chen, L., Wang, X., Xiang, B., Wu, X., et al. (2017a). Human menstrual blood-derived stem cells ameliorate liver fibrosis in mice by targeting hepatic stellate cells via paracrine mediators. *Stem Cells Transl. Med.* 6 (1), 272–284. doi:10.5966/sctm.2015-0265

Chen, Q., Yin, D., Zhang, Y., Yu, L., Li, X. D., Zhou, Z. J., et al. (2017b). MicroRNA-29a induces loss of 5-hydroxymethylcytosine and promotes metastasis of hepatocellular carcinoma through a TET-SOCS1-MMP9 signaling axis. *Cell. Death Dis.* 8 (6), e2906. doi:10.1038/cddis.2017.142

Chen, L., Xiang, B., Wang, X., and Xiang, C. (2017c). Exosomes derived from human menstrual blood-derived stem cells alleviate fulminant hepatic failure. *Stem Cell. Res. Ther.* 8 (1), 9. doi:10.1186/s13287-016-0453-6

Chen, X., Wu, Y., Wang, Y., Chen, L., Zheng, W., Zhou, S., et al. (2020a). Human menstrual blood-derived stem cells mitigate bleomycin-induced pulmonary fibrosis through anti-apoptosis and anti-inflammatory effects. *Stem Cell. Res. Ther.* 11 (1), 477. doi:10.1186/s13287-020-01926-x

Chen, J., Hu, C., Chen, L., Tang, L., Zhu, Y., Xu, X., et al. (2020b). Clinical study of mesenchymal stem cell treatment for acute Respiratory Distress syndrome induced by Epidemic influenza A (H7N9) infection: a Hint for COVID-19 treatment. *Eng. Beijing China* 6 (10), 1153–1161. doi:10.1016/j.eng.2020.02.006

Cordeiro, M. R., Carvalhos, C. A., and Figueiredo-Dias, M. (2022). The emerging role of menstrual-blood-derived stem cells in endometriosis. *Biomedicines* 11 (1), 39. doi:10.3390/biomedicines11010039

Cuenca, J., Le-Gatt, A., Castillo, V., Belletti, J., Díaz, M., Kurte, G. M., et al. (2018). The reparative Abilities of menstrual stem cells modulate the wound matrix Signals and improve cutaneous regeneration. *Front. Physiol.* 9, 464. doi:10.3389/fphys.2018.00464

Cuttle, L., Nataatmadja, M., Fraser, J. F., Kempf, M., Kimble, R. M., and Hayes, M. T. (2005). Collagen in the scarless fetal skin wound: detection with picrosirius-polarization. *Wound Repair Regen. Off. Publ. Wound Heal Soc. Eur. Tissue Repair Soc.* 13 (2), 198–204. doi:10.1111/j.1067-1927.2005.130211.x

Dalirfardouei, R., Jamialahmadi, K., Jafarian, A. H., and Mahdipour, E. (2019). Promising effects of exosomes isolated from menstrual blood-derived mesenchymal stem cell on wound-healing process in diabetic mouse model. *J. Tissue Eng. Regen. Med.* 13 (4), 555–568. doi:10.1002/term.2799

de Oliveira, R. Z., de Oliveira Buono, F., Cressoni, A. C. L., Penariol, L. B. C., Padovan, C. C., Tozetti, P. A., et al. (2022). Overexpression of miR-200b-3p in menstrual blood-derived mesenchymal stem cells from endometriosis women. *Reprod. Sci. Thousand Oaks Calif.* 29 (3), 734–742. doi:10.1007/s43032-022-00860-y

de Pedro, M. Á., Gómez-Serrano, M., Marinaro, F., López, E., Pulido, M., Preußer, C., et al. (2021). IFN-gamma and TNF-alpha as a priming strategy to enhance the immunomodulatory capacity of Secretomes from menstrual blood-derived stromal cells. *Int. J. Mol. Sci.* 22 (22), 12177. doi:10.3390/ijms222212177

Deans, R., and Abbott, J. (2010). Review of intrauterine adhesions. *J. Minim. Invasive Gynecol.* 17 (5), 555–569. doi:10.1016/j.jmig.2010.04.016

Du, J., Jiang, Y., Liu, X., Ji, X., Xu, B., Zhang, Y., et al. (2023). HGF secreted by menstrual blood-derived endometrial stem cells ameliorates non-alcoholic fatty liver disease through downregulation of hepatic Rnf186. *Stem Cells Dayt Ohio* 41 (2), 153–168. doi:10.1093/stmcls/sxac091

D'Arcangelo, D., Gaetano, C., and Capogrossi, M. C. (2002). Acidification prevents endothelial cell apoptosis by Axl activation. *Circ. Res.* 91 (7), e4–e12. doi:10.1161/01.res.0000036753.50601.e9

Ekström, P., Alm, P., and Akerlund, M. (1991). Differences in vasomotor responses between main stem and smaller branches of the human uterine artery. *Acta Obstet. Gynecol. Scand.* 70 (6), 429–433. doi:10.3109/00016349109007155

Eming, S. A., Krieg, T., and Davidson, J. M. (2007). Inflammation in wound repair: molecular and cellular mechanisms. *J. Investig. Dermatol.* 127 (3), 514–525. doi:10.1038/sj.jid.5700701

Emmerson, S., Mukherjee, S., Melendez-Munoz, J., Cousins, F., Edwards, S. L., Karjalainen, P., et al. (2019). Composite mesh design for delivery of autologous mesenchymal stem cells influences mesh integration, exposure and biocompatibility in an ovine model of pelvic organ prolapse. *Biomaterials* 225, 119495. doi:10.1016/j.biomaterials.2019.119495

Eyni, H., Ghorbani, S., Shirazi, R., Salari Asl, L., P Beiranvand, S., and Soleimani, M. (2017). Three-dimensional wet-electrospun poly(lactic acid)/multi-wall carbon

nanotubes scaffold induces differentiation of human menstrual blood-derived stem cells into germ-like cells. *J. Biomater. Appl.* 32 (3), 373–383. doi:10.1177/0885328217723179

Falcone, T., and Flyckt, R. (2018). Clinical management of endometriosis. *Obstet. Gynecol.* 131 (3), 557–571. doi:10.1097/AOG.0000000000002469

Fan, C., Li, X., Xiao, Z., Zhao, Y., Liang, H., Wang, B., et al. (2017). A modified collagen scaffold facilitates endogenous neurogenesis for acute spinal cord injury repair. *Acta Biomater.* 51, 304–316. doi:10.1016/j.actbio.2017.01.009

Fan, X. L., Zhang, Y., Li, X., and Fu, Q. L. (2020). Mechanisms underlying the protective effects of mesenchymal stem cell-based therapy. *Cell. Mol. Life Sci. CMLS* 77 (14), 2771–2794. doi:10.1007/s00018-020-03454-6

Fard, M., Akhavan-Tavakoli, M., Khanjani, S., Zare, S., Edalatkhah, H., Arasteh, S., et al. (2018). Bilayer amniotic membrane/Nano-fibrous fibroin scaffold promotes differentiation capability of menstrual blood stem cells into keratinocyte-like cells. *Mol. Biotechnol.* 60 (2), 100–110. doi:10.1007/s12033-017-0049-0

Fathi-Kazerooni, M., Fattah-Ghazi, S., Darzi, M., Makarem, J., Nasiri, R., Salahshour, F., et al. (2022). Safety and efficacy study of allogeneic human menstrual blood stromal cells secretome to treat severe COVID-19 patients: clinical trial phase I and II. *Stem Cell. Res. Ther.* 13 (1), 96. doi:10.1186/s13287-022-02771-w

Feng, P., Li, P., and Tan, J. (2019). Human menstrual blood-derived stromal cells promote recovery of premature ovarian insufficiency via regulating the ECM-dependent FAK/AKT signaling. *Stem Cell. Rev. Rep.* 15 (2), 241–255. doi:10.1007/s12015-018-9867-0

Finley, P. J., DeClue, C. E., Sell, S. A., DeBartolo, J. M., and Shornick, L. P. (2016). Diabetic wounds exhibit decreased Ym1 and Arginase expression with increased expression of IL-17 and IL-20. *Adv. Wound Care* 5 (11), 486–494. doi:10.1089/wound.2015.0676

Ghaemi, A., Ghiasvand, M., Omraninava, M., Merza, M. Y., Alkhafaji, A. T., Raoofi, A., et al. (2023). Hyperbaric oxygen therapy and coenzyme Q10 synergistically attenuates damage progression in spinal cord injury in a rat model. *J. Chem. Neuroanat.* 132, 102322. doi:10.1016/j.jchemneu.2023.102322

Guo, S., and Dipietro, L. A. (2010). Factors affecting wound healing. *J. Dent. Res.* 89 (3), 219–229. doi:10.1177/0022034509359125

Hao, J., Ma, A., Sun, C., Qin, H., Zhu, Y., Li, G., et al. (2024). Melatonin pretreatment improves endometrial regenerative cell-mediated therapeutic effects in experimental colitis. *Int. Immunopharmacol.* 133, 112092. doi:10.1016/j.intimp.2024.112092

Harro, C. D., Pang, Y. Y., Roden, R. B., Hildesheim, A., Wang, Z., Reynolds, M. J., et al. (2001). Safety and immunogenicity trial in adult volunteers of a human papillomavirus 16 L1 virus-like particle vaccine. *J. Natl. Cancer Inst.* 93 (4), 284–292. doi:10.1093/jnci/93.4.284

Heneidi, S., Simerman, A. A., Keller, E., Singh, P., Li, X., Dumesic, D. A., et al. (2013). Awakened by cellular stress: isolation and characterization of a novel population of pluripotent stem cells derived from human adipose tissue. *PloS One* 8 (6), e64752. doi:10.1371/journal.pone.0064752

Hjazi, A., Alghamdi, A., Aloraini, G. S., Alshehri, M. A., Alsuwat, M. A., Albelasi, A., et al. (2024). Combination use of human menstrual blood stem cell-derived exosomes and hyperbaric oxygen therapy, synergistically promote recovery after spinal cord injury in rats. *Tissue Cell.* 88, 102378. doi:10.1016/j.tice.2024.102378

Hockemeyer, D., Soldner, F., Cook, E. G., Gao, Q., Mitalipova, M., and Jaenisch, R. (2008). A drug-inducible system for direct reprogramming of human somatic cells to pluripotency. *Cell. Stem Cell.* 3 (3), 346–353. doi:10.1016/j.stem.2008.08.014

Holowaty, P., Miller, A. B., Rohan, T., and To, T. (1999). Natural history of dysplasia of the uterine cervix. *J. Natl. Cancer Inst.* 91 (3), 252–258. doi:10.1093/jnci/91.3.252

Hong, S., Tian, H., Lu, Y., Laborde, J. M., Muhale, F. A., Wang, Q., et al. (2014). Neuroprotectin/protectin D1: endogenous biosynthesis and actions on diabetic macrophages in promoting wound healing and innervation impaired by diabetes. *Am. J. Physiol. Cell. Physiol.* 307 (11), C1058–C1067. doi:10.1152/ajpcell.00270.2014

Hosoya, S., Yokomizo, R., Kishigami, H., Fujiki, Y., Kaneko, E., Amita, M., et al. (2023). Novel therapeutic strategies for injured endometrium: intrauterine transplantation of menstrual blood-derived cells from infertile patients. *Stem Cell. Res. Ther.* 14 (1), 297. doi:10.1186/s13287-023-03524-z

Hosseini, S., Shokri, F., Ansari Pour, S., Jeddi-Tehrani, M., Nikoo, S., Yousefi, M., et al. (2016). A shift in the balance of T17 and Treg cells in menstrual blood of women with unexplained recurrent spontaneous abortion. *J. Reprod. Immunol.* 116, 13–22. doi:10.1016/j.jri.2016.03.001

Hosseini, S., Shokri, F., Pour, S. A., Khoshnoodi, J., Jeddi-Tehrani, M., and Zarnani, A. H. (2019). Diminished frequency of menstrual and peripheral blood NKT-like cells in patients with unexplained recurrent spontaneous abortion and infertile women. *Reprod. Sci. Thousand Oaks Calif.* 26 (1), 97–108. doi:10.1177/1933719118766261

Hu, Z., and Ma, D. (2018). The precision prevention and therapy of HPV-related cervical cancer: new concepts and clinical implications. *Cancer Med.* 7 (10), 5217–5236. doi:10.1002/cam4.1501

Hu, L., Wang, J., Zhou, X., Xiong, Z., Zhao, J., Yu, R., et al. (2016). Exosomes derived from human adipose mensenchymal stem cells accelerates cutaneous wound healing via optimizing the characteristics of fibroblasts. *Sci. Rep.* 6, 32993. doi:10.1038/srep32993

Huang, J. J., Shi, Y. Q., Li, R. L., Hu, A., Lu, Z. Y., Weng, L., et al. (2015). Angiogenesis effect of therapeutic ultrasound on HUVECs through activation of the PI3K-Akt-eNOS signal pathway. *Am. J. Transl. Res.* 7 (6), 1106–1115.

Huangfu, D., Osafune, K., Maehr, R., Guo, W., Eijkelenboom, A., Chen, S., et al. (2008). Induction of pluripotent stem cells from primary human fibroblasts with only Oct4 and Sox2. *Nat. Biotechnol.* 26 (11), 1269–1275. doi:10.1038/nbt.1502

Humphries, B., and Yang, C. (2015). The microRNA-200 family: small molecules with novel roles in cancer development, progression and therapy. *Oncotarget* 6 (9), 6472–6498. doi:10.18632/oncotarget.3052

Ichim, T. E., Alexandrescu, D. T., Solano, F., Lara, F., Campion, R. D. N., Paris, E., et al. (2010). Mesenchymal stem cells as anti-inflammatories: implications for treatment of Duchenne muscular dystrophy. *Cell. Immunol.* 260 (2), 75–82. doi:10.1016/j.cellimm.2009.10.006

Iribarne-Durán, L. M., Domingo-Piñar, S., Peinado, F. M., Vela-Soria, F., Jiménez-Díaz, I., Barranco, E., et al. (2020). Menstrual blood concentrations of parabens and benzophenones and related factors in a sample of Spanish women: an exploratory study. *Environ. Res.* 183, 109228. doi:10.1016/j.envres.2020.109228

Ji, S., Liu, Y., Yan, L., Zhang, Y., Li, Y., Zhu, Q., et al. (2023). DIA-based analysis of the menstrual blood proteome identifies association between CXCL5 and IL1RN and endometriosis. *J. Proteomics* 289, 104995. doi:10.1016/j.jprot.2023.104995

Jiménez-Díaz, I., Iribarne-Durán, L. M., Ocón, O., Salamanca, E., Fernández, M. F., Olea, N., et al. (2016). Determination of personal care products -benzophenones and parabens-in human menstrual blood. *J. Chromatogr. B Anal. Technol. Biomed. Life Sci.* 1035, 57–66. doi:10.1016/j.jchromb.2016.09.035

Jin, X. W., Cash, J., and Kennedy, A. W. (1999). Human papillomavirus typing and the reduction of cervical cancer risk. *Cleve Clin. J. Med.* 66 (9), 533–539. doi:10.3949/ccjm.66.9.533

Khademi, F., Soleimani, M., Verdi, J., Tavangar, S. M., Sadroddiny, E., Massumi, M., et al. (2014). Human endometrial stem cells differentiation into functional hepatocyte-like cells. *Cell. Biol. Int.* 38 (7), 825–834. doi:10.1002/cbin.10278

Khanjani, S., Khanmohammadi, M., Zarnani, A. H., Akhondi, M. M., Ahani, A., Ghaempanah, Z., et al. (2014). Comparative evaluation of differentiation potential of menstrual blood-versus bone marrow-derived stem cells into hepatocyte-like cells. *PloS One* 9 (2), e86075. doi:10.1371/journal.pone.0086075

Khanmohammadi, M., Khanjani, S., Edalatkhah, H., Zarnani, A. H., Heidari-Vala, H., Soleimani, M., et al. (2014). Modified protocol for improvement of differentiation potential of menstrual blood-derived stem cells into adipogenic lineage. *Cell. Prolif.* 47 (6), 615–623. doi:10.1111/cpr.12133

Khoury, M., Drake, A., Chen, Q., Dong, D., Leskov, I., Fragoso, M. F., et al. (2011). Mesenchymal stem cells secreting angiopoietin-like-5 support efficient expansion of human hematopoietic stem cells without compromising their repopulating potential. *Stem Cells Dev.* 20 (8), 1371–1381. doi:10.1089/scd.2010.0456

Khoury, M., Alcayaga-Miranda, F., Illanes, S. E., and Figueroa, F. E. (2014). The promising potential of menstrual stem cells for antenatal diagnosis and cell therapy. *Front. Immunol.* 5, 205. doi:10.3389/fimmu.2014.00205

Kim, J. B., Greber, B., Araúzo-Bravo, M. J., Meyer, J., Park, K. I., Zaehres, H., et al. (2009). Direct reprogramming of human neural stem cells by OCT4. *Nature* 461 (7264), 649–643. doi:10.1038/nature08436

Ko, M., Huang, Y., Jankowska, A. M., Pape, U. J., Tahiliani, M., Bandukwala, H. S., et al. (2010). Impaired hydroxylation of 5-methylcytosine in myeloid cancers with mutant TET2. *Nature* 468 (7325), 839–843. doi:10.1038/nature09586

Kunte, H., Farhadi, H. F., Sheth, K. N., Simard, J. M., and Kronenberg, G. (2015). Sulfonylureas–a novel treatment to reduce tissue damage after acute spinal cord injury? *Lancet Neurol.* 14 (4), 352. doi:10.1016/S1474-4422(15)70013-X

Kushida, Y., Wakao, S., and Dezawa, M. (2018). Muse cells are endogenous reparative stem cells. *Adv. Exp. Med. Biol.* 1103, 43–68. doi:10.1007/978-4-431-56847-6_3

Li, Y., Li, X., Zhao, H., Feng, R., Zhang, X., Tai, D., et al. (2013a). Efficient induction of pluripotent stem cells from menstrual blood. *Stem Cells Dev.* 22 (7), 1147–1158. doi:10.1089/scd.2012.0428

Lai, D., Wang, F., Yao, X., Zhang, Q., Wu, X., and Xiang, C. (2015). Human endometrial mesenchymal stem cells restore ovarian function through improving the renewal of germline stem cells in a mouse model of premature ovarian failure. *J. Transl. Med.* 13, 155. doi:10.1186/s12967-015-0516-y

Lai, D., Guo, Y., Zhang, Q., Chen, Y., and Xiang, C. (2016). Differentiation of human menstrual blood-derived endometrial mesenchymal stem cells into oocyte-like cells. *Acta Biochim. Biophys. Sin.* 48 (11), 998–1005. doi:10.1093/abbs/gmw090

Landén, N. X., Li, D., and Ståhle, M. (2016). Transition from inflammation to proliferation: a critical step during wound healing. *Cell. Mol. Life Sci. CMLS* 73 (20), 3861–3885. doi:10.1007/s00018-016-2268-0

Larson, B. J., Longaker, M. T., and Lorenz, H. P. (2010). Scarless fetal wound healing: a basic science review. *Plast. Reconstr. Surg.* 126 (4), 1172–1180. doi:10.1097/PRS.0b013e3181eae781

Lengerke, C., and Daley, G. Q. (2010). Autologous blood cell therapies from pluripotent stem cells. *Blood Rev.* 24 (1), 27–37. doi:10.1016/j.blre.2009.10.001

Li, S., and Hu, G. F. (2012). Emerging role of angiogenin in stress response and cell survival under adverse conditions. *J. Cell. Physiol.* 227 (7), 2822–2826. doi:10.1002/jcp.23051

Li, Y., Zhao, H., Lan, F., Lee, A., Chen, L., Lin, C., et al. (2010). Generation of human-induced pluripotent stem cells from gut mesentery-derived cells by ectopic expression of OCT4/SOX2/NANOG. *Cell. Reprogr.* 12 (3), 237–247. doi:10.1089/cell.2009.0103

Li, X., Xiao, Z., Han, J., Chen, L., Xiao, H., Ma, F., et al. (2013b). Promotion of neuronal differentiation of neural progenitor cells by using EGFR antibody functionalized collagen scaffolds for spinal cord injury repair. *Biomaterials* 34 (21), 5107–5116. doi:10.1016/j.biomaterials.2013.03.062

Li, X., Lan, X., Zhao, Y., Wang, G., Shi, G., Li, H., et al. (2019). SDF-1/CXCR4 axis enhances the immunomodulation of human endometrial regenerative cells in alleviating experimental colitis. *Stem Cell. Res. Ther.* 10 (1), 204. doi:10.1186/s13287-019-1298-6

Li, H., Wei, J., Li, M., Li, Y., Zhang, T., Tian, J., et al. (2024). Biological characteristics of Muse cells derived from MenSCs and their application in acute liver injury and intracerebral hemorrhage diseases. *Regen. Ther.* 27, 48–62. doi:10.1016/j.reth.2024.03.003

Liang, X., Ding, Y., Zhang, Y., Tse, H. F., and Lian, Q. (2014). Paracrine mechanisms of mesenchymal stem cell-based therapy: current status and perspectives. *Cell. Transpl.* 23 (9), 1045–1059. doi:10.3727/096368913X667709

Liang, X., Zhang, L., Wang, S., Han, Q., and Zhao, R. C. (2016). Exosomes secreted by mesenchymal stem cells promote endothelial cell angiogenesis by transferring miR-125a. *J. Cell. Sci.* 129 (11), 2182–2189. doi:10.1242/jcs.170373

Liu, Y., Prasad, R., and Wilson, S. H. (2010). HMGB1: roles in base excision repair and related function. *Biochim. Biophys. Acta* 1799 (1–2), 119–130. doi:10.1016/j.bbagrm.2009.11.008

Liu, T., Huang, Y., Zhang, J., Qin, W., Chi, H., Chen, J., et al. (2014). Transplantation of human menstrual blood stem cells to treat premature ovarian failure in mouse model. *Stem Cells Dev.* 23 (13), 1548–1557. doi:10.1089/scd.2013.0371

Liu, T., Zhang, L., Joo, D., and Sun, S. C. (2017). NF-κB signaling in inflammation. *Signal Transduct. Target Ther.* 2, 17023-. doi:10.1038/sigtrans.2017.23

Liu, Y., Niu, R., Yang, F., Yan, Y., Liang, S., Sun, Y., et al. (2018). Biological characteristics of human menstrual blood-derived endometrial stem cells. *J. Cell. Mol. Med.* 22 (3), 1627–1639. doi:10.1111/jcmm.13437

Lopez-Verrilli, M. A., Caviedes, A., Cabrera, A., Sandoval, S., Wyneken, U., and Khoury, M. (2016). Mesenchymal stem cell-derived exosomes from different sources selectively promote neuritic outgrowth. *Neuroscience* 320, 129–139. doi:10.1016/j.neuroscience.2016.01.061

Lowry, W. E., Richter, L., Yachechko, R., Pyle, A. D., Tchieu, J., Sridharan, R., et al. (2008). Generation of human induced pluripotent stem cells from dermal fibroblasts. *Proc. Natl. Acad. Sci. U. S. A.* 105 (8), 2883–2888. doi:10.1073/pnas.0711983105

Lu, L., Liu, M., Sun, R., Zheng, Y., and Zhang, P. (2015). Myocardial infarction: symptoms and treatments. *Cell. Biochem. Biophys.* 72 (3), 865–867. doi:10.1007/s12013-015-0553-4

Luz-Crawford, P., Torres, M. J., Noël, D., Fernandez, A., Toupet, K., Alcayaga-Miranda, F., et al. (2016). The immunosuppressive signature of menstrual blood mesenchymal stem cells entails opposite effects on experimental arthritis and graft versus host diseases. *Stem Cells Dayt Ohio* 34 (2), 456–469. doi:10.1002/stem.2244

Lv, M., Xia, Y., Li, B., Liu, H., Pan, J., bei, L., et al. (2016). Serum amyloid A stimulates vascular endothelial growth factor receptor 2 expression and angiogenesis. *J. Physiol. Biochem.* 72 (1), 71–81. doi:10.1007/s13105-015-0462-4

Lv, H., Hu, Y., Cui, Z., and Jia, H. (2018). Human menstrual blood: a renewable and sustainable source of stem cells for regenerative medicine. *Stem Cell. Res. Ther.* 9 (1), 325. doi:10.1186/s13287-018-1067-y

Mahdipour, E., Salmasi, Z., and Sabeti, N. (2019). Potential of stem cell-derived exosomes to regenerate β islets through Pdx-1 dependent mechanism in a rat model of type 1 diabetes. *J. Cell. Physiol.* 234 (11), 20310–20321. doi:10.1002/jcp.28631

Male, V., and Moffett, A. (2023). Natural killer cells in the human uterine Mucosa. *Annu. Rev. Immunol.* 41, 127–151. doi:10.1146/annurev-immunol-102119-075119

Malik, R., Chauhan, G., Traylor, M., Sargurupremraj, M., Okada, Y., Mishra, A., et al. (2018). Multiancestry genome-wide association study of 520,000 subjects identifies 32 loci associated with stroke and stroke subtypes. *Nat. Genet.* 50 (4), 524–537. doi:10.1038/s41588-018-0058-3

Margiana, R., Markov, A., Zekiy, A. O., Hamza, M. U., Al-Dabbagh, K. A., Al-Zubaidi, S. H., et al. (2022). Clinical application of mesenchymal stem cell in regenerative medicine: a narrative review. *Stem Cell. Res. Ther.* 13 (1), 366. doi:10.1186/s13287-022-03054-0

Marinaro, F., Pericuesta, E., Sánchez-Margallo, F. M., Casado, J. G., Álvarez, V., Matilla, E., et al. (2018). Extracellular vesicles derived from endometrial human mesenchymal stem cells improve IVF outcome in an aged murine model. *Reprod. Domest. Anim. Zuchthyg* 53 (Suppl. 2), 46–49. doi:10.1111/rda.13314

Marinaro, F., Macías-García, B., Sánchez-Margallo, F. M., Blázquez, R., Álvarez, V., Matilla, E., et al. (2019). Extracellular vesicles derived from endometrial human mesenchymal stem cells enhance embryo yield and quality in an aged murine model. *Biol. Reprod.* 100 (5), 1180–1192. doi:10.1093/biolre/ioy263

Matsumoto, J., Iwano, H., Inoue, H., Iwano, N., Yamashiki, N., and Yokota, H. (2007). Metabolic barrier against bisphenol A in rat uterine endometrium. *Toxicol. Sci. Off. J. Soc. Toxicol.* 99 (1), 118–125. doi:10.1093/toxsci/kfm148

Meola, J., Rosa, E., Silva, J. C., Dentillo, D. B., da Silva, W. A., Veiga-Castelli, L. C., et al. (2010). Differentially expressed genes in eutopic and ectopic endometrium of women with endometriosis. *Fertil. Steril.* 93 (6), 1750–1773. doi:10.1016/j.fertnstert.2008.12.058

Micutkova, L., Diener, T., Li, C., Rogowska-Wrzesinska, A., Mueck, C., Huetter, E., et al. (2011). Insulin-like growth factor binding protein-6 delays replicative senescence of human fibroblasts. *Mech. Ageing Dev.* 132 (10), 468–479. doi:10.1016/j.mad.2011.07.005

Mihalas, B. P., Redgrove, K. A., McLaughlin, E. A., and Nixon, B. (2017). Molecular mechanisms responsible for increased Vulnerability of the ageing oocyte to oxidative damage. *Oxid. Med. Cell. Longev.* 2017, 4015874. doi:10.1155/2017/4015874

Mirzadegan, E., Golshahi, H., and Kazemnejad, S. (2020). Current evidence on immunological and regenerative effects of menstrual blood stem cells seeded on scaffold consisting of amniotic membrane and silk fibroin in chronic wound. *Int. Immunopharmacol.* 85, 106595. doi:10.1016/j.intimp.2020.106595

Mirzadegan, E., Golshahi, H., Saffarian, Z., Darzi, M., Khorasani, S., Edalatkhah, H., et al. (2022). The remarkable effect of menstrual blood stem cells seeded on bilayer scaffold composed of amniotic membrane and silk fibroin aiming to promote wound healing in diabetic mice. *Int. Immunopharmacol.* 102, 108404. doi:10.1016/j.intimp.2021.108404

Murray, P. J., Allen, J. E., Biswas, S. K., Fisher, E. A., Gilroy, D. W., Goerdt, S., et al. (2014). Macrophage activation and polarization: nomenclature and experimental guidelines. *Immunity* 41 (1), 14–20. doi:10.1016/j.immuni.2014.06.008

Na, J., Lee, K., Na, W., Shin, J. Y., Lee, M. J., Yune, T. Y., et al. (2016). Histone H3K27 Demethylase JMJD3 in Cooperation with NF-κB regulates keratinocyte wound healing. *J. Investig. Dermatol* 136 (4), 847–858. doi:10.1016/j.jid.2015.11.029

Na, J., Shin, J. Y., Jeong, H., Lee, J. Y., Kim, B. J., Kim, W. S., et al. (2017). JMJD3 and NF-κB-dependent activation of Notch1 gene is required for keratinocyte migration during skin wound healing. *Sci. Rep.* 7 (1), 6494. doi:10.1038/s41598-017-06750-7

Namavar, J. B., Parsanezhad, M. E., and Ghane-Shirazi, R. (2001). Female genital tuberculosis and infertility. *Int. J. Gynaecol. Obstet. Off. Organ Int. Fed. Gynaecol. Obstet.* 75 (3), 269–272. doi:10.1016/S0020-7292(01)00494-5

Nikoo, S., Ebtekar, M., Jeddi-Tehrani, M., Shervin, A., Bozorgmehr, M., Kazemnejad, S., et al. (2012). Effect of menstrual blood-derived stromal stem cells on proliferative capacity of peripheral blood mononuclear cells in allogeneic mixed lymphocyte reaction. *J. Obstet. Gynaecol. Res.* 38 (5), 804–809. doi:10.1111/j.1447-0756.2011.01800.x

Nikoo, S., Ebtekar, M., Jeddi-Tehrani, M., Shervin, A., Bozorgmehr, M., Vafaei, S., et al. (2014). Menstrual blood-derived stromal stem cells from women with and without endometriosis reveal different phenotypic and functional characteristics. *Mol. Hum. Reprod.* 20 (9), 905–918. doi:10.1093/molehr/gau044

Noble, L. S., Simpson, E. R., Johns, A., and Bulun, S. E. (1996). Aromatase expression in endometriosis. *J. Clin. Endocrinol. Metab.* 81 (1), 174–179. doi:10.1210/jcem.81.1.8550748

Paine, S. K., Basu, A., Choudhury, R. G., Bhattacharya, B., Chatterjee, S., and Bhattacharya, C. (2018). Multiplex PCR from menstrual blood: a non-invasive Cost-effective approach to reduce diagnostic Dilemma for genital tuberculosis. *Mol. Diagn Ther.* 22 (3), 391–396. doi:10.1007/s40291-018-0322-3

Parasar, P., Ozcan, P., and Terry, K. L. (2017). Endometriosis: Epidemiology, diagnosis and clinical management. *Curr. Obstet. Gynecol. Rep.* 6 (1), 34–41. doi:10.1007/s13669-017-0187-1

Park, I. H., Arora, N., Huo, H., Maherali, N., Ahfeldt, T., Shimamura, A., et al. (2008a). Disease-specific induced pluripotent stem cells. *Cell.* 134 (5), 877–886. doi:10.1016/j.cell.2008.07.041

Park, I. H., Zhao, R., West, J. A., Yabuuchi, A., Huo, H., Ince, T. A., et al. (2008b). Reprogramming of human somatic cells to pluripotency with defined factors. *Nature* 451 (7175), 141–146. doi:10.1038/nature06534

Patel, A. N., Park, E., Kuzman, M., Benetti, F., Silva, F. J., and Allickson, J. G. (2008). Multipotent menstrual blood stromal stem cells: isolation, characterization, and differentiation. *Cell. Transpl.* 17 (3), 303–311. doi:10.3727/096368908784153922

Pei, X. M., Yeung, M. H. Y., Wong, A. N. N., Tsang, H. F., Yu, A. C. S., Yim, A. K. Y., et al. (2023). Targeted sequencing approach and its clinical applications for the molecular diagnosis of human diseases. *Cells* 12 (3), 493. doi:10.3390/cells12030493

Penariol, L. B. C., Thomé, C. H., Tozetti, P. A., Paier, C. R. K., Buono, F. O., Peronni, K. C., et al. (2022). What do the transcriptome and proteome of menstrual blood-derived mesenchymal stem cells Tell Us about endometriosis? *Int. J. Mol. Sci.* 23 (19), 11515. doi:10.3390/ijms231911515

Piersma, B., Bank, R. A., and Boersema, M. (2015). Signaling in fibrosis: TGF-β, WNT, and YAP/TAZ Converge. *Front. Med.* 2, 59. doi:10.3389/fmed.2015.00059

Pittenger, M. F., Discher, D. E., Péault, B. M., Phinney, D. G., Hare, J. M., and Caplan, A. I. (2019). Mesenchymal stem cell perspective: cell biology to clinical progress. *NPJ Regen. Med.* 4, 22. doi:10.1038/s41536-019-0083-6

Qin, W., Xiong, Y., Chen, J., Huang, Y., and Liu, T. (2018). DC-CIK cells derived from ovarian cancer patient menstrual blood activate the TNFR1-ASK1-AIP1 pathway to kill autologous ovarian cancer stem cells. *J. Cell. Mol. Med.* 22 (7), 3364–3376. doi:10.1111/jcmm.13611

Qiu, J., Ma, X. L., Wang, X., Chen, H., and Huang, B. R. (2012). Insulin-like growth factor binding protein-6 interacts with the thyroid hormone receptor α1 and modulates the thyroid hormone-response in osteoblastic differentiation. *Mol. Cell. Biochem.* 361 (1–2), 197–208. doi:10.1007/s11010-011-1104-y

Rajabi, Z., Yazdekhasti, H., Noori Mugahi, S. M. H., Abbasi, M., Kazemnejad, S., Shirazi, A., et al. (2018). Mouse preantral follicle growth in 3D co-culture system using human menstrual blood mesenchymal stem cell. *Reprod. Biol.* 18 (1), 122–131. doi:10.1016/j.repbio.2018.02.001

Ratajczak, M. Z., Zuba-Surma, E. K., Wysoczynski, M., Wan, W., Ratajczak, J., Wojakowski, W., et al. (2008). Hunt for pluripotent stem cell – regenerative medicine search for almighty cell. *J. Autoimmun.* 30 (3), 151–162. doi:10.1016/j.jaut.2007.12.003

Razavi, M., Rezaee, M., Telichko, A., Inan, H., Dahl, J., Demirci, U., et al. (2020). The paracrine function of mesenchymal stem cells in response to Pulsed focused ultrasound. *Cell. Transpl.* 29, 963689720965478. doi:10.1177/0963689720965478

Ren, H., Zhang, Q., Wang, J., and Pan, R. (2018). Comparative effects of umbilical cord- and menstrual blood-derived MSCs in repairing acute lung injury. *Stem Cells Int.* 2018, 7873625. doi:10.1155/2018/7873625

Robeldo, T., Canzi, E. F., de Andrade, P. M., Santana, J. P. P., Teixeira, F. R., Spagnol, V., et al. (2020). Effect of Tahiti lime (Citrus latifolia) juice on the production of the PGF2α/PGE2 and pro-inflammatory cytokines involved in menstruation. *Sci. Rep.* 10 (1), 7063. doi:10.1038/s41598-020-63477-8

Schwab, J. M., Chiang, N., Arita, M., and Serhan, C. N. (2007). Resolvin E1 and protectin D1 activate inflammation-resolution programmes. *Nature* 447 (7146), 869–874. doi:10.1038/nature05877

Seo, J. H., Yu, J. H., Suh, H., Kim, M. S., and Cho, S. R. (2013). Fibroblast growth factor-2 induced by enriched environment enhances angiogenesis and motor function in chronic hypoxic-ischemic brain injury. *PloS One* 8 (9), e74405. doi:10.1371/journal.pone.0074405

Seo, Y., Kang, M. J., and Kim, H. S. (2021). Strategies to potentiate paracrine therapeutic efficacy of mesenchymal stem cells in inflammatory diseases. *Int. J. Mol. Sci.* 22 (7), 3397. doi:10.3390/ijms22073397

Shao, B., Wang, H., Ren, S. H., Chen, Q., Wang, Z. B., Xu, Y. N., et al. (2025). Exosomes derived from a mesenchymal-like endometrial regenerative cells ameliorate renal ischemia reperfusion injury through delivery of CD73. *Stem Cell. Res. Ther.* 16 (1), 148. doi:10.1186/s13287-025-04275-9

Shi, Y., Shu, B., Yang, R., Xu, Y., Xing, B., Liu, J., et al. (2015). Wnt and Notch signaling pathway involved in wound healing by targeting c-Myc and Hes1 separately. *Stem Cell. Res. Ther.* 6 (1), 120. doi:10.1186/s13287-015-0103-4

Shimizu, K., Kamada, Y., Sakamoto, A., Matsuda, M., Nakatsuka, M., and Hiramatsu, Y. (2017). High expression of high-mobility group box 1 in menstrual blood: implications for endometriosis. *Reprod. Sci. Thousand Oaks Calif.* 24 (11), 1532–1537. doi:10.1177/1933719117692042

Sinaii, N., Plumb, K., Cotton, L., Lambert, A., Kennedy, S., Zondervan, K., et al. (2008). Differences in characteristics among 1,000 women with endometriosis based on extent of disease. *Fertil. Steril.* 89 (3), 538–545. doi:10.1016/j.fertnstert.2007.03.069

Skliutė, G., Baušytė, R., Borutinskaitė, V., Valiulienė, G., Kaupinis, A., Valius, M., et al. (2021). Menstrual blood-derived endometrial stem cells' Impact for the treatment perspective of female infertility. *Int. J. Mol. Sci.* 22 (13), 6774. doi:10.3390/ijms22136774

Spitzer, M. (1998). Cervical screening adjuncts: recent advances. *Am. J. Obstet. Gynecol.* 179 (2), 544–556. doi:10.1016/s0002-9378(98)70393-x

Sun, N., Panetta, N. J., Gupta, D. M., Wilson, K. D., Lee, A., Jia, F., et al. (2009). Feeder-free derivation of induced pluripotent stem cells from adult human adipose stem cells. *Proc. Natl. Acad. Sci. U. S. A.* 106 (37), 15720–15725. doi:10.1073/pnas.0908450106

Sun, L., Zhu, M., Feng, W., Lin, Y., Yin, J., Jin, J., et al. (2019). Exosomal miRNA let-7 from menstrual blood-derived endometrial stem cells alleviates pulmonary fibrosis through regulating mitochondrial DNA damage. *Oxid. Med. Cell. Longev.* 2019, 4506303. doi:10.1155/2019/4506303

Sziksz, E., Pap, D., Lippai, R., Béres, N. J., Fekete, A., Szabó, A. J., et al. (2015). Fibrosis related inflammatory Mediators: role of the IL-10 cytokine family. *Mediat. Inflamm.* 2015, 764641. doi:10.1155/2015/764641

Takahashi, K., Tanabe, K., Ohnuki, M., Narita, M., Ichisaka, T., Tomoda, K., et al. (2007). Induction of pluripotent stem cells from adult human fibroblasts by defined factors. *Cell.* 131 (5), 861–872. doi:10.1016/j.cell.2007.11.019

Tan, J., Li, P., Wang, Q., Li, Y., Li, X., Zhao, D., et al. (2016). Autologous menstrual blood-derived stromal cells transplantation for severe Asherman's syndrome. *Hum. Reprod. Oxf Engl.* 31 (12), 2723–2729. doi:10.1093/humrep/dew235

Tsang, H. F., Yu, A. C. S., Jin, N., Yim, A. K. Y., Leung, W. M. S., Lam, K. W., et al. (2022). The clinical application of metagenomic next-generation sequencing for detecting pathogens in bronchoalveolar lavage fluid: case reports and literature review. *Expert Rev. Mol. Diagn* 22 (5), 575–582. doi:10.1080/14737159.2022.2071607

Tsang, H. F., Cheung, Y. S., Yu, C. S. A., Chan, C. S. S., Wong, C. B. T., Yim, K. Y. A., et al. (2024). Menstrual blood as a diagnostic specimen for human papillomavirus genotyping and genital tract infection using next-generation sequencing as a novel diagnostic tool. *Diagn Basel Switz.* 14 (7), 686. doi:10.3390/diagnostics14070686

Uchida, S., Hayakawa, K., Ogata, T., Tanaka, S., Kataoka, K., and Itaka, K. (2016). Treatment of spinal cord injury by an advanced cell transplantation technology using brain-derived neurotrophic factor-transfected mesenchymal stem cell spheroids. *Biomaterials* 109, 1–11. doi:10.1016/j.biomaterials.2016.09.007

van der Molen, R. G., Schutten, J. H. F., van Cranenbroek, B., ter Meer, M., Donckers, J., Scholten, R. R., et al. (2014). Menstrual blood closely resembles the uterine immune micro-environment and is clearly distinct from peripheral blood. *Hum. Reprod. Oxf Engl.* 29 (2), 303–314. doi:10.1093/humrep/det398

Volk, S. W., Wang, Y., Mauldin, E. A., Liechty, K. W., and Adams, S. L. (2011). Diminished type III collagen promotes myofibroblast differentiation and increases scar deposition in cutaneous wound healing. *Cells Tissues Organs* 194 (1), 25–37. doi:10.1159/000322399

Wang, Z., Wang, Y., Wang, Z., Gutkind, J. S., Wang, Z., Wang, F., et al. (2015). Engineered mesenchymal stem cells with enhanced tropism and paracrine secretion of cytokines and growth factors to treat traumatic brain injury. *Stem Cells Dayt Ohio* 33 (2), 456–467. doi:10.1002/stem.1878

Wang, K., Jiang, Z., Webster, K. A., Chen, J., Hu, H., Zhou, Y., et al. (2017). Enhanced cardioprotection by human endometrium mesenchymal stem cells driven by exosomal MicroRNA-21. *Stem Cells Transl. Med.* 6 (1), 209–222. doi:10.5966/sctm.2015-0386

Wellner, U., Schubert, J., Burk, U. C., Schmalhofer, O., Zhu, F., Sonntag, A., et al. (2009). The EMT-activator ZEB1 promotes tumorigenicity by repressing stemness-inhibiting microRNAs. *Nat. Cell. Biol.* 11 (12), 1487–1495. doi:10.1038/ncb1998

Wiwatpanit, T., Murphy, A. R., Lu, Z., Urbanek, M., Burdette, J. E., Woodruff, T. K., et al. (2020). Scaffold-free endometrial organoids Respond to excess Androgens associated with Polycystic ovarian syndrome. *J. Clin. Endocrinol. Metab.* 105 (3), 769–780. doi:10.1210/clinem/dgz100

Wong, S. C. C., Au, T. C. C., Chan, S. C. S., Ng, L. P. W., and Tsang, H. F. (2018). Menstrual blood human papillomavirus DNA and TAP1 gene polymorphisms as potential biomarkers for screening and Monitoring of cervical squamous intraepithelial lesion. *J. Infect. Dis.* 218 (11), 1739–1745. doi:10.1093/infdis/jiy369

Wu, Q., Wang, Q., Li, Z., Li, X., Zang, J., Wang, Z., et al. (2018). Human menstrual blood-derived stem cells promote functional recovery in a rat spinal cord hemisection model. *Cell. Death Dis.* 9 (9), 882. doi:10.1038/s41419-018-0847-8

Wu, Y., Chen, X., Zhao, Y., Wang, Y., Li, Y., and Xiang, C. (2019). Genome-wide DNA methylation and hydroxymethylation analysis reveal human menstrual blood-derived stem cells inhibit hepatocellular carcinoma growth through oncogenic pathway suppression via regulating 5-hmC in enhancer elements. *Stem Cell. Res. Ther.* 10 (1), 151. doi:10.1186/s13287-019-1243-8

Xiang, B., Chen, L., Wang, X., Zhao, Y., Wang, Y., and Xiang, C. (2017). Transplantation of menstrual blood-derived mesenchymal stem cells promotes the repair of LPS-induced acute lung injury. *Int. J. Mol. Sci.* 18 (4), 689. doi:10.3390/ijms18040689

Xu, X., Li, X., Gu, X., Zhang, B., Tian, W., Han, H., et al. (2017). Prolongation of cardiac Allograft survival by endometrial regenerative cells: focusing on B-cell responses. *Stem Cells Transl. Med.* 6 (3), 778–787. doi:10.5966/sctm.2016-0206

Xu, X., Jiang, W., Chen, L., Xu, Z., Zhang, Q., Zhu, M., et al. (2021). Evaluation of the safety and efficacy of using human menstrual blood-derived mesenchymal stromal cells in treating severe and critically ill COVID-19 patients: an exploratory clinical trial. *Clin. Transl. Med.* 11 (2), e297. doi:10.1002/ctm2.297

Yang, H., Zhou, B., Prinz, M., and Siegel, D. (2012). Proteomic analysis of menstrual blood. *Mol. Cell. Proteomics MCP* 11 (10), 1024–1035. doi:10.1074/mcp.M112.018390

Yang, R. Q., Teng, H., Xu, X. H., Liu, S. Y., Wang, Y. H., Guo, F. J., et al. (2016). Microarray analysis of microRNA deregulation and angiogenesis-related proteins in endometriosis. *Genet. Mol. Res. GMR* 15 (2). doi:10.4238/gmr.15027826

Yang, Y., Chen, Y., Zhao, Y., Ji, F., Zhang, L., Tang, S., et al. (2022). Human menstrual blood-derived stem cell transplantation suppresses liver injury in DDC-induced chronic cholestasis. *Stem Cell. Res. Ther.* 13 (1), 57. doi:10.1186/s13287-022-02734-1

Yates, C. C., Hebda, P., and Wells, A. (2012). Skin wound healing and scarring: fetal wounds and regenerative restitution. *Birth Defects Res. Part C Embryo Today Rev.* 96 (4), 325–333. doi:10.1002/bdrc.21024

Ye, L., Chang, J. C., Lin, C., Sun, X., Yu, J., and Kan, Y. W. (2009). Induced pluripotent stem cells offer new approach to therapy in thalassemia and sickle cell anemia and option in prenatal diagnosis in genetic diseases. *Proc. Natl. Acad. Sci. U. S. A.* 106 (24), 9826–9830. doi:10.1073/pnas.0904689106

Yu, J., Vodyanik, M. A., Smuga-Otto, K., Antosiewicz-Bourget, J., Frane, J. L., Tian, S., et al. (2007). Induced pluripotent stem cell lines derived from human somatic cells. *Science* 318 (5858), 1917–1920. doi:10.1126/science.1151526

Yu, D., Zhao, Y., Wang, H., Kong, D., Jin, W., Hu, Y., et al. (2021). IL-1β pre-stimulation enhances the therapeutic effects of endometrial regenerative cells on experimental colitis. *Stem Cell. Res. Ther.* 12 (1), 324. doi:10.1186/s13287-021-02392-9

Zafardoust, S., Kazemnejad, S., Darzi, M., Fathi-Kazerooni, M., Rastegari, H., and Mohammadzadeh, A. (2020). Improvement of pregnancy rate and live birth rate in poor ovarian responders by intraovarian Administration of autologous menstrual blood derived- mesenchymal stromal cells: phase I/II clinical trial. *Stem Cell. Rev. Rep.* 16 (4), 755–763. doi:10.1007/s12015-020-09969-6

Zafardoust, S., Kazemnejad, S., Fathi-Kazerooni, M., Darzi, M., Sadeghi, M. R., Sadeghi Tabar, A., et al. (2023a). The effects of intraovarian injection of autologous menstrual blood-derived mesenchymal stromal cells on pregnancy outcomes in women with poor ovarian response. *Stem Cell. Res. Ther.* 14 (1), 332. doi:10.1186/s13287-023-03568-1

Zafardoust, S., Kazemnejad, S., Darzi, M., Fathi-Kazerooni, M., Saffarian, Z., Khalili, N., et al. (2023b). Intraovarian Administration of autologous menstrual blood derived-mesenchymal stromal cells in women with premature ovarian failure. *Arch. Med. Res.* 54 (2), 135–144. doi:10.1016/j.arcmed.2022.12.015

Zafardoust, S., Didar, H., Ganagard, M. G., Tavakoli, M., Arefi, S., Arjmandinaloo, S., et al. (2025). Intra-ovarian injection of autologous menstrual blood-derived-mesenchymal stromal cells: a safe and promising method to improve pregnancy rate in poor ovarian responders. *Stem Cell. Res. Ther.* 16 (1), 171. doi:10.1186/s13287-025-04278-6

Zhang, Q. Z., Su, W. R., Shi, S. H., Wilder-Smith, P., Xiang, A. P., Wong, A., et al. (2010). Human gingiva-derived mesenchymal stem cells elicit polarization of m2 macrophages and enhance cutaneous wound healing. *Stem Cells Dayt Ohio* 28 (10), 1856–1868. doi:10.1002/stem.503

Zhang, J., Guan, J., Niu, X., Hu, G., Guo, S., Li, Q., et al. (2015). Exosomes released from human induced pluripotent stem cells-derived MSCs facilitate cutaneous wound healing by promoting collagen synthesis and angiogenesis. *J. Transl. Med.* 13, 49. doi:10.1186/s12967-015-0417-0

Zhang, Y., Lin, X., Dai, Y., Hu, X., Zhu, H., Jiang, Y., et al. (2016). Endometrial stem cells repair injured endometrium and induce angiogenesis via AKT and ERK pathways. *Reprod. Camb Engl.* 152 (5), 389–402. doi:10.1530/REP-16-0286

Zhang, J., Tian, X., Chen, Y., Huang, S., Cui, Z., Tian, R., et al. (2021). Feasibility and accuracy of menstrual blood testing for high-risk human papillomavirus detection with Capture sequencing. *JAMA Netw. Open* 4 (12), e2140644. doi:10.1001/jamanetworkopen.2021.40644

Zhao, H., Li, Y., Jin, H., Xie, L., Liu, C., Jiang, F., et al. (2010). Rapid and efficient reprogramming of human amnion-derived cells into pluripotency by three factors OCT4/SOX2/NANOG. *Differ. Res. Biol. Divers.* 80 (2–3), 123–129. doi:10.1016/j.diff.2010.03.002

Zhao, G. N., Zhang, P., Gong, J., Zhang, X. J., Wang, P. X., Yin, M., et al. (2017). Tmbim1 is a multivesicular body regulator that protects against non-alcoholic fatty liver disease in mice and monkeys by targeting the lysosomal degradation of Tlr4. *Nat. Med.* 23 (6), 742–752. doi:10.1038/nm.4334

Zhao, Y., Lan, X., Wang, Y., Xu, X., Lu, S., Li, X., et al. (2018a). Human endometrial regenerative cells attenuate bleomycin-induced pulmonary fibrosis in mice. *Stem Cells Int.* 2018, 3475137. doi:10.1155/2018/3475137

Zhao, Y., Chen, X., Wu, Y., Wang, Y., Li, Y., and Xiang, C. (2018b). Transplantation of human menstrual blood-derived mesenchymal stem cells alleviates Alzheimer's disease-like pathology in APP/PS1 transgenic mice. *Front. Mol. Neurosci.* 11, 140. doi:10.3389/fnmol.2018.00140

Zhao, X., Zhao, X., and Wang, Z. (2021). Synergistic neuroprotective effects of hyperbaric oxygen and N-acetylcysteine against traumatic spinal cord injury in rat. *J. Chem. Neuroanat.* 118, 102037. doi:10.1016/j.jchemneu.2021.102037

Zhong, Z., Patel, A. N., Ichim, T. E., Riordan, N. H., Wang, H., Min, W. P., et al. (2009). Feasibility investigation of allogeneic endometrial regenerative cells. *J. Transl. Med.* 7, 15. doi:10.1186/1479-5876-7-15

Zhou, T., Benda, C., Duzinger, S., Huang, Y., Li, X., Li, Y., et al. (2011). Generation of induced pluripotent stem cells from urine. *J. Am. Soc. Nephrol. JASN* 22 (7), 1221–1228. doi:10.1681/ASN.2011010106

Zhu, H., Pan, Y., Jiang, Y., Li, J., Zhang, Y., and Zhang, S. (2019). Activation of the Hippo/TAZ pathway is required for menstrual stem cells to suppress myofibroblast and inhibit transforming growth factor β signaling in human endometrial stromal cells. *Hum. Reprod. Oxf Engl.* 34 (4), 635–645. doi:10.1093/humrep/dez001

Zucherato, V. S., Penariol, L. B. C., Silva, LECM, Padovan, C. C., Poli-Neto, O. B., Rosa-E-Silva, J. C., et al. (2021). Identification of suitable reference genes for mesenchymal stem cells from menstrual blood of women with endometriosis. *Sci. Rep.* 11 (1), 5422. doi:10.1038/s41598-021-84884-5

frontiers | Frontiers in Cell and Developmental Biology

TYPE Review
PUBLISHED 03 September 2025
DOI 10.3389/fcell.2025.1595897

OPEN ACCESS

EDITED BY
Valerie Kouskoff,
The University of Manchester,
United Kingdom

REVIEWED BY
Rossella Labella,
Columbia University, United States
Naseem Ahamad,
The University of Texas Health Science Center at San Antonio, United States

*CORRESPONDENCE
Yan Chen,
cyz600@163.com
Zhixu He,
hzx@gmc.edu.cn

RECEIVED 18 March 2025
ACCEPTED 24 June 2025
PUBLISHED 03 September 2025

CITATION
Shu J, Xie X, Wang S, Du Z, Huang P, Chen Y and He Z (2025) CRISPR/Cas-edited iPSCs and mesenchymal stem cells: a concise review of their potential in thalassemia therapy. *Front. Cell Dev. Biol.* 13:1595897. doi: 10.3389/fcell.2025.1595897

CRISPR/Cas-edited iPSCs and mesenchymal stem cells: a concise review of their potential in thalassemia therapy

Jiaojiao Shu[1], Xin Xie[1], Sixi Wang[1], Zuochen Du[2], Pei Huang[2], Yan Chen[2]* and Zhixu He[1,3]*

[1]Department of Pediatrics, Affiliated Hospital of Zunyi Medical University, Zunyi, China, [2]Department of Pediatric, Affiliated Hospital of Zunyi Medical University, Guizhou Children's Hospital, Zunyi, China, [3]Department of Pediatrics, Affiliated Hospital of Guizhou Medical University, Guiyang, China

Thalassemia, a prevalent single-gene inherited disorder, relies on hematopoietic stem cell or bone marrow transplantation as its definitive treatment. However, the scarcity of suitable donors and the severe complications from anemia and iron overload pose significant challenges. An immediate need exists for a therapeutic method that addresses both the illness and its associated complications. Advancements in stem cell technology and gene-editing methods, such as clustered regularly interspaced short palindromic repeats along with its associated protein (CRISPR/Cas), offer encouraging prospects for a therapy that could liberate patients from the need for ongoing blood transfusions and iron chelation treatments. The potential of genetic reprogramming using induced pluripotent stem cells (iPSCs) to address thalassemia is highly promising. Furthermore, mesenchymal stem cells (MSCs), recognized for their capacity to self-renew and differentiate into multiple lineages that include bone, cartilage, adipose tissue, and liver, demonstrate potential in alleviating several complications faced by thalassemia patients, including osteoporosis, cirrhosis, heart conditions, respiratory issues, and immune-related disorders. In this review, we synthesize and summarize relevant studies to assess the therapeutic potential and predict the curative effects of these cellular approaches.

KEYWORDS

thalassemia, gene therapy, iPSC, MSC, complication

1 Introduction

Initially identified along the Mediterranean coast, thalassemia is considered one of the most common autosomal recessive disorders stemming from single-gene inheritance (Zakaria et al., 2022). Annually, approximately 300,000 to 500,000 infants are born with serious types of homozygous thalassemia, and it is estimated that approximately 7% of the worldwide population holds the thalassemia gene (Liu et al., 2024; Tran et al., 2023; Saleemi, 2014). There are regional differences in China; thalassemia patients or carriers mainly live in the south of the Yangtze River, such as Guangxi Province, where the proportion of carriers reaches 20%–25% (Chen et al., 2022). Major thalassemia patients require blood diffusion and iron chelation therapy to survive, which has no cure other than allogeneic hematopoietic stem cell transplantation (HSCT); however, the challenge

of identifying a suitably matched donor significantly restricts the accessibility of this therapeutic approach (Zakaria et al., 2022).

Stem cell therapy utilizes the natural abilities of stem cells, such as their inherent capacity for proliferation, differentiation, and self-renewal, to repair damaged cells and promote the healing of organs, providing therapeutic advantages and improving physical development (Mousaei G et al., 2022). Currently, allogeneic HSCT is the primary stem cell treatment for thalassemia and the only recognized potentially curative method for individuals with transfusion-dependent major thalassemia (Farmakis et al., 2022). Furthermore, various research efforts are investigating the combination of gene therapy and mesenchymal stem cells (MSCs) with induced pluripotent stem cells for treating thalassemia (Li et al., 2022a). Clustered regularly interspaced short palindromic repeats along with its associated protein 9 (CRISPR/Cas9) gene-edited induced pluripotent stem cells (iPSCs) from patients can have normal genes and are hopefully capable of differentiating into normal hematopoietic cells and red blood cells (Zakaria et al., 2022). MSCs, which derive from the mesoderm, exhibit significant differentiation capabilities and low levels of immunogenicity (Rudnitsky et al., 2025). MSCs are valuable for therapeutic applications due to their potential to evolve into various adult stem cells, address complications like liver cirrhosis and osteoporosis, facilitate bone healing and liver function improvement in animal studies, and exhibit minimal immunogenicity, reducing the risk of immune rejection (Chen et al., 2023; Huang et al., 2025; Yang et al., 2020). Nevertheless, the relevant research on treating thalassemia with iPSCs and MSCs remains limited. Therefore, in this review, we aim to summarize studies on the application of these stem cells in thalassemia treatment.

2 Thalassemia and its complication

2.1 Thalassemia pathogenesis

Thalassemia is considered one of the most common genetic disorders inherited in an autosomal recessive manner, distinguished by a defect in the production (resulting from mutations or deletions) of one or several globin peptide chains (α, β, γ, and δ). This alteration creates an imbalance in the hemoglobin structure, which eventually results in the transformation or destruction of red blood cells (Kattamis et al., 2022). Due to decreased normal hemoglobin levels, red blood cells have a shorter lifespan and reduced oxygen transport capacity, and may rupture when passing through the marrow or spleen, leading to hemolytic anemia (Thiagarajan et al., 2021). Thus, the patients exhibit anemic symptoms, for instance, pallor, developmental retardation, and hepatosplenomegaly, due to chronic hypoxia. These symptoms can have a remission through blood transfusion (Musallam et al., 2024).

2.2 Clinical manifestation of thalassemia

Thalassemia can result from mutations or deletions in chromosome 16 or chromosome 11, referred to as α-thalassemia and β-thalassemia, respectively; if both chromosomes are mutated, the condition is known as αβ-thalassemia. In clinical practice, γ-thalassemia, δ-thalassemia, and δβ-thalassemia (or εγδβ-thalassemia) also exist; however, they are less prevalent than α-thalassemia and β-thalassemia (Table 1) (Taher et al., 2021).

α-Thalassemia is caused by insufficient production of α-globin peptides, which arises from genes found on chromosome 16. This chromosome typically harbors four α-globin alleles, and the condition's severity correlates with the number of affected alleles (Harewood and Azevedo, 2024). A single mutation or deletion, known as silent carrier status, is asymptomatic. When two alleles are compromised, the condition is classified as α-thalassemia minor, which is generally mild or without clinical signs. The intermedia form, known as hemoglobin H disease, occurs when three alleles are defective; it can lead to severe symptoms, with some patients requiring blood transfusions (Musallam et al., 2024). Major α-thalassemia, also known as Hb Bart's hydrops fetalis, often results in miscarriage in the early stages of pregnancy (Tesio and Bauer, 2023). Pregnant women affected by fetal hydrops may experience a condition known as mirror syndrome, which can lead to maternal edema, proteinuria, and hypertension. Additionally, there is an increased risk of dystocia (difficult labor) and postpartum hemorrhage due to the enlarged placenta (Biswas et al., 2023). Unfortunately, because many couples are unaware of their α-thalassemia carrier status and lack access to prenatal screening, most fetuses with α-thalassemia major (ATM) are diagnosed with hydrops or other abnormalities detected through routine prenatal ultrasound examinations (Winger et al., 2025; Tamary et al., 1993). Another kind of thalassemia in hospital is β-thalassemia, and the global morbidity rate of β-thalassemia is approximately 1.5% (Cri et al., 2019). According to available statistics, approximately 4 million infants are born with β-thalassemia (Kattamis et al., 2020), which is mainly distributed in the Mediterranean and Southeast Asia, and a few β-thalassemia infants die before they are diagnosed in some areas with poor medical resources (Taher et al., 2021; Angastiniotis and Lobitz, 2019). β-Thalassemia is difficult to be detected *in utero*, and most patients begin to present clinical symptoms after 6 months of age. Unlike α-thalassemia, β-thalassemia is divided into three types (Zakaria et al., 2022) based on mutation in two alleles on human chromosome 11 (Origa, 2017). Minor thalassemia, known as β-thalassemia carriers, presents with either mild anemia or no clinical symptoms. In contrast, β-thalassemia intermedia involves individuals who are double heterozygotes and exhibit clinical features ranging from mild to severe, potentially resulting in moderate anemia and hepatosplenomegaly (Origa, 2017). Severe β-thalassemia, also known as Cooley's anemia (Khan and Shaikh, 2023), is associated with the possibility of severe anemia, jaundice, hepatosplenomegaly, growth retardation, and facial skeletal deformity; these patients require regular lifelong blood transfusions, iron chelation therapy, or hematopoietic stem cell transplantation (Needs et al., 2024). Certain patients with severe β-thalassemia may not survive into their twenties due to complications like arrhythmia and heart failure, which can lead to critical deterioration from iron overload within a span of 6 months (Coates, 2014).

TABLE 1 Thalassemia types and their genetic defects, clinical manifestations, severity, and complications.

Type and genetic deficiency	Clinical manifestation	Severity	Complication	Reference
α-Thalassemia (α-globin gene deletion or deficiency)	a. Silent type: asymptomatic b. Mild type: mild anemia c. Intermediate type (hemoglobin H disease): moderate anemia (may present with jaundice and hepatomegaly) d. Severe type (hydrops fetalis syndrome): severe fetal anemia, generalized edema, and hepatomegaly, often leading to fetal death	Silent and mild types are mild; intermediate type is moderate; severe type is severe	Jaundice, hepatomegaly, hydrops fetalis syndrome, cardiac enlargement, skeletal deformities, delayed growth and development, and iron overload	Musallam et al. (2024), Li et al. (2024), Winger et al. (2025), Farashi and Harteveld (2018), and Tamary et al. (1993)
β-Thalassemia (β-globin gene deletion or deficiency)	a. Mild type: mild anemia; b. Intermediate type: may present with jaundice, hepatomegaly, and delayed growth and development; c. Severe type: severe anemia, pale complexion, hepatomegaly, jaundice, and poor development, with typical facial features, require long-term blood transfusions	Mild type is mild; intermediate and severe types are more severe	Jaundice, hepatomegaly, delayed growth and development, skeletal deformities, heart enlargement, and iron overload	Bajwa and Basit (2025), Makis et al., 2021; Origa (2017), Cao and Galanello (2010), Dordevic et al. (2025), Langer et al. (1993), and Cappellini et al. (2014)
δβ-Thalassemia (δ- and β-globin gene deletion or deficiency)	Mild anemia	Relatively mild	Slight jaundice and hepatomegaly	De Simone et al. (2022)
γ-Thalassemia (γ -globin chain deletion or deficiency)	Usually presents with mild anemia	Relatively mild	Slight jaundice and hepatomegaly	De Simone et al. (2022)
δ-Thalassemia (δ gene mutation)	Mild anemia	Relatively mild	Slight jaundice and hepatomegaly	De Simone et al. (2022)

2.3 Current treatments of thalassemia

Various therapeutic strategies are available for the management of thalassemia, encompassing blood transfusions, iron chelation therapy, splenectomy, bone marrow transplantation, HSCT, gene editing methods, and the induced synthesis of fetal hemoglobin (Wang et al., 2023; Khan and Shaikh, 2024), and medications such as hydroxyurea (Ali et al., 2021), which prolong the life of the patient at the different way. However, some of the treatments pose some challenges that urgently need to be addressed. For example, blood transfusion and iron removal are two symptomatic treatments for major thalassemia (Hodroj et al., 2023); however, frequent or excessive transfusions can lead to iron overload as iron released from the breakdown of red blood cells may deposit in various tissues and organs, resulting in serious complication.

2.4 Complications of thalassemia

Although patients with major thalassemia receive the treatments mentioned above, they may still experience numerous complications, including thromboembolic events, organ dysfunction, endocrinopathies, cardiovascular disease, and osteoporosis (Kattamis et al., 2022; Wood, 2023; Gaudio et al., 2019). A cohort study showed that 480 of 709 patients (67.7%) with β-thalassemia have developed at least one complication and 93 β-thalassemia patients died due to heart diseases (57.0%), complications from bone marrow transplantation (10.8%), infections (8.6%), liver diseases (4.3%), cancers (3.2%), thrombus embolism (2.2%), and severe anemia (1.1%) (Forni et al., 2023). These complications are mostly caused by anemia and the occurrence of iron overload resulting from long-term and massive blood transfusions (Yousuf et al., 2022). The accumulation of iron in various organs could result in several types of organ dysfunction, potentially leading to considerable damage and failure of those organs (Wang et al., 2025a). Complications that may arise from this include arrhythmias, dysfunction of the left ventricle (Fu and Yang, 2025), fibrosis or cirrhosis (Langer et al., 1993), osteoporosis (Bhardwaj et al., 2023), kidney disorders (Demosthen et al., 2019), and abnormalities in respiratory function (Bou-Fakhredin et al., 2023). Additionally, endocrine disorders are largely related to iron accumulation in crucial glands such as the pituitary, thyroid, and adrenal glands, significantly impacting the growth and development of patients with thalassemia (Tenuta et al., 2024; Venou et al., 2024; Evangelidis et al., 2023). In addition to other complications,

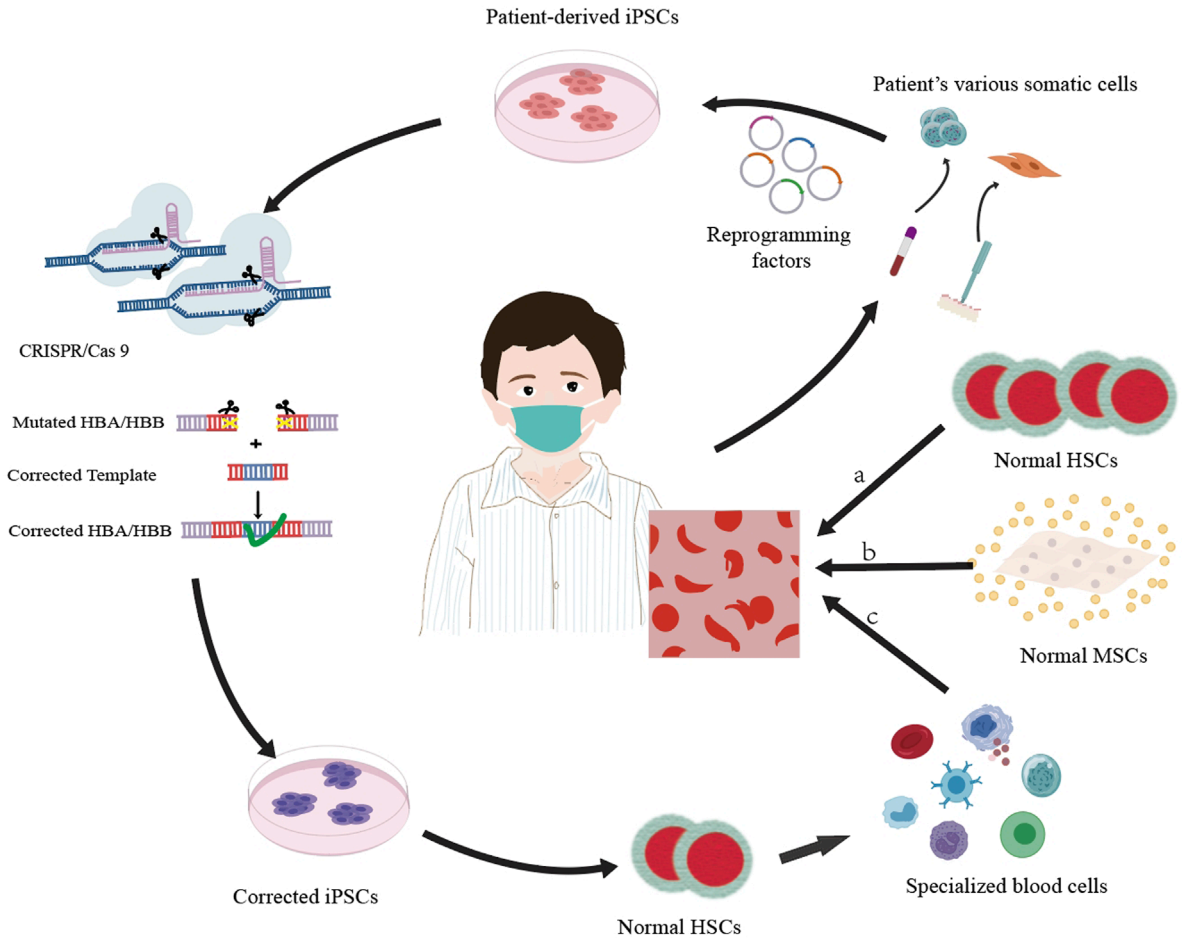

FIGURE 1
Overview of three cell therapy approaches for thalassemia treatment: a. allogeneic hematopoietic stem cell (HSC) transplantation, where healthy HSCs are transplanted into the patient to replace the defective cells; b. allogeneic mesenchymal stem cell (MSC) transplantation, which utilizes healthy MSCs to enhance the function of HSCs and may help in remedying the condition; c. by using CRISPR/Cas9 technology to modify the mutated HBA/HBB gene in the induced pluripotent stem cells (iPSCs) of the patient, differentiating these corrected iPSCs into healthy hematopoietic stem cells (HSCs), and subsequently transplanting the normal HSCs back into the patient's body to substitute the defective cells, a targeted gene therapy approach is achieved.

patients may face infections and Graft-versus-Host Disease (GVHD) (Vento et al., 2006; Akbayram et al., 2022), as well as cancer and alloimmunization, which can further threaten the life of the patient.

3 The overview of stem cell therapies for thalassemia

Stem cell treatments encompass allogeneic stem cell therapy, which involves the transplantation of the bone marrow, peripheral blood, and umbilical cord blood sourced from relatives of the patient or from a human leukocyte antigen (HLA)-matched donor (Karponi and Zogas, 2019), as well as autologous stem cell therapy, wherein the patient's own stem cells are grafted following gene reprogramming (Srivastava and Shaji, 2017); these approaches mainly include hematopoietic stem cell transplantation, mesenchymal stem cell transplantation, and gene-edited stem cell transplantation (Figure 1; Table 2). It is meaningful to develop autologous stem cell transplantation that can correct the genetic defect.

3.1 The source of stem cells: stem cell bank

Stem cells have the ability to renew themselves and can be classified into two categories depending on their source (Brignier and Gewirtz, 2010), namely, embryonic and adult stem cells. Additionally, stem cells are classified into totipotent, pluripotent, multipotent, and unipotent cells, according to their differentiation potential (Wen and Wang, 2025). A zygote, which is an example of a totipotent stem cell, has the capacity to develop into a fully formed organism. In contrast, a pluripotent stem cell can differentiate into several types of tissues, but it cannot generate an entire individual (Malik and Wang, 2022). Two categories of human pluripotent stem cells exist: human embryonic stem cells (hESCs), originating from the inner cell mass of embryos, and human induced pluripotent stem cells (hiPSCs), obtained through the reprogramming of somatic cells

TABLE 2 Comparison of the therapies of HSCs, MSCs, and iPSCs.

Stem cell type	Advantage	Disadvantage	Reference
HSCs	a. Currently the only method capable of curing transfusion-dependent thalassemia (TDT) b. Relatively mature technology	a. Donor limitations b. Transplant risks of GVHD. c. Toxicity of conditioning regimens	Wood, (2023), Aljagthmi and Abdel-Aziz (2025), and Hoang et al. (2025)
MSCs	a. Immunomodulation, which can reduce the risk of GVHD. b. Hematopoiesis promotion c. Diverse sources: comprise bone marrow, umbilical cord blood, and adipose tissue, among others	a. Efficacy uncertainty b. Technical challenge c. Long-term safety	Wiewiórska-Krata et al. (2025), Terai et al. (2025), Mousavi et al. (2023), and Levy et al. (2020)
iPSCs	a. Personalized therapy b. Genetic modification: integrating CRISPR/Cas9 with alternative gene editing methods c. Research potential	a. Technical complexity b. Ethical issues: involves ethical debates about embryonic stem cells c. Safety issues: gene editing may introduce off-target effects	Hardouin et al. (2025) and Yamanaka (2020)

(Tian et al., 2023). In 2006, Takahashi and Yamanaka found that fibroblasts obtained from mice could be converted into specialized cells, reflecting the three germ layers by applying four specific transcription factors: Oct4, Sox-2, Klf4, and c-Myc (Takahashi and Yamanaka, 2006); this technology involving induced pluripotent stem cells has slowly been utilized in the therapy for certain human ailments (Huang et al., 2020). A multipotent stem cell has the ability to develop into one or more specific tissues (Aprile et al., 2024). For instance, hematopoietic stem cells are capable of transforming into erythrocytes, leukocytes, and platelets, whereas mesenchymal stem cells primarily reside in connective tissue and interstitial spaces of organs (Zhang et al., 2018). Unipotent stem cell like myoblast can only differentiate into muscle cells.

Typically, stem cells used to treat thalassemia come from matched donors or the patients themselves, but technological advancements now enable the cultivation of stem cells from biological materials like umbilical cord blood under strict safety and quality regulations (Sharma et al., 2021). Stem cells can be stored in cell banks for future applications (Table 3) and are also used in research and treatment of various diseases (Stacey and Healy, 2021). At present, Zunyi Medical University has cooperated with enterprises to establish the first placental stem cell bank and seven autologous stem cell banks in China, and set up two public stem cell banks in Guizhou Province to provide perinatal stem cell storage services and store important stem cell medicine treatment needs. Ossium Health has established a cryopreserved bone marrow cell repository recovered from deceased organ vertebrae, referred to as hematopoietic progenitor cell bone marrow (Johnstone et al., 2021).

3.2 Allogeneic stem cell transplantation for thalassemia

Currently, the only curative treatment for severe thalassemia is allogeneic hematopoietic stem cell transplantation (Srivastava and Shaji, 2017). This process involves utilizing hematopoietic stem cells obtained from external sources, such as the bone marrow, peripheral blood, or umbilical cord blood of relatives (Wei et al., 2024). The aim is to restore the blood and immune systems of the patient, with the success of the treatment being affected by variables including the recipient's age, compatibility with the donor, and medical care provided prior to the transplant.

3.2.1 Bone marrow transplantation

Clinically, the initiation of bone marrow transplantation for disease treatment occurred in 1957 (Simpson and Dazzi, 2019). Bone marrow serves as a primary source of hematopoietic stem cells (Agarwal et al., 2023), and this procedure stands as the definitive treatment for thalassemia, particularly among individuals suffering from severe β-thalassemia (Ali et al., 2021). Bone marrow transplantation can help patients with thalassemia restore normal red blood cell production by providing healthy hematopoietic stem cells, thereby improving anemia symptoms and potentially achieving a cure, but it also involves inherent challenges and risks (Oikonomopoulou and Goussetis, 2021). Post-transplantation, patients might experience complications, including GVHD and hepatobiliary disorders (Dezan et al., 2023).

3.2.2 Umbilical cord blood transplantation

Umbilical cord blood contains a large number of hematopoietic stem cells, and it can be used in patients with no compatible donor (Hordyjewska et al., 2015). For more than 30 years, the transplantation of umbilical cord blood has been used in medical practices (Gupta and Wagner, 2020). Although it was initially regarded as medical waste, a thorough investigation into its biological characteristics and immunogenicity has revealed that umbilical cord blood is abundant in hematopoietic stem cells, which tend to proliferate and survive more effectively than other types of stem cells (Zhu et al., 2021a). Furthermore, it exhibits low immunogenicity, does not require strict HLA matching, causes no harm to donors, and is associated with a lower incidence of GVHD in transplant recipients (Zhu et al., 2021b). Compared to bone marrow, the matching process for cord blood demands a lesser degree of site matching, thereby making it easier to find a compatible donor (Sanchez-Petitto et al., 2023). Although umbilical cord blood transplantation has distinct benefits, it is utilized less often in clinical

TABLE 3 Founding time, source, and reason for establishment of Stem Cell Banks.

Stem cell bank	Founding time	Source	Reason for establishment	Reference
UK Stem Cell Bank(UKSCB)	2003	Approximately 100 research-grade hESC lines and several human pluripotent stem cell lines	Foster the advancement of scientific research and the clinical application of stem cell treatments	O'Shea and Abranches (2020)
Korea National Stem Cell Bank (KSCB)	2005	17 tissue-derived adult stem cells and 228 primary genetic disease cells	Supply stem cell resources, regenerative medicine information, and hESC registry	Kim et al. (2021)
Karolinska Institute Human Embryonic Stem Cell Bank (KISCB)	2002	60 hESC lines	Set up hESC lines for clinical use: remove xeno, chemical conditions, and ensure GMP.	Main et al. (2020)
Spanish National Stem Cell Bank (BNLC)	2006	40 hESC lines and 171 hiPSC lines, including cord blood and adipose-derived MSCs	Advance stem cell and regenerative medicine; establish hiPSC bank from homozygous cord blood	Aran et al. (2020)

settings than bone marrow and peripheral blood hematopoietic stem cell transplants. This is attributable to factors such as the possibility of delayed engraftment, the risk of graft failure, elevated non-relapse mortality rates, a heightened susceptibility to infections, and the considerable expenses involved in procuring umbilical cord blood (Sirinoglu Demiriz et al., 2012; Kindwall-Keller and Ballen, 2020).

3.2.3 Peripheral blood stem cell transplantation

The use of peripheral blood stem cell transplantation (PBSCT) from a matched sibling donor has been suggested as an alternative to bone marrow transplantation to reduce the risk of transplant failure in patients with major thalassemia (Körbling et al., 2011). PBSCT is a vital treatment method for thalassemia, which involves collecting hematopoietic stem cells from a donor, who can be the patient themselves or a matched donor, and then transfusing them intravenously into the patient's body (Angelucci et al., 2014). These stem cells migrate to the bone marrow, replacing the patient's abnormal hematopoietic cells and restoring normal red blood cell production (Körblin et al., 2011). This method holds promise for treating thalassemia; however, it requires finding an appropriate donor and addressing complications associated with transplantation (Angelucci et al., 2014). A successful transplant can greatly enhance the patient's quality of life, potentially decreasing or even removing the requirement for blood transfusions and iron chelation therapy. However, not all of the transplant patients can be saved; some of them die from complications after transplantation like GVHD, osteonecrosis, and infection (Kuci et al., 2020). However, the failure rate of allograft is approximately 25% (Marziali et al., 2017). Transplants of hematopoietic stem cells sourced from siblings who share identical HLA profiles show notably improved success rates when contrasted with those obtained from unrelated donors. However, it is important to note that merely 35%-40% of patients with thalassemia are able to find a sibling donor with matching HLA (O'Reilly, 1983). In addition, Jagasia demonstrated that approximately 40% HSCT of identical siblings will get GVHD, whereas 59% will get GVHD in the transplantation of the unrelated donor hematopoietic stem cells (Jagasia et al., 2012). A research indicates that approximately 15%-16% of patients experience grades II-IV acute GVHD and 4%-12% experience chronic GVHD after transplantation for thalassemia (Mahmoud et al., 2015).

3.3 Autologous stem cell transplantation and gene-editing therapy for thalassemia

Transplantation of autologous hematopoietic stem cells or therapy involving gene editing represents a novel approach that functions by modifying a patient's own blood stem cells to correct the genetic mutation responsible for thalassemia (Zeng et al., 2023). This approach avoids donor-matching problems in allogeneic transplantation and may reduce the occurrence rate of GVHD and infectious diseases (Li and Yang, 2023). Autologous hematopoietic stem cell transplantation typically involves collecting hematopoietic stem cells from a person, using gene-editing techniques such as CRISPR-Cas9 to amend the genetic mutation, and then reinfusing the altered stem cells into the same individual (Wilkinson et al., 2021).

4 CRISPR/Cas-edited induced pluripotent stem cells

So far, gene-editing technology to treat thalassemia has been widely used in research and is considered one of the most promising therapies for diseases resulting from single-gene inheritance (Khiabani et al., 2023). Gene editing represents an advanced therapeutic approach that focuses on cultivating patients' hematopoietic stem cells. Following this, the edited stem cells containing the corrected gene are injected back into the patients' bodies to achieve complete healing (Ali et al., 2021). At present, gene therapy is in the experimental stage and has made some progress. Some research works have pointed out that

TABLE 4 Comparison of gene therapy strategies for thalassemia.

Therapeutic approach	Principle	Advantage	Disadvantage	Correction of known pathogenic mutations	Safety	Reference
CRISPR/Cas9 gene editing	Utilizes the CRISPR/Cas system to directly repair or insert target genes, correcting mutations	a. Precise correction of mutations b. Low risk of immune reactions c. Applicable to various cell types	a. Unintended effects b. The efficiency of delivery and specificity for cells need additional refinement	Suitable for cases requiring long-term stable expression of normal genes	a. Off-target effects and long-term safety b. Delivery system safety requires optimization	Paolini Sguazzi et al. (2021), Wang et al. (2025b), Butterfield et al. (2025), Gao et al. (2025), John and Czechowicz (2025), and Ali et al. (2025)
Lentiviral vectors	Introduces normal genes into cells via viral vectors to replace defective genes	a. Efficient gene insertion b. Long-term stable expression c. Extensive clinical experience	a. Potential for immune reactions b. Risk of insertional mutagenesis	Correction of single-base mutations	a. Long-term monitoring required b. Safety relatively mature but still with risks	Williams et al. (2025), Ottaviano and Qasim (2025), and Hackett and Crystal (2025)
Base editing	Chemically alters one base to another, which can be divided into two primary categories: those that target DNA and those that focus on RNA.	a. No double-strand breaks b. High efficiency for single-base conversions	a. Lower technological maturity b. Limited scope of application	a. Still in preclinical research stages b. Not yet widely applied clinically	a. Long-term stability and potential side effects b. Off-target effects	Porto et al. (2020), Komor et al. (2016), Gaudelli et al. (2017), and Rees and Liu (2018)

gene-editing technologies like CRISPR/Cas 9 (Zeng et al., 2023) can accurately modify or replace defective genes and ultimately restore the function of red blood cells (Traeger-Synodinos et al., 2024). Although gene therapy offers certain advantages over other therapies, it is not suitable for all thalassemia patients, and its high cost makes it inaccessible to many patients; moreover, the therapy becomes ineffective if the corrected gene is inserted off-target (Christakopoulos et al., 2023).

4.1 CRISPR/Cas9 gene-editing technology

The CRISPR/Cas9 system was initially used by bacteria and archaea for adaptive immune responses against foreign DNA sources like plasmids and viruses. It has now become a potent instrument for gene editing (Deltcheva et al., 2011). With the introduction of CRISPR/Cas9 technology in 2012 (Jinek et al., 2012), this method has shown considerable promise in addressing genetic disorders, including thalassemia. Although CRISPR/Cas9 has limitations in off-target effects and editing efficiency, its flexibility and programmability have spurred next-generation, more precise tools like Base Editing, offering broader strategies for treating monogenic diseases such as thalassemia (Table 4) (Greco et al., 2024). The CRISPR/Cas9 system, guided by RNA, is notable for being easy to use, economical, and versatile (Anurogo et al., 2021). However, despite its broad application prospects, gene therapy raises concerns about its safety and ethical implications, particularly the risk of off-target effects, which require rigorous ethical review and regulatory oversight (Hryhorowicz et al., 2023).

4.2 Human induced pluripotent stem cell

In 2006, Shinya Yamanaka et al. found that it was possible to reprogram adult skin fibroblasts into hiPSCs by incorporating four transcription factors: Oct4, Sox2, Klf4, and c-Myc (Takahashi and Yamanaka, 2006). iPSCs closely resemble embryonic stem cells regarding their morphological characteristics, patterns of gene expression, and capabilities for differentiation, which have been validated in various 3D cardiac tissue models (Campostrini et al., 2021). These cells exhibit remarkable self-renewal capabilities and have the potential for multipotent differentiation, rendering them a valuable resource for various applications, including regenerative medicine, drug development, and disease modeling (Poetsch et al., 2022). iPSCs derived from an individual's own cells provide considerable medical benefits by reducing the likelihood of immune rejection. Their capacity for self-renewal and differentiation into diverse cell types positions them as essential tools in regenerative medicine, drug discovery, and disease modeling (Cerneckis et al., 2024). iPSCs possess the ability to replicate and grow indefinitely in a laboratory setting, thus offering a substantial source of cells for applications in tissue engineering and cellular therapies (Mattis and Svendsen, 2011). This property is essential for producing the required cell populations for regenerative medicine (Rowe and Daley, 2019). However, iPSCs encounter challenges including potential genetic mutations and chromosomal abnormalities arising from reprogramming, which can compromise cell quality and safety (Kavyasudha et al., 2018). Additionally, effective differentiation into specific cell types and achieving targeted differentiation with functional integration *in vivo* present ongoing research challenges (Lee and Son, 2021).

4.2.1 Gene-editing strategies

Technologies for gene editing offer considerable promise for utilizing iPSCs (McTague et al., 2021). For instance, CRISPR/Cas9 tools can be utilized to modify iPSCs by either knocking out genes that hinder nerve regeneration (like Nogo-A) or inserting genes that encourage nerve repair (such as the neurotrophic factor BDNF) (Hsu et al., 2019). Additionally, for allogeneic iPSCs, HLA genes can be edited to match those of the patient or to create universal donor cells, thereby reducing the risk of immune rejection (Xu et al., 2019; Song et al., 2022). It is necessary to conduct sequencing, flow cytometry and other analyses on the verified edited iPS cells to verify the accuracy of the modification and the normal differentiation ability of the cells (Maurissen and Woltjen, 2020).

4.2.2 Strategy for differentiating hiPSCs into HSCs

A fundamental approach to differentiating iPSCs into hematopoietic stem cells (HSCs) involves the creation of embryoid bodies (EBs), induction of mesoderm, formation of hematopoietic endothelium, and the process of endothelial-to-hematopoietic transition (EHT) (Ng et al., 2024). This process also encompasses the utilization of various elements, such as cytokines [interleukin (IL)-3, IL-6], dexamethasone, stem cell factor (SCF), recombinant human erythropoietin (EPO), vascular endothelial growth factor (VEGF), insulin-like growth factor I (IGF-I), Fms-like tyrosine kinase 3 (FLT3), bone morphogenetic protein 4 (BMP4), albumin, and transferrin (Lapillonne et al., 2010; Bernecker et al., 2019; Rowe et al., 2016; Oguro, 2019). In addition, retinoic acid and its precursors (such as retinol) play important roles in the mesoderm patterning stage, significantly enhancing the efficiency of iPSC differentiation into hematopoietic cells (Grace et al., 2018). However, the differentiation of iPSCs into functional HSCs still faces challenges such as cell functional stability and immunogenicity (Wattanapanitch et al., 2019).

4.3 CRISPR/Cas-edited induced pluripotent stem cell for thalassemia

iPSCs utilizing CRISPR/Cas gene-editing techniques present an innovative strategy for treating thalassemia (Wattanapanitch et al., 2018). In the context of thalassemia management, the CRISPR/Cas technology is capable of correcting genetic mutations within iPSCs, which restores their erythropoietic function and allows for the production of healthy red blood cells through *in vitro* cultivation and differentiation into erythroid lineages (Xie et al., 2014). These differentiated red blood cells can subsequently be reintroduced into the patient, acting as a form of cellular therapy that either supplements or replaces the malfunctioning cells, thereby alleviating the symptoms related to the genetic mutation (Ou et al., 2016). This approach is particularly advantageous as it utilizes the patient's own cells, reducing the risk of immune rejection. Moreover, this technique could be applied to the treatment of various other genetic conditions (Li et al., 2023). The CRISPR/Cas9 technique for editing genes related to thalassemia poses numerous challenges, especially regarding safety considerations and the potential long-term consequences of this new technology, which have not yet been completely determined (Frangoul et al., 2021). Overall, using CRISPR/Cas gene-editing techniques on induced pluripotent stem cells exhibits potential as a therapy for thalassemia; nonetheless, further studies and confirmations are necessary prior to its widespread adoption in clinical applications (Zeng et al., 2023).

4.3.1 Delivery methods

The methods of delivering the CRISPR/Cas system play a vital role in the effectiveness of gene editing (Du et al., 2023). Typical methods of delivery encompass viral vectors such as adeno-associated virus (AAV) (Naso et al., 2017), adenovirus (AdV), lentivirus, Sendai virus, and retrovirus (Tong et al., 2019; Park et al., 2016), along with nonviral systems including lipid nanoparticles (Li et al., 2018; Sinclair et al., 2023). Although viral vectors offer high delivery efficiency, they are associated with risks of immune responses and insertional mutagenesis. In contrast, nonviral delivery systems are safer but less efficient (Seijas et al., 2025).

4.3.2 Editing efficiency

Editing efficiency directly impacts the therapeutic outcome. Improvements in the efficiency of the CRISPR/Cas9 system can be achieved through the optimization of sgRNA design, expression levels of Cas9 protein, and the selection of cell types (Agrawal et al., 2021). Utilizing high-precision variants of Cas9, such as eSpCas9 or SpCas9-HF1, can reduce off-target effects while also enhancing the safety of the editing procedure (Kleinstiver et al., 2021; Yin et al., 2016). In iPSCs, increased editing efficiency ensures more successful cell repair, fewer residual mutant cells, and better therapeutic efficacy, as shown by Singh et al. (2024), using p53 inhibition and pro-survival molecules to achieve over 90% CRISPR/Cas9 efficiency.

4.3.3 Differentiation into functional hematopoietic stem cells

The process of transforming corrected iPSCs into functional hematopoietic stem cells represents a crucial aspect of cellular therapy (Table 5). At present, by replicating the *in vivo* microenvironment that supports hematopoietic development and integrating specific cytokines (like BMP4, SCF, and TPO) with small molecular compounds (Bello et al., 2024; Jeong et al., 2020a; Kayama et al., 2024), iPSCs can be effectively guided to develop into the hematopoietic lineage. Further optimization of differentiation protocols, such as adjusting culture conditions, adding functional small molecules, and utilizing three-dimensional culture systems, holds promise for improving differentiation efficiency and cell quality (Rahman et al., 2025; Meng et al., 2014). Additionally, verifying the functionality of the differentiated cells through flow cytometry and *in vivo* transplantation experiments is an essential step to ensure therapeutic efficacy (Bhattacharya et al., 2014).

TABLE 5 The treatment and therapeutic effect of using iPSC to treat the thalassemia patients.

Disease	iPSC source	Treatment	Therapeutic effect	Reference
β-Thalassemia (homozygous 41/42 deletion)	β-Thal patient	CRISPR/Cas9+ iPSCs	Effectively fixes β-thal mutations in patient iPSCs	Ou et al. (2016)
β-Thalassemia [β17/17 (A→T) in HBB]	β-Thal patient	CRISPR/Cas9	Edited cells show normal karyotypes, pluripotency, and no off-target.	Song et al. (2015)
β-Thalassemia [IVS2-654(C>T)]	β-Thal patient	CRISPR/Cas9 + piggyBac	CRISPR/Cas9 detected off-target.	Xu et al. (2015)
HbE mutation	β-Thal patient	CRISPR/Cas9 plasmid + ssODN	Achieves one-step HbE correction in iPSCs	Wattanapanitch (2021)
β-Thalassemia (a homozygous β41-42 del and heterozygous Westmead mut in HBA2)	Fetal amnion	CRISPR/Cas9+ iPSCs	Mutations fixed; hiPSCs kept normal pluripotency and could become hematopoietic progenitors	Li et al. (2022a)
β-Thalassemia [β17/17 (A→T) in HBB]	β-Thal patient	CRISPR/Cas9 + iPSCs	Normal karyotype, maintained pluripotency, and no off-target effects	Song et al. (2015)
β-Thalassemia [−28 (A>G) and the 4-bp (TCTT) del at CD41-42 in exon 2]	β-Thal patient	CRISPR/Cas9 + iPSCs + piggyBac	Seamless HBB mutation correction via HDR; no off-target effects	Xie et al. (2014)
β-Thalassemia [4-bp del (−TCTT) and (−CTTT) at CD41-42 mut]	β-Thal patients	CRISPR/Cas9 + ssODNs	Repaired cells had normal β-globin transcripts, low mutation load, and no off-target mutagenesis	Niu et al. (2016)
β-Thalassemia (CD26 G>A mut in in HBB)	HbE/β-thalassemia patient's dermal fibroblasts with CD41/42 and CD26 mut	Cas9 + ssODNs via HDR	HBB protein restored; single CD26 allele fix normalizes β-globin in HbE/β-thalassemia	Wattanapanitch et al. (2018)

4.4 Barriers to translating research into clinical applications

4.4.1 Technical challenges and strategies for mitigation

One of the primary challenges in applying gene-editing technologies such as CRISPR/Cas9 to clinical treatments is the technical barriers associated with off-target effects (Concordet and Haeussler, 2018). Unplanned alterations to genes that are not the intended targets may heighten the risks linked to therapeutic treatments. To reduce these unintended effects, various strategies have been formulated.

High-fidelity Cas9 variants: the use of high-fidelity Cas9 variants (Zuo et al., 2022), such as eSpCas9, SpCas9-HF1, dCas9-FokI and evoCas9 (Allemailem et al., 2023; Wyvekens et al., 2015), has been extensively acknowledged in academic writings as an approach to enhance the accuracy of CRISPR/Cas9-editing systems (Naeem et al., 2020). The highly accurate version of Cas9, referred to as Hypa-Cas9, has demonstrated enhanced on-target effectiveness in human cells while minimizing off-target impacts (Chen et al., 2017).

Optimized sgRNA design: the careful design of single-guide RNA (sgRNA) improves the accuracy of gene editing and reduces off-target consequences (Doench et al., 2016). Using bioinformatic tools to predict and select sgRNA sequences with low off-target risks is an effective method to improve specificity (Concordet and Haeussler, 2018; Doench et al., 2016). Recent developments in the methods of delivering CRISPR/Cas9 for therapeutic gene editing in stem cells have been examined, emphasizing the significance of well-designed sgRNA in improving the efficiency of genome editing while minimizing off-target impacts (Lotfi et al., 2023).

Delivery approaches for CRISPR/Cas9 systems: enhancing the delivery mechanisms for the CRISPR/Cas9 system, using nonviral strategies like lipid nanoparticles (Kazemian et al., 2022) or electroporation (Hussen et al., 2024) as nonviral delivery systems, can lead to improved editing efficiency and a decrease in off-target effects.

Precise control of editing windows: introducing mutations into the deaminase allows for the narrowing of the editing window while still preserving significant editing activity (Jeong et al., 2020b). A study used adenine base editors (ABEs) to accurately correct the IVSI-110(G>A) mutation associated with beta-thalassemia, attaining a 90% efficiency in editing (Naiisseh et al., 2024). By precisely controlling the editing window, that is, performing edits during specific cell cycle stages, off-target effects can be minimized, as certain cell cycle stages are more precise in DNA damage repair mechanisms (Fichter et al., 2023).

Using these approaches allows us to more precisely modify mutations that lead to diseases, like thalassemia, while minimizing the potential for off-target effects.

4.4.2 Ethical and regulatory considerations

The translation of gene-editing technologies into clinical applications faces significant technical, ethical, and regulatory challenges (Ledford, 2020). The swift advancement of these technologies raises ethical concerns regarding safety, equity, privacy, and societal impact (Greely, 2019). The establishment of a unified global regulatory system faces challenges, as more countries become open to gene-editing technology (Sprink et al., 2022). Ethical reviews are crucial for ensuring research integrity and participant rights, and research workers must comply with laws including clinical trial regulations and data protection (Joseph et al., 2022). Public engagement and transparency are key factors to fostering understanding and discourse on these issues (Parikh et al., 2025). Overcoming these challenges is vital for advancing gene-editing technology in clinical settings (Wiley et al., 2025), potentially offering novel treatments for diseases like thalassemia.

5 Biological characteristics and function of MSCs

5.1 Biological properties

MSCs are a type of multipotent stem cell that was first discovered in the bone marrow by Friedenstein and are derived from the dental pulp, umbilical cord blood, amniotic membrane, placenta, mobilised peripheral blood, synovium and synovial fluid, endometrium, skin and muscle (Berebichez-Fridman and Montero-Olvera, 2018), which possess the ability to self-renew and differentiate into various cell types (Kolf et al., 2007). MSCs, mainly found in connective tissue and apparatus mesenchyme, are an important cell repository involved in tissue regeneration; MSCs are also a significant type of seed cell used in tissue engineering (Adil et al., 2022). MSCs proliferate rapidly and are easily isolated and cultured. These cells may be sourced from multiple origins, including bone marrow, periosteum, adipose tissue (Deo et al., 2022), umbilical cord tissue (Wu et al., 2023), dental tissue (Gan et al., 2020), and amniotic fluid (Gholami Farashah et al., 2023). Additionally, MSCs contribute to immune modulation by interacting with T cells (Kuca-Warnawin et al., 2021), B cells, NK cells (Abbasi et al., 2022), and other types of immune cells. Importantly, MSCs have little or no immunogenicity (Chen et al., 2024b) and the tolerance of immunity, which can reduce the risk of graft rejective reaction. Recently, a study found that higher-level TNF-α-induced protein 6 (TSG6) enhanced the anti-inflammatory function of CD317(+) MSCs, suggesting that CD317(+) MSCs may be a promising candidate for treating the immune-related diseases (Song et al., 2024). MSCs can repair tissues and differentiate into osteoblast, chondroblast, nerve cells, myoblast, and adipose tissues (Kim et al., 2023). Given the capabilities of MSCs, extensive research has been conducted on them, leading to their increasing implementation in clinical settings.

5.2 The possibility of MSC transplantation to treat thalassemia

A study has indicated that MSCs can enhance the homing of hematopoietic stem cells and boost their hematopoietic capacity (Aqmasheh et al., 2017). Given their role in immunological regulation, MSCs can inhibit NK cell activity and reduce T-cell proliferation by releasing specific cytokines and facilitating cell interactions, which is beneficial for minimizing rejection responses and enhancing survival rates (Johnstone et al., 2021). In patients with β-thalassemia, the MSCs in the bone marrow are functionally impaired due to iron overload and oxidative stress, leading to a decrease in their proliferation, differentiation capacity, and hematopoietic supportive function (Cri et al., 2019). The alteration of the bone marrow microenvironment in patients with thalassemia leads to a significant increase in the lipid, protein, glycogen and nucleic acid content of bone marrow mesenchymal stem cells (BM-MSCs), which is related to enhanced cell proliferation and bone marrow activity (Aksoy et al., 2012). Moreover, studies have shown that the vertebral body - adherent mesenchymal stromal cells (vBA - MSCs) extracted from donor vertebral fragments have similar characteristics to traditional bone marrow - derived mesenchymal stromal cells (BM - MSCs), but with a significantly higher abundance (Johnstone et al., 2020). Additionally, they are matched with hematopoietic progenitor cells (HPCs), which helps promote the formation of mixed chimerism, enhance peripheral immune regulatory functions, and improve the safety of transplantation (Johnstone et al., 2021).

5.3 Research on using MSCs to treat the complication of thalassemia

MSCs have shown potential therapeutic values in treating multiple complications of thalassemia, including heart disease (Szaraz et al., 2017), liver disease (Banas et al., 2007; Ortuño-Costela et al., 2025), bone destruction (Afflerbach et al., 2020), lung disease (Mansouri et al., 2019), endocrine abnormalities (Sarvari et al., 2021), and other diseases (Hoang et al., 2022) (Figure 2). First, thalassemia patients face a long-term anemic state and need regular blood transfusion, which may lead to increased heart burden, causing heart enlargement, cardiac hypertrophy, and other heart diseases (Berdoukas et al., 2015), and MSCs play a role in protecting and repairing the heart. They facilitate the regeneration and repair of injured myocardial tissue, enhancing cardiac function by differentiating into both cardiomyocytes and vascular smooth muscle cells (Ala, 2023; An et al., 2025). Second, chronic anemia and increased red blood cell destruction in individuals with thalassemia can place a greater strain on the liver, potentially leading to liver diseases such as hepatic fibrosis (Papastamataki et al., 2010). MSCs have the ability to release various growth factors and cytokines, aiding in the regeneration and repair of liver cells, minimizing liver inflammation, and enhancing liver function (Rostami et al., 2021; Wen et al., 2025). Third, patients with thalassemia may have bone destruction and osteoporosis due to chronic anemia and myelodysplasia (Bhardwaj et al., 2023), and MSCs have the ability of osteogenic differentiation, can promote the regeneration and repair of bone tissue, can increase bone density and bone strength, and can improve bone condition (Jiang et al., 2021). Fourth, thalassemia patients receiving chronic transfusions are

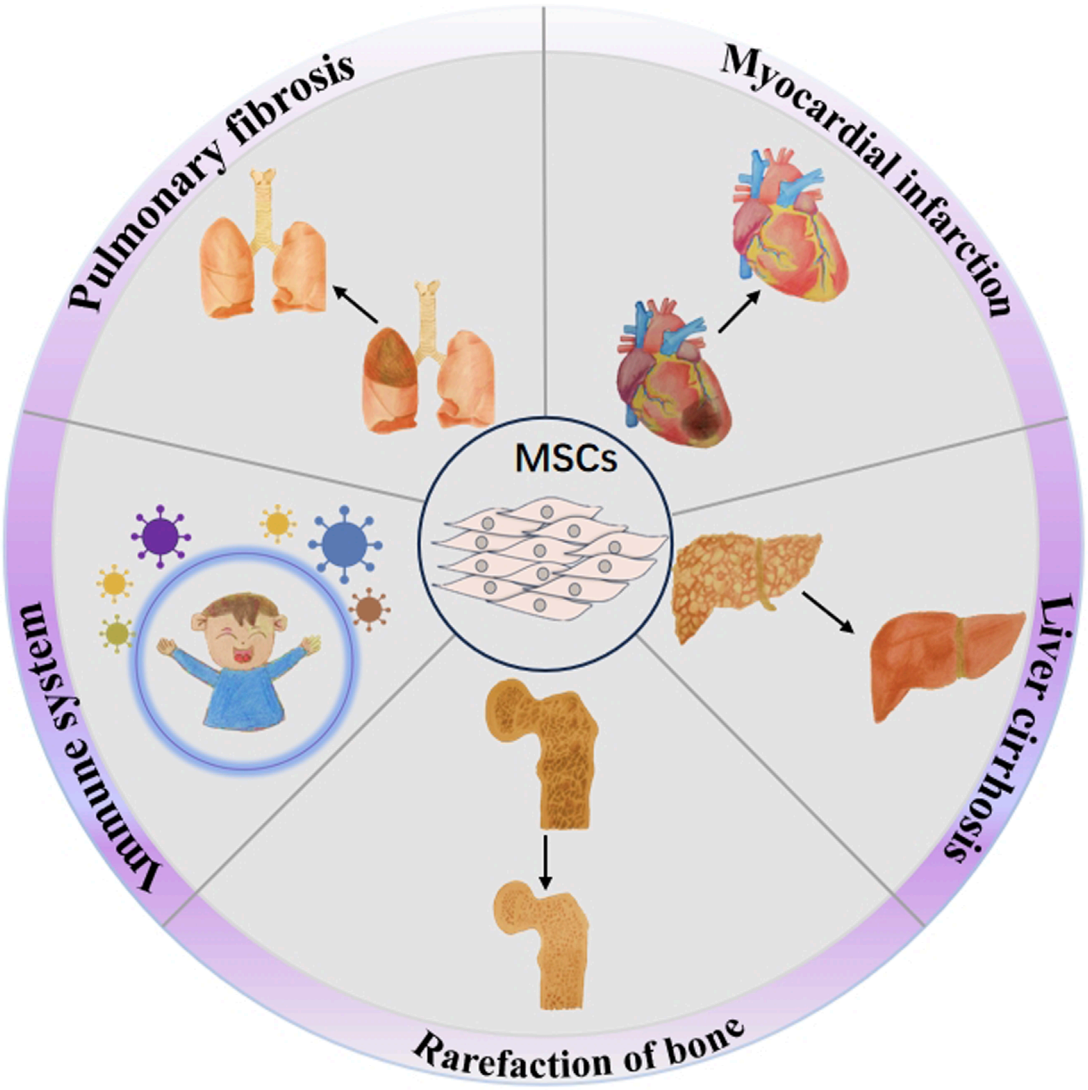

FIGURE 2
Therapeutic potential of MSCs in addressing thalassemia-related complications. The potential of MSCs to treat the complications of thalassemia including myocardial infarction, liver cirrhosis, rarefaction of bone, pulmonary fibrosis, and immune system damage.

at risk of iron overload and pulmonary fibrosis (Carnelli et al., 2003). MSCs have the potential to address these respiratory concerns by transforming into alveolar and lung epithelial cells, facilitating the repair of lung tissue, minimizing fibrosis, and enhancing overall lung performance (Doherty et al., 2024; Antoniou et al., 2010), offering a new therapeutic strategy for lung diseases associated with thalassemia. Additionally, thalassemia patients may experience endocrine system dysfunction due to long-term anemia, malnutrition, and other factors (Carsote et al., 2022). Endocrine abnormalities and MSCs can regulate the balance between the immune and endocrine systems, promote the functional recovery of endocrine glands, and improve the symptoms associated with endocrine abnormalities (Hoang et al., 2022). In addition to these challenges, individuals with thalassemia who have undergone blood transfusions, iron chelation therapy, or bone marrow transplantation might experience adverse effects resulting from these treatments (Yousuf et al., 2022). Current research on using MSCs to treat thalassemia-related complications is still in the early stages, with further exploration needed in areas such as specific treatment mechanisms, optimal administration methods, and efficacy evaluation (Li et al., 2024). Moreover, addressing the challenges related to the sourcing, preparation, and quality assurance of MSCs is essential to ensure the safety and effectiveness of these treatments (Guadix et al., 2019). In summary, MSCs demonstrate considerable potential as a therapy for various complications linked to thalassemia, and it is expected that they will provide enhanced treatment alternatives for these individuals moving forward.

5.4 Challenges in translational application: technical, ethical, and regulatory aspects

During the process of transplanting allogeneic MSCs into patients, challenges in technology, ethics, and regulations must be addressed (Velikova et al., 2024). Technically, it is

crucial to guarantee the viability, homing ability, and long-term stability of the cells, which includes optimizing cell isolation, expansion, and cryopreservation techniques (Wang and Li, 2024). Additionally, utilizing the patient's own MSCs after genetic modification and subsequent autologous transplantation offers a promising approach to potentially reduce the risk of immune rejection and GVHD (Večerić-Haler et al., 2022; Li et al., 2022b). Ethical considerations involve obtaining fully informed consent from patients, safeguarding patient privacy, and ensuring equitable access to treatment (Lo et al., 2009). Regulatory compliance requires adherence to international and local regulatory standards, navigating the approval process, and conducting long-term surveillance to evaluate the safety and efficacy of the therapy (Farmakis et al., 2022). Overcoming these challenges necessitates interdisciplinary collaboration, technological advancement, ethical review, and strict regulatory compliance to enhance the feasibility and acceptance of the treatment, ultimately aiming to improve therapeutic outcomes for patients with thalassemia.

6 Conclusion

6.1 The current status and challenges of stem cell therapy

Currently, in the area of stem cell therapy, the management of thalassemia mainly relies on hematopoietic stem cells, whereas MSCs and iPSCs demonstrate considerable promise for a range of uses (Muthu et al., 2022). Nonetheless, there are variations in both therapeutic effectiveness and safety among stem cells derived from different origins. For example, MSCs obtained from umbilical cord blood present advantages like reduced immunogenicity (Um et al., 2020); however, they may not exhibit the same level of cell activity and functionality as MSCs obtained from bone marrow (Shang et al., 2021). Despite their low immunogenicity, MSCs can still trigger immune responses under certain conditions, and the performance and longevity of stem cells *in vivo* can be affected by factors such as inflammation and hypoxia (Chen et al., 2023). Furthermore, the attributes and size of the patient cohort (including factors like age, severity of the disease, and genetic background) might also influence the comparability of the research findings (Česnik et al., 2024). The constraints of existing technologies, such as the accuracy of gene-editing instruments and inconsistencies in cell culture conditions, can also contribute to varying results (Česnik and Švajger, 2024; Mushahary et al., 2018). Although advancements have been achieved, obstacles continue to exist: iPSCs encounter problems related to epigenetic instability and the potential for tumor formation, whereas adult stem cells struggle to accomplish successful differentiation (Su et al., 2025). Ongoing assessment of long-term safety and effectiveness is essential for further verification.

6.2 The capabilities and constraints of gene-editing technology

Regarding gene-editing technology, CRISPR/Cas9 has demonstrated remarkable promise in correcting gene mutations related to thalassemia, but there are still significant differences in off-target effects and editing efficiency across different studies. Some report high editing efficiency but note potential off-target effects, whereas others manage to minimize off-target effects but still face challenges in enhancing editing efficiency (Zeng et al., 2023). These inconsistent outcomes may result from differences in experimental design, cell sources, gene-editing methods, or animal models, given that viral vectors have high delivery efficiency but are associated with risks such as immune reactions and insertional mutations, whereas nonviral delivery systems, although safer, tend to have lower efficiency (Taghdiri and Mussolino, 2024). The potential impact of the limitations of current technologies on research outcomes cannot be ignored. Despite advancements in CRISPR/Cas9 technology aimed at minimizing off-target effects, including the development of high-fidelity Cas9 variants and enhanced sgRNA designs, the total eradication of off-target effects remains a significant challenge (Guo et al., 2023).

6.3 Future directions for the development of thalassemia treatment technologies

To address these challenges, future studies should implement more standardized experimental frameworks and methods to minimize variability in outcomes while simultaneously promoting the advancement of safer and more effective gene-editing technologies and delivery systems (Lino et al., 2018). Furthermore, the significance of collaboration across multiple disciplines should not be underestimated, as integrating knowledge from gene editing, cell biology, clinical practice, and other areas can collaboratively enhance the progression of thalassemia treatment technologies (Christakopoulos et al., 2023).

Author contributions

JS: Conceptualization, Visualization, Writing – original draft, Writing – review and editing. XX: Conceptualization, Writing – original draft, Writing – review and editing. SW: Visualization, Writing – original draft. ZD: Supervision, Project administration, Writing – review and editing. PH: Supervision, Project administration, Writing – review and editing. YC: Conceptualization, Supervision, Funding acquisition, Writing – review and editing. ZH: Conceptualization, Supervision, Funding acquisition, Writing – review and editing.

Funding

The author(s) declare that financial support was received for the research and/or publication of this article. This study was supported by the National Natural Science Foundation joint fund project (U23A20498), Kweichow Moutai Hospital Research and Talent Training Fund Project (MTyk2022-01), and Guizhou Provincial Science and Technology Project (QKHCG[2024]ZD012).

Conflict of interest

The authors declare that the research was conducted in the absence of any commercial or financial relationships that could be construed as a potential conflict of interest.

Generative AI statement

The author(s) declare that Generative AI was used in the creation of this manuscript. Generative AI was used for language enhancement services. Specifically, the manuscript was refined with the assistance of Kimi, an AI developed by Moonshot AI, to improve the linguistic quality and clarity of the writing.

Publisher's note

All claims expressed in this article are solely those of the authors and do not necessarily represent those of their affiliated organizations, or those of the publisher, the editors and the reviewers. Any product that may be evaluated in this article, or claim that may be made by its manufacturer, is not guaranteed or endorsed by the publisher.

References

Abbasi, B., Shamsasenjan, K., Ahmadi, M., Beheshti, S. A., and Saleh, M. (2022). Mesenchymal stem cells and natural killer cells interaction mechanisms and potential clinical applications. *Stem Cell Res. Ther.* 13 (1), 97. doi:10.1186/s13287-022-02777-4

Adil, A., Xu, M., and Haykal, S. (2022). Recellularization of bioengineered scaffolds for vascular composite allotransplantation. *Front. Surg.* 9, 843677. doi:10.3389/fsurg.2022.843677

Afflerbach, A. K., Kiri, M. D., Detinis, T., and Maoz, B. M. (2020). Mesenchymal stem cells as a promising cell source for integration in novel In Vitro models. *Biomolecules* 10 (9), 1306. doi:10.3390/biom10091306

Agarwal, R. K., Dhanya, R., Sedai, A., Ankita, K., Parmar, L., Ramprakash, S., et al. (2023). Bone marrow quality index: a predictor of acute graft-versus-host disease in hematopoietic stem cell transplantation for thalassemia. *Transpl. Cell Ther.* 29 (11), 711.e1–711.e6. doi:10.1016/j.jtct.2023.07.014

Agrawal, S., Padmaswari, M. H., Stokes, A. L., Maxenberger, D., Reese, M., Khalil, A., et al. (2024). Optimizing Recombinant Cas9 Expression: Insights from E. coliBL21(DE3) Strains for Enhanced Protein Purification and Genome Editing. *Biomedicines.* 12 (6), 1226–711.e6. doi:10.3390/biomedicines12061226

Akbayram, S., Demir, H. A., Kılıç, A. L., Güneş, A. M., Zengin, E., Özmen, S., et al. (2022). Thalassemia-free and graft-versus-host-free survival: outcomes of hematopoietic stem cell transplantation for thalassemia major, Turkish experience. *Bone Marrow Transplant.* 57 (5), 760–767. doi:10.1038/s41409-022-01613-w

Aksoy, C., Guliyev, A., Kilic, E., Uckan, D., and Severcan, F. (2012). Bone marrow mesenchymal stem cells in patients with beta thalassemia major: molecular analysis with attenuated total reflection-Fourier transform infrared spectroscopy study as a novel method. *Stem Cells Dev.* 21 (11), 2000–2011. doi:10.1089/scd.2011.0444

Ala, M. (2023). The beneficial effects of mesenchymal stem cells and their exosomes on myocardial infarction and critical considerations for enhancing their efficacy. *Ageing Res. Rev.* 89, 101980. doi:10.1016/j.arr.2023.101980

Algeri, M., Lodi, M., and Locatelli, F. (2023). Hematopoietic stem cell transplantation in thalassemia. *Hematol. Oncol. Clin. North Am.* 37 (2), 413–432. doi:10.1016/j.hoc.2022.12.009

Ali, A., Azmat, U., Khatoon, A., Akbar, K., Murtaza, B., Ji, Z., et al. (2025). From gene editing to tumor eradication: the CRISPR revolution in cancer therapy. *Prog. Biophys. Mol. Biol.* 196, 114–131. doi:10.1016/j.pbiomolbio.2025.04.003

Ali, S., Mumtaz, S., Shakir, H. A., Khan, M., Tahir, H. M., Mumtaz, S., et al. (2021). Current status of beta-thalassemia and its treatment strategies. *Mol. Genet. Genomic Med.* 9 (12), e1788. doi:10.1002/mgg3.1788

Aljagthmi, A. A., and Abdel-Aziz, A. K. (2025). Hematopoietic stem cells: understanding the mechanisms to unleash the therapeutic potential of hematopoietic stem cell transplantation. *Stem Cell Res. Ther.* 16 (1), 60. doi:10.1186/s13287-024-04126-z

Allemailem, K. S., Almatroodi, S. A., Almatroudi, A., Alrumaihi, F., Al Abdulmonem, W., Al-Megrin, W. A. I., et al. (2023). Recent advances in genome-editing technology with CRISPR/Cas9 variants and stimuli-responsive targeting approaches within tumor cells: a future perspective of cancer management. *Int. J. Mol. Sci.* 24 (8), 7052. doi:10.3390/ijms24087052

An, C., Zhao, Y., Guo, L., Zhang, Z., Yan, C., Zhang, S., et al. (2025). Innovative approaches to boost mesenchymal stem cells efficacy in myocardial infarction therapy. *Mater Today Bio* 31, 101476. doi:10.1016/j.mtbio.2025.101476

Angastiniotis, M., and Lobitz, S. (2019). Thalassemias: an overview. *Int. J. Neonatal Screen* 5 (1), 16. doi:10.3390/ijns5010016

Angelucci, E., Matthes-Martin, S., Baronciani, D., Bernaudin, F., Bonanomi, S., Cappellini, M. D., et al. (2014). Hematopoietic stem cell transplantation in thalassemia major and sickle cell disease: indications and management recommendations from an international expert panel. *Haematologica* 99 (5), 811–20. doi:10.3324/haematol.2013.099747

Antoniou, K. M., Papadaki, H. A., Soufla, G., Kastrinaki, M. C., Damianaki, A., Koutala, H., et al. (2010). Investigation of bone marrow mesenchymal stem cells (BM MSCs) involvement in idiopathic pulmonary fibrosis (IPF). *Respir. Med.* 104 (10), 1535–1542. doi:10.1016/j.rmed.2010.04.015

Anurogo, D., Yuli Prasetyo Budi, N., Thi Ngo, M. H., Huang, Y. H., and Pawitan, J. A. (2021). Cell and gene therapy for anemia: hematopoietic stem cells and gene editing. *Int. J. Mol. Sci.* 22 (12), 6275. doi:10.3390/ijms22126275

Aprile, D., Patrone, D., Peluso, G., and Galderisi, U. (2024). Multipotent/pluripotent stem cell populations in stromal tissues and peripheral blood: exploring diversity, potential, and therapeutic applications. *Stem Cell Res. & Ther.* 15 (1), 139. doi:10.1186/s13287-024-03752-x

Aran, B., Lukovic, D., Aguilar-Quesada, R., and Veiga, A. (2020). Pluripotent stem cell regulation in Spain and the Spanish National Stem Cell Bank. *Stem Cell Res.* 48, 101956. doi:10.1016/j.scr.2020.101956

Aqmasheh, S., Shamsasanjan, K., Akbarzadehlaleh, P., Pashoutan Sarvar, D., and Timari, H. (2017). Effects of mesenchymal stem cell derivatives on hematopoiesis and hematopoietic stem cells. *Adv. Pharm. Bull.* 7(2), 165–177. doi:10.15171/apb.2017.021

Azvolinsky, A. (2019). Molecular scissors cut in on stem cells. *Nat. Med.* 25 (6), 864–866. doi:10.1038/s41591-019-0467-6

Bajwa, H., and Basit, H. (2025). "Thalassemia," in *StatPearls*. Treasure Island, FL: StatPearls Publishing LLC.

Banas, A., Teratani, T., Yamamoto, Y., Tokuhara, M., Takeshita, F., Quinn, G., et al. (2007). Adipose tissue-derived mesenchymal stem cells as a source of human hepatocytes. *Hepatology.* 46(1), 219–228. doi:10.1002/hep.21704

Bello, A. B., Canlas, K. K. V., Kim, D., Park, H., and Lee, S. H. (2024). Stepwise dual-release microparticles of BMP-4 and SCF in induced pluripotent stem cell spheroids enhance differentiation into hematopoietic stem cells. *J. Control. Release* 371, 386–405. doi:10.1016/j.jconrel.2024.06.011

Berdoukas, V., Coates, T. D., and Cabantchik, Z. I. Iron and oxidative stress in cardiomyopathy in thalassemia. (2015). *Free Radic. Biol. Med.* 88(Pt A):3–9. doi:10.1016/j.freeradbiomed.2015.07.019

Berebichez-Fridman, R., and Montero-Olvera, P. R. (2018). Sources and clinical applications of mesenchymal stem cells: State-of-the-art review. *Sultan Qaboos Univ. Med. J.* 18 (3), e264–e277. doi:10.18295/squmj.2018.18.03.002

Bernecker, C., Ackermann, M., Lachmann, N., Rohrhofer, L., Zaehres, H., Araúzo-Bravo, M. J., et al. (2019). Enhanced *Ex Vivo* generation of erythroid cells from human induced pluripotent stem cells in a simplified cell culture system with low cytokine support. *Stem Cells Dev.* 28 (23), 1540–1551. doi:10.1089/scd.2019.0132

Bhardwaj, A., Swe, K. M. M., and Sinha, N. K. (2023). Treatment for osteoporosis in people with beta-thalassaemia. *Cochrane Database Syst. Rev.* 5 (5), Cd010429. doi:10.1002/14651858.CD010429.pub3

Bhardwaj, A., Swe, K. M. M., and Sinha, N. K. (2023). Treatment for osteoporosis in people with beta-thalassaemia. *Cochrane Database Syst. Rev.* 5(5), CD010429. doi:10.1002/14651858.CD010429.pub3

Bhattacharya, S., Burridge, P. W., Kropp, E. M., Chuppa, S. L., Kwok, W. M., Wu, J. C., et al. (2014). High efficiency differentiation of human pluripotent stem cells to cardiomyocytes and characterization by flow cytometry. *J. Vis. Exp.* 23(91), 52010. doi:10.3791/52010

Biswas, S., Gomez, J., Horgan, R., Sibai, B. M., Saad, A., Powel, J. E., et al. (2023). Mirror syndrome: a systematic literature review. *Am. J. Obstet. Gynecol. MFM* 5 (9), 101067. doi:10.1016/j.ajogmf.2023.101067

Bou-Fakhredin, R., Motta, I., Cappellini, M. D., and Taher, A. T. (2023). Clinical complications and their management. *Hematol. Oncol. Clin. North Am.* 37 (2), 365–378. doi:10.1016/j.hoc.2022.12.007

Brignier, AC, and Gewirtz, AM (2010). Embryonic and adult stem cell therapy. *J. Allergy Clin. Immunol.* 125 (2), S336–44. doi:10.1016/j.jaci.2009.09.032

Butterfield, G. L., Reisman, S. J., Iglesias, N., and Gersbach, C. A. (2025). Gene regulation technologies for gene and cell therapy. *Mol. Ther.* 33 (5), 2104–2122. doi:10.1016/j.ymthe.2025.04.004

Campostrini, G., Windt, L. M., van Meer, B. J., Bellin, M., and Mummery, C. L. (2021). Cardiac tissues from stem cells: new routes to maturation and cardiac regeneration. *Circ. Res.* 128 (6), 775–801. doi:10.1161/CIRCRESAHA.121.318183

Cao, A., and Galanello, R. (2010). Beta-thalassemia. *Genet. Med.* 12 (2), 61–76. doi:10.1097/GIM.0b013e3181cd68ed

Caocci, G., La Nasa, G., d'Aloja, E., Vacca, A., Piras, E., Pintor, M., et al. (2011). Ethical issues of unrelated hematopoietic stem cell transplantation in adult thalassemia patients. *BMC Med. Ethics* 12, 4. doi:10.1186/1472-6939-12-4

Cappellini, M. D., Cohen, A., Porter, J., Taher, A., and Viprakasit, V. (2014). *Guidelines for the management of transfusion dependent thalassaemia (TDT)*. Nicosia, CY: Thalassaemia International Federation.

Carnelli, V., D'Angelo, E., Pecchiari, M., Ligorio, M., and D'Angelo, E. (2003). Pulmonary dysfunction in transfusion-dependent patients with thalassemia major. *Am. J. Respir. Crit. Care Med.* 168(2), 180–184. doi:10.1164/rccm.200211-1292OC

Cerneckis, J., Cai, H., and Shi, Y. (2024). Induced pluripotent stem cells (iPSCs): molecular mechanisms of induction and applications. *Signal Transduct. Target Ther.* 9 (1), 112. doi:10.1038/s41392-024-01809-0

Cetin, B., Erendor, F., Eksi, Y. E., Sanlioglu, A. D., and Sanlioglu, S. (2025). Advancing CRISPR genome editing into gene therapy clinical trials: progress and future prospects. *Expert Rev. Mol. Med.* 27, e16. doi:10.1017/erm.2025.10

Chen, A. P., Gao, P., Lin, L., Ashok, P., He, H., Ma, C., et al. (2024a). An improved approach to generate IL-15(+/+)/TGFβR2(-/-) iPSC-derived natural killer cells using TALEN. *Cell Rep. Methods* 4 (9), 100857. doi:10.1016/j.crmeth.2024.100857

Chen, J. S., Dagdas, Y. S., Kleinstiver, B. P., Welch, M. M., Sousa, A. A., Harrington, L. B., et al. (2017). Enhanced proofreading governs CRISPR-Cas9 targeting accuracy. *Nature* 550 (7676), 407–410. doi:10.1038/nature24268

Chen, P., Lin, W. X., and Li, S. Q. (2022). THALASSEMIA in ASIA 2021: thalassemia in Guangxi Province, People'S Republic of China. *Hemoglobin* 46 (1), 33–35. doi:10.1080/03630269.2021.2008960

Chen, W., Lv, L., Chen, N., and Cui, E. (2023). Immunogenicity of mesenchymal stromal/stem cells. *Scand. J. Immunol.* 97 (6), e13267. doi:10.1111/sji.13267

Chen, Y., Xu, Y., Chi, Y., Sun, T., Gao, Y., Dou, X., et al. (2024b). Efficacy and safety of human umbilical cord-derived mesenchymal stem cells in the treatment of refractory immune thrombocytopenia: a prospective, single arm, phase I trial. *Signal Transduct. Target Ther.* 9 (1), 102. doi:10.1038/s41392-024-01793-5

Carsote, M., Vasiliu, C., Trandafir, A. I., Albu, S. E., Dumitrascu, M. C., Popa, A., et al. (2022). New entity-thalassemic endocrine disease: major beta-thalassemia and endocrine involvement. *Diagn. (Basel)*. 12(8), 1921. doi:10.3390/diagnostics12081921

Česnik, A. B., and Švajger, U. (2024). The issue of heterogeneity of MSC-based advanced therapy medicinal products-a review. *Front. Cell Dev. Biol.* 12, 1400347. doi:10.3389/fcell.2024.1400347

Česnik, A. B., and Švajger, U. (2024). The issue of heterogeneity of MSC-based advanced therapy medicinal products-a review. *Front. Cell. Dev. Biol.* 12, 1400347. doi:10.3389/fcell.2024.1400347

Christakopoulos, G. E., Telange, R., Yen, J., and Weiss, M. J. (2023). Gene therapy and gene editing for β-Thalassemia. *Hematol. Oncol. Clin. North Am.* 37 (2), 433–447. doi:10.1016/j.hoc.2022.12.012

Chukwuemeka, C. G., Ndubueze, C. W., Kolawole, A. V., Joseph, J. N., Oladipo, I. H., Ofoezie, E. F., et al. (2025). In vitro erythropoiesis: the emerging potential of induced pluripotent stem cells (iPSCs). *Blood Sci.* 7 (1), e00215. doi:10.1097/BS9.0000000000000215

Coates, T. D. (2014). Physiology and pathophysiology of iron in hemoglobin-associated diseases. *Free Radic. Biol. Med.* 72, 23–40. doi:10.1016/j.freeradbiomed.2014.03.039

Concordet, J. P., and Haeussler, M. (2018). CRISPOR: intuitive guide selection for CRISPR/Cas9 genome editing experiments and screens. *Nucleic Acids Res.* 46 (W1), W242–W245. doi:10.1093/nar/gky354

Crippa, S., Rossella, V., Aprile, A., Silvestri, L., Rivis, S., Scaramuzza, S., et al. (2019). Bone marrow stromal cells from β-thalassemia patients have impaired hematopoietic supportive capacity. *J. Clin. Invest* 129 (4), 1566–1580. doi:10.1172/JCI123191

Demirci, S., Leonard, A., and Tisdale, J. F. (2020). Hematopoietic stem cells from pluripotent stem cells: clinical potential, challenges, and future perspectives. *Stem Cells Transl. Med.* 9 (12), 1549–1557. doi:10.1002/sctm.20-0247

Demosthenous, C., Vlachaki, E., Apostolou, C., Eleftheriou, P., Kotsiafti, A., Vetsiou, E., et al. (2019). Beta-thalassemia: renal complications and mechanisms: a narrative review. *Hematology* 24 (1), 426–438. doi:10.1080/16078454.2019.1599096

Deltcheva, E., Chylinski, K., Sharma, C. M., Gonzales, K., Chao, Y., and Pirzada, Z. A. (2011). CRISPR RNA maturation by trans-encoded small RNA and host factor RNase III. *Nature* 471 (7340), 602–7. doi:10.3390/pharmaceutics14040791

Deo, D., Marchioni, M., and Rao, P. (2022). Mesenchymal stem/stromal cells in organ transplantation. *Pharmaceutics* 14 (4), 791. doi:10.3390/pharmaceutics14040791

De Simone, G., Quattrocchi, A., Mancini, B., di Masi, A., Nervi, C., and Ascenzi, P. (2022). Thalassemias: from gene to therapy. *Mol. Asp. Med.* 84, 101028. doi:10.1016/j.mam.2021.101028

Dezan, M. G. F., Cavalcante, L. N., Cotrim, H. P., and Lyra, A. C. (2023). Hepatobiliary disease after bone marrow transplant. *Expert Rev. Gastroenterol. Hepatol.* 17 (2), 129–143. doi:10.1080/17474124.2023.2169671

Dobner, J., Diecke, S., Krutmann, J., Prigione, A., and Rossi, A. (2024). Reassessment of marker genes in human induced pluripotent stem cells for enhanced quality control. *Nat. Commun.* 15 (1), 8547. doi:10.1038/s41467-024-52922-1

Doench, J. G., Fusi, N., Sullender, M., Hegde, M., Vaimberg, E. W., Donovan, K. F., et al. Optimized sgRNA design to maximize activity and minimize off-target effects of CRISPR-Cas9. (2016). *Nat. Biotechnol.* 34(2), 184–191. doi:10.1038/nbt.3437

Doench, J. G., Fusi, N., Sullender, M., Hegde, M., Vaimberg, E. W., Donovan, K. F., et al. (2016). Optimized sgRNA design to maximize activity and minimize off-target effects of CRISPR-Cas9. *Nat. Biotechnol.* 34 (2), 184–191. doi:10.1038/nbt.3437

Doherty, D. F., Roets, L. E., Dougan, C. M., Brown, R. R., Hawthorne, I. J., O'Kane, C., et al. (2024). Mesenchymal stromal cells reduce inflammation and improve lung function in a mouse model of cystic fibrosis lung disease. *Sci. Rep.* 14 (1), 30899. doi:10.1038/s41598-024-81276-3

Dordevic, A., Mrakovcic-Sutic, I., Pavlovic, S., Ugrin, M., and Roganovic, J. (2025). Beta thalassemia syndromes: new insights. *World J. Clin. Cases* 13 (10), 100223. doi:10.12998/wjcc.v13.i10.100223

Du, Y., Liu, Y., Hu, J., Peng, X., and Liu, Z. (2023). CRISPR/Cas9 systems: delivery technologies and biomedical applications. *Asian J. Pharm. Sci.* 18 (6), 100854. doi:10.1016/j.ajps.2023.100854

Evangelidis, P., Venou, T. M., Fani, B., Vlachaki, E., Gavriilaki, E., and on behalf of the International Hemoglobinopathy Research Network INHERENT (2023). Endocrinopathies in hemoglobinopathies: what is the role of iron? *Int. J. Mol. Sci.* 24 (22), 16263. doi:10.3390/ijms242216263

Farashi, S., and Harteveld, C. L. (2018). Molecular basis of α-thalassemia. *Blood Cells Mol. Dis.* 70, 43–53. doi:10.1016/j.bcmd.2017.09.004

Farmakis, D., Porter, J., Taher, A., Domenica Cappellini, M., Angastiniotis, M., and Eleftheriou, A. (2022). 2021 thalassaemia international Federation guidelines for the management of transfusion-dependent thalassemia. *Hemasphere* 6 (8), e732. doi:10.1097/HS9.0000000000000732

Fichter, K. M., Setayesh, T., and Malik, P. (2023). Strategies for precise gene edits in mammalian cells. *Mol. Ther. Nucleic Acids* 32, 536–552. doi:10.1016/j.omtn.2023.04.012

Forni, G. L., Gianesin, B., Musallam, K. M., Longo, F., Rosso, R., Lisi, R., et al. (2023). Overall and complication-free survival in a large cohort of patients with β-thalassemia major followed over 50 years. *Am. J. Hematol.* 98 (3), 381–387. doi:10.1002/ajh.26798

Frangoul, H., Altshuler, D., Cappellini, M. D., Chen, Y. S., Domm, J., Eustace, B. K., et al. (2021). CRISPR-Cas9 gene editing for sickle cell disease and β-Thalassemia. *N. Engl. J. Med.* 384 (3), 252–260. doi:10.1056/NEJMoa2031054

Gan, L., Liu, Y., Cui, D., Pan, Y., Zheng, L., and Wan, M. (2020). Dental tissue-derived human mesenchymal stem cells and their potential in therapeutic application. *Stem Cells Int.* 2020, 8864572. doi:10.1155/2020/8864572

Gao, X., Zhou, C., Feng, Y., Ye, B., Zhao, Z., Qi, L., et al. (2025). Research progress of gene editing technology in neurological diseases. *Gene* 962, 149534. doi:10.1016/j.gene.2025.149534

Gaudelli, N. M., Komor, A. C., Rees, H. A., Packer, M. S., Badran, A. H., Bryson, D. I., et al. (2017). Programmable base editing of A•T to G•C in genomic DNA without DNA cleavage. *Nature* 551 (7681), 464–471. doi:10.1038/nature24644

Gaudio, A., Morabito, N., Catalano, A., Rapisarda, R., Xourafa, A., and Lasco, A. (2019). Pathogenesis of thalassemia major-associated osteoporosis: a review with insights from clinical experience. *J. Clin. Res. Pediatr. Endocrinol.* 11 (2), 110–117. doi:10.4274/jcrpe.galenos.2018.2018.0074

Gholami Farashah, M. S., Mohammadi, A., Javadi, M., Soleimani Rad, J., Shakouri, S. K., Meshgi, S., et al. (2023). Bone marrow mesenchymal stem cells' osteogenic potential: superiority or non-superiority to other sources of mesenchymal stem cells? *Cell Tissue Bank.* 24 (3), 663–681. doi:10.1007/s10561-022-10066-w

Gluckman, E., Cappelli, B., Bernaudin, F., Labopin, M., Volt, F., Carreras, J., et al. (2017). Sickle cell disease: an international survey of results of HLA-identical sibling hematopoietic stem cell transplantation. *Blood* 129 (11), 1548–1556. doi:10.1182/blood-2016-10-745711

Grace, C. S., Mikkola, H. K. A., Dou, D. R., Calvanese, V., Ronn, R. E., and Purton, L. E. (2018). Protagonist or antagonist? The complex roles of retinoids in the regulation of hematopoietic stem cells and their specification from pluripotent stem cells. *Exp. Hematol.* 65, 1–16. doi:10.1016/j.exphem.2018.06.287

Greco, F., Cosentino, M., and Marino, F. (2024). The Italian breakthrough in CRISPR trials for rare diseases: a focus on beta-thalassemia and sickle cell disease treatment. *Front. Med. (Lausanne)* 11, 1356578. doi:10.3389/fmed.2024.1356578

Greely, H. T. (2019). CRISPR'd babies: human germline genome editing in the 'He Jiankui affair. *J. Law Biosci.* 6 (1), 111–183. doi:10.1093/jlb/lsz010

Guadix, J. A., López-Beas, J., Clares, B., Soriano-Ruiz, J. L., Zugaza, J. L., and Gálvez-Martín, P. (2019). Principal criteria for evaluating the quality, safety and efficacy of hmsc-based products in clinical practice: current approaches and challenges. *Pharmaceutics.* 11 (11), 552. doi:10.3390/pharmaceutics11110552

Guo, C., Ma, X., Gao, F., and Guo, Y. (2023). Off-target effects in CRISPR/Cas9 gene editing. *Front. Bioeng. Biotechnol.* 11, 1143157. doi:10.3389/fbioe.2023.1143157

Gupta, A. O., and Wagner, J. E. (2020). Umbilical cord blood transplants: current status and evolving therapies. *Front. Pediatr.* 8, 570282. doi:10.3389/fped.2020.570282

Hackett, N. R., and Crystal, R. G. (2025). Four decades of adenovirus gene transfer vectors: history and current use. *Mol. Ther.* 33 (5), 2192–2204. doi:10.1016/j.ymthe.2025.03.062

Hardouin, G., Miccio, A., and Brusson, M. (2025). Gene therapy for β-thalassemia: current and future options. *Trends Mol. Med.* 31 (4), 344–358. doi:10.1016/j.molmed.2024.12.001

Harewood, J., and Azevedo, A. M. (2024). "Alpha thalassemia," in *StatPearls*. Treasure Island, FL: StatPearls Publishing LLC.

Hoang, D. M., Pham, P. T., Bach, T. Q., Ngo, A. T. L., Nguyen, Q. T., Phan, T. T. K., et al. (2022). Stem cell-based therapy for human diseases. *Signal Transduct. Target Ther.* 7 (1), 272. doi:10.1038/s41392-022-01134-4

Hoang, D. M., Pham, P. T., Bach, T. Q., Ngo, A. T. L., Nguyen, Q. T., Phan, T. T. K., et al.(2022). Stem cell-based therapy for human diseases. *Signal Transduct. Target Ther.* 7(1), 272. doi:10.1038/s41392-022-01134-4

Hoang, V. T., Nguyen, Q. T., Phan, T. T. K., Pham, T. H., Dinh, N. T. H., Anh, L. P. H., et al. (2025). Tissue engineering and regenerative medicine: perspectives and challenges. *MedComm (2020)* 6 (5), e70192. doi:10.1002/mco2.70192

Hodroj, M. H., Akiki, N., Bou-Fakhredin, R., and Taher, A. T. (2023). Beta-thalassemia: is cure still a dream? *Minerva Med.* 114 (6), 850–860. doi:10.23736/S0026-4806.23.08501-4

Hordyjewska, A., Popiołek, Ł., and Horecka, A. (2015). Characteristics of hematopoietic stem cells of umbilical cord blood. *Cytotechnology* 67 (3), 387–96. doi:10.1007/s10616-014-9796-y

Hryhorowicz, M., Lipiński, D., and Zeyland, J. (2023). Evolution of CRISPR/Cas systems for precise genome editing. *Int. J. Mol. Sci.* 24 (18), 14233. doi:10.3390/ijms241814233

Hsu, M. N., Liao, H. T., Truong, V. A., Huang, K. L., Yu, F. J., Chen, H. H., et al. (2019). CRISPR-based activation of endogenous neurotrophic genes in adipose stem cell sheets to stimulate peripheral nerve regeneration. *Theranostics* 9 (21), 6099–6111. doi:10.7150/thno.36790

Hussen, B. M., Najmadden, Z. B., Abdullah, S. R., Rasul, M. F., Mustafa, S. A., Ghafouri-Fard, S., et al. (2024). CRISPR/Cas9 gene editing: a novel strategy for fighting drug resistance in respiratory disorders. *Cell. Commun. Signal.* 22(1):329. doi:10.1186/s12964-024-01713-8

Huang, C. Y., Li, L. H., Hsu, W. T., Cheng, Y. C., Nicholson, M. W., Liu, C. L., et al. (2020). Copy number variant hotspots in Han Taiwanese population induced pluripotent stem cell lines - lessons from establishing the Taiwan human disease iPSC Consortium Bank. *J. Biomed. Sci.* 27 (1), 92. doi:10.1186/s12929-020-00682-7

Jagasia, M., Arora, M., Flowers, M. E. D., Chao, N. J., McCarthy, P. L., Cutler, C. S., et al. (2012). Risk factors for acute GVHD and survival after hematopoietic cell transplantation. *Blood* 119 (1), 296–307. doi:10.1182/blood-2011-06-364265

Jeong, S., An, B., Kim, J. H., Han, H. W., Kim, J. H., Heo, H. R., et al. (2020a). BMP4 and perivascular cells promote hematopoietic differentiation of human pluripotent stem cells in a differentiation stage-specific manner. *Exp. & Mol. Med.* 52 (1), 56–65. doi:10.1038/s12276-019-0357-5

Jeong, Y. K., Song, B., and Bae, S. (2020b). Current status and challenges of DNA base editing tools. *Mol. Ther.* 28 (9), 1938–1952. doi:10.1016/j.ymthe.2020.07.021

Jiang, Y., Zhang, P., Zhang, X., Lv, L., and Zhou, Y. (2021). Advances in mesenchymal stem cell transplantation for the treatment of osteoporosis. *Cell. Prolif.* 54(1), e12956. doi:10.1111/cpr.12956

Jinek, M., Chylinski, K., Fonfara, I., Hauer, M., Doudna, J. A., and Charpentier, E. (2012). A programmable dual-RNA-guided DNA endonuclease in adaptive bacterial immunity. *Science* 337 (6096), 816–821. doi:10.1126/science.1225829

John, T., and Czechowicz, A. (2025). Clinical hematopoietic stem cell-based gene therapy. *Mol. Ther.* 33, 2663–2678. doi:10.1016/j.ymthe.2025.04.029

Johnstone, B. H., Messner, F., Brandacher, G., and Woods, E. J. (2021). A large-scale bank of organ donor bone marrow and matched mesenchymal stem cells for promoting immunomodulation and transplant tolerance. *Front. Immunol.* 12, 622604. doi:10.3389/fimmu.2021.622604

Johnstone, B. H., Miller, H. M., Beck, M. R., Gu, D., Thirumala, S., LaFontaine, M., et al. (2020). Identification and characterization of a large source of primary mesenchymal stem cells tightly adhered to bone surfaces of human vertebral body marrow cavities. *Cytotherapy* 22 (11), 617–628. doi:10.1016/j.jcyt.2020.07.003

Joseph, A. M., Karas, M., Ramadan, Y., Joubran, E., and Jacobs, R. J. (2022). Ethical perspectives of therapeutic human genome editing from multiple and diverse viewpoints: a scoping review. *Cureus* 14 (11), e31927. doi:10.7759/cureus.31927

Karponi, G., and Zogas, N. (2019). Gene therapy for beta-thalassemia: updated perspectives. *Appl. Clin. Genet.* 12, 167–180. doi:10.2147/TACG.S178546

Kattamis, A., Forni, G. L., Aydinok, Y., and Viprakasit, V. (2020). Changing patterns in the epidemiology of β-thalassemia. *Eur J Haematol* 105 (6), 692–703. doi:10.1111/ejh.13512

Kattamis, A., Kwiatkowski, J. L., and Aydinok, Y. (2022). Thalassaemia. *Lancet* 399 (10343), 2310–2324. doi:10.1016/S0140-6736(22)00536-0

Kavyasudha, C., Macrin, D., ArulJothi, K. N., Joseph, J. P., Harishankar, M. K., and Devi, A. (2018). Clinical applications of induced pluripotent stem cells - Stato attuale. *Adv. Exp. Med. Biol.* 1079, 127–149. doi:10.1007/5584_2018_173

Kayama, A., and Eto, K. (2024). Mass production of iPSC-derived platelets toward the clinical application. *Regen. Ther.* 25, 213–219. doi:10.1016/j.reth.2023.12.009

Kazemian, P., Yu, S. Y., Thomson, S. B., Birkenshaw, A., Leavitt, B. R., and Ross, C. J. D. (2022). Lipid-nanoparticle-based delivery of CRISPR/Cas9 genome-editing components. *Mol. Pharm.* 19 (6), 1669–1686. doi:10.1021/acs.molpharmaceut.1c00916

Khan, I., and Shaikh, H. (2023). "Beta thalassemia major (Cooley Anemia)," in *StatPearls*. Treasure Island, FL: StatPearls Publishing LLC.

Khiabani, A., Kohansal, M. H., Keshavarzi, A., Shahraki, H., Kooshesh, M., Karimzade, M., et al. (2023). CRISPR/Cas9, a promising approach for the treatment of β-thalassemia: a systematic review. *Mol. Genet. Genomics* 298 (1), 1–11. doi:10.1007/s00438-022-01978-z

Kim, J. H., Jo, H. Y., Ha, H. Y., and Kim, Y. O. (2021). Korea national stem cell bank. *Stem Cell Res.* 53, 102270. doi:10.1016/j.scr.2021.102270

Kim, M., Jang, H. J., Baek, S. Y., Choi, K. J., Han, D. H., and Sung, J. S. (2023). Regulation of base excision repair during adipogenesis and osteogenesis of bone marrow-derived mesenchymal stem cells. *Sci. Rep.* 13 (1), 16384. doi:10.1038/s41598-023-43737-z

Kindwall-Keller, T. L., and Ballen, K. K. (2020). Umbilical cord blood: the promise and the uncertainty. *Stem Cells Transl. Med.* 9 (10), 1153–1162. doi:10.1002/sctm.19-0288

Kleinstiver, B. P., Prew, M. S., Tsai, S. Q., Topkar, V. V., Nguyen, N. T., Zheng, Z., et al. (2015). Engineered CRISPR-Cas9 nucleases with altered PAM specificities. *Nature* 523 (7561), 481–485. doi:10.1038/nature14592

Kleinstiver, B. P., Pattanayak, V., Prew, M. S., Tsai, S. Q., Nguyen, N. T., Zheng, Z., et al. (2016). High-fidelity CRISPR-Cas9 nucleases with no detectable genome-wide off-target effects. *Nature*. 529(7587), 490–495. doi:10.1038/nature16526

Komor, A. C., Kim, Y. B., Packer, M. S., Zuris, J. A., and Liu, D. R. (2016). Programmable editing of a target base in genomic DNA without double-stranded DNA cleavage. *Nature* 533 (7603), 420–424. doi:10.1038/nature17946

Kolf, C. M., Cho, E., and Tuan, R. S. (2007). Mesenchymal stromal cells. Biology of adult mesenchymal stem cells: regulation of niche, self-renewal and differentiation. *Arthritis Res. Ther.* 9(1), 204. doi:10.1186/ar2116

Körbling, M., and Freireich, E. J. (2011). Twenty-five years of peripheral blood stem cell transplantation. *Blood* 117 (24), 6411–6416. doi:10.1182/blood-2010-12-322214

Kuca-Warnawin, E., Plebańczyk, M., Bonek, K., and Kontny, E. (2021). Inhibition of allogeneic and autologous T cell proliferation by adipose-derived mesenchymal stem cells of ankylosing spondylitis patients. *Stem Cells Int.* 2021, 6637328. doi:10.1155/2021/6637328

Kuci, Z., Jordan, C., Wehner, S., Sörensen, J., Jarisch, A., Salzmann-Manrique, E., et al. (2020). The phenotype and functional activity of mesenchymal stromal cells in pediatric patients with non-malignant hematological diseases. *Cells* 9 (2), 431. doi:10.3390/cells9020431

Langer, A. L., Adam, M. P., Feldman, J., Mirzaa, G. M., Pagon, R. A., Wallace, S. E., et al. (1993). "Beta-thalassemia," in *GeneReviews (®)*. Editor M. P. Adam, Seattle, WA: University of Washington.

Lapillonne, H., Kobari, L., Mazurier, C., Tropel, P., Giarratana, M. C., Zanella-Cleon, I., et al. (2010). Red blood cell generation from human induced pluripotent stem cells: perspectives for transfusion medicine. *Haematologica* 95 (10), 1651–1659. doi:10.3324/haematol.2010.023556

Ledford, H. (2020). CRISPR gene editing in human embryos wreaks chromosomal mayhem. *Nature* 583 (7814), 17–18. doi:10.1038/d41586-020-01906-4

Lee, H., and Son, M. Y. (2021). Current challenges associated with the use of human induced pluripotent stem cell-derived organoids in regenerative medicine. *Int. J. Stem Cells* 14 (1), 9–20. doi:10.15283/ijsc20140

Levy, O., Kuai, R., Siren, E. M. J., Bhere, D., Milton, Y., Nissar, N., et al. (2020). Shattering barriers toward clinically meaningful MSC therapies. *Sci. Adv.* 6 (30), eaba6884. doi:10.1126/sciadv.aba6884

Li, L., Hu, S., and Chen, X. (2018). Non-viral delivery systems for CRISPR/Cas9-based genome editing: challenges and opportunities. *Biomaterials* 171, 207–218. doi:10.1016/j.biomaterials.2018.04.031

Li, L., Yi, H., Liu, Z., Long, P., Pan, T., Huang, Y., et al. (2022a). Genetic correction of concurrent α- and β-thalassemia patient-derived pluripotent stem cells by the CRISPR-Cas9 technology. *Stem Cell Res. Ther.* 13 (1), 102. doi:10.1186/s13287-022-02768-5

Li, T., Yang, Y., Qi, H., Cui, W., Zhang, L., Fu, X., et al. (2023). CRISPR/Cas9 therapeutics: progress and prospects. *Signal Transduct. Target Ther.* 8 (1), 36. doi:10.1038/s41392-023-01309-7

Li, Y., Hao, J., Hu, Z., Yang, Y. G., Zhou, Q., Sun, L., et al. (2022b). Current status of clinical trials assessing mesenchymal stem cell therapy for graft versus host disease: a systematic review. *Stem Cell Res. Ther.* 13 (1), 93. doi:10.1186/s13287-022-02751-0

Li, Z., and Yang, L. (2023). Current status of producing autologous hematopoietic stem cells. *Curr. Res. Transl. Med.* 71 (1), 103377. doi:10.1016/j.retram.2023.103377

Li, Z., Yao, X., Zhang, J., Yang, J., Ni, J., and Wang, Y. (2024). Exploring the bone marrow micro environment in thalassemia patients: potential therapeutic alternatives. *Front. Immunol.* 15, 1403458. doi:10.3389/fimmu.2024.1403458

Lidonnici, M. R., Scaramuzza, S., and Ferrari, G. (2023). Gene therapy for hemoglobinopathies. *Hum. Gene Ther.* 34 (17-18), 793–807. doi:10.1089/hum.2023.138

Lino, C. A., Harper, J. C., Carney, J. P., and Timlin, J. A. (2018). Delivering CRISPR: a review of the challenges and approaches. *Drug Deliv.* 25 (1), 1234–1257. doi:10.1080/10717544.2018.1474964

Liu, S., Shi, J., Lin, Y., Luo, H., Wu, Y., Yan, J., et al. (2024). A sandwich-type dual-mode biosensor based on graphdiyne and DNA nanoframework for ultra-sensitive detection of CD142 gene. *Biosens. Bioelectron.* 248, 115962. doi:10.1016/j.bios.2023.115962

Lo, B., and Parham, L. (2009). Ethical issues in stem cell research. *Endocr. Rev.* 30(3):204–213. doi:10.1210/er.2008-0031

Lotfi, M., Morshedi Rad, D., Mashhadi, S. S., Ashouri, A., Mojarrad, M., Mozaffari-Jovin, S., et al. (2023). Recent advances in CRISPR/Cas9 delivery approaches for therapeutic gene editing of stem cells. *Stem Cell. Rev. Rep.* 19(8), 2576–2596. doi:10.1007/s12015-023-10585-3

Mahmoud, H. K., Elhaddad, A. M., Fahmy, O. A., Samra, M. A., Abdelfattah, R. M., El-Nahass, Y. H., et al. (2015). Allogeneic hematopoietic stem cell transplantation for non-malignant hematological disorders. *J. Adv. Res.* 6 (3), 449–458. doi:10.1016/j.jare.2014.11.001

Main, H., Hedenskog, M., Acharya, G., Hovatta, O., and Lanner, F. (2020). Karolinska institutet human embryonic stem cell bank. *Stem Cell Res.* 45, 101810. doi:10.1016/j.scr.2020.101810

Makis, A., Voskaridou, E., Papassotiriou, I., and Hatzimichael, E. (2021). Novel therapeutic advances in β-Thalassemia. *Biol. (Basel)* 10 (6), 546. doi:10.3390/biology10060546

Malik, V., and Wang, J. (2022). Pursuing totipotency: authentic totipotent stem cells in culture. *Trends Genet.* 38 (7), 632–636. doi:10.1016/j.tig.2022.03.012

Mansouri, N., Willis, G. R., Fernandez-Gonzalez, A., Reis, M., Nassiri, S., Mitsialis, S. A., et al. (2019). Mesenchymal stromal cell exosomes prevent and revert experimental pulmonary fibrosis through modulation of monocyte phenotypes. *JCI Insight* 4 (21), e128060. doi:10.1172/jci.insight.128060

Marziali, M., Isgrò, A., Gaziev, J., Lucarelli, G., Nassiri, S., Mitsialis, S. A., et al. (2009). Hematopoietic stem cell transplantation in thalassemia and sickle cell disease. Unicenter experience in a multi-ethnic population. *Mediterr J Hematol Infect Dis* 1 (1), e2009027. doi:10.4084/MJHID.2009.027

Maurissen, T. L., and Woltjen, K. (2020). Synergistic gene editing in human iPS cells via cell cycle and DNA repair modulation. *Nat Commun* 11 (1), 2876. doi:10.1038/s41467-020-16643-5

Mattis, V. B., and Svendsen, C. N. (2011). Induced pluripotent stem cells: a new revolution for clinical neurology? *Lancet Neurology* 10 (4), 383–394. doi:10.1016/S1474-4422(11)70022-9

McTague, A., Rossignoli, G., Ferrini, A., Barral, S., and Kurian, M. A. (2021). Genome editing in iPSC-Based neural systems: from disease models to future therapeutic strategies. *Front. Genome* 3, 630600. doi:10.3389/fgeed.2021.630600

Meng, X., Leslie, P., Zhang, Y., and Dong, J. (2014). Stem cells in a three-dimensional scaffold environment. *SpringerPlus* 3, 80. doi:10.1186/2193-1801-3-80

Mettananda, S., Gibbons, R. J., and Higgs, D. R. (2015). α-Globin as a molecular target in the treatment of β-thalassemia. *Blood* 125 (24), 3694–3701. doi:10.1182/blood-2015-03-633594

Mousaei Ghasroldasht, M., Seok, J., Park, H. S., Liakath Ali, F. B., and Al-Hendy, A. (2022). Stem cell therapy: from idea to clinical practice. *Int. J. Mol. Sci.* 23 (5), 2850. doi:10.3390/ijms23052850

Mousavi, E., Khosravi, A., Sedigh, S. S., Mayanei, S. A. T., Banakar, M., Karimzadeh, M., et al. (2023). Exosomes derived from mesenchymal stem cells: heralding a new treatment for periodontitis? *Tissue Cell* 82, 102070. doi:10.1016/j.tice.2023.102070

Musallam, K. M., Cappellini, M. D., Coates, T. D., Kuo, K. H. M., Al-Samkari, H., Sheth, S., et al. (2024). Alpha-thalassemia: a practical overview. *Blood Rev.* 64, 101165. doi:10.1016/j.blre.2023.101165

Mushahary, D., Spittler, A., Kasper, C., Weber, V., and Charwat, V. (2018). Isolation, cultivation, and characterization of human mesenchymal stem cells. *Cytom. A* 93 (1), 19–31. doi:10.1002/cyto.a.23242

Musharraf, S. G., Iqbal, A., Ansari, S. H., Parveen, S., Khan, I. A., and Siddiqui, A. J. (2017). β-Thalassemia patients revealed a significant change of untargeted metabolites in comparison to healthy individuals. *Sci. Rep.* 7, 42249. doi:10.1038/srep42249

Muthu, S., Jeyaraman, M., Kotner, M. B., Jeyaraman, N., Rajendran, R. L., Sharma, S., et al. (2022). Evolution of mesenchymal stem cell therapy as an advanced therapeutic medicinal product (ATMP)-an Indian perspective. *Bioengineering (Basel)* 9 (3), 111. doi:10.3390/bioengineering9030111

Naeem, M., Majeed, S., Hoque, M. Z., and Ahmad, I. (2020). Latest developed strategies to minimize the off-target effects in CRISPR-Cas-Mediated genome editing. *Cells* 9 (7), 1608. doi:10.3390/cells9071608

Naiisseh, B., Papasavva, P. L., Papaioannou, N. Y., Tomazou, M., Koniali, L., Felekis, X., et al. (2024). Context base editing for splice correction of IVSI-110 β-thalassemia. *Mol. Ther. Nucleic Acids* 35 (2), 102183. doi:10.1016/j.omtn.2024.102183

Naso, M. F., Tomkowicz, B., Perry, W. L., and Strohl, W. R. (2017). Adeno-associated virus (AAV) as a vector for gene therapy. *BioDrugs* 31 (4), 317–334. doi:10.1007/s40259-017-0234-5

Needs, T., Gonzalez-Mosquera, L. F., and Lynch, D. T. (2024). "Beta thalassemia," in *StatPearls*. Treasure Island, FL: StatPearls Publishing LLC.

Ng, E. S., Sarila, G., Li, J. Y., Edirisinghe, H. S., Saxena, R., Sun, S., et al. (2024). Long-term engrafting multilineage hematopoietic cells differentiated from human induced pluripotent stem cells. *Nat Biotechnol.* doi:10.1038/s41587-024-02360-7

Niu, X., He, W., Song, B., Ou, Z., Fan, D., Chen, Y., et al. (2016). Combining single strand oligodeoxynucleotides and CRISPR/Cas9 to correct gene mutations in β-Thalassemia-induced pluripotent stem cells. *J. Biol. Chem.* 291 (32), 16576–16585. doi:10.1074/jbc.M116.719237

Oguro, H. (2019). Generation of Hematopoietic Stem and Progenitor Cells from Human Pluripotent Stem Cells. *Methods Mol Biol.* 2048, 245–257. doi:10.1007/978-1-4939-9728-2_19

Oikonomopoulou, C., and Goussetis, E. (2021). HSCT remains the only cure for patients with transfusion-dependent thalassemia until gene therapy strategies are proven to be safe. *Bone Marrow Transpl.* 56 (12), 2882–2888. doi:10.1038/s41409-021-01461-0

O'Reilly, R. J. (1983). Allogenic bone marrow transplantation: current status and future directions. *Blood* 62 (5), 941–964. doi:10.1182/blood.v62.5.941.941

Origa, R. (2017). β-Thalassemia. *Genet. Med.* 19 (6), 609–619. doi:10.1038/gim.2016.173

Ortuño-Costela, M. C., Pinzani, M., and Vallier, L. (2025). Cell therapy for liver disorders: past, present and future. *Nat. Rev. Gastroenterol. Hepatol.* 22 (5), 329–342. doi:10.1038/s41575-025-01050-2

O'Shea, O., and Abranches, E. (2020). UK stem cell bank. *Stem Cell Res.* 49, 102019. doi:10.1016/j.scr.2020.102019

Ottaviano, G., and Qasim, W. (2025). Current landscape of vector safety and genotoxicity after hematopoietic stem or immune cell gene therapy. *Leukemia* 39, 1325–1333. doi:10.1038/s41375-025-02585-8

Ou, Z., Niu, X., He, W., Chen, Y., Song, B., Xian, Y., et al.(2016). The combination of CRISPR/Cas9 and iPSC technologies in the gene therapy of human β-thalassemia in mice. *Sci. Rep.* 6, 32463. doi:10.1038/srep32463

Paolini Sguazzi, G., Muto, V., Tartaglia, M., Bertini, E., and Compagnucci, C. (2021). Induced pluripotent stem cells (iPSCs) and gene therapy: a new era for the treatment of neurological diseases. *Int. J. Mol. Sci.* 22 (24), 13674. doi:10.3390/ijms222413674

Papastamataki, M., Delaporta, P., Premetis, E., Kattamis, A., Ladis, V., and Papassotiriou, I. (2010). Evaluation of liver fibrosis in patients with thalassemia: the important role of hyaluronic acid. *Blood Cells, Mol. Dis.* 45 (3), 215–218. doi:10.1016/j.bcmd.2010.06.002

Parikh, M. C. (2025). Gene editing: developments, ethical considerations, and future directions. *J. Community Hosp. Intern Med. Perspect.* 15(1), 1–4. doi:10.55729/2000-9666.1445

Park, A., Hong, P., Won, S. T., Thibault, P. A., Vigant, F., Oguntuyo, K. Y., et al. (2016). Sendai virus, an RNA virus with no risk of genomic integration, delivers CRISPR/Cas9 for efficient gene editing. *Mol. Ther. Methods Clin. Dev.* 3, 16057. doi:10.1038/mtm.2016.57

Park, S. H., and Bao, G. (2021). CRISPR/Cas9 gene editing for curing sickle cell disease. *Transfus. Apher. Sci.* 60 (1), 103060. doi:10.1016/j.transci.2021.103060

Poetsch, M. S., Strano, A., and Guan, K. (2022). Human induced pluripotent stem cells: from cell origin, genomic stability, and epigenetic memory to translational medicine. *Stem Cells* 40 (6), 546–555. doi:10.1093/stmcls/sxac020

Rahman, M. S., Qi, G., Li, Q., Liu, X., Bai, J., Chen, M., et al. (2025). Three-Dimensional trilineage differentiation conditions for human induced pluripotent stem cells. *Bioeng. (Basel)*. 12(5), 503. doi:10.3390/bioengineering12050503

Rees, H. A., and Liu, D. R. (2018). Base editing: precision chemistry on the genome and transcriptome of living cells. *Nat. Rev. Genet.* 19 (12), 770–788. doi:10.1038/s41576-018-0059-1

Rivella, S. (2019). Iron metabolism under conditions of ineffective erythropoiesis in β-thalassemia. *Blood* 133 (1), 51–58. doi:10.1182/blood-2018-07-815928

Rostami, T., Kasaeian, A., Maleki, N., Nikbakht, M., Kiumarsi, A., Tavangar, S. M., et al. (2021). The effect of bone marrow-derived mesenchymal stem cell co-transplantation with hematopoietic stem cells on liver fibrosis alleviation and survival in patients with class III β-thalassemia major. *Stem Cell Res. Ther.* 12 (1), 213. doi:10.1186/s13287-021-02242-8

Rowe, R. G., and Daley, G. Q. (2019). Induced pluripotent stem cells in disease modelling and drug discovery. *Nat. Rev. Genet.* 20 (7), 377–388. doi:10.1038/s41576-019-0100-z

Rowe, R. G., Mandelbaum, J., Zon, L. I., and Daley, G. Q. (2016). Engineering hematopoietic stem cells: lessons from development. *Cell Stem Cell* 18 (6), 707–720. doi:10.1016/j.stem.2016.05.016

Rudnitsky, E., Braiman, A., Wolfson, M., Muradian, K. K., Gorbunova, V., Turgeman, G., et al. (2025). Mesenchymal stem cells and their derivatives as potential longevity-promoting tools. *Biogerontology* 26 (3), 96. doi:10.1007/s10522-025-10240-z

Szaraz, P., Gratch, Y. S., Iqbal, F., and Librach, C. L. (2017). *In vitro* differentiation of human mesenchymal stem cells into functional cardiomyocyte-like cells. *J. Vis. Exp.* (126), 55757. doi:10.3791/55757

Saleemi, S. (2014). Saudi guidelines on the diagnosis and treatment of pulmonary hypertension: pulmonary hypertension associated with hemolytic anemia. *Ann. Thorac. Med.* 9 (Suppl. 1), S67–S73. doi:10.4103/1817-1737.134039

Sanchez-Petitto, G., Rezvani, K., Daher, M., Rafei, H., Kebriaei, P., Shpall, E. J., et al. (2023). Umbilical cord blood transplantation: connecting its origin to its future. *Stem Cells Transl. Med.* 12 (2), 55–71. doi:10.1093/stcltm/szac086

Santarone, S., Angelini, S., Natale, A., Vaddinelli, D., Spadano, R., Casciani, P., et al. (2022). Survival and late effects of hematopoietic cell transplantation in patients with thalassemia major. *Bone Marrow Transpl.* 57 (11), 1689–1697. doi:10.1038/s41409-022-01786-4

Sarvari, M., Alavi-Moghadam, S., Aghayan, H. R., Tayanloo-Beik, A., Payab, M., Tootee, A., et al. (2021). Stem cells researches and therapies towards endocrine diseases treatment; strategies, challenges, and opportunities. *J. Diabetes Metab. Disord.* 23(2), 1461–1467. doi:10.1007/s40200-020-00674-2

Seijas, A., Cora, D., Novo, M., Al-Soufi, W., Sánchez, L., and Arana, Á. J. (2025). CRISPR/Cas9 delivery systems to enhance gene editing efficiency. *Int. J. Mol. Sci.* 26(9), 4420. doi:10.3390/ijms26094420

Shang, Y., Guan, H., and Zhou, F. (2021). Biological characteristics of umbilical cord mesenchymal stem cells and its therapeutic potential for hematological disorders. *Front. Cell Dev. Biol.* 9, 570179. doi:10.3389/fcell.2021.570179

Sharma, A., Jagannath, VA., and Puri, L. (2021). Hematopoietic stem cell transplantation for people with β-thalassaemia. *Cochrane Database Syst. Rev.* 4(4), CD008708. doi:10.1002/14651858.CD008708.pub5

Simpson, E., and Dazzi, F. (2019). Bone marrow transplantation 1957-2019. *Front. Immunol.* 10, 1246. doi:10.3389/fimmu.2019.01246

Sinclair, F., Begum, A. A., Dai, C. C., Toth, I., and Moyle, P. M. (2023). Recent advances in the delivery and applications of nonviral CRISPR/Cas9 gene editing. *Drug Deliv. Transl. Res.* 13 (5), 1500–1519. doi:10.1007/s13346-023-01320-z

Singh, A., Babu, S., Phan, M., and Yuan, S. H. (2024). CRISPR/Cas9-Based protocol for precise genome editing in induced pluripotent stem cells. *Bio Protoc.* 14(24), e5141. doi:10.21769/BioProtoc.5141

Sirinoglu Demiriz, I., Tekgunduz, E., and Altuntas, F. (2012). What is the most appropriate source for hematopoietic stem cell transplantation? Peripheral stem cell/bone marrow/cord blood. *Bone Marrow Res.* 2012, 834040. doi:10.1155/2012/834040

Song, B., Fan, Y., He, W., Zhu, D., Niu, X., Wang, D., et al. (2015). Improved hematopoietic differentiation efficiency of gene-corrected beta-thalassemia induced pluripotent stem cells by CRISPR/Cas9 system. *Stem Cells Dev.* 24 (9), 1053–1065. doi:10.1089/scd.2014.0347

Song, C., Wang, L., Li, Q., Liao, B., Qiao, W., Dong, N., et al. (2022). Generation of individualized immunocompatible endothelial cells from HLA-I-matched human pluripotent stem cells. *Stem Cell Res Ther.* 13 (1), 48. doi:10.1186/s13287-022-02720-7

Song, J., Ma, Q., Li, Y., Wang, X., Chen, S., Liang, B., et al. (2024). CD317(+) MSCs expanded with chemically defined media have enhanced immunological anti-inflammatory activities. *Stem Cell Res. Ther.* 15 (1), 2. doi:10.1186/s13287-023-03618-8

Sprink, T., Wilhelm, R., and Hartung, F. (2022). Genome editing around the globe: an update on policies and perceptions. *Plant Physiol.* 190 (3), 1579–1587. doi:10.1093/plphys/kiac359

Srivastava, A., and Shaji, R. V. (2017). Cure for thalassemia major - from allogeneic hematopoietic stem cell transplantation to gene therapy. *Haematologica* 102 (2), 214–223. doi:10.3324/haematol.2015.141200

Stacey, G. N., and Healy, L. (2021). The International Stem Cell Banking Initiative (ISCBI). *Stem Cell Res.* 53, 102265. doi:10.1016/j.scr.2021.102265

Su, Z., Dong, H., Fang, X., Zhang, W., and Duan, H. (2025). Frontier progress and translational challenges of pluripotent differentiation of stem cells. *Front. Genet.* 16, 1583391. doi:10.3389/fgene.2025.1583391

Taghdiri, M., and Mussolino, C. (2024). Viral and non-viral systems to deliver gene therapeutics to clinical targets. *Int. J. Mol. Sci.* 25 (13), 7333. doi:10.3390/ijms25137333

Taher, A. T., Musallam, K. M., and Cappellini, M. D. (2021). β-Thalassemias. *N. Engl. J. Med.* 384 (8), 727–743. doi:10.1056/NEJMra2021838

Takahashi, K., and Yamanaka, S. (2006). Induction of pluripotent stem cells from mouse embryonic and adult fibroblast cultures by defined factors. *Cell* 126 (4), 663–676. doi:10.1016/j.cell.2006.07.024

Tamary, H., Dgany, O., Adam, M. P., Feldman, J., Mirzaa, G. M., Pagon, R. A., et al. (1993). "Alpha-thalassemia," in *GeneReviews (®)*. Editor M. P. Adam, Seattle, WA: University of Washington).

Tenuta, M., Cangiano, B., Rastrelli, G., Carlomagno, F., Sciarra, F., Sansone, A., et al. (2024). Iron overload disorders: growth and gonadal dysfunction in childhood and adolescence. *Pediatr. Blood Cancer* 71 (7), e30995. doi:10.1002/pbc.30995

Terai, S., Ezoe, S., Mano, K., Matsuzaki, Y., Sato, Y., Yamahara, K., et al. (2025). Recommendations for the safe implementation of intravenous administration of mesenchymal stromal cells. *Regen. Ther.* 29, 171–176. doi:10.1016/j.reth.2025.01.024

Tesio, N., and Bauer, D. E. (2023). Molecular basis and genetic modifiers of thalassemia. *Hematol. Oncol. Clin. North Am.* 37 (2), 273–299. doi:10.1016/j.hoc.2022.12.001

Thiagarajan, P., Parker, C. J., and Prchal, J. T. (2023). How Do Red Blood Cells Die?. *Front Physiol.* 12, 655393. doi:10.3389/fphys.2021.655393

Tian, Z., Yu, T., Liu, J., Wang, T., and Higuchi, A. (2023). Introduction to stem cells. *Prog. Mol. Biol. Transl. Sci.* 199, 3–32. doi:10.1016/bs.pmbts.2023.02.012

Tong, S., Moyo, B., Lee, C. M., Leong, K., and Bao, G. (2019). Engineered materials for in vivo delivery of genome-editing machinery. *Nat. Rev. Mater* 4, 726–737. doi:10.1038/s41578-019-0145-9

Traeger-Synodinos, J., Vrettou, C., Sofocleous, C., Zurlo, M., Finotti, A., Gambari, R., et al. (2024). Impact of α-Globin gene expression and α-Globin modifiers on the phenotype of β-Thalassemia and other hemoglobinopathies: implications for patient management. *Int. J. Mol. Sci.* 25 (6), 3400. doi:10.3390/ijms25063400

Tran, D. C., Dang, A. L., Hoang, T. N. L., Nguyen, C. T., Le, T. M. P., Dinh, T. N. M., et al. (2023). Prevalence of thalassemia in the Vietnamese population and building a clinical decision support system for prenatal screening for thalassemia. *Mediterr. J. Hematol. Infect. Dis.* 15 (1), e2023026. doi:10.4084/MJHID.2023.026

Um, S., Ha, J., Choi, S. J., Oh, W., and Jin, H. J. (2020). Prospects for the therapeutic development of umbilical cord blood-derived mesenchymal stem cells. *World J. Stem Cells* 12 (12), 1511–1528. doi:10.4252/wjsc.v12.i12.1511

Večerić-Haler, Ž., Sever, M., Kojc, N., Halloran, P. F., Boštjančič, E., Mlinšek, G., et al. (2022). Autologous mesenchymal stem cells for treatment of chronic active antibody-mediated kidney graft rejection: report of the phase I/II clinical trial case series. *Transpl. Int.* 35, 10772. doi:10.3389/ti.2022.10772

Velikova, T., Dekova, T., and Miteva, D. G. (2024). Controversies regarding transplantation of mesenchymal stem cells. *World J. Transpl.* 14(2), 90554. doi:10.5500/wjt.v14.i2.90554

Venou, T. M., Barmpageorgopoulou, F., Peppa, M., and Vlachaki, E. (2024). Endocrinopathies in beta thalassemia: a narrative review. *Horm. (Athens)* 23 (2), 205–216. doi:10.1007/s42000-023-00515-w

Vento, S., Cainelli, F., and Cesario, F. (2006). Infections and thalassaemia. *Lancet Infect. Dis.* 6 (4), 226–233. doi:10.1016/S1473-3099(06)70437-6

Wang, J., and Li, R. (2024). Effects, methods and limits of the cryopreservation on mesenchymal stem cells. *Stem Cell Res. & Ther.* 15 (1), 337. doi:10.1186/s13287-024-03954-3

Wang, K. C., Zheng, T., and Hubbard, B. P. (2025b). CRISPR/Cas technologies for cancer drug discovery and treatment. *Trends Pharmacol. Sci.* 46 (5), 437–452. doi:10.1016/j.tips.2025.02.009

Wang, W. D., Hu, F., Zhou, D. H., Gale, R. P., Lai, Y. R., Yao, H. X., et al. (2023). Thalassaemia in China. *Blood Rev.* 60, 101074. doi:10.1016/j.blre.2023.101074

Wattanapanitch, M. (2019). Recent Updates on Induced Pluripotent Stem Cells in Hematological Disorders. *Stem Cells Int.* , 5171032. doi:10.1155/2019/5171032

Wattanapanitch, M. (2021). Correction of hemoglobin E/Beta-Thalassemia patient-derived iPSCs using CRISPR/Cas9. *Methods Mol. Biol.* 2211, 193–211. doi:10.1007/978-1-0716-0943-9_14

Wattanapanitch, M., Damkham, N., Potirat, P., Trakarnsanga, K., Janan, M., U-Pratya, Y., et al. (2018). One-step genetic correction of hemoglobin E/beta-thalassemia patient-derived iPSCs by the CRISPR/Cas9 system. *Stem Cell Res. Ther.* 9 (1), 46. doi:10.1186/s13287-018-0779-3

Wei, L., Yan, W., Shah, W., Zhang, Z., Wang, M., Liu, B., et al. (2024). Advancements and challenges in stem cell transplantation for regenerative medicine. *Heliyon* 10 (16), e35836. doi:10.1016/j.heliyon.2024.e35836

Wen, D., and Wang, J. (2025). Totipotency or plenipotency: rethinking stem cell bipotentiality. *Curr. Opin. Genet. Dev.* 92, 102342. doi:10.1016/j.gde.2025.102342

Wen, Y., Li, J., Mukama, O., Huang, R., Deng, S., and Li, Z. (2025). New insights on mesenchymal stem cells therapy from the perspective of the pathogenesis of nonalcoholic fatty liver disease. *Dig. Liver Dis.* 57, 1107–1118. doi:10.1016/j.dld.2025.03.007

Wiewiórska-Krata, N., Foroncewicz, B., Mucha, K., and Zagożdżon, R. (2025). Cell therapies for immune-mediated disorders. *Front. Med. (Lausanne)* 12, 1550527. doi:10.3389/fmed.2025.1550527

Wiley, L., Cheek, M., LaFar, E., Ma, X., Sekowski, J., Tanguturi, N., et al. (2025). The ethics of human embryo editing via CRISPR-Cas9 technology: a systematic review of ethical arguments, reasons, and concerns. *HEC Forum* 37 (2), 267–303. doi:10.1007/s10730-024-09538-1

Wilkinson, A. C., Dever, D. P., Baik, R., Camarena, J., Hsu, I., Charlesworth, C. T., et al. (2021). Cas9-AAV6 gene correction of beta-globin in autologous HSCs improves sickle cell disease erythropoiesis in mice. *Nat. Commun.* 12 (1), 686. doi:10.1038/s41467-021-20909-x

Williams, D. A., Kohn, D. B., and Thrasher, A. J. (2025). *Ex vivo* modification of hematopoietic stem and progenitor cells for gene therapy. *Mol. Ther.* 33 (5), 2141–2153. doi:10.1016/j.ymthe.2025.03.058

Winger, B. A., Ajayi, A., and Vichinsky, E. (2025). Diagnosis and treatment of alpha thalassemia major. *Hemoglobin* 49 (1), 3–9. doi:10.1080/03630269.2024.2432899

Wood, J. C. (2023). Cardiac complications in thalassemia throughout the lifespan: victories and challenges. *Ann. N. Y. Acad. Sci.* 1530 (1), 64–73. doi:10.1111/nyas.15078

Wu, S. C. M., Zhu, M., Chik, S. C. C., Kwok, M., Javed, A., Law, L., et al. (2023). Adipose tissue-derived human mesenchymal stromal cells can better suppress complement lysis, engraft and inhibit acute graft-versus-host disease in mice. *Stem Cell Res. Ther.* 14 (1), 167. doi:10.1186/s13287-023-03380-x

Wyvekens, N., Topkar, V. V., Khayter, C., Joung, J. K., and Tsai, S. Q. (2015). Dimeric CRISPR RNA-guided FokI-dCas9 nucleases directed by truncated gRNAs for highly specific genome editing. *Hum. Gene Ther.* 26 (7), 425–431. doi:10.1089/hum.2015.084

Xie, F., Ye, L., Chang, J. C., Beyer, A. I., Wang, J., Muench, M. O., et al. (2014). Seamless gene correction of β-thalassemia mutations in patient-specific iPSCs using CRISPR/Cas9 and piggyBac. *Genome Res.* 24 (9), 1526–1533. doi:10.1101/gr.173427.114

Xu, P., Tong, Y., Liu, X. z., Wang, T. t., Cheng, L., Wang, B. y., et al. (2015). Both TALENs and CRISPR/Cas9 directly target the HBB IVS2-654 (C > T) mutation in β-thalassemia-derived iPSCs. *Sci. Rep.* 5, 12065. doi:10.1038/srep12065

Xu, H., Wang, B., Ono, M., Kagita, A., Fujii, K., Sasakawa, N., et al. (2019). Targeted Disruption of HLA Genes via CRISPR-Cas9 Generates iPSCs with Enhanced Immune Compatibility. *Cell Stem Cell.* 24 (4), 566–578. doi:10.1016/j.stem.2019.02.005

Yamanaka, S. (2020). Pluripotent stem cell-based cell therapy-promise and challenges. *Cell Stem Cell* 27 (4), 523–531. doi:10.1016/j.stem.2020.09.014

Yang, X., Meng, Y., Han, Z., Ye, F., Wei, L., and Zong, C. (2020). Mesenchymal stem cell therapy for liver disease: full of chances and challenges. *Cell Biosci.* 10, 123. doi:10.1186/s13578-020-00480-6

Ye, L., Chang, J. C., Lin, C., Sun, X., Yu, J., and Kan, Y. W. (2009). Induced pluripotent stem cells offer new approach to therapy in thalassemia and sickle cell anemia and option in prenatal diagnosis in genetic diseases. *Proc. Natl. Acad. Sci. U. S. A.* 106 (24), 9826–9830. doi:10.1073/pnas.0904689106

Yin, S., Zhang, M., Liu, Y., Sun, X., Guan, Y., Chen, X., et al. (2023). Engineering of efficiency-enhanced Cas9 and base editors with improved gene therapy efficacies. *Mol. Ther.* 31(3), 744–759. doi:10.1016/j.ymthe.2022.11.014

Yong, J., Tao, J., Wang, K., Li, X., and Yang, Y. (2025). Post-myocardial infarction cardiac remodeling: multidimensional mechanisms and clinical prospects of stem cell therapy. *Stem Cell Rev. Rep.* doi:10.1007/s12015-025-10888-7

Yousuf, R., Akter, S., Wasek, S. M., Sinha, S., Ahmad, R., and Haque, M. (2022). Thalassemia: a review of the challenges to the families and caregivers. *Cureus* 14 (12), e32491. doi:10.7759/cureus.32491

Zakaria, N. A., Bahar, R., Abdullah, W. Z., Mohamed Yusoff, A. A., Shamsuddin, S., Abdul Wahab, R., et al. (2022). Genetic manipulation strategies for β-Thalassemia: a review. *Front. Pediatr.* 10, 901605. doi:10.3389/fped.2022.901605

Zeng, S., Lei, S., Qu, C., Wang, Y., Teng, S., and Huang, P. (2023). CRISPR/Cas-based gene editing in therapeutic strategies for beta-thalassemia. *Hum. Genet.* 142 (12), 1677–1703. doi:10.1007/s00439-023-02610-9

Zhang, Y., Gao, S., Xia, J., and Liu, F. (2018). Hematopoietic hierarchy - an updated roadmap. *Trends Cell Biol.* 28 (12), 976–986. doi:10.1016/j.tcb.2018.06.001

Zhu, X., Tang, B., and Sun, Z. (2021a). Umbilical cord blood transplantation: still growing and improving. *Stem Cells Transl. Med.* 10 (Suppl. 2), S62–s74. doi:10.1002/sctm.20-0495

Zuo, Z., Babu, K., Ganguly, C., Zolekar, A., Newsom, S., Rajan, R., et al. (2022). Rational engineering of CRISPR-Cas9 nuclease to attenuate position-dependent off-target effects. *Crispr J.* 5 (2), 329–340. doi:10.1089/crispr.2021.0076

frontiers | Frontiers in Cell and Developmental Biology

TYPE Original Research
PUBLISHED 18 September 2025
DOI 10.3389/fcell.2025.1564382

OPEN ACCESS

EDITED BY
Sukhbir Kaur,
National Institutes of Health (NIH), United States

REVIEWED BY
Wen Li,
University at Buffalo, United States
Marcin Kaminski,
St. Jude Children's Research Hospital, United States
Shijie Qi,
University of Montreal Hospital Centre (CRCHUM), Canada

*CORRESPONDENCE
Hao Wang,
hwangca272@hotmail.com,
hwang1@tmu.edu.cn

†These authors share first authorship

RECEIVED 21 January 2025
ACCEPTED 27 August 2025
PUBLISHED 18 September 2025

CITATION
Liu T, Sun C, Liu X, Zhao P, Shao B, Xu Y, Xiao Y, Wang H, Chen Q, Yang G and Wang H (2025) Sirtuin 6 mediates the therapeutic effect of endometrial regenerative cell-derived exosomes in alleviation of acute transplant rejection by weakening c-myc-dependent glutaminolysis. *Front. Cell Dev. Biol.* 13:1564382. doi: 10.3389/fcell.2025.1564382

Sirtuin 6 mediates the therapeutic effect of endometrial regenerative cell-derived exosomes in alleviation of acute transplant rejection by weakening c-myc-dependent glutaminolysis

Tong Liu[1,2†], Chenglu Sun[1,2†], Xu Liu[1,2†], Pengyu Zhao[1,2], Bo Shao[1,2], Yini Xu[1,2], Yiyi Xiao[1,2], Hongda Wang[1,2], Qiang Chen[1,2], Guangmei Yang[1,2] and Hao Wang[1,2,3]*

[1]Department of General Surgery, Tianjin Medical University General Hospital, Tianjin, China, [2]Tianjin General Surgery Institute, Tianjin, China, [3]Tianjin Key Laboratory of Precise Vascular Reconstruction and Organ Function Repair, Tianjin, China

Background: Despite the rapid development of immunosuppressive drugs, acute rejection (AR) remains a cause of allograft dysfunction and allograft failure. Although endometrial regenerative cell-derived exosomes (ERC-Exos) effectively alleviate AR, more research is required to fully understand the underlying mechanisms. Thus, this study aimed to determine whether sirtuin 6 (SIRT6) mediates the therapeutic effect of ERC-Exos on AR and elucidate the underlying mechanisms.

Methods: The expression of SIRT6 was verified in ERC-Exos by Western blot. ERC-Exos with extremely low expression of SIRT6 (SIRT6-KD-ERC-Exos) were obtained by transducing shRNA-SIRT6 in ERCs. C57BL/6 recipient mice were transplanted with heart grafts from BALB/c donor mice and divided into three groups: untreated, ERC-Exo-treated, and SIRT6-KD-ERC-Exo-treated groups. Recipient mice were sacrificed on post-operative day 8 for the determination of graft pathological changes, intra-graft immunocyte infiltration, splenic $CD4^+$ T cell populations, and serum cytokine levels *in vivo*. The proportion of $CD4^+$ T cells and their secreting cytokine levels were determined *in vitro*. Besides, the underlying mechanisms were also investigated *in vitro*.

Results: ERC-Exos expressed SIRT6, and cardiac graft survival was increased by SIRT6-expressing ERC-Exos. Graft pathological damage, intra-graft $CD4^+$ T cell infiltration, and intra-graft inflammatory (Th1 and Th17) cell infiltration decreased, and intra-graft and serum inflammatory cytokine (interferon (IFN)-γ and interleukin (IL)-17) levels decreased in the SIRT6-expressing ERC-Exo-treated mice. Furthermore, in the recipient mice, ERC-Exo treatment markedly increased the differentiation of regulatory T cells (Tregs) while significantly decreasing that of Th1 and Th17 cells. In a similar vein,

ERC-Exo therapy raised the levels of the anti-inflammatory cytokine IL-10 *in vitro* while decreasing those of IFN-γ and IL-17. By suppressing the expression of important proteins linked to glutaminolysis and further deactivating the mammalian target of rapamycin complex 1 (mTORC1) pathway, ERC-Exos reduced the uptake and use of glutamine in naïve $CD4^+$ T cells, according to mechanism exploration. In contrast, SIRT6-KD-ERC-Exos considerably reversed these trends and changes both *in vivo* and *in vitro*.

Conclusion: SIRT6 is crucial in mediating ERC-Exos to remodel $CD4^+$ T cell differentiation by weakening c-Myc-dependent glutaminolysis, thereby alleviating AR.

KEYWORDS

endometrial regenerative cells, exosomes, SIRT6, CD4 + T cell differentiation, glutaminolysis, acute rejection

Introduction

Despite the availability of alternative treatments, organ transplantation remains the most reliable means to treat end-stage organ failure (Shah et al., 2022; Kittleson and Kobashigawa, 2017). Acute rejection (AR) usually occurs from a few days to 2 weeks after transplantation, which is the most common rejection in organ transplantation and affects transplanted organs' early survival (Stewart et al., 2007). AR is mainly caused by the HLA complex incompatibility between donor and recipient, and more involved in T cells (Stewart et al., 2007). Besides, long-term use of immunosuppressive drugs will lead to many negative effects, including tumorigenesis and lethal infections (Söderlund and Rådegran, 2015). Hence, safer and more effective immunotherapeutic methods should be explored to alleviate AR.

Due to their extremely low expression of major histocompatibility complex (MHC) class II and absence of MHC class I as well as co-stimulatory molecules, mesenchymal stem cells (MSCs) are classified as "immune privileged cells" (Quaranta et al., 2016). MSCs are immune-privileged, so they cannot induce rejection and can perform their original functions, such as tissue repair and immune regulation. As a result, MSC injection is thought to be a viable therapy option for a variety of disorders. For instance, the preliminary findings of a multicenter randomized controlled trial revealed that injecting umbilical cord-derived MSCs following kidney transplantation is safe and effective in reducing AR incidence (Sun et al., 2018). However, the invasive harvesting procedure, restricted availability, and potential risk of allogeneic use limit the method's widespread clinical adoption.

Endometrial regenerative cells (ERCs) are a new type of MSCs collected from menstrual blood with the advantages of non-invasive acquisition and autologous stem cell reinfusion therapy (Darzi et al., 2016). We previously reported that ERC therapy can ameliorate a variety of immune-related disorders *in vivo*, including transplant rejection, ulcerative colitis, and autoimmune hepatitis, via modulating $CD4^+$ T cells (Hu et al., 2021; Li et al., 2019; Wang et al., 2021). In heart transplantation model mice, ERC therapy can alleviate transplantation rejection by decreasing the helper T cell 1 (Th1) and 17 (Th17) proportion, while increasing the percentage of regulatory T cells (Tregs) (Hu et al., 2021). Although ERC treatment shows promise, its clinical uses have some limits. As a kind of MSC, ERCs are inevitably associated with certain common problems of cell therapy, such as diminished therapeutic efficacy caused by pulmonary network blockage or cell embolism from repeated injections (Klabukov et al., 2023). Therefore, cell-free therapeutic strategies are being developed. Similarly, our prior research found that ERC-derived exosomes (ERC-Exos) show a significant therapeutic effect on AR, which could be attributed to their regulatory function in $CD4^+$ T cell differentiation.

Sirtuin 6 (SIRT6), an important member of the NAD^+-dependent histone deacetylase SIRT family, is a multifunctional protein involved in various enzymatic activities, including histone deacetylation, de-fatty acylation, and mono-ADP-ribosylation (Li et al., 2022). It was initially identified as an anti-aging protein, but more investigations have revealed numerous activities of SIRT6, such as regulating the inflammatory response, resisting oxidative stress, and maintaining metabolism (Li et al., 2022; Guo et al., 2022). For example, SIRT6 inhibits IL-6 secretion in macrophages by weakening the NF-κB pathway and downregulating STAT3 mRNA transcription, thus preventing macrophages from polarizing towards a pro-inflammatory phenotype (Lee et al., 2017). Aside from its regulatory function on macrophage polarization, considering that NF-κB pathway activation is important in T cell activation (Schmitz et al., 2003), SIRT6 may have some regulatory effects on T cells. A follow-up study showed that in rheumatoid arthritis, SIRT6 inhibition reduces the percentage of Tregs in the peripheral blood and synovial fluid (Wang et al., 2019), indicating that SIRT6 has the potential to regulate $CD4^+$ T cell differentiation. Studies have also shown that SIRT6 can negatively regulate c-Myc, a key target expressed in large quantities during naïve $CD4^+$ T cell activation, through histone deacetylation (mainly histone H3 lysine K9 and histone H3 lysine K56) (Sebastián et al., 2012). Specifically, the upregulation of c-Myc during naïve $CD4^+$ T cell activation can promote the transcription of downstream glutaminolysis-related genes, such as glutaminase 1 (*GLS1*) and solute carrier family 1 member 5 (*SCL1A5*), an encoding gene of alanine-serine-cysteine transporter system 2 (ASCT2) protein (Wang et al., 2011). This process is also known as c-Myc-dependent glutaminolysis (Marchingo et al., 2020). Thus, SIRT6 shows great potential in the regulation of glutaminolysis in naïve $CD4^+$ T cells.

Glutamine, an immune regulatory nutrient, is frequently used in large amounts for cellular energy and facilitates the intracellular synthesis of genetic material via glutaminolysis in rapidly proliferating and dividing cells (Yang et al., 2017). For naïve $CD4^+$ T cells to proliferate and differentiate, they need to rapidly take up a large amount of glutamine right after activation and subsequently initiate glutaminolysis (Geltink et al., 2018). Naïve $CD4^+$ T cells can differentiate into different subtypes following antigen stimulation via different metabolic patterns (Liu et al., 2023). Specifically, the differentiation of Th1 and Th17 cells tends to involve glutaminolysis, whereas that of Tregs does not (Geltink et al., 2018). Even under specific cell differentiation conditions, impaired glutaminolysis can substantially affect the fate of peripheral naïve $CD4^+$ T cells during differentiation (Yang et al., 2021). For example, even under Th1 polarization, naïve $CD4^+$ T cells with glutamine deficiency also tilt toward $Foxp3^+$ Tregs and hinder their differentiation into Th1 cells (Klysz et al., 2015). AR is accompanied by disordered $CD4^+$ T cell differentiation, especially increased Th1 and Th17 cell proportions and decreased Treg proportions. Therefore, remodeling disordered $CD4^+$ T cell differentiation by modulating glutaminolysis appears to be a viable way to alleviate AR.

Early research found that SIRT6 is widely expressed in various cells and is mainly localized in the nucleus (Pillai and Gupta, 2020). However, subsequent research showed that SIRT6 is also expressed and accumulated in cytoplasm (Hou et al., 2022). Thus, research on SIRT6 gradually shifted from intracellular to extracellular investigations. A recent study has reported that SIRT6 can express in the bone marrow-derived MSC exosomes and exert its deacetylation to inhibit phosphate-induced aortic calcification (Wei WQ. et al., 2021). Given SIRT6's encouraging immunomodulatory potential, we looked into how it might mediate the therapeutic effects of ERC-Exos. As mentioned previously, SIRT6 shows a promising ability to remodel disordered $CD4^+$ T cell differentiation by regulating c-Myc-dependent glutaminolysis. Therefore, this study aimed to explore whether ERC-Exos expresses SIRT6 and whether the ERC-Exo therapy effect in alleviating allogeneic immune response is mediated by SIRT6. We also investigated whether SIRT6-expressing ERC-Exos can improve aberrant $CD4^+$ T cell differentiation on AR by weakening glutaminolysis.

Materials and methods

Isolation, culture, and detection of ERCs

All human ERCs used in this study were isolated from menstrual blood provided by healthy female volunteers aged 20–30 years, and the procedure was approved by Tianjin Medical University General Hospital (IRB2024-YX-013-01, Tianjin, China). First, menstrual blood is filtered to remove blood clots, and the bottom red precipitate is obtained by centrifugation. Then, these red precipitates were resuspended by PBS, slowly added to the same volume of human peripheral blood lymphocyte separation solution, and ERCs were obtained by density gradient centrifugation. Finally, the extracted ERCs were cultured in Dulbecco's modified Eagle's medium/Ham's F12 (DMEM/F12) nutrient medium supplemented with 10% fetal bovine serum (FBS) and 1% P/S solution in a 37 °C 5% CO_2 incubator. After being incubated for approximately 1–2 ° weeks, ERCs were harvested and phenotypically identified using flow cytometry. The identified ERCs were then used for further studies.

Three-lineage experiment

In order to further identify the stem cell characteristics of ERCs, the three-line differentiation experiments were carried out. 1. Osteogenic differentiation: 0.1% gelatin was added into a 12-well plate, with 500 μL in each hole, so that it covered the whole bottom surface. Then the gelatin coated 12-well plate was placed in a 37 °C incubator for at least 30 min. After 30 min, the gelatin was discarded and used to inoculate cells after the Petri dish was dried. ERCs were inoculated into a 12-well plate coated with gelatin in the amount of 4×10^4 cells per well, and cultured in serum-free medium, and the medium was changed once a day. When the confluence degree of ERCs reached 70%, the medium was discarded by suction, and 1 mL of human mesenchymal stem cells osteogenic differentiation medium was added to each well to start the induced differentiation. After 21–30 days of ERC osteogenesis induction, the precipitation of calcium nodules was observed under the microscope, and the osteogenic differentiation was identified by alizarin red S staining. 2. Chondrogenic differentiation: 3×10^5 ERCs were transferred to a 15 mL centrifuge tube, and the centrifuge was 300 *g* for 5 min. After centrifugation, the supernatant was poured out, 500 μL of human mesenchymal stem cells were added into chondrogenic differentiation medium, and the cells were resuspended. Centrifuge: 300 *g* for 5 min. The centrifuge tube cover was unscrewed for gas exchange, and it was kept in a cell incubator for 24 h. After 24–48 °h, when the cells aggregated, the bottom of the centrifuge tube was flicked to make the cartilage ball separate from the bottom of the tube and suspend in the liquid. The cell culture medium was changed every 2–3° days to prevent the cartilage ball from being scattered. After 21–28° days of chondrogenic differentiation of ERCs, the differentiation medium was discarded, and the chondrocytes were washed twice with 3 mL PBS, and then fixed with 3 mL 4% paraformaldehyde. The fixed chondrocytes were embedded in paraffin, and the chondrogenic differentiation was identified by alixin blue staining. 3. Adipogenic differentiation: ERCs were inoculated into 12-well plates with the number of 4×10^4 cells per well, and cultured in serum-free medium. When the confluence of ERCs reached 100%, the medium was discarded, and 1 mL of adipogenic differentiation medium was added to each well to start differentiation induction. Adipogenic differentiation was induced for 9–35° days. After the formation of lipid droplets was observed under the microscope, the adipogenic differentiation was identified by oil red O staining.

Construction of ERCs with low expression of SIRT6 (SIRT6-KD-RECs)

To knock down SIRT6 in ERCs and further obtain ERC-Exos with low expression of SIRT6 (SIRT6-KD-ERC-Exos), We bought shRNA-SIRT6 lentivirus containing green fluorescent protein (GFP) and puromycin resistance gene from Gene-Chem company (Shanghai, China).

The sequence of shRNA-SIRT6 was as follows: 5′-CGAGGATGTCGGTGAATTATTCAAGAGATAATTCACCGAC ATCCTCG-3′. Specifically, the SIRT6-Knockdown virus consisted of Lv-hU6-MCS (shRNA-SIRT6 sequence insertion site) -CBh-gcGFP-IRES-puromycin. Similarly, the empty vector virus had the same architecture. Empty vector virus inserted an unintentional sequence (5′-TTCTCCGAACGTGTCACGT-3′) at MSC site, which would not affect the expression of SIRT6. Lentiviral transduction was carried out following the instructions from Gene-Chem, using an optimal multiplicity of infection (MOI = 20). ERCs at passage 2 were plated onto a 6-well plate with a density of 15,000/well, and lentiviral transduction was carried out when the confluence reached 50%–60%. The transduction time was 12–16 °h, and the transduction is terminated according to the cell condition. After transduction, the cells were washed by PBS and replaced with fresh medium without lentivirus. To select for successfully transduced cells, puromycin (2 μg/mL, Solarbio, China) was incorporated into the culture medium. At the same time, puromycin was added to the ERCs of un-transduced lentivirus with the same generation and density, and the screening was finished when it died completely. After the cell screening, the GFP positive cells were detected by fluorescence microscope to be more than 90%, and then Western blot was carried out to detect SIRT6 expression level in ERCs. After successfully constructing SIRT6-KD-ERCs, the supernatant was collected to isolate SIRT6-KD-ERC-Exos. Besides, SIRT6-NC-ERCs could be obtained by successfully transducing ERCs with empty vector virus. Similarly, the further obtained exosome was SIRT6-NC-ERC-Exos.

Isolation and characterization of ERC-derived exosomes

ERCs were cultured in 10-cm dishes, washed with phosphate buffered saline (PBS), and maintained in FBS-free medium (Transgen, Beijing, China) for 48 h upon reaching nearly 90%–95% confluence. Then, the exosomes were obtained by centrifugation (Beckman centrifuge, United States) under the following conditions: 3,000 *g*, 4 °C, 10 °min; 10,000 *g*, 4 °C, 30 °min; 130,000 *g*, 4 °C, 70 min. The exosomes were resuspended with PBS and stored at −80 °C. The morphology of ERC-Exos was observed using transmission electron microscopy (TEM) (HT7700-SS, HITACHI, Japan). The size distribution of ERC-Exos was measured using nanoparticle tracking analysis (NTA) (Malvern Instruments Ltd., Malvern, United Kingdom). The concentration of ERC-Exos was determined using a bicinchoninic acid (BCA) protein assay kit (Solarbio, Beijing, China). In addition, exosomal markers, including CD9, CD63, TSG101, and calnexin, were detected using Western blot assay with the corresponding antibodies (dilution at 1:2000, 1:2,500, 1:2,000, and 1:3,000 respectively, abcam).

Animals

Adult C57BL/6 and BALB/c mice (male, 6–8 ° weeks old, weighing 23–26 g) were obtained from the China Food and Drug Inspection Institute (Beijing, China). All animals used in this study were housed in a conventional experimental environment with sufficient space, water, food, and appropriate temperature at the Tianjin General Surgery Institute (Tianjin, China). All animal procedures followed the animal use protocol approved by the Animal Care and Use Committee of Tianjin Medical University (Tianjin, China), and all the experiments were performed in accordance with the guidelines of the Chinese Council on Animal Care.

Allogeneic cardiac transplantation and experimental groups

C57BL/6 mouse recipients were randomly assigned to three experimental groups (n = 5): untreated, ERC-Exo-treated, and SIRT6-KD-ERC-Exo-treated groups (exosomes were obtained through ERC transduction by shRNA-SIRT6 lentivirus). As described in our previous study (Hu et al., 2021), an intra-abdominal heterotopic cardiac transplantation model was adopted, in which the hearts of BALB/c mice were transplanted into the abdomen of C57BL/6 mouse recipients. Specifically, the donor aorta and the recipient abdominal aorta, and the donor pulmonary artery and the recipient inferior vena cava anastomosed end to side. After the operation, the recipient mice were fed separately under appropriate conditions. In ERC-Exo and SIRT6-KD-ERC-Exo treatment groups, the corresponding exosome treatment was given respectively by tail vein injection on the first, third and fifth day after operation. In detail, each mouse was injected with 200 μg exosomes at a time on the injection day. The heartbeats of the grafts were recorded daily by the same member of our research team who was blinded to the treatment details. According to the force of the graft heartbeat, the pulsation was divided into three degrees: A, beating strongly; B, noticeable decline in the intensity of pulsation; and C, complete arrest of the graft heartbeat. For the graft survival time (n = 5), the days until the graft heartbeat was completely arrested were recorded. Based on our previous experience (Hu et al., 2021), for the assessment of efficacy and immune microenvironment, the recipient mice were euthanized on post-operative day (POD) 8, and the grafts and spleens were extracted for subsequent analyses.

Histology assessment

After being formalin-fixed, dehydrated, and paraffin-embedded, the heart graft samples were sliced into sections with 5-μm thickness. The sections were stained with hematoxylin and eosin (H&E). All the finished products were used to evaluate the severity of rejection under a light microscope. The presence of myocyte necrosis, interstitial hemorrhage, lymphocyte infiltration, vasculitis, and intravascular thrombosis was detected and scored in accordance with previously described criteria (Wang et al., 2003). On comparison with normal tissues, the following scores can be obtained: 0, no rejection; 1, mild interstitial or perivascular infiltrate without necrosis; 2, focal interstitial or perivascular infiltrate with necrosis; 3, multifocal interstitial or perivascular infiltrate with necrosis; and 4, widespread infiltrate with hemorrhage and/or vasculitis. The pathological score was calculated according to the degree of heart graft injury in each recipient mouse.

Immunohistochemistry assessment

As described above, 5-μm heart tissue slices were obtained from the paraffin-embedded grafts. After programmed dewaxing, the slices were first incubated with ethylene diamine tetra-acetic acid (EDTA) antigen repair solution (Solarbio, Beijing, China), and antigen repair was conducted for 15 min at 100 °C in a microwave oven. They were then cultured with 3% hydrogen peroxide to eliminate endogenous peroxides. After being blocked with 10% goat serum, the sections were incubated with rabbit anti-mouse CD4 (dilution at 1:1,000, Abcam), IFN-γ (dilution at 1:100, ABclonal), IL-17A (dilution at 1:100, ABclonal), and Foxp3 (dilution at 1:100, affinity) antibody overnight at 4 °C and then with 100 μL of enhanced enzyme-labeled goat anti-rabbit IgG polymer (DAB kit, ZSGB-BIO, Beijing, China) for 20 min the next day at room temperature. Finally, the slices were stained with hematoxylin for 1 min and then observed under an optical microscope to evaluate the severity of $CD4^+$ T cell infiltration. The percentage of the area of the section occupied by positive staining using ImageJ software.

Enzyme-linked immunosorbent assay

The serum levels of interferon gamma (IFN-γ), IL-17, and IL-10 in the recipient mice were measured using their corresponding ELISA kits (DAKEWE, Shenzhen, China) in accordance with the manufacturer's instructions. In this experiment, 100 μL serum samples were required for each test well, and three representative cytokines were tested in this experiment. $CD4^+$ T cells were isolated from the C57BL/6 mice and co-cultured with or without ERC-Exos or SIRT6-KD-ERC-Exos in 12-well plates. Then, the levels of IFN-γ, IL-17, and IL-10 in the cell supernatants were detected using their corresponding ELISA kits (DAKEWE, Shenzhen, China) in accordance with the manufacturer's instructions.

Glutamine uptake analysis

The extracted mouse naïve $CD4^+$ T cells were placed in 24-well plates, with about 10^6 cells per well, which were set into three groups, namely, untreated group, ERC-Exo treatment group, and ERC-SIRT6-KD-Exo treatment group. Each group was added with the same components necessary for $CD4^+$ T cell activation, including but not limited to glutamine (2 mM), CD3 (5 μg/mL), CD28 (3 μg/mL), and IL-2 (50 U/mL). After 24 h of different treatments, supernatant and cells were collected separately. Glutamine contents of naïve $CD4^+$ T cells were measured by use of a glutamine content measuring kit (Solarbio, Cat. NO.: BC5305, Beijing) in accordance with the manufacturer's protocol. The OD value of samples at A450 was tested by using a multifunctional enzyme label instrument. Then, the glutamine content was calculated according to the manufacturer's protocol. Additionally, the content of glutamine in the supernatant was also detected. Because the total glutamine content added to the culture medium among the three groups is the same, the difference of glutamine uptake by naïve $CD4^+$ T cells can be obtained by comparing the glutamine content in supernatant and cells, respectively.

α-ketoglutaric acid (α-KG) content detection

Naïve $CD4^+$ T cells were collected after 24 h of different treatments, as in the previous treatment of glutamine content detection. α-KG contents of naïve $CD4^+$ T cells were measured by use of an α-KG content measuring kit (Solarbio, Cat. NO.: BC5425, Beijing) in accordance with the manufacturer's protocol. The OD value of samples at A340 was tested by using a multifunctional enzyme label instrument. Then, the α-KG content was calculated according to the manufacturer's protocol.

Flow cytometry analysis

Flow cytometry was performed to identify the phenotype of the ERCs and detect the immune cell population in the spleens of the recipient mice. The collected cells were divided into 100 μL single cell suspensions and then stained with fluorescent-labeled antibodies, including Zombie Dye, anti-CD14-FITC, anti-CD90-PE, anti-CD-79a-PE, anti-HLA-DR-FITC, anti-CD73-FITC, anti-CD44-APC, anti-CD4-FITC, anti-CD25-PE, anti-IL-17A-Percp-cy5.5, anti-FOXP3-APC, and anti-IFN-γ-PE, which were purchased from eBioscience (Thermofisher, United States) and BioLegend (Biolegend, United States). Finally, the percentage of different cells was analyzed using FlowJ software. The columnar statistical chart was made by Graphpad V8.0 software.

Immunofluorescence staining

ERCs with a good growth state at passage 5 were adopted. The day before, the suspended ERCs were inoculated in a 12-well plate containing round coverslips, with a density of about 5×10^4 cells/mL/well. When the cell aggregation reached 80%–90%, the cells were taken out and washed twice with PBS, then 1 mL of 4% paraformaldehyde fixed solution was added to each well for cell fixation at room temperature for 15 min, then PBS was washed twice, and 1% BSA blocking solution was added for nonspecific antigen blocking at room temperature for 1 h. Subsequently, the excess BSA blocking solution was sucked off, and CD73 antibody (dilution at 1:100, Abcam) was added for incubation at 4 °C overnight. The next day, the incubated antibody was taken out and returned to room temperature for 30 min. After PBS washing twice, the corresponding cy3-labeled secondary antibody (dilution at 1:50, Proteintech) was incubated for 1 h at room temperature in the dark. After PBS washing twice, the round coverslip was taken out and dripped with neutral resin containing 4,6-diamino-2-phenyl indole (DAPI) staining for sealing. The cells were observed under a fluorescence microscope.

Exosome phagocytosis detection

The uptake of exosomes by naïve $CD4^+$ T cells was determined as follows. ERC-Exos and SIRT6-KD-ERC-Exos were incubated with 1 μM PKH26 (Solarbio, Beijing, China) for 15 min at 37 °C and then centrifuged at 100,000 *g* for 70 min to remove unbound dye.

Naïve CD4$^+$ T cells were acquired from C57BL/6 mouse spleens and co-cultured with PKH-26 labeled exosomes for 6 h. The treated cells were washed twice with PBS and fixed with 4% paraformaldehyde. Following DAPI staining, the cells were observed under a confocal microscope.

Co-culture of ERC-Exos and C57BL/6 mouse naïve CD4$^+$ T cells *in vitro*

Naïve CD4$^+$ T cells were extracted from C57BL/6 mice and co-cultured with or without ERC-Exos or SIRT6-KD-ERC-Exos in 96-well plates to investigate whether SIRT6-expressing ERC-Exos can influence CD4$^+$ T cell differentiation *in vitro*. In brief, a suspension of naïve CD4$^+$ T cells was prepared. The sacrificed spleens were ground and individually filtered using sterilized meshes (100 meshes). After the red blood cells were lysed, the remaining cells were resuspended and counted. Based on the number of cells, CD4$^+$ (L3T4) T cell-sorting magnetic beads (Miltenyi biotec, Germany) with corresponding volumes were added and allowed to stand for 10 min for complete mixing. The mixed liquid was then filtered twice by gravity under a magnetic field. Subsequently, the filter column was washed with culture medium to obtain naïve CD4$^+$ T cells. Each well was covered with 2×10^5 naïve CD4$^+$ T cells, and the cells were cultured in 200 μL of Roswell Park Memorial Institute 1,640 (RPMI-1640) medium. Finally, ERC-Exos or SIRT6-KD-ERC-Exos were added to different groups for co-culture, and flow cytometry was conducted after 72 h.

Naïve CD4$^+$ T cell activation detection

To explore whether SIRT6-expressing ERC-Exos affect naïve CD4$^+$ T cell activation *in vitro*, we extracted naïve CD4$^+$ T cells from C57BL/6 mice and co-cultured them with or without ERC-Exos or SIRT6-KD-ERC-Exos in 96-well plates for 12–24 h. After being co-cultured, T cells were collected for flow cytometry. Specifically, the collected cells were divided into 100 μL single cell suspensions and then stained with fluorescent-labeled antibodies, including anti-CD4-FITC and anti-CD25-PE, which were purchased from eBioscience (Thermofisher, United States) and BioLegend (Biolegend, United States). Finally, the percentage of different cells was analyzed using FlowJ software.

Western blot

CD4$^+$ T cells *in vitro* from the untreated, ERC-Exo-treated, and SIRT6-KD-ERC-Exo-treated groups were washed and then lysed in radio immunoprecipitation assay (RIPA) lysis buffer containing a protease inhibitor. After the lysis, the lysate was centrifuged, then the supernatant was sucked, and the concentration of the sample was measured by the BCA protein assay kit. Subsequently, loading buffer (Solarbio, Beijing, China) was added and the protein sample was denatured by boiling. The equal mass protein samples were separated by sodium dodecyl sulfate polyacrylamide gel electrophoresis (SDS-PAGE) and then transferred to a polyvinylidene fluoride (PVDF) membrane. The protein-containing membrane after transfer was blocked with bovine serum albumin solution and then incubated with primary antibodies at appropriate dilution (SIRT6, 1:2000, abcam; c-Myc, 1:3,000, Affinity; ASCT2, 1:750, ABclonal; GLS1, 1:1,000, Affinity; p-S6K1, 1:500, ABclonal; S6K1, 1:1,000, ABclonal) at 4 °C overnight. The next day, the membrane was washed in tris-buffered saline with tween-20 (TBST) and then incubated in the corresponding secondary antibody dilution (goat anti-rabbit, 1:2000, Affinity) at room temperature. Finally, the membrane was washed with TBST and incubated with an enhanced chemiluminescence solution (Sparkjade, Jinan, China) for several seconds. The membrane was photographed and analyzed on an exposure platform. The quantitative analysis was performed by comparing the ratio of target proteins/internal proteins in different groups using ImageJ.

Statistical analysis

Experimental data are presented as mean ± SD. Differences between multiple groups were calculated using one-way analysis of variance (ANOVA). The survival curve of the heart graft was constructed using the Kaplan–Meier cumulative survival method, and differences among groups were analyzed using the log-rank (Mantel–Cox) test. In the data charts, one asterisk represents $p \leq 0.05$, two asterisks represent $p \leq 0.01$, and three asterisks represent $p \leq 0.001$. Differences with $p \leq 0.05$ were considered statistically significant. GraphPad Prism (version 8.0) was used for the statistical analyses.

Results

Characterization of ERCs

The ERCs' morphology at passages 3–5 was used to assess their purity after being extracted from the volunteers' menstrual blood. Results showed that the ERCs were spindle shaped, fibroblast-like, and colony-forming (Figure 1A). Furthermore, a significant rate of proliferation was indicated by the doubling time, which was roughly 24 h. The stem cell characteristics of the ERCs were further evaluated using common MSC surface markers. At passage 5, the ERCs were detached and stained with the MSC surface markers CD14, CD79a, HLA-DR, CD44, CD73, and CD90. Consistent with our previous reports, the ERCs showed high expression levels of CD44, CD73, and CD90 but no expression of CD14, CD79a, and HLA-DR (Figure 1B). Among these MSC surface markers, CD73, a representative ERC positive marker, was also selected for immunofluorescence staining (Figure 1C) to further verify the stem cell characteristics of ERCs for supporting these flow cytometry analyses. Additionally, ERCs' strong osteogenic, chondrogenic, and adipogenic differentiation abilities were confirmed by the three-lineage differentiation experiment (Figure 1D). These findings demonstrated that the ERCs used in our study were MSCs with stable stem cell properties, the ability to cling to the culture dish, and the capacity to multiply quickly.

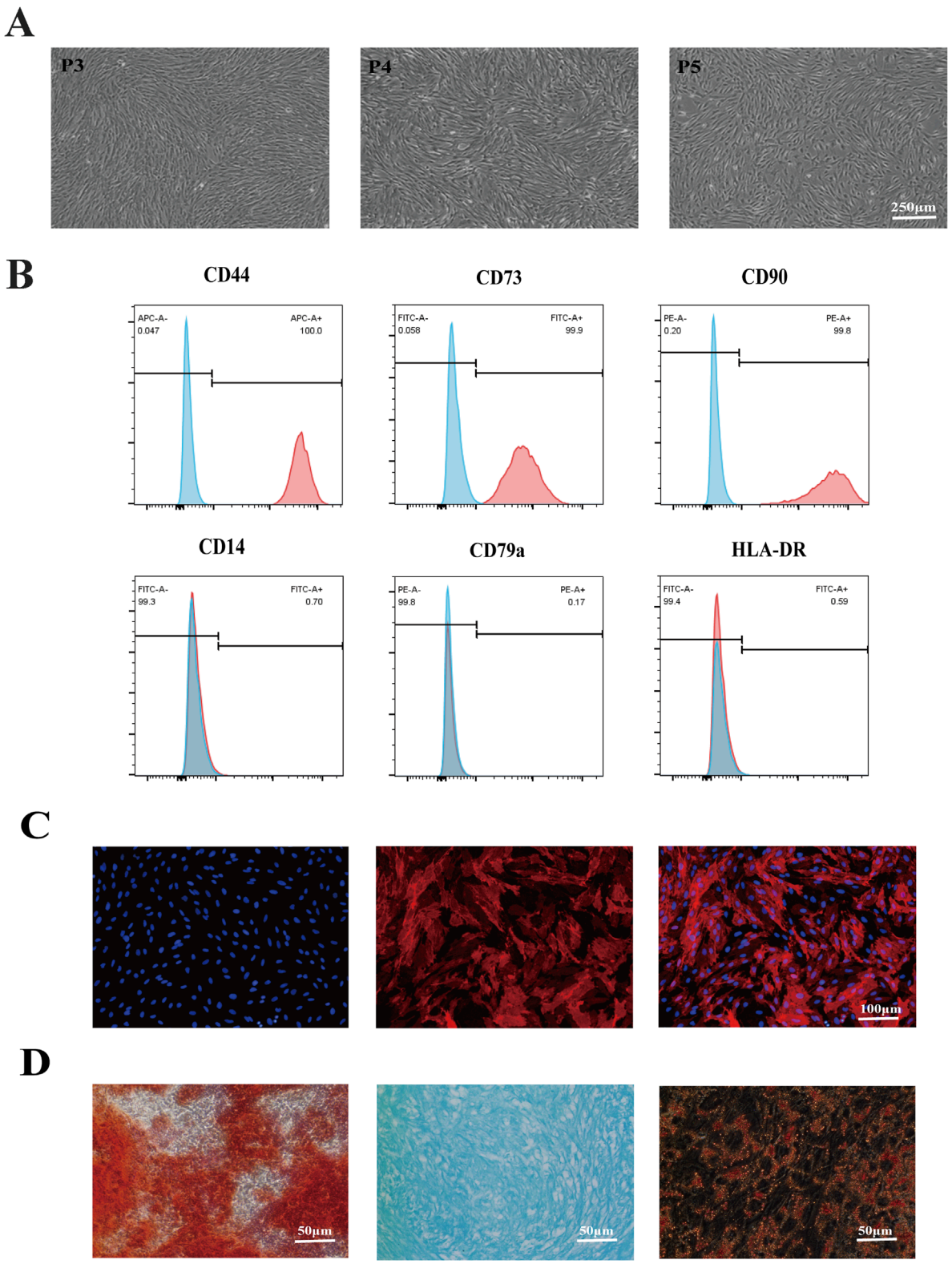

FIGURE 1
Identification of ERC features. **(A)** Morphology of ERCs at passage 3 to passage 5 (magnification 40×). ERCs were spindle-shaped, fibroblast-like, colony-forming ability and the doubling time was about 24 h. **(B)** Flow cytometry analysis of surface markers of ERCs. **(C)** Immunofluorescence staining of surface markers CD73 of ERCs (magnification 100×). **(D)** The results of three-lineage (osteogenic, chondrogenic, and adipogenic) differentiation of ERCs were stained by alizarin red, alixin blue and oil red O respectively (magnification 200×).

Construction of ERC-Exos with low expression of SIRT6

In order to determine whether ERC-Exos can express SIRT6, we first identified the subcellular localization of SIRT6 in ERCs. The results showed that, consistent with previous reports, SIRT6 could be expressed in the nucleus and cytoplasm of ERCs (Supplementary Figure S1). The expression of SIRT6 in the ERC-Exos was measured using Western blot analysis. Results showed that SIRT6 did express in ERC-Exos (Figure 2A). To construct ERC-Exos with low SIRT6 expression, ERCs were transduced using a shRNA-SIRT6 lentivirus. At 72 h after transduction, GFP expression was detected in more than 90% SIRT6-KD-ERCs, and knocking down SIRT6 in ERCs would not cause changes in cell morphology (Figure 2B). Further examination showed that the expression of SIRT6 in ERCs was significantly decreased after transduction (Figure 2C). Subsequently, the supernatants were centrifuged to obtain SIRT6-KD-ERC-Exos. The result showed that SIRT6 expression was significantly knocked down and almost undetectable in SIRT6-KD-ERC-Exos (Figure 2D). Subsequently, exosomes purified from the supernatant of ERCs were identified using TEM and NTA. As previously described, TEM found that ERC-Exos exhibited a bilayer membrane structure with a typical cup-shaped morphology (Figure 2E). NTA showed that the majority of ERC-Exos were in the size range of 30–200 nm (Figure 2F). Moreover, the characteristics of SIRT6-KD-ERC-Exos were identified, and the findings were consistent with those of exosomes obtained from un-transfected ERCs. The results suggested that knocking down SIRT6 in ERC-Exos did not affect the morphological characteristics or size distribution of these exosomes (Figures 2E,F). Meanwhile, Western blot analysis identified exosome-specific markers, including CD9, CD63, and TSG101, but not the non-exosome marker calnexin in the ERC-Exo and SIRT6-KD-ERC-Exo groups (Figure 2G). These data indicated that ERC-Exos could express SIRT6 and that knocking down SIRT6 did not alter the basic characteristics of ERC-Exos.

Then, at the beginning of subsequent experiments, we set up three groups (ERC-Exos, SIRT6-NC-ERC-Exos, and SIRT6-KD-ERC-Exos) to identify exosomes and compare their functions. Results, as shown in the Supplementary Figure S2A, there was no difference in exosome morphology, particle size distribution, and surface protein markers among the three groups. Subsequently, we also compared the functions of the three groups. We executed the naïve $CD4^+$ T cell differentiation experiment *in vitro*. The results showed that there was no difference in differentiation of $CD4^+$ T cells between ERC-Exos and SIRT6-NC-ERC-Exos groups after treatment (Supplementary Figure S2B). Taken together, these data indicated that ERC-Exos and SIRT6-NC-ERC-Exos were identical in shape, size, and function.

SIRT6 mediated ERC-Exos to alleviate AR in transplant recipients

To determine whether SIRT6 mediates the therapeutic effect of ERC-Exos on AR, C57BL/6 recipient mice were transplanted with heart grafts from BALB/c donor mice and divided into three groups, namely, untreated, ERC-Exo-treated, and SIRT6-KD-ERC-Exo-treated group. As shown in Figure 3A, C57BL/6 recipient mice were injected with ERC-Exos or SIRT6-KD-ERC-Exos on the first, third and fifth day after operation, and at the same time, the untreated group mice were injected with the same volume of PBS. The results showed that ERC-Exos significantly prolonged allograft survival, and this effect was related to SIRT6 expression (Figure 3B). Specifically, the allograft survival time was significantly longer ($p < 0.05$) in the ERC-Exo-treated group (20.2 ± 2.4° days) than in the untreated group (8.2 ± 1.6° days). However, the allograft survival time was significantly shorter ($p < 0.05$) in the SIRT6-KD-ERC-Exo-treated group (14 ± 2° days) than in the ERC-Exo-treated group (20.2 ± 2.4° days). Graft pathology (Figure 3C) revealed that the grafts in the untreated group showed severe rejection with vasculitis and massive cell infiltration. After ERC-Exo treatment, the lesions in the grafts were significantly attenuated, with almost normal pathology on POD 8. However, SIRT6 knockdown reduced the therapeutic effect of ERC-Exos in mediating allograft protection, and the grafts showed typical features of AR. Graft pathology was scored according to accepted diagnostic criteria for heart rejection (Stewart et al., 2005). According to the findings, the untreated group had the highest pathological lesion score, followed by the SIRT6-KD-ERC-Exo-treated group. According to Figure 3D, the group that received ERC-Exo had the lowest pathological lesion score. In addition, ERC-Exo treatment significantly reduced intra-graft $CD4^+$ T cell infiltration, but this effect was markedly inhibited when SIRT6 was knocked down in ERC-Exos (Figures 3E,F).

In order to further verify whether the therapeutic effect of ERC-Exos is related to its regulation of $CD4^+$ T cell differentiation in the graft, we performed immunohistochemical staining in different (untreated, ERC-Exo treated, and SIRT6-KD-ERC-Exo treated) groups of mouse heart grafts. Different from the detection of $CD4^+$ T cell infiltration level, we paid more attention to the different subtypes and cytokine levels of $CD4^+$ T cells in the grafts. Results showed that in the untreated group, more inflammatory cytokines such as IFN-γ and IL-17A were found in the transplanted heart of mice, and the levels of these two cytokines decreased significantly after ERC-Exo treatment (Figures 4A,B,D,E). However, when SIRT6 was knocked down in ERC-Exos, this trend was obviously reversed (Figures 4A,B,D,E). In addition, we also detected the infiltration of anti-inflammatory cell Tregs in the graft. The infiltration distribution of Tregs showed an opposite trend. Treg infiltration was less in untreated grafts, but the proportion of Tregs in grafts increased significantly after ERC-Exo treatment. Remarkably, compared to the ERC-Exo treatment group, Treg infiltration in these grafts dramatically diminished after SIRT6-KD-ERC-Exos were administered (Figures 4C,F). These findings indicated that via modulating the proportion between different $CD4^+$ T cell subtypes in the graft, SIRT6 mediated the therapeutic benefits of ERC-Exos in alleviating AR of cardiac allografts.

SIRT6 mediated ERC-Exos to remodel the proportion of different $CD4^+$ T cell subtypes in transplant recipients

The above results showed that the SIRT6-expressing ERC-Exos affected the $CD4^+$ T cell infiltration and the degree of

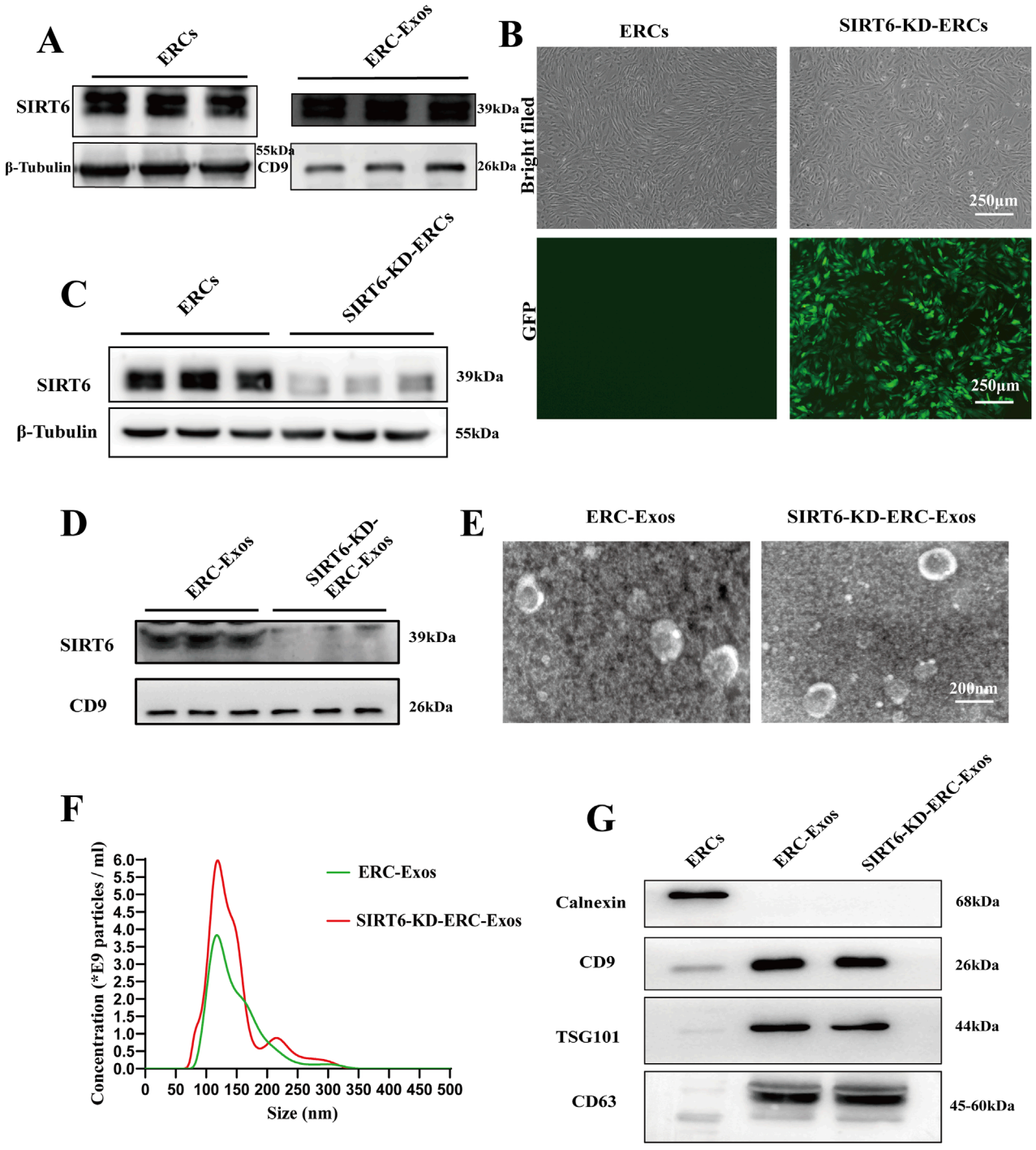

FIGURE 2
Isolation and identification of ERC-Exos and SIRT6-KD-ERC-Exos. **(A)** The expression level of SIRT6 in ERCs and ERC-Exos. **(B)** Morphology of ERCs and SIRT6-KD-ERCs at passage 2 (magnification 40×). The successful transduction of ERCs with shRNA-SIRT6 lentivirus was shown by GFP. **(C)** The expression level of SIRT6 in ERCs and SIRT6-KD-ERCs. **(D)** The expression level of SIRT6 in ERC-Exos and SIRT6-KD-ERC-Exos. **(E)** TEM revealed that both ERC-Exos and SIRT6-KD-ERC-Exos exhibited a bilayer membrane structure with a typical cup-shaped morphology. **(F)** Nanoparticle tracking analysis images of ERC-Exos and SIRT6-KD-ERC-Exos. Both ERC-Exos and SIRT6-KD-ERC-Exos were in the size range from 30 to 200 nm, and there is no difference between the two groups. **(G)** Western blot analysis of Calnexin, CD9, TSG101, and CD63 in ERCs, ERC-Exos, and SIRT6-KD-ERC-Exos (representative of three independent experiments).

pathological damage in these grafts. To explore the reasons behind this therapeutic effect, we determined the proportions of $CD4^+$ T cell subtypes, including Th1, Th17, and Tregs, in the peripheral lymphoid organs of recipient mice. As shown in Figures 5A–D, the proportions of Th1 and Th17 cells were significantly lower in the ERC-Exo-treated and SIRT6-KD-ERC-Exo-treated groups than in

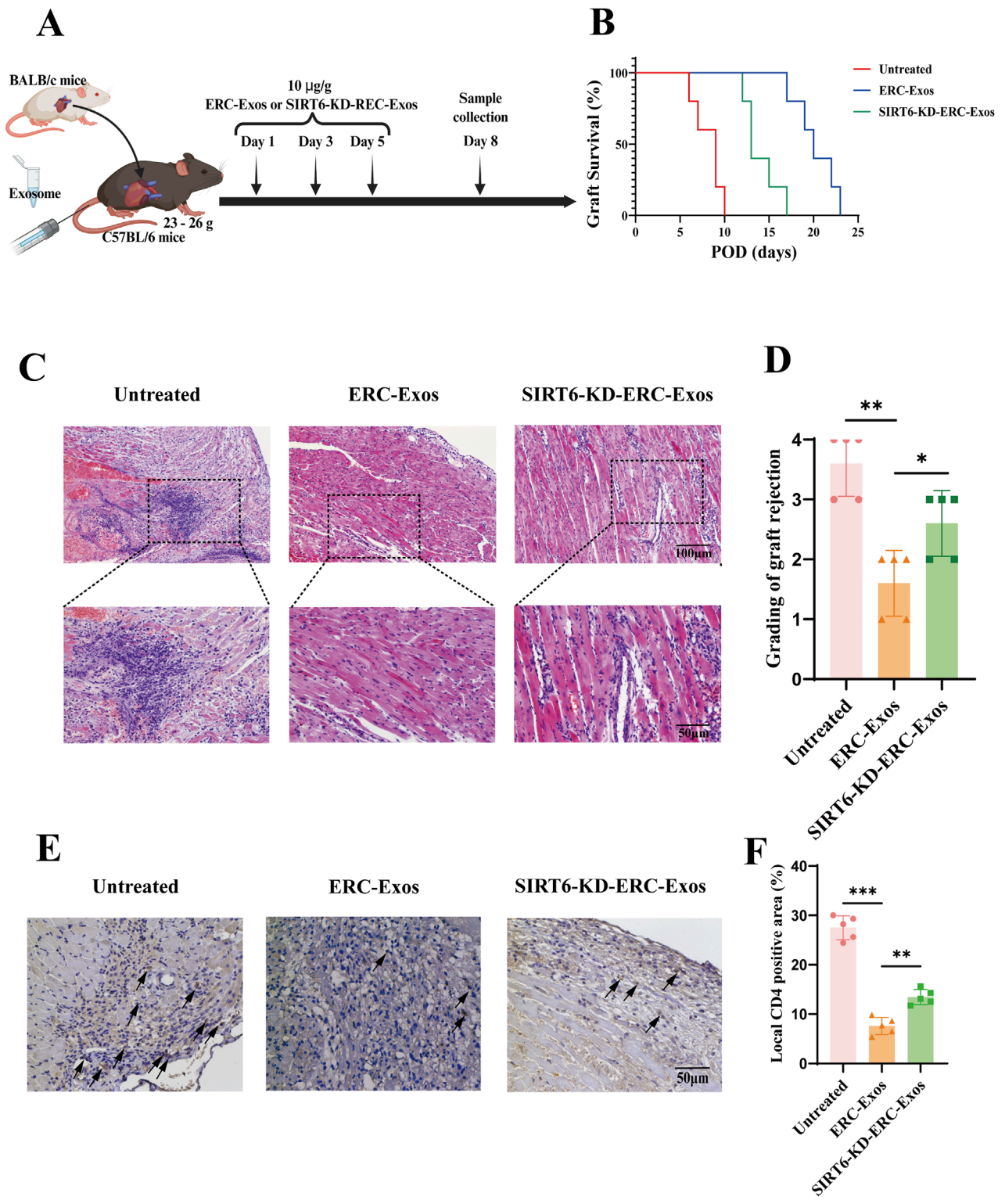

FIGURE 3
SIRT6 mediated ERC-Exos to prolong graft survival and alleviate acute allograft rejection. **(A)** A schema of *in vivo* study design. **(B)** Kaplan-Meier curves of allograft survival of cardiac transplants, in which BALB/c hearts were transplanted into C57BL/6 recipients. The allograft survival was significantly prolonged in ERC-Exo-treated group when compared with the untreated group, and the therapeutic effect was weakened in the SIRT6-KD-ERC-Exo-treated group (n = 5 per group). Statistics by Log-rank test. **(C)** Representative histology of cardiac allografts on post-operative day (POD) 8 (magnification 100× and 200× respectively). ERC-Exo-treated recipients showed a milder lymphocytes infiltration and myocyte damage compared with untreated mice, while SIRT6-KD-ERC-Exo treatment slightly reversed these changes (n = 5 per group). **(D)** Pathological score of graft rejection in different groups (n = 5 per group). Score criteria: 0, no change; 1, minimum change; 2, mild change; 3, moderate change; and 4, marked change compared with normal tissues. **(E)** Representative graft sections for immunohistological staining of intra-graft $CD4^+$ T cell infiltration (magnification 200×). ERC-Exo-treated recipients revealed a milder $CD4^+$ T cell infiltration compared with untreated mice, while knocking down
(*Continued*)

FIGURE 3 (Continued)
SIRT6 in ERC-Exos slightly reversed these changes (n = 5 per group). The positive staining areas were shown by arrows. **(F)** Quantitative analysis of $CD4^+$ T cell proportion in IHC. Statistics by one-way ANOVA. $^*p < 0.05$, $^{**}p < 0.01$, $^{***}p < 0.001$, ns = non-significant. For all panels, the bar graphs represent mean ± SD.

the untreated group. Compared with the ERC-Exo-treated group, the SIRT6-KD-ERC-Exo-treated group had significantly higher proportions of Th1 and Th17 cells in the spleens of the recipient mice. Meanwhile, the Treg proportion was significantly higher ($p < 0.001$) in the ERC-Exo-treated group than in the untreated group (Figures 5E,F). Similarly, the Treg population was significantly lower ($p < 0.01$) in the SIRT6-KD-ERC-Exo-treated group than in the ERC-Exo-treated group (Figures 5E,F). Subsequently, the serum levels of cytokines, including IFN-γ, IL-17, and IL-10, were examined in the different groups. Compared with the other groups, the ERC-Exo-treated group had the lowest levels of the pro-inflammatory cytokines IFN-γ and IL-17 (IFN-γ: untreated group vs. ERC-Exo-treated group, $p < 0.001$; ERC-Exo-treated group vs. SIRT6-KD-ERC-Exo-treated group, $p < 0.001$; IL-17: untreated group vs. ERC-Exo-treated group, $p < 0.001$; ERC-Exo-treated group vs. SIRT6-KD-ERC-Exo-treated group, $p < 0.01$) and the highest anti-inflammatory cytokine IL-10 (untreated group vs. ERC-Exo-treated group, $p < 0.001$; ERC-Exo-treated group vs. SIRT6-KD-ERC-Exo-treated group, $p < 0.01$, Figure 5G). Although the SIRT6-KD-ERC-Exo-treated group had lower IFN-γ and IL-17 secretion and higher IL-10 secretion than that in the untreated group, the therapeutic effect was still stronger in the ERC-Exo-treated group than in the SIRT6-KD-ERC-Exo-treated group (IFN-γ: ERC-Exo-treated group vs. SIRT6-KD-ERC-Exo-treated group, $p < 0.001$; IL-17: ERC-Exo-treated group vs. SIRT6-KD-ERC-Exo-treated group, $p < 0.01$; IL-10: ERC-Exo-treated group vs. SIRT6-KD-ERC-Exo-treated group, $p < 0.01$, Figure 5G). These data indicated that SIRT6 mediated ERC-Exos to remodel the proportion of different $CD4^+$ T cell subtypes and serum cytokine levels in transplant recipients.

SIRT6 mediated ERC-Exos to modulate naïve $CD4^+$ T cell differentiation *in vitro*

To further explore the role of SIRT6 in mediating ERC-Exo-induced naïve $CD4^+$ T cell differentiation *in vitro*, we co-cultured ERC-Exos with naïve $CD4^+$ T cells from the peripheral lymphoid organs of the C57BL/6 recipient mice. Firstly, the purity of isolated naïve $CD4^+$ T cells was detected by flow cytometry after isolation. The results (Supplementary Figure S3) showed that the purity of $CD4^+$ T cells isolated from C57BL/c mice spleens was more than 98%. Besides, the recognized markers of naïve $CD4^+$ T cells ($CD44^{lo}CD62L^{hi}$) in mice were also used for staining, and the results showed that the purity of naïve $CD4^+$ T cells was over 96% (Supplementary Figure S3). Because CD44CD62L can be used not only to identify naïve $CD4^+$ T cells but also to identify effector T cells ($CD44^{hi}CD62L^{lo}$), the data show that effector T cells (0.02%) could be almost ignored in the newly extracted naïve $CD4^+$ T cells of mice. Then, on the basis of the experimental grouping *in vivo*, the T-cell, T-cell + ERC-Exo, and T-cell + SIRT6-KD-ERC-Exo groups were established *in vitro*. Subsequently, the proportions of different $CD4^+$ T cell subtypes were determined *in vitro* in the three groups. The T-cell group had the highest proportions of Th1 and Th17 cells and the lowest Treg proportion, whereas the T-cell + ERC-Exo group showed the opposite trend. Compared with the T-cell + ERC-Exo group, the T-cell + SIRT6-KD-ERC-Exo group had significantly higher proportions of Th1 and Th17 cells and lower Treg proportion (T-cell + ERC-Exo group vs. T-cell + SIRT6-KD-ERC-Exo group, Th1 cells: $p < 0.05$; Th17 cells: $p < 0.05$; Tregs: $p < 0.01$; Figures 6A–F). Finally, the secretion levels of cytokines IFN-γ, IL-17, and IL-10 were detected in the different groups. As shown in Figure 6G, the results were consistent with the experimental results *in vivo*; that is, ERC-Exo treatment induced cytokines to tilt in the direction of anti-inflammation, while the absence of SIRT6 in exosomes weakened this effect. These results indicated that SIRT6 mediated ERC-Exos to modulate naïve $CD4^+$ T cell differentiation and cytokine secretion *in vitro*.

Subsequently, we further detected the level of cell death and proliferation during $CD4^+$ T cell differentiation *in vitro*. We explored it by Annexin V/7-AAD dye and the results showed that there would be some cell death in the process of T cell differentiation. When ERC-Exo treatment was given, the proportion of apoptotic cells in T cells decreased obviously, and when SIRT6 was knocked down, the decreasing trend increased again (Supplementary Figure S4A,B). These data indicated that SIRT6 also played a certain role in mediating ERC-Exos to inhibit T cell death. As to proliferation during *in vitro* T cell differentiation experiments, we used Ki67 dye to detect the proliferation of different treatment groups. The results, as shown in the Supplementary Figure S4C, showed that ERC-Exo treatment obviously inhibited the excessive proliferation of T cells under inflammatory conditions, while the knockdown of SIRT6 in exosomes reversed this trend, which indicated that SIRT6 mediated its regulation of T cell proliferation in ERC-Exos.

SIRT6 mediated ERC-Exos to inhibit naïve $CD4^+$ T cell activation and mTORC1 activity by weakening c-Myc-dependent glutaminolysis

To further explore the mechanisms by which SIRT6 mediates ERC-Exos to modulate $CD4^+$ T cell differentiation, we conducted an exosome phagocytosis experiment. Both ERC-Exos and SIRT6-KD-ERC-Exos were phagocytosed by naïve $CD4^+$ T cells, with no significant difference in the level of phagocytosis (Figure 7A). Subsequently, the SIRT6 protein level in naïve $CD4^+$ T cells were measured after co-culturing with ERC-Exos or SIRT6-KD-ERC-Exos for 12 h. Western blot analysis showed that ERC-Exo treatment significantly increased SIRT6 protein expression in naïve $CD4^+$ T cells (Figures 7B,C). However, treatment with SIRT6-KD-ERC-Exos did not significantly change SIRT6 protein expression level in naïve $CD4^+$ T cells (Figures 7B,C).

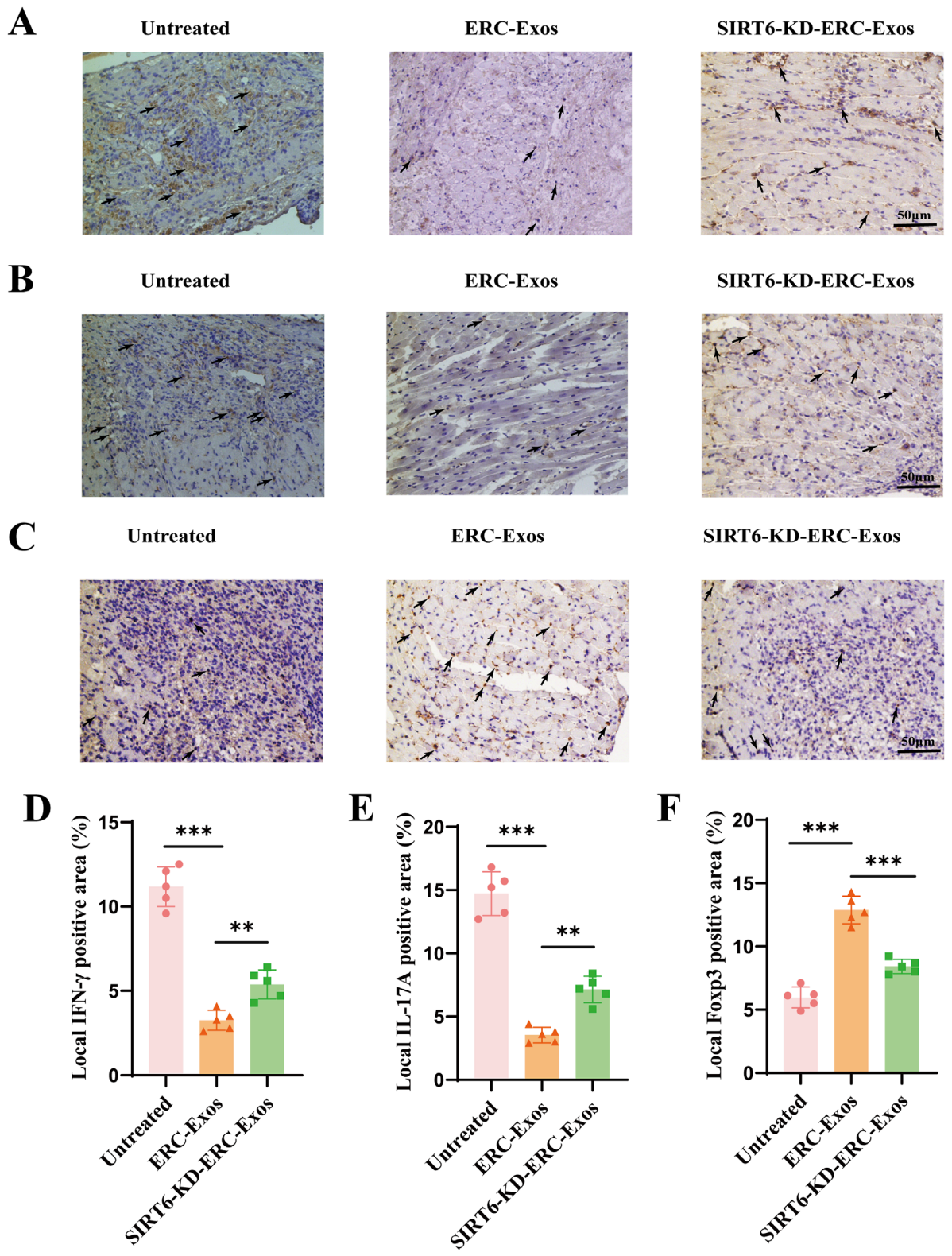

FIGURE 4
SIRT6 mediated ERC-Exos to regulate CD4$^+$ T cell differentiation in the graft, alleviating the inflammatory infiltration. Representative graft sections for infiltration of different subsets of CD4$^+$ T cells and immunohistochemical staining of cytokines in the graft (magnification 200×). IFN-γ **(A)** and IL-17A **(B)** were used to stain Th1 and Th17 cells and their corresponding cytokines in the graft, respectively. Foxp3 **(C)** was used to stain the Treg infiltration in the graft. The positive staining areas were shown by arrows. Quantitative analysis of IFN-γ **(D)**, IL-17A **(E)**, and Foxp3 **(F)** positive cell proportion in IHC via ImageJ software.

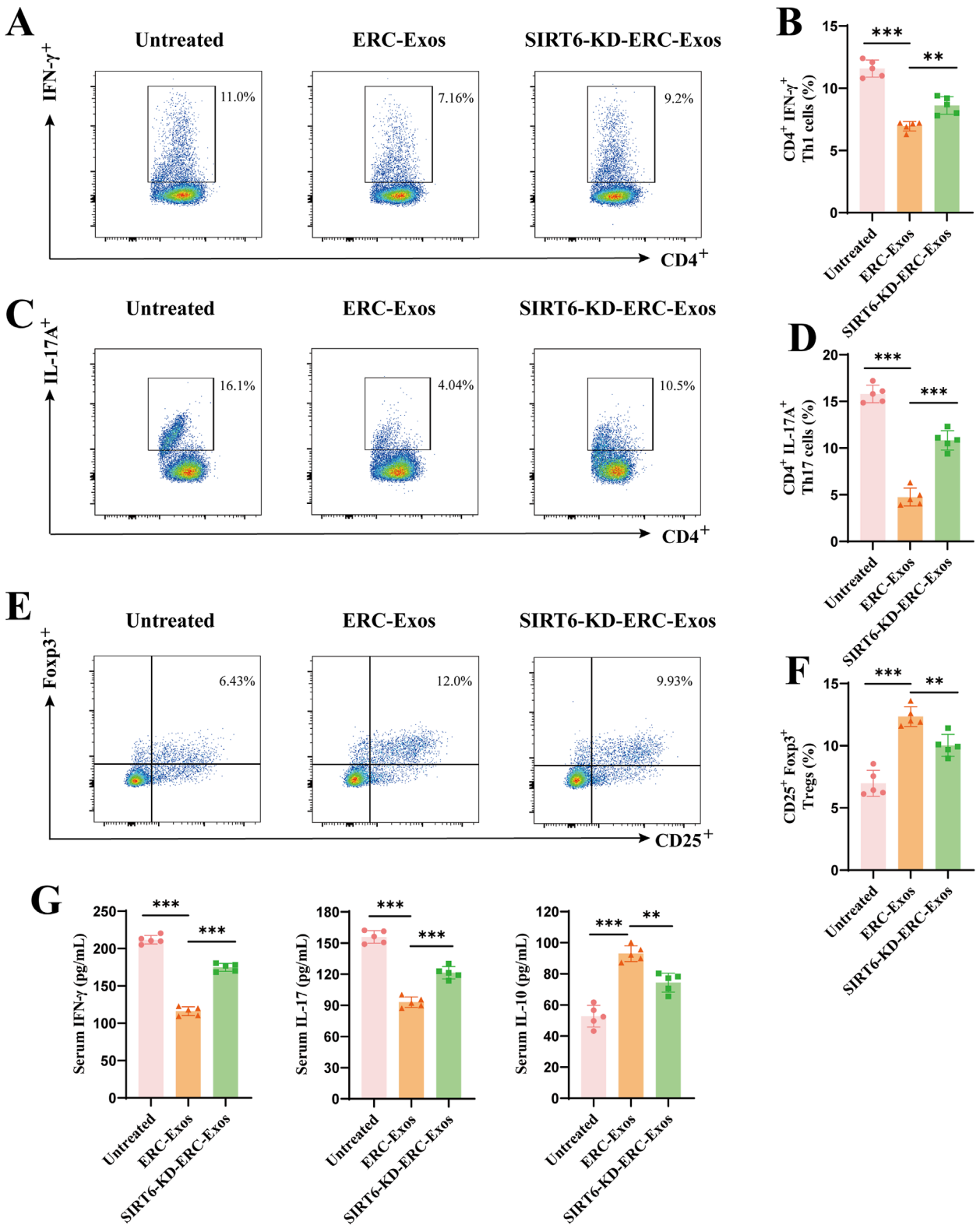

FIGURE 5
SIRT6 mediated ERC-Exos to remodel CD4$^+$ T cell differentiation and serum cytokine secretion level in recipient mice. Single-cell suspensions of splenocytes obtained from the untreated, ERC-Exo-treated, and SIRT6-KD-ERC-Exo-treated groups were analyzed for the frequency of CD4$^+$IFN-γ$^+$, and CD4$^+$IL-17A$^+$ cells by flow cytometry, gated on live cells. The representative pseudocolor plots **(A,C)** and statistical graphs **(B,D)** were depicted (n = 5 per group). In addition, the frequency of CD25$^+$Foxp3$^+$ cells obtained from the three groups were also analyzed by flow cytometry, gated on live cells and CD4$^+$ cells. The representative pseudocolor plots **(E)** and statistical graphs **(F)** were depicted (n = 5 per group). **(G)** The representative CD4$^+$ T cell serum cytokine levels in the recipient mice across the three groups (n = 5 per group). Specifically, compared with untreated group, ERC-Exo treatment could significantly decrease serum pro-inflammatory cytokine (IFN-γ and IL-17) level and increase IL-10 secretion, while knocking down SIRT6 in ERC-Exos slightly reversed these trends. Statistics by one-way ANOVA.$^*p < 0.05$,$^{**}p < 0.01$,$^{***}p < 0.001$, ns = non-significant. For all panels, the bar graphs represent mean ± SD.

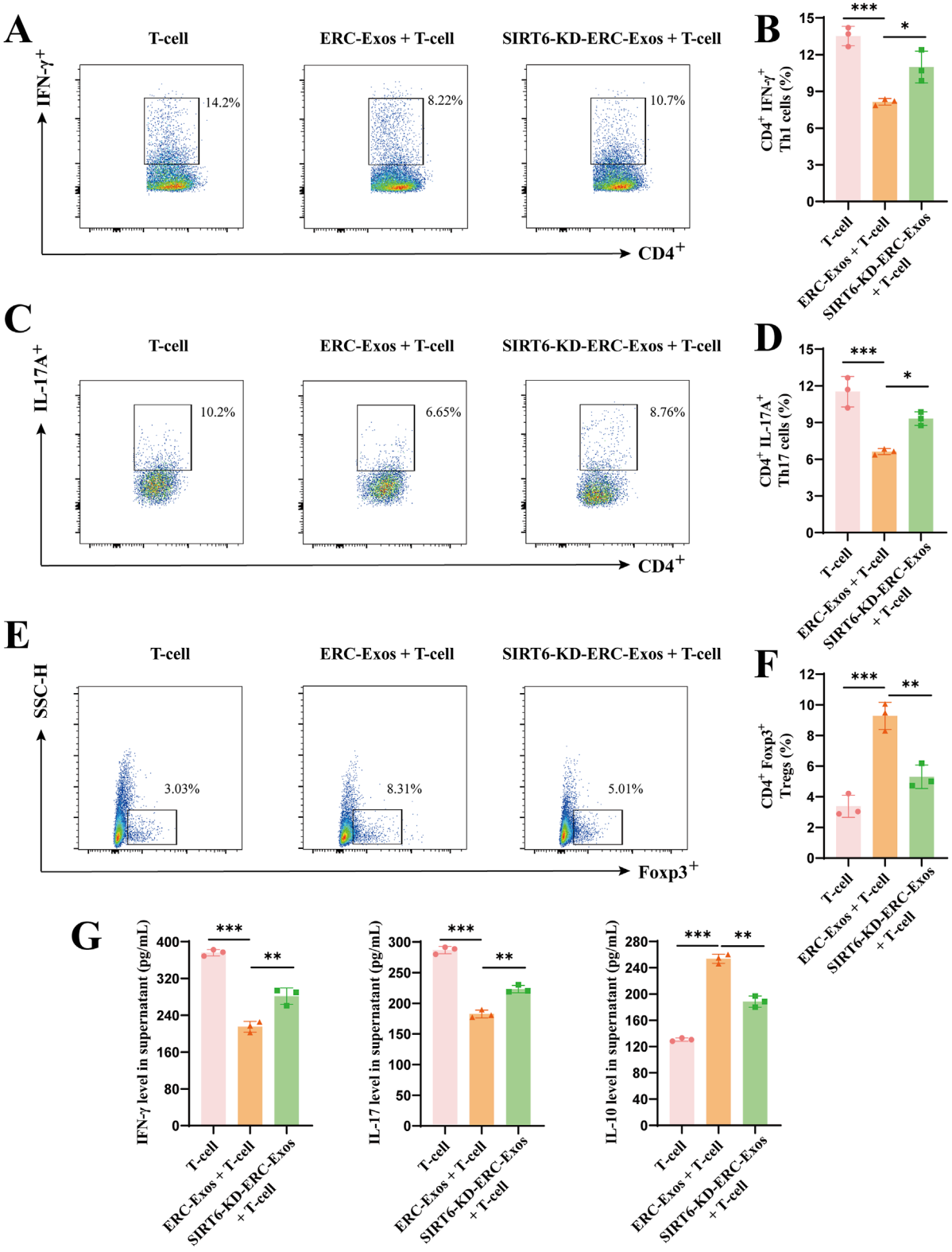

FIGURE 6
SIRT6 mediated ERC-Exos to modulate CD4$^+$ T cell differentiation and cytokine secretion level *in vitro*. Naïve CD4$^+$ T cells were extracted from C57BL/6 mice. In the medium added with CD3/CD28, they were co-cultured with/withou ERC-Exos and SIRT6-KD-ERC-Exo for 72 h. Single-cell suspensions were obtained from the T-cell, T-cell + ERC-Exo, and T-cell + SIRT6-KD-ERC-Exo groups and then were analyzed for the frequency of CD4$^+$IFN-γ$^+$, and CD4$^+$IL-17A$^+$ cells by flow cytometry, gated on live cells. The representative pseudocolor plots **(A,C)** and statistical graphs **(B,D)** were depicted (Repeat three independent holes). Similarly, the frequency of Foxp3$^+$ cells obtained from the three groups were also analyzed by flow cytometry, gated on live cells and CD4$^+$ cells. The representative pseudocolor plots **(E)** and statistical graphs **(F)** were depicted (Repeat three

(*Continued*)

FIGURE 6 (Continued)
independent holes). **(G)** The representative cytokine levels of $CD4^+$ T cell supernatant in the three groups (Repeat three independent holes). Compared with untreated group, ERC-Exo treatment could significantly decrease serum pro-inflammatory cytokine (IFN-γand IL-17) level and increase IL-10 secretion, while absence of SIRT6 in ERC-Exos slightly reversed these trends. Statistics by one-way ANOVA. $^*p < 0.05$, $^{**}p < 0.01$, $^{***}p < 0.001$, ns = non-significant. For all panels, the bar graphs represent mean ± SD.

SIRT6 has been shown in earlier research to be able to block c-Myc transcription and translation in a variety of cell types. The transcription factor c-Myc is essential for T cell proliferation and differentiation. According to prior proteomic researches, c-Myc regulates the expression of important proteinases and amino acid transporters in immunocompetent T cells, with ASCT2 and GLS1 displaying the most notable alterations (Wang et al., 2011; Marchingo et al., 2020). To find out this change, we first used CD3/CD28 to stimulate the activation of naïve $CD4^+$ T cells, and then treated them with ERC-Exos/SIRT6-KD-ERC-Exos, respectively, and then detected the transcription level of c-Myc in T cells. The results showed that after ERC-Exo treatment, the transcription level of c-Myc mRNA in naïve $CD4^+$ T cells decreased significantly, and this decrease would be reversed with the knock-down of SIRT6 in exosomes (Supplementary Figure S5). Besides, the transcription level of ASCT2 and GLS1 mRNA in naïve $CD4^+$ T cells also showed the same trend (Supplementary Figure S5). Then, we further use Western blot to analyze their expression at the translation level. The results showed that ERC-Exo treatment significantly inhibited c-Myc expression, whereas SIRT6-KD-ERC-Exo treatment restored this inhibitory function (Figures 7D,E). The downstream target proteins of c-Myc, including ASCT2 and GLS1, were also detected, and the result was consistent with the change in c-Myc protein expression (Figures 7D,E). In order to further clarify that this change is indeed related to SIRT6, we further explored it by using SIRT6 inhibitor OSS_128,167. In the experimental group where SIRT6 inhibitor interfered with ERC-Exo treatment, the protein levels of c-Myc, ASCT2, and GLS1 increased compared with ERC-Exo treatment (Supplementary Figure S6A,B). Subsequently, we detected the glutamine uptake of $CD4^+$ T cells in different treatment groups. These results are consistent with the above changes in protein levels. Compared with the other two groups, the untreated group showed the highest glutamine intake level (Figure 7F). However, after ERC-Exo treatment, the glutamine uptake level of T cells decreased obviously, showing the lowest level (Figure 7F). Compared with ERC-Exo treatment, the uptake level of glutamine in T cells treated with SIRT6-KD-ERC-Exo increased, but it was still lower than that in the untreated group (Figure 7F). In addition, the content of α-KG in $CD4^+$ T cells was further detected in the three groups, respectively. Consistent with the level of glutamine intake, the highest level of α-KG content was displayed in $CD4^+$ T cells of the untreated group (Figure 7G). After ERC-Exo treatment, the content of α-KG in $CD4^+$ T cells decreased significantly, but when SIRT6 in ERC-Exo was knocked down, the content of α-KG in T cells increased (Figure 7G). Similarly, after OSS_128,167 treatment, glutamine uptake and intracellular α-KG production of naïve $CD4^+$ T cells were significantly inhibited compared with ERC-Exo treatment group (Supplementary Figure S6C,D). Previous studies have revealed that the activation state of mammalian target of rapamycin complex 1 (mTORC1) is regulated by glutaminolysis in various cells. Considering the decrease of glutamine uptake and its metabolite α-KG, we further explored the activation state of the mTORC1 signaling pathway through Western blot analysis. Similarly, the data showed that the ERC-Exo treatment inhibited the activation of the mTORC1 pathway in naïve $CD4^+$ T cells, and this effect was related to the expression of SIRT6 in exosomes (Figures 7H,I). Administration of SIRT6-KD-ERC-Exos significantly reversed the inhibition of the mTORC1 pathway (Figures 7H,I). The Supplementary Figure S6E,F further proved this effect mediated by SIRT6 in ERC-Exos.

In order to further clarify that this effect is mediated by SIRT6, we used SIRT6 activator and SIRT6 inhibitor in Jurkat cell to explore the activated state of c-Myc/glutaminolysis/mTORC1 status respectively. The results showed that the level of c-Myc-dependent glutaminolysis increased after the activation of CD3/CD28 in Jurkat cell, which led to the activation of mTORC1 (Supplementary Figure S7). When SIRT6 activator was given, these effects were obviously inhibited (Supplementary Figure S7), indicating that SIRT6 did play a key role in inhibiting c-Myc-dependent glutaminolysis of T cells. Similarly, the opposite trend after administration of SIRT6 inhibitor further proves this effect (Supplementary Figure S7). These data demonstrated that SIRT6 did regulate the c-Myc/glutaminolysis/mTORC1 status in activated T cells.

We measured the activation level of naïve $CD4^+$ T cells in light of earlier research showing that the production of important proteins linked to glutaminolysis is suppressed and that T cell activation is linked to glutaminolysis. The results showed that administration of ERC-Exos significantly restrained the activation of naïve $CD4^+$ T cells compared with untreated T cells (T-cell + ERC-Exo group vs. T-cell group, $p < 0.01$, Figures 7J,K; Supplementary Figure S8). However, SIRT6 knockdown in ERC-Exos led to an increased activation of naïve $CD4^+$ T cells (T-cell + ERC-Exo group vs. T-cell + SIRT6-KD-ERC-Exo group, $p < 0.05$, Figures 7J,K; Supplementary Figure S8). Taken together, these data showed that SIRT6 mediated ERC-Exos to inhibit naïve $CD4^+$ T cell activation and mTORC1 activity by weakening c-Myc-dependent glutaminolysis.

Discussion

Immunosuppressive medications are currently the primary strategy for managing AR following transplantation. As previously mentioned, it is impossible to overlook these medications' limits with regard to infection, carcinogenesis, and chronic graft failure (Söderlund and Rådegran, 2015). So, safe and effective methods to alleviate AR must be explored. Clinical trials have shown that MSCs from different sources, such as umbilical cord-derived MSCs or bone marrow-derived MSCs, can be administered as injection therapy

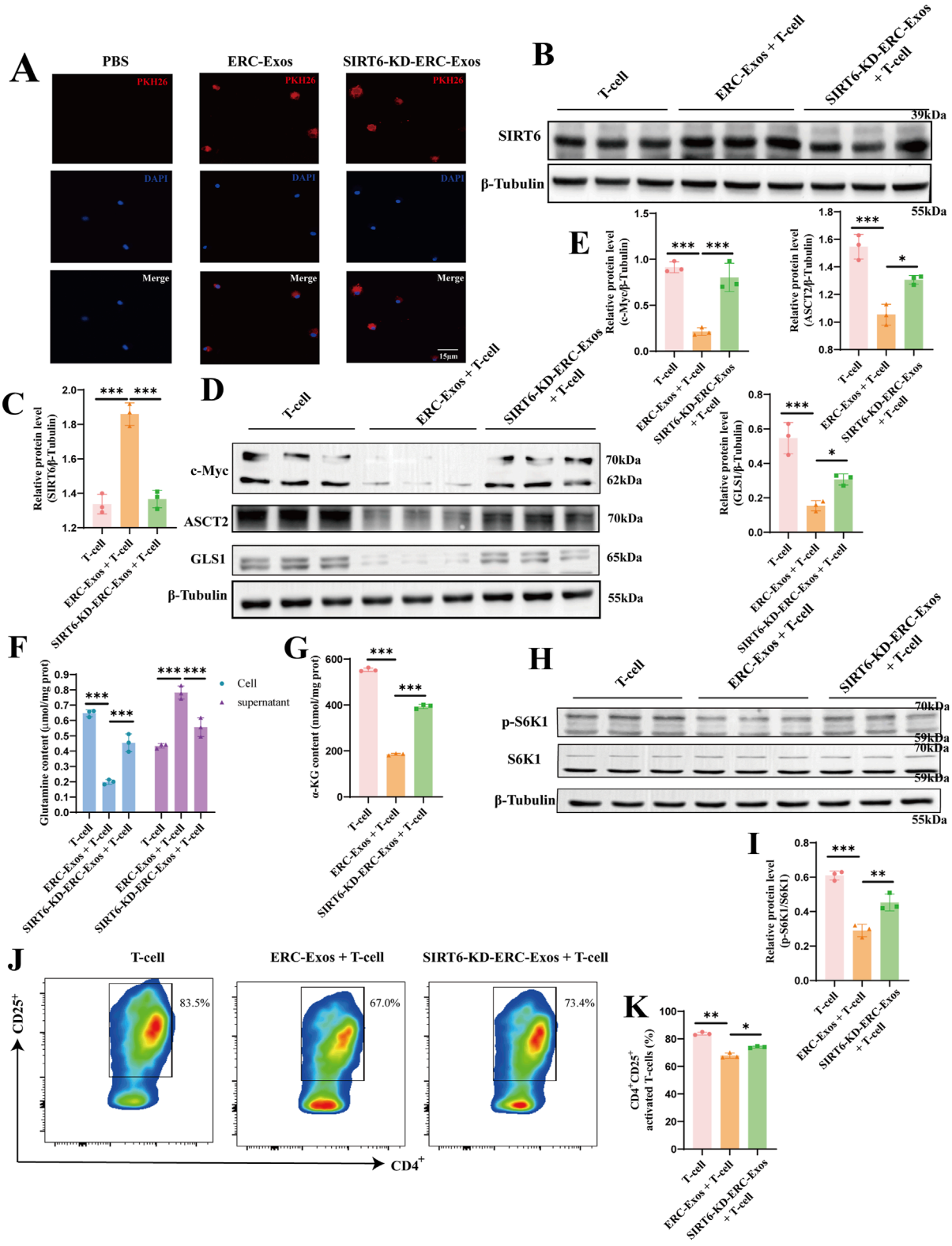

FIGURE 7
SIRT6 mediated ERC-Exos to inhibit naïve CD4$^+$ T cell activation and mTORC1 activation via weakening c-Myc-dependent glutaminolysis. Firstly, naïve CD4$^+$ T cells were acquired from C57BL/6 mouse spleen, then were co-cultured with PKH-26 labeled exosomes for 6 h. **(A)** Representative diagrams of ERC-Exos and SIRT6-KD-ERC-Exos phagocytosed by CD4$^+$ T cells (red represents exosomes-labeled by PKH26, blue represents the naïve CD4$^+$ T cell nucleus-labeled by DAPI; magnification 630×). Subsequently, ERC-Exos or SIRT6-KD-ERC-Exos were added into naïve CD4$^+$ T cells respectively for 12 h, and then detected the expression level of SIRT6 in naïve CD4$^+$ T cells via Western blot **(B)**. **(C)** Quantitative analysis of SIRT6 protein level. The key proteins of c-Myc-induced glutaminolysis **(D)** were detected via Western blot. **(E)** Quantitative analysis of c-Myc, ASCT2, and GLS1 protein level.
(*Continued*)

FIGURE 7 (Continued)
Besides, the content of glutamine was detected in $CD4^+$ T cells and supernatant 24 h after different treatments **(F)**. Because the glutamine contentadded in the culture medium was consistent, the glutamine uptake level of $CD4^+$ T cells in different treatment groups could be evaluated by comparing the glutamine content in cells and supernatant, respectively. **(G)** The decomposition product α-KG of glutamine was further detected in these $CD4^+$ T cells. **(h)** The activation state of mTORC1 in $CD4^+$ T cells of different treatment groups was further detected. Finally, the activation level of naïve $CD4^+$ T cells was analyzed for the frequency of $CD25^+$via flow cytometry. **(I)** Quantitative analysis of p-S6K1 protein level. The representative pseudocolor plots **(J)** and statistical graphs **(K)** were depicted (Repeat three independent holes). Statistics by one-way ANOVA. $^*p < 0.05$, $^{**}p < 0.01$, $^{***}p < 0.001$, ns = non-significant. For all panels, the bar graphs represent mean ± SD.

after kidney transplantation, and they all have obvious therapeutic effects in reducing the dosage of immunosuppressive drugs with no adverse reactions (Sun et al., 2018; Wei YC. et al., 2021). Besides, our preliminary work confirmed that ERCs and ERC-Exos can alleviate AR and prolong cardiac allograft survival in a mouse cardiac allograft model (Hu et al., 2021; Xu et al., 2024). Notably, previous studies have confirmed that the therapeutic effect of ERCs is gender-independent (Izawa et al., 2025; Lu et al., 2024), and it can play a therapeutic role in both female and male mice (Fathi-Kazerooni and Tavoosidana, 2019). Considering that female mice may have some extra-experimental interference due to the changes of the menstrual cycle and hormone level, this experiment adopts male mice for heart transplantation.

In this study, we first found that SIRT6 expressed in ERC-Exos. We then used the shRNA-SIRT6 lentiviral to successfully obtain SIRT6-KD-ERC-Exos, a type of ERC-Exo with extremely low SIRT6 expression. Though using these two different exosomes to treat intra-abdominal heterotopic cardiac transplantation mice, we found that ERC-Exo treatment alleviated AR in these model mice. Specifically, ERC-Exo treatment prolonged graft survival, reduced the infiltration of inflammatory cell as well as cytokines in the graft, remodeled $CD4^+$ T cell differentiation, and rectified the inordinate secretion of $CD4^+$ T cell inflammatory cytokines. However, when SIRT6 was knocked down in ERC-Exos, these therapeutic effects were significantly weakened, resulting in a shorter graft survival, heavier intra-graft inflammatory cell and cytokines infiltration, disordered $CD4^+$ T cell differentiation, and serum pro-inflammatory cytokine secretion. This cardioprotective effect may be attributed to the therapeutic effect of ERC-Exos mediated by SIRT6 on acute cardiac allograft rejection by remodeling peripheral $CD4^+$ T cell differentiation. Follow-up mechanistic studies demonstrated that ERC-Exo treatment downregulated c-Myc protein expression, thereby weakening the uptake and utilization of glutamine. As mentioned earlier, c-Myc is a hub protein that can regulate the relative expression of key proteins related to glutaminolysis, especially ASCT2 and GLS1 (Marchingo et al., 2020). The expression levels of ASCT2 and GLS1 were verified to be downregulated, and the activation of the mTORC1 pathway was suppressed. Likewise, the expression level of these proteins, the uptake rate, and the glutamine utilization rate were all reversed while SIRT6 was knocked out in ERC-Exos. Taken together, these results indicated that it was SIRT6 in ERC-Exos that alleviated AR by weakening c-Myc-dependent glutaminolysis (Figure 8).

Exosomes are 30–200 nm membrane extracellular vesicles composed of various proteins, enzymes, transcription factors, lipids, extracellular matrix proteins, receptors, and nucleic acids (Kalluri and LeBleu, 2020). Previous studies have shown that ERC-Exos can promote angiogenesis, anti-apoptosis, and immunoregulation through a variety of microRNAs and proteins contained in it (Marinaro et al., 2019). Our previous research found that loading siSLAMF6 within ERC-Exos can effectively prolong the graft survival time in cardiac transplantation mice (Xu et al., 2024). Interestingly, in this study, we found that compared with the untreated group, ERC-Exo treatment can also significantly prolong the graft survival time, and significantly inhibit the trend of $CD4^+$ T cells differentiating into pro-inflammatory subtypes (Xu et al., 2024). This means that there are some therapeutic molecules in ERC-Exos. Although ERC-Exos with artificial modification does show better therapeutic effect, its large-scale development is limited due to the complicated artificial modification process of foreign bodies. Therefore, exploring the self-mechanism of ERC-Exo therapeutic effect is imperative.

With the discovery of transcription factors in exosomes (Kalluri and LeBleu, 2020; Qiu et al., 2018), some proteins that were located in the nucleus and could enter/leave the nucleus, including the SIRT family proteins, were gradually explored in exosomes. The SIRT family proteins have seven members (SIRT1-7) with different subcellular localization and function (Warren and MacIver, 2019). These proteins play many important roles in cell metabolism, anti-oxidative stress and DNA repair (Warren and MacIver, 2019). Among them, the roles of SIRT1 and SIRT3 in adaptive immune regulation have been revealed (Warren and MacIver, 2019). A recent study found that the decrease of SIRT1 expression was related to the severity of inflammation and tubulitis after renal transplantation (Aksungur et al., 2025). Because SIRT1 and SIRT3 are located in the nucleus and mitochondria, respectively, there are few previous studies on them in exosomes. Encouragingly, with the development of research, the extracellular exploration of SIRT3 may be further developed with the help of the research hotspot of mitochondria transfer. Besides, SIRT6 also showed good anti-inflammatory potential (Pillai and Gupta, 2020). For instance, inhibiting SIRT6 reduced the percentage of Tregs in the peripheral blood and synovial fluid in rheumatoid arthritis (Wang et al., 2019). However, whether SIRT family proteins can be expressed in extracellular structure is still a puzzle. Until recent years, Chamberlain *et al.* found that SIRT2 is expressed in oligodendrocyte-derived exosomes and deacetylated (Chamberlain et al., 2021). Wei *et al.* also demonstrated that SIRT6 expressed in mouse bone marrow-derived MSC exosomes and alleviates aortic calcification by deacetylating HMGB1 (Wei WQ. et al., 2021). These reports aroused our interest in exploring the role and function of SIRT6 in ERC-Exos for immunotherapy. Hou *et al.* also reported that SIRT6 can be released from the nucleus and accumulate in the cytoplasm, and this effect can be amplified by palmitic acid treatment (Hou et al., 2022). Combining these reports with our results, we speculate that the therapeutic effect of ERC-Exos can be improved by pretreatment

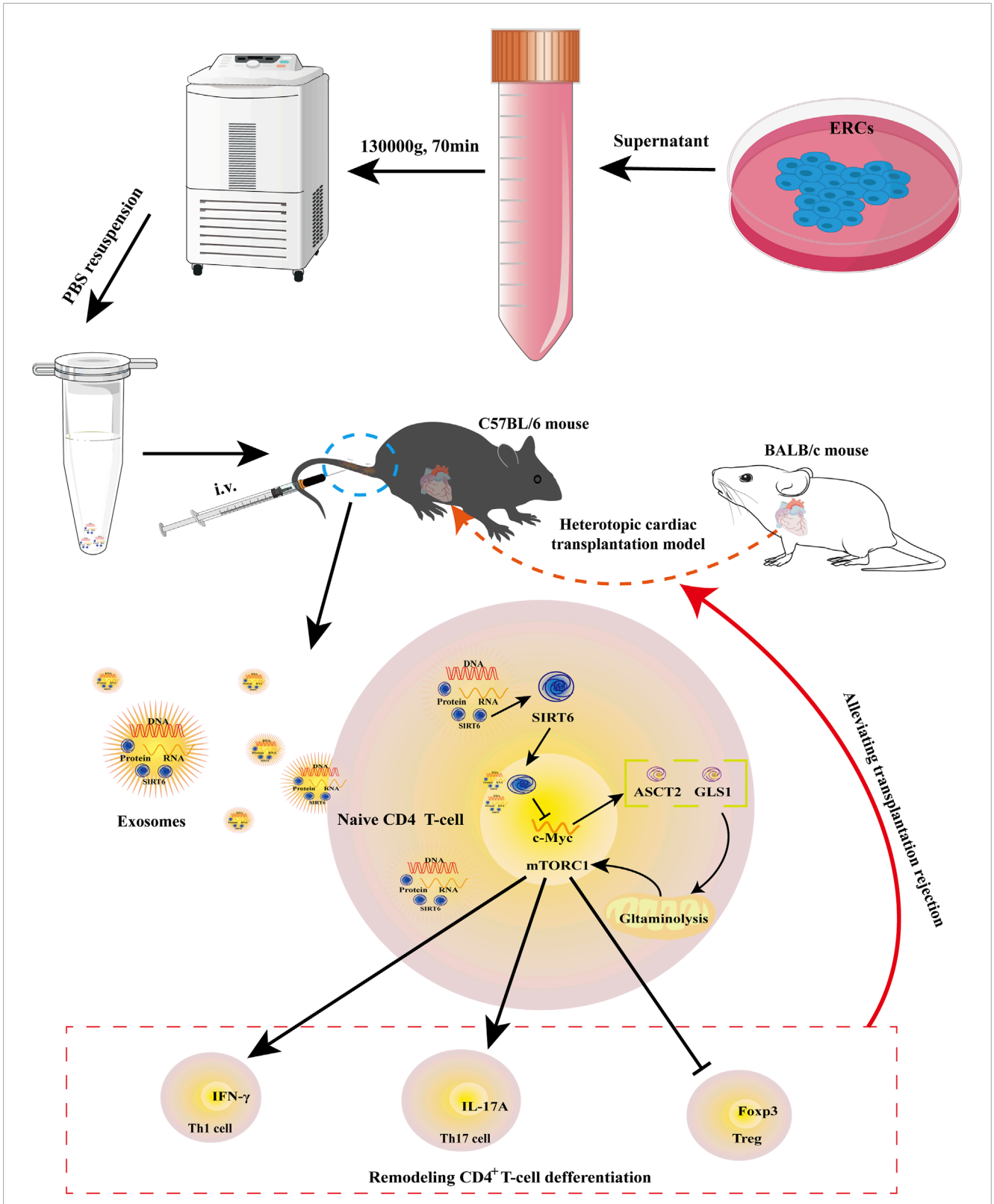

FIGURE 8
Schematic diagram of the therapeutic effects mediated by SIRT6-expressing ERC-Exos on AR. As previously described, ERC-Exos are obtained from the supernatant of ERCs by ultracentrifugation. Then, BALB/c hearts are transplanted into the abdomen of C57BL/6 recipients to construct a heterotopic cardiac transplantation model. And ERC-Exo treatment can alleviate AR in recipient mice by tail vein injection. In terms of mechanism, after the ERC-Exos are injected into recipient mice, they reach all parts of the body with blood circulation, including lesion sites or peripheral lymphoid organs, such as the spleen, and then can be phagocytized by peripheral naïve $CD4^+$ T cells, leading to an increased SIRT6 expression level in these T cells. Increased SIRT6 in naïve $CD4^+$ T cells can inhibit the transcription and translation of c-Myc through its histone deacetylation and then downregulate
(*Continued*)

FIGURE 8 (Continued)
the key proteins of glutaminolysis, ASCT2 and GLS1. Thus, SIRT6-expressing ERC-Exos can weaken c-Myc-dependent glutaminolysis in naïve $CD4^+$ T cells. Due to the weakened glutaminolysis, the activity of mTORC1, the downstream pathway of glutaminolysis process, is also inhibited, so the differentiation of naïve T cells into Th1/Th17 is weakened and Treg differentiation is increased.

with palmitic acid followed by exosome collection. As for other SIRT family proteins, based on their anti-oxidative stress function, they may also have the potential to regulate immunity through a series of intracellular physiological activities, but the specific mechanism may be different and needs further exploration.

Previous studies have reported that T cells can change their differentiation fate or function by phagocytosing exosomes secreted by other cells (Wang et al., 2018; Bolandi et al., 2020). In the present study, the ERC-Exos injected into the recipient mice were distributed into all parts of the body via blood circulation, including lesion sites or peripheral lymphoid organs, such as the spleen, and then phagocytosed by peripheral naïve $CD4^+$ T cells, leading to an increase in SIRT6 expression, thus exerting its therapeutic effects. As previously reported, SIRT6 may also play a deacetylating role in the exosomes (Wei WQ. et al., 2021). SIRT6 plays a therapeutic role in many immune-related diseases through deacetylation (Li et al., 2022; Pillai and Gupta, 2020). For example, Oraby *et al.* found that SIRT6 improves cell inflammation and blepharoptosis caused by ulcerative colitis in acetic acid-treated rats by deacetylating FoxC1 (Oraby et al., 2024). Studies have shown that SIRT6 can decrease c-Myc activity by promoting its deacetylation at the ninth lysine site of H3 histone (H3K9) and the 56th lysine site of H3 histone (H3K56) (Stewart et al., 2005; Tao et al., 2013). Although we did not detect H3K9 or H3K56 acetylation, our results did indicate that SIRT6 reduced c-Myc expression. Therefore, combined with previous reports, we deduced that ERC-Exo treatment increased SIRT6 expression in naïve $CD4^+$ T cells and then decreased the transcription and translation levels of c-Myc by promoting its deacetylation at the H3K9 or H3K56 sites, which consequently decreased the expression of key proteins ASCT2 and GLS1 for glutaminolysis.

ASCT2 is an important amino acid transporter for glutamine uptake into the cytoplasm, and GLS1 is the first rate-limiting enzyme for glutaminolysis after entering the cytoplasm (Liu et al., 2023). They control glutaminolytic uptake and enzymolysis, respectively. Previous studies have shown that glutaminolysis is closely related to the activation and differentiation of naïve $CD4^+$ T cells (Yu et al., 2022; Nakaya et al., 2014). For example, Yu *et al.* revealed that inhibiting the activation of naïve $CD4^+$ T cells and Th1/Th17 cell differentiation by blocking glutaminolysis play a therapeutic role in autoimmune hepatitis (Yu et al., 2022). Consistent with these reports, our study found that, even with the addition of CD3/CD28, SIRT6-expressing ERC-Exos inhibited naïve $CD4^+$ T cell activation. Additionally, previous studies have shown that Th1/Th17 cell generation requires mTORC1 activation, whereas Tregs do not (Nakaya et al., 2014; Delgoffe et al., 2009). Nakaya *et al.* also found that after the T cell receptor stimulation by CD3/CD28, naïve $CD4^+$ T cells begin to absorb large quantities of glutamine via ASCT2, thereby activating the downstream target mTORC1 and promoting the differentiation of naïve $CD4^+$ T cells into Th1 and Th17 cells (Nakaya et al., 2014). However, Treg differentiation is not affected by glutamine intake. Subsequently, the knockout experiment confirmed that the deletion of ASCT2 affected the differentiation of Th1 and Th17 cells by reducing glutamine uptake but had no effect on Treg differentiation, indicating that Tregs can differentiate normally under glutamine deficiency (Nakaya et al., 2014). Similarly, our data showed that SIRT6-expressing ERC-Exos inhibited mTORC1 activation by weakening glutaminolysis, thus reducing the differentiation of Th1/Th17 cells and increasing that of Tregs.

mTORC1, a center for sensing and integrating various signals from the environment to control metabolism, plays an indispensable role in integrating the metabolic spectrum and guiding the differentiation of naïve $CD4^+$ T cells (Huang et al., 2020). Previous studies have demonstrated that Ras homolog enriched in brain (Rheb) (an upstream activating protein of mTORC1)-deficient $CD4^+$ T cells suppress Th1 cell differentiation by weakening the T cell response to IL-12 and preventing T-bet transcription (Delgoffe et al., 2011; Chornoguz et al., 2017). Regarding Th17 cells, the activated mTORC1 can increase the phosphorylation level of STAT3 at tyrosine 705 (Tyr705) in naïve $CD4^+$ T cells, which is necessary for retinoic acid receptor-related orphan receptor gamma t (RORγt) expression (Wang et al., 2020). As a negative regulator of STAT3, activated mTORC1 also promotes STAT3 phosphorylation and upregulates RORγt expression by blocking suppressor of cytokine signaling 3 (SOCS3) (Wang et al., 2020). Then, activated mTORC1 upregulates HIF-1α expression to promote glycolysis in naïve $CD4^+$ T cells, consequently promoting Th17 cell differentiation (Dang et al., 2011). Finally, activated mTORC1 enhances Th17 cell differentiation in a ribosomal S6 kinase 1/2 (S6K1/2)-dependent manner. Specifically, S6K1 inhibits the expression of Gfi1, a negative regulator of Th17 cell differentiation, and S6K2 promotes the nuclear localization of RORγt, thereby upregulating RORγt expression (Kurebayashi et al., 2012). However, the function of mTORC1 is reversed during Treg differentiation. For example, activated mTORC1 can block Treg generation by preventing Smad3 phosphorylation or H3K4 methylation close to the Foxp3 transcription start site, both of which promote Foxp3 transcription (Kurebayashi et al., 2012). Moreover, mTORC1 improves glycolytic activity by inducing HIF-1α expression, but Treg differentiation does not rely on glycolytic metabolism to provide energy compared to Th17 cells, resulting in a significant difference in the differentiation of Th17 cells and Tregs (Dang et al., 2011; Shi et al., 2011). In summary, these reports showed the different roles of mTORC1 in $CD4^+$ T cell differentiation; that is, activated mTORC1 promotes the pro-inflammatory cell differentiation, such as Th1/Th17 cells, while inactivated mTORC1 promotes the differentiation of anti-inflammatory cells, such as Tregs.

Amino acids, especially glutamine, leucine, arginine, and methionine, play an important role in the activation of the

mTORC1 signaling pathway (Jewell et al., 2015; Meng et al., 2020; Gu et al., 2017). ASCT2, an essential amino acid transporter for Glutamine uptake, regulates the mTORC1 activation status (Nakaya et al., 2014). Nakaya *et al.* demonstrated that ASCT2 mediates TCR-stimulated mTORC1 activation in naïve $CD4^+$ T cells (Nakaya et al., 2014). As mentioned above, our results showed that the expression of ASCT2 in naïve $CD4^+$ T cells was downregulated after administration of ERC-Exos. Subsequently, we further detected that the glutamine uptake efficiency and α-KG content in these T cells also decrease. Therefore, we further explored mTORC1 activity, and our findings were consistent with those of previous studies showing that mTORC1 is inactivated when ASCT2 is downregulated in naïve $CD4^+$ T cells (Nakaya et al., 2014; Huang et al., 2020). α-KG, the metabolic product of glutamine, promotes mTORC1 assembly and positively regulates the mTORC1 pathway when present in lysosomes (Cabré et al., 2021; Durán et al., 2013). In addition to this direct effect, glutaminolysis also regulates the activation of mTORC1 by affecting energy generation in cells. In specific, glutaminolysis metabolic products such as α-KG can participate in tricarboxylic acid cycle, which is the main pathway to produce energy (Cabré et al., 2021). Excessive energy production in cells inhibits adenosine 5′-monophosphate (AMP)-activated protein kinase (AMPK), an upstream negative regulatory target of mTORC1 (González et al., 2020). Hence, combining these reports with our results, we speculate that α-KG inactivates mTORC1 by reducing energy generation in naïve $CD4^+$ T cells to activate AMPK or directly affecting mTORC1 assembly. Although we were not clear about how α-KG inactivates mTORC1 in $CD4^+$ T cells, our results showed that SIRT6-expressing ERC-Exos could indeed inactivate mTORC1 by reducing α-KG, a key metabolite of glutamine decomposition.

Previously, studies have revealed that $CD4^+$ effector T cell subsets participate in allograft rejection (Wa et al., 2011). Th1 and Th17 cells are closely related to the occurrence of transplant rejection, while Tregs are often related to the formation and maintenance of immune tolerance (Wa et al., 2011). When $CD4^+$ T cells are activated, they can produce IL-2, which can be used as a growth factor to induce the proliferation of Th1 cells expressing transcription factor T-bet expressed in T cells (Hall, 2015). And Th1 cells can become an important part of allograft rejection by secreting IFN-γ. On the one hand, when Th1 cells are recruited to inflammatory tissues, they can directly mediate tissue damage by releasing IFN-γ (Hall, 2015). On the other hand, IFN-γ can also be used as a bridge to connect Th1 cells and induce other anti-inflammatory cell activation, such as M1 macrophages (Hall et al., 1984). In addition, Th17 cells also play an important role in tissue injury on AR. IL-17A, a pro-inflammatory cytokine, can be produced by $CD8^+$ memory T cells, eosinophils, neutrophils, and monocytes, but its main secretory cell is still Th17 cells (Afzali et al., 2007). IL-17A can not only activate the inflammatory signal pathway (such as the mitogen-activated protein kinase (MAPK) and NF-κB pathways) of target cells by binding to its receptors but also induce further inflammatory response by recruiting neutrophils (Laan et al., 2001; Miyamoto et al., 2003). Besides, Li *et al.* also reported that the antagonism of IL-17A signaling pathway could reduce the IFN-γ production in the graft and prolong the graft survival (Li et al., 2006). As for Tregs, Tregs are one of the important factors to maintain immune tolerance, which inhibits excessive T cell activation and proliferation by secreting IL-10 (Afzali et al., 2007; Edemir et al., 2008). Specifically, IL-10 inhibits the response of antigen-specific effector cells by inhibiting the production of pro-inflammatory cytokines (Edemir et al., 2008). Studies had demonstrated that the upregulation of IL-10 gene could improve renal function and prolong the survival of renal allografts in a rat transplantation model (Chen et al., 2007). Our results are consistent with these previous reports. In our mouse transplantation model, IFN-γ and IL-17A showed high levels in serum and grafts, while IL-10 levels were relatively low in serum. After ERC-Exo treatment, the proinflammatory cytokines IFN-γ and IL-17 decreased in serum and grafts, but the level of IL-10 increased in serum. And this effect is obviously weakened with the knockdown of SIRT6 in ERC-Exos. Due to the massive secretion of these cytokines, the therapeutic effect of ERC-Exos on AR can be explained not only by $CD4^+$ T cells but also by other immune cells, which is also worth our further study.

In conclusion, we confirmed the therapeutic effects of targeting T cell glutaminolysis in allogeneic transplantation using ERC-Exo therapy. By inhibiting the c-Myc-dependent glutaminolysis of naïve $CD4^+$ T cells to remodel their differentiation, ERC-Exos can specifically alleviate acute transplant rejection, and this effect is mediated by SIRT6 in exosomes.

Conclusion

The present study affirmed the therapeutic effect of ERC-Exos in alleviating AR. Moreover, we emphasized the crucial role of SIRT6 in ERC-Exo-mediated immune tolerance formation via remodeling inordinate $CD4^+$ T differentiation. In a word, this study paves a way for the theoretical basis of the immunoregulatory potential of ERC-Exos and will guide the future clinical application of ERC-Exos in the treatment of AR.

Data availability statement

The raw data supporting the conclusions of this article will be made available by the authors, without undue reservation.

Ethics statement

The animal study was approved by the Animal Care and Use Committee of Tianjin Medical University. The study was conducted in accordance with the local legislation and institutional requirements.

Author contributions

TL: Conceptualization, Data curation, Software, Validation, Visualization, Writing – original draft, Writing – review

and editing. CS: Conceptualization, Data curation, Formal Analysis, Investigation, Methodology, Project administration, Supervision, Visualization, Writing – review and editing. XL: Data curation, Investigation, Methodology, Project administration, Software, Supervision, Validation, Visualization, Writing – review and editing. PZ: Conceptualization, Data curation, Investigation, Methodology, Software, Supervision, Writing – review and editing. BS: Conceptualization, Data curation, Investigation, Methodology, Software, Supervision, Writing – review and editing. YnX: Data curation, Formal Analysis, Methodology, Project administration, Software, Supervision, Writing – review and editing. YyX: Formal Analysis, Methodology, Project administration, Software, Supervision, Writing – review and editing. HoW: Conceptualization, Data curation, Investigation, Methodology, Software, Supervision, Writing – review and editing. QC: Conceptualization, Investigation, Methodology, Project administration, Supervision, Writing – review and editing. GY: Formal Analysis, Methodology, Project administration, Supervision, Validation, Writing – review and editing. HaW: Conceptualization, Funding acquisition, Methodology, Project administration, Resources, Supervision, Writing – review and editing.

Funding

The author(s) declare that financial support was received for the research and/or publication of this article. This work was supported by grants to HaW from the National Natural Science Foundation of China (No. 82071802 and 82270794), Natural Science Foundation of Tianjin (No. 21JCYBJC00850), Science and Technology Project of Tianjin Health Commission (No. TJWJ2021MS004), and Tianjin Key Medical Discipline (Specialty) Construction Project (TJYXZDXK-076C).

Conflict of interest

The authors declare that the research was conducted in the absence of any commercial or financial relationships that could be construed as a potential conflict of interest.

Generative AI statement

The author(s) declare that no Generative AI was used in the creation of this manuscript.

Any alternative text (alt text) provided alongside figures in this article has been generated by Frontiers with the support of artificial intelligence and reasonable efforts have been made to ensure accuracy, including review by the authors wherever possible. If you identify any issues, please contact us.

Publisher's note

All claims expressed in this article are solely those of the authors and do not necessarily represent those of their affiliated organizations, or those of the publisher, the editors and the reviewers. Any product that may be evaluated in this article, or claim that may be made by its manufacturer, is not guaranteed or endorsed by the publisher.

Supplementary material

The Supplementary Material for this article can be found online at: https://www.frontiersin.org/articles/10.3389/fcell.2025.1564382/full#supplementary-material

References

Afzali, B., Lombardi, G., Lechler, R. I., and Lord, G. M. (2007). The role of T helper 17 (Th17) and regulatory T cells (Treg) in human organ transplantation and autoimmune disease. *Clin. Exp. Immunol.* 148 (1), 32–46. doi:10.1111/j.1365-2249.2007.03356.x

Aksungur, N., Kizilkaya, M., Altundaş, N., Balkan, E., Kara, S., Demirci, E., et al. (2025). Molecular crosstalk between Sirt1, Wnt/B-Catenin signaling, and inflammatory pathways in renal transplant rejection: role of mirnas, lncrnas, Il-1, Il-6, and tubulointerstitial inflammation. *Med. Kaunas.* 61 (6), 1073. doi:10.3390/medicina61061073

Bolandi, Z., Mokhberian, N., Eftekhary, M., Sharifi, K., Soudi, S., Ghanbarian, H., et al. (2020). Adipose derived mesenchymal stem cell exosomes loaded with Mir-10a promote the differentiation of Th17 and treg from naive Cd4+ T cell. *Life Sci.*, 259. doi:10.1016/j.lfs.2020.118218

Cabré, N., Luciano-Mateo, F., Chapski, D. J., Baiges-Gaya, G., Fernández-Arroyo, S., Hernández-Aguilera, A., et al. (2021). Glutaminolysis-induced Mtorc1 activation drives non-alcoholic steatohepatitis progression. *J. hepatology*. doi:10.1016/j.jhep.2021.04.037

Chamberlain, K. A., Huang, N., Xie, Y. X., LiCausi, F., Li, S. N., Li, Y., et al. (2021). Oligodendrocytes enhance axonal energy metabolism by deacetylation of mitochondrial proteins through transcellular delivery of Sirt2. *Neuron* 109 (21), 3456–3472.e8. doi:10.1016/j.neuron.2021.08.011

Chen, B., Kapturczak, M. H., Joseph, R., George, J. F., Campbell-Thompson, M., Wasserfall, C. H., et al. (2007). Adeno-associated viral vector-mediated Interleukin-10 prolongs allograft survival in a rat kidney transplantation model. *Am. J. Transplant.* 7 (5), 1112–1120. doi:10.1111/j.1600-6143.2007.01772.x

Chornoguz, O., Hagan, R. S., Haile, A., Arwood, M. L., Gamper, C. J., Banerjee, A., et al. (2017). Mtorc1 promotes T-Bet phosphorylation to regulate Th1 differentiation. *J. Immunol.* 198 (10), 3939–3948. doi:10.4049/jimmunol.1601078

Dang, E. V., Barbi, J., Yang, H. Y., Jinasena, D., Yu, H., Zheng, Y., et al. (2011). Control of T_H17/T_{Reg} balance by hypoxia-Inducible factor 1. *Cell* 146 (5), 772–784. doi:10.1016/j.cell.2011.07.033

Darzi, S., Werkmeister, J. A., Deane, J. A., and Gargett, C. E. (2016). Identification and characterization of human endometrial mesenchymal stem/stromal cells and their potential for cellular therapy. *Stem Cells Transl. Med.* 5 (9), 1127–1132. doi:10.5966/sctm.2015-0190

Delgoffe, G. M., Pollizzi, K. N., Waickman, A. T., Heikamp, E., Meyers, D. J., Horton, M. R., et al. (2011). The kinase mtor regulates the differentiation of helper T cells through the selective activation of signaling by Mtorc1 and Mtorc2. *Nat. Immunol.* 12 (4), 295–303. doi:10.1038/ni.2005

Delgoffe, G. M., Kole, T. P., Zheng, Y., Zarek, P. E., Matthews, K. L., Xiao, B., et al. (2009). The mtor kinase differentially regulates effector and regulatory T cell lineage commitment. *Immunity* 30 (6), 832–844. doi:10.1016/j.immuni.2009.04.014

Durán, R. V., MacKenzie, E. D., Boulahbel, H., Frezza, C., Heiserich, L., Tardito, S., et al. (2013). Hif-independent role of prolyl hydroxylases in the cellular response to amino acids. *Oncogene* 32 (38), 4549–4556. doi:10.1038/onc.2012.465

Edemir, B., Kurian, S. M., Eisenacher, M., Lang, D., Müller-Tidow, C., Gabriels, G., et al. (2008). Activation of counter-regulatory mechanisms in a rat renal acute rejection model. *Bmc Genomics*, 9. doi:10.1186/1471-2164-9-71

Fathi-Kazerooni, M., and Tavoosidana, G. (2019). Menstrual blood stem cell transplantation in mice model of acute liver failure: does gender of recipient affect the outcome? *Avicenna J. Med. Biotechnol.* 11 (4), 308–316.

Geltink, R. I. K., Kyle, R. L., and Pearce, E. L. (2018). Unraveling the complex interplay between T cell metabolism and function. *Annu. Rev. Immunol.* 36, 461–488. doi:10.1146/annurev-immunol-042617-053019

González, A., Hall, M. N., Lin, S. C., and Hardie, D. G. (2020). Ampk and tor: the yin and yang of cellular nutrient sensing and growth control. *Cell Metab.* 31 (3), 472–492. doi:10.1016/j.cmet.2020.01.015

Gu, X., Orozco, J. M., Saxton, R. A., Condon, K. J., Liu, G. Y., Krawczyk, P. A., et al. (2017). Samtor is an *S*-Adenosylmethionine sensor for the Mtorc1 pathway. *Science* 358 (6364), 813–818. doi:10.1126/science.aao3265

Guo, Z. Y., Li, P., Ge, J. B., and Li, H. (2022). Sirt6 in aging, metabolism, inflammation and cardiovascular diseases. *Aging Dis.* 13, 1787–1822. doi:10.14336/AD.2022.0413

Hall, B. M. (2015). T cells: soldiers and spies-the surveillance and control of effector T cells by regulatory T cells. *Clin. J. Am. Soc. Nephrol.* 10 (11), 2050–2064. doi:10.2215/CJN.06620714

Hall, B. M., Bishop, G. A., Duggin, G. G., Horvath, J. S., Philips, J., and Tiller, D. J. (1984). Increased expression of Hla-Dr antigens on renal tubular cells in renal transplants: relevance to the rejection response. *Lancet* 2 (8397), 247–251. doi:10.1016/s0140-6736(84)90297-6

Hou, T. Y., Tian, Y., Cao, Z. Y., Zhang, J., Feng, T. T., Tao, W. H., et al. (2022). Cytoplasmic Sirt6-Mediated Acsl5 deacetylation impedes nonalcoholic fatty liver disease by facilitating hepatic fatty acid oxidation. *Mol. Cell* 82 (21), 4099–4115.e9. doi:10.1016/j.molcel.2022.09.018

Hu, Y. H., Kong, D. J., Qin, Y. F., Yu, D. D., Jin, W., Li, X., et al. (2021). Cd73 expression is critical to therapeutic effects of human endometrial regenerative cells in inhibition of cardiac allograft rejection in mice. *Stem Cells Transl. Med.* 10 (3), 465–478. doi:10.1002/sctm.20-0154

Huang, H. L., Long, L. Y., Zhou, P. P., Chapman, N. M., and Chi, H. B. (2020). Mtor signaling at the crossroads of environmental signals and T-Cell fate decisions. *Immunol. Rev.* 295 (1), 15–38. doi:10.1111/imr.12845

Izawa, H., Xiang, C., Ogawa, S., Hisanaga, I., and Yoshimoto, T. (2025). Amelioration of female menopausal syndrome by intravenous administration of autologous menstrual blood-derived stem cells. *Regen. Ther.* 29, 192–201. doi:10.1016/j.reth.2025.03.009

Jewell, J. L., Kim, Y. C., Russell, R. C., Yu, F. X., Park, H. W., Plouffe, S. W., et al. (2015). Metabolism. Differential regulation of mTORC1 by leucine and glutamine. *Science* 347 (6218), 194–198. doi:10.1126/science.1259472

Kalluri, R., and LeBleu, V. S. (2020). The biology, function, and biomedical applications of exosomes. *Science* 367 (6478), eaau6977. doi:10.1126/science.aau6977

Kittleson, M. M., and Kobashigawa, J. A. (2017). Cardiac transplantation current outcomes and contemporary controversies. *Jacc-Heart Fail.* 5 (12), 857–868. doi:10.1016/j.jchf.2017.08.021

Klabukov, I., Yatsenko, E., and Baranovskii, D. (2023). The effects of mesenchymal stromal cells and platelet-rich plasma treatments on cutaneous wound healing: ignoring the possibility of adverse events and side effects could compromise study results. *Archives Dermatological Res.* 316 (1), 35. doi:10.1007/s00403-023-02783-3

Klysz, D., Tai, X. G., Robert, P. A., Craveiro, M., Cretenet, G., Oburoglu, L., et al. (2015). Glutamine-dependent A-Ketoglutarate production regulates the balance between T helper 1 cell and regulatory T cell generation. *Sci. Signal.* 8 (396), ra97. doi:10.1126/scisignal.aab2610

Kurebayashi, Y., Nagai, S., Ikejiri, A., Ohtani, M., Ichiyama, K., Baba, Y., et al. (2012). Pi3k-Akt-Mtorc1-S6k1/2 axis controls Th17 differentiation by regulating Gfi1 expression and nuclear translocation of Rorγ. *Cell Rep.* 1 (4), 360–373. doi:10.1016/j.celrep.2012.02.007

Laan, M., Lötvall, J., Chung, K. F., and Lindén, A. (2001). Il-17-Induced cytokine release in human bronchial epithelial cells *in vitro*:: role of mitogen-activated protein (map) kinases. *Br. J. Pharmacol.* 133 (1), 200–206. doi:10.1038/sj.bjp.0704063

Lee, Y., Ka, S. O., Cha, H. N., Chae, Y. N., Kim, M. K., Park, S. Y., et al. (2017). Myeloid sirtuin 6 deficiency causes insulin resistance in high-fat diet-fed mice by eliciting macrophage polarization toward an M1 phenotype. *Diabetes* 66 (10), 2659–2668. doi:10.2337/db16-1446

Li, J., Simeoni, E., Fleury, S., Dudler, J., Fiorini, E., Kappenberger, L., et al. (2006). Gene transfer of soluble Interleukin-17 receptor prolongs cardiac allograft survival in a rat model. *Eur. J. Cardio-Thoracic Surg.* 29 (5), 779–783. doi:10.1016/j.ejcts.2006.01.052

Li, X., Lan, X., Zhao, Y. M., Wang, G., Shi, G. G., Li, H. Y., et al. (2019). Sdf-1/Cxcr4 axis enhances the immunomodulation of human endometrial regenerative cells in alleviating experimental colitis. *Stem Cell Res. and Ther.*, 10. doi:10.1186/s13287-019-1298-6

Li, Y. J., Jin, J., and Wang, Y. (2022). Sirt6 widely regulates aging, immunity, and cancer. *Front. Oncol.*, 12. doi:10.3389/fonc.2022.861334

Liu, T., Ren, S. H., Sun, C. L., Zhao, P. Y., and Wang, H. (2023). Glutaminolysis and peripheral Cd4+ T cell differentiation: from mechanism to intervention strategy. *Front. Immunol.*, 14. doi:10.3389/fimmu.2023.1221530

Lu, Y., Liu, R., Kang, X., Zhang, S., Sun, Y., Fan, W., et al. (2024). Menstrual blood-derived endometrial stem cell transplantation improves Male reproductive dysfunction in T1d mice by enhancing antioxidative capacity. *Reprod. Sci.* 31 (6), 1719–1731. doi:10.1007/s43032-024-01498-8

Marchingo, J. M., Sinclair, L. V., Howden, A. J. M., and Cantrell, D. A. (2020). Quantitative analysis of how myc controls T cell proteomes and metabolic pathways during T cell activation. *Elife* 9, e53725. doi:10.7554/eLife.53725

Marinaro, F., Gómez-Serrano, M., Jorge, I., Silla-Castro, J. C., Vázquez, J., Sánchez-Margallo, F. M., et al. (2019). Unraveling the molecular signature of extracellular vesicles from endometrial-derived mesenchymal stem cells: potential modulatory effects and therapeutic applications. *Front. Bioeng. Biotechnol.* 7, 431. doi:10.3389/fbioe.2019.00431

Meng, D. L., Yang, Q. M., Wang, H. Y., Melick, C. H., Navlani, R., Frank, A. R., et al. (2020). Glutamine and asparagine activate Mtorc1 independently of rag gtpases. *J. Biol. Chem.* 295 (10), 2890–2899. doi:10.1074/jbc.AC119.011578

Miyamoto, M., Prause, O., Sjöstrand, M., Laan, M., Lötvall, J., and Lindén, A. (2003). Endogenous Il-17 as a mediator of neutrophil recruitment caused by endotoxin exposure in mouse airways. *J. Immunol.* 170 (9), 4665–4672. doi:10.4049/jimmunol.170.9.4665

Nakaya, M., Xiao, Y. C., Zhou, X. F., Chang, J. H., Chang, M., Cheng, X. H., et al. (2014). Inflammatory T cell responses rely on amino acid transporter Asct2 facilitation of glutamine uptake and Mtorc1 kinase activation. *Immunity* 40 (5), 692–705. doi:10.1016/j.immuni.2014.04.007

Oraby, M. A., Mageed, S. S. A., Raouf, A. A., Abdelshafy, D. A., Ahmed, E. F., Khalil, R. T., et al. (2024). Remdesivir ameliorates ulcerative colitis-propelled cell inflammation and pyroptosis in acetic acid rats by restoring Sirt6/Foxc1 pathway. *Int. Immunopharmacol.* 137, 112465. doi:10.1016/j.intimp.2024.112465

Pillai, V. B., and Gupta, M. P. (2020). Is nuclear sirtuin Sirt6 a master regulator of immune function? *Am. J. Physiology-Endocrinology Metabolism* 320 (3), E399–E414. doi:10.1152/ajpendo.00483.2020

Qiu, J. J., Lin, X. J., Tang, X. Y., Zheng, T. T., Lin, Y. Y., and Hua, K. Q. (2018). Exosomal metastasis-associated lung adenocarcinoma transcript 1 promotes angiogenesis and predicts poor prognosis in epithelial ovarian cancer. *Int. J. Biol. Sci.* 14 (14), 1960–1973. doi:10.7150/ijbs.28048

Quaranta, P., Focosi, D., Freer, G., and Pistello, M. (2016). Tweaking mesenchymal stem/progenitor cell immunomodulatory properties with viral vectors delivering cytokines. *Stem Cells Dev.* 25 (18), 1321–1341. doi:10.1089/scd.2016.0145

Schmitz, M. L., Bacher, S., and Dienz, O. (2003). NF-kappaB activation pathways induced by T cell costimulation. *Faseb J.* 17 (15), 2187–2193. doi:10.1096/fj.02-1100rev

Sebastián, C., Zwaans, B. M. M., Silberman, D. M., Gymrek, M., Goren, A., Zhong, L., et al. (2012). The histone deacetylase Sirt6 is a tumor suppressor that controls cancer metabolism. *Cell* 151 (6), 1185–1199. doi:10.1016/j.cell.2012.10.047

Shah, P., Yuzefpolskaya, M., Hickey, G. W., Breathett, K., Wever-Pinzon, O., Ton, V. K., et al. (2022). Twelfth interagency registry for mechanically assisted circulatory support report: readmissions after left ventricular assist device. *Ann. Thorac. Surg.* 113 (3), 722–737. doi:10.1016/j.athoracsur.2021.12.011

Shi, L. Z., Wang, R. N., Huang, G. H., Vogel, P., Neale, G., Green, D. R., et al. (2011). HIF1alpha-dependent glycolytic pathway orchestrates a metabolic checkpoint for the differentiation of TH17 and treg cells. *J. Exp. Med.* 208 (7), 1367–1376. doi:10.1084/jem.20110278

Söderlund, C., and Rådegran, G. (2015). Immunosuppressive therapies after heart transplantation - the balance between under- and over-immunosuppression. *Transplant. Rev.* 29 (3), 181–189. doi:10.1016/j.trre.2015.02.005

Stewart, S., Winters, G. L., Fishbein, M. C., Tazelaar, H. D., Kobashigawa, J., Abrams, J., et al. (2005). Revision of the 1990 working formulation for the standardization of nomenclature in the diagnosis of heart rejection. *J. Heart Lung Transplant.* 24 (11), 1710–1720. doi:10.1016/j.healun.2005.03.019

Stewart, S., Fishbein, M. C., Snell, G. I., Berry, G. J., Boehler, A., Burke, M. M., et al. (2007). Revision of the 1996 working formulation for the standardization of nomenclature in the diagnosis of lung rejection. *J. Heart Lung Transplant.* 26 (12), 1229–1242. doi:10.1016/j.healun.2007.10.017

Sun, Q. P., Huang, Z. Y., Han, F., Zhao, M., Cao, R. H., Zhao, D. Q., et al. (2018). Allogeneic mesenchymal stem cells as induction therapy are safe and feasible in renal allografts: pilot results of a multicenter randomized controlled trial. *J. Transl. Med.* 16, 52. doi:10.1186/s12967-018-1422-x

Tao, R. Y., Xiong, X. W., DePinho, R. A., Deng, C. X., and Dong, X. C. (2013). Foxo3 transcription factor and Sirt6 deacetylase regulate low density lipoprotein (Ldl)-Cholesterol homeostasis *via* control of the proprotein convertase Subtilisin/kexin type 9 (*Pcsk9*) gene expression. *J. Biol. Chem.* 288 (41), 29252–29259. doi:10.1074/jbc.M113.481473

Wang, S. H., Li, J., Xie, A. N., Wang, G. H., Xia, N., Ye, P., et al. (2011). Dynamic changes in Th1, Th17, and Foxp3+T cells in patients with acute cellular rejection after cardiac transplantation. *Clin. Transplant.* 25 (2), E177–E186. doi:10.1111/j.1399-0012.2010.01362.x

Wang, H., Hosiawa, K. A., Garcia, B., Shum, J. B., Dutartre, P., Kelvin, D. J., et al. (2003). Attenuation of acute xenograft rejection by short-term treatment with Lf15-0195 and monoclonal antibody against Cd45rb in a rat-to-mouse cardiac Transplantation model. *Transplantation* 75 (9), 1475–1481. doi:10.1097/01.TP.0000057245.59998.95

Wang, R. N., Dillon, C. P., Shi, L. Z., Milasta, S., Carter, R., Finkelstein, D., et al. (2011). The transcription factor myc controls metabolic reprogramming upon T lymphocyte activation. *Immunity* 35 (6), 871–882. doi:10.1016/j.immuni.2011.09.021

Wang, X. C., Shen, H. Y., Zhangyuan, G., Huang, R. Y., Zhang, W. J., He, Q. F., et al. (2018). 14-3-3ζ delivered by hepatocellular carcinoma-derived exosomes impaired anti-tumor function of tumor-infiltrating T lymphocytes. *Cell Death and Dis.* 9, 159. doi:10.1038/s41419-017-0180-7

Wang, H. X., Li, S. T., Zhang, G. Q., Wu, H., and Chang, X. T. (2019). Potential therapeutic effects of *Cyanidin-3-O*-Glucoside on rheumatoid arthritis by relieving inhibition of Cd38+Nk cells on treg cell differentiation. *Arthritis Res. and Ther.* 21 (1), 220. doi:10.1186/s13075-019-2001-0

Wang, P., Zhang, Q., Tan, L., Xu, Y. N., Xie, X. B., and Zhao, Y. (2020). The regulatory effects of mtor complexes in the differentiation and function of Cd4+ T cell subsets. *J. Immunol. Res.*, 2020. doi:10.1155/2020/3406032

Wang, H. D., Zhao, Y. M., Ren, B. B., Qin, Y. F., Li, G. M., Kong, D. J., et al. (2021). Endometrial regenerative cells with Galectin-9 high-expression attenuate experimental autoimmune hepatitis. *Stem Cell Res. and Ther.* 12 (1), 541. doi:10.1186/s13287-021-02604-2

Warren, J. L., and MacIver, N. J. (2019). Regulation of adaptive immune cells by sirtuins. *Front. Endocrinol. (Lausanne)* 10, 466. doi:10.3389/fendo.2019.00466

Wei, W. Q., Guo, X. D., Gu, L. J., Jia, J. S., Yang, M., Yuan, W. J., et al. (2021a). Bone marrow mesenchymal stem cell exosomes suppress phosphate-induced aortic calcification *via* Sirt6-Hmgb1 deacetylation. *Stem Cell Res. and Ther.* 12 (1), 235. doi:10.1186/s13287-021-02307-8

Wei, Y. C., Chen, X. Y., Zhang, H. X., Su, Q., Peng, Y. W., Fu, Q., et al. (2021b). Efficacy and safety of bone marrow-derived mesenchymal stem cells for chronic antibody-mediated rejection after kidney Transplantation-a single-arm, two-dosing-regimen, phase I/Ii study. *Front. Immunol.*, 12. doi:10.3389/fimmu.2021.662441

Xu, Y., Ren, S., Wang, H., Qin, Y., Liu, T., Sun, C., et al. (2024). Endometrial regeneration cell-derived exosomes loaded with Sislamf6 inhibit cardiac allograft rejection through the suppression of desialylation modification. *Cell Mol. Biol. Lett.* 29 (1), 128. doi:10.1186/s11658-024-00645-y

Yang, L. F., Venneti, S., and Nagrath, D. (2017). Glutaminolysis: a hallmark of cancer metabolism. *Annu. Rev. Biomed. Eng.* 19, 163–194. doi:10.1146/annurev-bioeng-071516-044546

Yang, G., Xia, Y. Y., and Ren, W. K. (2021). Glutamine metabolism in Th17/Treg cell fate: applications in Th17 cell-associated diseases. *Sci. China-Life Sci.* 64 (2), 221–233. doi:10.1007/s11427-020-1703-2

Yu, Q., Tu, H. H., Yin, X. Y., Peng, C., Dou, C. Y., Yang, W. H., et al. (2022). Targeting glutamine metabolism ameliorates autoimmune hepatitis *via* inhibiting T cell activation and differentiation. *Front. Immunol.* 13, 880262. doi:10.3389/fimmu.2022.880262

frontiers | Frontiers in Cell and Developmental Biology

TYPE Original Research
PUBLISHED 08 October 2025
DOI 10.3389/fcell.2025.1651658

OPEN ACCESS

EDITED BY
Valerie Kouskoff,
The University of Manchester,
United Kingdom

REVIEWED BY
Anca M. Colita,
Carol Davila University of Medicine and Pharmacy, Romania
Yongsheng Ruan,
Southern Medical University, China

*CORRESPONDENCE
Yunyan He,
yunyanhe@aliyun.com
Jianming Luo,
jmluo@aliyun.com

†These authors have contributed equally to this work

RECEIVED 22 June 2025
ACCEPTED 23 September 2025
PUBLISHED 08 October 2025

CITATION
Pang G, Wang X, Jia W, Li M, Zhou T, Luo J and He Y (2025) Risk factors and prognosis of poor graft function after allogeneic hematopoietic stem cell transplantation in pediatric: a retrospective study.
Front. Cell Dev. Biol. 13:1651658.
doi: 10.3389/fcell.2025.1651658

Risk factors and prognosis of poor graft function after allogeneic hematopoietic stem cell transplantation in pediatric: a retrospective study

Guanxiu Pang[1,2†], Xiaobo Wang[3†], Wenguang Jia[1,2], Mengchen Li[1,2], Tianyuan Zhou[1,2], Jianming Luo[1,2*] and Yunyan He[1,2*]

[1]Department of Pediatrics, The First Affiliated Hospital of Guangxi Medical University, Nanning, China, [2]The First Affiliated Hospital of Guangxi Medical University / Difficult and Critical Illness Center, Pediatric Clinical Medical Research Center of Guangxi, Nanning, China, [3]Department of Hematology, The Seventh Affiliated Hospital of Sun Yat-sen University, Shenzhen, China

Introduction: Poor graft function (PGF) represents a serious and potentially life-threatening complication following allogeneic hematopoietic stem cell transplantation (allo-HSCT); however, its etiological risk factors and prognostic implications remain inadequately defined within pediatric populations.
Methods: A retrospective cohort study was conducted on 175 pediatric patients undergoing allo-HSCT between 30 June 2018, and 31 December 2022. Patients were stratified into PGF (n = 30) and good graft function (GGF, n = 145) groups. Multivariate logistic regression identified risk factors for PGF, while Cox proportional hazards models evaluated mortality-associated variables. Survival outcomes were analyzed using Kaplan-Meier curves.
Results: Key findings encompass: (1) PGF Risk Factors: Multivariable analysis identified four independent predictors of PGF: age ≥10 years at transplantation (OR = 29.27, 95%CI: 5.70–150.21, P < 0.001), HLA mismatch (OR = 4.11, 95%CI: 1.45–11.65, P = 0.008), cytomegalovirus (CMV) infection (OR = 7.64, 95%CI: 2.31–25.21, P = 0.001), and BK virus (BKV) infection (OR = 12.22, 95%CI: 2.49–59.89, P = 0.002); The model's predictive performance by ROC analysis yielded an AUC of 0.886 (95%CI: 0.83–0.94; P < 0.001). (2) Survival Analysis: the 4-year overall survival (OS) was profoundly inferior in the PGF cohort compared to the GGF cohort (49.4% ± 10.3% vs. 90.2% ± 2.5%, P < 0.001). (3) Predictors of Mortality: Cox regression identified PGF (HR = 2.39, 95%CI: 1.02–5.59, P = 0.044), acute graft-versus-host disease (grade I/II, HR = 3.43, 95%CI: 1.29–9.15, P = 0.014; grade III/IV, HR = 8.92, 95%CI: 3.19–24.96, P < 0.001), hemorrhagic cystitis (HR = 3.18, 95%CI: 1.37–7.39, P = 0.007), and severe pneumonia (HR = 4.42, 95%CI: 1.92–10.19, P < 0.001) as independent predictors of early mortality.
Conclusion: Age ≥10 years at transplantation, HLA mismatch, CMV infection, or BK viremia identifies a high-risk cohort of pediatric allo-HSCT recipients who require intensified monitoring for PGF,

underscoring an urgent need for effective preventive and therapeutic interventions.

KEYWORDS

children, allogeneic hematopoietic stem cell transplantation, poor graft function, risk factors, prognosis

Introduction

Allogeneic hematopoietic stem cell transplantation (allo-HSCT) remains a definitive treatment for hematologic malignancies, marrow failure syndromes, and inherited disorders. Despite achieving long-term remission in over 40,000 annual recipients globally (Passweg et al., 2021), poor graft function (PGF)—characterized by full donor chimerism (≥95%) with sustained multilineage cytopenia (neutrophils $<0.5 \times 10^9$/L, platelets $<20 \times 10^9$/L, hemoglobin <70 g/L) —confers substantial mortality risks through hemorrhagic complications and opportunistic infections (Prabahran et al., 2022; Kong, 2019). Clinically, PGF manifests as either primary (failed engraftment by day +28) or secondary (cytopenias post-initial engraftment) subtypes (Kong, 2019; Sun et al., 2015; Zhao et al., 2019). Epidemiological analyses reveal cumulative incidence rates of 5%–27% (Dominietto et al., 2001; Man et al., 2022), with primary and secondary PGF affecting 1.5%–12.1% and 12.7%–16.3% of recipients (Zhao et al., 2019; Xiao et al., 2014), respectively. Prognostically, primary PGF was associated with markedly reduced overall survival (OS: 25%–34.6% at 1 year; 6% at 2 years), whereas secondary PGF shows partial hematopoietic recovery (53.6%) but limited survival benefit compared to those with GGF (5,9,10), highlighting the urgent need for improved management strategies.

Contemporary research identifies multiple peritransplant risk modifiers for PGF development, including but not limited to splenic enlargement (Zhao et al., 2019; Chen et al., 2022), elevated pretransplant serum ferritin levels (Zhao et al., 2019; Taoka et al., 2012), HLA mismatch (Sun et al., 2015; Taoka et al., 2012), ABO incompatibility (Xiao et al., 2014; Chen et al., 2022), low $CD34^+$ cell doses (Zhao et al., 2019; Sun et al., 2019), and cytomegalovirus (CMV) reactivation episodes (Lv et al., 2021; Lin et al., 2022). Nevertheless, existing evidence remains constrained by heterogeneous findings across studies and a paucity of pediatric-specific data. This investigation proposes to conduct a comprehensive retrospective cohort analysis of pediatric allo-HSCT recipients, employing multivariate regression models to systematically evaluate modifiable risk parameters of PGF. The ultimate objectives encompass refinement of transplantation protocols, implementation of risk-adapted preventive strategies, and consequent improvement in long-term survival metrics for this vulnerable patient population.

Materials and methods

Patients

A retrospective analysis was conducted on the clinical data of 175 pediatric patients who underwent allo-HSCT at the Pediatric Transplant Center of the First Affiliated Hospital of Guangxi Medical University between 30 June 2018, and 31 December 2022. Inclusion criteria: Recipients undergoing their first allo-HSCT and their respective donors, age under 18 years, and with guardians having signed consent forms acknowledging transplant-related risks. Exclusion criteria: Incomplete clinical data. Finally, a total of 175 patients met these criteria and were enrolled in the study. The study was reviewed and approved by the ethics committees of The First Affiliated Hospital of Guangxi Medical University.

Data collection

Demographic characteristics of recipients (sex, age), primary disease type, splenomegaly status, splenectomy history, pre-transplant serum ferritin levels, donor-recipient matching parameters (sex, blood type, HLA matching), graft source, conditioning regimens, transplantation approach, $CD34^+$ cell dose (x 10^6/kg), total nucleated cell dose (x 10^6/kg), as well as neutrophil and platelet engraftment times were systematically documented. Post-transplant complications data encompassing hemorrhagic cystitis, secondary hypertension, secondary hyperglycemia, acute graft-versus-host disease (aGVHD), chronic graft-versus-host disease (cGVHD), CMV infection, Epstein-Barr virus (EBV) infection, BK virus (BKV) infection, and severe pneumonia were stratified based on temporal occurrence relative to PGF development and OS endpoints. The primary endpoint was OS duration, calculated from transplantation date until death or last follow-up. Secondary endpoints included PGF incidence rates and time-to-PGF, defined as the interval between hematopoietic stem cell infusion and PGF diagnosis. All patients were followed through 31 December 2023.

Transplantation conditioning regimen

All patients underwent conditioning regimens to eradicate abnormal clones and disrupt disease mechanisms. The regimens varied based on patient tolerance and disease status, with 10 specific combinations listed (Supplementary Table S1).

Post-transplant complications management

The basic GVHD prevention regimen consists of cyclosporine A and mycophenolate mofetil (Penack et al., 2020; Brown et al., 2020). For haploidentical donor transplants, additional post-transplant cyclophosphamide is used on days +3 and +4 for prevention (M et al., 2016; Anurathapan et al., 2016). The GVHD grading system follows the modified Glucksberg

criteria and the international consensus grading system (Schoemans et al., 2018; Stem Cell Application Group, Hematology Branch of Chinese Medical Association, 2020). Other preventive measures include appropriate antibiotic use during conditioning to prevent infections, the administration of low-molecular-weight heparin, prostaglandin E1, and ursodeoxycholic acid to prevent transplant-associated hepatic veno-occlusive disease, proper hydration and alkalinization to prevent hemorrhagic cystitis, and oral phenytoin to prevent reversible posterior leukoencephalopathy syndrome.

Treatment of PGF

All patients diagnosed with PGF received standardized supportive care comprising blood product transfusions, anti-infective prophylaxis, and intravenous immunoglobulin administration for immunomodulatory support. First-line cytokine therapy comprised subcutaneous granulocyte colony-stimulating factor combined with thrombopoietin receptor agonists (TPO-RAs, e.g.,,eltrombopag). For refractory cases, cellular therapies were initiated: donor lymphocyte infusion at escalating doses (1×10^6 to 1×10^7 $CD3^+$ cells/kg), $CD34^+$ stem cell boosts ($>2 \times 10^6$ $CD34^+$ cells/kg), and third-party mesenchymal stromal cell (MSC) infusions ($1–2 \times 10^8$ viable cells/kg/dose administered every 14 ± 2 days for 2-3 cycles) to facilitate hematopoietic niche reconstitution.

Statistical methods

Statistical analyses were performed using SPSS 26.0 software (IBM, United States). Continuous variables with normal distribution are expressed as mean ± standard deviation and were compared using independent samples t-tests. Non-normally distributed continuous data are summarized as median (interquartile range) and compared using the Mann–Whitney U test. Categorical variables are presented as number (percentage) and analyzed with the Pearson χ^2 test or Fisher's exact test, as appropriate. Multivariable logistic regression was used to identify independent risk factors for PGF. The discriminative ability of the regression model was assessed using receiver operating characteristic (ROC) curve analysis. Survival distributions were estimated by the Kaplan-Meier method and compared with the log-rank test. A two-sided p-value <0.05 was considered statistically significant.

Results

Incidence and characteristics

Among 175 patients, neutrophil engraftment was achieved in 172 (98.3%), and platelet engraftment was achieved in 162 (92.3%). The mean time to neutrophil engraftment was 14.0 ± 0.40 days, while the median time to platelet engraftment was 16.0 days (range, 6–89 days). The median infused $CD34^+$ cell dose was 6.65×10^6/kg (range, 0.84–40.77 $\times$ 10^6/kg). 3 patients failed to achieve engraftment of both neutrophils and platelets by day 28 and were diagnosed with primary PGF.

By 31 December 2023, PGF occurred in 30 patients (17.1%) among the 175 analyzed cohort, while GGF was observed in 145 patients (82.9%). Of the PGF cases, 3 (10.0%) were classified as primary PGF and 27 (90.0%) as secondary PGF. Comparative analysis revealed that PGF patients were significantly older at transplantation (mean age 9.8 ± 0.7 years vs. 6.5 ± 0.3 years; P < 0.001) and exhibited higher rates of splenectomy (43.3% vs. 16.6%; P = 0.001). Additionally, the PGF cohort demonstrated greater prevalence of malignant comorbidities (26.7% vs. 10.3%; P = 0.016), increased HLA mismatch frequency (50.0% vs. 27.6%; P = 0.016), and higher incidence of post-transplant complications, including BKV infection (26.7% vs. 4.8%; P < 0.001), hemorrhagic cystitis (56.7% vs. 31.7%; P = 0.010), severe cGVHD (10.0% vs. 2.0%; P = 0.025) and severe pneumonia (26.7% vs. 11.0%; P = 0.048) (Table 1).

Risk factors for PGF

Univariate analysis identified advanced transplantation age (≥10 years, P < 0.001), HLA mismatch (P = 0.018), pre-PGF CMV infection (P = 0.007), and BKV infection (P = 0.001) as significant predictors of PGF. These factors were then analyzed using multivariate logistic regression. The results showed that age ≥10 years at the time of transplantation (OR = 29.27, 95%CI: 5.70–150.21, P < 0.001), HLA mismatch (OR = 4.11, 95%CI: 1.45–11.65, P = 0.008), CMV infection (OR = 7.64, 95%CI: 2.31–25.21, P = 0.001), and BKV infection (OR = 12.22, 95%CI: 2.49–59.89, P = 0.002) were identified as independent risk factors for PGF (Table 2).

The predictive performance of the model was assessed via ROC curve analysis, yielding an area under the curve (AUC) of 0.886 (95%CI: 0.83–0.94; P < 0.001). This model exhibits a relatively high level of diagnostic accuracy, with sensitivity and specificity values of 80.0% and 84.1%, respectively, demonstrating robust utility for PGF risk stratification (Figure 1).

Survival analyses

As of 31 December 2023, the median follow-up duration for post-transplant OS was 24.97 months (range: 1.33–59.87 months). Of the 175 enrolled patients, 28 (16.0%) had died and 147 (84.0%) remained alive. The estimated 4-year OS rate for the entire cohort was 84.3% ± 2.8% (Figure 2A).

Stratified by graft function outcomes, the PGF group (n = 30) exhibited significantly poorer survival, with 14 deaths (46.7%) and 16 survivors (53.3%) at the end of follow-up, yielding a median survival of 13.5 months (range: 1.33–54.63 months). In contrast, the GGF group (n = 145) demonstrated markedly better outcomes, with 14 deaths (9.7%) and 131 survivors (90.3%). Consequently, the 4-year OS rate was substantially lower in the PGF group compared to the GGF group (49.4% ± 10.3% vs. 90.2% ± 2.5%, P < 0.001; Figure 2B).

When stratified by pre-transplant primary disease type, the cohort included 22 patients with malignant diseases and 153 patients with non-malignant diseases. By the end of follow-up, 2 deaths (9.1%) were recorded in the malignant disease group, with 20 patients (90.9%) surviving. In the non-malignant disease group,

10.3389/fcell.2025.1651658

TABLE 1 Clinical characteristics of the PGF and GGF patients.

Characteristics	PGF (n = 30)	GGF (n = 145)	P Value
Disease n (%)			0.102
Thalassemia	14 (46.7)	104 (71.7)	
AA	4 (13.3)	14 (9.7)	
AL	5 (16.7)	14 (9.7)	
HLH	2 (6.6)	5 (3.4)	
others	5 (16.7)	8 (5.5)	
Gender n (%)			0.581
Male	17 (57.1)	90 (62.1)	
Female	13 (42.9)	55 (37.9)	
Age (years, mean ± SD)	9.8 ± 0.7	6.5 ± 0.3	<0.001
SF level (ug/L, median, range)	3027.1 (66.7–15151.0)	2751.9 (35.9–14463.1)	0.765
Splenomegaly			0.001
Yes	13 (43.3)	24 (16.6)	
No	17 (56.7)	121 (83.4)	
Types of primary onset n (%)			0.035
Malignant	8 (26.7)	15 (10.3)	
Non-malignant	22 (73.3)	130 (89.7)	
Blood mismatch n (%)			0.279
Identical	15 (50.0)	88 (60.7)	
Mismatch	15 (50.0)	57 (39.3)	
HLA disparity n (%)			0.016
Matched	15 (50.0)	105 (72.4)	
Mismatched	15 (50.0)	40 (27.6)	
Source of stem cell n (%)			0.084
BM	4 (13.3)	15 (10.4)	
BM + UCB	3 (10.0)	35 (24.1)	
BM + PB	21 (70.0)	94 (64.8)	
PB	2 (6.7)	1 (0.7)	
Neutrophil recovery (days, mean ± SD)	17.1 ± 0.8	17.0 ± 0.5	0.936
Platelet recovery (days, median, range)	19.0 (8.0–89.0)	17.0 (8.0–32.0)	0.017
$CD34^+$ cell dose (10^6/kg, median, range)	5.5 (2.0–34.3)	7.10 (0.8–40.8)	0.485
CMV infection n (%)			0.108

(Continued on the following page)

10.3389/fcell.2025.1651658

TABLE 1 (*Continued*) Clinical characteristics of the PGF and GGF patients.

Characteristics	PGF (n = 30)	GGF (n = 145)	P Value
Yes	21 (70.0)	120 (82.8)	
No	9 (30.0)	25 (17.2)	
EBV infection n (%)			0.236
Yes	14 (46.7)	51 (35.2)	
No	16 (53.3)	94 (64.8)	
BKV infection n (%)			<0.001
Yes	8 (26.7)	7 (4.8)	
No	22 (73.3)	138 (95.2)	
Hemorrhagic cystitis n (%)			0.010
Yes	17 (56.7)	46 (31.7)	
No	13 (43.3)	99 (68.3)	
aGVHD n (%)			0.450
No	22 (73.3)	120 (82.8)	
Grade I-II	5 (16.7)	18 (12.4)	
Grade III-IV	3 (10.0)	7 (4.8)	
cGVHD n (%)			0.025
No	24 (80.0)	138 (95.2)	
Mild	2 (6.7)	2 (1.4)	
Moderate	1 (3.3)	2 (1.4)	
Severe	3 (10.0)	3 (2.0)	
Severe pneumonia n (%)			0.048
Yes	8 (26.7)	16 (11.0)	
No	22 (73.3)	129 (89.0)	

PGF, poor graft function; GGF, goor graft function; AA, aplastic anemia; AL, acute leukemia; HLH, hemophagocytic lymphohistiocytosis; SF, serum ferritin; HLA, human leukocyte antigen; BM, bone marrow; UCB, umbilical cord blood; PB, peripheral blood; CMV, cytomegalovirus; EBV, Epstein-Barr virus; BKV, BK, virus; aGVHD, Acute graft-versus-host disease; cGVHD, Chronic graft-versus-host disease.

26 deaths (17.0%) occurred, and 127 patients (83.0%) remained alive. In the malignant disease subgroup, the 2-year OS rate was significantly lower in patients with PGF than in those with GGF (42.9% ± 31.0% vs. 100%, P = 0.0314; Figure 2C). Conversely, within the non-malignant disease subgroup, the 4-year OS rate remained significantly reduced in the PGF group compared to the GGF group (47.4% ± 10.5% vs. 89.1% ± 2.7%, P < 0.001; Figure 2D).

To identify clinical factors associated with reduced OS, Cox proportional hazards regression analyses were performed. Univariate analysis revealed significant associations between decreased OS and the following risk factors: HLA mismatch (P = 0.005), PGF (P < 0.001), post-transplant EBV infection (P = 0.025), hemorrhagic cystitis (P = 0.013), aGVHD (grade I-II, P < 0.001; grade III-IV, P < 0.001), and severe pneumonia (p < 0.001). Variables with P < 0.05 in univariate analysis were subsequently included in multivariate modeling, which identified four independent predictors of diminished OS: post-transplant PGF (HR = 2.39, 95%CI: 1.02–5.59, P = 0.044), aGVHD (grade I/II, HR = 3.43, 95%CI: 1.29–9.15, P = 0.014; grade III/IV, HR = 8.92, 95%CI: 3.19–24.96, P < 0.001), hemorrhagic cystitis (HR = 3.18, 95%CI: 1.37–7.39, P = 0.007), and severe pneumonia (HR = 4.42, 95%CI: 1.92–10.19, P < 0.001). These results highlight the substantial prognostic impact of post-transplant complications, underscoring the importance of early detection and

10.3389/fcell.2025.1651658

TABLE 2 Univariate-multivariate analysis of risk factors for PGF.

Variables	Univariate analysis for PGF		Multivariate analysis for PGF	
	Or (95%CI)	P Value	Or (95%CI)	P Value
Gender				
Male	1.00		-	
Female	1.25 (0.56–2.77)	0.581	-	
Age (years)				
<5	1.00		1.00	
≥5, <10	2.02 (0.51–8.00)	0.317	2.79 (0.56–14.02)	0.212
≥10	10.92 (2.97–40.10)	<0.001	29.27 (5.70–150.21)	<0.001
SF level, ng/mL				
<2000	1.00		-	
≥2000	1.000 (0.45–2.31)	1.000	-	
Splenomegaly				
No	1.00		-	
Yes	1.12 (0.50–2.47)	0.789	-	
Types of primary onset				
Malignant	1.00		-	
Non-malignant	0.38 (0.14–1.03)	0.057	-	
Blood mismatch				
Identical	1.00		-	
Mismatch	1.54 (0.70–3.40)	0.281	-	
HLA disparity				
Matched	1.00		1.00	
Mismatched	2.63 (1.18–5.86)	0.018	4.11 (1.45–11.65)	0.008
Source of stem cell				
BM	1.00		-	
BM + UCB	0.32 (0.06–1.62)	0.168	-	
BM + PB	0.84 (0.25–2.78)	0.773	-	
PB	7.50 (0.53–105.28)	0.135	-	
$CD34^+$ cell dose, 10^6/kg				
<5	1.00		-	
≥5, <10	0.50 (0.18–1.43)	0.198	-	
≥10	0.81 (0.33–1.99)	0.650	-	

(Continued on the following page)

10.3389/fcell.2025.1651658

TABLE 2 (*Continued*) Univariate-multivariate analysis of risk factors for PGF.

Variables	Univariate analysis for PGF		Multivariate analysis for PGF	
	Or (95%CI)	P Value	Or (95%CI)	P Value
TNC dose, 10^8/kg				
<10	1.00			
≥10	2.178 (0.93–5.08)	0.071		
CMV infection before PGF				
No	1.00		1.00	
Yes	3.20 (1.37–7.47)	0.007	7.64 (2.31–25.21)	0.001
EBV infection before PGF				
No	1.00		-	
Yes	1.61 (0.73–3.57)	0.238	-	
BKV infection before PGF				
No	1.00		1.00	
Yes	7.17 (2.37–21.75)	0.001	12.22 (2.49–59.89)	0.002
Hemorrhagic cystitis before PGF				
No	1.00		-	
Yes	2.15 (0.97–4.77)	0.059	-	
aGVHD before PGF				
No	1.00		-	
Grade I-II	0.98 (0.27–3.65)	0.981	-	
Grade III-IV	1.41 (0.28–7.17)	0.682	-	
cGVHD before PGF				
No	1.00		-	
Mild	2.56 (0.22–29.19)	0.450	-	
Moderate	2.56 (0.22–29.19)	0.450	-	
Severe	1.70 (0.17–17.00)	0.650	-	
Severe pneumonia before PGF				
No	1.00		-	
Yes	1.61 (0.54–4.80)	0.391	-	

PGF, poor graft function; GGF, goor graft function; SF, serum ferritin; HLA, human leukocyte antigen; BM, bone marrow; UCB, umbilical cord blood; PB, peripheral blood; TNC, total nucleated cell.
CMV, cytomegalovirus; EBV, Epstein-Barr virus; BKV, BK, virus; aGVHD, Acute graft-versus-host disease; cGVHD, Chronic graft-versus-host disease.

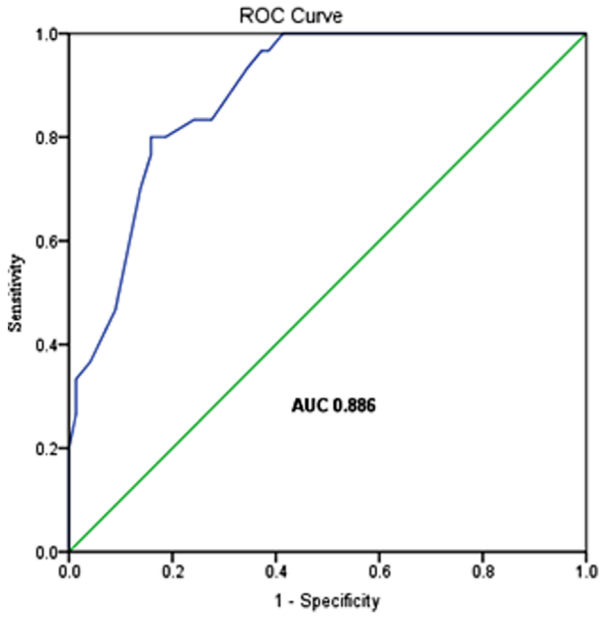

FIGURE 1
The ROC curve of the logistic regression model.

aggressive management of these conditions to optimize survival outcomes (Table 3).

Discussion

Advances in transplantation protocols have improved the prevention and management of complications following allo-HSCT. Nevertheless, PGF remains a critical complication that negatively impacts outcomes in pediatric patients. Inconsistent definitions of PGF contribute to significant variability in reported incidence rates and associated risk factors. In this cohort, the overall incidence of PGF was 17.1%, consistent with the previously reported range of 5.0%–27.0% (Dominietto et al., 2001; Man et al., 2022). Primary PGF constituted 1.7% of cases, closely aligning with the 1.5% reported by Zhao et al. 2019. But markedly lower than the 5.6% observed by Sun et al. 2015. Secondary PGF occurred in 15.4% of cases, matching the findings of Zhao et al. 2019.

Higher recipient age has been established as a risk factor for PGF in prior studies (Xiao et al., 2014; Alchalby et al., 2016). In our pediatric cohort, recipients aged ≥10 years exhibited a significantly increased risk of PGF. This association may be attributable to the high prevalence of transfusion-dependent thalassemia major (67.4%) in the cohort, where older recipient typically experience cumulative transfusion burden, leading to parenchymal iron deposition. Iron overload generates reactive oxygen species (ROS) via Haber-Weiss/Fenton reactions, inducing oxidative stress that suppresses BCL2 expression and promotes erythroid apoptosis (Taoka et al., 2012). Additionally, it triggers DNA damage and $CD34^{+}$ cell depletion in bone marrow (Ohmoto et al., 2017), potentially mediating PGF pathogenesis. However, definitive validation of this mechanism requires confirmation through large-scale prospective studies. Furthermore, our findings highlight the importance of performing HSCT before the age of 10 years in thalassemia patients, whenever clinically feasible, to mitigate iron accumulation and preempt microenvironmental damage.

With the continuous refinement of haploidentical hematopoietic stem cell transplantation protocols, pediatric patients undergoing this approach can achieve long-term outcomes comparable to those of matched sibling donor HSCT (Lv et al., 2019). However, a subset of patients still experience PGF following hematopoietic reconstitution, which poses a significant threat to long-term survival. In our study, HLA mismatch was identified as an independent risk factor for PGF development, consistent with previous findings (Sun et al., 2019; Lv et al., 2021; Alchalby et al., 2016). Nevertheless, the precise mechanisms by which HLA disparity mediates PGF remain incompletely elucidated, warranting further exploration and validation through additional clinical research.

CMV infection following allo-HSCT can involve critical organs and increase the risk of PGF and GVHD, which is closely associated with the immune reconstitution of CMV-specific T cells (Reddehase et al., 2021; Degli-Esposti and Hill, 2022). During the first year post-transplantation, clonal expansion of CMV-specific effector memory T cells drives this process. Our analyses, consistent with prior retrospective studies, demonstrated CMV reactivation as an independent risk factor of PGF in both univariate and multivariate models (Lv et al., 2021; Lin et al., 2022). However, conflicting data exist; another study identified CMV infection as a risk factor for primary PGF in univariate analysis, but this association did not persist after multivariate adjustment (Zhao et al., 2019). These discrepant findings suggest that whether CMV infection constitutes a risk factor for PGF remains controversial, underscoring the need for rigorous validation through well-designed prospective multicenter cohort studies.

BKV typically remains latent in immunocompetent individuals, with primary infections often asymptomatic. In pediatric allo-HSCT recipients, however, treatment-induced immunosuppression frequently reactivates latent BKV, leading to clinical complications. While BKV is a well-known cause of post-transplant hemorrhagic cystitis (McCaffrey et al., 2021; Janeczko-Czarnecka et al., 2020), its role in other allo-HSCT-related outcomes remains poorly understood. This study identifies BKV reactivation as an independent risk factor of PGF, extending its clinical relevance beyond hemorrhagic cystitis. These findings suggest that early BKV monitoring and preemptive therapy during the post-transplant period may reduce PGF incidence. However, the causal relationship between the reactivation of latent viruses (such as CMV and BKV) and the occurrence of PGF remains controversial, as PGF can lead to delayed hematopoietic and immune reconstitution, thereby increasing susceptibility to viral infections. Definitive establishment of causality requires large-scale, multi-center prospective cohort studies incorporating protocol-based virological surveillance and rigorously standardized clinical endpoints.

Furthermore, the severity of the underlying disease may substantially increase the risk of PGF through multiple synergistic pathways, including direct impairment of hematopoietic stem cell and microenvironmental reserves. Concurrently, high-intensity pre-transplant conditioning regimens may exacerbate PGF risk via direct cytotoxic effects and immune dysregulation. Future studies

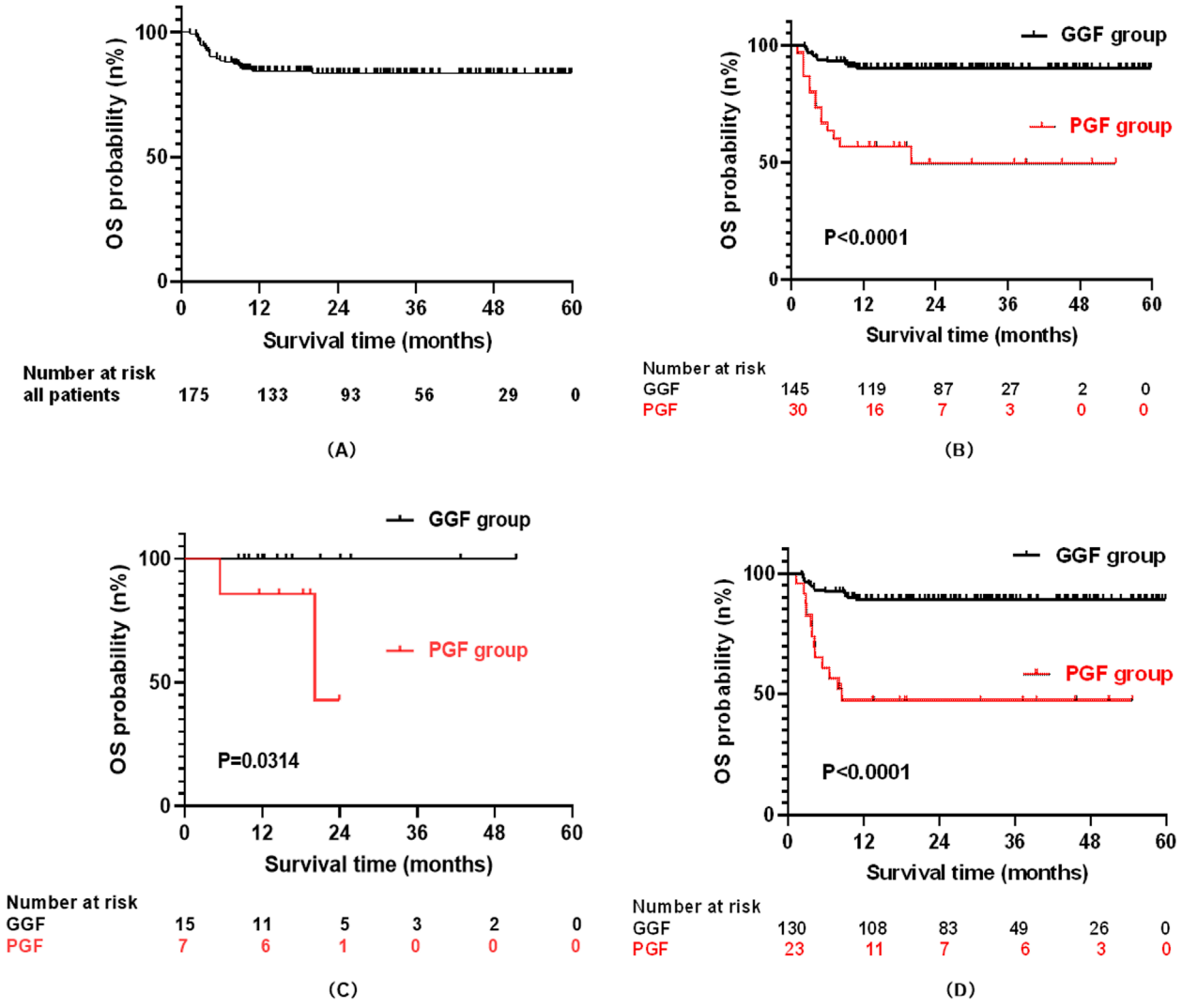

FIGURE 2
The curve for overall survival (OS): All patients **(A)**; PGF and GGF patients **(B)**; Patients with PGF and GGF in the malignant group **(C)**; Patients with PGF and GGF in the no-malignant group **(D)**.

should incorporate detailed stratification based on disease risk indices and conditioning intensity, to better isolate independent predictors of PGF.

Patients who develop PGF following transplantation are associated with a poor prognosis. In this study, the 4-year OS was significantly lower in the PGF group compared to the GGF group among pediatric recipients, consistent with prior reports (Zhao et al., 2019; Sun et al., 2019; Prabahran et al., 2021). However, the management of PGF remains investigational. Currently, therapeutic strategies for PGF are primarily developed based on its underlying pathological mechanisms. These include interventions such as second donor stem cell infusion, purified $CD34^+$ cell infusion, MSC transfusion, and thrombopoietin receptor agonists (e.g., eltrombopag) (Shahzad et al., 2021; Servais et al., 2023; Mahat et al., 2020). Univariate-multivariate analysis in this study identified PGF as an independent risk factor for reduced OS, alongside hemorrhagic cystitis, grade I-II aGVHD, grade III-IV aGVHD, and severe pneumonia. These findings highlight the critical need to mitigate PGF occurrence through targeted preventive strategies, which may substantially improve survival outcomes in this vulnerable population.

In conclusion, PGF is characterized by high incidence and poor prognosis. This study demonstrates that PGF is an independent risk factor for reduced OS, underscoring the imperative to mitigate PGF occurrence as a key strategy to improve clinical outcomes. The study also identified recipient age ≥10 years, HLA mismatching, and post-transplant CMV or BKV infections as independent risk factors for PGF after allo-HSCT in pediatric. Optimizing transplantation protocols to address these risk factors—such as performing allo-HSCT at a younger age, improving HLA compatibility, and enhancing antiviral prophylaxis—may reduce PGF incidence. Furthermore, investigating early predictive biomarkers for PGF could guide timely clinical interventions, enabling proactive management to enhance OS in affected patients.

10.3389/fcell.2025.1651658

TABLE 3 Univariate-multivariate analysis of risk factors for OS.

Variables	Univariate analysis for OS		Multivariate analysis for OS	
	HR (95%CI)	P Value	HR (95%CI)	P Value
Gender n (%)				
Male	1.00		-	
Female	0.85 (0.39–1.83)	0.673	-	
Age (years)				
<5	1.00		-	
≥5, <10	1.75 (0.62–4.97)	0.292	-	
≥10	2.61 (0.91–7.52)	0.075	-	
SF level, ng/mL				
<2000	1.00		-	
≥2000	1.18 (0.53–2.55)	0.681	-	
Types of primary onset				
Malignant	1.00		-	
Non-malignant	1.95 (0.46–8.21)	0.364	-	
Blood mismatch				
Identical	1.00		-	
Mismatch	1.29 (0.62–2.70)	0.507	-	
HLA disparity				
Matched	1.00		1.00	
Mismatched	2.90 (1.38–6.09)	0.005	1.64 (0.66–4.07)	0.288
Source of stem cell				
BM	1.00		-	
BM + UCB	0.70 (0.20–2.47)	0.574	-	
BM + PB	0.66 (0.22–1.95)	0.449	-	
PB	2.07 (0.23–18.56)	0.517	-	
$CD34^+$ cell dose, 10^6/kg				
<5	1.00		-	
≥5, <10	0.93 (0.37–2.30)	0.870	-	
≥10	0.82 (0.34–1.97)	0.649	-	
TNC dose, 10^8/kg				
<10	1.00			
≥10	1.09 (0.52–2.31)	0.816		

(Continued on the following page)

10.3389/fcell.2025.1651658

TABLE 3 (*Continued*) Univariate-multivariate analysis of risk factors for OS.

Variables	Univariate analysis for OS		Multivariate analysis for OS	
	HR (95%CI)	P Value	HR (95%CI)	P Value
PGF before OS				
No	1.00		1.00	
Yes	6.06 (2.88–12.75)	<0.001	2.39 (1.02–5.59)	0.044
CMV infection before OS				
No	1.00		-	
Yes	1.403 (0.60–3.30)	0.438	-	
EBV infection before OS				
No	1.00		1.00	
Yes	2.35 (1.11–4.97)	0.025	1.50 (0.63–3.59)	0.360
BKV infection before OS				
No	1.00		-	
Yes	2.50 (0.95–6.58)	0.064	-	
Hemorrhagic cystitis before OS				
No	1.00		1.00	
Yes	2.58 (1.22–5.46)	0.013	3.18 (1.37–7.39)	0.007
aGVHD before OS				
No	1.00			
Grade I-II	4.93 (2.01–12.08)	<0.001	3.43 (1.29–9.15)	0.014
Grade III-IV	22.58 (9.03–56.47)	<0.001	8.92 (3.19–24.96)	<0.001
cGVHD before OS				
No	1.00		-	
Mild	1.73 (0.23–12.83)	0.591	-	
Moderate	2.20 (0.30–16.32)	0.440	-	
Severe	3.02 (0.91–10.05)	0.072	-	
Severe pneumonia before OS				
No	1.00		1.00	
Yes	10.37 (4.91–21.89)	<0.001	4.42 (1.92–10.19)	<0.001

OS, over survival; PGF, poor graft function; GGF, goor graft function; SF, serum ferritin; HLA, human leukocyte antigen; BM, bone marrow; UCB, umbilical cord blood; PB, peripheral blood; TNC, total nucleated cell; CMV, cytomegalovirus; EBV, Epstein-Barr virus; BKV, BK, virus; aGVHD, Acute graft-versus-host disease; cGVHD, Chronic graft-versus-host disease.

However, this study has several limitations. First, as a retrospective investigation, it may be subject to selection bias due to the exclusion of cases with incomplete information. Second, the sample size from a single center was insufficient to develop separate risk models for primary and secondary PGF. Future multi-center prospective studies are warranted to further elucidate the mechanisms underlying PGF and to identify predictive biomarkers for its occurrence,

thereby providing a basis for early clinical intervention and treatment.

Data availability statement

The original contributions presented in the study are included in the article/Supplementary Material, further inquiries can be directed to the corresponding authors.

Ethics statement

The studies involving humans were approved by Institutional Review Board of First Affiliated Hospital of Guangxi Medical University [2021-EC-(098)]. The studies were conducted in accordance with the local legislation and institutional requirements. Written informed consent for participation in this study was provided by the participants' legal guardians/next of kin.

Author contributions

GP: Formal Analysis, Methodology, Software, Writing – original draft. XW: Conceptualization, Formal Analysis, Software, Validation, Writing – original draft. WJ: Data curation, Writing – review and editing. ML: Data curation, Writing – original draft. TZ: Data curation, Writing – original draft. JL: Project administration, Resources, Supervision, Writing – review and editing. YH: Funding acquisition, Methodology, Project administration, Resources, Supervision, Writing – review and editing.

Funding

The author(s) declare that financial support was received for the research and/or publication of this article. The study was supported by the Guangxi Project for the Development, Promotion and Application of Appropriate Health Technologies (No. S2019091), NHC Key Laboratory of Thalassemia Medicine and Guangxi Key laboratory of Thalassemia Research, and Guangxi Clinical Research Center for Pediatric disease (No. AD22035219).

Acknowledgments

We are grateful for the efforts made by peer colleague to collect the data and for all the data provided by the patients included in the study. We also acknowledge the support from the Key Laboratory of Children's Disease Research in Guangxi's Colleges and Universities, Education Department of Guangxi Zhuang Autonomous Region.

Conflict of interest

The authors declare that the research was conducted in the absence of any commercial or financial relationships that could be construed as a potential conflict of interest.

Generative AI statement

The author(s) declare that no Generative AI was used in the creation of this manuscript.

Any alternative text (alt text) provided alongside figures in this article has been generated by Frontiers with the support of artificial intelligence and reasonable efforts have been made to ensure accuracy, including review by the authors wherever possible. If you identify any issues, please contact us.

Publisher's note

Supplementary material

The Supplementary Material for this article can be found online at: https://www.frontiersin.org/articles/10.3389/fcell.2025.1651658/full#supplementary-material

References

Alchalby, H., Yunus, D. R., Zabelina, T., Ayuk, F., and Kröger, N. (2016). Incidence and risk factors of poor graft function after allogeneic stem cell transplantation for myelofibrosis. *Bone Marrow Transpl.* 51 (9), 1223–1227. doi:10.1038/bmt.2016.98

Anurathapan, U., Hongeng, S., Pakakasama, S., Sirachainan, N., Songdej, D., Chuansumrit, A., et al. (2016). Hematopoietic stem cell transplantation for homozygous β-thalassemia and β-thalassemia/hemoglobin E patients from haploidentical donors. *Bone Marrow Transpl.* 51 (6), 813–818. doi:10.1038/bmt.2016.7

Brown, P., Inaba, H., Annesley, C., Beck, J., Colace, S., Dallas, M., et al. (2020). Pediatric acute lymphoblastic leukemia, version 2.2020, NCCN clinical practice guidelines in oncology. *J. Natl. Compr. Canc Netw.* 18 (1), 81–112. doi:10.6004/jnccn.2020.0001

Chen, J., Pang, A., Zhao, Y., Liu, L., Ma, R., Wei, J., et al. (2022). Primary graft failure following allogeneic hematopoietic stem cell transplantation: risk factors, treatment and outcomes. *Hematology* 27 (1), 293–299. doi:10.1080/16078454.2022.2042064

Degli-Esposti, M. A., and Hill, G. R. (2022). Immune control of cytomegalovirus reactivation in stem cell transplantation. *Blood* 139 (9), 1277–1288. doi:10.1182/blood.2020010028

Dominietto, A., Raiola, A. M., van Lint, M. T., Lamparelli, T., Gualandi, F., Berisso, G., et al. (2001). Factors influencing haematological recovery after allogeneic haemopoietic stem cell transplants: Graft-Versus-Host disease, donor type, cytomegalovirus infections and cell dose. *Br. J. Haematol.* 112 (1), 219–227. doi:10.1046/j.1365-2141.2001.02468.x

Janeczko-Czarnecka, M., Rybka, B., Ryczan-Krawczyk, R., KałWak, K., and Ussowicz, M. (2020). Thymic activity in immune recovery after allogeneic hematopoietic stem cell transplantation in children. *Cent. Eur. J. Immunol.* 45 (2), 151–159. doi:10.5114/ceji.2019.89843

Kong, Y. (2019). Poor graft function after allogeneic hematopoietic stem cell transplantation-an old complication with new insights. *Semin. Hematol.* 56 (3), 215–220. doi:10.1053/j.seminhematol.2018.08.004

Lin, F., Han, T., Zhang, Y., Cheng, Y., Xu, Z., Mo, X., et al. (2022). The incidence, outcomes, and risk factors of secondary poor graft function in haploidentical hematopoietic stem cell transplantation for acquired aplastic anemia. *Front. Immunol.* 13, 896034. doi:10.3389/fimmu.2022.896034

Lv, M., Chang, Y., and Huang, X. (2019). Everyone has a donor: contribution of the Chinese experience to global practice of haploidentical hematopoietic stem cell transplantation. *Front. Med.* 13 (1), 45–56. doi:10.1007/s11684-017-0595-7

Lv, W. R., Zhou, Y., Xu, J., Fan, Z. P., Huang, F., Xu, N., et al. (2021). Haploidentical donor transplant is associated with secondary poor graft function after allogeneic stem cell transplantation: a single-center retrospective study. *Cancer Med.* 10 (23), 8497–8506. doi:10.1002/cam4.4353

M, B., E, L., S, C., M, Z., E, V., M, F., et al. (2016). Feasibility and outcome of haploidentical hematopoietic stem cell transplantation with post-transplant high-dose cyclophosphamide for children and adolescents with hematologic malignancies: an AIEOP-GITMO retrospective multicenter study. *Biol. blood marrow Transplant. J. Am. Soc. Blood Marrow Transplant.* 22 (5), 902–909. doi:10.1016/j.bbmt.2016.02.002

Mahat, U., Rotz, S. J., and Hanna, R. (2020). Use of thrombopoietin receptor agonists in prolonged thrombocytopenia after hematopoietic stem cell transplantation. *Biol. Blood Marrow Transplant.* 26 (3), e65–e73. doi:10.1016/j.bbmt.2019.12.003

Man, Y., Lu, Z., Yao, X., Gong, Y., Yang, T., and Wang, Y. (2022). Recent advancements in poor graft function following hematopoietic stem cell transplantation. *Front. Immunol.* 13, 911174. doi:10.3389/fimmu.2022.911174

McCaffrey, J., Bhute, V. J., and Shenoy, M. (2021). BK virus infection and outcome following kidney transplantation in childhood. *Sci. Rep.* 11 (1), 2468. doi:10.1038/s41598-021-82160-0

Ohmoto, A., Fuji, S., Miyagi-Maeshima, A., Kim, S. W., Tajima, K., Tanaka, T., et al. (2017). Association between pretransplant iron overload determined by bone marrow pathological analysis and bacterial infection. *Bone Marrow Transpl.* 52 (8), 1201–1203. doi:10.1038/bmt.2017.93

Passweg, J. R., Baldomero, H., Chabannon, C., Basak, G. W., de la Cámara, R., Corbacioglu, S., et al. (2021). Hematopoietic cell transplantation and cellular therapy survey of the EBMT: monitoring of activities and trends over 30 years. *Bone Marrow Transpl.* 56 (7), 1651–1664. doi:10.1038/s41409-021-01227-8

Penack, O., Marchetti, M., Ruutu, T., Aljurf, M., Bacigalupo, A., Bonifazi, F., et al. (2020). Prophylaxis and management of graft *versus* host disease after stem-cell transplantation for haematological malignancies: updated consensus recommendations of the european society for blood and marrow transplantation. *Lancet Haematol.* 7 (2), e157–e167. doi:10.1016/S2352-3026(19)30256-X

Prabahran, A., Koldej, R., Chee, L., Wong, E., and Ritchie, D. (2021). Evaluation of risk factors for and subsequent mortality from poor graft function (PGF) post allogeneic stem cell transplantation. *Leuk. Lymphoma* 62 (6), 1482–1489. doi:10.1080/10428194.2021.1872072

Prabahran, A., Koldej, R., Chee, L., and Ritchie, D. (2022). Clinical features, pathophysiology, and therapy of poor graft function post-allogeneic stem cell transplantation. *Blood Adv.* 6 (6), 1947–1959. doi:10.1182/bloodadvances.2021004537

Reddehase, M. J., Holtappels, R., and Lemmermann, N. A. W. (2021). Consequence of histoincompatibility beyond GvH-Reaction in cytomegalovirus disease associated with allogeneic hematopoietic cell transplantation: change of paradigm. *Viruses* 13 (8), 1530. doi:10.3390/v13081530

Schoemans, H. M., Lee, S. J., Ferrara, J. L., Wolff, D., Levine, J. E., Schultz, K. R., et al. (2018). EBMT-NIH-CIBMTR task force position statement on standardized terminology and guidance for graft-versus-host disease assessment. *Bone Marrow Transpl.* 53 (11), 1401–1415. doi:10.1038/s41409-018-0204-7

Servais, S., Baron, F., Lechanteur, C., Seidel, L., Baudoux, E., Briquet, A., et al. (2023). Multipotent mesenchymal stromal cells as treatment for poor graft function after allogeneic hematopoietic cell transplantation: a multicenter prospective analysis. *Front. Immunol.* 14, 1106464. doi:10.3389/fimmu.2023.1106464

Shahzad, M., Siddiqui, R. S., Anwar, I., Chaudhary, S. G., Ali, T., Naseem, M., et al. (2021). Outcomes with CD34-Selected stem cell boost for poor graft function after allogeneic hematopoietic stem cell transplantation: a systematic review and meta-analysis. *Transplant. Cell. Ther.* 27 (10), 877.e1–877.e8. doi:10.1016/j.jtct.2021.07.012

Stem Cell Application Group, Hematology Branch of Chinese Medical Association (2020). Expert consensus on allogeneic hematopoietic stem cell Transplantation in China for the treatment of hematological diseases (III.) - acute graft-versus-host disease (2020 Edition). *Chin. J. Hematol.* 41 (7), 529–536. doi:10.3760/cma.j.issn.0253-2727.2020.07.001

Sun, Y. Q., He, G. L., Chang, Y. J., Xu, L. P., Zhang, X. H., Han, W., et al. (2015). The incidence, risk factors, and outcomes of primary poor graft function after unmanipulated haploidentical stem cell transplantation. *Ann. Hematol.* 94 (10), 1699–1705. doi:10.1007/s00277-015-2440-x

Sun, Y. Q., Wang, Y., Zhang, X. H., Xu, L. P., Liu, K. Y., Yan, C. H., et al. (2019). Virus reactivation and low dose of CD34+ cell, rather than haploidentical transplantation, were associated with secondary poor graft function within the first 100 days after allogeneic stem cell transplantation. *Ann. Hematol.* 98 (8), 1877–1883. doi:10.1007/s00277-019-03715-w

Taoka, K., Kumano, K., Nakamura, F., Hosoi, M., Goyama, S., Imai, Y., et al. (2012). The effect of iron overload and chelation on erythroid differentiation. *Int. J. Hematol.* 95 (2), 149–159. doi:10.1007/s12185-011-0988-3

Xiao, Y., Song, J., Jiang, Z., Li, Y., Gao, Y., Xu, W., et al. (2014). Risk-factor analysis of poor graft function after allogeneic hematopoietic stem cell transplantation. *Int. J. Med. Sci.* 11 (6), 652–657. doi:10.7150/ijms.6337

Zhao, Y., Gao, F., Shi, J., Luo, Y., Tan, Y., Lai, X., et al. (2019). Incidence, risk factors, and outcomes of primary poor graft function after allogeneic hematopoietic stem cell transplantation. *Biol. Blood Marrow Transpl.* 25 (9), 1898–1907. doi:10.1016/j.bbmt.2019.05.036

frontiers | Frontiers in Cell and Developmental Biology

TYPE Original Research
PUBLISHED 25 November 2025
DOI 10.3389/fcell.2025.1616235

OPEN ACCESS

EDITED BY
Yu Liu,
University of Houston, United States

REVIEWED BY
Zhen Guo,
Washington University in St. Louis, United States
Vitalina Gryshkova,
UCB Biopharma SPRL, Belgium

*CORRESPONDENCE
Nianmin Qi,
Drqi@163.com
Yuehong Wu,
wuyuehong2003@163.com

†These authors have contributed equally to this work

RECEIVED 22 April 2025
REVISED 21 September 2025
ACCEPTED 04 November 2025
PUBLISHED 25 November 2025

CITATION
Ke M, Wang H, Yang K, Ji M, Qi N and Wu Y (2025) Doxorubicin induces cardiotoxicity by enhancing autophagy via mTOR signaling in hiPSC- and hESC-derived cardiomyocytes. *Front. Cell Dev. Biol.* 13:1616235. doi: 10.3389/fcell.2025.1616235

Doxorubicin induces cardiotoxicity by enhancing autophagy via mTOR signaling in hiPSC- and hESC-derived cardiomyocytes

Minxia Ke[1†], Hao Wang[2,3†], Kailun Yang[1], Meng Ji[2], Nianmin Qi[2,3*] and Yuehong Wu[1*]

[1]Department of Biochemistry and Molecular Biology, College of Life Science and Medicine, Zhejiang Sci-Tech University, Hangzhou, Zhejiang, China, [2]Hangzhou Biaomo Biosciences Co., Ltd., Hangzhou, Zhejiang, China, [3]Asia Stem Cell Therapies Co., Limited, Shanghai, China

Introduction: Doxorubicin (DOX) is a highly effective anti-cancer drug, but its clinical applications are limited by its cardiotoxicity. The mechanisms underlying DOX-induced cardiotoxicity (DIC) remain incompletely understood. Human induced pluripotent stem cells (hiPSCs) and human embryonic stem cells (hESCs) offer an advanced platform for investigating DIC, as they accurately recapitulate human cardiac physiology and pathology. However, the roles and mechanisms of DIC in hiPSC-CMs and hESC-CMs, especially regarding autophagy dynamics and regulation, are still not well-defined.

Methods: Cell viability, apoptosis, reactive oxygen species production, and DNA damage were assessed. Autophagy was evaluated by transmission electron microscope, LC3-II/LC3-I ratio, and autophagy flux assays. The role of autophagy and mTOR signaling was investigated using 3-methyladenine (3-MA) and rapamycin (RAPA), respectively.

Results: DOX reduced cell viability and induced apoptosis in hiPSC-CMs and hESC-CMs. Additionally, DOX caused an increase in reactive oxygen species production and DNA damage. Furthermore, DOX significantly upregulated autophagy, confirmed by the accumulation of autophagosomes and autolysosomes, and an increase in the LC3-II/LC3-I ratio. Autophagy flux assays showed that DOX induced autophagy in a time-dependent manner. The autophagy mediated by DOX was partially attenuated by 3-MA. Moreover, this activation was due to mTOR signaling inhibition. The downregulation of mTOR signaling by RAPA increased cell death of hESC-CMs. Interestingly, minor variations in injury severity and cellular sensitivity were observed between these two models.

Conclusion: Our study uncovered the multifaceted effects of DOX on hiPSC-CMs and hESC-CMs, revealing a shared mechanism in which DOX enhances autophagy via inhibition of the mTOR signaling pathway. These findings reveal key insights into DIC pathogenesis and suggest that autophagy modulation may be a promising therapeutic strategy.

KEYWORDS

doxorubicin, cardiomyocytes, autophagy, MTOR signaling, human induced pluripotent stem cells, human embryonic stem cells

1 Introduction

Doxorubicin (DOX) is an effective anti-cancer agent for treating a wide range of malignancies, but its cumulative and dose-dependent cardiotoxicity limits its clinical application (Abdullah et al., 2019; Jones and Dass, 2022). Despite decades of studies, the mechanisms underlying DOX-induced cardiotoxicity (DIC) have not been fully elucidated, and predicting or preventing DIC in individual patients remains challenging.

Several different molecular mechanisms have been proposed for DIC in both experimental and clinical studies. The dominant mechanism is associated with DNA damage and reactive oxygen species (ROS) production, which leads to cardiomyocyte death (Li et al., 2020; L'Ecuyer et al., 2006). Other hypotheses have been proposed, including mitochondrial dysfunction and the modulation of intracellular calcium release (Hanna et al., 2014; Ichikawa et al., 2014). In addition, autophagy has also been proposed to serve a dual role in DIC (Sun et al., 2023; Xiao et al., 2019). Autophagy, a multistep and dynamic biological process, plays a crucial role in maintaining cellular homeostasis (Wang et al., 2024). Many studies indicate that autophagy is involved in several physiological and pathological processes in the heart (Li et al., 2024; Yamaguchi, 2019). Several studies have shown that DOX suppresses basal autophagy in rat cardiomyocytes, suggesting that activation of autophagy may protect against DIC (Pizarro et al., 2016; Sishi et al., 2013; Zilinyi et al., 2018). In contrast, other studies report that DOX upregulates autophagy in rat cardiomyocytes, contributing to detrimental effects and cell death (Kobayashi et al., 2010; Scicchitano et al., 2021; Wang et al., 2018). The conflicting findings regarding DOX's role in cardiac autophagy regulation highlight the need for further investigation.

The conflicting results regarding autophagy may be attributed to multiple factors, including variations in experiment models. Most methodologies for analyzing DIC, which employ models such as ion channel–overexpressing cells or animal models, frequently fail to fully and accurately replicate the effects of cardiac drugs in humans (Protze et al., 2019; McSweeney et al., 2019). This is due to interspecies differences in drug metabolism, cardiac structure and function. Recently, human induced pluripotent stem cells (hiPSCs) and human embryonic stem cells (hESCs) represent attractive cell sources for cell therapy and drug development (Cerneckis et al., 2024). hiPSC- and hESC-derived cardiomyocytes (hiPSC-CMs and hESC-CMs), which express key human cardiac ion channels and sarcomeric proteins, demonstrate contractile function, gene expression profiles, and electrophysiological phenotypes that closely resemble those of native human cardiomyocytes. Moreover, hiPSC-CMs and hESC-CMs offer a robust platform for large-scale drug screening and compound testing. hiPSC-CMs and hESC-CMs have been used to test drug-induced cardiac toxicity including DIC in recent works (Burridge et al., 2016; Maillet et al., 2016; Zhao and Zhang, 2017; Cui et al., 2019; Yang et al., 2022). However, the role and mechanisms of DIC in different CM models, particularly its multifaceted roles and mechanisms, including the dynamic changes and regulatory processes of autophagy, remain incompletely understood.

In the present study, we investigated the role and mechanisms of DIC using the hiPSC- and hESC-CM model system. Our results suggested DOX triggered apoptosis, ROS production and DNA damage in both hiPSC-CMs and hESC-CMs. Moreover, DOX enhanced autophagy via inhibiting mTOR signaling in hiPSC-CMs and hESC-CMs, ultimately leading to CM damage.

2 Materials and methods

2.1 Cardiomyocyte differentiation of hiPSCs and hESCs

The hiPSCs (American Type Culture Collection, ATCC) cell line present in this study were obtained from Stem Cell Bank of Chinese Academy of Sciences. The hESCs (H9 cell line, WA09, WiCell Research Institute) (Thomson et al., 1998) cell line present in this study were obtained from Shanghai Zhong Qiao Xin Zhou Biotechnology Co. Ltd. hiPSCs and hESCs were routinely cultured at 37 °C and 5% CO_2 in mTeSR™ one complete maintenance medium (Stemcell Technologies, Inc.) on 6-well plates coated with Matrigel (BD Biosciences, Bedford, MA). Cells were passaged every 2–3 days using ACCUTASE™ cell detachment solution (Stemcell Technologies, Inc.). In order to direct differentiation into CMs as our previous work described (Ke et al., 2020), hiPSCs and hESCs were split at a 1:6 ratio and plated onto Matrigel-coated 12-well plates cultured for 3 days. When the hiPSCs and hESCs reached 85% confluence, 6 μM CHIR99021 (MedChemExpress) was added to RPMI/B27 without insulin medium (Gibco, Invitrogen, USA) to initiate the differentiation. On day 2, the medium was changed to RPMI/B27 minus insulin medium supplement with 3 μg/mL IWP2 (MedChemExpress). On day 5, the medium was changed to RPMI/B27 without insulin. On day 7, the differentiating cells were cultured in RPMI/B27 plus insulin medium (Gibco, Invitrogen, USA). On day 15, the cells were cultured with purification medium (Tohyama et al., 2013), which are comprised of glucose-depleted DMEM (Gibco, Invitrogen, USA), 213 μg/mL of l-ascorbic acid 2-phosphate supplemented (Sigma-Aldrich; Merck KGaA), and 500 μg/mL of recombinant human albumin (Oryzogen; Wuhan Healthgen Biotechnology, Corp.) combining with 4 mM L-lactic acid (Sigma-Aldrich; Merck KGaA). The medium was refreshed every 2 days during the purification process. On day 19, cells were maintained in RPMI/B27 plus insulin media. To investigate the effect of DOX (MedChemExpress) in hiPSC-CMs and hESC-CMs, cells at differentiation day 21 were dissociated by using 0.25% Trypsin-EDTA (Gibco, Invitrogen, USA) for 3 min at 37 °C and then centrifuged at 1,000 rpm for 5 min. Cells were replanted in DMEM (Gibco, Invitrogen, USA) containing 20% FBS (Gibco, Invitrogen, USA) for 24 h and changed in a chemically defined medium (CDM3) for maintenance. CDM3 medium consists of DMEM, 500 μg/mL of Oryza sativa–derived recombinant human albumin (Sigma-Aldrich; Merck KGaA), and 213 μg/mL of L-ascorbic acid 2-phosphate (Sigma-Aldrich; Merck KGaA).

2.2 Immunocytochemical staining

For immunocytochemical staining, we fixed cells with 4% PFA (Sigma), permeabilized them with 0.4% Triton X-100 (Sigma), and then incubated them with the primary antibody anti-cTnT (Abcam, USA, 1:400) and anti-Cx43 (Abcam, USA, 1:400) overnight at 4 °C.

The nucleus was stained with DAPI (Invitrogen, USA). All samples were imaged with a Carl Zeiss microscope and processed with ZEN software.

2.3 Flow cytometry

For characterization of hiPSC-CMs and hESC-CMs, the differentiated CMs were collected after dissociation with 0.25% Trypsin-EDTA for 3 min. The cells were fixed and permeabilized with the Foxp3 Staining Buffer kit (Invitrogen, USA) for 30 min, followed by incubation with the primary antibody (anti-cTnT, Abcam, 1:100) for 1 h at room temperature. The PE-conjugated secondary antibody (Biolegend, 1:400) was added to the cells for 1 h at 4 °C. Apoptosis was assessed by flow cytometry, using an Annexin V-FITC Apoptosis Detection Kit (BD Pharmingen). The assay was conducted based on the instructions which were provided by the manufacturer. Briefly, after treatment with DOX, 5×10^5 cells were rinsed twice in PBS and incubated in 100 μ L one x binding buffer. Five μ L of Annexin V-FITC was added to the cells and incubated at RT for 15 min in the dark. Propidium iodide was not added because of DOX autofluorescence which may interfere with its detection. All samples were analyzed with a flow cytometer (BD Accuri™ C6, BD Biosciences) and quantified with FlowJo software.

2.4 CCK8 assay

The viability of cells was evaluated by CCK8 assay (Beyotime Institute of Biotechnology, Jiangsu, China). Briefly, 1×10^4 cells/well CM cells were seeded into 96-well plates (Gibco, Invitrogen, USA) and cultured for 3 days. The cells were then treated with the different doses (0, 0.1, 0.25, 0.5, 1, 1.5, 2.5, 5.0, 10, 25, 50, 100 μM) of DOX for 24 h. 24 h later, the medium was exchanged with a fresh medium containing CCK8 reagent and incubated for an additional 4 h at 37 °C. By using an enzyme-linked immunosorbent assay reader (Thermo Fisher Scientific, Inc.), the data were read at an absorbance of 450 nm wavelength.

2.5 LDH assay

Cells seeded on a 96-well culture plate were treated with DOX for 24 h. The LDH release assay was performed to detect cell cytotoxicity, following the manufacturer's instructions (Beyotime Institute of Biotechnology, Jiangsu, China). Briefly, the culture medium was collected and incubated with the working mixture (lactate, INT solution and diaphorase) at 37 °C for 30 min in dark. The absorbance of the sample was measured by an enzyme-linked immunosorbent assay reader at 490 nm. First, cardiomyocytes were incubated with 5 mM 3-MA (MedChemExpress) (Hou et al., 2012) or 2.5 μM Rapamycin (MedChemExpress) (Zhou et al., 2007) for 12 h, then stimulated with 0.25 μM, 0.5 μM and 1 μM DOX, after that both were maintained for 24 h. The LDH release assay was conducted to detect cell cytotoxicity, following the manufacturer's instructions as previously described.

2.6 Detection of reactive oxygen species (ROS)

Intracellular ROS generation was analyzed using a ROS Assay Kit (Beyotime Institute of Biotechnology, Jiangsu, China). In accordance with instructions, after treatment with different concentrations (0, 0.25, 0.5, 1 μM) of DOX for 24 h, cells were incubated with DCFH-DA for 30 min at 37 °C and then washed three times with the medium. The fluorescence intensity was measured using the fluorospectrophotometer at 488 nm excitation and 525 nm emission wavelengths (PerkinElmer, Canada). The ROS fluorescence intensity was normalized relative to the mean Hoechst fluorescence intensity. Meanwhile, the cells were detected by flow cytometry. For further analysis of mitochondrial ROS in hiPSC-CMs and hESC-CMs, the live cells were stained with MitoSOX Red dye (ThermoFisher, Life Technologies, USA) according to the manufacturer's instructions. The images were obtained with Fluorescence microscopy, and analyzed with Image J software.

2.7 DNA damage

hiPSC-CMs or hESC-CMs were seeded on gelatin-coated coverslips and treated with or without DOX in 12-well plates. After 24 h, cells were washed twice with PBS, fixed in 4% formaldehyde in PBS at RT for 30 min, and then permeated with 0.1% Triton-100X at RT for 15 min. Next, the coverslips were washed, and blocked with 10% goat serum for 1 h at RT and then incubated with the first antibody (γ-H2AX, 1:200) overnight at 4 °C. The cells were then washed thrice for 5 min and stained with Alexa Fluor™ 555-conjugated antibody (1:500; Beyotime Institute of Biotechnology). After staining for 10 min with DAPI, cells were analyzed by an Optiphot-2 microscope (Nikon Corporation) equipped with a CCD video camera system (Optronics Engineering, Ltd.) or a confocal laser scanning microscopy (Optronics Engineering, Ltd.).

2.8 Analysis of autophagic flux

To analyze autophagic flux, hiPSC-CMs or hESC-CMs were replanted on Laser confocal dishes (JingAn Biological Technology Co., Ltd, Shanghai, China). Cells were washed twice with PBS and infected with adenovirus expressing mCherry-GFP-LC3B fusion protein (Ad-mCherry-GFP-LC3B; Beyotime Institute of Biotechnology, Jiangsu, China) at an MOI of 20 for 24 h. After infection, the cells were treated with 0.5 μM of DOX for 6, 12 and 24 h. Then, cells were fixed with 4% paraformaldehyde, and then visualized with a confocal laser scanning microscopy (Olympus). We measured autophagic flux at different time points by observing the color change of mCherry/GFP.

2.9 Transmission electron microscope

hiPSC-CMs or hESC-CMs prepared for TEM were treated with or without DOX for 24 h. The cells were harvested, fixed with 5% glutaraldehyde (Sigma-Aldrich; Merck KGaA) at 4 °C

overnight, and then postfixed with 1% osmium tetroxide (Sigma-Aldrich; Merck KGaA) at RT for 1 h. After fixation, the cells were dehydrated through a graded series of ethanol (Sinopharm Chemical Reagent Co., Ltd). Subsequently, the samples were treated with Spurr embedding agents mixed with various specifications of acetone (Sigma-Aldrich; Merck KGaA). Then, the ultrathin sections were mounted on nickel grids, followed by staining with lead citrate, uranyl acetate and 50% ethanol solution (Sigma-Aldrich; Merck KGaA). Thin sections of each sample were observed and analyzed under a transmission electron microscope (Hitachi H −7,650).

2.10 Western blot analysis

Proteins were extracted from hiPSC-CMs or hESC-CMs with RIPA lysis buffer then centrifuged at 120,00× g for 30 min. The concentration was quantified with Bradford assay (Thermo-Fisher Biochemical Co. Ltd, Beijing, China). For immunoblotting analysis, 30 μg of total proteins were loaded into the PAGE-SDS gels. The proteins were separated and transferred to a nitrocellulose membrane (Millipore, Billerica, MA, USA). Next, the membrane was blocked in 5% Nonfat dry milk in PBST and then incubated overnight at 4 °C followed by primary antibodies against GAPDH (1:5000), mTOR (1:500), p-mTOR (1:500) and LC3B (1:1,000) purchased from Cell Signaling Technology. Subsequently, the membrane was rinsed with PBST and incubated with horseradish peroxidase-conjugated goat anti-rabbit or mouse immunoglobulin G (IgG) antibody (Proteintech) for 1 h at RT. Afterward, the membrane was then washed with PBST three times and visualized with enhanced chemiluminescence (ECL) reagent (Amersham; GE Healthcare Life Sciences), and images were captured with the ECL Tanon 5500 system (Tanon Science and Technology Co., Ltd.).

2.11 Statistical analysis

In all experiments, data were detected by three or four independent biological replicates (n = 3–4) and presented as means ± standard deviation (SD). Grayscale analysis was quantified using ImageJ software. Prior to parametric testing, the Shapiro–Wilk test confirmed normal distribution and the Brown–Forsythe test confirmed homogeneity of variances for all datasets. Data Statistical significance was analyzed by using the unpaired Student's t-test or one-way ANOVA followed by Dunnett's *post hoc* multiple comparison test. Two-way ANOVA was employed to analyze the effects of two independent variables. Differences were considered statistically significant when $p < 0.05$.

3 Results

3.1 Differentiation and characterization of hiPSC-CMs and hESC-CMs

hiPSCs and hESCs were differentiated to CMs as described previously (Ke et al., 2020) with slight modifications (Figure 1A). Immunocytochemical staining results showed that the cardiomyocyte-specific marker cTnT and the mature gap-junction marker Cx43 were expressed in hiPSC-CMs and hESC-CMs (Figure 1B). Flow cytometry analysis revealed that over 97% of the hiPSC-CMs and hESC-CMs were expressing the cTnT, indicating that these cells represent a highly pure cardiomyocyte population (Figure 1C). By day 10 post-differentiation, both hiPSC-CMs and hESC-CMs exhibited robust spontaneous contractions, providing qualitative evidence of electrophysiological activity (Supplementary Videos S1, S2).

3.2 DOX decreased the cell viability and induced cell apoptosis in hiPSC-CMs and hESC-CMs

In clinical studies, DOX can induce cardiomyocyte death within hours of intravenous administration in some patients at relatively low cumulative doses of 200–250 mg/m2 (Unverferth et al., 1983; Swain et al., 2003). The CCK8 results showed that DOX treatment resulted in a dose-dependent decrease in cell viability (Figure 2A). The cardiotoxicity was induced at a low concentration of DOX (0.1 μM for 24 h). We next investigated the cell damage caused by different concentrations of DOX (0–1 μM), which were chosen based on prior studies and are considered clinically relevant, as they fall well within the plasma concentration range observed in patients undergoing DOX therapy (Burridge et al., 2016; Frost et al., 2002). As shown in Figure 2B, LDH release significantly increased in a dose-dependent manner (0.25, 0.5 and 1 μM) following DOX treatment. Subsequently, we investigated the DOX-induced apoptosis in hiPSC-CMs and hESC-CMs. At a high concentration of 1 μM, DOX caused the most significant cell damage, prompting its use in the present study for apoptosis analysis. Flow cytometry analysis demonstrated that exposure of CMs to 1 μM DOX for 24 h resulted in a significant increase of Annexin V-FITC$^+$ cells (an indicator of total apoptotic cells) compared to vehicle-treated control cells (Figure 2C). Moreover, morphologies of nuclear shrinkage and apoptotic bodies, indicative of typical apoptotic features, were observed by TEM in the DOX-treated group (Figure 2D). These data demonstrate that DOX treatment decreases cell viability and induces apoptosis in hiPSC-CMs and hESC-CMs. Collectively, these results from our study align with previous cellular and human biopsy reports (Burridge et al., 2016; Maillet et al., 2016; Zhao and Zhang, 2017; Cui et al., 2019), confirming the cardiotoxic effects of DOX and establishing a reliable *in vitro* model for assessing DIC in hiPSC-CMs and hESC-CMs.

3.3 DOX increased cellular ROS production and triggered DNA damage of hiPSC-CMs and hESC-CMs

To investigate the damage role of DOX in hiPSC-CMs and hESC-CMs, we first measured intracellular ROS production following DOX treatment using the probe DCFH-DA. As shown in Figure 3A, compared with the control, DOX induced a significant increase in intracellular ROS in hiPSC-CMs at 0.25, 0.5, and 1 μM, whereas in hESC-CMs significance was observed only at 0.5 and 1 μM. Similarly, the results were confirmed by flow

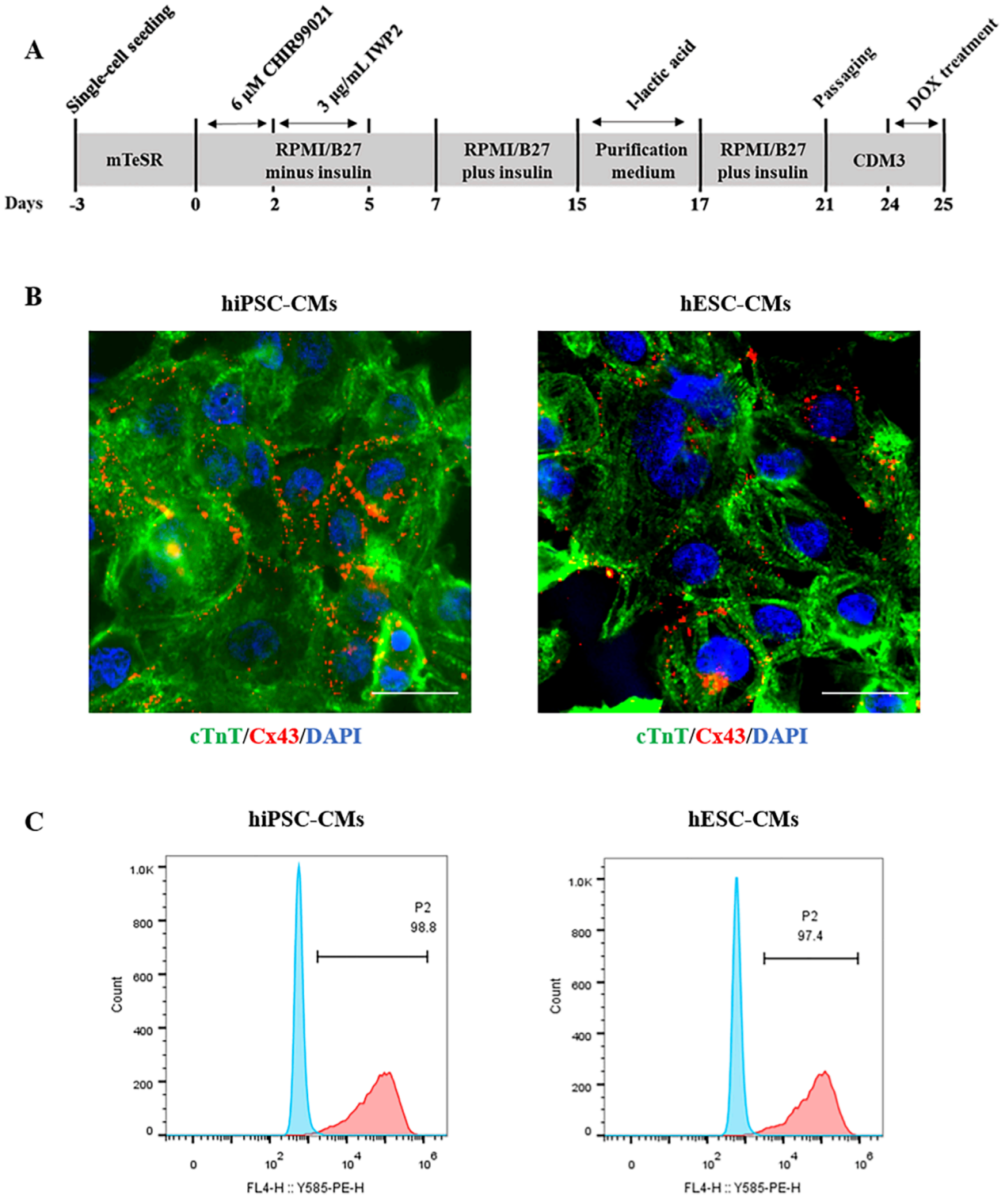

FIGURE 1
Differentiation and characterization of hiPSC-CMs and hESC-CMs. **(A)** Experimental scheme of differentiation protocol from hiPSCs and hESCs to differentiated cardiomyocytes. **(B)** Immunocytochemical staining of the cardiomyocyte marker cTnT in hiPSC-CMs and hESC-CMs at differentiation day 20. cTnT, green. CX43, red. DAPI, blue. Scar bar, 50 μm. **(C)** Flow cytometry analysis of the percentage of cTnT-positive ($cTnT^+$) CMs at differentiation day 20.

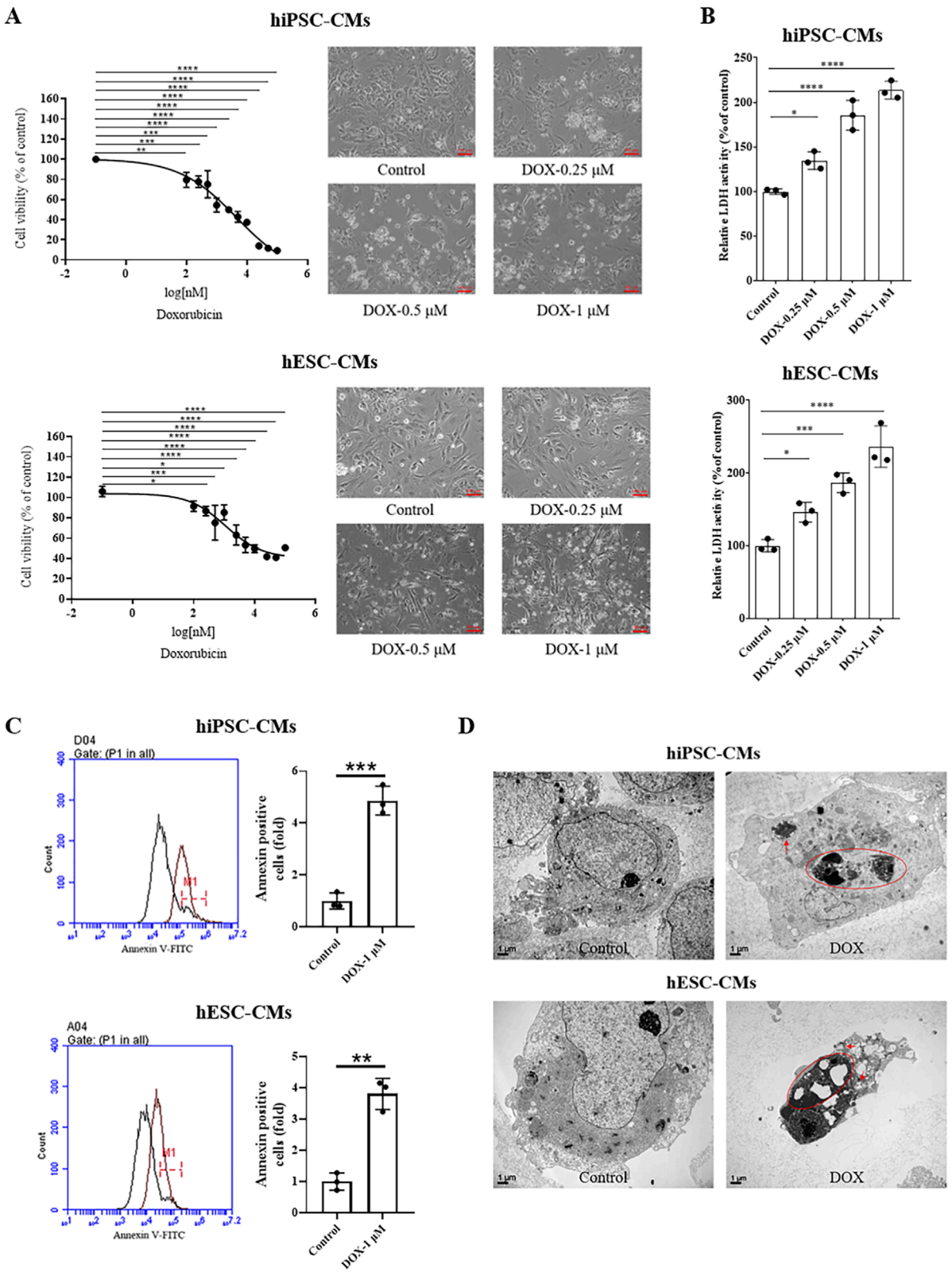

FIGURE 2
DOX decreased the cell viability and induced cell apoptosis of hiPSC-CMs and hESC-CMs. **(A)** hiPSC-CMs or hESC-CMs were treated with the different dose (0, 0.1, 0.25, 0.5, 1, 1.5, 2.5, 5.0, 10, 25, 50, 100 μM) DOX for 24 h. Cell viability was assessed by CCK-8 assay. Scale bar, 100 μm. P values were calculated using one-way ANOVA followed by Dunnett's *post hoc* test comparing each DOX-treated group vs. the vehicle control group.*P < 0.05,**P < 0.01,***P < 0.001,****P < 0.0001. **(B)** The LDH activity of hiPSC-CMs and hESC-CMs after treatment with DOX (0, 0.25, 0.5, 1 μM) for 24 h. P values were calculated using one-way ANOVA followed by Dunnett's *post hoc* test comparing each DOX-treated group vs. the vehicle control group.*P < (*Continued*)

FIGURE 2 (Continued)
0.05, ***P < 0.001, ****P < 0.0001. **(C)** Following treatment with 1 μM DOX for 24 h, cells were collected and analyzed by flow cytometry using Annexin V-FITC staining. P values were calculated using an unpaired two-tailed t-test comparing the DOX-treated group vs. the vehicle control group. **P < 0.01, ***P < 0.001. **(D)** Morphologies of nuclear shrinkage and apoptotic bodies were observed by TEM in 1 μM DOX treatment group. The red circle represents nuclear shrinkage and the red arrow indicates autophagosome. Scale bar, 1 μm. (n = 3, mean = S.D).

cytometry analysis (Figure 3B). Additionally, a dose-dependent increase in MitoSOX red fluorescence was observed in cells exposed to DOX (Figure 3C). Next, the level of double-stranded DNA damage was assessed through staining for phosphorylated H2A histone family member X (γ-H2AX) on serine 139. As shown in Figure 3D, DOX treatment induced γ-H2AX expression in hiPSC-CMs in a dose-dependent manner, with significant DNA damage evident at a concentration of 0.5 μM. Therefore, we evaluated γ-H2AX expression in hiPSC-CMs and hESC-CMs treated with 0.5 μM DOX using laser confocal microscopy. The results demonstrated that DOX induced an increase in γ-H2AX expression in both hiPSC-CMs and hESC-CMs groups (Figure 3E). These findings indicate that DOX increases ROS levels and triggers DNA damage, leading to apoptosis, which represents one of the mechanisms of DIC.

3.4 DOX induced autophagy of hiPSC-CMs and hESC-CMs

Autophagy has dual functions in both physiology and pathology. To evaluate the changes in autophagy, we first observed ultrastructure changes and autophagosome formation in hiPSC-CMs and hESC-CMs by TEM. The results revealed an accumulation of autophagosomes and autolysosomes in DOX-treated groups (Figure 4A). Western blots were performed to detect the changes in the ratios of LC3 II/LC3 I in hiPSC-CMs and hESC-CMs treated with or without DOX. We found that DOX significantly upregulated the ratio of LC3 II/LC3 I in the hiPSC-CMs and hESC-CMs (Figure 4B). The most pronounced changes in autophagy-related proteins were noted at a DOX concentration of 0.5 μM. Therefore, the concentration of 0.5 μM was utilized in subsequent studies to investigate the effects of DOX on autophagy and its underlying mechanisms. To further study DOX-induced autophagic flux, we detected autophagy in hiPSC-CMs and hESC-CMs infected with adenovirus expressing a dual-fluorescence reporter mCherry-GFP-LC3B fusion protein (Ad-mCherry-GFP-LC3B) at a different time point (6 h, 12 h, and 24 h). Treatment with DOX resulted in an increase of autophagic flux within 6 h, as indicated by the number of both yellow and red puncta, with the maximum effect observed at 24 h (Figure 4C). Moreover, the DOX-induced increases in the LC3 II/LC3 I ratio were attenuated by 3-MA, an autophagy inhibitor, as shown in Figure 4D. In addition, to assess the role of autophagy in DOX-induced cardiomyocyte death, we evaluated the effects of 3-MA on LDH release. In Figure 4E, compared with the control, DOX induced an increase in LDH level, indicating cellular damage. However, pretreatment with the autophagy inhibitor 3-MA led to a significant yet partial reduction in DOX-induced LDH release at both 0.5 and 1 μM, resulting in a partial rescue effect (Figure 4E; Supplementary Table S1). Collectively, these results suggest that DOX upregulates autophagy in both hiPSC-CMs and hESC-CMs, which partially contribute to cardiotoxicity.

3.5 DOX inhibited mTOR signaling in hiPSC-CMs and hESC-CMs

The kinase mTOR functions as a key signaling 'station' in the regulation of cellular metabolism, promoting protein synthesis while inhibiting the induction of autophagy (Liang, 2010). Although other pathways such as PI3K/AKT and AMPK also play roles in autophagy regulation, mTOR is widely recognized as one of the most pivotal and extensively studied mediators of autophagic processes (Shackebaei et al., 2024). Given the gatekeeper role of mTOR in autophagy regulation, we investigated whether DOX alters autophagy in hiPSC-CMs and hESC-CMs through mTOR signaling. We found that DOX treatment notably decreased mTOR activation in hiPSC-CMs and hESC-CMs, as evidenced by the reduced phosphorylation at Ser-2248 across various concentrations (Figure 5A). To further confirm the role of mTOR signaling in autophagy induced by DOX, we next treated hiPSC-CMs and hESC-CMs with rapamycin (RAPA), an mTOR inhibitor. In hiPSC-CMs, RAPA alone increased LDH release and exacerbated DOX-induced cell death, although without significant additive cytotoxicity (Figure 5B; Supplementary Table S1). In contrast, in hESC-CMs co-treatment with RAPA and DOX (0.25 and 0.5 μM) resulted in a significant additive increase in LDH release, suggesting the inhibition of mTOR enhances the cytotoxic effects of DOX (Figure 5B; Supplementary Table S1). Collectively, these experiments demonstrate that DOX stimulates autophagy in hiPSC-CMs and hESC-CMs through inhibiting mTOR signaling.

4 Discussion

DOX is one of the most effective anthracycline chemotherapy agents for treating a wide range of malignancies but causes cardiotoxicity in many patients (Jones and Dass, 2022). In the present study, our investigation focused on the features and mechanisms of DIC using the hiPSC- and hESC-CM model. Our results suggested that DOX treatment decreased cell viability and induced cell apoptosis via the accumulation of ROS and DNA damage. Notably, our study further investigated the function of autophagy in DIC and demonstrated that DOX promoted autophagy of hiPSC-CMs and hESC-CMs by inhibiting mTOR signaling.

The mechanism and pathogenesis of DIC remain controversial and obscure, despite extensive research over the last half-century. Animal and heterologous cell models help clarify DIC mechanisms but may not fully capture human cardiac complexities. hiPSC-CMs and hESC-CMs provide a human-based, high-throughput,

10.3389/fcell.2025.1616235

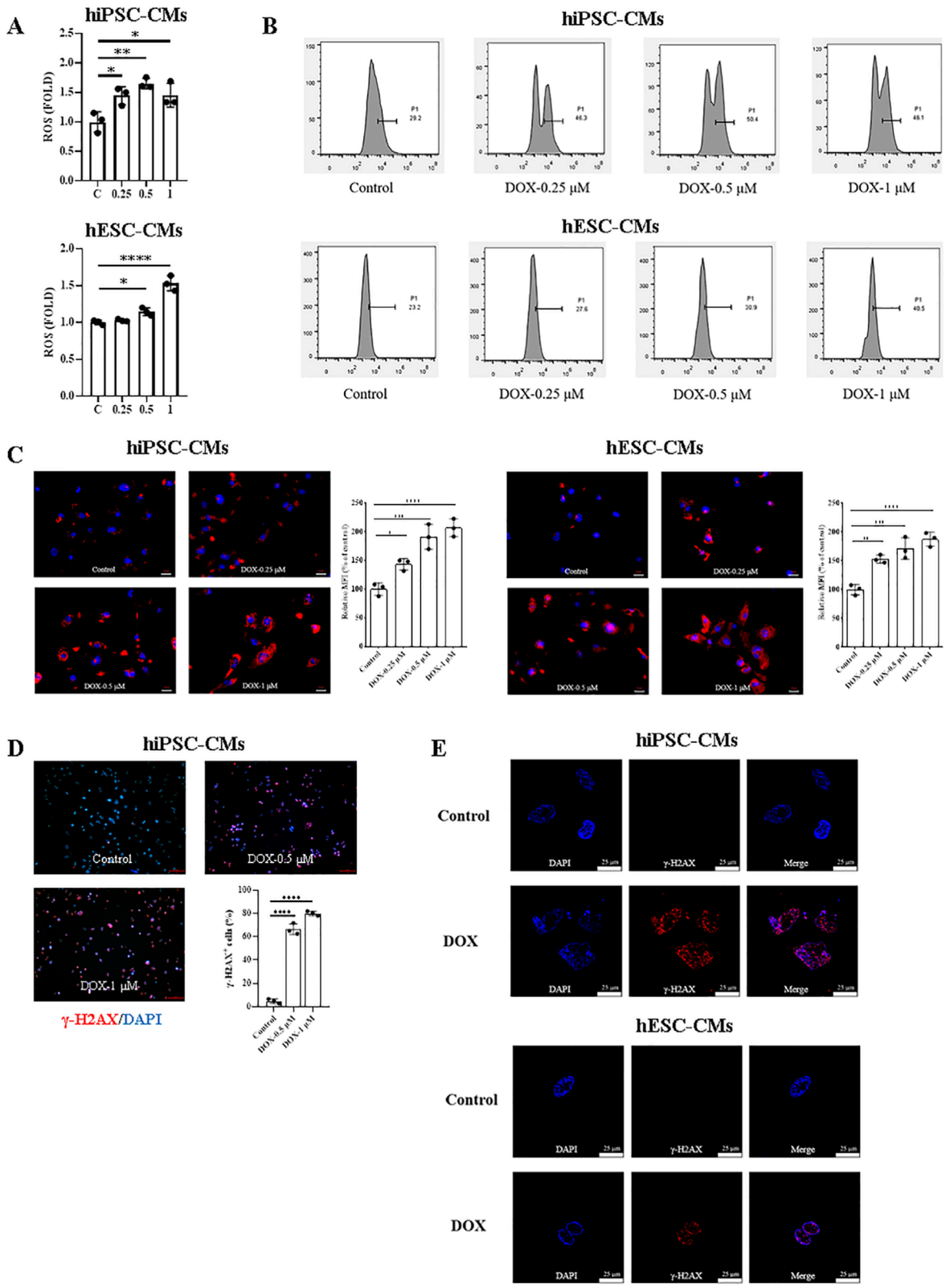

FIGURE 3
ROS production and DNA damage induced by DOX in hiPSC-CMs and hESC-CMs. **(A)** Exposure of hiPSC-CMs or hESC-CMs to different dose (0, 0.25, 0.5, 1 μM) DOX for 24 h resulted in a significant increase in ROS production as measured by the DCFH-DA probe. P values were calculated using one-way ANOVA followed by Dunnett's *post hoc* test comparing each DOX-treated group vs. the vehicle control group.*P < 0.05,**P < 0.01,****P <

(*Continued*)

FIGURE 3 (Continued)
0.0001. **(B)** The representative data of flow cytometry assessed by DCFH-DA in hiPSC-CMs and hESC-CMs with or without DOX treatment. **(C)** Mitochondrial ROS were quantified as relative median fluorescence intensity (MFI) of MitoSOX normalized to vehicle control in hiPSC-CMs and hESC-CMs treated overnight with 0.25, 0.5 and 1 μM DOX. MitoSOX is shown in red, and DAPI nuclear staining is shown in blue. Scale bars, 50 μm. Data were analyzed by one-way ANOVA with Dunnett's post-test; *P < 0.05, **P < 0.01, ***P < 0.001, ****P < 0.0001 *versus* control. **(D)** Representative fluorescence images and quantitative data of DNA double-stranded break in hiPSC-CMs treated overnight with 0.5 and 1 μM DOX. γ-H2AX staining is shown in red, and DAPI nuclear staining is shown in blue. Scale bars, 100 μm. Data were analyzed by one-way ANOVA with Dunnett's post-test; ****P < 0.0001 *versus* control. **(E)** Representative fluorescence images of DNA double-stranded break in hiPSC-CMs and hESC-CMs treated overnight with 0.5 μM DOX. γ-H2AX, red; DAPI, blue. Scale bars, 25 μm. (n = 3, mean = S.D).

and genetically diverse platform that can significantly enhance our understanding of DIC (Burridge et al., 2016; Maillet et al., 2016; Zhao and Zhang, 2017; Cui et al., 2019; Yang et al., 2022). In our research, we first utilized both hiPSC-CM and hESC-CM models to investigate the multifaceted effects and potential mechanisms of DIC, with a specific focus on the dynamic changes and regulatory processes associated with autophagy.

A commonly cited pathway involves the DOX-induced generation of ROS associated with mitochondrial dysfunction (Songbo et al., 2019; Yarmohammadi et al., 2021). Our data showed that DOX increased ROS production of hiPSC-CMs and hESC-CMs, in agreement with previous reports (Songbo et al., 2019). The generation of ROS by redox cycling causes DNA damage, an early event in DIC, which was also confirmed in our data (L'Ecuyer et al., 2006). DOX significantly increased ROS levels in both the intracellular and mitochondria of hiPSC-CMs and hESC-CMs; however, the magnitude and dose-response dynamics differed between the two models (Supplementary Table S1), highlighting the necessity for patient-specific or lineage-specific mechanistic profiling of oxidative stress responses. Moreover, mitochondrial ROS exhibited a greater increase compared to intracellular ROS (Supplementary Table S1), consistent with mitochondria representing the primary source of ROS generation in DIC (Songbo et al., 2019). DNA damage, one of the most significant effects induced by chemical agents, triggers different stress responses in various cell models, either repairing the damage or leading to cell death (Naselli et al., 2024). In our study, DOX induces DNA damage in hiPSC-CMs and hESC-CMs, which subsequently results in their apoptosis. In addition, DIC mediated by topoisomerase-IIβ causes transcriptional modulation of nuclear and mitochondrial genes and DNA-damage-induced apoptosis (Zhang et al., 2012). The ROS level was increased in H9c2 cells after treatment with DOX which promotes the NLRP3 inflammasome activation and secretion of IL-1β (Wei et al., 2020). The role of NLRP3 inflammasome in our cell model needs to be further evaluated.

Autophagy has dual functions, enhancing cellular survival by degrading damaged or obsoleted proteins and organelles under physiological conditions or inducing cell death under pathological conditions (Marshall and Vierstra, 2018). There are many steps involved in autophagy, as it comprises multiple steps such as membrane nucleation, elongation, and completion of the autophagosome, autophagosome fusion with the lysosome to form autolysosome, and autolysosomal degradation (Mizushima, 2007). LC3, an autophagy marker, plays a crucial role in autophagosome biogenesis and maturation (Mizushima, 2020). LC3 II is formed by LC3 I conjugated to phosphatidylethanolamine, which amount is related to the number of autophagosomes (Mizushima and Yoshimori, 2007). Advanced imaging and marker-based techniques have proven to be invaluable tools for precisely characterizing and deeply understanding the dual roles of autophagy in cellular stress and cardiotoxicity (Naselli et al., 2024; Klionsky et al., 2021). In our research, Western blot analysis demonstrated that DOX significantly upregulated the LC3 II/LC3 I ratio both hiPSC-CMs and hESC-CMs, with the maximal increase consistently observed at 0.5 μM (Supplementary Table S1). Furthermore, utilizing advanced imaging and marker-based techniques, TEM visualization revealed a significant increase in autophagosome formation in DOX-treated groups, and the results of autophagy flux assays using Ad-mCherry-GFP-LC3B indicated a time-dependent accumulation of autophagosomes. Thereby DOX can be considered to stimulate autophagy in hiPSC-CMs and hESC-CMs via increasing the number of autophagosomes. Although DOX enhanced autophagy in both hiPSC-CMs and hESC-CMs, static snapshots may bias quantification; higher-throughput and dynamic analyses are further required to accurately assess potential differences. Recently, some studies suggested that DOX treatment increased the accumulation of autophagosomes in response to the autophagic degradation process inhibition, such as impairing lysosomal function as well as autophagosome/autolysosome fusion, but has little effect on autophagosome formation *in vivo* (mice) and *in vitro* (NRCM) (Li et al., 2016; Abdullah et al., 2019). We did not directly assess lysosomal activity or the fusion of autophagosomes with autolysosomes using LysoTracker or chloroquine-based assays; thus, the possibility that DOX may impair autophagic degradation remains insufficiently investigated and warrants further research. Autophagy functions as a double-edged sword: on one hand, it protects cells by degrading and recycling damaged organelles and proteins; on the other hand, excessive autophagy can induce cell death. In our work, DOX-induced hyperactive autophagy exacerbated cellular damage, ultimately leading to cell death in hiPSC-CMs and hESC-CMs. Furthermore, we found that inhibition of autophagy formation induced by DOX using 3-MA, an autophagy inhibitor downregulating PI3 kinase complex, decreased expression of LC3 II/LC3 I and improved cell viability of hiPSC-CMs and hESC-CMs. Nevertheless, 3-MA only partially alleviated the injury, and cell viability remained below baseline levels. This indicates that autophagy may represent one aspect of the injury mechanism in DIC. The biological meaning of this effect and the precise contribution of autophagy to overall cell death remain to be fully elucidated. Our findings underscore the intricate and pivotal role of autophagy in DIC and highlight the therapeutic potential of modulating autophagy. However, we did not dissect the downstream of autophagy flux mediated by DOX.

10.3389/fcell.2025.1616235

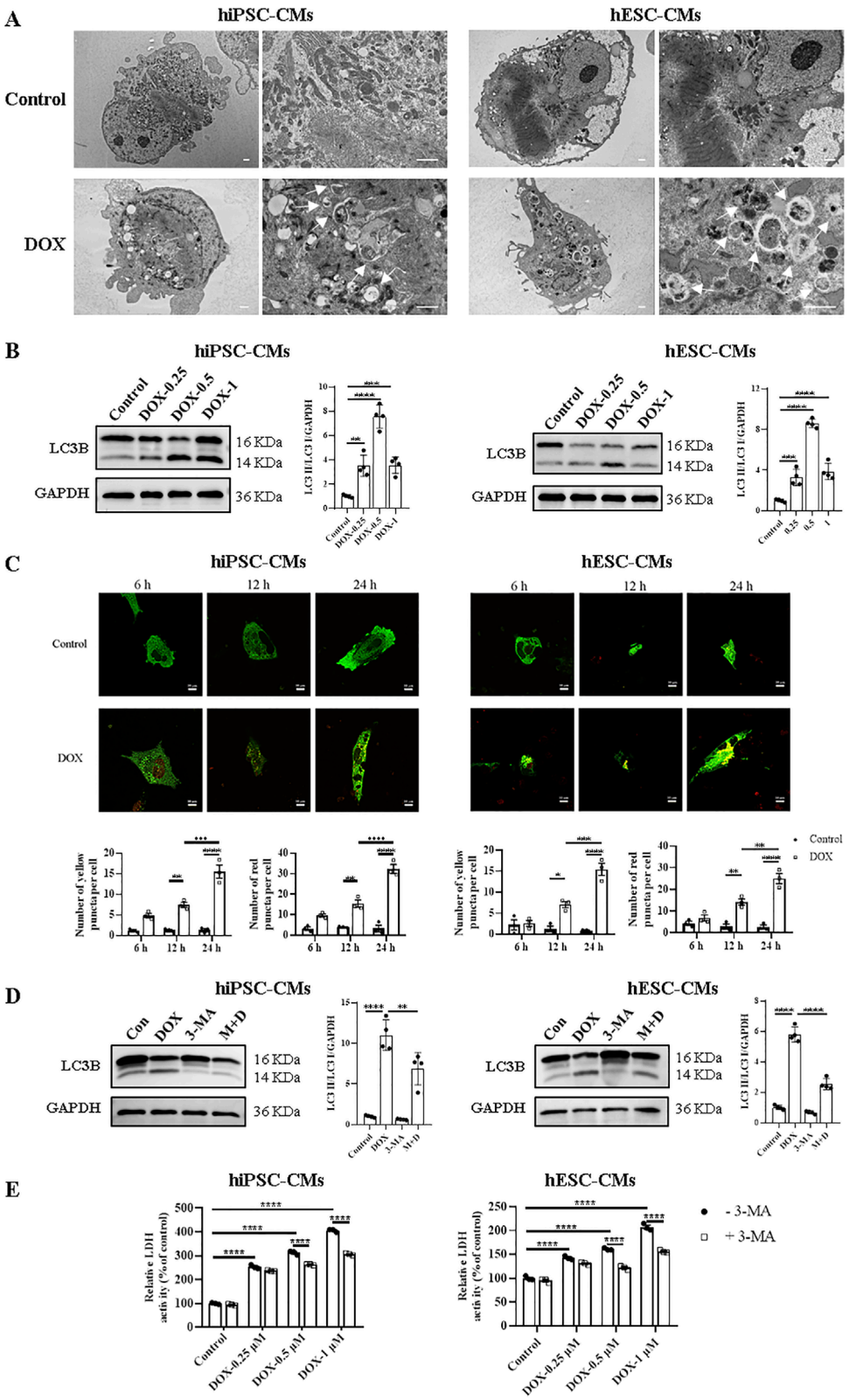

FIGURE 4
Treatment with DOX upregulated hiPSC-CMs and hESC-CMs autophagy. **(A)** Representative TEM images of hiPSC-CMs and hESC-CMs treated overnight with 0.5 μM DOX. Arrowhead, autophagosomes and autolysosomes. Scale bars, 1 μm. **(B)** Western blot analysis of LC3B in hiPSC-CMs and hESC-CMs following DOX (0, 0.25, 0.5, 1 μM) treatment. P values were calculated using one-way ANOVA followed by Dunnett's *post hoc* test comparing each DOX-treated group vs. the vehicle control group.***P < 0.001,****P < 0.0001. **(C)** Representative fluorescence images o and quantitative data f hiPSC-CMs and hESC-CMs expressing mCherry-GFP-LC3 and treated with 0.5 μM DOX for 6, 12 and 24 h, respectively.

(*Continued*)

FIGURE 4 (Continued)
Autophagosomes, yellow puncta; autolysosome, red puncta. Scale bars, 10 μm. Data were analyzed by two-way ANOVA; *P < 0.05, **P < 0.01, ***P < 0.001, ****P < 0.0001. **(D,E)** hiPSC-CMs and hESC-CMs were incubated with 5 mM 3-MA for 12 h prior to stimulation with 0.5 μM DOX or different concentrations of DOX (0, 0.25, 0.5, 1 μM), then both were maintained for 24 h. **(D)** The effect of 3-MA on the expression ratio of LC3 II/LC3 I in hiPSC-CMs and hESC-CMs analyzed by Western blotting. P values were calculated using one-way ANOVA followed by Dunnett's *post hoc* test for multiple comparisons among all groups (Control, DOX, 3-MA, M + D). **P < 0.01, ****P < 0.0001. **(E)** By spectrophotometry, LDH activity in the culture media was measured. P values were calculated using two-way ANOVA. ****P < 0.0001. The lower band is LC3 II and the higher one is LC3 I on LC3B membrane. GAPDH was used as a loading control and grayscale analysis was performed for statistics. (n = 3-4, mean = S.D.).

Moreover, previous studies have demonstrated that dox-induced activation of autophagy is likely pathological and contributes to cellular dysfunction and apoptosis (Dirks-Naylor, 2013). In our study, DOX at 0.5 μM induces peak autophagy and concurrently increases cell death in hiPSC-CMs and hESC-CMs, but apoptosis was not assessed (Supplementary Table S1). At 1 μM, DOX-induced autophagy remains elevated compared to controls but declines, while apoptosis markedly increases, with distinct fold changes in hiPSC-CMs *versus* hESC-CMs (Supplementary Table S1). A study reported that a high concentration of DOX (1 μM) was associated with DNA damage, PARP-1 dissociation, and severe apoptosis in mouse stem cell-derived cardiomyocytes (Cunha-Oliveira et al., 2018). Whether the apoptotic surge is caused by concurrent autophagic activation or occurs independently remains unclear. Future studies should combine apoptosis detection methods and inhibitors like caspase inhibitors to analyze the temporal dynamics of autophagic flux and apoptosis in DIC, clarify their interaction, and identify key mechanisms.

What mechanisms are involved in the stimulation of cardiac autophagy by DOX? The mTOR protein, an atypical serine/threonine kinase, exerts as a critical signaling 'station' in regulating cell homeostasis and stress responses, which stimulates protein synthesis and suppresses the induction of autophagy (Liang, 2010; Liu et al., 2024; Guseva et al., 2024). mTOR interacts with the ULK1-Atg13-FIP200 complex, which is essential for the onset of autophagosome formation in mammals, and phosphorylates ULK1 and Atg13 to inhibit autophagy (Ganley et al., 2009). It has been demonstrated that mTOR signaling is essential for heart physiological processes regulation such as growth, aging, and lifespan, as well as for playing a pivotal role in pathological conditions such as atherosclerosis and ischemia–reperfusion injury (Park et al., 2016; Yuan et al., 2014; Li et al., 2019; Gurusamy et al., 2010; Liu et al., 2021). Several studies have explored the impact of DOX on the mTOR signaling pathway (Yarmohammadi et al., 2023). However, the role and mechanisms of mTOR in DIC remain inconsistent and inconclusive (Shackebaei et al., 2024). Some studies have reported a reduction in mTOR protein activation within cardiac tissue, while others have observed an increase in activation (Yarmohammadi et al., 2023). Our findings indicate that following DOX treatment, p-mTOR levels decreased significantly, suggesting that DOX may induce autophagy by inhibiting mTOR signaling. RAPA, an mTOR inhibitor, further reduced cell viability, particularly at 0.25 μM DOX in hESC-CMs. hESC-CMs and hiPSC-CMs exhibit distinct responses to RAPA-induced injury. This difference may be attributed to DOX-mediated suppression of p-mTOR to a low baseline level in hiPSC-CMs, thereby limiting the potential for additional inhibitory effects by RAPA. Alternatively, the underlying injury mechanisms may differ between the 2 cell types. These findings highlight the need for further investigation to clarify the biological significance of these observations. This suppression of mTOR signaling may occur via several classical upstream regulatory pathways, including the activation of AMPK and the inhibition of the PI3K/AKT pathway (Shackebaei et al., 2025). DOX has been demonstrated to activate AMPK in both H9C2 cardiomyocytes and mouse hearts (Chen et al., 2011; Pointon et al., 2010). Furthermore, downregulation or disruption of the PI3K/AKT/mTOR signaling pathway is increasingly recognized as a critical mechanism in DIC (Yu et al., 2020; Zhang et al., 2020). Recently, a study utilizing GEO transcriptomic data and animal model validation has identified a 23-gene autophagy signature—including Akt1, Hif1a, and Mapk3—that highlights potential mechanistic and therapeutic targets (Wu et al., 2024). However, current understanding of the mTOR axis predominantly using cell lines or acute high-dose animal models, resulting in a significant gap in clinically relevant contexts. In this study, we demonstrate the essential role of mTOR in DIC using hiPSC-CMs and hESC-CMs. In future studies, we will use this model with multi-omics profiling—including transcriptomics, proteomics, and metabolomics—to develop precision mTOR-targeted therapies for DIC.

Li et al. reported that DOX blocked cardiomyocyte autophagic flux by altering lysosomal function in mice, independent of mTOR activation (Li et al., 2016). We hypothesize that DOX-induced activation of autophagosome synthesis promotes autophagy damage in CMs. It is plausible that the conclusions may come from differences in the cell models, the dose and time of DOX treatment, and so on. Recent studies have identified novel regulated cell death pathways and elucidated their involvement in the pathogenesis of DIC, including ferroptosis and pyroptosis. Ferroptosis is an iron-dependent form of cell death characterized by uncontrolled lipid peroxidation, which ultimately leads to membrane rupture (Ru et al., 2024). Lipid peroxides represent one of the major sources of ROS involved in DIC, and the role of iron in this process has been well established (Christidi and Brunham, 2021). Our study revealed a significant elevation in ROS levels in hiPSC-CMs and hESC-CMs exposed to DIC; however, the precise origin of this oxidative stress and its mechanistic link to ferroptosis remain to be fully elucidated. Pyroptosis is a novel form of programmed cell death that is mediated by caspase-1 activation and involves the release of substantial pro-inflammatory mediators (Bai et al., 2025). Evidence increasingly shows that DOX induces excessive autophagy through GSDMD or miR-34a-5p upregulation, promoting pyroptosis in mouse cardiomyocytes and contributing to cardiac toxicity (Qu et al., 2022; Zhong et al., 2023). In future studies, we aim to investigate the mechanistic crosstalk between DOX-induced autophagy and pyroptosis in hiPSC-CMs and hESC-CMs.

10.3389/fcell.2025.1616235

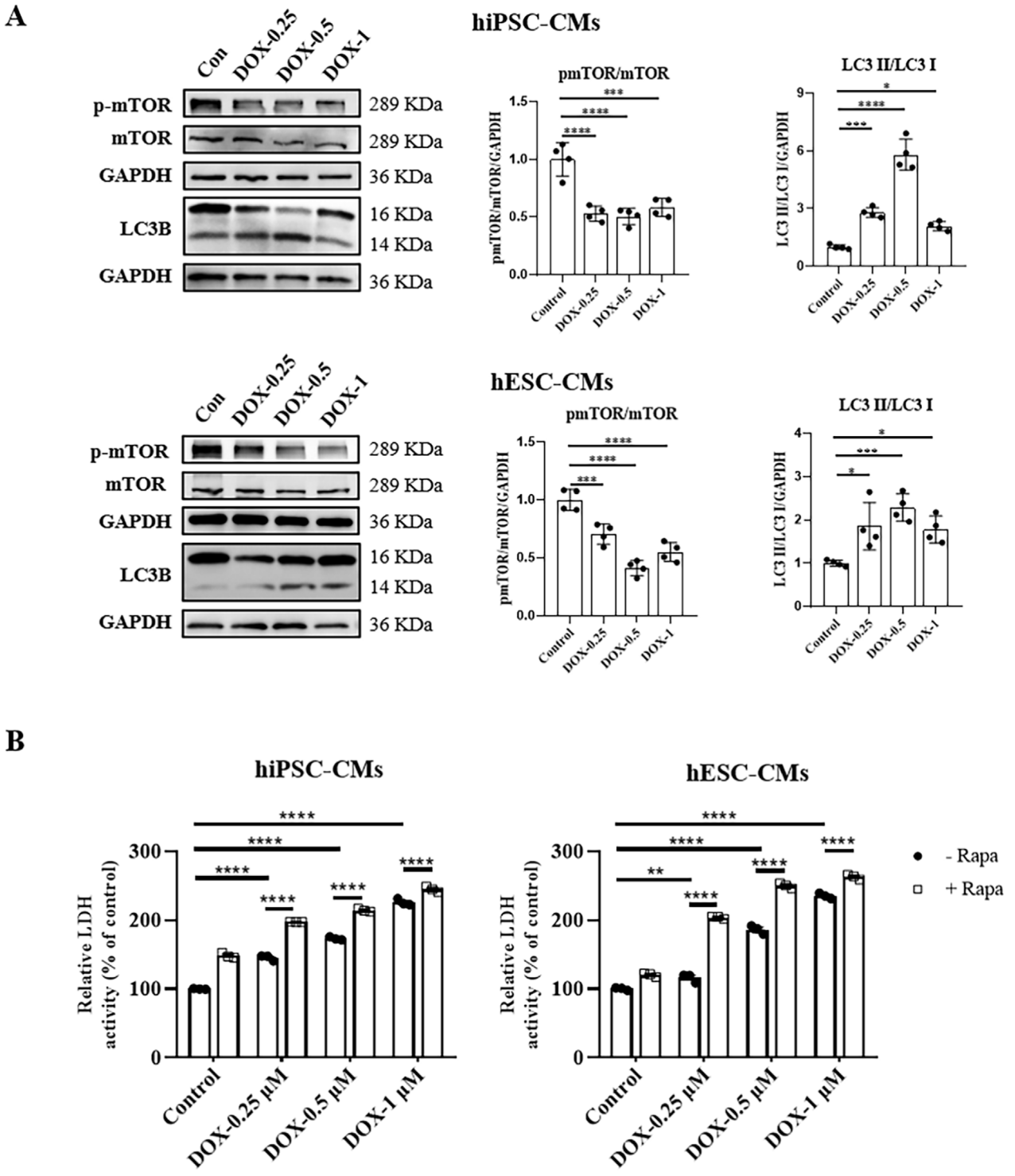

FIGURE 5
DOX inhibited mTOR signaling in hiPSC-CMs and hESC-CMs. **(A)** Western blot analysis of mTOR, p-mTOR, and LC3 II/LC3 I in hiPSC-CMs and hESC-CMs following DOX (0, 0.25, 0.5, 1 μM) treatment. P values were calculated using one-way ANOVA followed by Dunnett's *post hoc* test comparing each DOX-treated group vs. the vehicle control group.*P < 0.05,***P < 0.001,****P < 0.0001. **(B)** hiPSC-CMs or hESC-CMs were treated with 2.5 μM rapamycin for 24 h. Then CMs were exposed to different concentrations of DOX (0, 0.25, 0.5, 1 μM) for 24 h. In the culture media, LDH activity was assessed by spectrophotometry. P values were calculated using two-way ANOVA.**P < 0.01,****P < 0.0001. The lower band is LC3 II and the higher band is LC3 I on LC3B membrane. GAPDH was used as a loading control and grayscale analysis was performed for statistics. (n = 3-4, mean = S.D).

In conclusion, our work demonstrated DOX-induced cardiotoxicity via ROS production, DNA damage, apoptosis, and autophagy in hiPSC-CMs and hESC-CMs. Moreover, the present work suggested that DOX enhanced autophagy via inhibiting mTOR signaling in hiPSC-CMs and hESC-CMs. Overall, these data provide a better understanding of DIC and indicate that the mTOR signaling pathway and its modulation of autophagy represent a valuable therapeutic target of DIC.

Data availability statement

The original contributions presented in the study are included in the article/Supplementary Material, further inquiries can be directed to the corresponding authors.

Ethics statement

Ethical approval was not required for the studies on animals in accordance with the local legislation and institutional requirements because only commercially available established cell lines were used.

Author contributions

MK: Visualization, Investigation, Formal Analysis, Data curation, Conceptualization, Writing – original draft, Methodology. HW: Writing – original draft, Visualization, Conceptualization, Data curation, Investigation. KY: Data curation, Writing – original draft, Visualization. MJ: Writing – original draft, Conceptualization, Investigation. NQ: Writing – review and editing, Validation, Funding acquisition. YW: Writing – review and editing, Funding acquisition, Validation, Supervision.

Funding

The authors declare that financial support was received for the research and/or publication of this article. This research was funded by the Enterprise Commissioned R&D Project (grant no. 16040135-J).

Acknowledgements

We would like to acknowledge Stem Cell Bank of Chinese Academy of Sciences for providing us with human iPSCs. We would like to acknowledge Shanghai Zhong Qiao Xin Zhou Biotechnology Co. Ltd for providing us with human ESCs. We are grateful to the Faculty of Agriculture, Life and Environmental Sciences, Zhejiang University for their technical support in the detection of autophagy by Transmission electron microscope. Also, the authors would also like to thank Mr. Ahmed Salah for his critical review and helpful comments on the manuscript.

Conflict of interest

Authors HW, MJ, and NQ were employed by Hangzhou Biaomo Biosciences Co., Ltd. Authors HW and NQ were employed by Asia Stem Cell Therapies Co., Limited.

The remaining authors declare that the research was conducted in the absence of any commercial or financial relationships that could be construed as a potential conflict of interest.

Generative AI statement

The authors declare that no Generative AI was used in the creation of this manuscript.

Any alternative text (alt text) provided alongside figures in this article has been generated by Frontiers with the support of artificial intelligence and reasonable efforts have been made to ensure accuracy, including review by the authors wherever possible. If you identify any issues, please contact us.

Publisher's note

Supplementary material

The Supplementary Material for this article can be found online at: https://www.frontiersin.org/articles/10.3389/fcell.2025.1616235/full#supplementary-material

References

Abdullah, C. S., Alam, S., Aishwarya, R., Miriyala, S., Bhuiyan, M. A. N., Panchatcharam, M., et al. (2019). Doxorubicin-induced cardiomyopathy associated with inhibition of autophagic degradation process and defects in mitochondrial respiration. *Sci. Rep.* 9, 2002. doi:10.1038/s41598-018-37862-3

Bai, Y., Pan, Y., and Liu, X. (2025). Mechanistic insights into gasdermin-mediated pyroptosis. *Nat. Rev. Mol. Cell Biol.* 26, 501–521. doi:10.1038/s41580-025-00837-0

Burridge, P. W., Li, Y. F., Matsa, E., Wu, H., Ong, S. G., Sharma, A., et al. (2016). Human induced pluripotent stem cell-derived cardiomyocytes recapitulate the predilection of breast cancer patients to doxorubicin-induced cardiotoxicity. *Nat. Med.* 22, 547–556. doi:10.1038/nm.4087

Cerneckis, J., Cai, H., and Shi, Y. (2024). Induced pluripotent stem cells (iPSCs): molecular mechanisms of induction and applications. *Signal Transduct. Target Ther.* 9, 112. doi:10.1038/s41392-024-01809-0

Chen, M. B., Wu, X. Y., Gu, J. H., Guo, Q. T., Shen, W. X., and Lu, P. H. (2011). Activation of AMP-Activated protein kinase contributes to doxorubicin-induced cell

death and apoptosis in cultured myocardial H9c2 cells. *Cell Biochem. Biophys.* 60, 311–322. doi:10.1007/s12013-011-9153-0

Christidi, E., and Brunham, L. R. (2021). Regulated cell death pathways in doxorubicin-induced cardiotoxicity. *Cell Death Dis.* 12, 339. doi:10.1038/s41419-021-03614-x

Cui, N., Wu, F., Lu, W. J., Bai, R., Ke, B., Liu, T., et al. (2019). Doxorubicin-induced cardiotoxicity is maturation dependent due to the shift from topoisomerase IIα to IIβ in human stem cell derived cardiomyocytes. *J. Cell Mol. Med.* 23, 4627–4639. doi:10.1111/jcmm.14346

Cunha-Oliveira, T., Ferreira, L. L., Coelho, A. R., Deus, C. M., and Oliveira, P. J. (2018). Doxorubicin triggers bioenergetic failure and p53 activation in mouse stem cell-derived cardiomyocytes. *Toxicol. Appl. Pharmacol.* 348, 1–13. doi:10.1016/j.taap.2018.04.009

Dirks-Naylor, A. J. (2013). The role of autophagy in doxorubicin-induced cardiotoxicity. *Life Sci.* 93, 913–916. doi:10.1016/j.lfs.2013.10.013

Frost, B. M., Eksborg, S., Bjork, O., Abrahamsson, J., Behrendtz, M., Castor, A., et al. (2002). Pharmacokinetics of doxorubicin in children with acute lymphoblastic leukemia: multi-institutional collaborative study. *Med. Pediatr. Oncol.* 38, 329–337. doi:10.1002/mpo.10052

Ganley, I. G., Lam DU, H., Wang, J., Ding, X., Chen, S., and Jiang, X. (2009). ULK1.ATG13.FIP200 complex mediates mTOR signaling and is essential for autophagy. *J. Biol. Chem.* 284, 12297–12305. doi:10.1074/jbc.M900573200

Gurusamy, N., Lekli, I., Mukherjee, S., Ray, D., Ahsan, M. K., Gherghiceanu, M., et al. (2010). Cardioprotection by resveratrol: a novel mechanism *via* autophagy involving the mTORC2 pathway. *Cardiovasc Res.* 86, 103–112. doi:10.1093/cvr/cvp384

Guseva, E. A., Pavlova, J. A., Dontsova, O. A., and Sergiev, P. V. (2024). Synthetic activators of autophagy. *Biochem. (Mosc)* 89, 27–52. doi:10.1134/S0006297924010024

Hanna, A. D., Lam, A., Tham, S., Dulhunty, A. F., and Beard, N. A. (2014). Adverse effects of doxorubicin and its metabolic product on cardiac RyR2 and SERCA2A. *Mol. Pharmacol.* 86, 438–449. doi:10.1124/mol.114.093849

Hou, H., Zhang, Y., Huang, Y., Yi, Q., Lv, L., Zhang, T., et al. (2012). Inhibitors of phosphatidylinositol 3'-kinases promote mitotic cell death in HeLa cells. *PLoS One* 7, e35665. doi:10.1371/journal.pone.0035665

Ichikawa, Y., Ghanefar, M., Bayeva, M., Wu, R., Khechaduri, A., Naga Prasad, S. V., et al. (2014). Cardiotoxicity of doxorubicin is mediated through mitochondrial iron accumulation. *J. Clin. Invest* 124, 617–630. doi:10.1172/JCI72931

Jones, I. C., and Dass, C. R. (2022). Doxorubicin-induced cardiotoxicity: causative factors and possible interventions. *J. Pharm. Pharmacol.* 74, 1677–1688. doi:10.1093/jpp/rgac063

Ke, M., Ji, M., Wang, H., Yao, Y., Wu, Y., and Qi, N. (2020). Inhibition of rho-associated protein kinase improves the survival of human induced pluripotent stem cell-derived cardiomyocytes after dissociation. *Exp. Ther. Med.* 19, 1701–1710. doi:10.3892/etm.2020.8436

Klionsky, D. J., Abdel-Aziz, A. K., Abdelfatah, S., Abdellatif, M., Abdoli, A., Abel, S., et al. (2021). Guidelines for the use and interpretation of assays for monitoring autophagy (4th edition)[1]. *Autophagy* 17, 1–382. doi:10.1080/15548627.2020.1797280

Kobayashi, S., Volden, P., Timm, D., Mao, K., Xu, X., and Liang, Q. (2010). Transcription factor GATA4 inhibits doxorubicin-induced autophagy and cardiomyocyte death. *J. Biol. Chem.* 285, 793–804. doi:10.1074/jbc.M109.070037

L'Ecuyer, T., Sanjeev, S., Thomas, R., Novak, R., Das, L., Campbell, W., et al. (2006). DNA damage is an early event in doxorubicin-induced cardiac myocyte death. *Am. J. Physiol. Heart Circ. Physiol.* 291, H1273–H1280. doi:10.1152/ajpheart.00738.2005

Li, D. L., Wang, Z. V., Ding, G., Tan, W., Luo, X., Criollo, A., et al. (2016). Doxorubicin blocks cardiomyocyte autophagic flux by inhibiting lysosome acidification. *Circulation* 133, 1668–1687. doi:10.1161/CIRCULATIONAHA.115.017443

Li, X., Xie, X., Yu, Z., Chen, Y., Qu, G., Yu, H., et al. (2019). Bone marrow mesenchymal stem cells-derived conditioned medium protects cardiomyocytes from hypoxia/reoxygenation-induced injury through Notch2/mTOR/autophagy signaling. *J. Cell Physiol.* 234, 18906–18916. doi:10.1002/jcp.28530

Li, Z., Li, H., Liu, B., Luo, J., Qin, X., Gong, M., et al. (2020). Inhibition of miR-25 attenuates doxorubicin-induced apoptosis, reactive oxygen species production and DNA damage by targeting PTEN. *Int. J. Med. Sci.* 17, 1415–1427. doi:10.7150/ijms.41980

Li, L., XI, R., Gao, B., Zeng, Y., Ma, Q., Gong, T., et al. (2024). Research progress of autophagy in heart failure. *Am. J. Transl. Res.* 16, 1991–2000. doi:10.62347/OBXQ9477

Liang, C. (2010). Negative regulation of autophagy. *Cell Death Differ.* 17, 1807–1815. doi:10.1038/cdd.2010.115

Liu, C., Chen, G., Chen, Y., Dang, Y., Nie, G., Wu, D., et al. (2021). Danlou tablets inhibit atherosclerosis in apolipoprotein E-Deficient mice by inducing macrophage autophagy: the role of the PI3K-Akt-mTOR pathway. *Front. Pharmacol.* 12, 724670. doi:10.3389/fphar.2021.724670

Liu, X., Guo, B., Li, Q., and Nie, J. (2024). mTOR in metabolic homeostasis and disease. *Exp. Cell Res.* 441, 114173. doi:10.1016/j.yexcr.2024.114173

Maillet, A., Tan, K., Chai, X., Sadananda, S. N., Mehta, A., Ooi, J., et al. (2016). Modeling doxorubicin-induced cardiotoxicity in human pluripotent stem cell derived-cardiomyocytes. *Sci. Rep.* 6, 25333. doi:10.1038/srep25333

Marshall, R. S., and Vierstra, R. D. (2018). Autophagy: the master of bulk and selective recycling. *Annu. Rev. Plant Biol.* 69, 173–208. doi:10.1146/annurev-arplant-042817-040606

Mcsweeney, K. M., Bozza, W. P., Alterovitz, W. L., and Zhang, B. (2019). Transcriptomic profiling reveals p53 as a key regulator of doxorubicin-induced cardiotoxicity. *Cell Death Discov.* 5, 102. doi:10.1038/s41420-019-0182-6

Mizushima, N. (2007). Autophagy: process and function. *Genes Dev.* 21, 2861–2873. doi:10.1101/gad.1599207

Mizushima, N. (2020). The ATG conjugation systems in autophagy. *Curr. Opin. Cell Biol.* 63, 1–10. doi:10.1016/j.ceb.2019.12.001

Mizushima, N., and Yoshimori, T. (2007). How to interpret LC3 immunoblotting. *Autophagy* 3, 542–545. doi:10.4161/auto.4600

Naselli, F., Cardinale, P. S., Volpes, S., Martino, C., Cruciata, I., Valenti, R., et al. (2024). An alternative approach of TUNEL assay to specifically characterize DNA fragmentation in cell model systems. *Histochem. Cell Biol.* 162, 429–442. doi:10.1007/s00418-024-02306-9

Park, J. H., Choi, S. H., Kim, H., Ji, S. T., Jang, W. B., Kim, J. H., et al. (2016). Doxorubicin regulates autophagy signals *via* accumulation of cytosolic Ca(2+) in human cardiac progenitor cells. *Int. J. Mol. Sci.* 17, 1680. doi:10.3390/ijms17101680

Pizarro, M., Troncoso, R., Martinez, G. J., Chiong, M., Castro, P. F., and Lavandero, S. (2016). Basal autophagy protects cardiomyocytes from doxorubicin-induced toxicity. *Toxicology* 370, 41–48. doi:10.1016/j.tox.2016.09.011

Pointon, A. V., Walker, T. M., Phillips, K. M., Luo, J., Riley, J., Zhang, S. D., et al. (2010). Doxorubicin *in vivo* rapidly alters expression and translation of myocardial electron transport chain genes, leads to ATP loss and caspase 3 activation. *PLoS One* 5, e12733. doi:10.1371/journal.pone.0012733

Protze, S. I., Lee, J. H., and Keller, G. M. (2019). Human pluripotent stem cell-derived cardiovascular cells: from developmental biology to therapeutic applications. *Cell Stem Cell* 25, 311–327. doi:10.1016/j.stem.2019.07.010

Qu, Y., Gao, R., Wei, X., Sun, X., Yang, K., Shi, H., et al. (2022). Gasdermin D mediates endoplasmic reticulum stress *via* FAM134B to regulate cardiomyocyte autophagy and apoptosis in doxorubicin-induced cardiotoxicity. *Cell Death Dis.* 13, 901. doi:10.1038/s41419-022-05333-3

Ru, Q., Li, Y., Chen, L., Wu, Y., Min, J., and Wang, F. (2024). Iron homeostasis and ferroptosis in human diseases: mechanisms and therapeutic prospects. *Signal Transduct. Target Ther.* 9, 271. doi:10.1038/s41392-024-01969-z

Scicchitano, M., Carresi, C., Nucera, S., Ruga, S., Maiuolo, J., Macri, R., et al. (2021). Icariin protects H9c2 rat cardiomyoblasts from doxorubicin-induced cardiotoxicity: role of Caveolin-1 upregulation and enhanced autophagic response. *Nutrients* 13, 4070. doi:10.3390/nu13114070

Shackebaei, D., Hesari, M., Gorgani, S., Vafaeipour, Z., Salaramoli, S., and Yarmohammadi, F. (2024). The role of mTOR in the doxorubicin-induced cardiotoxicity: a systematic review. *Cell Biochem. Biophys.* 83, 43–52.

Shackebaei, D., Hesari, M., Gorgani, S., Vafaeipour, Z., Salaramoli, S., and Yarmohammadi, F. (2025). The role of mTOR in the doxorubicin-induced cardiotoxicity: a systematic review. *Cell Biochem. Biophys.* 83, 43–52. doi:10.1007/s12013-024-01475-7

Sishi, B. J., Loos, B., VAN Rooyen, J., and Engelbrecht, A. M. (2013). Autophagy upregulation promotes survival and attenuates doxorubicin-induced cardiotoxicity. *Biochem. Pharmacol.* 85, 124–134. doi:10.1016/j.bcp.2012.10.005

Songbo, M., Lang, H., Xinyong, C., Bin, X., Ping, Z., and Liang, S. (2019). Oxidative stress injury in doxorubicin-induced cardiotoxicity. *Toxicol. Lett.* 307, 41–48. doi:10.1016/j.toxlet.2019.02.013

Sun, X., DU, J., Meng, H., Liu, F., Yang, N., Deng, S., et al. (2023). Targeting autophagy with SAR405 alleviates doxorubicin-induced cardiotoxicity. *Cell Biol. Toxicol.* 39, 3255–3267. doi:10.1007/s10565-023-09831-8

Swain, S. M., Whaley, F. S., and Ewer, M. S. (2003). Congestive heart failure in patients treated with doxorubicin: a retrospective analysis of three trials. *Cancer* 97, 2869–2879. doi:10.1002/cncr.11407

Thomson, J. A., Itskovitz-Eldor, J., Shapiro, S. S., Waknitz, M. A., Swiergiel, J. J., Marshall, V. S., et al. (1998). Embryonic stem cell lines derived from human blastocysts. *Science* 282, 1145–1147. doi:10.1126/science.282.5391.1145

Tohyama, S., Hattori, F., Sano, M., Hishiki, T., Nagahata, Y., Matsuura, T., et al. (2013). Distinct metabolic flow enables large-scale purification of mouse and human pluripotent stem cell-derived cardiomyocytes. *Cell Stem Cell* 12, 127–137. doi:10.1016/j.stem.2012.09.013

Unverferth, B. J., Magorien, R. D., Balcerzak, S. P., Leier, C. V., and Unverferth, D. V. (1983). Early changes in human myocardial nuclei after doxorubicin. *Cancer* 52, 215–221. doi:10.1002/1097-0142(19830715)52:2<215::aid-cncr2820520206>3.0.co;2-f

Wang, H., Wang, H., Liang, E. Y., Zhou, L. X., Dong, Z. L., Liang, P., et al. (2018). Thrombopoietin protects H9C2 cells from excessive autophagy and apoptosis in doxorubicin-induced cardiotoxicity. *Oncol. Lett.* 15, 839–848. doi:10.3892/ol.2017.7410

Wang, H., Li, X., Zhang, Q., Fu, C., Jiang, W., Xue, J., et al. (2024). Autophagy in disease onset and progression. *Aging Dis.* 15, 1646–1671. doi:10.14336/AD.2023.0815

Wei, S., Ma, W., Li, X., Jiang, C., Sun, T., Li, Y., et al. (2020). Involvement of ROS/NLRP3 inflammasome signaling pathway in doxorubicin-induced cardiotoxicity. *Cardiovasc Toxicol.* 20, 507–519. doi:10.1007/s12012-020-09576-4

Wu, H., Chen, H., Ding, X., Kuang, X., Pang, M., Liu, S., et al. (2024). Identification of autophagy-related signatures in doxorubicin-induced cardiotoxicity. *Toxicol. Appl. Pharmacol.* 491, 117082. doi:10.1016/j.taap.2024.117082

Xiao, B., Hong, L., Cai, X., Mei, S., Zhang, P., and Shao, L. (2019). The true colors of autophagy in doxorubicin-induced cardiotoxicity. *Oncol. Lett.* 18, 2165–2172. doi:10.3892/ol.2019.10576

Yamaguchi, O. (2019). Autophagy in the heart. *Circ. J.* 83, 697–704. doi:10.1253/circj.CJ-18-1065

Yang, M., Fu, J. D., Zou, J., Sridharan, D., Zhao, M. T., Singh, H., et al. (2022). Assessment of mitophagy in human iPSC-derived cardiomyocytes. *Autophagy* 18, 2481–2494. doi:10.1080/15548627.2022.2037920

Yarmohammadi, F., Rezaee, R., and Karimi, G. (2021). Natural compounds against doxorubicin-induced cardiotoxicity: a review on the involvement of Nrf2/ARE signaling pathway. *Phytother. Res.* 35, 1163–1175. doi:10.1002/ptr.6882

Yarmohammadi, F., Hesari, M., and Shackebaei, D. (2023). The role of mTOR in doxorubicin-altered cardiac metabolism: a promising therapeutic target of natural compounds. *Cardiovasc. Toxicol.* 24, 146–157. doi:10.1007/s12012-023-09820-7

Yu, W., Qin, X., Zhang, Y., Qiu, P., Wang, L., Zha, W., et al. (2020). Curcumin suppresses doxorubicin-induced cardiomyocyte pyroptosis *via* a PI3K/Akt/mTOR-dependent manner. *Cardiovasc Diagn Ther.* 10, 752–769. doi:10.21037/cdt-19-707

Yuan, Q., Chen, Z., Santulli, G., Gu, L., Yang, Z. G., Yuan, Z. Q., et al. (2014). Functional role of Calstabin2 in age-related cardiac alterations. *Sci. Rep.* 4, 7425. doi:10.1038/srep07425

Zhang, S., Liu, X., Bawa-Khalfe, T., Lu, L. S., Lyu, Y. L., Liu, L. F., et al. (2012). Identification of the molecular basis of doxorubicin-induced cardiotoxicity. *Nat. Med.* 18, 1639–1642. doi:10.1038/nm.2919

Zhang, J., Wang, M., Ding, W., Zhao, M., Ye, J., Xu, Y., et al. (2020). Resolvin E1 protects against doxorubicin-induced cardiotoxicity by inhibiting oxidative stress, autophagy and apoptosis by targeting AKT/mTOR signaling. *Biochem. Pharmacol.* 180, 114188. doi:10.1016/j.bcp.2020.114188

Zhao, L., and Zhang, B. (2017). Doxorubicin induces cardiotoxicity through upregulation of death receptors mediated apoptosis in cardiomyocytes. *Sci. Rep.* 7, 44735. doi:10.1038/srep44735

Zhong, Z., Gao, Y., Zhou, J., Wang, F., Zhang, P., Hu, S., et al. (2023). Inhibiting mir-34a-5p regulates doxorubicin-induced autophagy disorder and alleviates myocardial pyroptosis by targeting Sirt3-AMPK pathway. *Biomed. Pharmacother.* 168, 115654. doi:10.1016/j.biopha.2023.115654

Zhou, J., Wulfkuhle, J., Zhang, H., Gu, P., Yang, Y., Deng, J., et al. (2007). Activation of the PTEN/mTOR/STAT3 pathway in breast cancer stem-like cells is required for viability and maintenance. *Proc. Natl. Acad. Sci. U. S. A.* 104, 16158–16163. doi:10.1073/pnas.0702596104

Zilinyi, R., Czompa, A., Czegledi, A., Gajtko, A., Pituk, D., Lekli, I., et al. (2018). The cardioprotective effect of metformin in doxorubicin-induced cardiotoxicity: the role of autophagy. *Molecules* 23, 1184. doi:10.3390/molecules23051184

Frontiers in
Cell and Developmental Biology

Explores the fundamental biological processes of life, covering intracellular and extracellular dynamics.

The world's most cited developmental biology journal, advancing our understanding of the fundamental processes of life. It explores a wide spectrum of cell and developmental biology, covering intracellular and extracellular dynamics.

Discover the latest Research Topics

See more →

Frontiers

Avenue du Tribunal-Fédéral 34
1005 Lausanne, Switzerland
frontiersin.org

Contact us

+41 (0)21 510 17 00
frontiersin.org/about/contact